Distribution Agreement

In presenting this thesis or dissertation as a partial fulfillment of the requirements for an advanced degree from Emory University, I hereby grant to Emory University and its agents the non-exclusive license to archive, make accessible, and display my thesis or dissertation in whole or in part in all forms of media, now or hereafter known, including display on the world wide web. I understand that I may select some access restrictions as part of the online submission of this thesis or dissertation. I retain all ownership rights to the copyright of the thesis or dissertation. I also retain the right to use in future works (such as articles or books) all or part of this thesis or dissertation.

Signature:

_____ _____

Thomas Pickel Date

Synthesis of bulky 1,4,7-triazacylcononanes, including asymmetric derivatives; Esterification by aryl-diselenide catalyzed redox condensation; 1-amino-3,4-difluorocyclopentane-1-carboxylic acids as PET imaging agents

By

Thomas Pickel
Doctor of Philosophy

Chemistry

_____

Lanny S. Liebeskind, Ph.D.
Advisor

_____

Frank E. McDonald, Ph.D.
Committee Member

_____

Nathan T. Jui, Ph.D.
Committee Member

Accepted:

_____

Lisa A. Tedesco, Ph.D.
Dean of the James T. Laney School of Graduate Studies

_____

Date

Synthesis of bulky 1,4,7-triazacylcononanes, including asymmetric derivatives; Esterification by aryl-diselenide catalyzed redox condensation; 1-amino-3,4-difluorocyclopentane-1-carboxylic acids as PET imaging agents

By

Thomas Pickel
B.A., Western Connecticut State University

Advisor: Lanny Liebeskind, Ph.D.

An abstract of
A dissertation submitted to the Faculty of the
James T. Laney School of Graduate Studies of Emory University
in partial fulfillment of the requirements for the degree of
Doctor of Philosophy
in Chemistry
2019

Abstract

Synthesis of bulky 1,4,7-triazacylcononanes, including asymmetric derivatives; Esterification by aryl-diselenide catalyzed redox condensation; 1-amino-3,4-difluorocyclopentane-1-carboxylic acids as PET imaging agents
By Thomas Pickel

Triazacyclononane and its N-substituted derivatives have been extensively applied as ligands in coordination chemistry and catalysis. While the coordination chemistry of tacn has reached a level of relative maturity, synthetic access to the tacn scaffold remains highly underdeveloped. To date, there are no examples of N-substituted tacn derivatives that contain a non-annulet stereocenter alpha to the annular N atoms, or unsymmetrically N-substituted derivatives where one or two R groups are tertiary. Reported herein is an efficient method for preparing the previously inaccessible derivatives of tacn described above, as well as improved routes to the industrially relevant compounds H_3tacn and H_4dtne.

The dehydrative condensation of alcohols and carboxylic acids to generate esters is classically performed in the presence of a Lewis or Brønsted acid, or by preactivation of the carboxylic acid to generate a powerful and highly acidic electrophile. An alternative approach to this transformation is reduction oxidation condensation (redox condensation), which involves the formal oxidative removal of "H_2" and reductive removal of "O", allowing for the coupling of carboxylic acids and alcohols under relatively milder conditions. Generally, esterification by redox condensation requires both a stoichiometric oxidant and reductant, rendering these protocols wasteful. In this work, a redox dehydration esterification of carboxylic acids and alcohols in the presence of a catalytic aryl diselenide oxidant with O_2 as a terminal oxidant and triethylphosphite as the terminal reductant is described.

Reported herein is the cold synthesis, ^{18}F radiosynthesis, and biological evaluation of the four stereoisomers of 1-amino-3,4-difluorocyclopentane-1-carboxylic acid (3,4-DFACPC), a series of non-natural amino acids for use in Positron Emission Tomography (PET). *In vitro* 9L, U87 ΔEGFR, and DU145 cancer cell line assays demonstrated that 3,4-DFACPCs are substrates primarily for system L transport, with some transport occurring via system ASC. In Fischer rats bearing 9L gliosarcoma tumors, [^{18}F]3,4-DFACPCs showed high levels of uptake in tumors and good tumor to normal brain tissue ratios, suggesting that these compounds may be useful as PET radiotracers for imaging brain tumors. Additionally, biodistribution studies in healthy Fischer rats as well as uptake in DU145 cells collectively imply that [^{18}F]3,4-DFACPCs may have promise for imaging prostate cancer.

Synthesis of bulky 1,4,7-triazacylcononanes, including asymmetric derivatives; Esterification by aryl-diselenide catalyzed redox condensation; 1-amino-3,4-difluorocyclopentane-1-carboxylic acids as PET imaging agents

By

Thomas Pickel
B.A., Western Connecticut State University

Advisor: Lanny S. Liebeskind, Ph.D.

A dissertation submitted to the Faculty of the
James T. Laney School of Graduate Studies of Emory University
in partial fulfillment of the requirements for the degree of
Doctor of Philosophy
in Chemistry
2019

Acknowledgements

As all who've sought a doctoral degree are aware, obtaining a PhD is a difficult endeavor that is completed in equal measure by the one pursuing the degree and by the friends, family, and mentors who support, guide, and teach them. I am certain that without the assistance of the many people who've stood behind me, I could not have succeeded in this program. Firstly, I would like to thank both of my advisors, Dr. Christopher Scarborough and Dr. Lanny Liebeskind. Most graduate students are lucky to have one advisor who takes an active role in their development; I had the good fortune of having two. Chris is a gifted speaker, teacher, and passionate student of chemistry whom I'm thankful to have had the opportunity to learn from during my first few years as a graduate student. Lanny is likewise a talented teacher and a steadying presence from whom I've learned a methodical and disciplined approach to research that I am certain will serve me well in my career. I would also like to thank my committee members Dr. Frank McDonald and Dr. Nate Jui, both of whom were always available to offer helpful advice at various stages of my time at Emory. I would be remiss if I failed to mention that Nate plays a mean right-center field, which I credit with getting me out of an inning or two. I owe a debt of gratitude to the faculty at Western Connecticut State University including Dr. Paul Hines, Dr. Anne Roberts, Dr. Russell Selzer, Dr. Richard Molinelli, Dr. Yuan Mei-Ratliff, Dr. Paula Secondo, and especially my advisor Dr. Nicholas Greco, for providing me with the opportunity to succeed as an undergraduate and encouraging me to pursue graduate studies. For more than three years at Emory, I was privileged to learn the crystallographic trade from John Bacsa, whose unique brand of humor I will greatly miss. As any chemist knows, at times the lab can be a trying place. My time in lab was made infinitely more enjoyable by the many wonderful labmates I've had, including Sriram, Pavan, Greg, Gouthami, Michele, Dan, Nuke, Cassandra, Martin, Eddy, Haleigh, and Christian. I'm grateful to have made some great friends here who helped me to enjoy time spent outside of the lab, especially Charlie, Spencer, Christian, Matt, and Adam. If not for my friends Nick and Peter, I would never have made it to Emory, and I owe them thanks as well. Lastly, I'd like to acknowledge my incredibly supportive family. Scott and Sandy made Atlanta feel like a home away from home. My brother Ryan, and my parents Jim, Michele, and Tom offered endless encouragement throughout my graduate studies, and have shared in each of the struggles I've encountered along the way. I owe a special thanks to my mom for always being patient and kind, for talking me off the proverbial ledge at any time of day or night, and for pushing me to be the best that I can be. Finally, Jessica, thank you for being the light at the end of the tunnel and for being a constant source of motivation to finish these studies. I have many things to be grateful for from my time at Emory, but I'm most grateful that it brought us together.

Tables of Contents

List of Figures

Chapter 1

Chapter 2

List of Schemes

Chapter 1

Chapter 2

Chapter 3

List of Tables

Chapter 2

Chapter 3

Chapter 1

Synthesis of Previously Inaccessible Derivatives of 1,4,7-*Tri*-R-1,4,7-Triazacyclononane, Including Chiral Examples, and a Rapid Synthesis of the HCl Salts of H_3tacn and H_4dtne

Adapted from: T. C. Pickel, G. J. Karahalis, C. T. Buru, J. Bacsa, C. C. Scarborough. Synthesis of Previously Inaccessible Derivatives of 1, 4, 7-Tri-(R*)*-1, 4, 7-Triazacyclononane, Including Chiral Examples, and a Rapid Synthesis of the HCl Salts of H_3tacn and H_4dtne. *Eur. J. Org. Chem.* **2018**, *2018*, 6876-6889.

G. J. Karahalis assisted in the synthesis and or characterization of $\mathbf{2^{Me}}$, $\mathbf{2^{Bn}}$, $\mathbf{2^{iPr}}$, $\mathbf{3^{tBu,Bn}}$, ***t*Bu$_2$Bntacn**, $\mathbf{3^{tBu,dmea}}$, ***t*Bu$_2$dmeatacn**, $\mathbf{3^{tBu,pic}}$, ***t*Bu$_2$pictacn**, compound **1.05,** and ***t*Bu$_4$dtne**.

C. T. Buru assisted in the synthesis of compound **1.05**.

1.1 Abstract: The synthesis of 1,4,-di-*tert*-butyl-7-R-1,4,7-triazacyclononane (tBu$_2$Rtacn) derivatives via a "crab-like" cyclization is reported. The *tert*-butyl groups were cleavable with concentrated hydrochloric acid, allowing for a facile and convenient synthesis of the HCl salt of H$_3$tacn and the most direct route to its industrially relevant binucleating N-ethylene bridged derivative, H$_4$dtne. The "crab-like" synthesis was also extended to the synthesis of chiral tacn derivatives with both one (tBu$_2$Rtacn) and two (tBuR$_2$tacn) stereocenters in non-annulet, alpha-N positions. Additionally, the synthesis of tBuH$_2$tacn is described, and its steric profile, along with that of tBu$_2$Htacn, was quantified and compared to known R$_3$tacn derivatives (R = Me, iPr, tBu) via the percent buried volume method.

1.2 Introduction

1,4,7-Triazacyclononane (H$_3$tacn) and its N-substituted derivatives (R$_3$tacn) have a rich history as ligands for transition metals owing to their nearly ideal *facial* coordination geometry which confers resistance to substitution. R$_3$tacn ligands, including R$_2$tacn(CH$_2$CH$_2$)R$_2$tacn (**R$_4$dtne**, Figure 1.1), have found applications in both coordination chemistry[1] and catalysis, with notable examples of the latter being (R$_3$tacn)Mn catalysts for bleaching cotton and wood pulp with H$_2$O$_2$.[2] A limitation in the application of R$_3$tacn ligands is the laborious and waste-intensive route by which these ligands are commonly synthesized[3] (the Richman-Atkins synthesis, Scheme 1-1a). Despite multiple reports describing improved syntheses of H$_3$tacn[4], the need for a more efficient, expedient, and atom economic synthesis remains. Furthermore, there have been comparatively few improvements in the syntheses of R$_3$tacn derivatives, most of which are synthesized by alkylation of H$_3$tacn, and several challenges associated with their preparation persist:

(1) The synthesis of R_3tacn ligands where one or more of the R groups is different from the others requires laborious and time-intensive protecting group manipulation.[5]

(2) Unsymmetrical R_3tacn ligands where one or two R groups are tertiary alkyl are not known.

(3) Current routes to chiral derivatives of R_3tacn are very limited and have found limited success,[6] likely owing to the non-ideal chiral environment established by ligands synthesized by current routes. These include (1) derivatives with chiral R groups where the chiral center is removed from the nitrogen atoms by one methylene unit,[6g, 7] and (2) derivatives where chirality comes from chiral centers on the 9-membered heterocycle,[6b-f, 8] where such chiral groups do not project toward the coordination sphere of the ligated metal.

R_3tacn ligands are typically synthesized via alkylation of H_3tacn by Eschweiler-Clarke methylation (to afford Me_3tacn),[9] by substitution of alkyl halides[4d] or by ring-opening of epoxides.[6g, 7a] The Richman-Atkins route to R_3tacn ligands is required because the synthesis of H_3tacn, which is derived directly from deprotection of Ts3tacn, precludes installing R groups prior to formation of the 9-membered heterocycle. Accordingly, R_3tacn derivatives with *tertiary* alkyl R groups are inaccessible by this route, and were unreported until 2013 when we demonstrated a short and efficient synthesis of *t*Bu_3tacn,[10] which we have shown to offer a unique steric and oxidatively robust coordination environment. The route we employed to access *t*Bu_3tacn was an extension of the so-called "crab-like" cyclization method originally reported by Izatt and co-workers,[11] and later utilized by Bolm[12] and Murray,[13] for the synthesis of Me_2Rtacn ligands (R = primary alkyl group, Scheme 1-1b). This route, which involves chloroacetylation of $\mathbf{1^R}$ derivatives, cyclization around an amine, and reduction of the diamide product with $LiAlH_4$, was ideally suited for the synthesis of R_3tacn derivatives bearing *tertiary* alkyl R groups because these groups could be

installed prior to cyclization (installation of *tertiary* alkyl groups after cyclization has not been reported because methods for alkylation of secondary amines with tertiary alkyl groups are exceptionally rare[14]).

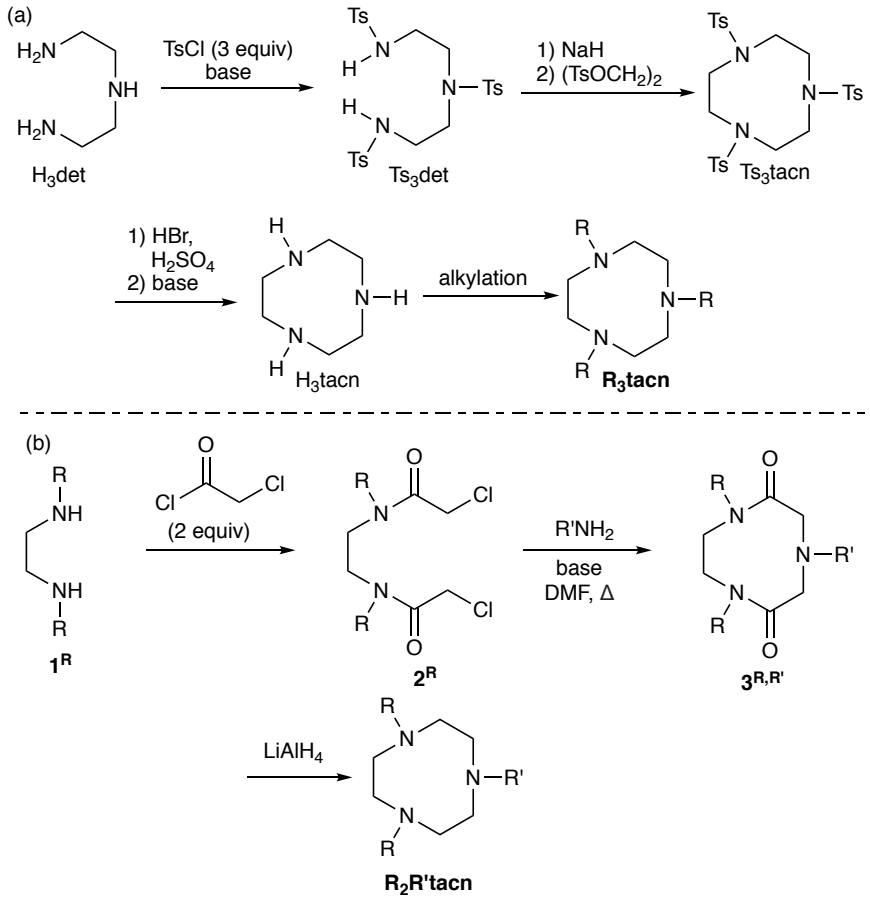

Scheme 1-1. Synthesis of R_3tacn derivatives by the (a) Richman-Atkins and (b) "crab-like" cyclization and reduction.

In this work, we demonstrate how this modified "crab-like" cyclization route may be employed for the synthesis of unsymmetrical *t*Bu$_2$Rtacn and *t*Bu$_4$dtne ligands, as well as for a rapid route to the HCl salts of H$_3$tacn and H$_4$dtne that involve significantly less waste than the Richman-Atkins route. Furthermore, we demonstrate the first syntheses of chiral R$_3$tacn ligands with chiral centers directly on the nitrogen substituent(s). A critical analysis of factors determining the accessibility of R$_3$tacn ligands by this route is included, which highlights both the scope and limitations of the

methodology. These studies open the possibility of investigating new and previously inaccessible R_3tacn ligands in catalysis, particularly in asymmetric catalysis where advances have been hindered by the nature of the currently accessible derivatives.

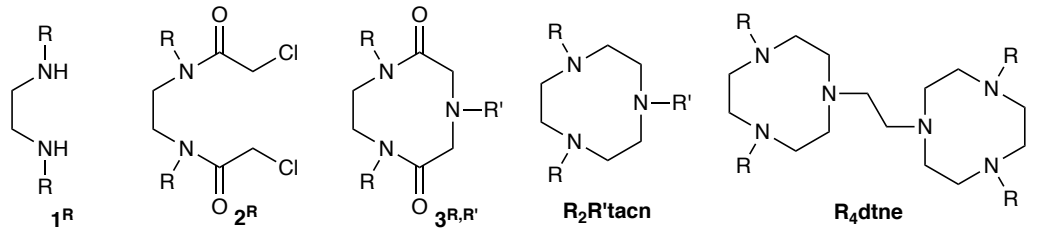

Figure 1-1. Numbering scheme for compounds described herein.

1.3 Results and Discussion

Synthesis of tBu_2Rtacn derivatives

Several routes for the synthesis of unsymmetrical R_3tacn ligands where no more than two R groups are the same have been reported in the decades since the discovery of H_3tacn. One notable technique includes the conversion of H_3tacn to the corresponding tricyclic orthoamide that can be alkylated only once and then deprotected to afford RH_2tacn (R is a primary or secondary alkyl group or a protecting group).[5a] Such derivatives can then be further elaborated, and this route has been applied to the synthesis of a derivative where all three R groups of R_3tacn are unique.[5a, 15] However, such compounds require many steps to access. Another notable route is mono de-tosylation of Ts_3tacn to afford Ts_2Htacn followed by alkylation and deprotection;[5b, c, 16] this route is used in the industrial production of Me_4dtne, which, along with Me_3tacn, is the most important industrial R_3tacn derivative owing to its success as a ligand for manganese in the H_2O_2 bleaching of cotton and wood pulp.[2b] Most recently, a promising route has been developed starting from diethylenetriamine and chloroacetaldehyde.[4c] Nonetheless, these syntheses cannot be used for the preparation of unsymmetrical R_3tacn derivatives where at least one R group is a tertiary alkyl

group because substitution of a tertiary alkyl group with a secondary nitrogen is not feasible. Therefore, this class of sterically unique and oxidatively resistant ligands has never been reported. It should be noted that an attempt to synthesize an unsymmetrical R_3tacn derivative from a diethylene triamine derivative bearing an alkyl group on the central nitrogen by a route analogous to the one shown in scheme 1-1a failed because of the nucleophilicity of the central nitrogen.[6b] The "crab-like" cyclization route to Me_2Rtacn derivatives with primary alkyl groups, developed by Izatt and co-workers,[11] involves cyclization of **2^{Me}** around primary amines followed by reduction with $LiAlH_4$ and is the only route with promise for the incorporation of at least one *t*Bu substituent on nitrogen. Consistent with this perspective, this route was successfully applied in the first synthesis of *t*Bu$_3$tacn[10] from **1^{tBu}**, chloroacetyl chloride and *t*BuNH$_2$ via **2^{tBu}**. We reasoned that this route could be applied broadly to the synthesis of *t*Bu$_2$Rtacn derivatives by cyclization of diamide **2^{tBu}** (prepared from chloroacetyl chloride and **1^{tBu}** in 94% yield) around various primary amines followed by reduction with $LiAlH_4$.

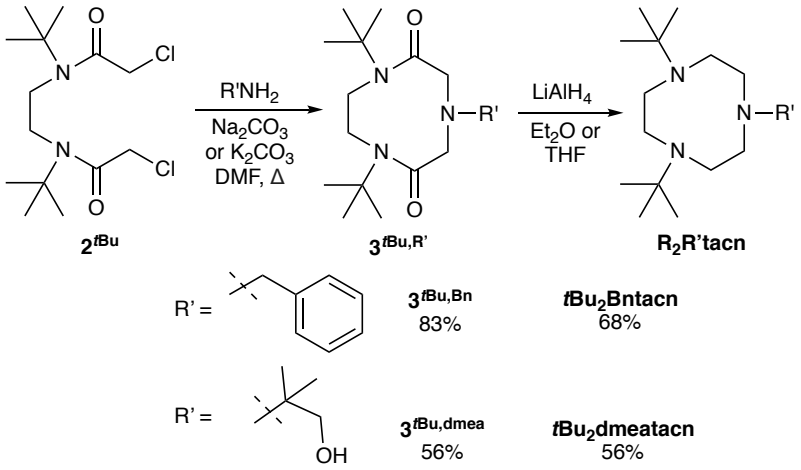

*Scheme 1-2. Synthesis of **R_2R'tacn** derivatives.*

Indeed, as shown in Scheme 1-2, *t*Bu$_2$Rtacn derivatives were prepared by this method, granting access to the first unsymmetrical R_3tacn derivatives bearing tertiary nitrogen substituents.

In addition to the novelty of the ligands provided through this route, our method is amenable to the facile preparation of sterically bulky analogues of well-known and highly useful tacn derivatives that are otherwise tedious to prepare. For example, **Me$_2$pictacn** (pic = 2-picolylamine) requires at least five working days and seven steps to synthesize, though it has nonetheless been used extensively in coordination chemistry and catalysis over the last decade.[17] In contrast, the synthesis of ***t*Bu$_2$pictacn** requires two working days and three steps, each of which was carried out successively without purification of any intermediates (Scheme 1-3).

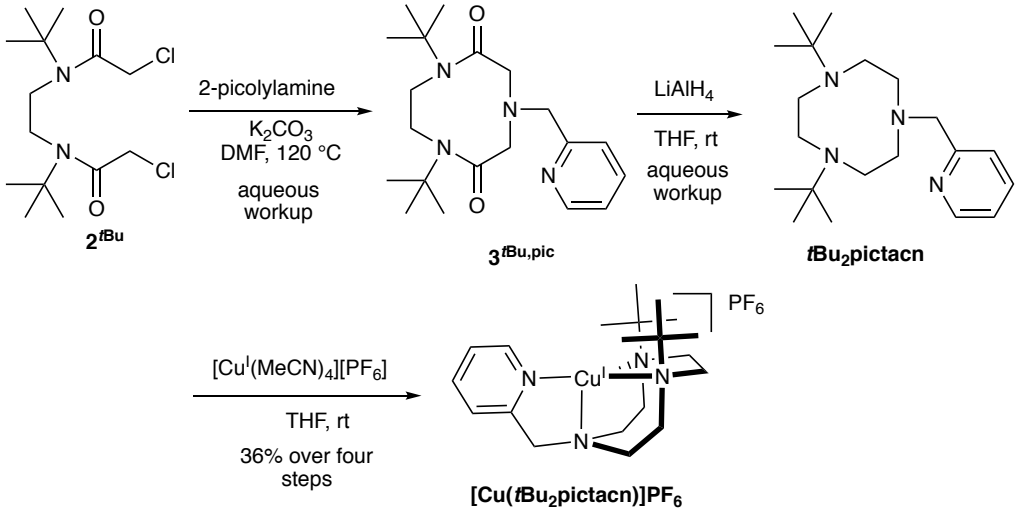

*Scheme 1-3. Synthesis of **tBu$_2$pictacn** and **[Cu(tBu$_2$pictacn)]PF$_6$**.*

As an added feature demonstrating the efficiency of this method, the otherwise challenging purification of ***t*Bu$_2$pictacn**, which is an oil at room temperature, was circumvented by metalation of the crude ligand with [Cu(MeCN)$_4$]PF$_6$ followed by crystallization to afford **[Cu(*t*Bu$_2$pictacn)]PF$_6$** (Figure 1-2) in 36% yield over four steps. Given its ease of synthesis, ***t*Bu$_2$pictacn** may be an attractive alternative to Me$_2$pictacn as a tetradentate ligand for supporting metal catalyzed oxidative transformations.

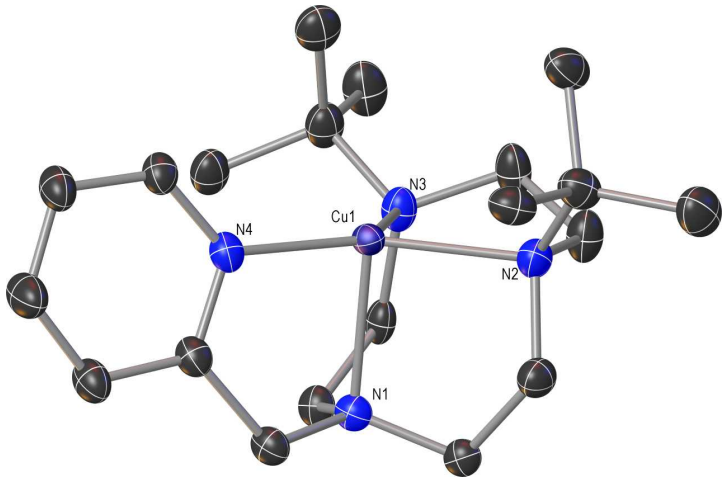

Figure 1-2. Molecular structure of ***[Cu(tBu$_2$pictacn)]PF$_6$****. Hydrogen atoms and PF_6^- counterion omitted for clarity.*

Remarkably, the synthesis of ***t*Bu$_2$Htacn** by this route through cyclization of **2$^{t\mathrm{Bu}}$** around NH_3 was also successful, requiring a large excess of ammonia to prevent oligomerization, and the use of a pressure vessel to accommodate heated solutions of NH_4OH. In our experience, ***t*Bu$_2$Htacn** is the most readily synthesized R_3tacn ligand; the three-step synthesis can be completed in 46% overall yield without any purification prior to distillation of the final product (Scheme 1-4). With the appropriate facilities, this ligand may be synthesized on large scale within two working days.

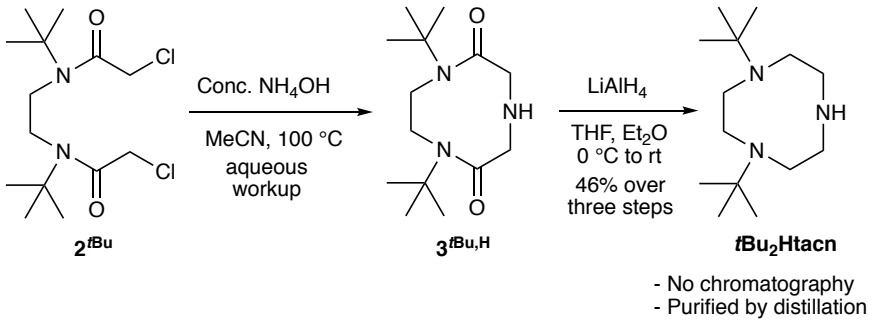

Scheme 1-4. Synthesis of ***tBu$_2$Htacn****.*

Efficient Synthesis of $[H_6tacn][Cl]_3$ from *t*Bu_2Htacn

From an industrial perspective, Me_3tacn is among the most important R_3tacn derivatives. It is an effective ligand for the large-scale manganese-catalyzed H_2O_2 bleaching of wood pulp and cotton for the paper and textile industries and is also used in commercial dishwasher detergents as H_2O_2 activators, processes that together utilize more than half of global H_2O_2 production [2b, 18]. Me_3tacn is presently produced through Eschweiler-Clarke methylation of H_3tacn, a process that proceeds in near-quantitative yields. Therefore, an improvement in the route to Me_3tacn likely requires an improved route to H_3tacn. Production of H_3tacn has been the subject of multiple patents in the past four decades, but nearly all methods have coalesced around the cyclization of twice-deprotonated Ts_3det with $TsOCH_2CH_2OTs$ to afford Ts_3tacn. Deprotection of the tosyl groups generally utilizes H_2SO_4 to form $[H_6tacn]_2[SO_4]_3$, an insoluble species that is more easily isolated when converted to $[H_6tacn][Cl]_3$ using concentrated hydrochloric acid.[3] Generally, $[H_6tacn][Cl]_3$ is subjected to Eschweiler-Clarke methylation without isolation by addition of sufficient base to deprotonate $[H_6tacn]^{3+}$.[1a, 4d, 19] While highly optimized, the Richman-Atkins route utilizes five equivalents of tosyl protecting groups per equivalent of Me_3tacn formed, where TsO^- and Me_3tacn both have molecular/ionic weights of 171 g/mol.

Given that ***t*Bu$_2$Htacn** is so readily accessible, we imagined that removal of the *tert*-butyl moieties may provide an attractive alternative route to H_3tacn. After screening several sets of conditions, we found that treatment of ***t*Bu$_2$Htacn** with conc. HCl at 95 °C overnight provided the desired **$[H_6tacn][Cl]_3$** in 89% yield (Scheme 1-5).

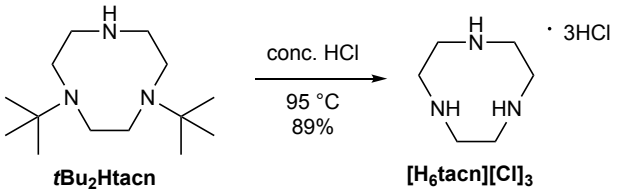

Scheme 1-5. Synthesis of ***[H$_6$tacn][Cl]$_3$*** *via acidic deprotection of* ***tBu$_2$Htacn***.

We assess that this route to **[H$_6$tacn][Cl]$_3$** is particularly attractive when compared to the conventional Richman-Atkins route for the following reasons:

(1) Upon deprotection of ^{t}Bu$_2$Htacn, 54% of the total mass is converted to an H$_3$tacn salt, compared to only 22% in the case of Ts$_3$tacn (assuming quantitative yields). Therefore, the route described here should be especially useful for large scale preparations of Me$_3$tacn, where atom economy and ease of scalability are particularly important.

(2) This synthesis of **[H$_6$tacn][Cl]$_3$** requires only one purification step: vacuum distillation of ^{t}Bu$_2$Htacn, as crystallization of **[H$_6$tacn][Cl]$_3$** occurs spontaneously upon cooling of the reaction mixture.

(3) The overall synthesis of **[H$_6$tacn][Cl]$_3$** from commercially available di-*tert*-butylethylenediamine can be accomplished within two days, including workups and purifications.

Below, we demonstrate the utility of this route in the practical and highly expedient synthesis of another industrially relevant tacn derivative, **Me$_4$dtne**.

Synthesis of chiral tacn derivatives with one chiral R group

One of the longest standing challenges in tacn synthesis is the development of effective chiral derivatives for asymmetric catalysis. To date, synthetic routes to chiral R$_3$tacn derivatives have

proceeded by one of two routes: (1) substitution of H_3tacn with an epoxide[6g] or lactone[7] or (2) introduction of annulet (ring) substituents during the Richman-Atkins synthesis of an H_3tacn derivative.[6b-f, 8] Tacn compounds generated by the former method possess a beta-N chiral center that is too remote to produce a significant stereoinductive influence on the coordination sphere of a coordinated metal, while the latter have stereocenters on the tacn annulus (ring), which projects away from the coordination sphere. These ligands have been employed in a number of reports, mainly in the pursuit of a Mn(R_3tacn) catalyzed asymmetric olefin epoxidation[6] based on the system developed by Hage.[2a] Only poor to moderate ee's were observed in these studies, consistent with the notion that such chiral tacn derivatives have a fundamental design flaw originating from the limitations associated with the available methods for their synthesis.

Asymmetric tacn derivatives with exocylic-N alpha stereocenters represent the ideal design for maximizing the stereoinductive influence of the tacn framework on the metal coordination sphere. To date, tacn derivatives of this type are unknown in the literature, likely due to the challenges associated with asymmetric functionalization of H_3tacn or its mono or di-protected analogues. We recognized that by employing the "crab-like" cyclization strategy, an amine with an alpha-N stereocenter could be incorporated into the tacn ring during the cyclization step, obviating the need for a direct asymmetric functionalization of tacn. To this end, **2**$^{t\mathbf{Bu}}$ was reacted with *sec*-phenethyl, *exo*-bornyl, and menthyl amine under our previously established cyclization conditions to provide the corresponding asymmetric diamides. Reduction of the diamides with $LiAlH_4$ furnished the first series of chiral tacn derivatives with non-annulet, alpha-N stereocenters (Scheme 1-6). Copper (I) complexes of ***t*Bu$_2$menthyltacn** and ***t*Bu$_2$*sec*-PhEttacn** have been prepared and characterized by single-crystal X-ray diffraction analysis (Figures 1-3 and 1-4, respectively).

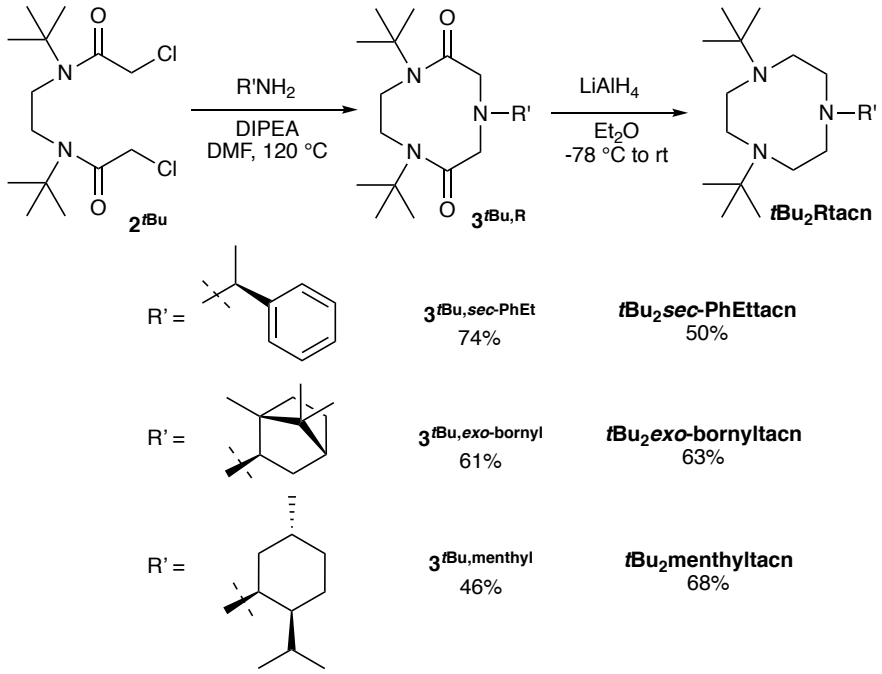

Scheme 1-6. Synthesis of tBu_2Rtacn derivatives where R' is a chiral group.

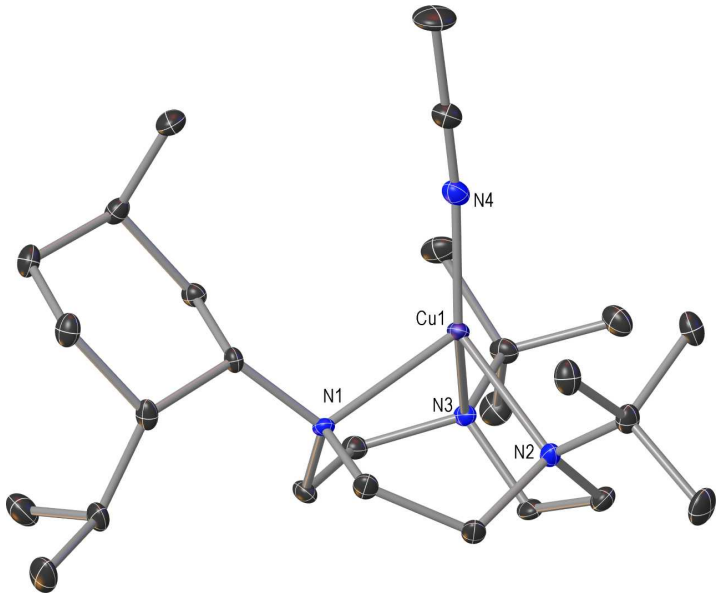

Figure 1-3. Molecular structure of ***[Cu(tBu_2menthyltacn)MeCN]PF_6****. Hydrogen atoms and PF_6^- counterion omitted for clarity.*

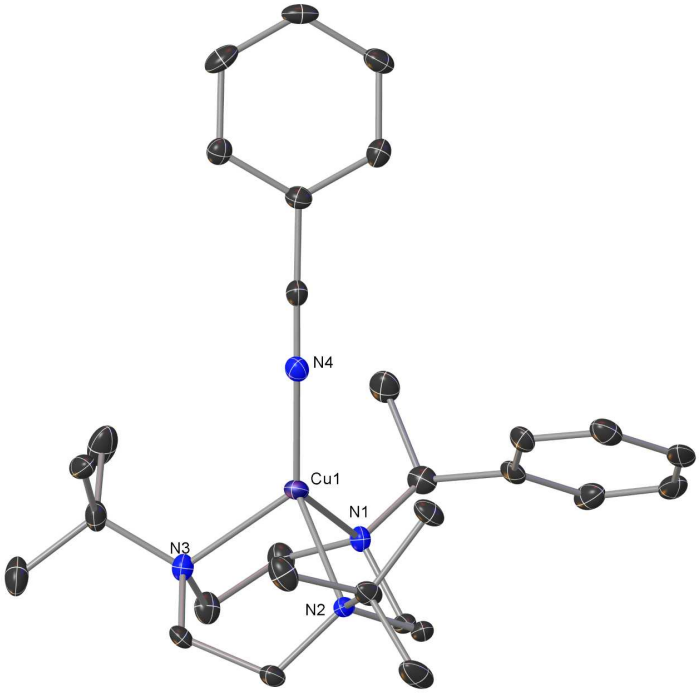

Figure 1-4. Molecular structure of ***[Cu(tBu$_2$sec-PhEttacn)(NCPh)]OTf.*** *Hydrogen atoms and OTf⁻ counterion omitted for clarity.*

Synthesis of a chiral tacn derivative with two chiral R groups

Having successfully utilized a "crab-like" cyclization in the preparation of tacn derivatives with one chiral R group, we sought to extend this method to the synthesis of tacn derivatives with two chiral R groups. In theory, the most straightforward route to such compounds proceeds through the synthesis of $\mathbf{2^{R}}$ derivatives where R is a chiral functionality with an alpha-N stereocenter. However, we have noted that $\mathbf{2^{tBu}}$ is unique, allowing facile ring closure around a range of primary amines where $\mathbf{2^{me}}$, $\mathbf{2^{Bn}}$, and $\mathbf{2^{iPr}}$ are generally ineffective as precursors to R_2R'tacn derivatives, with few exceptions.[11c, 12-13] This disparity is rationalized by considering the effect amide rotamers have on the ability of $\mathbf{2^{R}}$ derivatives to achieve the necessary conformation to undergo cyclization (*vide infra*). Therefore, we were presented with the difficult challenge of identifying

$\mathbf{2^R}$ derivatives where R is an alpha-N chiral moiety useful for stereoinduction but is also sterically bulky enough to allow for effective ring closure.

We began by preparing asymmetric $\mathbf{2^R}$ derivatives with secondary alpha-N stereocenters. However, in agreement with our previous observation that such $\mathbf{2^R}$ compounds undergo competitive oligomerization, attempted cyclization resulted in intractable mixtures of oligomeric byproducts with no trace of the desired $\mathbf{3^{R,R'}}$ product. Given that tertiary R groups seem to be indispensable in the cyclization of $\mathbf{2^R}$ compounds, we wondered if mixed a $\mathbf{2^{R,R'}}$ species containing one tertiary R group and one secondary R group might also undergo cyclization.

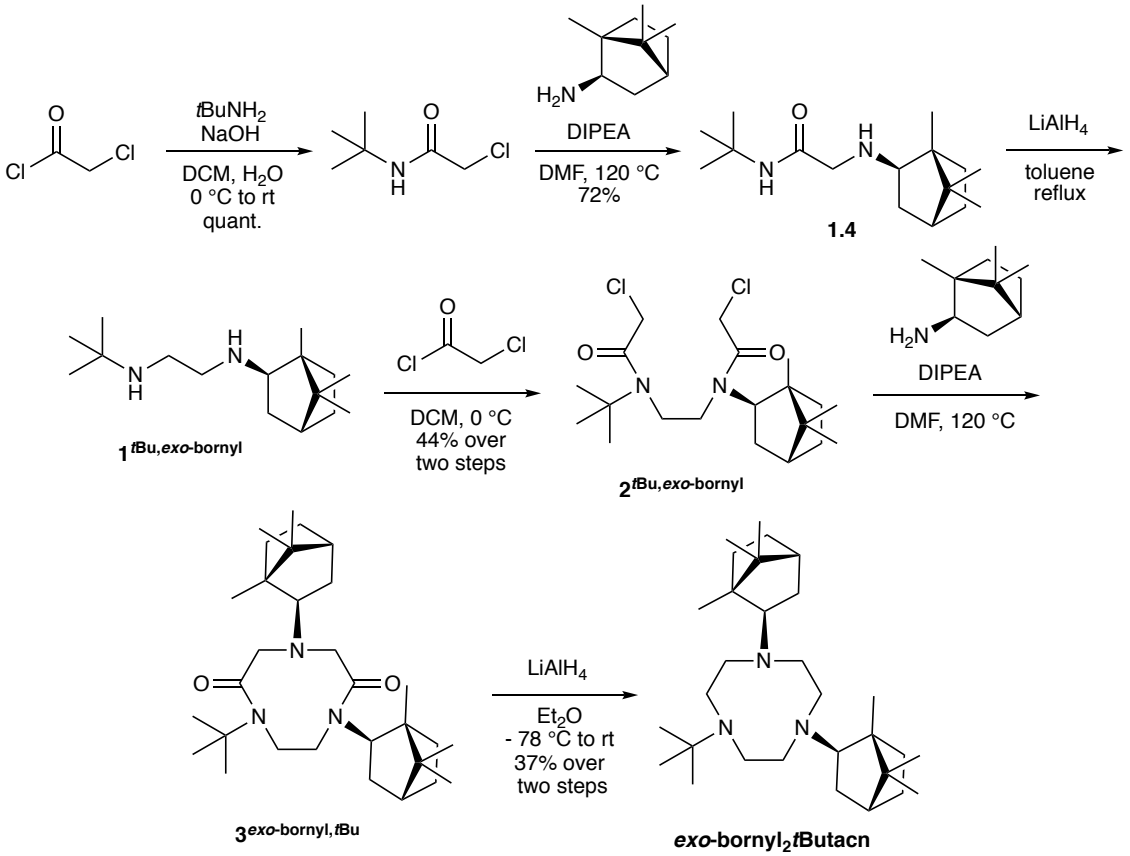

Scheme 1-7. Synthesis of ***exo-bornyl$_2$tButacn****.*

To probe this concept, unsymmetrical diamide $\mathbf{2^{tBu,exo\text{-}bornyl}}$ was prepared and subjected to cyclization conditions with exo-bornylamine and, to our delight, the reaction proceeded to give the

corresponding $\mathbf{3}^{exo\text{-}bornyl,tBu}$ diamide. LAH reduction of $\mathbf{3}^{exo\text{-}bornyl,tBu}$ furnished ***exo*-bornyl$_2$*t*Butacn**, the first tacn derivative with multiple exocyclic alpha-N stereocenters (Scheme 1-7, Figure 1-5).

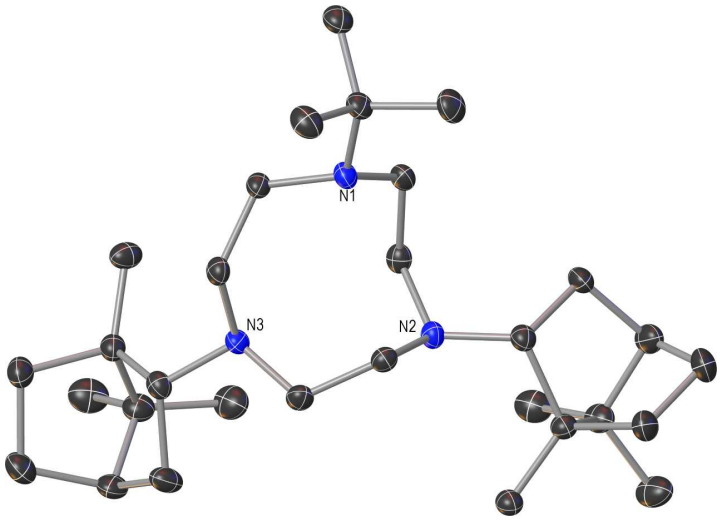

Figure 1-5. Molecular structure of ***exo-bornyl$_2$tButacn.*** *Hydrogen atoms omitted for clarity.*

To probe the generality of $\mathbf{2}^{tBu,R}$ (where R is a secondary alkyl group) as precursors to $\mathbf{3}^{tBu,R}$ products, we prepared the simplest $\mathbf{2}^{tBu,R}$ derivative, $\mathbf{2}^{tBu,iPr}$. Interestingly NMR spectra of this compound suggest that it samples only one rotamer on the NMR timescale (see supporting information: Figure S1-31), consistent with the spectra of $\mathbf{2}^{tBu,exo\text{-}bornyl}$ and $\mathbf{2}^{tBu}$. Exposure of $\mathbf{2}^{tBu,iPr}$ to S-(-)-alpha-methylbenzylamine (*sec*-PhEt) under the previously established cyclization conditions gave the triply unsymmetrically substituted tacn derivative $\mathbf{3}^{tBu,iPr,sec\text{PhEt}}$, and reduction with $LiAlH_4$ furnished the corresponding ***sec*-PhEt*i*Pr*t*Butacn** (Scheme 1-8). These results suggest that $\mathbf{2}^{tBu,R}$ derivatives may be generally useful as precursors to tacn compounds. Furthermore, in addition to providing a method for accessing chiral tacn derivatives with two chiral N-substituents, this route can be used to prepare tacn derivatives with three different N-substituents in only three steps from simple ethylenediamines. It is our hope that the disclosure of this method will stimulate the development of new tacn supported catalysts for asymmetric transformations.

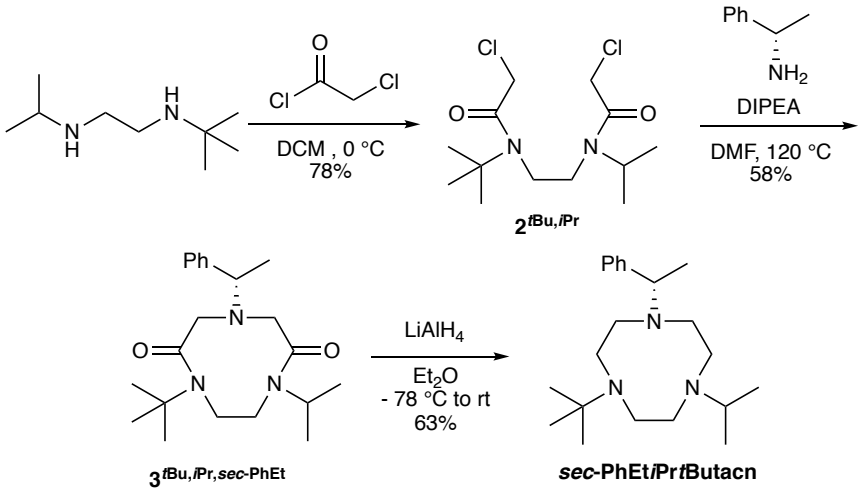

Scheme 1-8. Synthesis of ***sec-PhEtiPrtButacn****.*

Synthesis of *t*Bu$_4$dtne and [H$_{10}$dtne][Cl$_6$]

Because **[H$_6$tacn][Cl]$_3$** is so readily accessible through the route described above (vide supra), we questioned whether this route would be competitive with the current Richman-Atkins route in the synthesis Me$_4$dtne, a widely used and industrially relevant tacn derivative.[2b, 18] Me$_4$dtne is currently produced by selective deprotection of Ts$_3$tacn to [Ts$_2$H$_2$tacn][OTs], coupling of two Ts$_2$Htacn units with TsOCH$_2$CH$_2$OTs to afford Ts$_4$dtne, and tosyl deprotection to afford **[H$_{10}$dtne][Cl$_6$]**, which is subjected to one-pot neutralization/Eschwelier-Clark methylation to Me$_4$dtne[16]. Given that the Eschweiler-Clark methylation proceeds in nearly quantitative yield from **[H$_{10}$dtne][Cl$_6$]**, we targeted an improved synthesis of **[H$_{10}$dtne][Cl$_6$]** by exploring routes to generate **[H$_{10}$dtne][Cl$_6$]** using the methodology described above. To this end, the cyclization of diamide **2$^{t\mathrm{Bu}}$** around ethylenediamine was attempted, providing the desired tetraamide in 60% yield; however, reduction of the product to ***t*Bu$_4$dtne** using LiAlH$_4$ only occurred in 28% yield owing to isolation challenges (Scheme 1-9). Nonetheless, removal of the *tert*-butyl groups in ***t*Bu$_4$dtne** using concentrated hydrochloric acid at 95 ºC overnight afforded, upon cooling, 86% yield of **[H$_{10}$dtne][Cl$_6$]** without any detectable **[H$_6$tacn][Cl]$_3$** impurity, which is a common

impurity in the industrial synthesis of **[H$_{10}$dtne][Cl$_6$]**. While this four-step route is appealing when compared with the seven-step industrial route to this ligand, the purification of ***t*Bu$_4$dtne** is a major drawback. Therefore, we examined whether two ***t*Bu$_2$Htacn** groups could be coupled with 1,2-dibromoethane, a preferred source of the ethylene bridge in R$_4$dtne compared to TsOCH$_2$CH$_2$OTs, to afford ***t*Bu$_4$dtne**. Indeed, combining ***t*Bu$_2$Htacn** and 1,2-dibromoethane on saturated aqueous K_2CO_3 ("on water") for two hours in a 1:1 ratio afforded pure solid *t*Bu$_4$dtne in 96% isolated yield as a solid that is filtered directly from the reaction mixture.

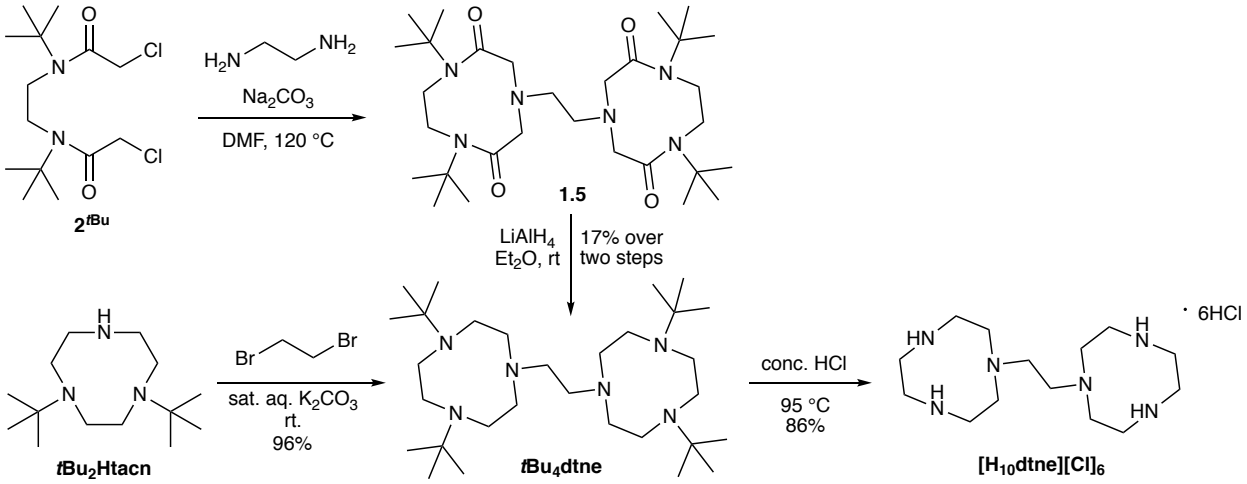

*Scheme 1-9. Synthesis of **tBu$_4$dtne** and deprotection to **[H$_{10}$dtne][Cl]$_6$**.*

As described above, the *tert*-butyl groups of ***t*Bu$_4$dtne** are readily removed with hydrochloric acid to afford **[H$_{10}$dtne][Cl$_6$]** in 86% yield. Thus we have developed a route to **[H$_{10}$dtne][Cl$_6$]** that provides several advantages over the traditional route including a shorter step count (five steps vs. seven steps), superior atom economy, and purification steps (one vs. four). We are optimistic that this advancement will encourage greater use of Me$_4$dtne in research settings and allow for more economical preparation on production scale.

Effect of tert-butyl substituted tertiary amides on 2^R ring closure

In the course of our work, we found that $\mathbf{2^R}$ derivatives, where at least one amide is substituted with a tertiary R group, undergo smooth cyclization to the corresponding diamide in good yield and with a broad range of sterically bulky amines. This finding stands in contrast to reports on the syntheses of tacn diamide derivatives from $\mathbf{2^{Me}}$, which proceed in modest yield and with only a narrow scope of sterically diminutive primary amines. In an effort to rationalize this disparity, we considered the effect of amide R groups on the conformation of $\mathbf{2^R}$ derivatives and the ability of the various possible conformers of $\mathbf{2^R}$ to undergo cyclization.

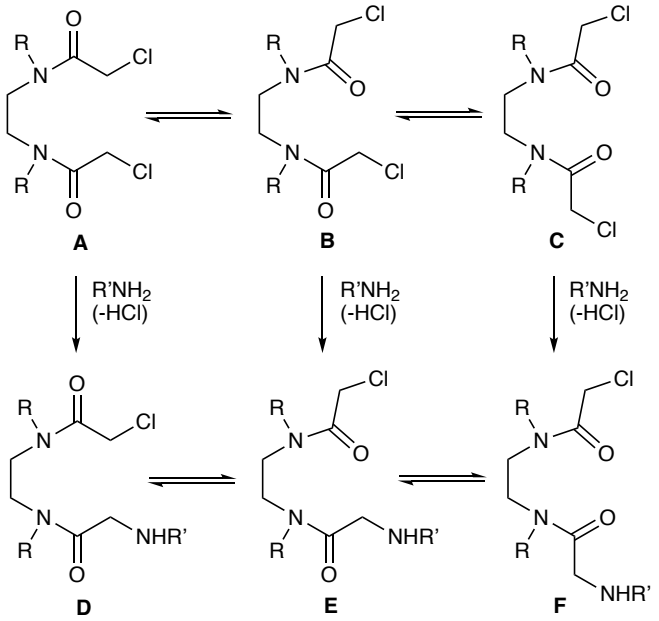

Scheme 1-10. Conformational isomerism in 2^R compounds and aminated intermediates.

An elementary analysis of the diamide $\mathbf{2^R}$ structure suggests that since both amides can adopt either the cis or trans rotamer, there are three possible molecular conformations: conformer **A** where both amides adopt the cis rotamer, conformer **B** where one amide is oriented cis and the other trans, and conformer **C** where both amides adopt the trans rotamer (Scheme 1-10). Following this line of reasoning, we assess that nucleophilic substitution of the aforementioned conformers with a primary amine gives rise to conformers **D**, **E**, and **F**. Conformer **D** is situated to allow cyclization,

owing to the close proximity of the amine and alkyl chloride moieties. Conversely, conformers **E** and **F** are unable to cyclize directly and are likely to form oligomeric byproducts. From this analysis, we conclude that cyclization will only occur directly from conformer **A**, and cyclization is therefore dependent on the ability of both amide moieties to adopt the cis rotamer conformation. Consequently, we speculate that $\mathbf{2^{R}}$ compounds with tert-butyl (and other sterically bulky functionalities) are relatively more competent for cyclization than their less bulky analogues due to the increased thermodynamic stability of the cis rotamer. To support this hypothesis, we were interested in experimentally identifying the conformers of a representative series of $\mathbf{2^{R}}$ derivatives. Understanding that amide rotamers generally equilibrate slowly enough at room temperature to be observable on the NMR timescale, we compared ^{1}H NMR spectra of $\mathbf{2^{R}}$ compounds with R groups of various sizes: $\mathbf{2^{Me}}$, $\mathbf{2^{Bn}}$, $\mathbf{2^{\textit{i}Pr}}$, and $\mathbf{2^{\textit{t}Bu}}$ (for the former three compounds, see supporting information: Figures S1-1, S1-3, and S1-5 respectively. The ^{1}H NMR spectrum of $\mathbf{2^{\textit{t}Bu}}$ has been reported previously[10]). Though we were unable to definitively identify any set of resonances as belonging to a particular rotamer, it was clear from the ^{1}H NMR spectra that $\mathbf{2^{Me}}$, $\mathbf{2^{Bn}}$, and $\mathbf{2^{\textit{i}Pr}}$ are able to access each of the three possible conformational isomers that arise from rotation about their N-C amide bonds. None of these compounds participated in cyclization with *tert*-butyl amine, instead providing oligomeric products. In contrast, the NMR spectrum of $\mathbf{2^{\textit{t}Bu}}$ suggests that it exists as a single conformer[10] and though we are unable to unequivocally identify it in solution phase as conformer **A**, it is noteworthy that this compound cyclizes reliably and efficiently with a range of amines, including *tert*-butyl amine. Furthermore, $\mathbf{2^{\textit{t}Bu,\textit{exo}\text{-bornyl}}}$ and $\mathbf{2^{\textit{t}Bu,\textit{i}Pr}}$, the only $\mathbf{2^{R}}$ derivatives without two tertiary R groups that we have observed to be competent for cyclization, were also found to exist as single conformers by ^{1}H NMR (see supporting information Figures S1-27 and S1-31, respectively). Taken together, these observations suggest that bulky amide R groups

stabilize the cis rotamer conformation, which allows for the unusually efficient cyclization of $\mathbf{2}^{t\mathbf{Bu}}$ and other bulky $\mathbf{2}^{\mathbf{R}}$ derivatives.

Synthesis of *t*BuH$_2$tacn

The "crab-like" cyclization reported here is amenable to the synthesis of tacn derivatives where two or three of the nitrogen substituents are bulky. However, because $\mathbf{2}^{\mathbf{R}}$ derivatives require two bulky R groups to favour cyclization over oligomerization, the direct synthesis of a tacn with only one bulky R group, such as *t*BuH$_2$tacn, is not readily achieved by this approach. Nonetheless, we were interested in the synthesis of *t*BuH$_2$tacn both as part of our broader efforts to provide access to otherwise inaccessible tacn derivatives, and because it was the only N-*tert*-butyl tacn derivative yet to be prepared. We concluded that the most efficient route to *t*BuH$_2$tacn was likely via the Richman-Atkins cyclization of **1.06** (Scheme 1-12) with ethylene glycol ditosylate. Notably, an attempt to prepare a benzyl substituted tacn derivative through a similar route resulted in the competitive formation of a piperazine, stemming from nucleophilic addition of the central nitrogen on one end of ethylene glycol ditosylate, followed by elimination of the ethylene tosamide moiety (Scheme 1-11).[6b]

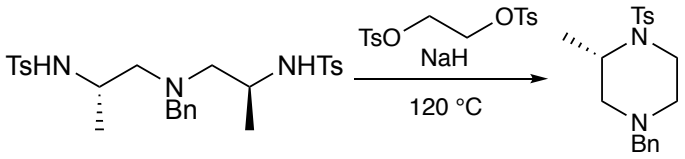

Scheme 1-11. Failed attempted Richman-Atkins cyclization.

Despite this precedent, we anticipated that the steric bulk of the *tert*-butyl substituent may attenuate the nucleophilicity of the central nitrogen in **1.06**, allowing the formation of the desired tacn. Thus, *tert*-butylamine was reacted with two equivalents of tosyl aziridine, providing intermediate **1.06** in near quantitative yield without purification. **1.06** was then subjected to Richman-Atkins

cyclization conditions with ethylene glycol ditosylate, resulting in the formation of **Ts$_2$*t*Butacn** in 74% yield with no trace of the piperazine byproduct. Deprotection of tosylated tacn derivatives typically proceeds in the presence of concentrated strong acids, though we demonstrated above that such conditions also remove *tert*-butyl groups. Instead, we surveyed many reducing conditions, ultimately finding that the tosyl groups were efficiently cleaved by reduction with sodium in a mixture of ammonia and THF, affording ***t*BuH$_2$tacn** in 53% isolated yield.

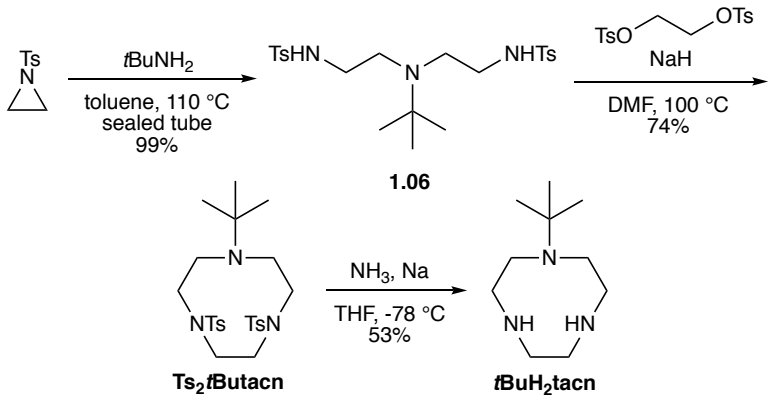

*Scheme 1-12. Synthesis of **tBuH$_2$tacn**.*

Percent Buried Volume Analysis

With the ligand series ***tBu$_2$Htacn*** and ***t*BuH$_2$tacn** in hand, we targeted a method to quantify the relative steric environment imposed by each ligand on a transition-metal ion to which they are coordinated. Thus, we synthesized and crystallographically characterized the $[Cu(R_3tacn)(MeCN)]^+$ species of ***t*Bu$_2$Htacn** and ***t*BuH$_2$tacn** (Figure 1-6), as such copper(I) species formed the basis for percent buried volume ($\%B_v$) calculations previously used to quantify the relative steric environment imposed by R_3tacn ligands (R = *t*Bu, *i*Pr, Me).[10]

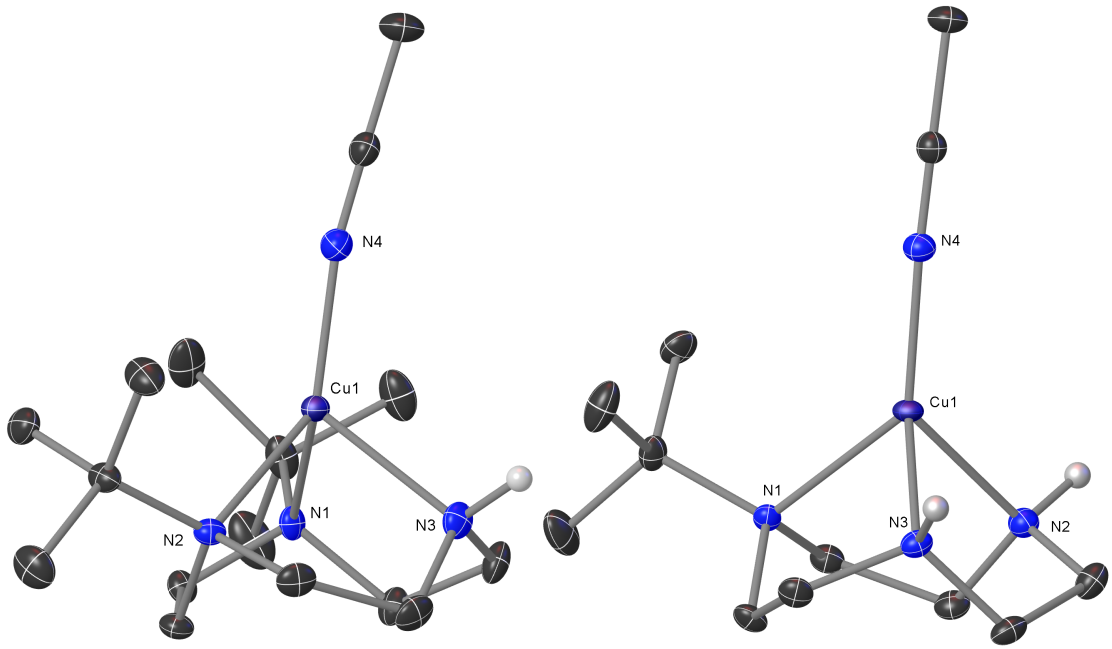

Figure 1-6. Molecular structures of the cations of ***[Cu(tBu$_2$Htacn)(MeCN)]PF$_6$*** *(left) and* ***[Cu(tBuH$_2$tacn)(MeCN)]OTf*** *(right). Hydrogen atoms, except those on nitrogen, are omitted for clarity. Cu–N–C angles of the MeCN are 170.2° (left) and 175.2° (right). The angle from the R$_3$tacn N$_3$ centroid through Cu to the MeCN nitrogen, a measure of the extent of leaning of the MeCN ligand away from the idealized pseudotetrahedral position, is 169.9° (left) and 177.2° (right).*

Utilizing this method, we demonstrate that ***t*Bu$_2$Htacn** is, on average, nearly isosteric with *i*Pr$_3$tacn, and that ***t*BuH$_2$tacn** is, on average, nearly isosteric with Me$_3$tacn (Figure 1-7). Given that the *tert*-butyl groups in ***t*Bu$_2$Htacn** and ***t*BuH$_2$tacn** are more oxidatively robust than the methyl and isopropyl groups in Me$_3$tacn and *i*Pr$_3$tacn, we anticipate that ***t*Bu$_2$Htacn** and ***t*BuH$_2$tacn** will be useful in oxidation reactions where Me$_3$tacn and *i*Pr$_3$tacn have also been employed, particularly where these ligands are degraded by oxidation of the N-alkyl substituent.

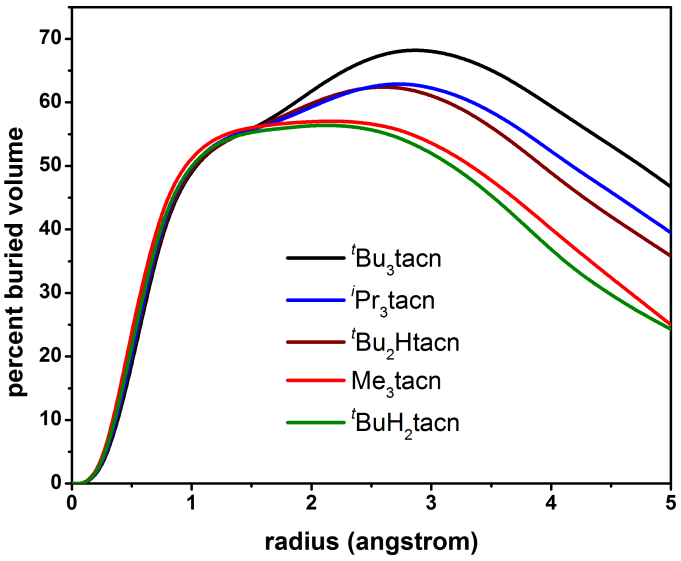

*Figure 1-7. Percent buried volume (%B_v) of the NR components of R_3tacn in $[Cu(R_3tacn)(MeCN)]^+$ cations as a function of sphere radius centered at the copper position. Acetonitrile ligand, counterion, and R_3tacn ethylene units are omitted in the calculated values. R_3tacn = tBu_3tacn (—), iPr_3tacn (—), **tBu_2Htacn** (—), Me_3tacn (—) and **$tBuH_2$tacn** (—).*

1.4 Conclusions

Three major limitations in the accessibility of R_3tacn derivatives have been overcome in the studies described above:

(1) A more efficient and less wasteful route to R_3tacn ligands where one or more of the R groups is unique is described.

(2) Unsymmetrical R_3tacn ligands where one or two R groups are tertiary alkyl are now accessible.

(3) The first chiral derivatives of R_3tacn with chiral centers alpha to the nitrogens on the R groups are described.

Furthermore, efficient routes to industrially important Me_3tacn and Me_4dtne are reported that produce significantly less waste compared with the conventional Richman-Atkins route. The results described herein detail routes to known as well as previously inaccessible R_3tacn ligands, particularly novel chiral examples, and are expected to promote increased utilization of such R_3tacn ligands in coordination chemistry and enable development of new and improved (asymmetric) catalytic methods for organic substrate transformations.

1.5 Experimental Information and Characterization Data

General Considerations:

All solvents were purchased from Fisher Scientific and dried over 4Å molecular sieves. N,N′-di-tert-butylethylenediamine (TCI America) was stored in a Strauss flask under N_2 to avoid decomposition. All other chemicals and solvents were obtained from commercial sources and used as received. Ultra-High Purity dry air was purchased from nexAir LLC. Thin layer chromatography was performed on Merck silica gel plates and visualized with potassium permanganate. ^{1}H NMR and ^{13}C NMR spectra were recorded on Bruker 600, Varian INOVA 600, INOVA 500 and INOVA 400 spectrometers. Residual solvent resonances were treated as internal reference signals. High resolution mass spectra were obtained from the Emory University Mass Spec Facility Inc. X-ray crystal structure data was obtained from Dr. John Bacsa of the Emory University X-ray Crystallography Center. *N*-(*tert*-butyl)-2-chloroacetamide,[20] (*S*)-*N*-((2*S*,5*R*)-2-isopropyl-5-methylcyclohexylidene)-2-methylpropane-2-sulfinamide[21], *N*-((1*R*, 2R, 4*R*)-1,7,7-trimethylbicyclo[2.2.1]heptan-2-yl)hydroxylamine[22], (1*R*, 2R, 4*R*)-1,7,7-trimethylbicyclo[2.2.1]heptan-2-amine[22], and N^1-(*tert*-butyl)-N^2-isopropylethane-1,2-diamine[23] were prepared according to literature procedures.

General synthesis of ***2^{R}***.

Chloroacetyl chloride (3.0 equiv) was added to CH_2Cl_2 in an oven-dried, N_2-purged round-bottom flask equipped with a stir bar to a concentration of 1.8 M. The flask was cooled on an ice bath while stirring for 15 minutes. **1^{R}** (1.0 equiv) was added to the reaction flask using a syringe pump over the course of 20 minutes. The ice bath was removed, and the reaction mixture was stirred overnight at room temperature. The next morning, the reaction mixture was added to a beaker pre-filled with ice and saturated K_2CO_3 (aq), and CH_2Cl_2 was used to rinse the residual reaction material into the beaker. The biphasic mixture was stirred for 30 minutes. The contents of the beaker were poured into a separatory funnel, the organic phase was isolated, and the aqueous phase was washed once with CH_2Cl_2. The combined organic extracts were washed with saturated K_2CO_3 (aq) followed by brine. The organic phase was then dried over anhydrous $MgSO_4$ and filtered. The filtrate was concentrated *in vacuo* to obtain the crude product as a white powder.

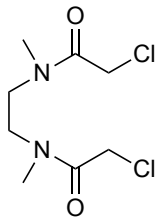

N,N'-(ethane-1,2-diyl)bis(2-chloro-N-methylacetamide) (**2^{Me}**). The crude product was crystallized from CH_2Cl_2/pentane to obtain pure product as a colorless crystalline solid (6.88 g, 72% yield). The ^{1}H and ^{13}C NMR spectra of this compound revealed the presence of a major symmetric amide rotamer and a minor unsymmetrical amide rotamer. Symmetric rotamer: ^{1}H NMR (400 MHz, Chloroform-*d*) δ 3.99 (s, 4 H), 3.54 (s, 4 H), 3.05 (s, 6 H); ^{13}C NMR (100 MHz, Chloroform-*d*) δ 167.17, 45.26, 41.54, 36.07; Unsymmetrical rotamer: ^{1}H NMR (400 MHz, Chloroform-*d*) δ 4.08 (s, 2 H), 4.04 (s, 2 H), 3.49 (s, 4 H), 3.08 (s, 3 H), 2.95 (s, 3 H); ^{13}C NMR (100 MHz, Chloroform-

d) δ 47.70, 47.25, 41.24, 40.82, 37.37, 34.29 (Note: carbonyl peaks not detected due to the lower concentration of the minor unsymmetrical rotamer). Positive Mode NSI-MS m/z: exact mass calculated for $C_8H_{15}Cl_2N_2O_2^+$ ($[M+H]^+$): 241.05106; found: 241.05064.[24]

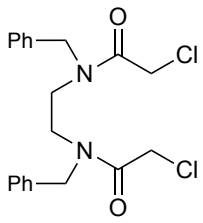

N,N'-(ethane-1,2-diyl)bis(N-benzyl-2-chloroacetamide) (**2**$^{\mathbf{Bn}}$). The crude product was crystallized from CH_2Cl_2/pentane to obtain pure product as colorless crystals (21.96 g, 66% yield). The ^{1}H and ^{13}C NMR spectra of this compound revealed the presence of a major symmetric amide rotamer, a minor unsymmetrical amide rotamer, and a minor symmetric amide rotamer. Major symmetric rotamer: ^{1}H NMR (400 MHz, Chloroform-*d*) δ 4.66 (s, 4 H), 4.06 (s, 4 H), 3.61 (s, 4 H). Unsymmetrical rotamer: ^{1}H NMR (400 MHz, Chloroform-*d*) δ 4.49 (s, 4 H), 4.13 (s, 2 H), 4.11 (s, 2 H), 3.39-3.33 (m, 2 H), 3.33-3.26 (m, 2 H). Minor symmetric rotamer: ^{1}H NMR (400 MHz, Chloroform-*d*) δ 4.56 (s, 4 H), 3.96 (s, 4 H), 3.41 (s, 4 H). Aryl C-H bonds of each amide rotamer were not distinguishable by ^{1}H NMR spectroscopy, where they combine as a complex multiplet at 7.42–7.10. Combined ^{13}C NMR (100 MHz, Chloroform-*d*) δ 167.56, 167.41, 167.14, 136.67, 135.90, 135.22, 129.30, 129.14, 128.73, 128.56, 128.23, 128.00, 127.74, 127.07, 126.46, 53.11, 51.50, 49.20, 45.88, 44.27, 43.09, 41.56, 41.17, 41.03. Positive Mode NSI-MS m/z: exact mass calculated for $C_{20}H_{23}Cl_2N_2O_2^+$ ($[M+H]^+$): 393.11366; found: 393.11293. [25]

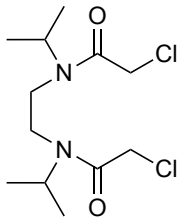

N,N'-(ethane-1,2-diyl)bis(2-chloro-N-isopropylacetamide) (**2**$^{i\mathbf{Pr}}$). The crude was purified through dissolution in minimal CH_2Cl_2 and precipitating the product with excess pentane to afford pure product as a white powder (25.72 g, 78% yield). The ^{1}H and ^{13}C NMR spectra of this compound revealed the presence of a major symmetric amide rotamer and a minor unsymmetrical amide rotamer. Symmetric rotamer: ^{1}H NMR (400 MHz, Chloroform-*d*) δ 4.11 (s, 4 H), 3.98 (sept, *J* = 6.6 Hz, 2 H), 3.34 (2, 4 H), 1.29 (d, *J* = 6.6 Hz, 12 H); ^{13}C NMR ($CDCl_3$) δ 166.55, 49.76, 42.01, 39.53, 21.05. Unsymmetrical rotamer: ^{1}H NMR (400 MHz, Chloroform-*d*) δ 4.64 (sept, *J* = 6.8 Hz, 2 H), 4.36 (s, 2 H), 4.10 (s, 2 H), 3.33-3.30 (m, 2 H), 3.30-3.28 (m, 2 H), 1.26 (d, *J* = 6.6 Hz, 6 H), 1.18 (d, *J* = 6.8 Hz, 6 H). Total ^{13}C NMR (100 MHz, Chloroform-*d*) δ 166.49, 49.69, 49.29, 46.52, 42.17, 41.98, 41.75, 41.54, 41.23, 39.49, 21.51, 21.01, 20.52. Positive Mode NSI-MS m/z: exact mass calculated for $C_{12}H_{21}O_2N_2Cl_2^+$ ($[M–H^–]^+$): 295.09801; found: 295.09740.

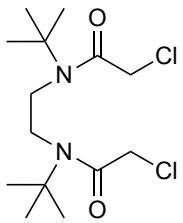

N,N'-(ethane-1,2-diyl)bis(N-(tert-butyl)-2-chloroacetamide) (**2**$^{t\mathbf{Bu}}$). This procedure represents an improvement to our previously published route. The crude product was found to be pure and was isolated as white powder (28.90 g, 94% yield). This material can be crystallized from

CH_2Cl_2/pentane to obtain colorless crystals if desired. Spectroscopic data matches reported literature values.[10]

General Synthesis of $\mathbf{3}^{tBu,R}$. $\mathbf{2}^{t\mathrm{Bu}}$ was dissolved in DMF to 1 M in a round-bottom flask equipped with a stir bar. The contents of the flask were stirred at room temperature, and Na_2CO_3 (2.5 equiv) was added. Primary amine (RNH_2, 1.1 equiv) was added, and the contents were stirred 30-60 minutes at room temperature. The reaction was then heated to 120 °C and stirred 3-12 hours. The flask was allowed to cool to room temperature, and the contents were poured into a separatory funnel, washing residual material from the reaction flask with EtOAc and water. The organic phase was separated, and the aqueous phase was washed with EtOAc. The combined organic phases were washed with five portions of brine to remove residual DMF. The organic phase was then dried with anhydrous $MgSO_4$ and filtered. The filtrate was concentrated *in vacuo* to yield a crude cyclic diamide, often of sufficient purity for subsequent reduction.

General Procedure for LAH Reduction of $\mathbf{3}^{tBu,R}$ *to* tBu_2Rtacn. In a glove box, lithium aluminum hydride pellets (5 equiv) were stirred in Et_2O (25 mL/g LAH) overnight. The grey suspension was then filtered over celite into a round-bottom flask equipped with a stir bar. With stirring, $\mathbf{3}^{t\mathrm{Bu,R}}$ (1 equiv) was added in small portions. The reaction was stirred 3-12 hours at room temperature, and then removed from the glove box and cooled on an ice bath. The stirred reaction was quenched by the Fieser method[26] (to quench n grams of $LiAlH_4$, carefully add by dropwise addition n mL of H_2O, n mL of 15% aqueous NaOH, and 3n mL of water). The quenched reaction was filtered, the filtered solid was washed with Et_2O, and the combined filtrate was concentrated in vacuo to afford product.

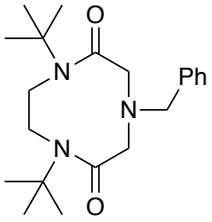

4-benzyl-1,7-di-tert-butyl-1,4,7-triazacyclononane-2,6-dione (**3**^{tBu,Bn}). **2**^{tBu} (500 mg, 1.54 mmol), DMF (15 mL), and potassium carbonate (639 mg, 4.62 mmol) were added to a round-bottom flask, which was then sparged with N_2 for 5 minutes. Benzylamine (173 mg, 0.18 mL, 1.61 mmol) was added and the mixture was heated to 120 °C for 4h. The mixture was cooled to room temperature, diluted with ethyl acetate and washed 3 times with ~50 mL portions of saturated aqueous LiCl. The organic phase was collected, dried over $MgSO_4$, filtered and concentrated *in vacuo*. Purification of this crude material by column chromatography (50/50 EtOAc/hexanes, R_f = 0.3) gave the product as a white powder (461 mg, 83% yield). ^{1}H NMR (400 MHz, Chloroform-*d*) δ 7.37-7.22 (m, 5 H), 3.80 (s, 2 H), 3.77 (s, 4 H), 3.46 (s, 4 H), 1.44 (s, 18 H); ^{13}C NMR (100 MHz, Chloroform-*d*) δ 171.56, 137.90, 129.31, 128.58, 127.40, 59.47, 59.35, 57.76, 48.23, 29.10. Positive Mode NSI-MS m/z: exact mass calculated for $C_{21}H_{34}N_3O_2^+$ ($[M+H]^+$): 360.26510; found 360.26510.

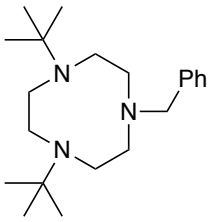

1-benzyl-4,7-di-tert-butyl-1,4,7-triazacyclononane (***t*Bu$_2$Bntacn**). Following the general reduction procedure, lithium aluminum hydride pellets (1.9 g, 50 mmol), diethyl ether (50mL) and **3**^{tBu,Bn}

(3.26 g, 9.1 mmol) were stirred overnight to produce a pale yellow oil after workup (3.45 g, 59% pure by ^{1}H NMR internal standard, 68% yield). ^{1}H NMR (400 MHz, Chloroform-*d*) δ 7.41 (d, *J* = 6.9 Hz, 2 H), 7.31 (t, *J* = 7.5 Hz, 2 H), 7.22 (t, *J* = 7.2 Hz, 1 H), 3.68 (s, 2 H), 2.97-2.90 (m, 4 H), 2.70-2.63 (m, 8 H), 1.06 (s, 18 H); ^{13}C NMR (100 MHz, Chloroform-*d*) δ 141.32, 128.96, 128.14, 126.60, 62.15, 55.62, 55.01, 53.05. 50.63, 27.21. Positive Mode NSI-MS m/z: exact mass calculated for $C_{21}H_{38}N_3^+$ ($[M+H]^+$): 332.30657; found 332.30584.

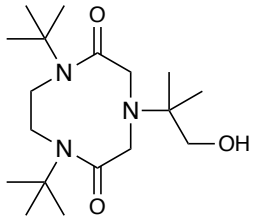

1,7-di-tert-butyl-4-(1-hydroxy-2-methylpropan-2-yl)-1,4,7-triazacyclononane-2,6-dione (**3**$^{t\mathbf{Bu,dmea}}$). Following the general cyclization procedure, **2**$^{t\mathbf{Bu}}$ (5.02 g, 15 mmol), DMF (16 mL), sodium carbonate (4.20 g, 39.7 mmol) and 2-amino-2-methyl-1-propanol (dmeaH_2, 1.6 mL,16.8 mmol) were heated overnight to produce an off-white crude solid after workup, which was purified by silica gel column chromatography (ethyl acetate, R_f = 0.4) to yield the product as a white solid (2.96 g, 56% yield). ^{1}H NMR (500 MHz, Chloroform-*d*) δ 3.78 (s, 4 H), 3.63 (s, 4 H), 3.46 (s, 2 H), 1.43 (s, 18 H), 1.12 (s, 6 H); ^{13}C NMR (100 MHz, Chloroform-*d*) δ 173.29, 69.69, 59.75, 58.68, 57.85, 47.14, 23.94, 21.24. Positive Mode NSI-MS m/z: exact mass calculated for $C_{18}N_{36}N_3O_3$ ($[M+H]^+$): 342.27567; found 342.27539.

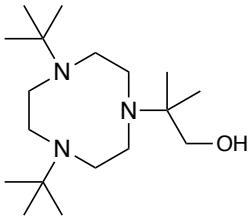

2-(4,7-di-tert-butyl-1,4,7-triazacyclononan-1-yl)-2-methylpropan-1-ol (***t*Bu$_2$dmeatacn**). Following the general reduction procedure with a slight modification, lithium aluminum hydride solution (4.0M in Et_2O, 10.5 mL), diethyl ether (25 mL), and **3^{tBu,dmea}** (2.88 g, 8.4 mmol) were stirred overnight. After quenching, the crude product was washed with chloroform. After filtration, the filtrate was concentrated *in vacuo* to produce a solid that was triturated with methanol and water to afford product as a white solid (1.45 g, 55% yield). ^{1}H NMR (400 MHz, Chloroform-*d*) δ 6.50 (br t, *J* = 6.6 Hz, 1 H), 3.50 – 2.00 (br m, 14 H) 0.95 (s, 24 H); ^{13}C NMR (100 MHz, Chloroform-*d*) δ 70.12, 57.95, 55.73, 54.21, 53.76, 51.65, 26.69, 18.53. Positive Mode NSI-MS m/z: exact mass calculated for $C_{18}H_{40}N_3O$ ($[M+H]^+$): 314.31714; found 314.31676.

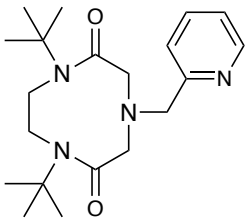

1,7-di-tert-butyl-4-(pyridin-2-ylmethyl)-1,4,7-triazacyclononane-2,6-dione (**3^{tBu,pic}**). **2^{tBu}** (1.88 g, 5.79 mmol), DMF (24 mL), water (8 mL) and potassium carbonate (2.55 g, 108.14 mmol) were added to a round-bottom flask, which was then sparged with N_2 for 15 minutes. 2-picolylamine (0.67 mL, 6.47 mmol) was added and the mixture was heated to 120 °C for 4h. The mixture was cooled to room temperature, diluted with ethyl acetate, and washed 3 times with ~50 mL of saturated aqueous LiCl. The organic phase was collected, dried over $MgSO_4$, filtered and

concentrated *in vacuo* to give 1.69g of a yellow solid. This crude material was found to be 85% pure by ^{1}H NMR internal standard (69% yield). The crude can be purified by silica gel column chromatography (ethyl acetate, R_f = 0.2) if desired. However, we found that using the crude material directly in the next step without further purification was most convenient. ^{1}H NMR (400 MHz, Chloroform-*d*) δ 8.53 (dtd, *J* = 5.1, 2.1, 1.0 Hz, 1 H), 7.68 (tt, *J* = 7.6, 2.0 Hz, 1 H), 7.52 (d, *J* = 7.6 Hz, 1 H), 7.16 (dddd, *J* = 7.2, 4.9, 2.3, 1.2 Hz, 1 H), 3.99 (s, 2 H), 3.75 (s, 4 H), 3.57 (s, 4 H), 1.44 (s, 18 H). ^{13}C NMR (100 MHz, Chloroform-*d*) δ 171.09, 158.39, 149.20, 136.61, 123.02, 122.11, 60.71, 59.07, 57.74, 48.25, 28.97. Positive Mode NSI-MS m/z: exact mass calculated for $C_{20}H_{33}N_4O_2^+$ ([M+H]$^+$): 361.26035; found 361.25946.

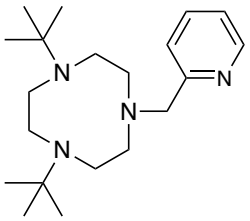

1,4-di-tert-butyl-7-(pyridin-2-ylmethyl)-1,4,7-triazacyclononane (***t*Bu$_2$pictacn**). Following a modified version of the general reduction procedure, crude **3**^{tBu,pic} (1.69g, 4.68 mmol) was dissolved in THF (50 mL) in a round-bottom flask inside a glove box. To this stirring solution, lithium aluminum hydride (755 mg, 19.9 mmol) was added. The mixture was stirred overnight then quenched in the glove box by the dropwise addition of methanol. The quenched reaction was filtered, and the solvent was removed *in vacuo*. The resulting viscous yellow oil with red solid was dissolved in dichloromethane and filtered to yield the product as a viscous yellow oil (1.13g, crude). This material is air sensitive, darkening to a red color upon removal from the glovebox and was not purified further. The yield of this compound is reported below as a two step yield based on crystalline **[Cu(*t*Bu$_2$pictacn)]PF$_6$**. ^{1}H NMR (300 MHz, Chloroform-*d*) δ 8.50 (ddd, *J* = 4.9,

1.9, 1.0 Hz, 1 H), 7.70 (d, *J* = 8.0 Hz, 1 H), 7.63 (td, *J* = 7.6, 1.8 Hz, 1 H), 7.11 (ddd, *J* = 7.4, 4.9, 1.4 Hz, 1 H), 3.85 (s, 2 H), 2.96-2.91 (m, 4 H), 2.70-2.66 (m, 4 H), 2.66 (s, 4 H), 1.03 (s, 18 H). ^{13}C NMR (100 MHz, Chloroform-*d*) δ 161.95, 148.91, 136.35, 123.14, 121.66, 63.90, 55.82, 55.11, 53.39, 50.60, 27.23. Positive Mode NSI-MS m/z: exact mass calculated for $C_{20}H_{37}N_4^+$ ($[M+H]^+$): 333.30182; found 333.30152 .

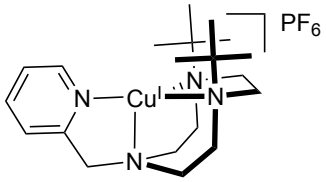

[Cu(tBu₂pictacn)]PF₆. Crude ***t*Bu₂pictacn** (1.13g, 3.40 mmol) and tetrahydrofuran (10 mL) were combined in a scintillation vial with a stir bar in a glovebox. A solution of $[Cu(MeCN)_4]PF_6$ (1.26 g, 3.40 mmol) in acetonitrile (5 mL) was added dropwise to the solution of crude ***t*Bu₂pictacn**. The reaction mixture was stirred for 2h then concentrated *in vacuo*. The concentrate was taken up in CH_2Cl_2, filtered, and recrystallized by layering with pentane to give 1.20 g of pure product as yellow/brown crystals (56% yield over two steps). ^{1}H NMR (400 MHz, Chloroform-*d*) δ 8.49 (d, J = 5.2 Hz, 1H), 7.78 (dt, J_1 = 8.0 Hz, J_2 = 1.2 Hz, 1H), 7.39-7.32 (m, 2H), 4.11 (s, 2H), 3.21-2.95 (m, 6H), 2.80-2.58 (m, 6H), 1.25 (s, 18H). ^{13}C NMR (100 MHz, Chloroform-*d*) δ 157.41, 147.76, 136.57, 124.14, 59.54, 57.96, 51.90, 44.01, 48.53, 27.01 (the resonance for the quaternary carbon of the picolyl moiety is not observed). Positive Mode NSI-MS m/z: exact mass calculated for $C_{20}H_{36}N_4Cu^+$ ($[M+H]^+$): 393.2230; found 395.2230. Anal. calc. for $C_{20}H_{36}N_4CuF_6P$: C, 44.40; H, 6.71; N, 10.36. Found: C, 44.41; H, 6.63; N, 10.50.

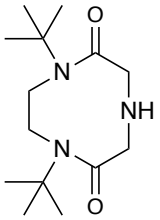

1,7-di-tert-butyl-1,4,7-triazacyclononane-2,6-dione (**3**^{tBu,H}). **2**^{tBu} (14.74 g, 54.72 mmol, 1 equiv) and 50 mL acetonitrile were added to a 500 mL thick walled glass pressure flask equipped with a stir bar *(Danger! Filling the pressure vessel more than half-way may result in explosion due to over-pressurization)*. Concentrated aqueous ammonium hydroxide (100 mL, 1.8 mol, 30 equiv) was then added, and the vessel was sealed with a screw cap. The mixture was heated to 100 °C for 6h, then allowed to cool to room temperature. The contents of the pressure flask were then transferred to a round bottom-flask and concentrated *in vacuo.* This concentrate was then taken up in CH_2Cl_2 and dried over Na_2SO_4 then filtered. Concentration of the filtrate *in* vacuo afforded a pale yellow solid (crude: 12.51 g). The crude can be purified by silica gel chromatography (3% methanol in ethyl acetate) if necessary; however, we found it to be more convenient to use this crude material in the next step without further purification. ^{1}H NMR (400 MHz, Chloroform-*d*) δ 3.68 (s, 4H), 3.54 (s, 4H), 2.23 (s, 1H), 1.43 (s, 18H). ^{13}C NMR (100 MHz, Chloroform-*d*) δ 172.57, 57.76, 52.57, 48.40, 28.94. Positive Mode NSI-MS m/z: exact mass calculated for $C_{14}H_{28}O_2N_3^+$ ($[M+H]^+$): 270.21815; found 270.21793.

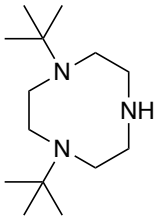

1,4-di-tert-butyl-1,4,7-triazacyclononane (***t*Bu$_2$Htacn**). Following a modified version of the general reduction procedure, crude **3^{tBu,H}** (12.51 g, 46.44 mmol, 1 equiv) and diethyl ether (125 mL) were added to a round-bottom flask containing a stir bar to create a suspension, then THF (125 mL) was added. The mixture was chilled with an ice bath and LAH pellets (17.5 g, 461.14 mmol, 10 equiv) were added in one portion. The mixture was allowed to stir overnight while warming slowly to room temperature. After stirring overnight, the reaction mixture was transferred to a beaker, cooled with an ice bath, and quenched by the Fieser method.[26] The mixture was then filtered and the insoluble residue was washed three times with 100 mL diethyl ether. The combined filtrates were then dried over Na_2SO_4, filtered, and concentrated *in vacuo.* The crude orange oil was purified by short path vacuum distillation (boiling point: 105°C at 0.30 bar) to give 5.18 g of pure product as a colorless oil (21.45 mmol, 46.2% yield over three steps). ^{1}H NMR (300 MHz, Chloroform-*d*) δ 2.74-2.71 (m, 4H), 2.63-2.60 (m, 4H), 2.55 (s, 4H), 1.05 (s, 18H). ^{13}C NMR (75 MHz, Chloroform-*d*) δ 58.84, 51.68, 48.97, 48.79, 27.15. Positive Mode NSI-MS m/z: exact mass calculated for $C_{14}H_{32}N_3^+$ ($[M+H]^+$): 242.2596; found 242.2591.

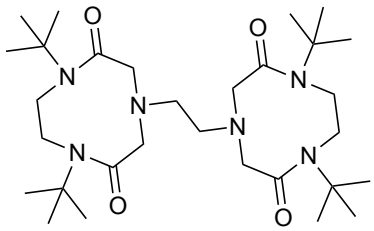

4,4'-(ethane-1,2-diyl)bis(1,7-di-tert-butyl-1,4,7-triazacyclononane-2,6-dione) (**1.05**). Following the general cyclization procedure, **2**$^{t\mathbf{Bu}}$ (10.09 g, 31 mmol, 1 equiv), DMF (31 mL), sodium carbonate (7.98g, 75 mmol, 2.4 equiv) and ethylenediamine (1.03 mL, 15 mmol, 0.50 equiv) were heated overnight to produce a crude orange solid (7.28g, 71% pure by internal standard) of sufficient purity for reduction (see reaction below). If necessary, the product can be purified by silica gel column chromatography (10% MeOH in DCM). ^{1}H NMR (400 MHz, Chloroform-*d*) δ 3.70 (s, 8 H), 3.50 (s, 8 H), 2.87 (s, 4 H), 1.41 (s, 36 H). ^{13}C NMR (75 MHz, Chloroform-*d*) δ 171.60, 60.39, 57.82, 52.31, 48.30, 29.10. Positive Mode NSI-MS m/z: exact mass calculated for $C_{30}H_{57}N_6O_4^+$ ($[M+H]^+$): 565.44413; found 565.44390.

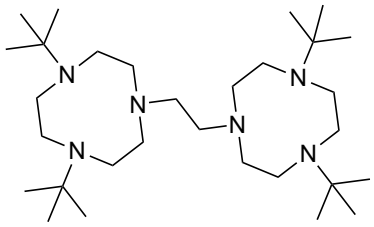

1,2-bis(4,7-di-tert-butyl-1,4,7-triazacyclononan-1-yl)ethane (***t*Bu$_4$dtne**). Following a modification of the general reduction procedure, crude **4** (7.28 g), lithium aluminum hydride solution (4.0 M in Et_2O, 34.6 mL) and diethyl ether (50 mL) were stirred together overnight to produce an off-white solid. This solid was purified by trituration with methanol/water to afford the product as a white solid (1.37 g, 17% yield over 2 steps).

Alternatively, ***t*Bu$_2$Htacn** (200 mg, 0.828 mmol, 1 equiv), saturated aqueous K_2CO_3 (10 mL) and a stir bar were added to a scintillation vial and the biphasic mixture was stirred. Dibromoethane (150 mg, 0.828 mmol, 1 equiv) was then added and the mixture was stirred for 2h. A white precipitate was observed. Another portion of dibromoethane (150 mg, 0.828 mmol, 1 equiv) was added, and the mixture was stirred until the precipitate coagulated into a single white mass. The aqueous solution was filtered off and the remaining solid material was taken up in dichloromethane, dried over Na_2SO_4, filtered, and concentrated *in vacuo* to afford 239 mg of white solid (88% pure by ^{1}H NMR internal standard with water as the only detectable impurity, 0.794 mmol, 96% yield). ^{1}H NMR (400 MHz, Chloroform-*d*) δ 3.00-2.94 (m, 8 H), 2.68-2.64 (m 8 H), 2.62 (s, 4 H), 2.58 (s, 8 H), 1.03 (s, 36 H). ^{13}C NMR (100 MHz, Chloroform-*d*) 56.45, 55.97, 55.03, 53.01, 50.69, 27.21. Positive Mode NSI-MS m/z: exact mass calculated for $C_{30}H_{65}N_6O^+$ ($[M+H]^+$): 509.52707; found 509.52721.

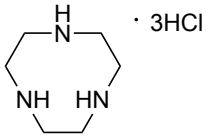

1,4,7-triazacyclononane-trihydrochloride (**[H$_6$tacn][Cl]$_3$**). ***t*Bu$_2$Htacn** (1.01 g, 4.18 mmol) and concentrated HCl (10 mL) were combined in a scintillation vial containing a stir bar. The vial was sealed with a teflon cap and allowed to stir at 95 °C overnight. The vial was removed from heat the following morning, and, upon cooling, white needles crystalized from the solution. The supernatant was decanted and concentrated via distillation at 100 °C. The crystalline material amounted to 961 mg and was 83% pure by internal standard with water as the only detectable impurity resulting in an 81% yield of crystalline material. The white, friable residue remaining after distillation of the supernatant accounted for 141 mg of material and was 56% pure by internal

standard, containing water as the only detectable impurity (baseline impurities are present), accounting for another 8% yield. Overall yield: 89%. ^{1}H NMR (300 MHz, D_2O/NaOD) δ 3.56 (s). Spectroscopic data matches reported literature values.[19c]

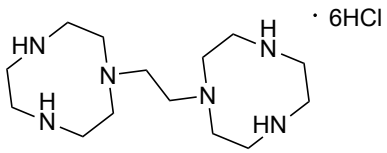

1,2-di(1,4,7-triazacyclononan-1-yl)ethane-hexahydrochloride **([H_{10}dtne][Cl]$_6$).** ***t*Bu$_4$dtne** (854 mg, 1.68 mmol) and 10 mL of HCl were added to a scintillation vial. The vial was sealed with a Teflon cap and heated to 95 °C overnight. The mixture was allowed to cool to r.t., and a white solid crystallized from solution. The solvent was removed by distillation into a beaker containing sat. aq. $NaHCO_3$, then further concentrated under high vacuum to give 0.835g of white powder/crystals (87% pure by internal standard with water as the major impurity, 86% yield). Spectral data matches reported literature values. [27]

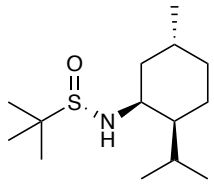

(S)-N-((1S,2S,5R)-2-isopropyl-5-methylcyclohexyl)-2-methylpropane-2-sulfinamide. To a flame dried round bottom flask under N_2 was added (*S*)-*N*-((2*S*,5*R*)-2-isopropyl-5-methylcyclohexylidene)-2-methylpropane-2-sulfinamide (1.93 g, 7.50 mmol, 1 equiv), then THF (50 mL) and MeOH (3.1 mL, 75 mmol, 10 equiv). This mixture was cooled to -78 °C, and $NaBH_4$ (570 mg, 15.11 mmol, 2 equiv) was added in portions over the course of an hour, then allowed to warm to room temperature overnight. The reaction was quenched by the addition of

water (20 mL), diluted with brine (50 mL), and extracted with EtOAc (3 × 50 mL). The organic phases were collected, dried over $MgSO_4$, filtered, and concentrated *in vacuo*. The crude mixture was purified by silica gel column chromatography, eluting with 30/70 EtOAc/hexanes (R_f = 0.3) to give 1.33 g (68% yield) of white solid. ^{1}H NMR (300 MHz, Chloroform-*d*) δ 3.73 (m, 1H), 3.07 (broad s, 1H), 1.98 (dq, *J* = 13.5, 3.1 Hz, 1H), 1.79 – 1.58 (m, 3H), 1.44 – 1.33 (m, 1H), 1.21 (s, 9H), 1.08 (m, 3H), 0.98 (d, *J* = 7.0 Hz, 3H), 0.93 (d, *J* = 7.0 Hz, 3H), 0.85 (d, *J* = 6.5 Hz, 4H). ^{13}C NMR (100 MHz, Chloroform-*d*) δ 55.22, 50.64, 47.74, 40.07, 35.10, 28.84, 25.55, 24.61, 22.60, 22.22, 21.30, 20.26. Positive Mode NSI-MS m/z: exact mass calculated for $C_{14}H_{30}NOS^+$ ($[M+H]^+$): 260.2042; found 260.204.

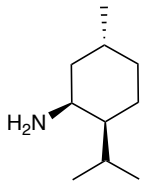

(1S,2S,5R)-2-isopropyl-5-methylcyclohexan-1-amine. In a round bottom flask, (*(S)-N*-((1S,2S,5R)-2-isopropyl-5-methylcyclohexyl)-2-methylpropane-2-sulfinamide (1.12 g, 4.32 mmol, 1 equiv) was diluted with MeOH (10 mL). To this mixture was added 3M methanolic HCl (7 mL, 21 mmol, ~5 equiv). The reaction was stirred at room temperature for 2 hours, then quenched by the addition of 2M NaOH (20 mL). The mixture was diluted with brine (50 mL) and extracted with DCM (3 × 50 mL), The organic phases were collected, dried over $MgSO_4$, filtered, and concentrated *in vacuo*. The crude was purified by silica gel column chromatography, eluting with a 4-9% 7M NH_3 in MeOH in DCM (5% 7M NH_3 in MeOH/DCM R_f = 0.2) to give 550 mg (82% yield) of colorless oil. ^{1}H NMR (300 MHz, Chloroform-*d*) δ 3.29 (s, 1H), 2.60-1.88 (broad s, 2H), 1.83-1.57 (m, 4H), 1.52 – 1.35 (m, 1H), 1.31-1.19 (m, 1H), 1.12 (td, *J* = 12.8, 3.4 Hz, 1H), 0.92 (apparent t, *J* = 6.7, Hz, 7H), 0.85 (d, *J* = 6.7 Hz, 4H).

^{1}H NMR data matches previously reported literature values.

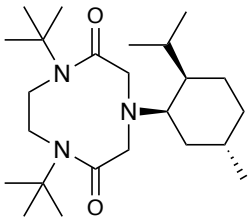

1,7-di-tert-butyl-4-((1S,2S,5R)-2-isopropyl-5-methylcyclohexyl)-1,4,7-triazacyclononane-2,6-dione (**3**$^{t\mathbf{Bu,menthyl}}$). To a flame dried round bottom flask under N_2, was added **2**$^{t\mathbf{Bu}}$ (1.05 g, 3.22 mmol, 1.0 equiv), DMF (30 mL), N,N-diisopropylethylamine (1.7 mL, 9.66 mmol, 3.0 equiv), and then (1S,2S,5R)-2-isopropyl-5-methylcyclohexan-1-amine (500 mg, 3.22 mmol, 1.0 equiv). The reaction was heated to 120 °C and allowed to stir at this temperature overnight. After cooling to room temperature, the mixture was diluted with brine (30 mL), extracted with EtOAc, and washed with water (5 × 30 mL). The organics were collected, dried over $MgSO_4$, and concentrated *in vacuo*. The crude was purified by silica gel column chromatography, eluting with 30/70 EtOAc/hexanes (Rf = 0.4) to give 608 mg (46% yield) of white solid. ^{1}H NMR (400 MHz, Chloroform-*d*) δ 4.09-3.96 (m, 2H), 3.72-3.55 (m, 6H), 3.21 (td, *J* = 5.1, 3.1 Hz, 1H), 2.15 (dq, *J* = 14.5, 3.1 Hz, 1H), 1.83 – 1.61 (m, 4H), 1.38 (s, 18H), 1.18 (ddd, *J* = 16.9, 8.9, 5.0 Hz, 1H), 0.99 (ddd, *J* = 14.5, 11.8, 5.0 Hz, 1H), 0.92 (d, *J* = 6.5 Hz, 3H), 0.88 (d, *J* = 6.5 Hz, 4H), 0.82 (d, *J* = 6.3 Hz, 3H). ^{13}C NMR (100 MHz, Chloroform-*d*) δ 172.04, 61.73, 57.48, 57.06, 47.11, 47.06, 35.52, 34.36, 28.79, 28.67, 28.21, 25.45, 22.76, 22.65, 21.46. Positive Mode NSI-MS m/z: exact mass calculated for $C_{24}H_{46}N_3O_2^+$ ($[M+H]^+$): 408.3585; found 408.3583.

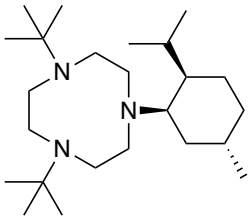

1,4-di-tert-butyl-7-((1S,2S,5R)-2-isopropyl-5-methylcyclohexyl)-1,4,7-triazacyclononane (***t*Bu$_2$menthyltacn**). To a flame dried round bottom flask under N_2, **3**^{tBu,menthyl} (223 mg, 0.547 mmol, 1.0 equiv) was added and taken up in Et_2O (20 mL). The mixture was cooled to -78 °C and white powdered lithium aluminum hydride (83 mg, 2.19 mmol, 4.0 equiv) was added under a stream of N_2. The reaction was allowed to stir overnight while warming slowly to room temperature. Excess lithium aluminum hydride was quenched via the Fieser method[26], and $MgSO_4$ was added directly to the reaction flask. The mixture was filtered, the solids were rinsed with Et_2O (3 × 10 mL), and the combined filtrates were concentrated *in vacuo.* The crude was purified by silica gel column chromatography eluting with 15% sat. aq. NH_4OH in MeCN (Rf = 0.4). Once eluted, the fractions containing the product were combined and concentrated. The concentrate was taken up in DCM (20 mL) and washed with 2M NaOH (20 mL), then the organics were dried over $MgSO_4$, filtered, and concentrated *in vacuo* to give 142 mg (68% yield) of colorless oil. ^{1}H NMR (300 MHz, Chloroform-*d*) δ 3.02 – 2.45 (m, 12H), 2.29 – 2.06 (m, 2H), 1.88 – 1.59 (m, 3H), 1.49 – 1.31 (m, 2H), 1.26-1.19 (m, 2H), 0.99 (m, 21H), 0.88 (d, *J* = 6.8 Hz, 3H), 0.82 (d, *J* = 6.3 Hz, 4H). ^{13}C NMR (100 MHz, Chloroform-*d*) δ 58.51, 57.43, 54.70, 52.41, 50.65, 47.91, 35.51, 35.41, 28.42, 27.53, 26.85, 26.61, 23.51, 22.87, 21.14. Positive Mode NSI-MS m/z: exact mass calculated for $C_{24}H_{50}N_3^+$ ($[M+H]^+$): 380.3999; found 380.3998.

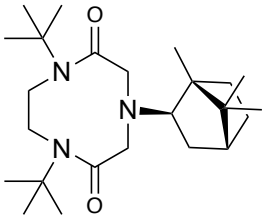

*1,7-di-tert-butyl-4-((1R,2R,4R)-1,7,7-trimethylbicyclo[2.2.1]heptan-2-yl)-1,4,7-triazacyclononane-2,6-dione (***3**$^{t\mathbf{Bu},exo\text{-}\mathbf{bornyl}}$). To a flame dried round bottom flask under N_2 was added **2**$^{t\mathbf{Bu}}$ (283 mg, 0.870 mmol, 1.0 equiv), DMF (20 mL), N,N-di-isopropylethylamine (0.45 mL, 2.61 mmol, 3.0 equiv), and then (1*R*,4*R*)-1,7,7-trimethylbicyclo[2.2.1]heptan-2-amine (172 mg, 1.13 mmol, 1.3 equiv). The reaction was heated to 120 °C and allowed to stir at this temperature overnight. After cooling to room temperature, the mixture was diluted with brine (30 mL), extracted with EtOAc, and washed with water (5 × 30 mL). The organics were collected, dried over $MgSO_4$, and concentrated *in vacuo*. The crude was purified by silica gel column chromatography, eluting with 40/60 EtOAc/hexanes (Rf = 0.2) to give 214 mg (61% yield) of white solid. ^{1}H NMR (400 MHz, Chloroform-*d*) δ 4.22-2.12 (m, 2H), 3.70 (d, *J* = 17.1 Hz, 2H), 3.61 – 3.46 (m, 4H), 2.83 (dd, *J* = 9.2, 6.0 Hz, 1H), 2.22 (ddt, *J* = 13.2, 7.0, 3.7 Hz, 1H), 1.71 – 1.55 (m, 4H), 1.40 (s, 18H), 1.07 (d, *J* = 8.5 Hz, 2H), 0.92 (apparent d, *J* = 2.1 Hz, 6H), 0.79 (s, 3H). ^{13}C NMR (75 MHz, Chloroform-*d*) δ 172.28, 75.85, 68.06, 57.27, 50.05, 46.95, 46.47, 44.75, 37.23, 35.99, 28.68, 27.06, 20.76, 20.72, 14.06. Positive Mode NSI-MS m/z: exact mass calculated for $C_{24}H_{44}N_3O_2^+$ ($[M+H]^+$): 406.3428; found 406.3427.

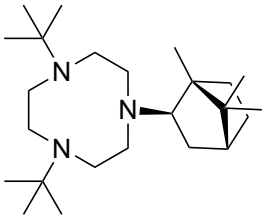

1,4-di-tert-butyl-7-((1R,2R,4R)-1,7,7-trimethylbicyclo[2.2.1]heptan-2-yl)-1,4,7-triazacyclononane (***t*Bu$_2$*exo*-bornyltacn**). To a flame dried round bottom flask under N_2, **3$^{tBu,exo\text{-}bornyl}$** (275 mg, 0.680 mmol, 1 equiv) was added and taken up in Et_2O (20 mL). The mixture was cooled to -78 °C and white powdered lithium aluminum hydride (103 mg, 2.72 mmol, 4.0 equiv) was added under a stream of N_2. The reaction was allowed to stir overnight while warming slowly to room temperature. Excess lithium aluminum hydride was quenched via the Fieser method[26], and $MgSO_4$ was added directly to the reaction flask. The mixture was filtered, the solids were rinsed with Et_2O (3 × 10 mL), and the combined filtrates were concentrated *in vacuo.* The crude was purified by silica gel column chromatography eluting with 10% sat. aq. NH_4OH in MeCN (Rf = 0.3). Once eluted, the fractions containing the product were combined and concentrated. The concentrate was taken up in DCM (30 mL) and washed with 2M NaOH (20 mL), then the organics were dried over $MgSO_4$, filtered, and concentrated *in vacuo* to give 161 mg (63% yield) of colorless oil. ^{1}H NMR (600 MHz, Acetone-d_6) δ 3.10 (s, 2H), 2.84 – 2.58 (m, 10H), 2.49 (dd, J = 8.9, 6.3 Hz, 1H), 1.84 (ddt, J = 12.2, 7.0, 3.7 Hz, 1H), 1.69 – 1.63 (m, 1H), 1.57 (t, J = 4.4 Hz, 1H), 1.50 – 1.39 (m, 2H), 1.02 (m, 23H), 0.94 (s, 3H), 0.79 (s, 3H). ^{13}C NMR (100 MHz, Acetone-d_6) δ 73.34, 56.47, 54.36, 52.23, 51.07, 49.19, 46.61, 44.85, 37.01, 35.34, 27.13, 26.29, 20.60, 19.67, 13.95. Positive Mode NSI-MS m/z: exact mass calculated for $C_{24}H_{49}N_3^+$ ([M+H]$^+$): 378.3843; found 378.3842.

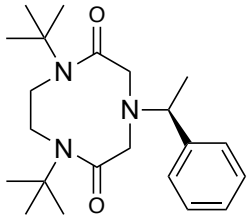

*(S)-1,7-di-tert-butyl-4-(1-phenylethyl)-1,4,7-triazacyclononane-2,6-dione (***3**$^{t\mathbf{Bu},sec\text{-}\mathbf{PhEt}}$). To a flame dried round bottom flask under N_2 was added **2**$^{t\mathbf{Bu}}$ (500 mg, 1.54 mmol, 1.0 equiv), DMF (25 mL), N,N-diisopropylethylamine (0.80 mL, 4.62 mmol, 3.0 equiv), and then (*S*)-(−)-α-Methylbenzylamine (196 mg, 1.61 mmol, 1.05 equiv). The reaction was heated to 120 °C and allowed to stir at this temperature overnight. After cooling to room temperature, the mixture was diluted with brine (30 mL), extracted with EtOAc, and washed with water (5 × 30 mL). The organics were collected, dried over $MgSO_4$, and concentrated *in vacuo*. The crude was purified by silica gel column chromatography, eluting with 50/50 EtOAc/hexanes (Rf = 0.3) to give 429 mg (74% yield) of off white solid.^{1}H NMR (600 MHz, Chloroform-*d*) δ 7.33 – 7.27 (m, 4H), 7.21 (tt, *J* = 6.1, 2.2 Hz, 1H), 4.00 (q, *J* = 6.8 Hz, 1H), 3.73 (s, 4H), 3.52 (d, *J* = 15.4 Hz, 2H), 3.44 (d, *J* = 15.4 Hz, 2H), 1.44 (d, *J* = 6.8 Hz, 3H), 1.38 (s, 18H). ^{13}C NMR (75 MHz, Chloroform-*d*) δ 172.12, 141.67, 128.38, 127.90, 127.23, 60.21, 57.81, 57.47, 47.65, 28.81, 16.89. Positive Mode NSI-MS m/z: exact mass calculated for $C_{22}H_{36}N_3O_2^+$ ($[M+H]^+$): 374.2802; found 374.2799.

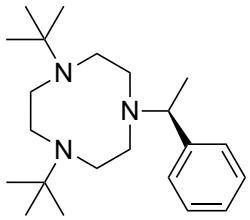

*(S)-1,4-di-tert-butyl-7-(1-phenylethyl)-1,4,7-triazacyclononane (***t**$\mathbf{Bu_2}$***sec*****-PhEttacn)**. To a flame dried round bottom flask under N_2, (S)-1,7-di-tert-butyl-4-(1-phenylethyl)-1,4,7-

triazacyclononane-2,6-dione (134 mg, 0.402 mmol, 1 equiv) was added and taken up Et_2O (5 mL). The mixture was cooled to -78 °C and white powdered lithium aluminum hydride (61 mg, 1.61 mmol, 4.0 equiv) was added under a stream of N_2. The reaction was allowed to stir overnight while warming slowly to room temperature. Excess lithium aluminum hydride was quenched via the Fieser method[26], and $MgSO_4$ was added directly to the reaction flask. The mixture was filtered, the solids were rinsed with Et_2O (3 × 5 mL), and the combined filtrates were concentrated *in vacuo.* The crude was purified by silica gel column chromatography eluting with 15% sat. aq. NH_4OH in MeCN (Rf = 0.2). Once eluted, the fractions containing the product were combined and concentrated. The concentrate was taken up in DCM (10 mL) and washed with 2M NaOH (10 mL), then the organics were dried over $MgSO_4$, filtered, and concentrated *in vacuo* to give 69 mg (50% yield) of pale yellow oil. ^{1}H NMR (600 MHz, Benzene-d_6) δ 7.50 (d, J = 7.8 Hz, 2H), 7.26 (td, J = 7.8, 1.8 Hz, 2H), 7.13 (t, J = 7.8, 1H), 3.69 (q, J = 6.7, 1H), 2.86 – 2.56 (m, 12H), 1.30 (d, J = 6.7, Hz, 3H), 1.03 (s, 18H). ^{13}C NMR (75 MHz, Benzene-d_6) δ 146.48, 128.22, 126.70, 63.40, 54.91, 54.52, 53.40, 52.06, 27.17, 18.03 – one aromatic C^{13} resonance is not observed (likely obscured by benzene). Positive Mode NSI-MS m/z: exact mass calculated for $C_{22}H_{40}N_3^+$ ($[M+H]^+$): 346.3217; found 346.3217.

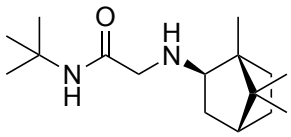

2-(tert-butylamino)-N-((1R,2R,4R)-1,7,7-trimethylbicyclo[2.2.1]heptan-2-yl)acetamide (**1.04**). To a flame dried round bottom flask under N_2 was added *N*-(*tert*-butyl)-2-chloroacetamide (753 mg, 5.04 mmol, 1.0 equiv), DMF (50 mL), N,N-diisopropylethylamine (1.32 mL, 7.56 mmol, 1.5 equiv), and then (1*R*, 2R, 4*R*)-1,7,7-trimethylbicyclo[2.2.1]heptan-2-amine (926 mg, 5.54 mmol,

1.1 equiv). This reaction was heated to 120 °C for 4 hours, then allowed to cool to room temperature. The mixture was diluted with brine (50 mL), then extracted with EtOAc (100 mL), and the organics washed with water (5 × 50 mL). The organics were dried over $MgSO_4$, filtered, and concentrated *in vacuo*. The crude was purified by silica gel column chromatography eluting with 40-70% EtOAc in hexanes (Rf = 0.3 in 50/50 EtOAc/hexanes) to give 970 mg (72% yield) of white solid. ^{1}H NMR (600 MHz, Chloroform-*d*) δ 7.22 (s, 1H), 3.11 (s, 2H), 2.48 (dd, *J* = 8.4, 4.9 Hz, 1H), 1.73 – 1.64 (m, 3H), 1.58 – 1.50 (m, 2H), 1.35 (s, 9H), 1.05 (td, *J* = 7.0, 2.7 Hz, 2H), 0.99 (s, 3H), 0.91 (s, 3H), 0.83 (s, 3H). ^{13}C NMR (100 MHz, Chloroform-*d*) δ 67.20, 52.19, 50.56, 48.58, 46.91, 45.07, 38.90, 36.91, 28.91, 27.26, 20.66, 20.62, 12.48 – carbonyl carbon ^{13}C resonance not observed. Positive Mode NSI-MS m/z: exact mass calculated for $C_{16}H_{30}N_2O^+$ ($[M+H]^+$): 267.2431; found 267.2428.

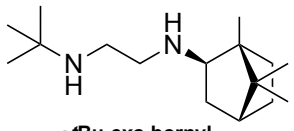

1 ***t*Bu,*exo*-bornyl**

N-(tert-butyl)-N′-((1R,2R,4R)-1,7,7-trimethylbicyclo[2.2.1]heptan-2-yl)ethane-1,2-diamine (**1** ***t*Bu,*exo*-bornyl**). To a flame dried round bottom flask under N_2 was added **5** (970 mg, 3.64 mmol, 1.0 equiv) and toluene (25 mL). Lithium aluminum hydride (275 mg, 7.28 mmol, 2.0 equiv) was added under a stream of N_2 and the mixture refluxed for 18 hours. After cooling to room temperature, excess lithium aluminum hydride was quenched via the Fieser method[26], and the reaction mixture was filtered. The solids were rinsed with Et_2O (3 × 10 mL) and the combined organics were washed with brine, dried over $MgSO_4$, filtered, and concentrated *in vacuo* to give 853 mg of pale yellow oil. The crude material was used in the next step without further purification.

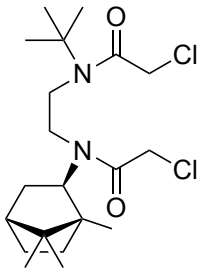

N-(tert-butyl)-2-chloro-N-(2-(2-chloro-N-((1R,2R,4R)-1,7,7-trimethylbicyclo[2.2.1]heptan-2-yl)acetamido)ethyl)acetamide (**2**$^{t\mathbf{Bu},exo\text{-}\mathbf{bornyl}}$). To a flame dried round bottom flask under N_2 was added chloroacetyl chloride (0.45 mL, 5.46 mmol, 1.5 equiv) and DCM (20 mL). The mixture was cooled to 0 °C and a solution of **1**$^{t\mathbf{Bu},exo\text{-}\mathbf{bornyl}}$ (5.04 mmol) in DCM (20 mL) was added dropwise over the course of 30 minutes. The reaction was allowed to warm to room temperature over the course of four hours. Sat. aq. K_2CO_3 (50 mL) was added to quench the reaction and the mixture was stirred vigorously for 10 minutes. The phases were separated, and the aqueous phase washed with DCM (2 × 20 mL). The organics were combined and washed with brine (50 mL), then dried over $MgSO_4$, filtered, and concentrated *in vacuo*. The crude was purified by silica gel column chromatography eluting with 30/70 EtOAc in hexanes (Rf = 0.3) to give 650 mg (44% yield over two steps) of white solid. ^{1}H NMR (400 MHz, Chloroform-*d*) δ 4.55 (d, *J* = 12.6 Hz, 1H), 4.28 (d, *J* = 12.6 Hz, 1H), 4.22 (d, *J* = 12.1 Hz, 1H), 4.07 (d, *J* = 12.1 Hz, 1H), 3.90 – 3.80 (m, 1 H), 3.70 (ddd, *J* = 13.3, 11.3, 4.4 Hz, 1H), 3.50 (ddd, *J* = 15.3, 11.3, 4.4 Hz, 1H), 3.29 – 3.06 (m, 2H), 1.99 – 1.74 (m, 4H), 1.69 – 1.57 (m, 1H), 1.44 (s, 9H), 1.35 – 1.09 (m, 2H), 0.93 (s, 3H), 0.89 (s, 3H), 0.76 (s, 3H). ^{13}C NMR (100 MHz, Chloroform-*d*) δ 169.60, 168.32, 64.73, 57.47, 51.07, 46.41, 44.18, 43.96, 43.18, 42.33, 38.22, 34.88, 29.02, 26.40, 21.94, 21.45, 11.65. Positive Mode NSI-MS m/z: exact mass calculated for $C_{20}H_{35}Cl_2N_2O_2^+$ ($[M+H]^+$): 405.2070; found 405.2069.

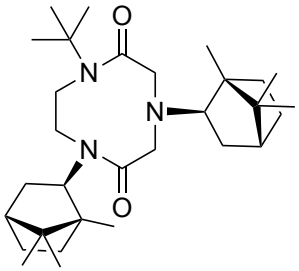

1-(tert-butyl)-4,7-bis((1R,2R,4R)-1,7,7-trimethylbicyclo[2.2.1]heptan-2-yl)-1,4,7-triazacyclononane-2,6-dione (**3**$^{exo\text{-bornyl},t\text{Bu}}$). To a flame dried round bottom flask under N_2 was added **2**$^{t\text{Bu},exo\text{-bornyl}}$ (200 mg, 0.493 mmol, 1 equiv), DMF (10 mL), N,N-diisopropylethylamine (0.26 mL, 1.48 mmol, 3.0 equiv), and then (1*R*, 2R, 4*R*)-1,7,7-trimethylbicyclo[2.2.1]heptan-2-amine (98 mg, 0.641 mmol, 1.3 equiv). This mixture was heated to reflux for 6 hours. After cooling to room temperature, the reaction was diluted with brine (10 mL) and extracted with EtOAc (20 mL). The organic phase was separated and washed with water (5 × 10 mL). The organics were dried over $MgSO_4$, filtered, and concentrated *in vacuo.* The crude was purified by silica gel column chromatography eluting with 20-60% EtOAc in hexanes (Rf = 0.3 in 40/60 EtOAc/hexanes) to give 155 mg of an impure white foam. This material was carried on without further purification (see supporting information: Figure S1-28 for ^{1}H NMR spectrum).

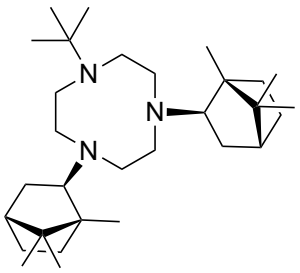

1-(tert-butyl)-4,7-bis((1R,2R,4R)-1,7,7-trimethylbicyclo[2.2.1]heptan-2-yl)-1,4,7-triazacyclononane (***exo*-bornyl$_2$*t*Bu*tacn***). To a flame dried round bottom flask under N_2 was added **3**$^{exo\text{-bornyl},t\text{Bu}}$ (155 mg, 0.493 mmol, 1 equiv) and Et_2O (20 mL). This mixture was cooled to

-78 °C and lithium aluminum hydride (80 mg, 2.11 mmol, 4.2 equiv) was added under a stream of N_2. The mixture was allowed to warm to room temperature while stirring overnight. Excess lithium aluminum hydride was quenched via the Fieser method.[26] The mixture was filtered and the solids rinsed with Et_2O (3 × 10 mL). After combining the filtrates, they were washed with brine (30 mL), dried over $MgSO_4$, filtered, and concentrated *in vacuo*. The crude was purified by silica gel column chromatography eluting with 3-6% 7M methanolic ammonia in DCM (Rf = 0.3 in 4% 7M methanolic ammonia in DCM. The fractions containing the product were collected and concentrated *in vacuo*. The concentrate was taken up in Et_2O (20 mL) and washed with 2M NaOH (20 mL). The organics were separated, dried over $MgSO_4$, filtered, and concentrated *in vacuo* to give 84 mg (37% yield for two steps) of an off white solid. An analytical sample was recrystallized from hot iPrOH (white solid). ^{1}H NMR (600 MHz, Benzene-d_6) δ 3.70 (broad s, 2H), 3.20 (broad s, 2H), 2.84 (t, J = 11.3 Hz, 2 H), 2.68 (dd, J = 14.3, 4.3 Hz, 2H), 2.60 (d, J = 13.3 Hz, 2H), 2.49 (dd, J = 9.0, 6.6 Hz, 2H), 2.45 (d, J = 11.3 Hz, 2H), 2.05 – 1.94 (m, 2H), 1.69 (dddt, J = 10.4, 7.1, 5.5, 2.9 Hz, 2H), 1.61 (t, J = 4.3 Hz, 2H), 1.52 – 1.44 (m, 4H), 1.16 (s, 6H), 1.11 – 1.08 (m, 4H), 1.07 (s, 6H), 1.05 (s, 9H), 0.84 (s, 6H). ^{13}C NMR (150 MHz, Benzene-d_6) δ 74.52, 55.37, 55.01, 52.00, 50.45, 48.49, 47.86, 46.00, 38.34, 36.84, 28.47, 27.61, 21.87, 20.82, 15.75. Positive Mode NSI-MS m/z: exact mass calculated for $C_{30}H_{56}N_3^+$ ([M+H]$^+$): 458.4469; found 458.4465.

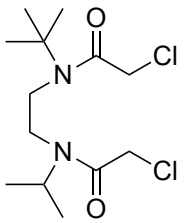

N-(tert-butyl)-2-chloro-N-(2-(2-chloro-N-isopropylacetamido)ethyl)acetamide (**2**$^{t\mathbf{Bu},i\mathbf{Pr}}$). To a flame dried round bottom flask under N_2 was added chloroacetyl chloride (8.0 mL, 101 mmol, 2.5

equiv) and DCM (80 mL). The mixture was cooled to 0 °C and N^1-(*tert*-butyl)-N^2-isopropylethane-1,2-diamine (6.40 g, 40.4 mmol, 1.0 equiv) was added dropwise over 20 minutes. The reaction was allowed to warm to room temperature over the course of four hours. Sat. aq. K_2CO_3 (200 mL) was added to quench the reaction and the mixture was stirred vigorously for 10 minutes. The phases were separated and the aqueous phase washed with DCM (2 × 80 mL). The organics were combined and washed with brine (200 mL), then dried over $MgSO_4$, filtered, and concentrated *in vacuo*. The pure compound was obtained by crystallization from EtOAc and hexanes to give 9.84 g, (78% yield) of white solid.^{1}H NMR (600 MHz, Chloroform-*d*) δ 4.45 (s, 1H), 4.11 (s, 1H), 4.08 (p, *J* = 6.6 Hz, 1H), 3.46 (s, 1H), 3.32 – 3.24 (m, 1H), 1.49 (s, 5H), 1.28 (d, *J* = 6.7 Hz, 4H). ^{13}C NMR (100 MHz, Chloroform-*d*) δ 168.31, 167.04, 57.79, 49.32, 44.16, 43.26, 42.90, 41.60, 29.01, 21.56. Positive Mode NSI-MS m/z: exact mass calculated for $C_{13}H_{25}O_2N_2Cl_2^+$ ($[M+H]^+$): 311.12876; found 311.12916.

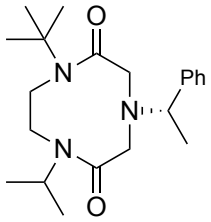

(S)-1-(tert-butyl)-4-isopropyl-7-(1-phenylethyl)-1,4,7-triazacyclononane-2,6-dione (**3**$^{t\mathbf{Bu},i\mathbf{Pr},sec\text{-}\mathbf{PhEt}}$). To a flame dried round bottom flask under N_2 was added **2**$^{t\mathbf{Bu},i\mathbf{Pr}}$ (150 mg, 0.483 mmol, 1 equiv), DMF (10 mL), N,N-diisopropylethylamine (0.13 mL, 0.725 mmol, 1,5 equiv), and then (*S*)-(−)-α-Methylbenzylamine (70 µL , 0.531 mmol, 1.1 equiv). This mixture was heated to 120 °C for 6 hours. After cooling to room temperature, the reaction was diluted with brine (10 mL) and extracted with EtOAc (20 mL). The organic phase was separated and washed with water (5 × 10 mL). The organics were dried over $MgSO_4$, filtered, and concentrated *in vacuo.* The crude was

purified by silica gel column chromatography eluting with 50% EtOAc in hexanes (Rf = 0.3 in 50/50 EtOAc/hexanes) to give 101 mg (58% yield) of an off white solid. ^{1}H NMR (400 MHz, Chloroform-*d*) δ 7.35 – 7.28 (m, 4H), 7.26 – 7.22 (m, 1H), 4.88 (p, *J* = 6.8 Hz, 1H), 4.00 (q, *J* = 6.8 Hz, 1H), 3.77 – 3.40 (m, 8H), 1.47 (d, *J* = 6.8 Hz, 3H), 1.44 (s, 9H), 1.05 (d, *J* = 6.8 Hz, 3H), 0.97 (d, *J* = 6.8 Hz, 3H). ^{13}C NMR (100 MHz, Chloroform-*d*) δ 172.94, 170.15, 141.92, 128.60, 127.95, 127.49, 60.81, 60.06, 57.25, 57.07, 48.20, 44.78, 44.64, 28.82, 20.48, 20.33, 17.60. Positive Mode NSI-MS m/z: exact mass calculated for $C_{21}H_{34}O_2N_3^+$ ([M+H]$^+$): 360.26455; found 360.26506.

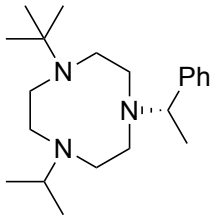

(S)-1-(tert-butyl)-4-isopropyl-7-(1-phenylethyl)-1,4,7-triazacyclononane (***sec*-PhEt*t*Bu*i*Prtacn**).

To a flame dried round bottom flask under N_2 was added **3**$^{t\mathbf{Bu},i\mathbf{Pr},sec\text{-}\mathbf{PhEt}}$ (99 mg, 0.275 mmol, 1 equiv) and Et_2O (20 mL). This mixture was cooled to -78 °C and lithium aluminum hydride (45 mg, 1.16 mmol, 4.2 equiv) was added under a stream of N_2. The mixture was allowed to warm to room temperature while stirring overnight. Excess lithium aluminum hydride was quenched via the Fieser method.[26] The mixture was filtered and the solids rinsed with Et_2O (3 × 10 mL). After combining the filtrates, they were washed with brine (30 mL), dried over $MgSO_4$, filtered, and concentrated *in vacuo*. The crude was purified by silica gel column chromatography eluting with 15% NH_4OH (saturated aqueous) in MeCN. The fractions containing the product were collected and concentrated *in vacuo*. The concentrate was taken up in Et_2O (20 mL) and washed with 2M NaOH (20 mL). The organics were separated, dried over $MgSO_4$, filtered, and concentrated *in*

vacuo to give 72 mg (63% yield) of a colorless oil. ^{1}H NMR (400 MHz, Benzene-d_6) δ 7.49 (d, J = 7.1 Hz, 2H), 7.25 (dd, J = 8.4, 6.9 Hz, 2H), 7.15 – 7.10 (m, 1H), 3.71 (q, J = 6.7 Hz, 1H), 2.92 – 2.51 (m, 13H), 1.31 (d, J = 6.7 Hz, 3H), 1.03 (s, 9H), 0.95 (d, J = 2.0 Hz, 3H), 0.94 (d, J = 2.0 Hz, 3H). ^{13}C NMR (100 MHz, Chloroform-d) δ 146.00, 128.00, 127.97, 126.34, 63.01, 54.98, 54.33, 53.61, 53.56, 53.06, 53.04, 52.30, 51.50, 27.11, 18.92, 18.28, 17.90. Positive Mode NSI-MS m/z: exact mass calculated for $C_{21}H_{38}N_3^+$ ([M+H]$^+$): 332.30602; found 332.30654.

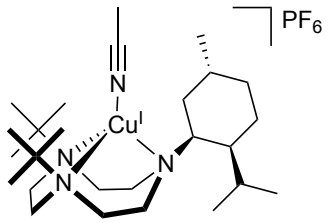

[Cu(tBu$_2$menthyltacn)(MeCN)]PF$_6$. To a scintillation vial in the glovebox containing 1,4-di-tert-butyl-7-((1S,2S,5R)-2-isopropyl-5-methylcyclohexyl)-1,4,7-triazacyclononane *(*165 mg, 0.435 mmol, 1.0 equiv) was added tetrakisacetonitrile copper(I) hexafluorophosphate (165 mg, 0.442 mmol, 1.0 equiv) as a solution in THF (5 mL). The mixture was stirred for two hours at room temperature, then concentrated *in vacuo*. The crude concentrate was purified by crystallization from THF/pentane vapor diffusion to give 96 mg (33% yield) of colorless crystals suitable for x-ray diffraction. ^{1}H NMR (400 MHz, Acetonitrile-d_3) δ 3.27 (dt, J = 12.9, 4.5 Hz, 1H), 3.18 – 3.05 (m, 2H), 3.03 – 2.90 (m, 4H), 2.86 – 2.69 (m, 3H), 2.62 – 2.45 (m, 2H), 2.31 (tdd, J = 10.6, 4.8, 2.7 Hz, 2H), 2.23 – 1.99 (m, 3H), 1.79 – 1.65 (m, 3H), 1.58 (dt, J = 14.3, 5.3 Hz, 1H), 1.25 (s, 9H), 1.24 (s, 9H), 1.07 (d, J = 6.9 Hz, 3H), 1.04 (d, J = 6.9 Hz, 3H), 0.94 (d, J = 6.7 Hz, 4H). ^{13}C NMR (100 MHz, Acetonitrile-d_3) δ 64.87, 59.41, 59.32, 57.76, 53.57, 52.76, 47.80, 47.65, 47.24, 41.77, 35.47, 29.12, 29.00, 27.74, 27.15, 24.30, 21.95, 20.87, 18.99. See supporting information Figure S1-42 for powder XRD.

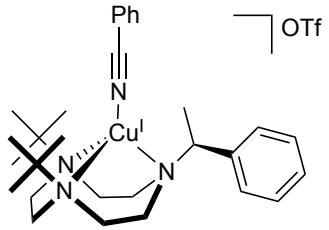

[Cu(tBu₂sec-PhEttacn)(NCPh)]OTf. To a scintillation vial in the glovebox containing (S)-1,4-di-tert-butyl-7-(1-phenylethyl)-1,4,7-triazacyclononane (186 mg, 0.538 mmol, 1.0 equiv) and MeCN (~ 4 mL) was added tetrakisacetonitrile copper(I) triflate (203 mg, 0.538 mmol, 1.0 equiv). The mixture was stirred overnight at room temperature, then concentrated *in vacuo*. The crude concentrate was taken up in a minimum quantity of benzonitrile, and vapor diffused with a mixture of Et_2O and pentane to give 220 mg (64% yield) of yellow needles suitable for x-ray diffraction. ^{1}H NMR (300 MHz, Acetonitrile-d_3) δ 7.84 – 7.25 (m, 10H), 3.97 (q, J = 6.8 Hz, 1H), 3.13 – 2.82 (m, 6H), 2.67 – 2.31 (m, 6H), 2.30 – 2.15 (m, 1H), 1.64 (d, J = 6.8 Hz, 3H), 1.26 (s, 9H), 1.20 (s, 9H). ^{13}C NMR (75 MHz, Acetonitrile-d_3) δ 141.38, 133.98, 133.10, 130.21, 130.05, 129.17, 129.00, 112.94, 67.41, 59.42, 59.36, 56.52, 51.41, 51.04, 50.34, 48.92, 48.29, 26.94, 20.44. Nitrile carbon ^{13}C resonance not observed. Anal. calc. for: $C_{30}H_{44}CuF_3N_4O_3S$: C, 54.49; H, 6.71; N, 8.47. Found: C, 54.55; H, 6.53; N, 8.43.

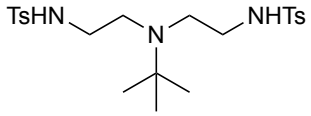

N,N''-di-tosyl-N'-tert-butyldiethylenetriamine (**1.06**). N-tosylaziridine (3.68 g, 18.66 mmol, 2.0 equiv) and toluene (20 mL) were combined in a thick-walled glass vessel. *tert*-Butylamine (680 mg, 0.975 mL, 9.33 mmol, 1.0 equiv) was added and the vessel was immediately sealed with a screw cap. The mixture was heated to 110 °C for six hours. After cooling to room temperature, the

mixture was transferred to a round-bottom flask and concentrated *in vacuo* to give the crude product as a colorless oil (4.35 g, 9.30 mmol, >99% yield), which was found to be pure by ^{1}H NMR spectroscopy. This material was used without purification but can be purified by filtration over silica gel with ethyl acetate if desired (Rf = 0.4 in 50/50 EtOAc/hexanes). ^{1}H NMR (400 MHz, Chloroform-*d*) δ 7.73 (d, J = 8.4 Hz, 2H), 7.29 (d, J = 8.4 Hz, 2H), 4.99 (s, 2H), 2.81 (t, J = 6.6 Hz, 4H), 2.53 (t, J = 6.6 Hz, 4H), 2.41 (s, 6H), 0.948 (s, 9H). ^{13}C NMR (75 MHz, Chloroform-*d*) δ 143.42, 136.81, 129.73, 127.06, 55.13, 50.32, 43.19, 26.99, 21.53. Positive Mode NSI-MS m/z: exact mass calculated for $C_{22}H_{34}N_3O_4S_2^+$ ($[M+H]^+$): 468.19852; found 468.19875.

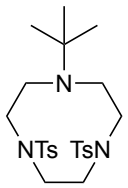

1-(tert-butyl)-4,7-ditosyl-1,4,7-triazacyclononane (**Ts$_2$*t*Butacn**). To a solution of N,N'-((tert-butylazanediyl)bis(ethane-2,1-diyl))bis(4-methylbenzenesulfonamide) (2.32 g, 4.96 mmol, 1.0 equiv) in DMF (50 mL), NaH (250 mg, 10.17 mmol, 2.05 equiv) was added under a stream of nitrogen and the mixture was stirred for 30 minutes. The mixture was heated to 100 °C and ethylene glycol ditosylate (1.84 g, 4.96 mmol, 1.0 equiv) in DMF (25 mL) was added over the course of two hours via syringe pump. The reaction was allowed to stir overnight at 100 °C. After cooling to room temperature, the reaction was quenched by the addition of water (5 mL) and was diluted with ethyl acetate (200 mL) and washed with brine (100-200 mL) then three portions of sat. aq. LiCl (100 mL). The organics were collected, dried over Na_2SO_4, filtered, and concentrated *in vacuo*. Purification by silica gel column chromatography (70/30 hexanes/ethyl acetate) afforded the product as a white foam (1.82 g, 3.69 mmol, 74% yield). ^{1}H NMR (400 MHz, Chloroform-*d*)

δ 7.65 (d, J = 8.0 Hz, 4H), 7.31 (d, J = 8.0 Hz, 4H), 3.54 (s, 4H), 3.15 (t, J = 4.1 Hz, 4H), 2.83 (t, J = 4.1 Hz, 4H), 2.42 (s, 6H), 1.05 (s, 9H). ^{13}C NMR (100 MHz, Chloroform-*d*) δ 143.54, 135.14, 129.86, 127.40, 55.31, 52.53, 27.08, 26.46, 21.62. Positive Mode NSI-MS m/z: exact mass calculated for $C_{24}H_{36}N_3O_4S_2^+$ ($[M+H]^+$): 494.21472; found 494.21475.

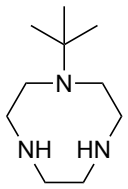

1-(tert-butyl)-1,4,7-triazacyclonane (***t*BuH$_2$tacn**). A round bottomed flask, under N_2, containing **Ts$_2$*t*Butacn** (5.38 g, 10.89 mmol, 1.0 equiv) dissolved in THF (100 mL), was cooled to –78 °C and fitted with a condensing jacket that was also cooled to –78 °C. Ammonia (100 mL) was condensed into the reaction flask, and freshly cut sodium strips (5.00 g, 217.8 mmol, 20 equiv) were then added under a stream of nitrogen. The mixture was stirred vigorously and allowed to warm to room temperature over the course of five hours. After reaching room temperature, the mixture took on a gel like consistency and was carefully treated with methanol (10 mL) and then water until all residual reductant had been quenched, as evidenced by a lack of effervescence. The mixture was then diluted with 200 mL of ethyl acetate and washed with brine. The organic phase was collected, dried over Na_2SO_4, filtered, and concentrated *in vacuo*. The crude product was purified by silica gel column chromatography (15% concentrated ammonium hydroxide in acetonitrile, Rf = 0.55). The pure fractions were collected, diluted with DCM, and washed with 2M sodium hydroxide. The organic phase was collected, dried over Na_2SO_4, filtered, and concentrated to afford the product as a colorless oil (1.06 g, 5.77 mmol, 53% yield). In lieu of chromatography, the crude mixture can be purified by distillation under high vacuum (0.1 mbar)

at 150 °C. ^{1}H NMR (400 MHz, Chloroform-*d*) δ 2.79 (s, 4H), 2.74 (t, J = 5.54 4H), 2.62-2.58 (m, 4H), 1.08 (s, 9H). ^{13}C NMR (100 MHz, Chloroform-*d*) δ 54.88, 49.07, 48.59, 47.29, 27.15. Positive Mode NSI-MS m/z: exact mass calculated for $C_{10}H_{24}N_3^+$ ([M+H]$^+$): 186.19651; found 186.19641.

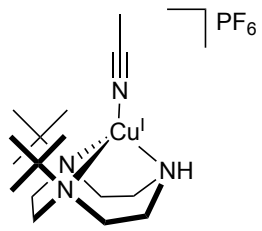

[Cu(tBu₂Htacn)(MeCN)]PF₆. ***t*Bu₂Htacn** (1.10 g, 4.56 mmol, 1.1 equiv) and acetonitrile (5 mL) were added to a scintillation vial with stir bar inside a glovebox. In a separate vial in the glovebox, $[Cu(MeCN)_4]PF_6$ was taken up in acetonitrile (5 mL). The copper solution was then added dropwise to the vial containing ***t*Bu₂Htacn**. The reaction was allowed to stir for 2 hours, and then the mixture was concentrated in vacuo. The resulting yellow oil was dissolved in CH_2Cl_2 and recrystallized by vapor diffusion with ether to give 1.105g of pure product (2.25 mmol, 54% yield) as light yellow translucent crystals of suitable quality for x-ray diffraction. Anal. Calculated for $C_{16}H_{34}CuF_6N_4P$: C, 39.14; H, 6.98; N, 11.41. Found: C, 39.44; H, 6.78; N, 11.47. ^{1}H NMR (400 MHz, Chloroform-*d*) δ 3.24 – 3.07 (m, 3H), 3.04 – 2.80 (m, 5H), 2.71 – 2.62 (m, 2H), 2.48 – 2.30 (m, 4H), 2.22 (s, 3H), 1.26 (s, 18H). ^{13}C NMR (100 MHz, Chloroform-*d*) δ 116.24 (bound acetonitrile), 58.38, 49.31, 47.99, 47.06, 27.00, 2.99 (bound acetonitrile).

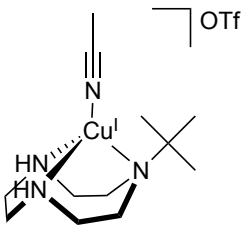

[Cu(tBuH$_2$tacn)(MeCN)]OTf. ***t*BuH$_2$tacn** (20 mg, 0.108 mmol, 1.1 equiv) and acetonitrile (1 mL) were combined in a scintillation vial equipped with a stir bar in a glovebox. In a separate vial in the glovebox, [Cu(MeCN)$_4$]OTf (36.9 mg, 0.098 mmol, 1.0 equiv) was dissolved in 1mL acetonitrile. The copper solution was added dropwise to the ligand solution. The reaction was allowed to stir overnight. The following afternoon, the solvent was removed in vacuo. The resulting colorless oily residue was taken up in a few drops of acetonitrile. Vapor diffusion with ether furnished 26.2 mg (0.060 mmol, 61% yield) of translucent, block-shaped crystals suitable for x-ray diffraction. ^{1}H NMR (400 MHz, Acetonitrile-d_3) δ 3.17 (s, 2H), 2.99-2.83 (m, 6H), 2.63–2.49 (m, 4H), 2.37-2.30 (m, 2H), 1.26 (s, 9H). ^{13}C NMR (100 MHz, Acetonitrile-d_3) δ 58.81, 48.23, 48.06, 46.05, 27.27. See supporting information Figure S1-43 for powder XRD.

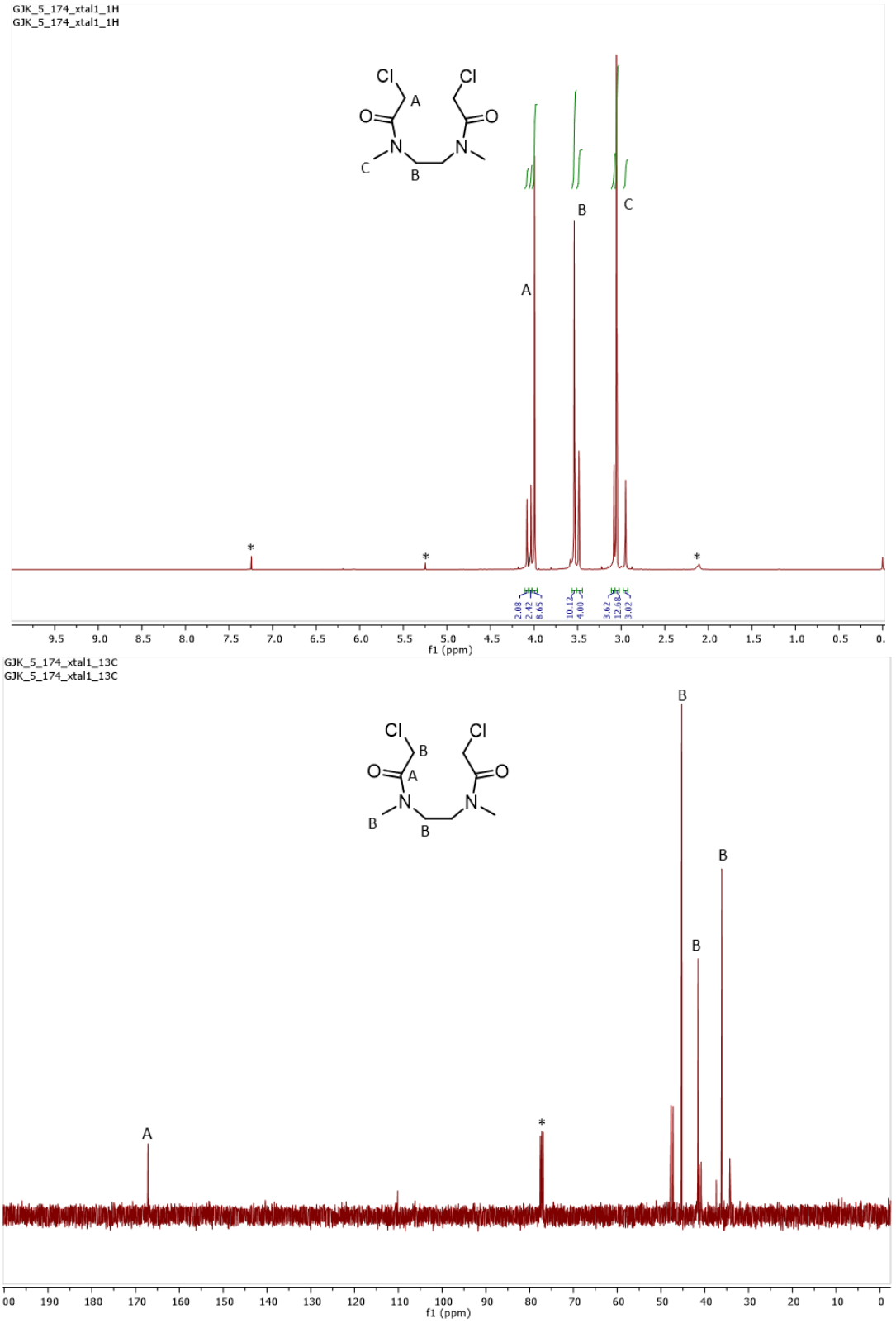

Figure S1-1. ^{1}H NMR spectrum (top) and ^{13}C NMR spectrum (bottom) of **2**^{Me} in $CDCl_3$.

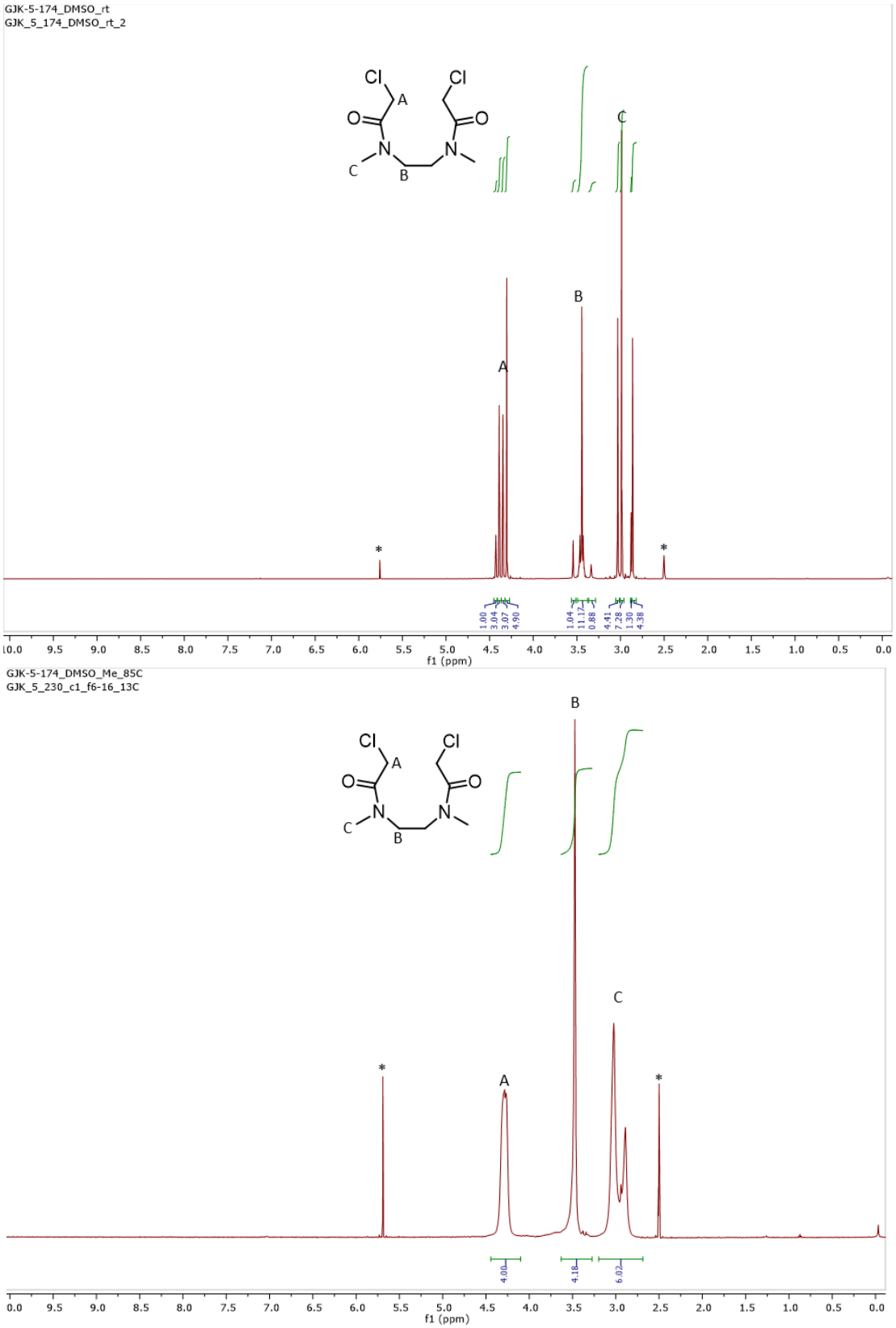

Figure S1-2. ^{1}H NMR spectrum of **2**$^{\mathbf{Me}}$ in DMSO at rt (top) and at 85 °C (bottom).

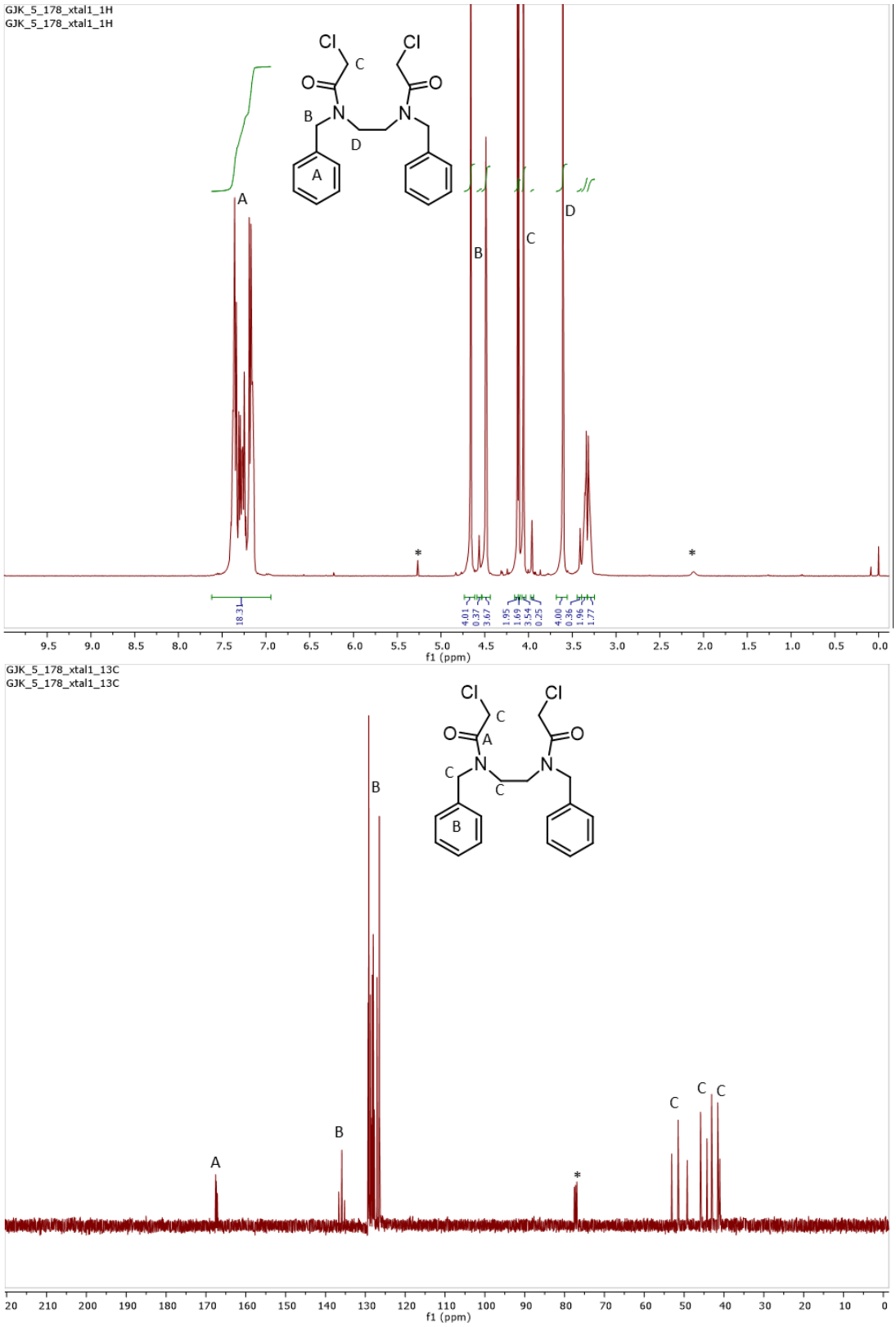

Figure S1-3. ^{1}H NMR spectrum (top) and ^{13}C NMR spectrum (bottom) of **2^{Bn}** in $CDCl_3$.

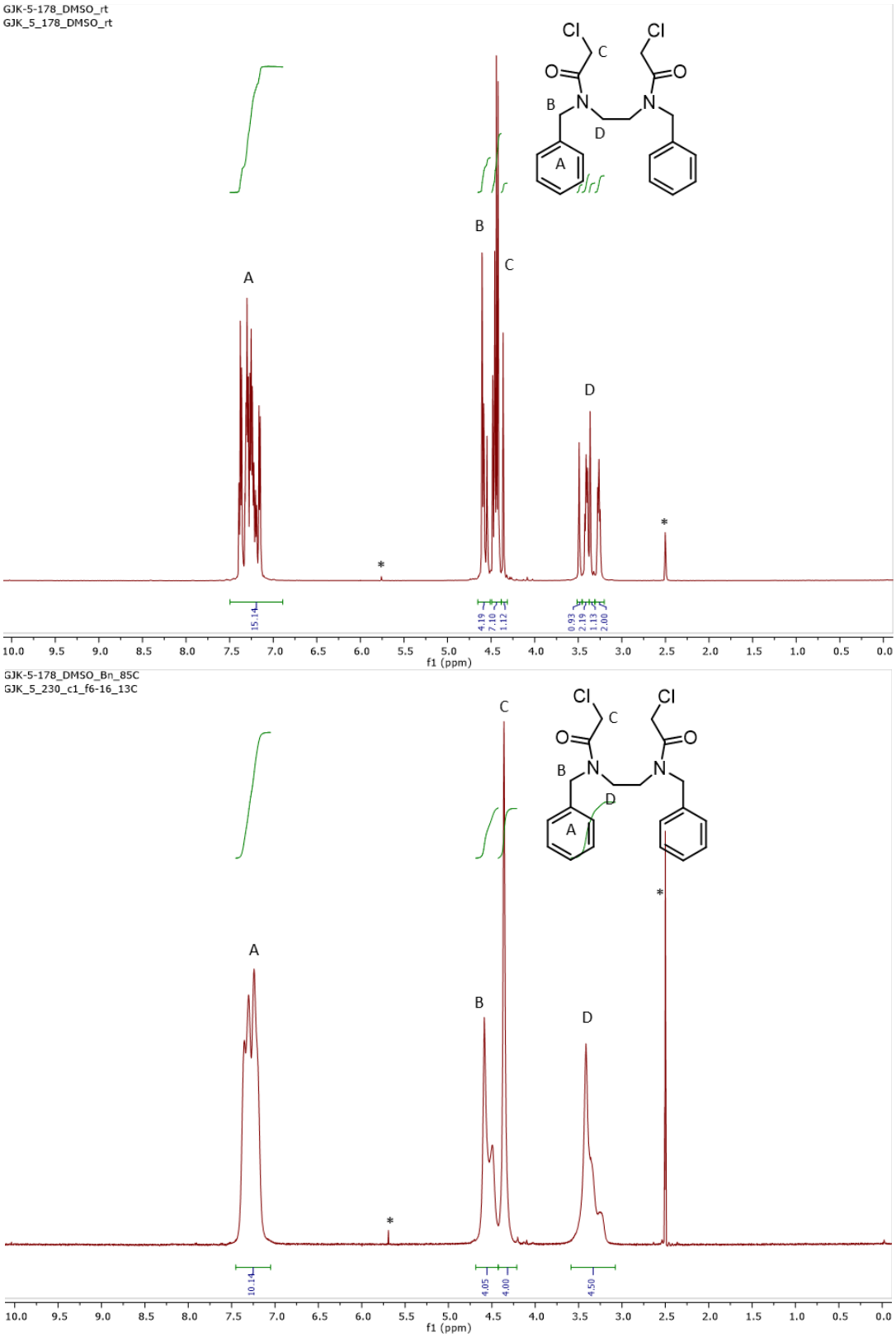

Figure S1-4. ^{1}H NMR spectrum of **2^{Bn}** in DMSO at rt (top) and at 85 °C (bottom).

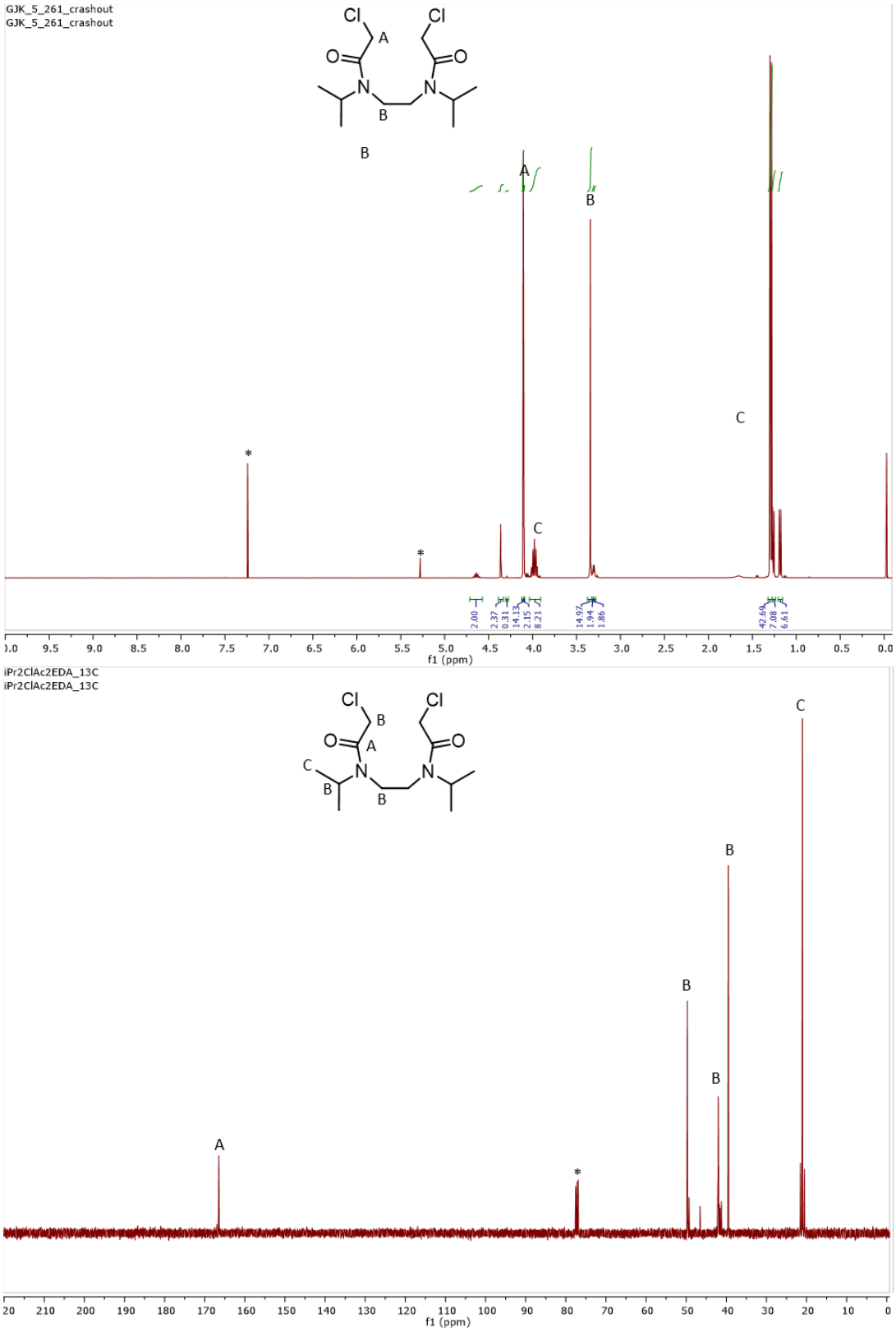

Figure S1-5. ^{1}H NMR spectrum (top) and ^{13}C NMR spectrum (bottom) of $\mathbf{2}^{\mathbf{iPr}}$ in $CDCl_3$.

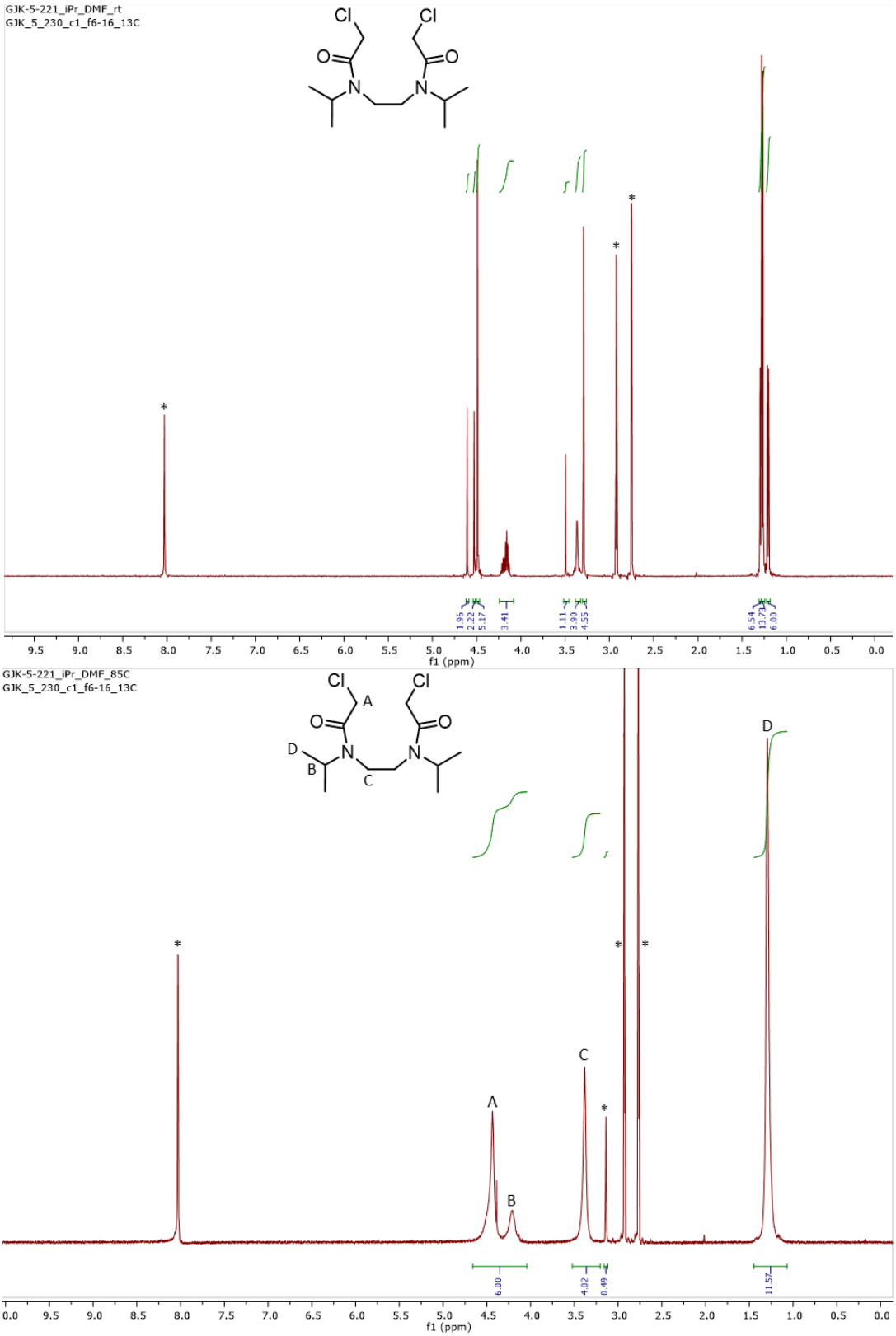

Figure S1-6. ^{1}H NMR spectrum **2**^{iPr} in DMF at rt (top) and at 85 °C (bottom).

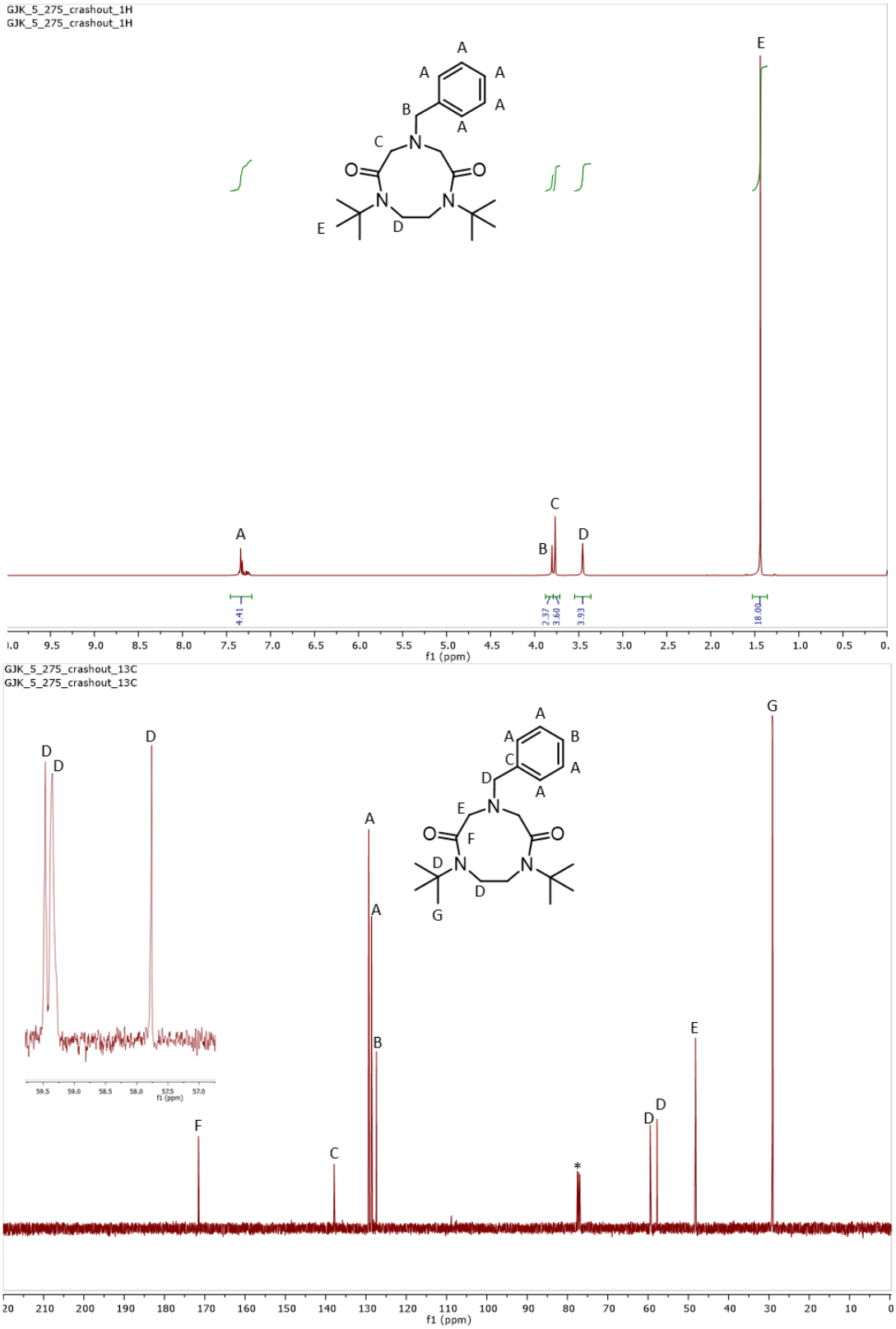

Figure S1-7. ^{1}H NMR spectrum (top) and ^{13}C NMR spectrum (bottom) of **3**^{tBu,Bn} in $CDCl_3$.

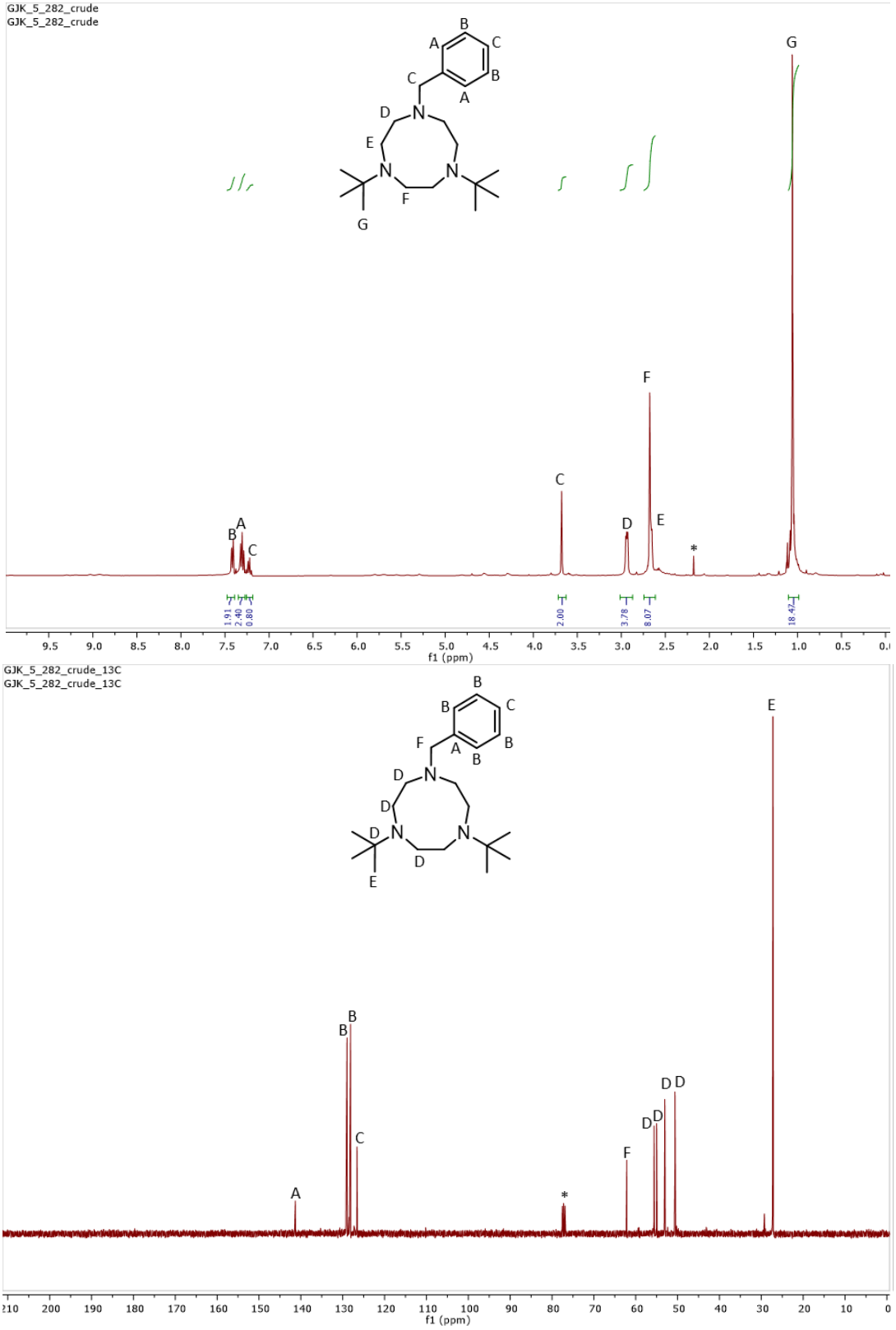

Figure S1-8. ^{1}H NMR spectrum (top) and ^{13}C NMR spectrum (bottom) of ***t*Bu$_2$Bntacn** in $CDCl_3$.

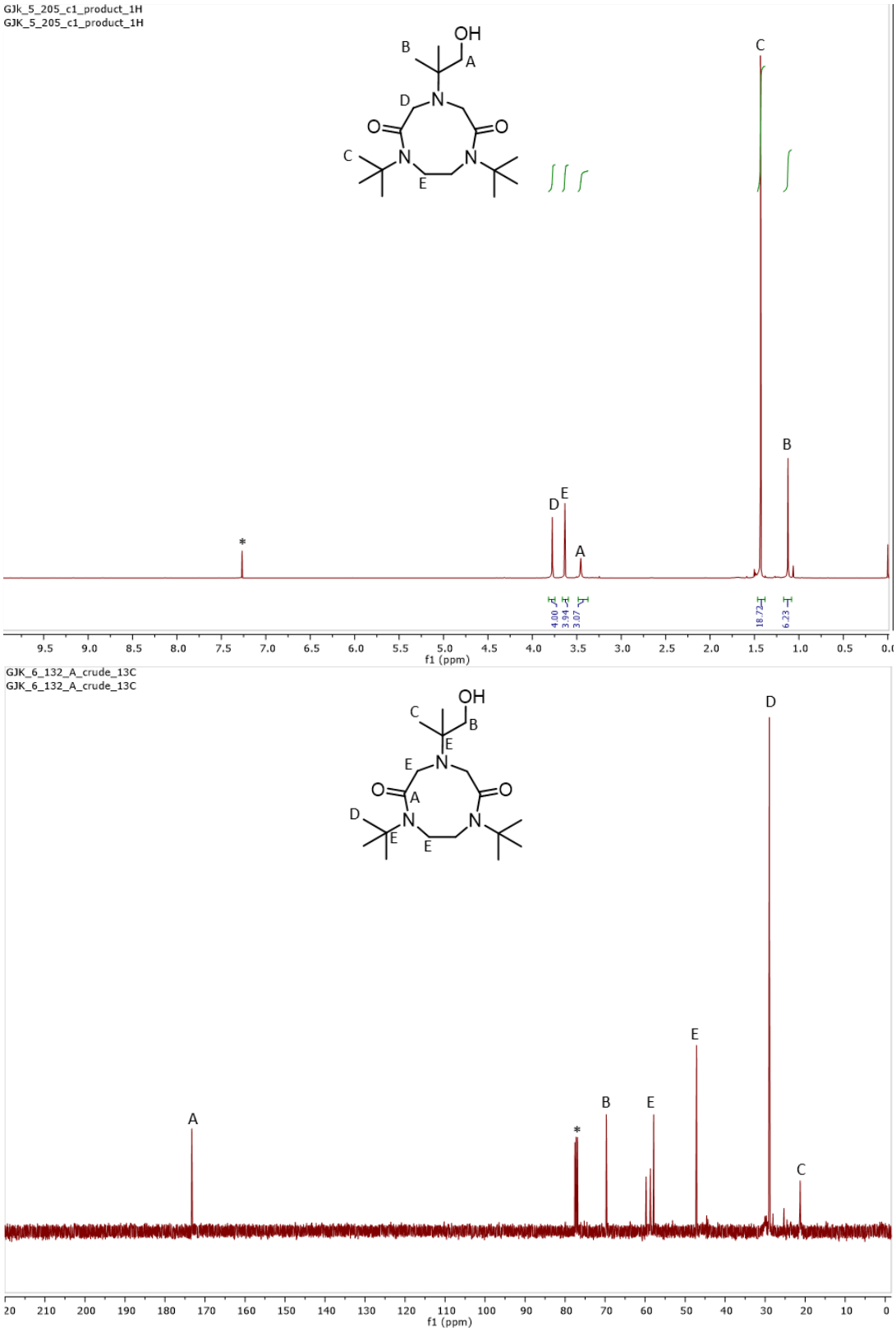

Figure S1-9. ^{1}H NMR spectrum (top) and ^{13}C NMR spectrum (bottom) of **3**$^{t\mathbf{Bu,dmea}}$ in $CDCl_3$.

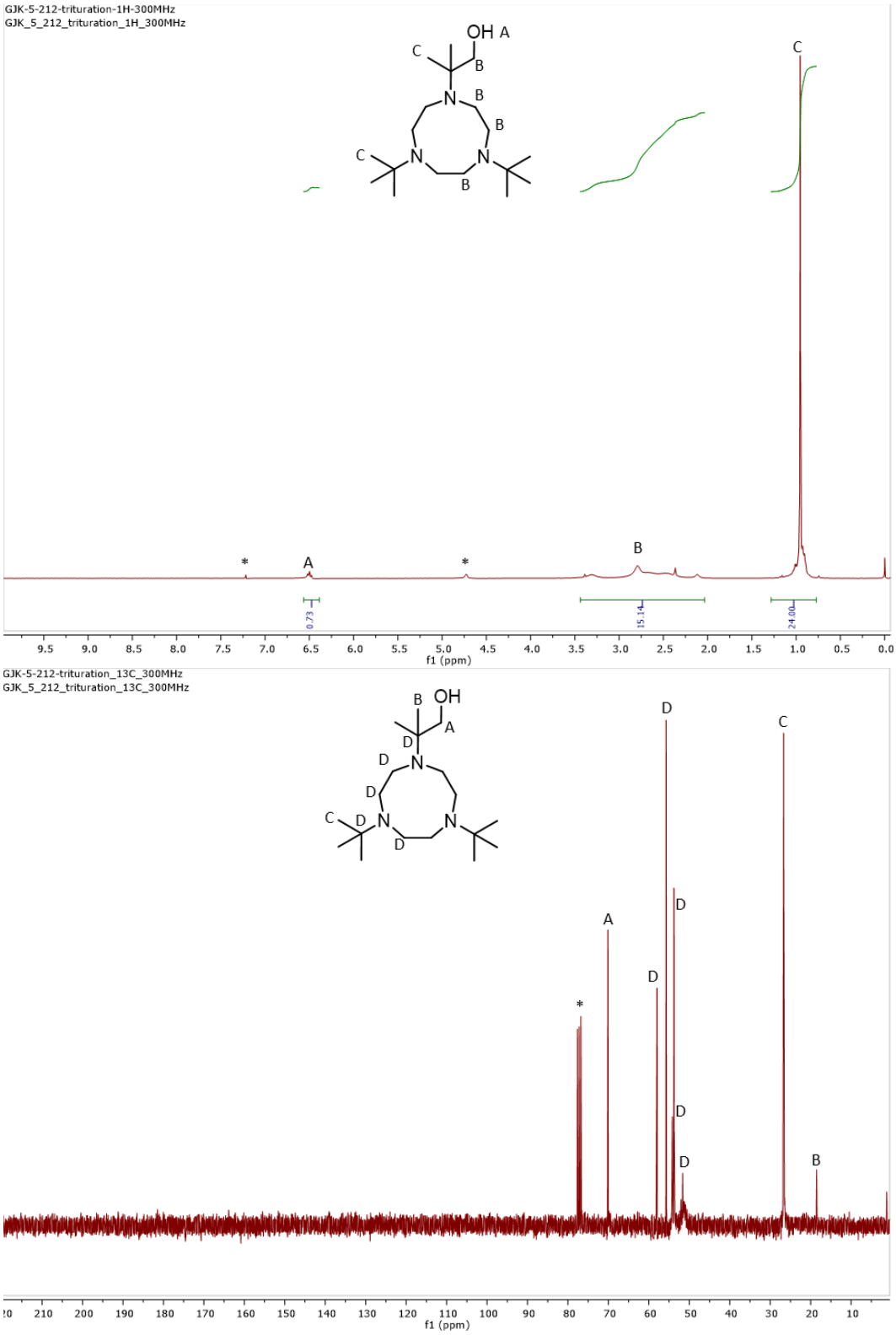

Figure S1-10. ^{1}H NMR spectrum (top) and ^{13}C NMR spectrum (bottom) of ***t*Bu$_2$dmeatacn** in $CDCl_3$.

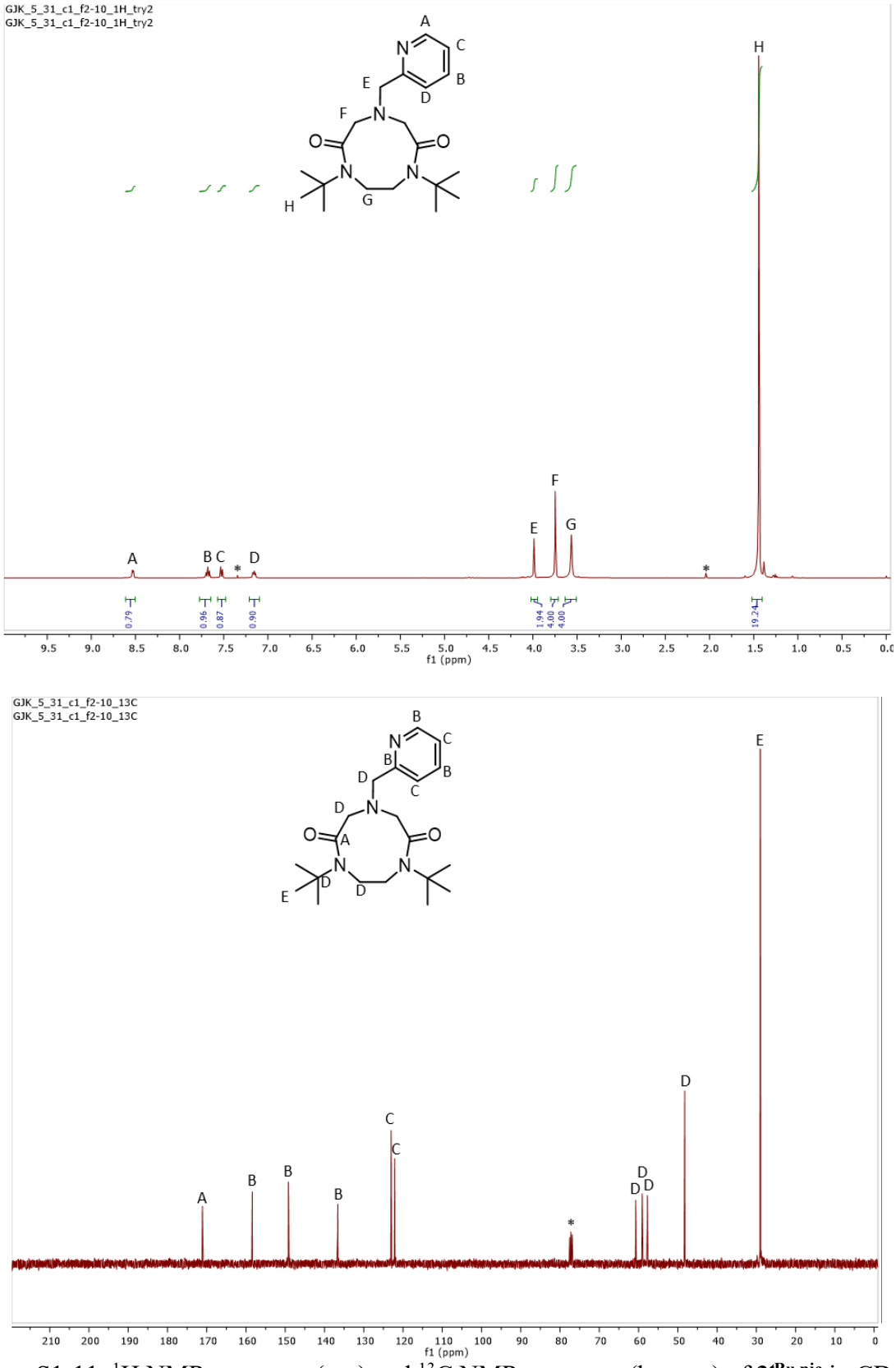

Figure S1-11. ^{1}H NMR spectrum (top) and ^{13}C NMR spectrum (bottom) of **3**$^{t\mathbf{Bu,pic}}$ in $CDCl_3$.

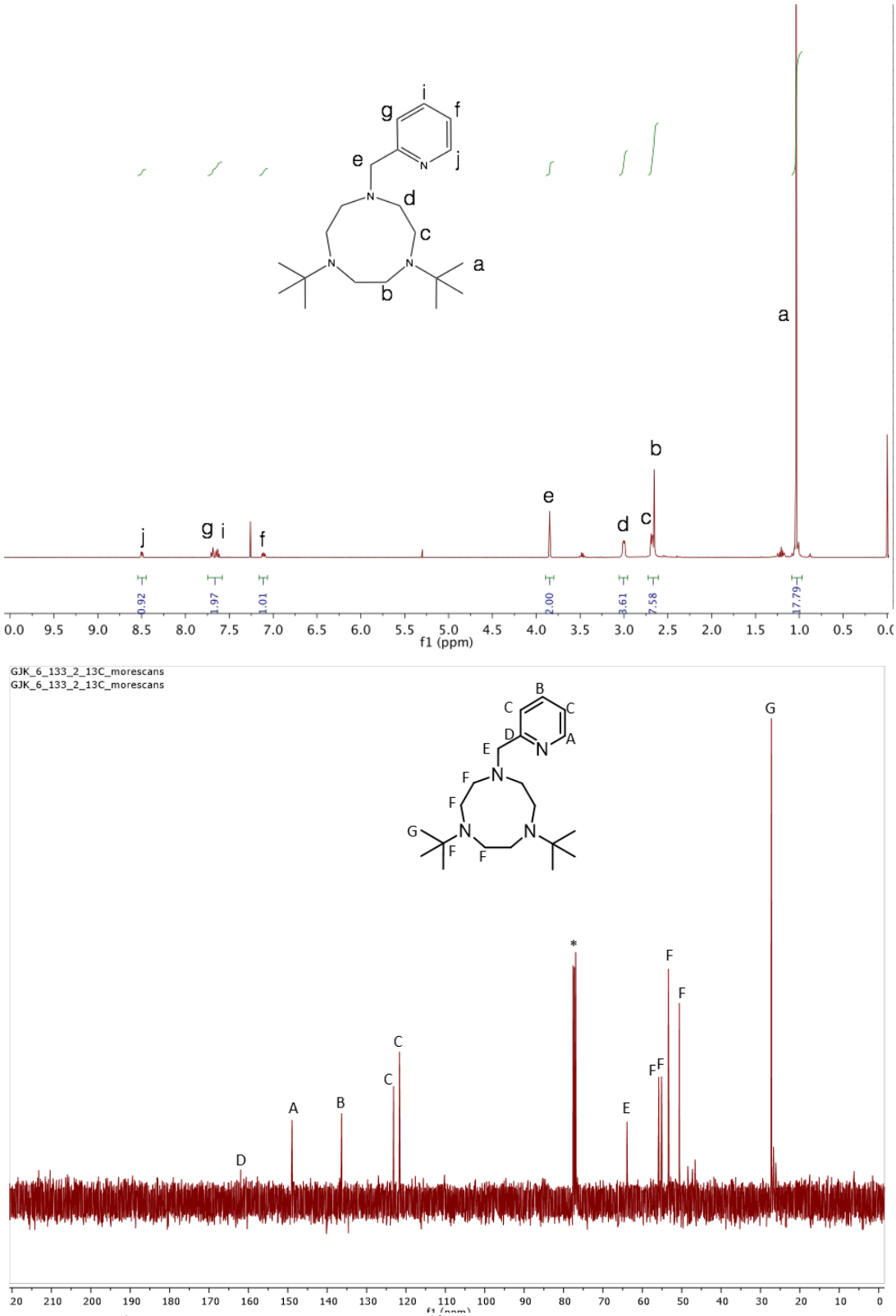

Figure S1-12. ^{1}H NMR spectrum (top) and ^{13}C NMR spectrum (bottom) of ***t*Bu$_2$pictacn** in $CDCl_3$.

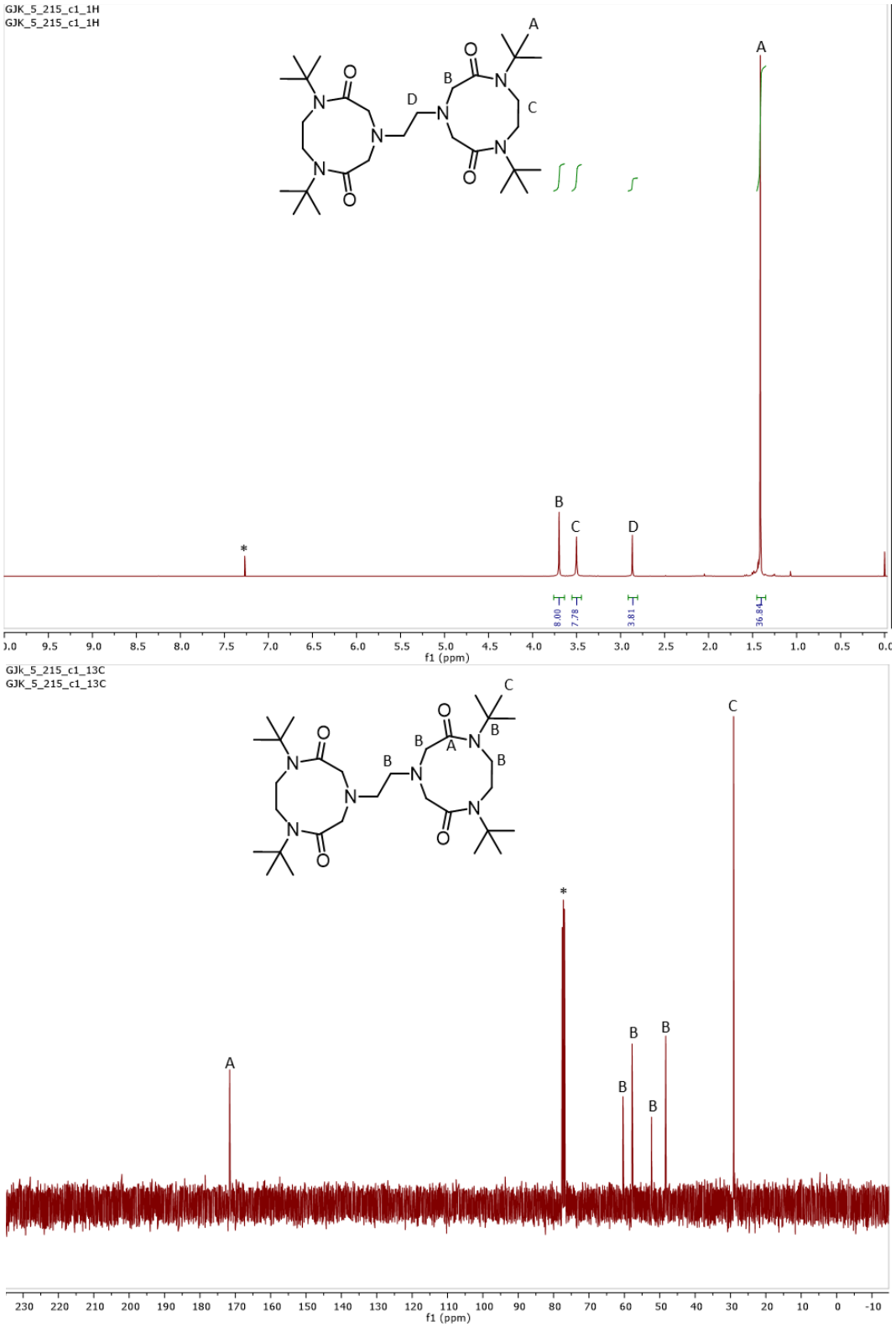

Figure S1-13. ^{1}H NMR spectrum (top) and ^{13}C NMR spectrum (bottom) of 4,4'-(ethane-1,2-diyl)bis(1,7-di-*tert*-butyl-1,4,7-triazonane-2,6-dione*)* (**1.05**) in $CDCl_3$.

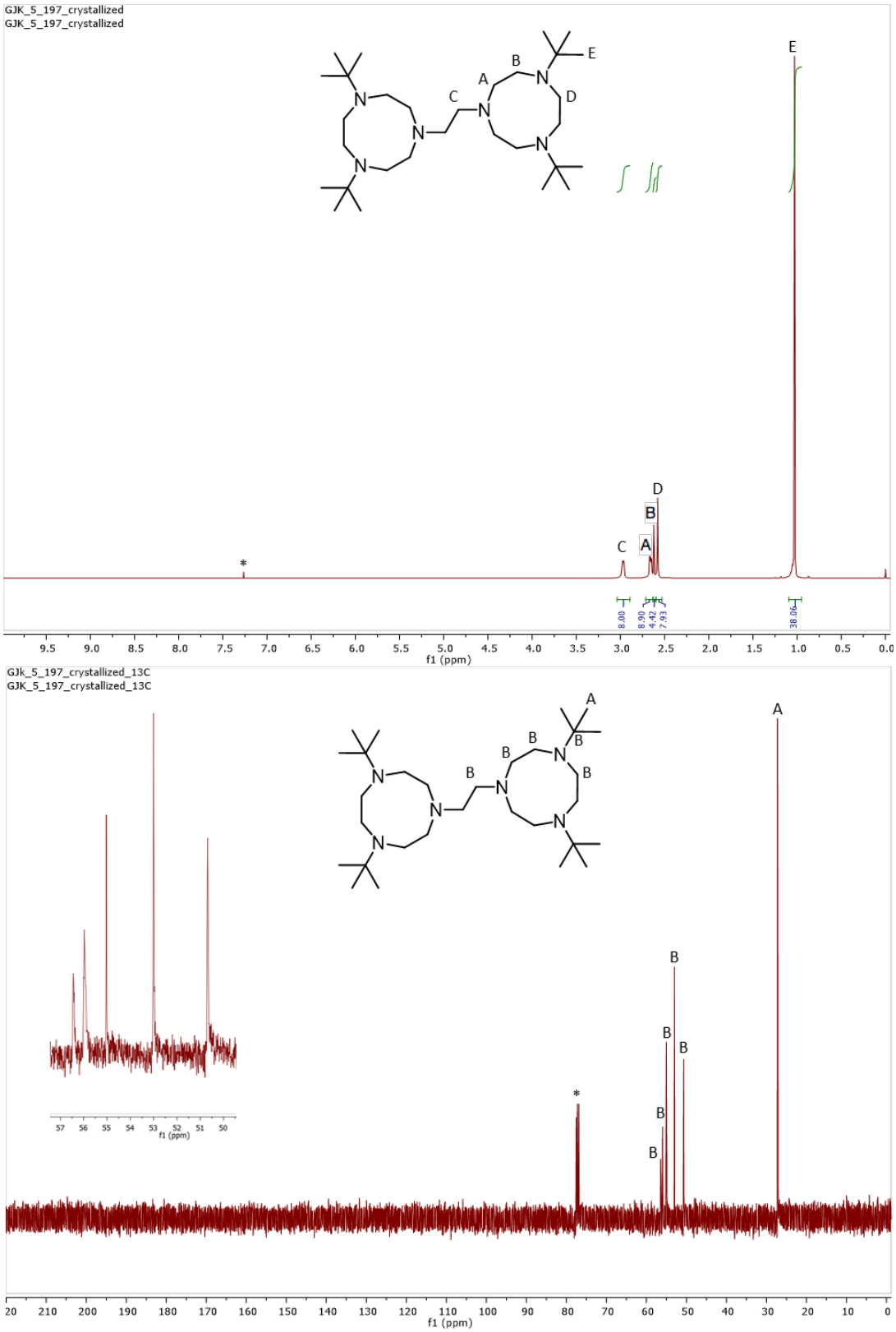

Figure S1-14. ^{1}H NMR spectrum (top) and ^{13}C NMR spectrum (bottom) of ***t*Bu$_4$dtne** in $CDCl_3$.

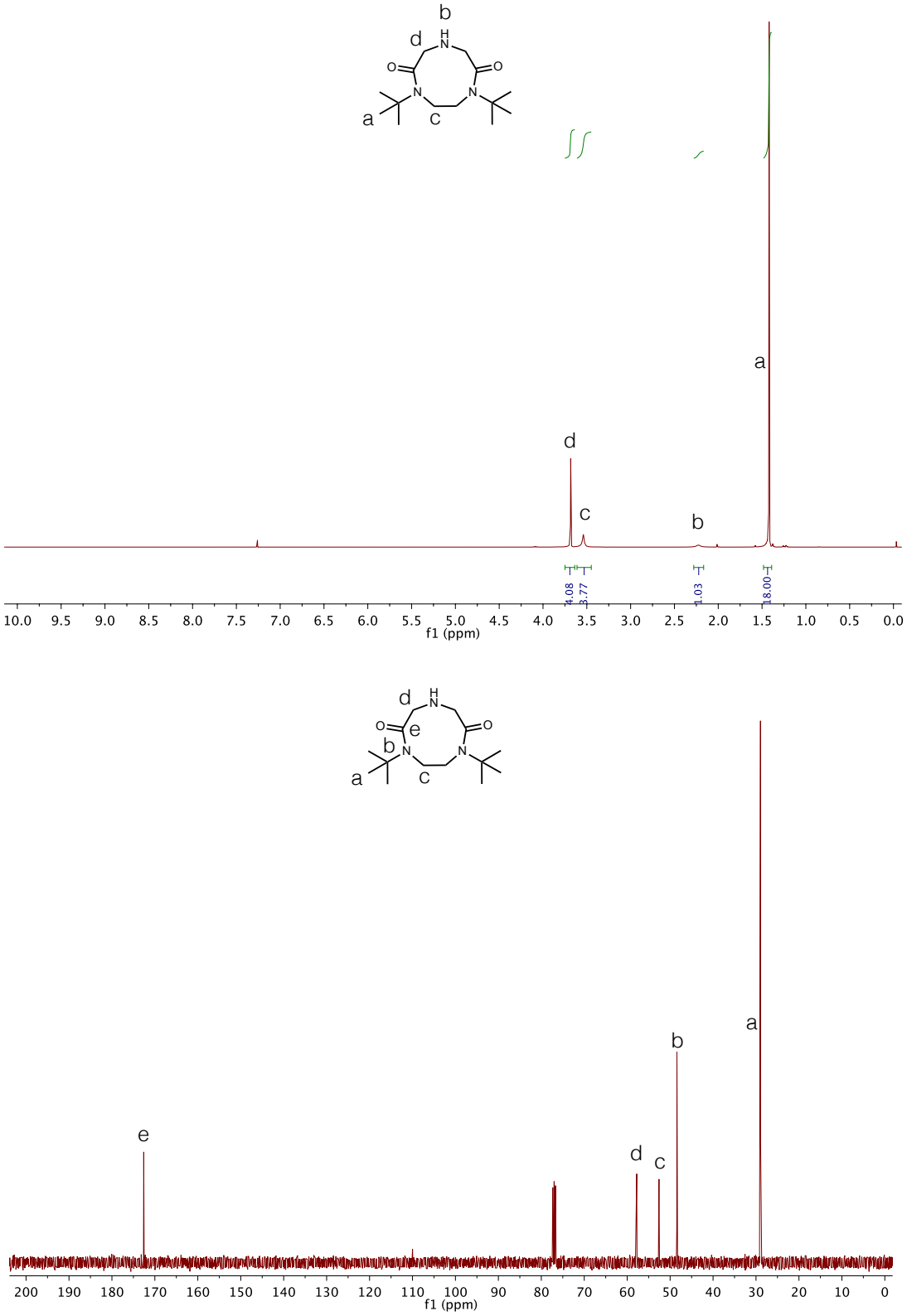

Figure S1-15. ^{1}H NMR spectrum (top) and ^{13}C NMR spectrum (bottom) of $\mathbf{3}^{t\mathbf{Bu,H}}$ in $CDCl_3$.

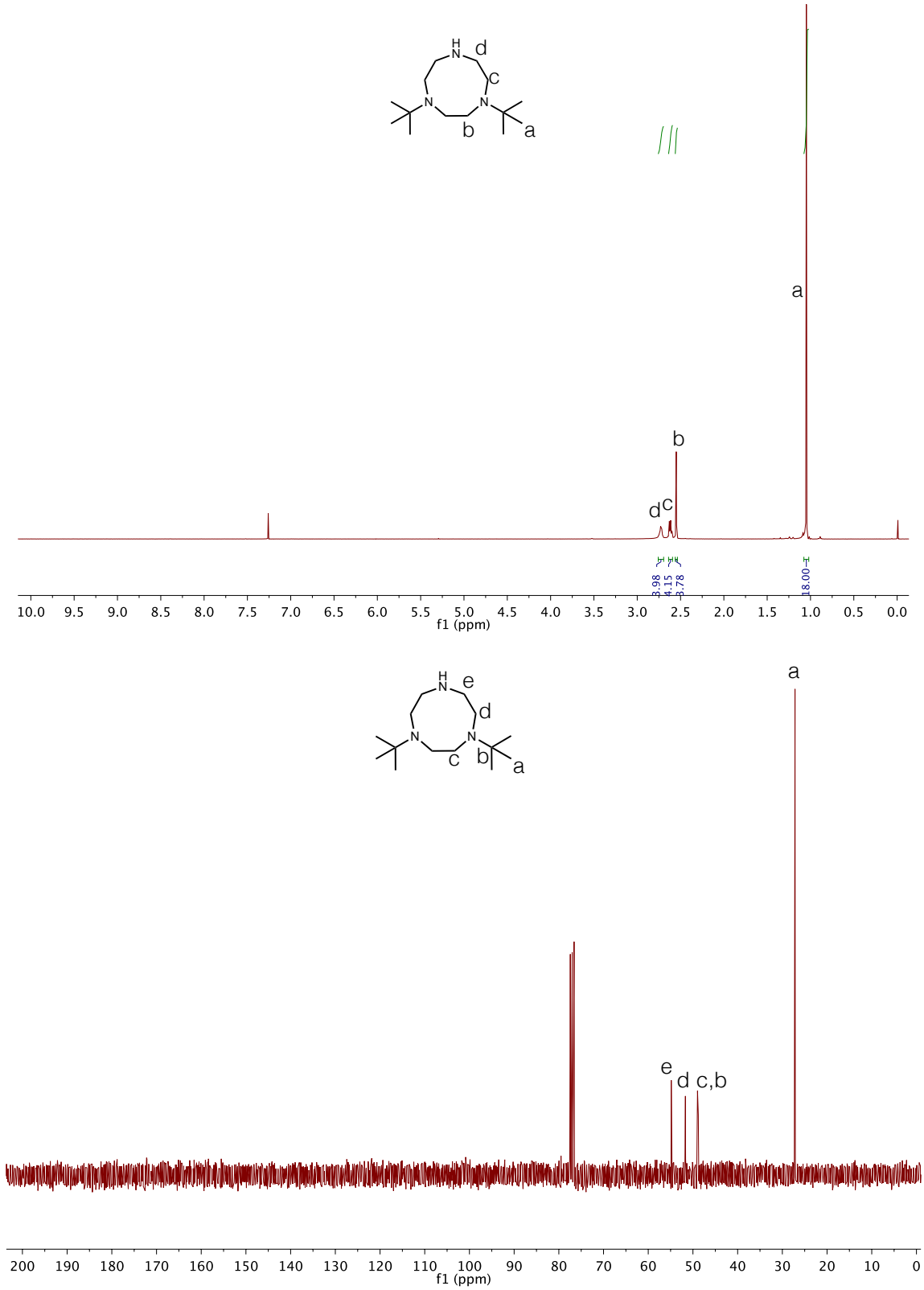

Figure S1-16. ^{1}H NMR spectrum (top) and ^{13}C NMR spectrum (bottom) of ***t*Bu$_2$Htacn** in $CDCl_3$.

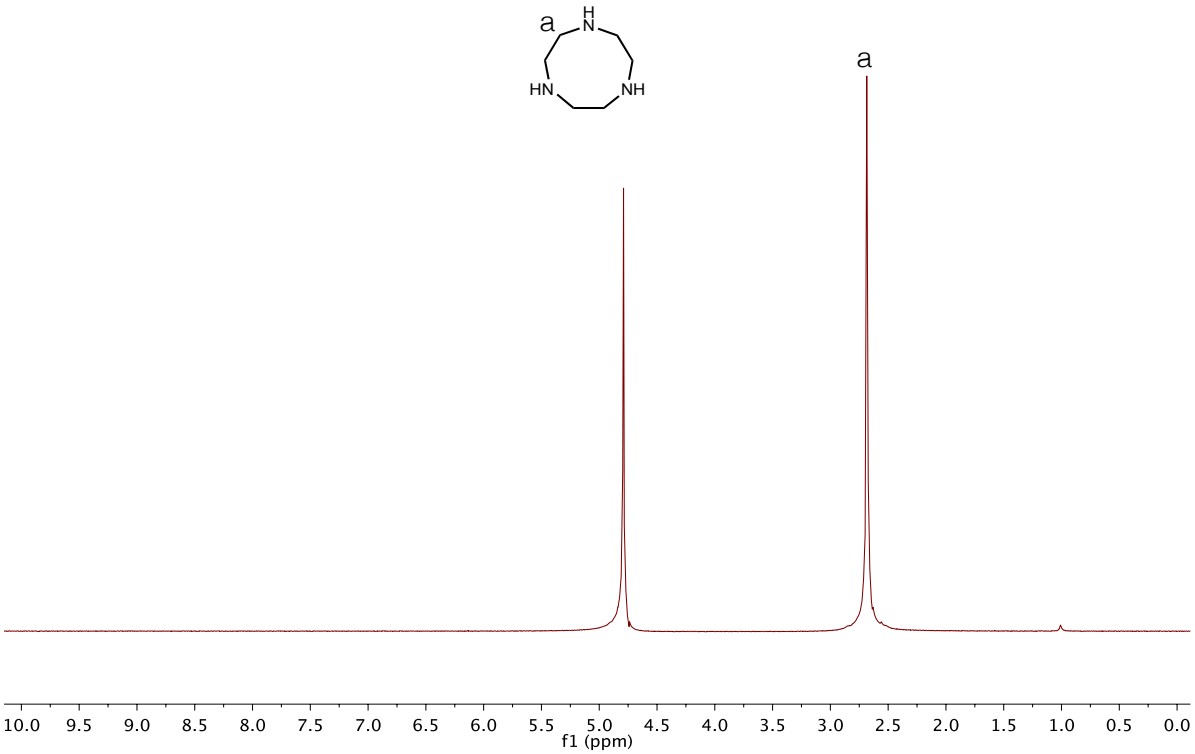

Figure S1-17. ^{1}H NMR spectrum of **[H_6tacn][Cl]$_3$** in NaOD.
^{1}H NMR data matches previously reported literature values.[19c]

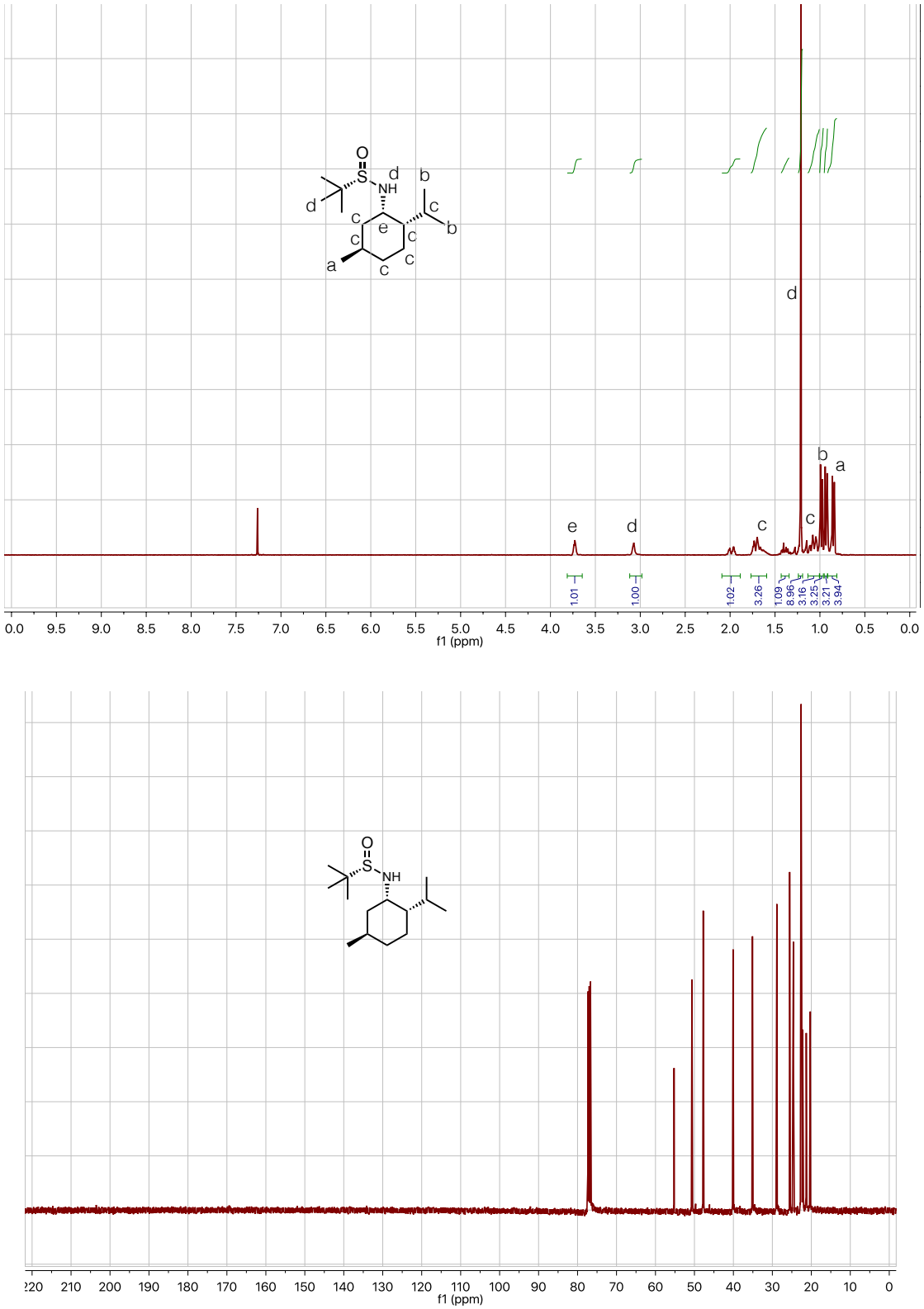

Figure S1-18. ^{1}H NMR spectrum (top) and ^{13}C NMR spectrum (bottom) of (S)-N-((1S,2S,5R)-2-isopropyl-5-methylcyclohexyl)-2-methylpropane-2-sulfinamide in $CDCl_3$.

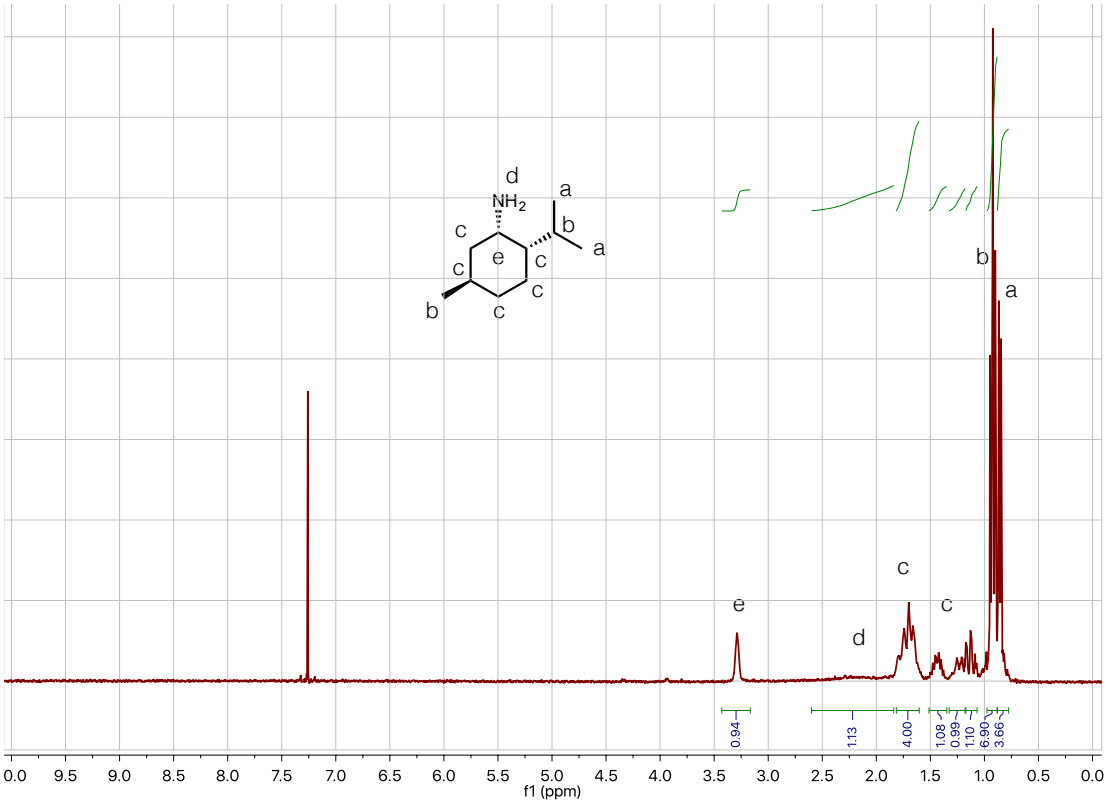

Figure S1-19. ^{1}H NMR spectrum of (1S,2S,5R)-2-isopropyl-5-methylcyclohexan-1-amine in $CDCl_3$. ^{1}H NMR data matches previously reported literature values.[28]

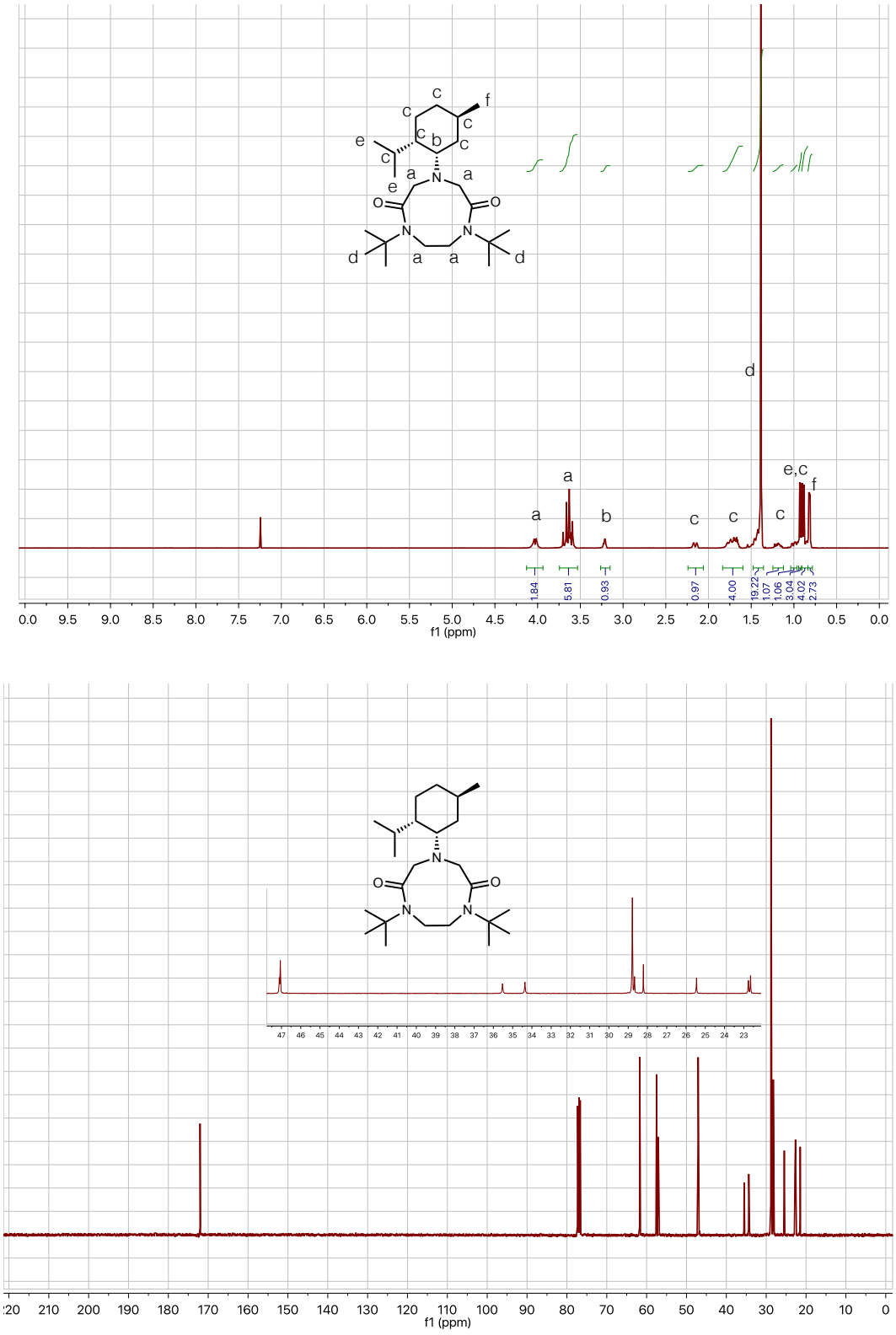

Figure S1-20. ^{1}H NMR spectrum (top) and ^{13}C NMR spectrum (bottom) of $\mathbf{3}^{t\mathbf{Bu,menthyl}}$ in $CDCl_3$.

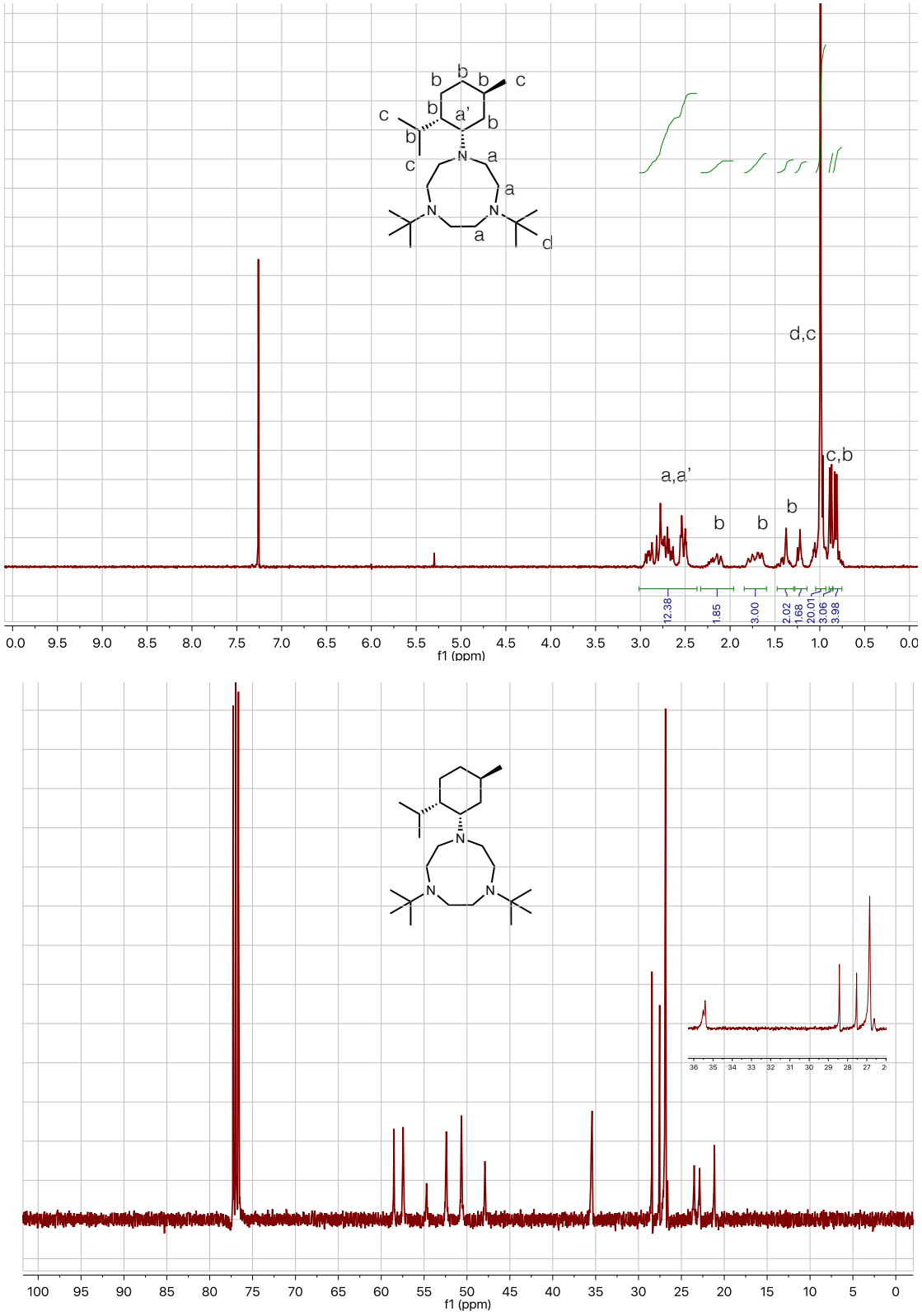

Figure S1-21. ^{1}H NMR spectrum (top) and ^{13}C NMR spectrum (bottom) of ***t*Bu$_2$menthyltacn** in $CDCl_3$.

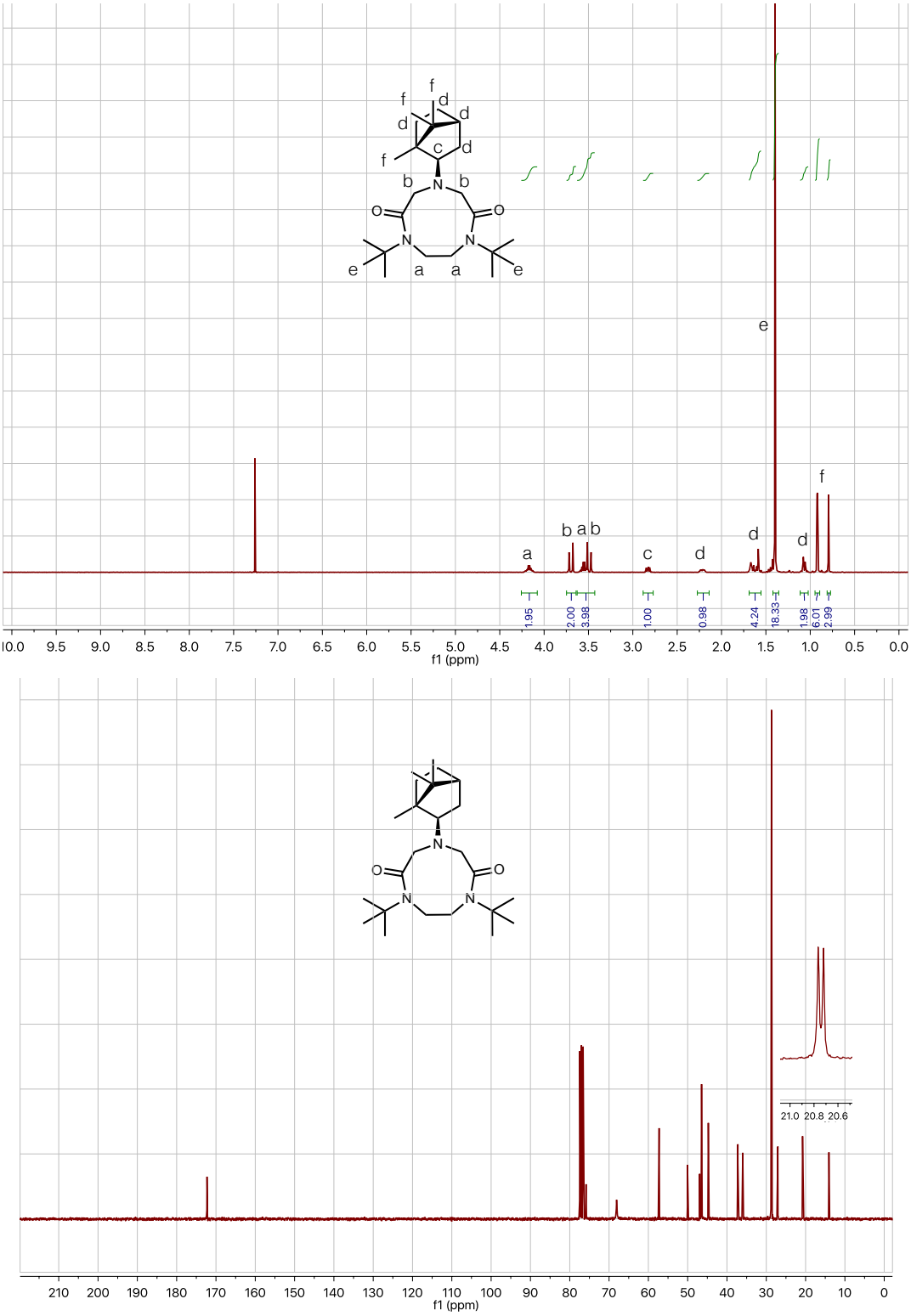

Figure S1-22. ^{1}H NMR spectrum (top) and ^{13}C NMR spectrum (bottom) of **3**$^{t\mathbf{Bu},exo\text{-}\mathbf{bornyl}}$ in $CDCl_3$.

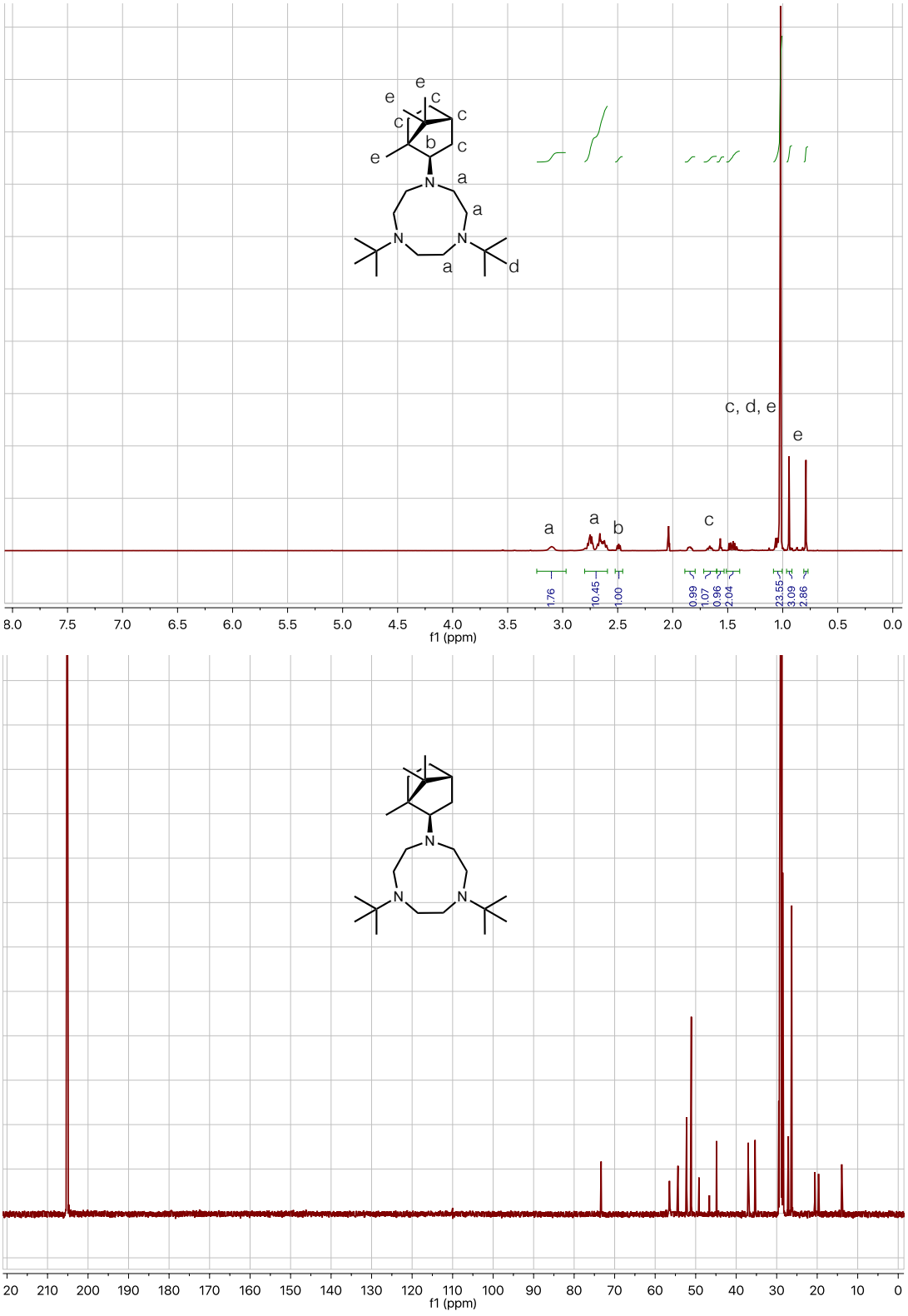

Figure S1-23. ^{1}H NMR spectrum (top) and ^{13}C NMR spectrum (bottom) of ***t*Bu$_2$*exo*-bornyltacn** in acetone-d$_6$.

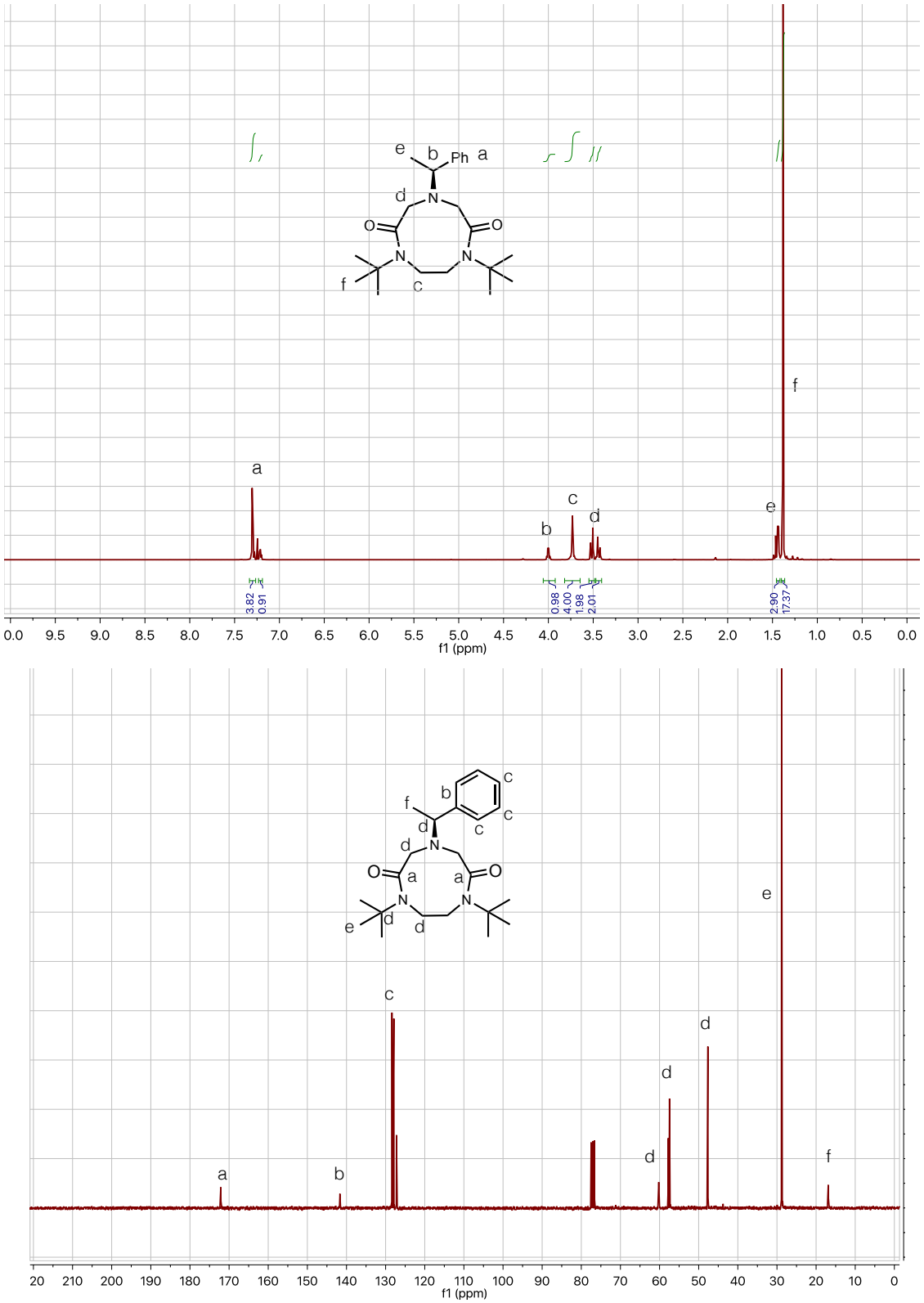

Figure S1-24. ^{1}H NMR spectrum (top) and ^{13}C NMR spectrum (bottom) of **3**$^{t\mathbf{Bu},sec\text{-}\mathbf{PhEt}}$ in $CDCl_3$.

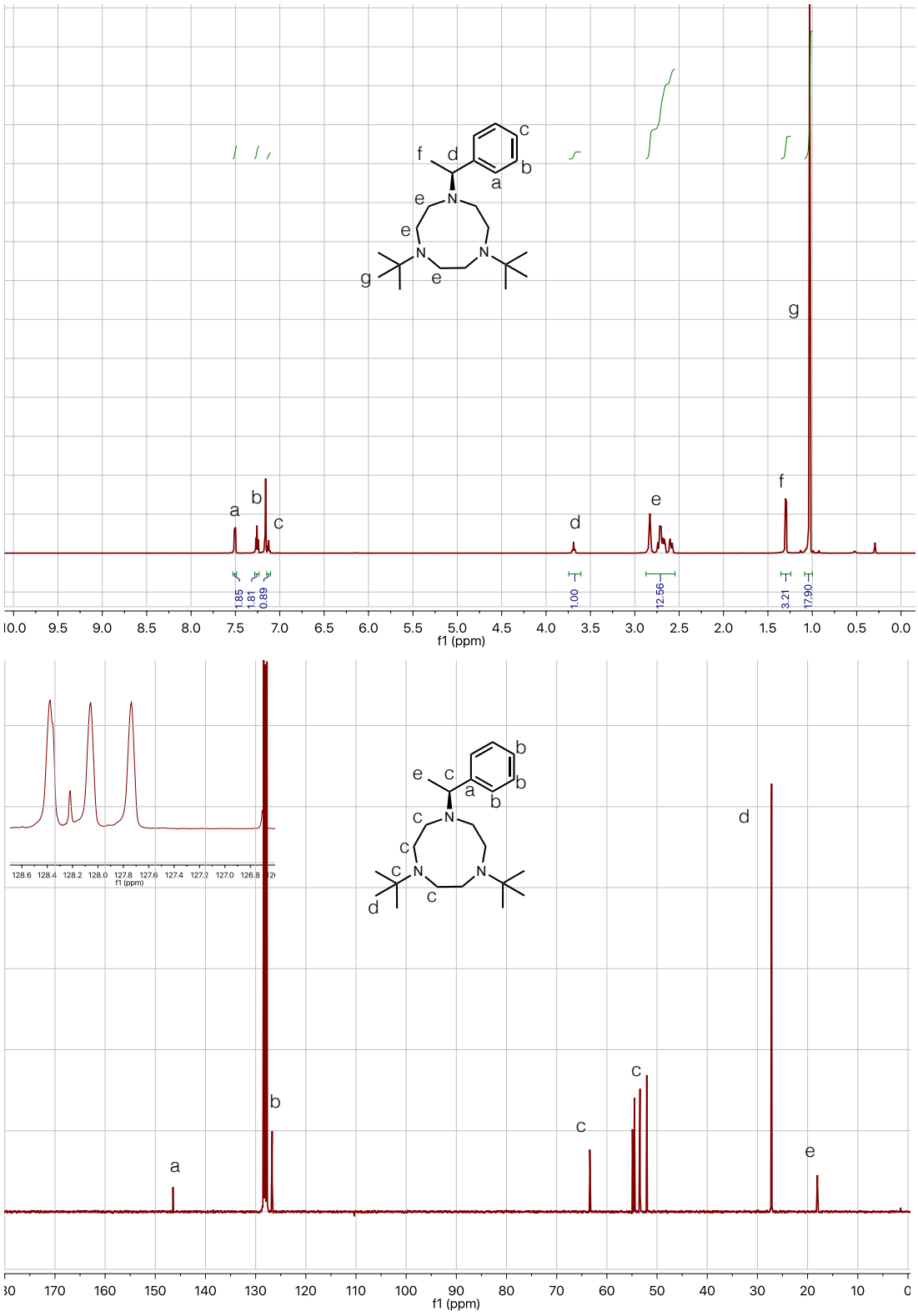

Figure S1-25. ^{1}H NMR spectrum (top) and ^{13}C NMR spectrum (bottom) of ***t*Bu$_2$*sec*-PhEttacn** in Benzene-d_6.

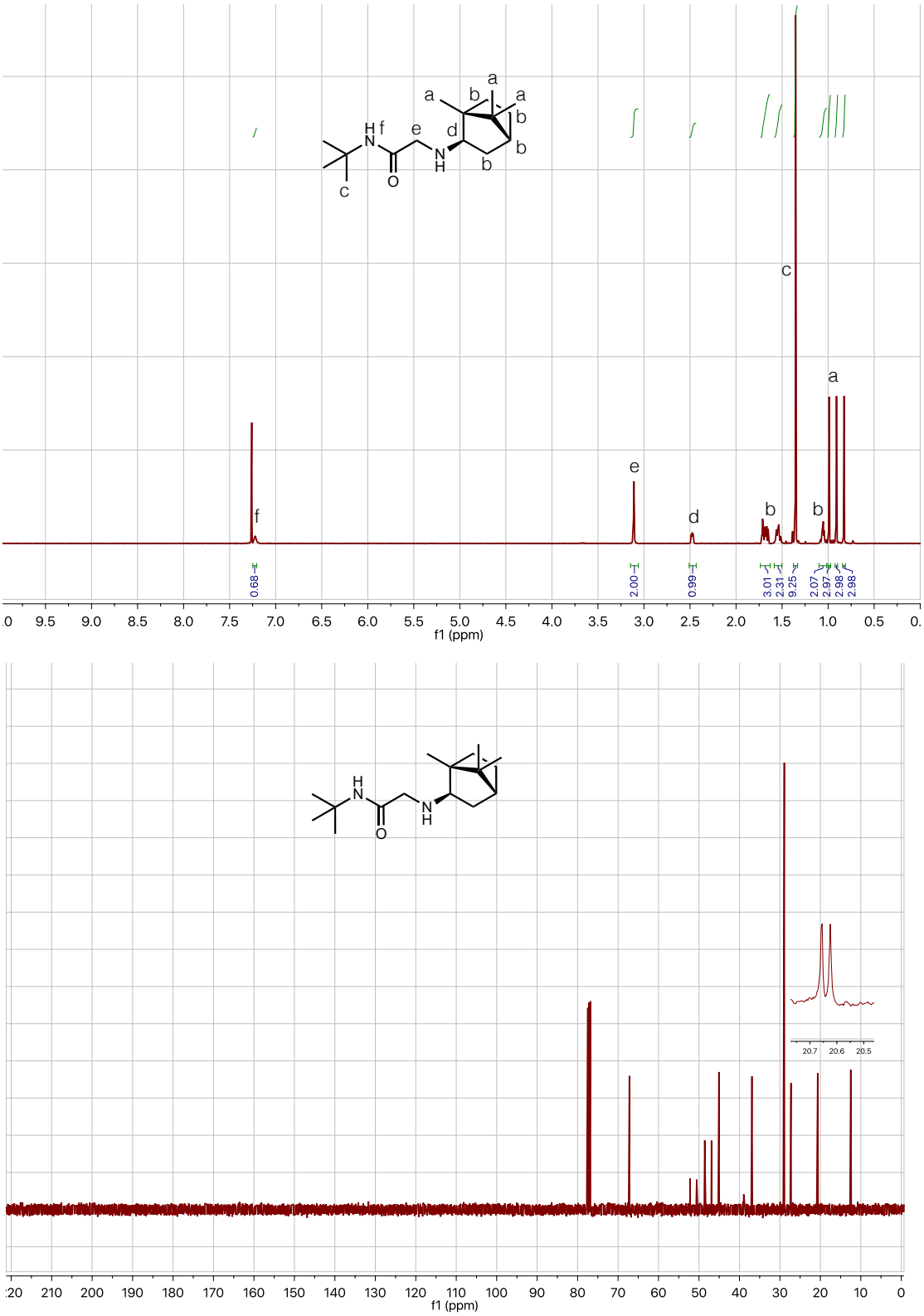

Figure S1-26. ^{1}H NMR spectrum (top) and ^{13}C NMR spectrum (bottom) of 2-(*tert*-butylamino)-N-((1R,2R,4R)-1,7,7-trimethylbicyclo[2.2.1]heptan-2-yl)acetamide (**1.04**) in $CDCl_3$.

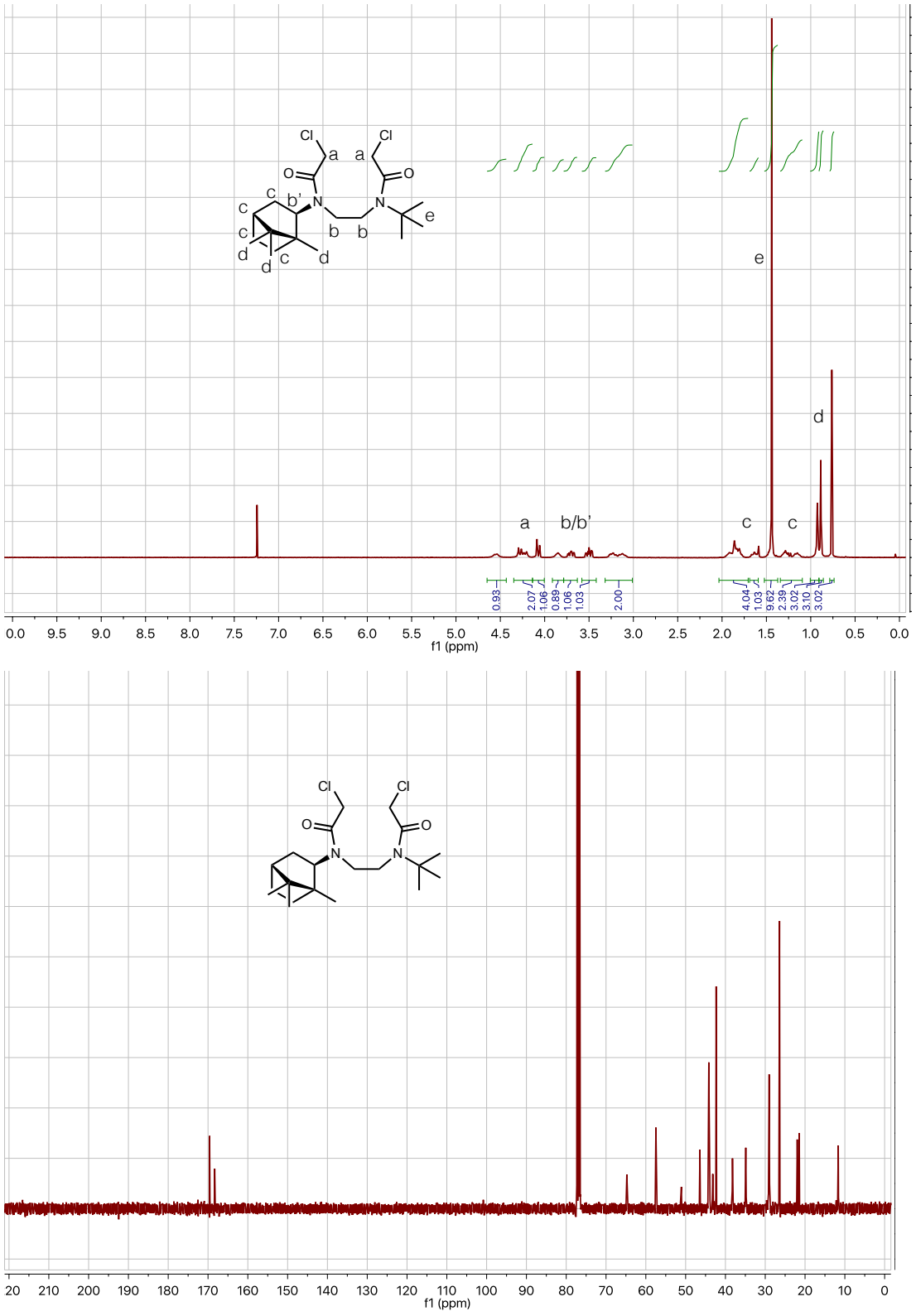

Figure S1-27. ^{1}H NMR spectrum (top) and ^{13}C NMR spectrum (bottom) of **2**$^{t\mathbf{Bu},exo\text{-}\mathbf{bornyl}}$ in $CDCl_3$.

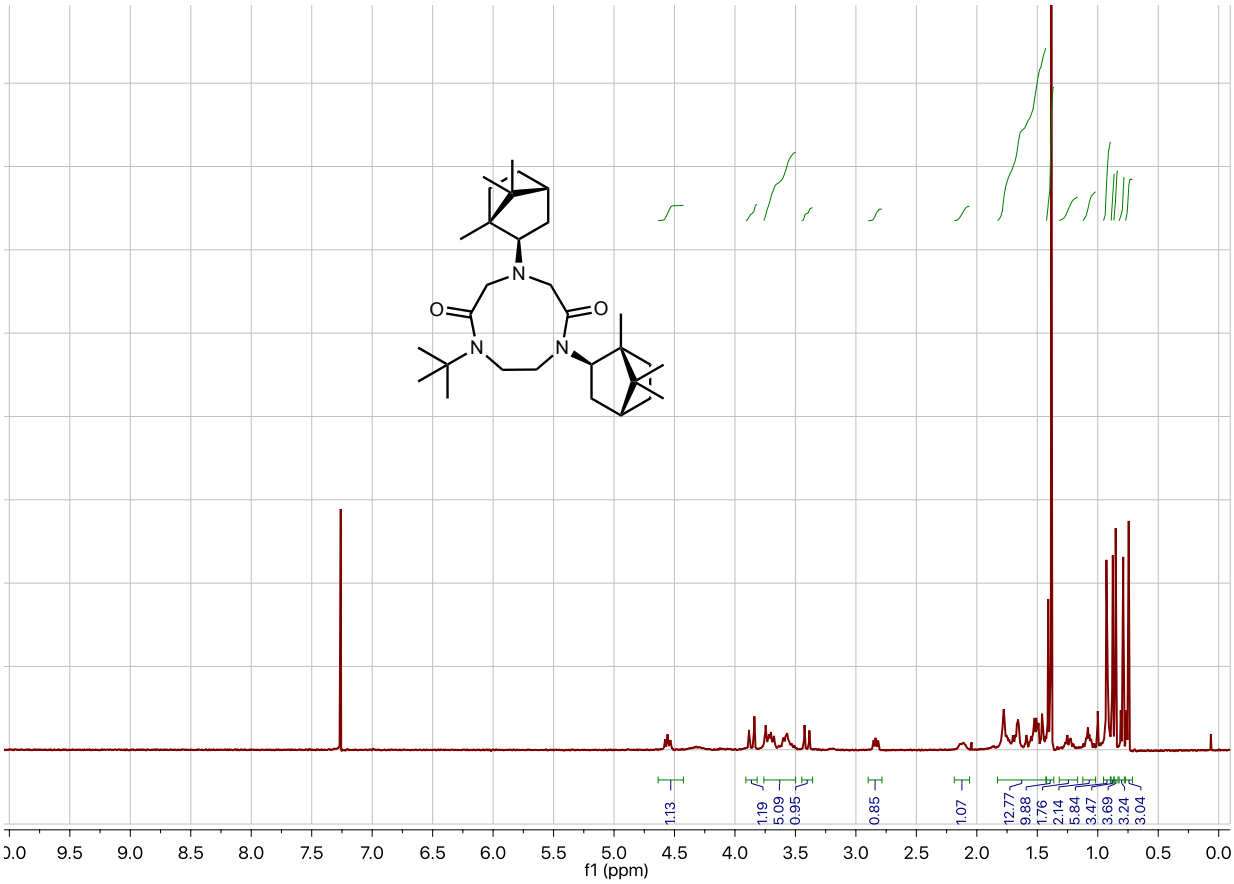

Figure S1-28. ^{1}H NMR spectrum of **3**$^{exo\text{-}bornyl,tBu}$ in $CDCl_3$.

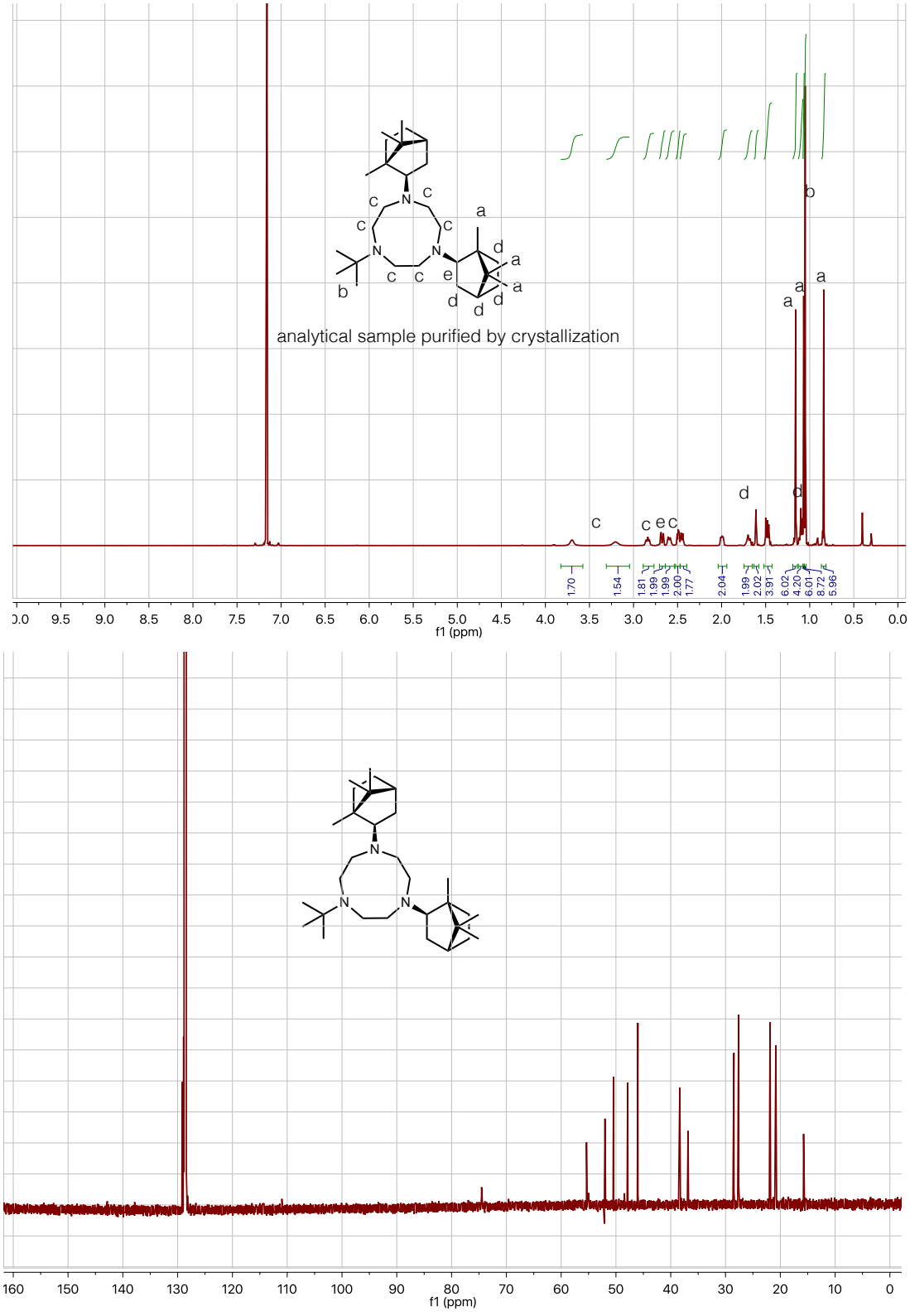

Figure S1-29. ^{1}H NMR spectrum (top, analytical sample purified by crystallization) and ^{13}C NMR spectrum (bottom, purified by chromatography) of ***exo*-bornyl$_2$*tButacn*** in Benzene-d_6.

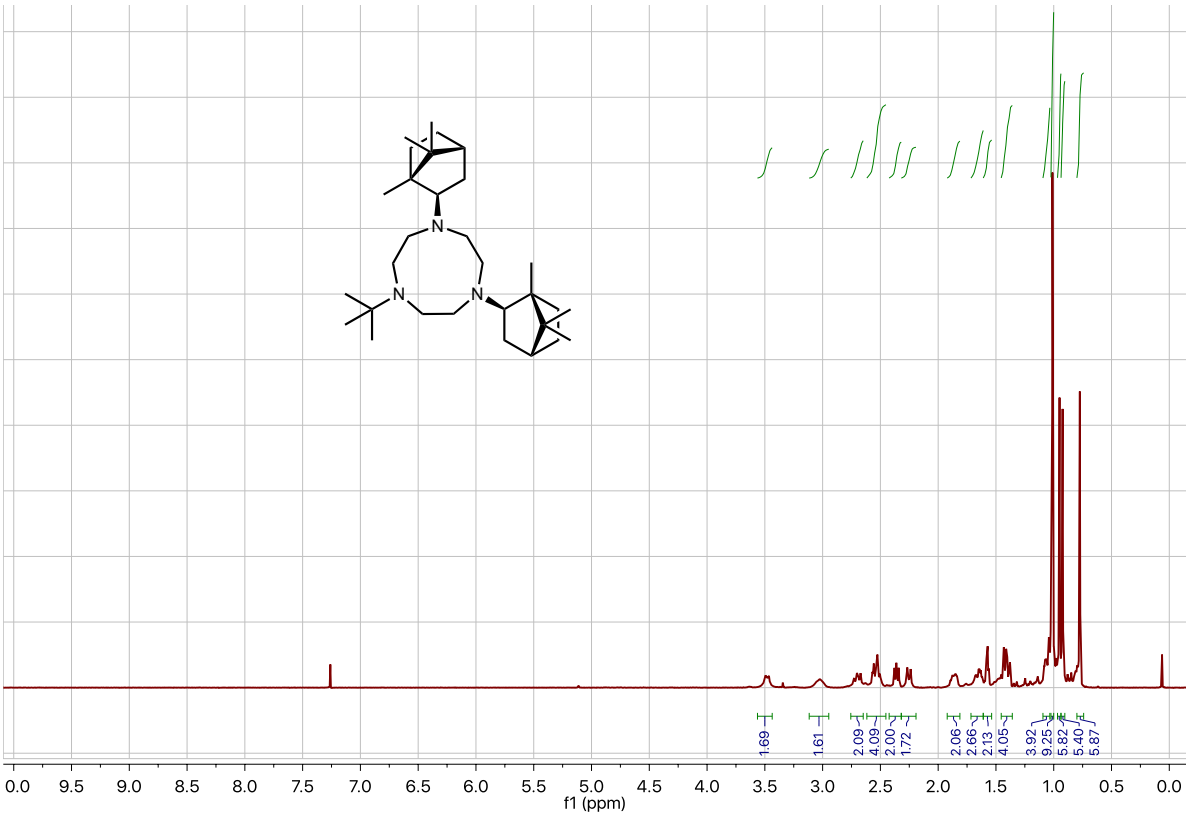

Figure S1-30. ^{1}H NMR spectrum of ***exo*-bornyl$_2$*tButacn*** (purified by chromatography) in $CDCl_3$.

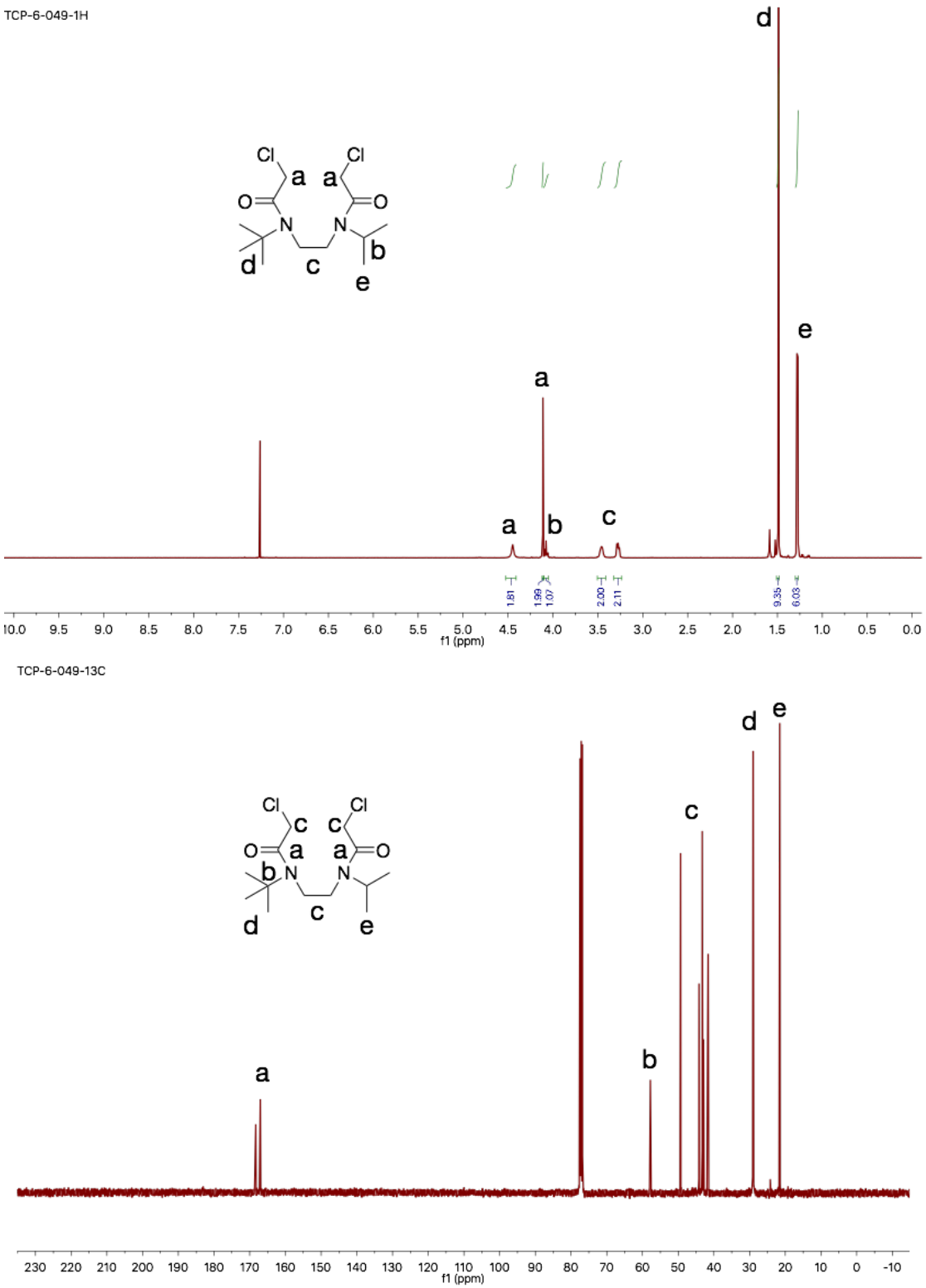

Figure S1-31. ^{1}H NMR spectrum (top) and ^{13}C NMR spectrum (bottom) of **2**$^{t\mathbf{Bu},i\mathbf{Pr}}$ in $CDCl_3$.

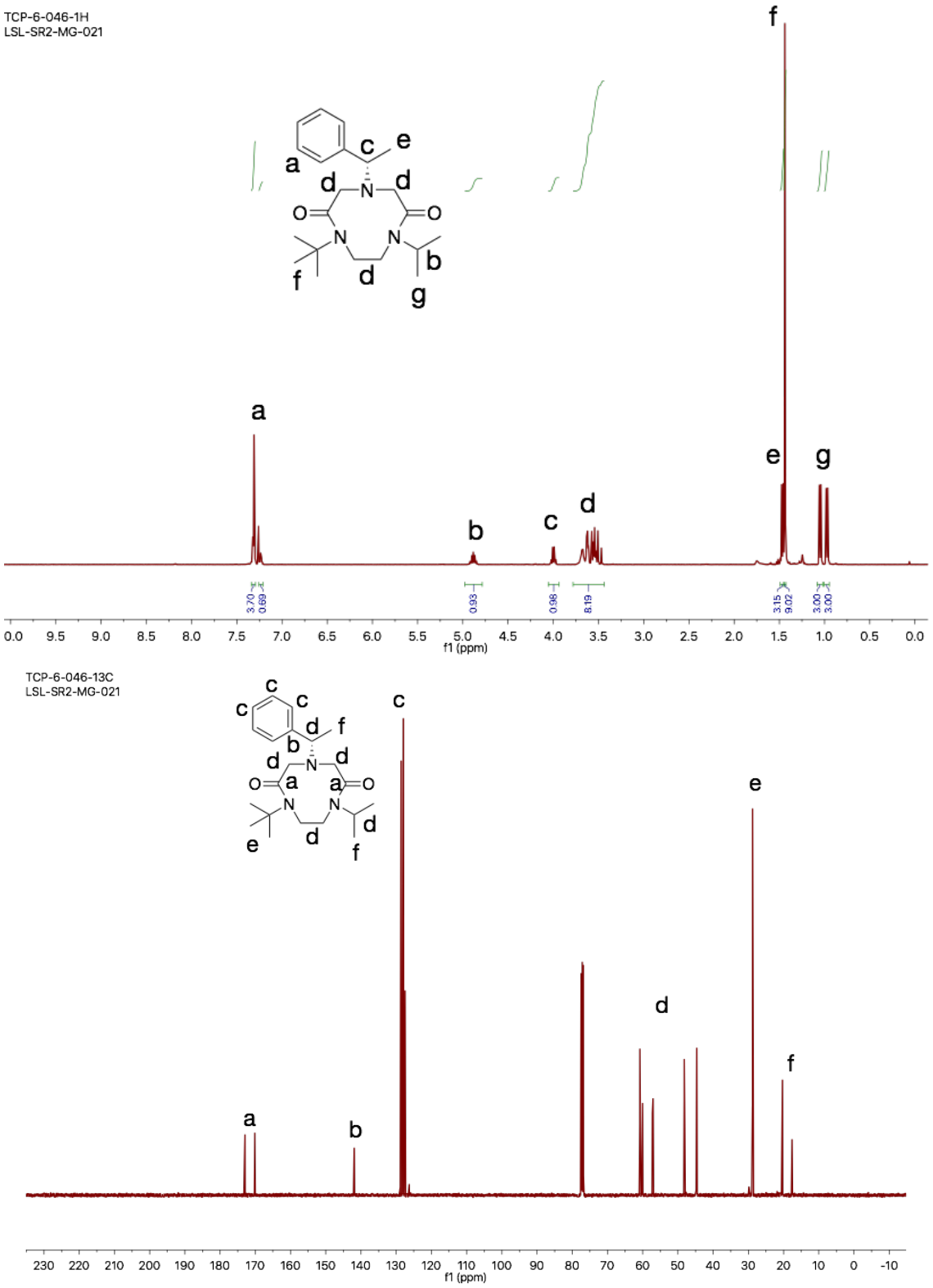

Figure S1-32. ^{1}H NMR spectrum (top) and ^{13}C NMR spectrum (bottom) of **3**$^{t\mathbf{Bu},i\mathbf{Pr},sec\text{-}\mathbf{PhEt}}$ in $CDCl_3$.

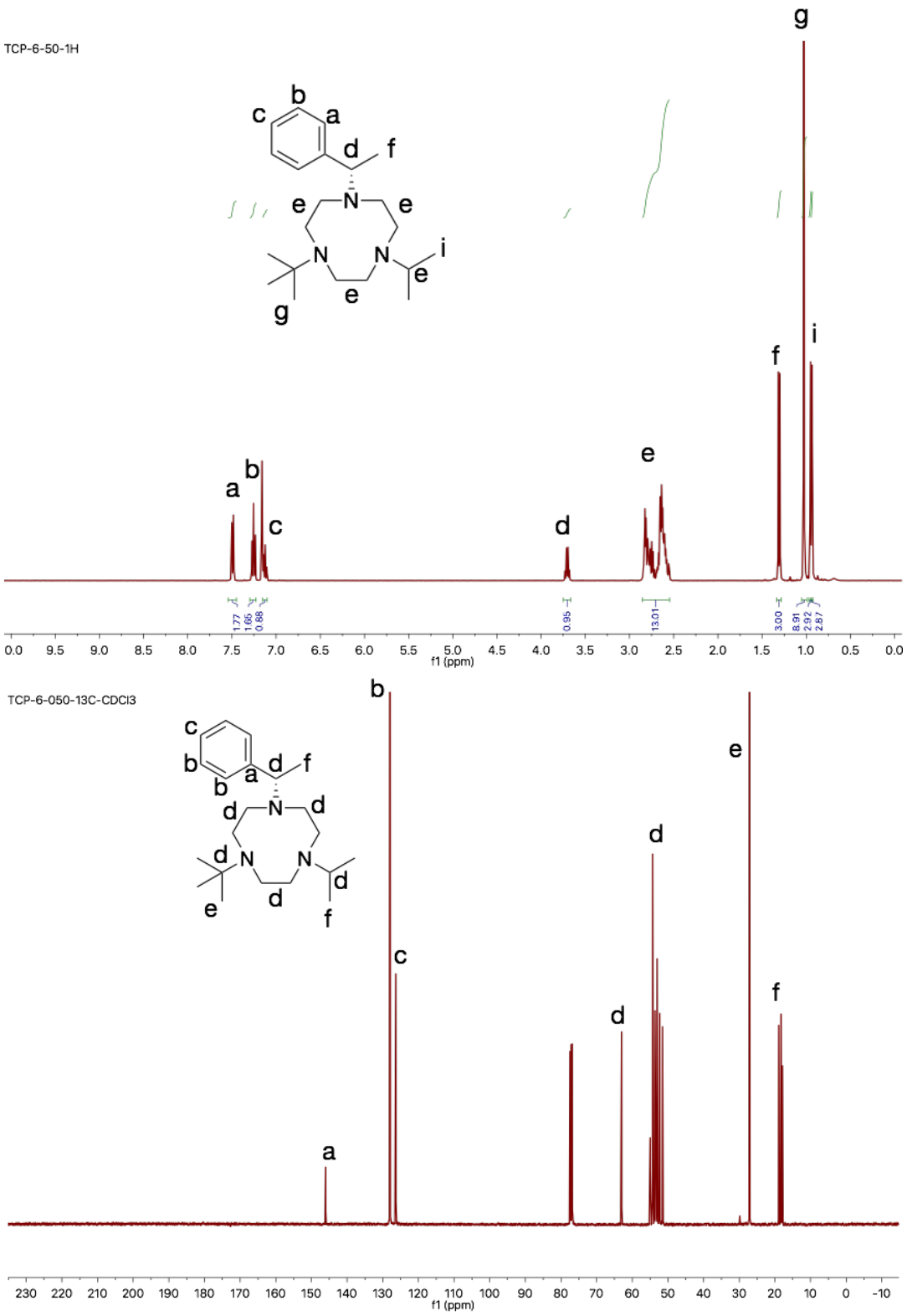

Figure S1-33. ^{1}H NMR spectrum (top) and ^{13}C NMR spectrum (bottom) of ***sec*-PhEt*t*Bu*i*Prtacn** in $CDCl_3$.

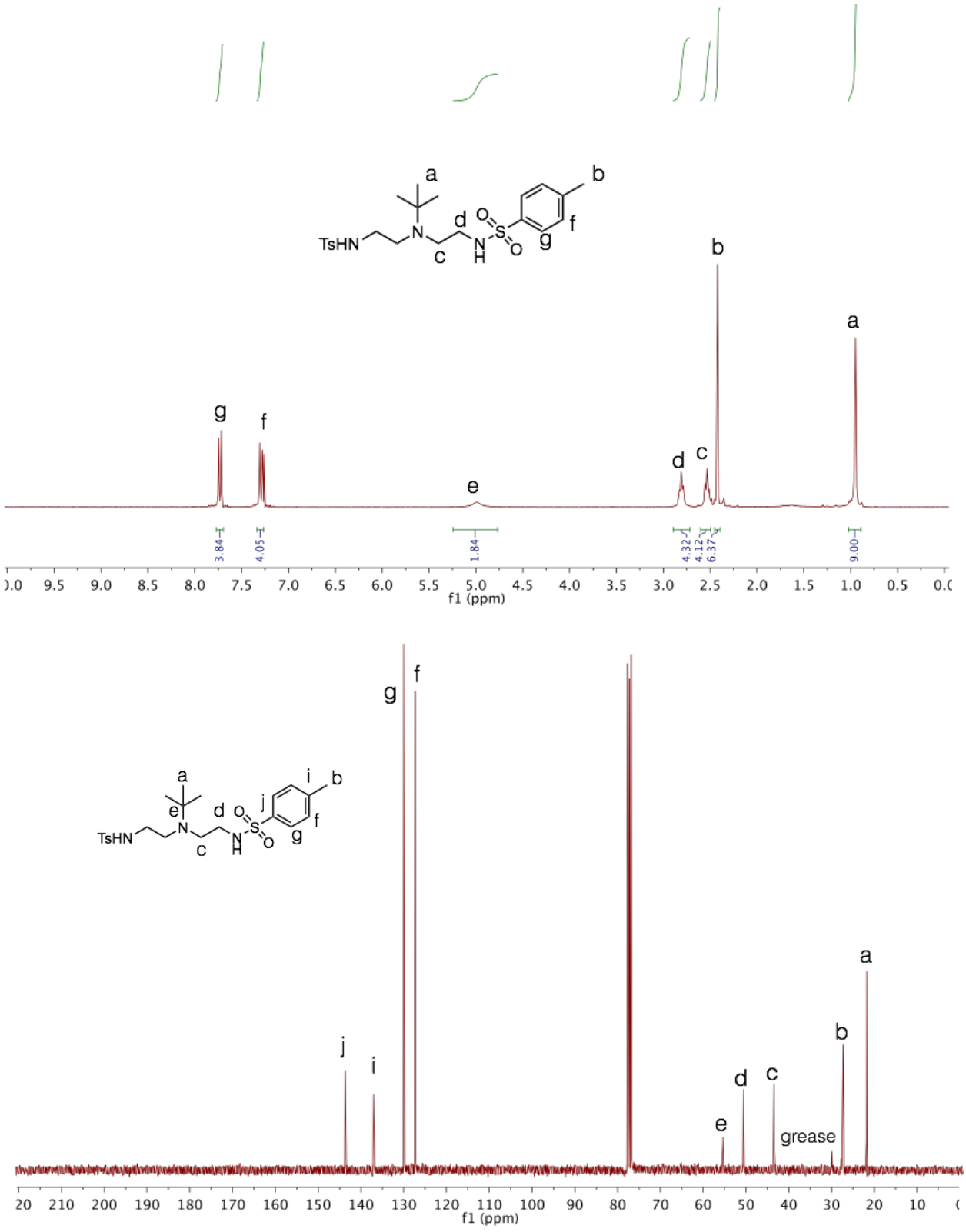

Figure S1-34. ^{1}H NMR spectrum (top) and ^{13}C NMR spectrum (bottom) of N,N''-*di*-tosyl-N'-*tert*-butyldiethylenetriamine (**1.06**) in $CDCl_3$.

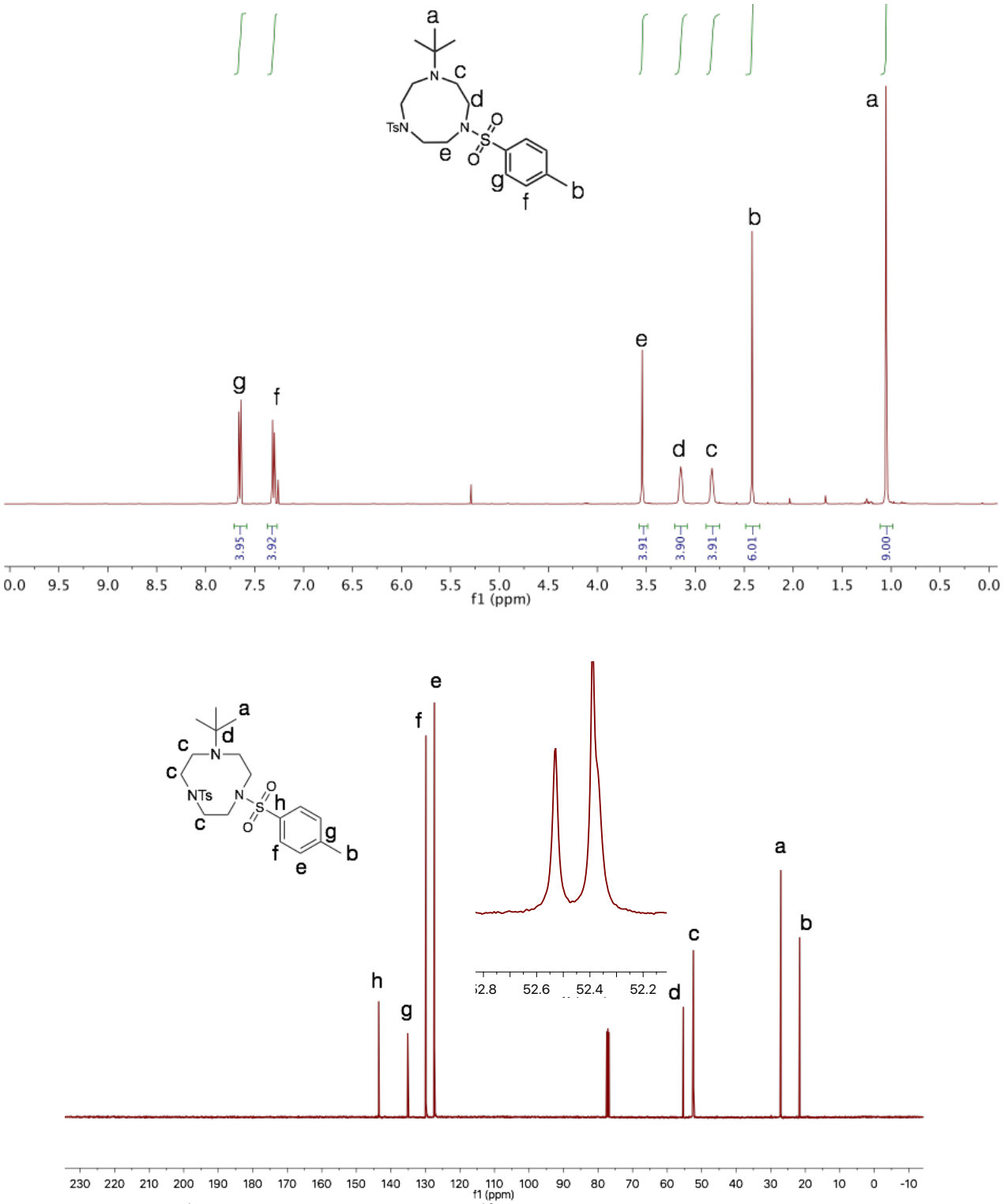

Figure S1-35. ^{1}H NMR spectrum (top) and ^{13}C NMR spectrum (bottom) of **Ts_2*t*Butacn** in $CDCl_3$.

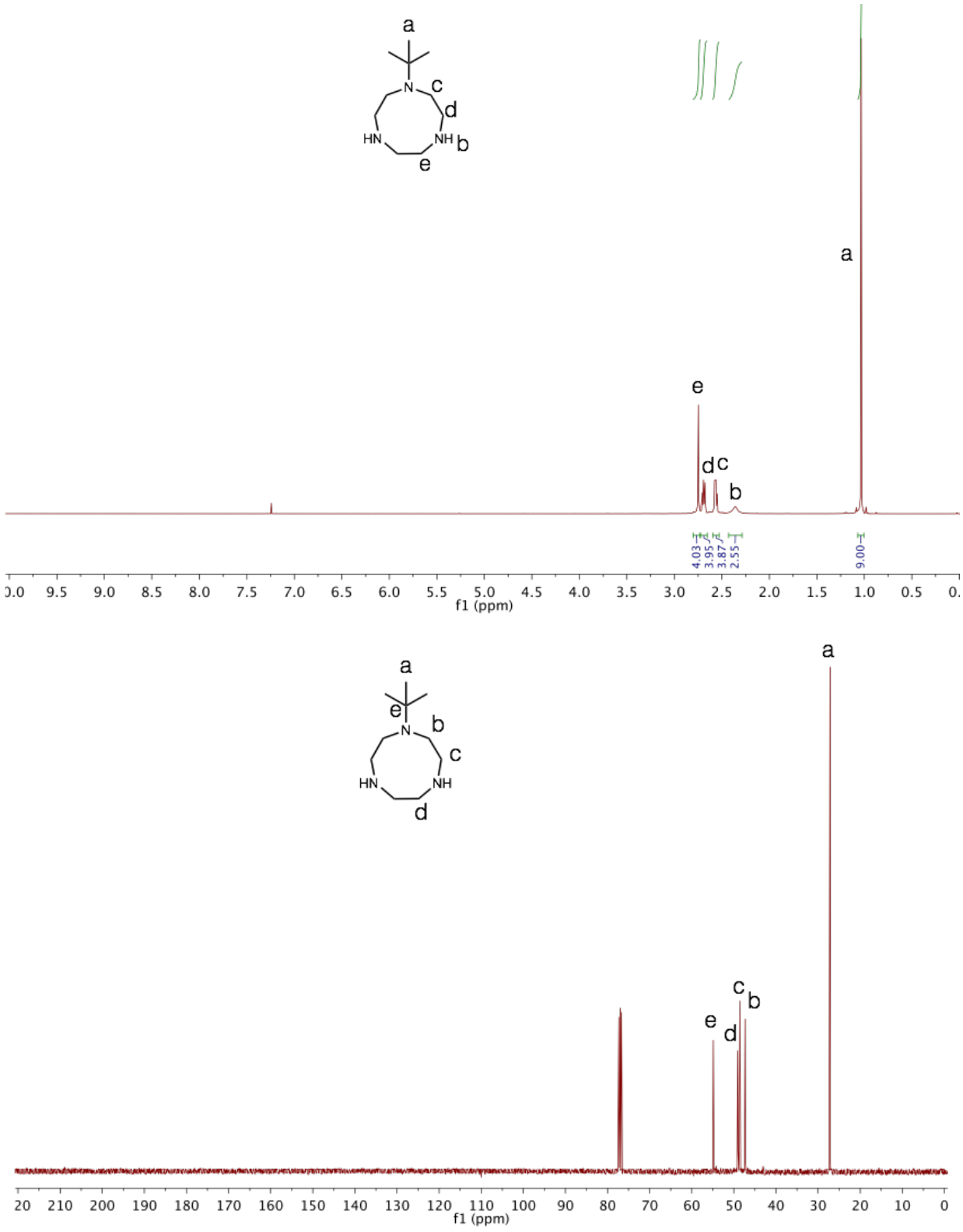

Figure S1-36. ^{1}H NMR spectrum (top) and ^{13}C NMR spectrum (bottom) of ***t*BuH$_2$tacn** in $CDCl_3$.

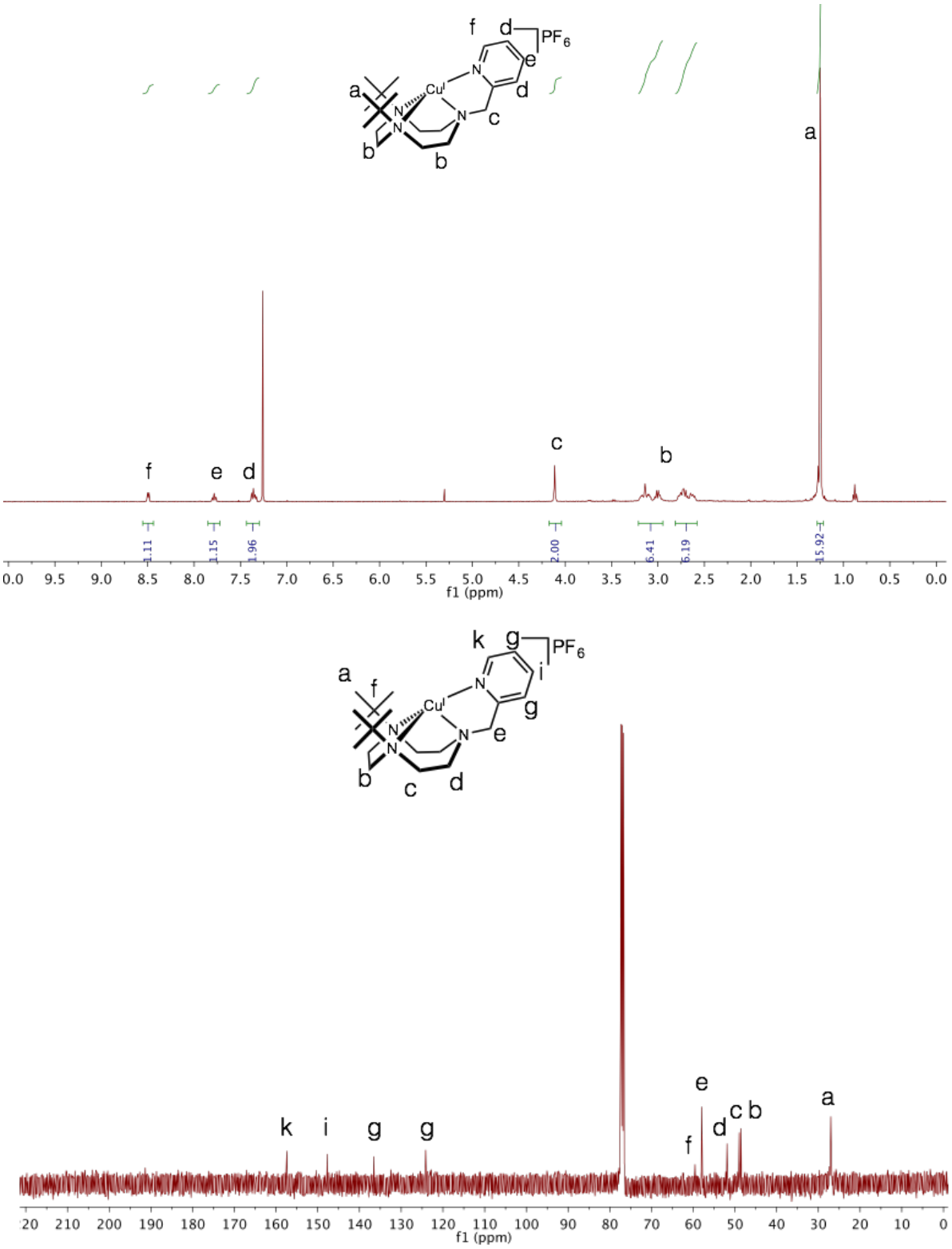

Figure S1-37. ^{1}H NMR spectrum (top) and ^{13}C NMR spectrum (bottom) of **[Cu(*t*Bu$_2$pictacn)]PF$_6$** in $CDCl_3$.

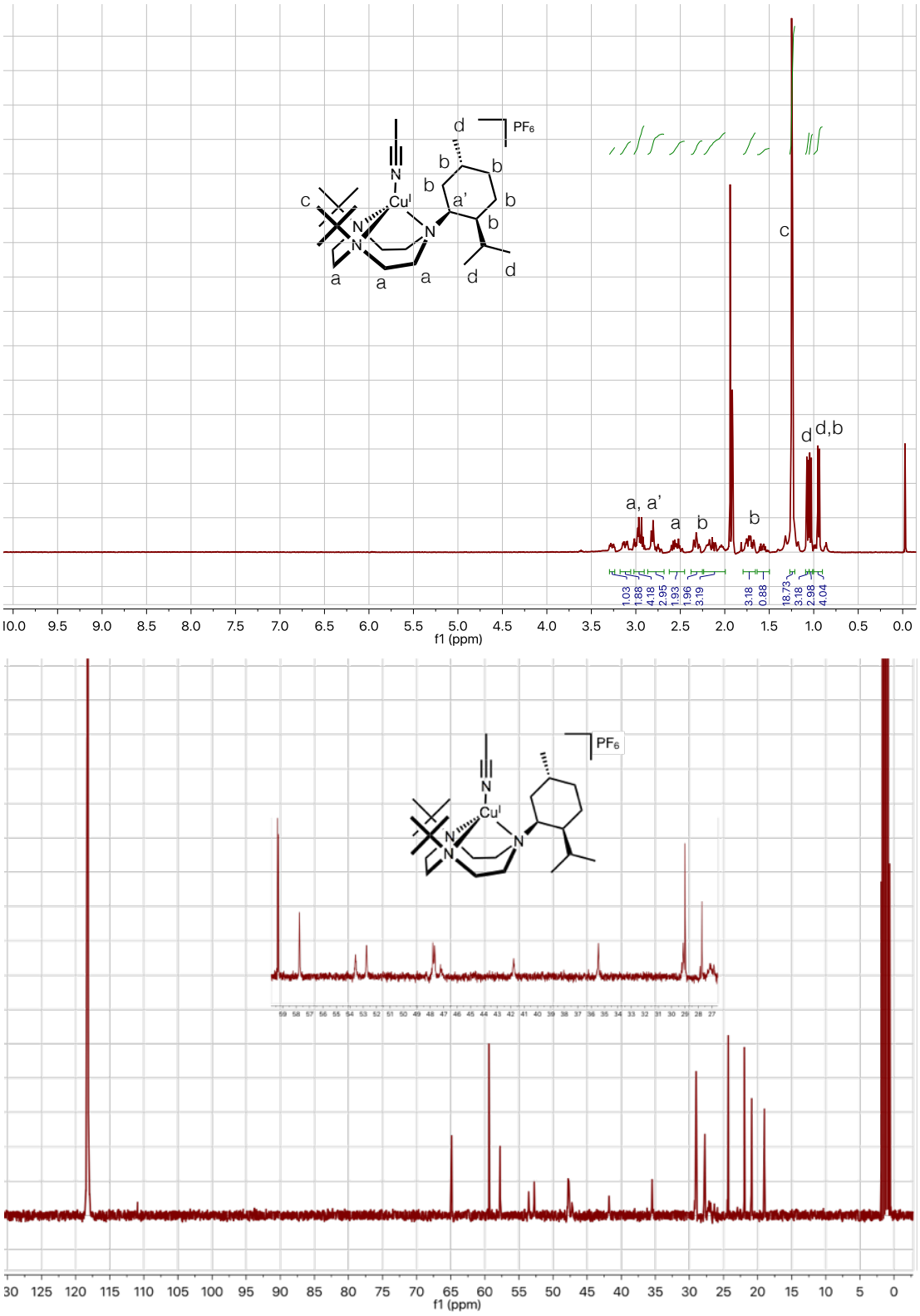

Figure S1-38. ^{1}H NMR spectrum (top) and ^{13}C NMR spectrum (bottom) of **[Cu(*t*Bu$_2$menthyltacn)(MeCN)]PF$_6$** in Acetonitrile-d_3.

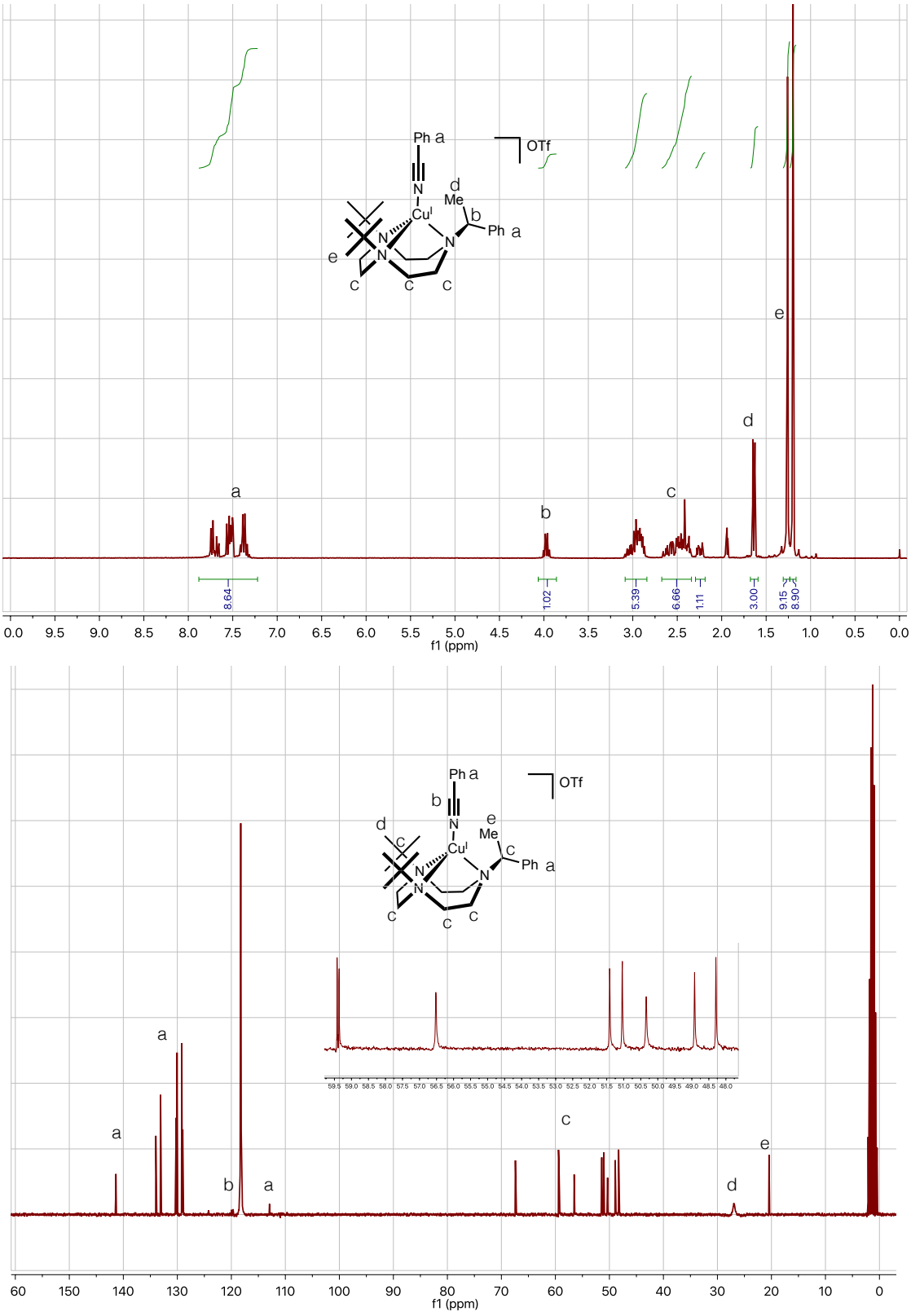

Figure S1-39. ^{1}H NMR spectrum (top) and ^{13}C NMR spectrum (bottom) of **[Cu(*t*Bu$_2$*sec*-PhEttacn)(NCPh)]OTf** in Acetonitrile-d_3.

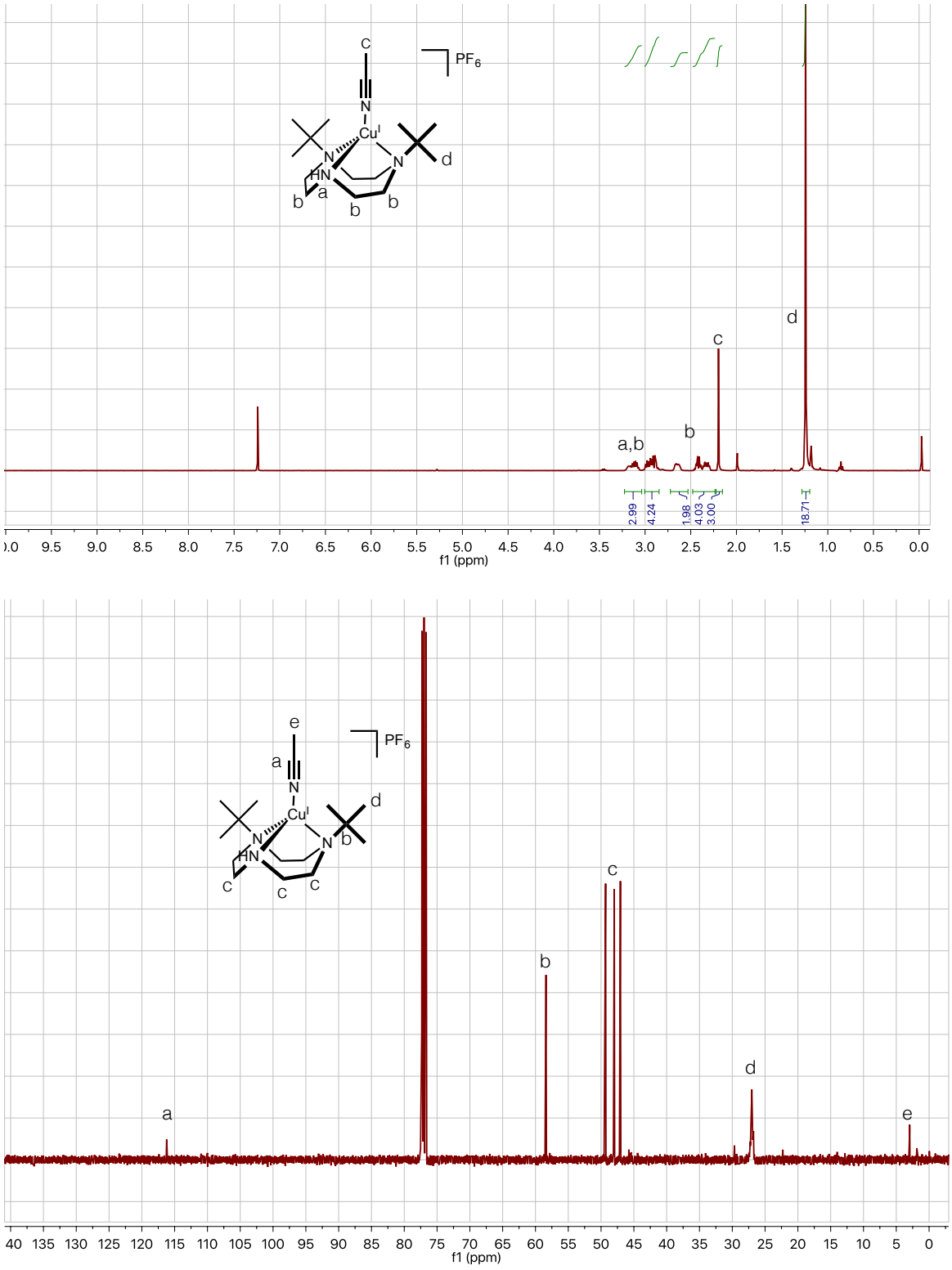

Figure S1-40. ^{1}H NMR spectrum (top) and ^{13}C NMR spectrum (bottom) of **[Cu(*t*Bu$_2$Htacn)(MeCN)]PF$_6$** in $CDCl_3$.

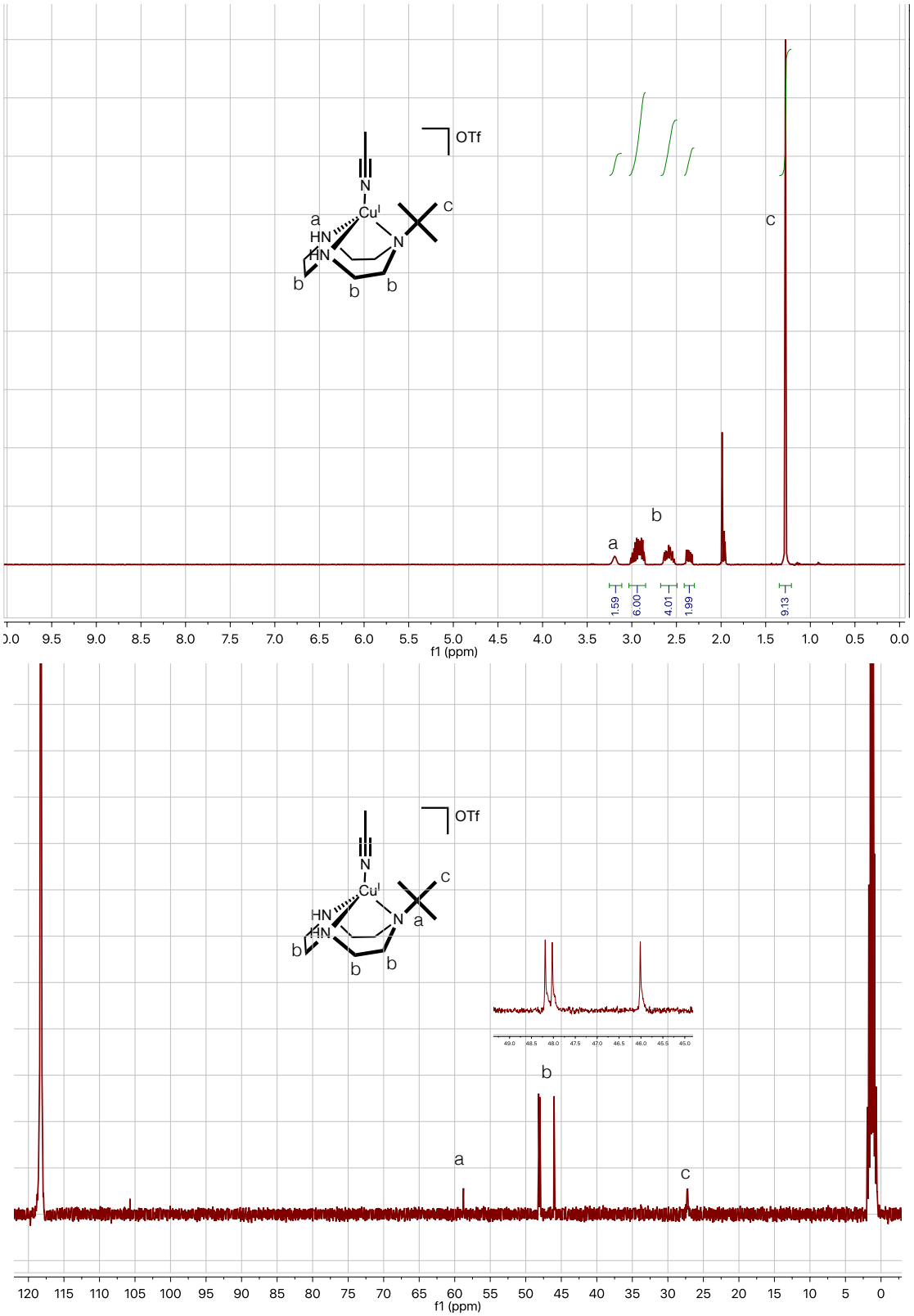

Figure S1-41. ^{1}H NMR spectrum (top) and ^{13}C NMR spectrum (bottom) of **[Cu(*t*BuH$_2$tacn)(MeCN)]OTf** in Acetonitrile-d_3.

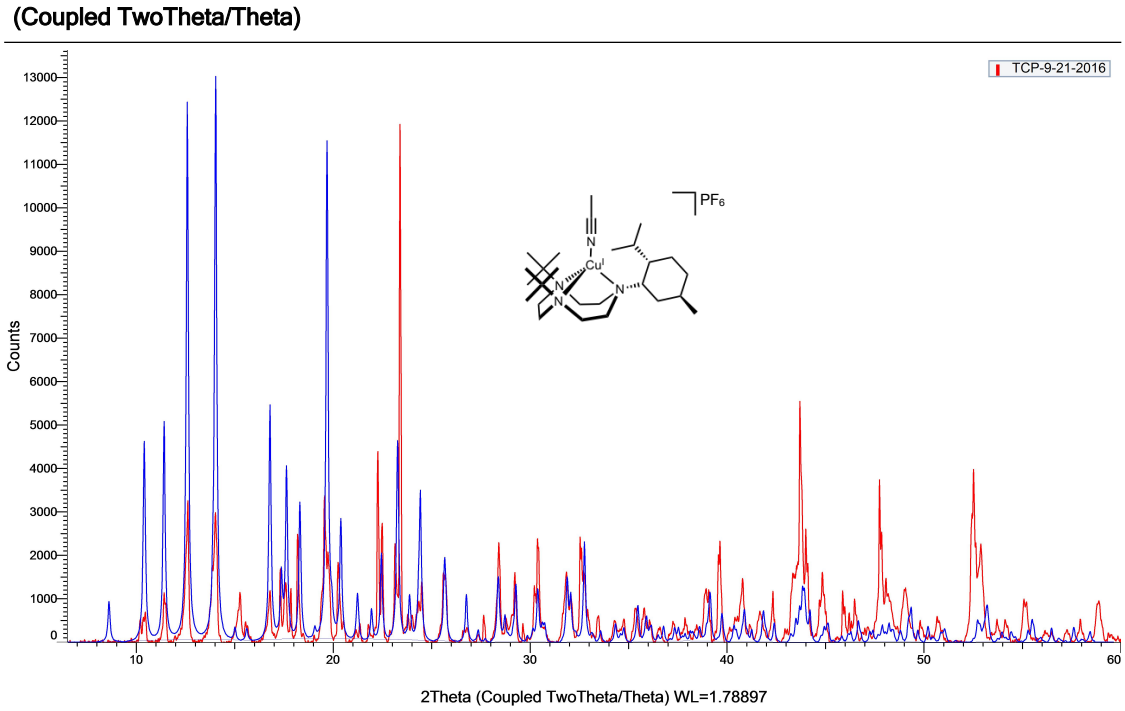

Figure S1-42. Theoretical (blue) and experimental (red) x-ray powder diffraction pattern of **[Cu(*t*Bu$_2$menthyltacn)(MeCN)]PF$_6$**. y axis: intensity, x axis: 2θ.

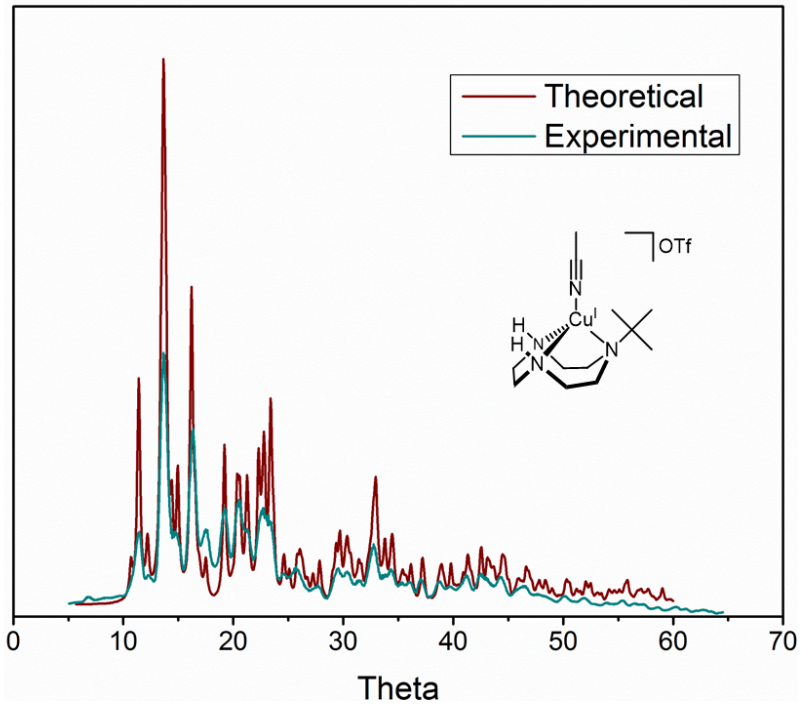

Figure S1-43. Theoretical (brown) and experimental (green) x-ray powder diffraction pattern of **[Cu(*t*BuH$_2$tacn)(MeCN)]OTf**. y axis: intensity, x axis: 2θ.

Compound Name: **[Cu*t*Bu$_2$pictacn]PF$_6$**

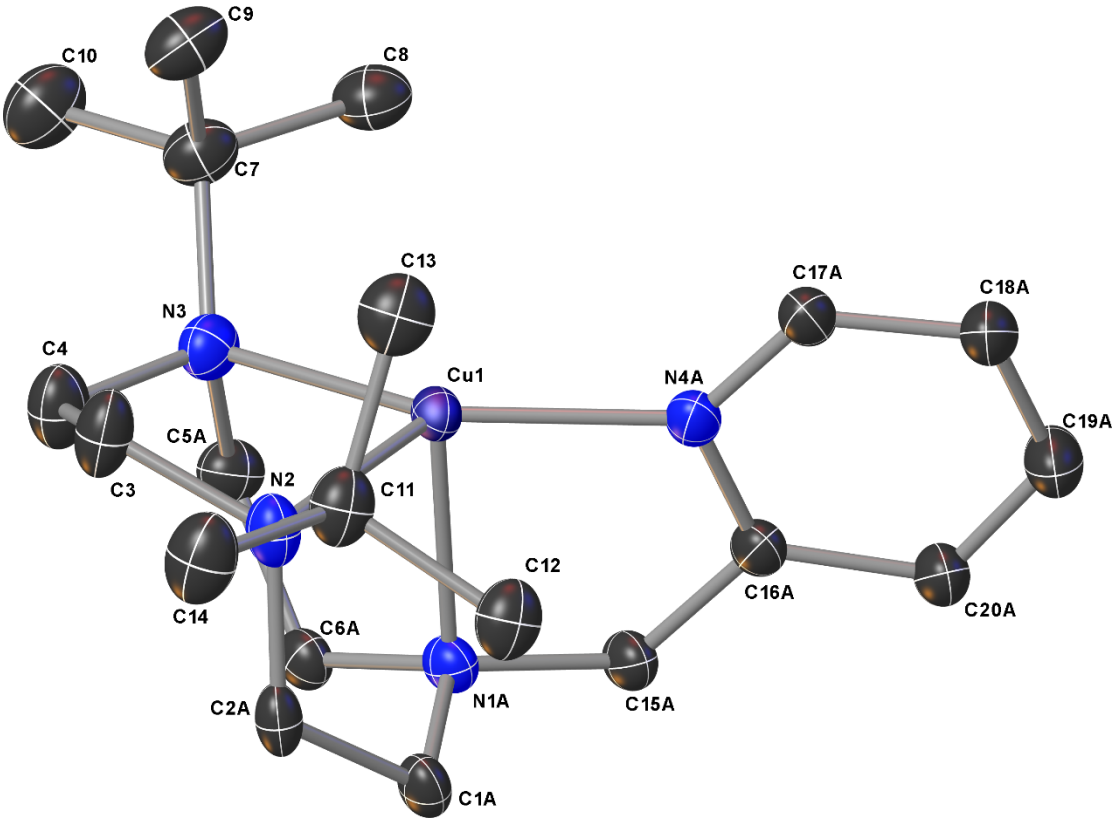

Table 1 Crystal data and structure refinement for A459.

Identification code	A459
Empirical formula	$C_{20}H_{36}CuF_6N_4P$
Formula weight	541.05
Temperature/K	100(2)
Crystal system	monoclinic
Space group	$P2_1/c$
a/Å	8.7758(10)
b/Å	17.933(2)
c/Å	15.6343(18)
α/°	90
β/°	97.725(2)
γ/°	90
Volume/Å^3	2438.1(5)
Z	4
ρ_{calc}g/cm^3	1.474
μ/mm^{-1}	1.022
F(000)	1128.0
Crystal size/mm^3	0.329 × 0.236 × 0.1
Radiation	MoKα (λ = 0.71073)
2Θ range for data collection/°	5.206 to 51.362
Index ranges	$-10 \le h \le 10$, $-21 \le k \le 21$, $-19 \le l \le 19$
Reflections collected	23119
Independent reflections	4614 [R_{int} = 0.0578, R_{sigma} = 0.0428]

Data/restraints/parameters	4614/702/468
Goodness-of-fit on F^2	1.229
Final R indexes [I>=2σ (I)]	R_1 = 0.0848, wR_2 = 0.1838
Final R indexes [all data]	R_1 = 0.0954, wR_2 = 0.1884
Largest diff. peak/hole / e $Å^{-3}$	0.80/-0.59

Table 2 Fractional Atomic Coordinates (×10^4) and Equivalent Isotropic Displacement Parameters ($Å^2$×10^3) for A459. U_{eq} is defined as 1/3 of of the trace of the orthogonalised U_{IJ} tensor.

Atom	*x*	*y*	*z*	U(eq)
C(3)	7674(8)	3663(4)	3551(5)	32.8(12)
C(4)	6611(8)	3000(4)	3271(5)	32.5(12)
C(7)	4063(8)	2930(4)	3832(4)	29.3(10)
C(8)	2432(8)	3241(4)	3683(5)	31.7(13)
C(9)	4853(9)	3262(4)	4689(5)	34.7(14)
C(10)	3982(10)	2082(4)	3918(5)	39.2(15)
C(11)	7992(8)	5032(4)	3472(5)	29.5(10)
C(12)	7642(8)	5708(4)	2881(5)	30.3(13)
C(13)	7255(9)	5178(4)	4280(5)	33.7(13)
C(14)	9740(8)	4942(4)	3709(5)	37.8(15)
Cu(1)	4846.9(8)	4331.3(4)	2913.4(5)	18.0(2)
N(2)	7271(6)	4344(3)	3027(4)	24.8(8)
N(3)	4952(6)	3186(3)	3117(4)	24.5(8)
C(1A)	6156(13)	4510(7)	1383(7)	22.4(15)
C(2A)	7464(12)	4304(10)	2086(5)	22.8(15)
C(5A)	4290(30)	2936(7)	2232(5)	26.4(14)
C(6A)	4639(17)	3336(6)	1413(8)	21.1(15)
C(15A)	3298(13)	4557(7)	1194(6)	22.8(15)
C(16A)	2903(14)	5186(7)	1764(8)	22.9(18)
C(17A)	3107(18)	5719(7)	3118(9)	25(2)
C(18A)	2192(18)	6322(7)	2850(9)	30(2)
C(19A)	1560(19)	6313(8)	1989(9)	36(3)
C(20A)	1942(16)	5769(7)	1427(9)	28(2)
N(1A)	4690(11)	4147(5)	1528(4)	20.5(11)
N(4A)	3484(15)	5171(6)	2612(6)	21.4(15)
C(1B)	6524(11)	4383(6)	1466(6)	22.9(18)
C(2B)	7812(11)	4172(7)	2178(6)	23.9(18)
C(5B)	4228(19)	2860(6)	2281(5)	27.4(17)
C(6B)	5115(14)	3189(5)	1589(7)	21.5(18)
C(15B)	3682(12)	4340(7)	1094(5)	23.2(17)
C(16B)	3059(12)	5005(6)	1523(7)	22.5(17)
C(17B)	2797(14)	5646(6)	2775(8)	26.5(19)
C(18B)	1772(15)	6158(7)	2371(9)	32(2)
C(19B)	1415(15)	6070(7)	1487(8)	37(3)
C(20B)	2023(13)	5495(7)	1050(8)	29(2)
N(1B)	5055(10)	4007(5)	1585(4)	21.1(14)
N(4B)	3409(12)	5079(5)	2391(5)	22.3(15)
P(1A)	9834(8)	2701(4)	656(5)	30.8(12)
F(1A)	9970(12)	2628(5)	1683(5)	37.8(16)

F(2A)	8032(8)	2794(5)	574(7)	39.0(17)
F(3A)	10042(10)	3587(4)	747(6)	37.6(15)
F(4A)	9790(10)	2767(6)	-369(5)	39.3(16)
F(5A)	11668(8)	2610(6)	736(5)	37.7(16)
F(6A)	9674(11)	1822(4)	554(6)	38.8(16)
P(1B)	9723(10)	2629(5)	671(6)	33.5(15)
F(1B)	9748(14)	2772(7)	1677(5)	40.2(18)
F(2B)	8031(10)	2998(6)	502(8)	39.8(18)
F(3B)	10451(12)	3417(5)	548(7)	40.2(17)
F(4B)	9550(12)	2451(7)	-336(5)	38.5(17)
F(5B)	11366(11)	2252(7)	818(6)	38.7(18)
F(6B)	8968(13)	1814(4)	770(7)	40.0(18)

Table 3 Anisotropic Displacement Parameters ($Å^2×10^3$) for A459. The Anisotropic displacement factor exponent takes the form: $-2\pi^2[h^2a^{*2}U_{11}+2hka^*b^*U_{12}+\ldots]$.

Atom	U_{11}	U_{22}	U_{33}	U_{23}	U_{13}	U_{12}
C(3)	26(2)	23.7(18)	47(2)	7.7(16)	-2.4(16)	0.8(13)
C(4)	27.5(17)	22.6(18)	47(3)	3.2(17)	3.2(15)	0.5(12)
C(7)	30(2)	31(2)	26.9(18)	2.2(14)	2.5(14)	-5.3(15)
C(8)	33(2)	38(3)	24(3)	0(2)	3.1(17)	-3.4(18)
C(9)	42(3)	33(3)	28(2)	3.8(18)	-0.3(18)	-8(2)
C(10)	43(3)	32(2)	41(3)	3.7(17)	1(3)	-7.6(17)
C(11)	27.0(19)	23.5(17)	36(2)	0.7(14)	-1.8(15)	-2.7(13)
C(12)	29(3)	24(2)	37(3)	-0.1(19)	-2(2)	-2.7(18)
C(13)	31(3)	31(3)	38(2)	-2.6(19)	-1.2(19)	-6(2)
C(14)	27.2(19)	34(3)	50(3)	6(3)	-3.6(17)	-3.8(16)
Cu(1)	17.7(4)	19.3(4)	16.7(4)	-0.6(3)	0.9(3)	2.8(3)
N(2)	18.8(14)	21.1(15)	34.0(16)	0.9(12)	1.3(11)	1.5(11)
N(3)	27.2(16)	20.1(14)	26.0(15)	-0.1(11)	2.7(12)	0.0(11)
C(1A)	16(2)	23(3)	29(2)	0.8(18)	4.7(14)	3.4(19)
C(2A)	17(2)	16(4)	35.0(18)	1.0(16)	1.8(13)	2.7(19)
C(5A)	29(3)	24(2)	26.7(18)	-1.0(13)	5.6(15)	-2.1(19)
C(6A)	15(4)	24(2)	24(2)	-0.5(13)	1.8(19)	2.2(17)
C(15A)	17(3)	28(3)	23(2)	2.1(17)	3.0(16)	4.8(19)
C(16A)	20(3)	26(3)	25(2)	3.9(17)	6.4(19)	4(2)
C(17A)	26(4)	23(2)	27(3)	4(2)	9(2)	4(3)
C(18A)	34(5)	27(3)	30(3)	6(2)	10(3)	9(3)
C(19A)	42(5)	36(3)	31(3)	4(2)	7(3)	18(4)
C(20A)	27(4)	31(3)	29(3)	6(2)	8(3)	10(3)
N(1A)	16(2)	24.1(19)	22.0(16)	0.3(12)	3.0(12)	2.0(14)
N(4A)	19(3)	22(2)	25(2)	4.1(16)	6.6(17)	2(2)
C(1B)	17(3)	24(4)	29(3)	0(3)	7(2)	3(2)
C(2B)	17(3)	18(4)	37(3)	1(2)	3(2)	4(3)
C(5B)	32(3)	25(3)	27(3)	-4(2)	10(2)	-6(3)
C(6B)	18(4)	24(3)	22(3)	0(2)	1(3)	2(2)
C(15B)	18(3)	29(3)	22(3)	2(2)	2(2)	4(2)
C(16B)	20(3)	25(3)	24(3)	5(2)	8(2)	3(3)

C(17B)	28(4)	24(3)	29(3)	4(3)	11(3)	3(3)
C(18B)	36(5)	32(4)	31(4)	7(3)	13(3)	10(3)
C(19B)	42(5)	39(4)	32(4)	6(3)	11(3)	19(4)
C(20B)	28(4)	33(4)	29(3)	8(3)	10(3)	10(3)
N(1B)	17(3)	26(3)	21(2)	1.4(19)	3.1(18)	1.6(19)
N(4B)	20(3)	23(3)	25(3)	4(2)	7(2)	1(2)
P(1A)	25(2)	40(2)	28(2)	-9.5(14)	4.9(15)	4.1(15)
F(1A)	38(3)	43(3)	33(2)	-9.3(17)	7.5(17)	4(2)
F(2A)	31(2)	43(3)	44(3)	-7(2)	7.4(18)	3.5(17)
F(3A)	33(3)	42(2)	39(3)	-9.3(17)	10(2)	2.4(17)
F(4A)	38(3)	47(3)	34(2)	-9.0(17)	5.6(17)	3(2)
F(5A)	31(2)	46(3)	37(3)	-10(2)	5.8(17)	3.8(17)
F(6A)	37(3)	42(2)	38(3)	-10.6(17)	7(2)	3.8(17)
P(1B)	33(3)	36(2)	29(2)	-4.2(17)	-4.5(18)	8.5(17)
F(1B)	43(3)	41(3)	35(2)	-4.4(19)	-2(2)	10(2)
F(2B)	38(3)	39(3)	41(3)	-2(2)	-2(2)	9(2)
F(3B)	41(3)	39(3)	39(3)	-4(2)	-1(2)	6(2)
F(4B)	41(3)	38(3)	34(2)	-4.3(19)	-3.8(19)	7(2)
F(5B)	37(3)	40(3)	37(3)	-3(2)	-3(2)	9(2)
F(6B)	40(3)	39(3)	39(3)	-3(2)	-1(2)	7(2)

Table 4 Bond Lengths for A459.

Atom	Atom	Length/Å	Atom	Atom	Length/Å
C(3)	C(4)	1.537(10)	C(17A)	C(18A)	1.378(13)
C(3)	N(2)	1.487(9)	C(17A)	N(4A)	1.331(11)
C(4)	N(3)	1.481(9)	C(18A)	C(19A)	1.386(17)
C(7)	C(8)	1.525(10)	C(19A)	C(20A)	1.384(16)
C(7)	C(9)	1.543(10)	C(1B)	C(2B)	1.523(12)
C(7)	C(10)	1.529(10)	C(1B)	N(1B)	1.489(9)
C(7)	N(3)	1.518(9)	C(5B)	C(6B)	1.534(11)
C(11)	C(12)	1.531(10)	C(6B)	N(1B)	1.469(10)
C(11)	C(13)	1.518(10)	C(15B)	C(16B)	1.506(14)
C(11)	C(14)	1.537(10)	C(15B)	N(1B)	1.466(11)
C(11)	N(2)	1.512(9)	C(16B)	C(20B)	1.402(12)
Cu(1)	N(2)	2.111(5)	C(16B)	N(4B)	1.357(11)
Cu(1)	N(3)	2.079(5)	C(17B)	C(18B)	1.378(13)
Cu(1)	N(1A)	2.177(6)	C(17B)	N(4B)	1.330(11)
Cu(1)	N(4A)	1.941(6)	C(18B)	C(19B)	1.385(17)
Cu(1)	N(1B)	2.187(6)	C(19B)	C(20B)	1.383(16)
Cu(1)	N(4B)	1.944(6)	P(1A)	F(1A)	1.599(8)
N(2)	C(2A)	1.504(9)	P(1A)	F(2A)	1.579(8)
N(2)	C(2B)	1.501(9)	P(1A)	F(3A)	1.605(9)
N(3)	C(5A)	1.495(9)	P(1A)	F(4A)	1.603(9)
N(3)	C(5B)	1.493(9)	P(1A)	F(5A)	1.606(8)
C(1A)	C(2A)	1.524(12)	P(1A)	F(6A)	1.588(9)
C(1A)	N(1A)	1.486(9)	P(1B)	F(1B)	1.591(10)
C(5A)	C(6A)	1.534(11)	P(1B)	F(2B)	1.615(10)

C(6A)	N(1A)	1.465(10)	P(1B)	F(3B)	1.574(10)
C(15A)	C(16A)	1.506(14)	P(1B)	F(4B)	1.593(10)
C(15A)	N(1A)	1.462(11)	P(1B)	F(5B)	1.582(9)
C(16A)	C(20A)	1.401(12)	P(1B)	F(6B)	1.620(10)
C(16A)	N(4A)	1.356(11)			

Table 5 Bond Angles for A459.

Atom	Atom	Atom	Angle/°	Atom	Atom	Atom	Angle/°
N(2)	C(3)	C(4)	112.8(6)	C(15A)	N(1A)	Cu(1)	102.5(5)
N(3)	C(4)	C(3)	114.7(6)	C(15A)	N(1A)	C(1A)	115.1(7)
C(8)	C(7)	C(9)	107.2(6)	C(15A)	N(1A)	C(6A)	116.5(7)
C(8)	C(7)	C(10)	108.9(6)	C(16A)	N(4A)	Cu(1)	113.0(6)
C(10)	C(7)	C(9)	109.1(6)	C(17A)	N(4A)	Cu(1)	128.5(7)
N(3)	C(7)	C(8)	110.0(6)	C(17A)	N(4A)	C(16A)	118.4(8)
N(3)	C(7)	C(9)	107.9(6)	N(1B)	C(1B)	C(2B)	111.5(6)
N(3)	C(7)	C(10)	113.6(6)	N(2)	C(2B)	C(1B)	107.7(7)
C(12)	C(11)	C(14)	109.9(6)	N(3)	C(5B)	C(6B)	105.7(8)
C(13)	C(11)	C(12)	107.0(6)	N(1B)	C(6B)	C(5B)	111.4(6)
C(13)	C(11)	C(14)	109.9(6)	N(1B)	C(15B)	C(16B)	114.3(6)
N(2)	C(11)	C(12)	109.3(6)	C(20B)	C(16B)	C(15B)	120.6(10)
N(2)	C(11)	C(13)	109.0(6)	N(4B)	C(16B)	C(15B)	118.4(7)
N(2)	C(11)	C(14)	111.6(6)	N(4B)	C(16B)	C(20B)	120.7(11)
N(2)	Cu(1)	N(1A)	90.8(3)	N(4B)	C(17B)	C(18B)	125.5(12)
N(2)	Cu(1)	N(1B)	82.6(3)	C(17B)	C(18B)	C(19B)	115.3(11)
N(3)	Cu(1)	N(2)	88.5(2)	C(20B)	C(19B)	C(18B)	121.8(10)
N(3)	Cu(1)	N(1A)	89.9(3)	C(19B)	C(20B)	C(16B)	118.2(11)
N(3)	Cu(1)	N(1B)	82.8(3)	C(1B)	N(1B)	Cu(1)	100.6(5)
N(4A)	Cu(1)	N(2)	126.4(5)	C(6B)	N(1B)	Cu(1)	105.6(5)
N(4A)	Cu(1)	N(3)	144.8(5)	C(6B)	N(1B)	C(1B)	114.9(7)
N(4A)	Cu(1)	N(1A)	85.5(3)	C(15B)	N(1B)	Cu(1)	102.8(5)
N(4B)	Cu(1)	N(2)	128.2(4)	C(15B)	N(1B)	C(1B)	114.5(6)
N(4B)	Cu(1)	N(3)	139.3(4)	C(15B)	N(1B)	C(6B)	115.8(7)
N(4B)	Cu(1)	N(1B)	85.2(3)	C(16B)	N(4B)	Cu(1)	113.6(6)
C(3)	N(2)	C(11)	111.3(5)	C(17B)	N(4B)	Cu(1)	128.0(7)
C(3)	N(2)	Cu(1)	101.5(4)	C(17B)	N(4B)	C(16B)	118.4(8)
C(3)	N(2)	C(2A)	116.7(8)	F(1A)	P(1A)	F(3A)	90.0(6)
C(3)	N(2)	C(2B)	103.8(7)	F(1A)	P(1A)	F(4A)	177.1(6)
C(11)	N(2)	Cu(1)	113.7(4)	F(1A)	P(1A)	F(5A)	88.6(5)
C(2A)	N(2)	C(11)	113.2(7)	F(2A)	P(1A)	F(1A)	91.7(5)
C(2A)	N(2)	Cu(1)	99.3(5)	F(2A)	P(1A)	F(3A)	90.2(6)
C(2B)	N(2)	C(11)	114.3(6)	F(2A)	P(1A)	F(4A)	91.2(5)
C(2B)	N(2)	Cu(1)	111.0(5)	F(2A)	P(1A)	F(5A)	179.6(8)
C(4)	N(3)	C(7)	113.8(5)	F(2A)	P(1A)	F(6A)	91.3(6)
C(4)	N(3)	Cu(1)	105.6(4)	F(3A)	P(1A)	F(5A)	89.6(6)
C(4)	N(3)	C(5A)	109.5(10)	F(4A)	P(1A)	F(3A)	90.1(6)
C(4)	N(3)	C(5B)	110.3(9)	F(4A)	P(1A)	F(5A)	88.5(5)
C(7)	N(3)	Cu(1)	113.3(4)	F(6A)	P(1A)	F(1A)	90.8(6)

C(5A)	N(3)	C(7)	114.6(8)	F(6A)	P(1A)	F(3A)	178.3(7)
C(5A)	N(3)	Cu(1)	98.7(6)	F(6A)	P(1A)	F(4A)	89.0(6)
C(5B)	N(3)	Cu(1)	104.3(5)	F(6A)	P(1A)	F(5A)	89.0(6)
N(1A)	C(1A)	C(2A)	111.6(6)	F(1B)	P(1B)	F(2B)	89.2(6)
N(2)	C(2A)	C(1A)	121.4(9)	F(1B)	P(1B)	F(4B)	174.8(8)
N(3)	C(5A)	C(6A)	122.4(9)	F(1B)	P(1B)	F(6B)	90.1(6)
N(1A)	C(6A)	C(5A)	111.6(6)	F(2B)	P(1B)	F(6B)	90.4(6)
N(1A)	C(15A)	C(16A)	114.5(7)	F(3B)	P(1B)	F(1B)	91.4(7)
C(20A)	C(16A)	C(15A)	120.7(10)	F(3B)	P(1B)	F(2B)	89.5(6)
N(4A)	C(16A)	C(15A)	118.5(7)	F(3B)	P(1B)	F(4B)	92.6(7)
N(4A)	C(16A)	C(20A)	120.7(11)	F(3B)	P(1B)	F(5B)	91.4(7)
N(4A)	C(17A)	C(18A)	125.4(11)	F(3B)	P(1B)	F(6B)	178.5(8)
C(17A)	C(18A)	C(19A)	115.3(11)	F(4B)	P(1B)	F(2B)	87.6(6)
C(20A)	C(19A)	C(18A)	121.7(10)	F(4B)	P(1B)	F(6B)	85.9(6)
C(19A)	C(20A)	C(16A)	118.2(11)	F(5B)	P(1B)	F(1B)	91.9(6)
C(1A)	N(1A)	Cu(1)	98.3(6)	F(5B)	P(1B)	F(2B)	178.6(8)
C(6A)	N(1A)	Cu(1)	105.6(6)	F(5B)	P(1B)	F(4B)	91.3(6)
C(6A)	N(1A)	C(1A)	115.4(7)	F(5B)	P(1B)	F(6B)	88.7(7)

Table 6 Torsion Angles for A459.

A	B	C	D	Angle/°	A	B	C	D	Angle/°
C(3)	C(4)	N(3)	C(7)	-104.5(7)	C(2A)	C(1A)	N(1A)	C(15A)	150.9(10)
C(3)	C(4)	N(3)	Cu(1)	20.4(7)	C(5A)	C(6A)	N(1A)	Cu(1)	14.8(13)
C(3)	C(4)	N(3)	C(5A)	125.8(7)	C(5A)	C(6A)	N(1A)	C(1A)	122.2(12)
C(3)	C(4)	N(3)	C(5B)	132.6(7)	C(5A)	C(6A)	N(1A)	C(15A)	-98.2(14)
C(3)	N(2)	C(2A)	C(1A)	127.3(11)	C(15A)	C(16A)	C(20A)	C(19A)	177.0(14)
C(3)	N(2)	C(2B)	C(1B)	133.1(7)	C(15A)	C(16A)	N(4A)	Cu(1)	3.1(13)
C(4)	C(3)	N(2)	C(11)	162.8(6)	C(15A)	C(16A)	N(4A)	C(17A)	-178.6(15)
C(4)	C(3)	N(2)	Cu(1)	41.5(7)	C(16A)	C(15A)	N(1A)	Cu(1)	25.4(9)
C(4)	C(3)	N(2)	C(2A)	-65.2(9)	C(16A)	C(15A)	N(1A)	C(1A)	-80.2(11)
C(4)	C(3)	N(2)	C(2B)	-73.7(8)	C(16A)	C(15A)	N(1A)	C(6A)	140.1(10)
C(4)	N(3)	C(5A)	C(6A)	-72.4(18)	C(17A)	C(18A)	C(19A)	C(20A)	-6(2)
C(4)	N(3)	C(5B)	C(6B)	-58.3(10)	C(18A)	C(17A)	N(4A)	Cu(1)	176.3(14)
C(7)	N(3)	C(5A)	C(6A)	158.3(14)	C(18A)	C(17A)	N(4A)	C(16A)	-2(2)
C(8)	C(7)	N(3)	C(4)	171.9(6)	C(18A)	C(19A)	C(20A)	C(16A)	5(3)
C(8)	C(7)	N(3)	Cu(1)	51.2(6)	C(20A)	C(16A)	N(4A)	Cu(1)	-177.6(12)
C(8)	C(7)	N(3)	C(5A)	-61.0(11)	C(20A)	C(16A)	N(4A)	C(17A)	1(2)
C(9)	C(7)	N(3)	C(4)	55.3(7)	N(1A)	C(1A)	C(2A)	N(2)	-47.8(17)
C(9)	C(7)	N(3)	Cu(1)	-65.4(6)	N(1A)	C(15A)	C(16A)	C(20A)	159.0(12)
C(9)	C(7)	N(3)	C(5A)	-177.6(10)	N(1A)	C(15A)	C(16A)	N(4A)	-21.6(13)
C(10)	C(7)	N(3)	C(4)	-65.9(8)	N(4A)	C(16A)	C(20A)	C(19A)	-2(2)
C(10)	C(7)	N(3)	Cu(1)	173.5(5)	N(4A)	C(17A)	C(18A)	C(19A)	4(3)
C(10)	C(7)	N(3)	C(5A)	61.3(11)	C(2B)	C(1B)	N(1B)	Cu(1)	53.3(8)
C(11)	N(2)	C(2A)	C(1A)	-101.6(11)	C(2B)	C(1B)	N(1B)	C(6B)	-59.6(10)
C(11)	N(2)	C(2B)	C(1B)	-105.5(7)	C(2B)	C(1B)	N(1B)	C(15B)	162.8(8)
C(12)	C(11)	N(2)	C(3)	175.9(6)	C(5B)	C(6B)	N(1B)	Cu(1)	29.4(9)
C(12)	C(11)	N(2)	Cu(1)	-70.2(6)	C(5B)	C(6B)	N(1B)	C(1B)	139.2(9)

C(12)	C(11)	N(2)	C(2A)	42.2(9)	C(5B)	C(6B)	N(1B)	C(15B)	-83.7(10)
C(12)	C(11)	N(2)	C(2B)	58.7(8)	C(15B)	C(16B)	C(20B)	C(19B)	176.2(11)
C(13)	C(11)	N(2)	C(3)	-67.4(7)	C(15B)	C(16B)	N(4B)	Cu(1)	5.3(11)
C(13)	C(11)	N(2)	Cu(1)	46.4(6)	C(15B)	C(16B)	N(4B)	C(17B)	-176.8(11)
C(13)	C(11)	N(2)	C(2A)	158.8(7)	C(16B)	C(15B)	N(1B)	Cu(1)	25.0(8)
C(13)	C(11)	N(2)	C(2B)	175.4(7)	C(16B)	C(15B)	N(1B)	C(1B)	-83.1(9)
C(14)	C(11)	N(2)	C(3)	54.1(8)	C(16B)	C(15B)	N(1B)	C(6B)	139.6(8)
C(14)	C(11)	N(2)	Cu(1)	168.0(5)	C(17B)	C(18B)	C(19B)	C(20B)	2(2)
C(14)	C(11)	N(2)	C(2A)	-79.7(9)	C(18B)	C(17B)	N(4B)	Cu(1)	-179.6(11)
C(14)	C(11)	N(2)	C(2B)	-63.1(8)	C(18B)	C(17B)	N(4B)	C(16B)	3(2)
Cu(1)	N(2)	C(2A)	C(1A)	19.3(13)	C(18B)	C(19B)	C(20B)	C(16B)	-2(2)
Cu(1)	N(2)	C(2B)	C(1B)	24.7(9)	C(20B)	C(16B)	N(4B)	Cu(1)	179.2(10)
Cu(1)	N(3)	C(5A)	C(6A)	37.6(18)	C(20B)	C(16B)	N(4B)	C(17B)	-2.8(16)
Cu(1)	N(3)	C(5B)	C(6B)	54.7(10)	N(1B)	C(1B)	C(2B)	N(2)	-54.7(11)
N(2)	C(3)	C(4)	N(3)	-45.0(9)	N(1B)	C(15B)	C(16B)	C(20B)	163.3(9)
N(3)	C(5A)	C(6A)	N(1A)	-39(2)	N(1B)	C(15B)	C(16B)	N(4B)	-22.8(12)
N(3)	C(5B)	C(6B)	N(1B)	-58.0(13)	N(4B)	C(16B)	C(20B)	C(19B)	2.4(18)
C(2A)	C(1A)	N(1A)	Cu(1)	42.8(11)	N(4B)	C(17B)	C(18B)	C(19B)	-2(2)
C(2A)	C(1A)	N(1A)	C(6A)	-69.0(12)					

Table 7 Hydrogen Atom Coordinates (Å×10^4) and Isotropic Displacement Parameters (Å^2×10^3) for A459.

Atom	*x*	*y*	*z*	U(eq)
H(3A)	7615	3776	4165	39
H(3B)	8748	3520	3499	39
H(4A)	6913	2787	2735	39
H(4B)	6773	2611	3723	39
H(8A)	1866	3011	3167	48
H(8B)	2471	3782	3602	48
H(8C)	1910	3130	4184	48
H(9A)	4954	3803	4629	52
H(9B)	5875	3039	4834	52
H(9C)	4231	3154	5150	52
H(10A)	3447	1955	4410	59
H(10B)	5026	1876	4011	59
H(10C)	3421	1871	3389	59
H(12A)	6528	5753	2719	45
H(12B)	8136	5643	2359	45
H(12C)	8039	6160	3185	45
H(13A)	7603	5661	4525	51
H(13B)	7551	4783	4703	51
H(13C)	6133	5184	4132	51
H(14A)	10211	4859	3184	57
H(14B)	9954	4515	4098	57
H(14C)	10169	5396	3997	57
H(1AA)	6018	5057	1373	27
H(1AB)	6427	4354	815	27
H(2AA)	7770	3786	1971	27

H(2AB)	8347	4627	2004	27
H(5AA)	3159	2938	2215	32
H(5AB)	4600	2409	2179	32
H(6AA)	5640	3160	1264	25
H(6AB)	3837	3208	928	25
H(15A)	2424	4204	1112	27
H(15B)	3426	4763	621	27
H(17A)	3501	5692	3714	30
H(18A)	2008	6716	3229	36
H(19A)	845	6690	1779	43
H(20A)	1564	5791	828	34
H(1BA)	6375	4930	1466	27
H(1BB)	6821	4239	899	27
H(2BA)	8055	3635	2142	29
H(2BB)	8751	4462	2116	29
H(5BA)	3127	2998	2166	33
H(5BB)	4313	2310	2293	33
H(6BA)	6201	3025	1699	26
H(6BB)	4670	2999	1015	26
H(15C)	2868	3955	999	28
H(15D)	3933	4494	521	28
H(17B)	3091	5702	3379	32
H(18B)	1340	6544	2678	39
H(19B)	734	6414	1171	44
H(20B)	1746	5433	446	35

Table 8 Atomic Occupancy for A459.

Atom	***Occupancy***	**Atom**	***Occupancy***	**Atom**	***Occupancy***
C(1A)	0.440(8)	H(1AA)	0.440(8)	H(1AB)	0.440(8)
C(2A)	0.440(8)	H(2AA)	0.440(8)	H(2AB)	0.440(8)
C(5A)	0.440(8)	H(5AA)	0.440(8)	H(5AB)	0.440(8)
C(6A)	0.440(8)	H(6AA)	0.440(8)	H(6AB)	0.440(8)
C(15A)	0.440(8)	H(15A)	0.440(8)	H(15B)	0.440(8)
C(16A)	0.440(8)	C(17A)	0.440(8)	H(17A)	0.440(8)
C(18A)	0.440(8)	H(18A)	0.440(8)	C(19A)	0.440(8)
H(19A)	0.440(8)	C(20A)	0.440(8)	H(20A)	0.440(8)
N(1A)	0.440(8)	N(4A)	0.440(8)	C(1B)	0.560(8)
H(1BA)	0.560(8)	H(1BB)	0.560(8)	C(2B)	0.560(8)
H(2BA)	0.560(8)	H(2BB)	0.560(8)	C(5B)	0.560(8)
H(5BA)	0.560(8)	H(5BB)	0.560(8)	C(6B)	0.560(8)
H(6BA)	0.560(8)	H(6BB)	0.560(8)	C(15B)	0.560(8)
H(15C)	0.560(8)	H(15D)	0.560(8)	C(16B)	0.560(8)
C(17B)	0.560(8)	H(17B)	0.560(8)	C(18B)	0.560(8)
H(18B)	0.560(8)	C(19B)	0.560(8)	H(19B)	0.560(8)
C(20B)	0.560(8)	H(20B)	0.560(8)	N(1B)	0.560(8)
N(4B)	0.560(8)	P(1A)	0.539(12)	F(1A)	0.539(12)
F(2A)	0.539(12)	F(3A)	0.539(12)	F(4A)	0.539(12)
F(5A)	0.539(12)	F(6A)	0.539(12)	P(1B)	0.461(12)
F(1B)	0.461(12)	F(2B)	0.461(12)	F(3B)	0.461(12)

F(4B)	0.461(12)	F(5B)	0.461(12)	F(6B)	0.461(12)

Crystal Data for $C_{20}H_{36}CuF_6N_4P$ (M =541.05 g/mol): monoclinic, space group $P2_1/c$ (no. 14), a = 8.7758(10) Å, b = 17.933(2) Å, c = 15.6343(18) Å, β = 97.725(2)°, V = 2438.1(5) Å^3, Z = 4, T = 100(2) K, μ(MoKα) = 1.022 mm^{-1}, *Dcalc* = 1.474 g/cm^3, 23119 reflections measured (5.206° ≤ 2Θ ≤ 51.362°), 4614 unique (R_{int} = 0.0578, R_{sigma} = 0.0428) which were used in all calculations. The final R_1 was 0.0848 (I > 2σ(I)) and wR_2 was 0.1884 (all data)

Compound Name: **[Cu(*t*Bu$_2$*sec*-PhEttacn)(NCPh)]OTf**

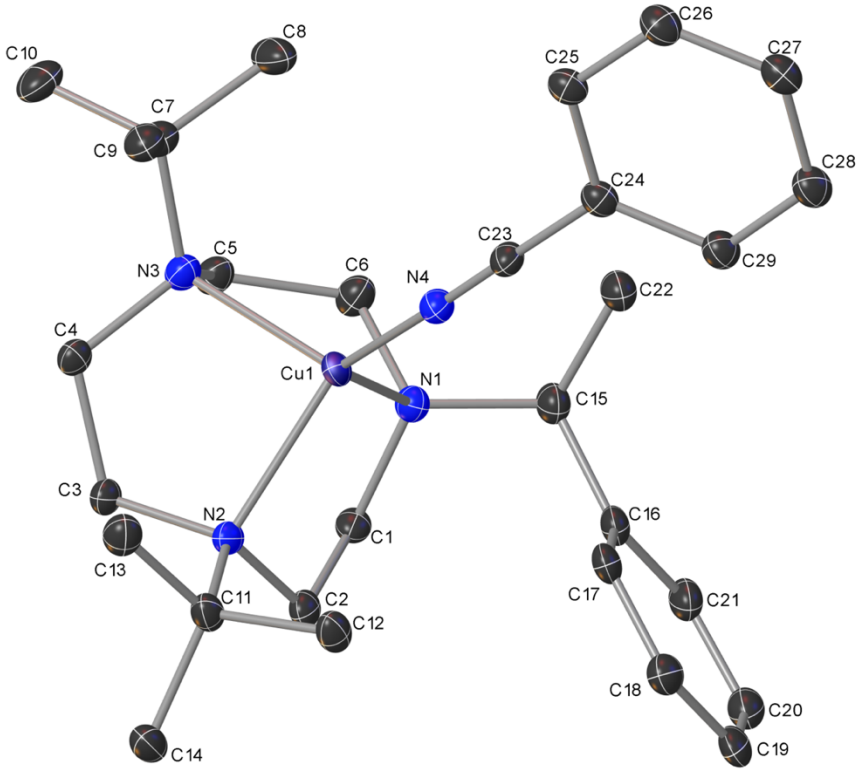

Table 1 Crystal data and structure refinement for **[Cu(*t*Bu$_2$*sec*-PhEttacn)(NCPh)]OTf**.

Identification code	CutBu2sec-PhEttacnNCPhOTf
Empirical formula	$C_{30}H_{44}CuF_3N_4O_3S$
Formula weight	661.29
Temperature/K	100(2)
Crystal system	monoclinic
Space group	$P2_1$
a/Å	8.9545(15)
b/Å	16.264(3)
c/Å	11.0384(18)
α/°	90
β/°	102.006(3)
γ/°	90
Volume/Å^3	1572.4(4)
Z	2
ρ_{calc}g/cm^3	1.397
μ/mm^{-1}	0.816
F(000)	696.0
Crystal size/mm^3	0.355 × 0.155 × 0.064
Radiation	MoKα (λ = 0.71073)
2Θ range for data collection/°	4.528 to 61.324
Index ranges	$-12 \le h \le 12$, $-23 \le k \le 22$, $-15 \le l \le 15$
Reflections collected	13943
Independent reflections	8349 [R_{int} = 0.0475, R_{sigma} = 0.0962]
Data/restraints/parameters	8349/196/387
Goodness-of-fit on F^2	1.025
Final R indexes [I>=2σ (I)]	R_1 = 0.0583, wR_2 = 0.1158
Final R indexes [all data]	R_1 = 0.0809, wR_2 = 0.1283

Largest diff. peak/hole / e Å^{-3}	0.79/-0.45
Flack parameter	0.049(18)

Table 2 Fractional Atomic Coordinates (×10^4) and Equivalent Isotropic Displacement Parameters (Å^2×10^3) for CutBu2sec-PhEttacnNCPhOTf. U_{eq} is defined as 1/3 of of the trace of the orthogonalised U_{IJ} tensor.

Atom	***x***	***y***	***z***	**U(eq)**
Cu1	4117.5(6)	6123.2(4)	7712.9(5)	13.04(13)
N2	4079(5)	7223(3)	6651(4)	14.6(6)
N3	4291(5)	6911(3)	9293(4)	16.4(6)
N4	3056(5)	5124(3)	7445(4)	15.4(8)
N1	6561(4)	6186(3)	8002(3)	15.4(6)
C17	6011(6)	5216(3)	5543(5)	18.5(8)
C25	1113(6)	3378(3)	8115(5)	16.7(8)
C2	5567(6)	7185(3)	6257(5)	16.8(9)
C5	5963(6)	7033(3)	9762(5)	18.1(8)
C16	7381(6)	5333(3)	6364(5)	17.9(7)
C12	2603(6)	6489(3)	4810(5)	19.2(8)
C21	8725(7)	5313(3)	5911(5)	21.9(9)
C24	2076(6)	3629(3)	7342(5)	15.9(7)
C23	2581(6)	4468(3)	7387(5)	15.6(9)
C20	8674(7)	5179(3)	4665(5)	23.6(9)
C18	5964(7)	5101(3)	4288(5)	21.7(9)
C19	7306(7)	5081(3)	3855(6)	22.5(9)
C1	6889(6)	6922(3)	7293(5)	16.4(10)
C22	6938(6)	4657(3)	8277(5)	21.2(9)
C7	3492(6)	6592(3)	10285(5)	20.2(7)
C29	2602(6)	3072(3)	6570(5)	18.2(8)
C6	6965(6)	6367(3)	9360(5)	19.6(10)
C4	3599(6)	7682(3)	8735(4)	15.1(8)
C27	1222(6)	1995(3)	7358(5)	19.4(8)
C26	698(6)	2552(3)	8110(5)	20.0(8)
C8	4270(7)	5797(4)	10828(6)	26.7(9)
C13	1279(6)	7362(3)	6070(5)	20.6(8)
C15	7458(6)	5449(3)	7746(5)	18.7(7)
C28	2179(6)	2253(3)	6584(5)	20.4(9)
C3	4130(6)	7921(3)	7558(4)	15.6(9)
C9	1837(6)	6377(3)	9688(5)	20.8(9)
C11	2738(6)	7281(3)	5570(5)	17.5(6)
C14	2878(7)	8006(3)	4704(5)	22.3(8)
C10	3498(7)	7218(4)	11307(5)	24.8(9)
S1	-65.1(15)	4077.2(8)	1172.9(12)	19.1(3)
F1	1488(4)	5094(2)	2822(3)	29.9(8)
F2	2835(4)	4135(2)	2246(4)	34.6(9)
F3	1363(5)	3863(2)	3494(3)	40.3(10)
O1	257(5)	4626(3)	239(4)	28.2(9)
O2	-1402(5)	4274(3)	1628(4)	29.9(10)
O3	151(5)	3220(2)	947(4)	29.3(10)
C30	1477(7)	4303(3)	2494(6)	23.9(12)

Table 3 Anisotropic Displacement Parameters ($Å^2×10^3$) for CutBu2sec-PhEttacnNCPhOTf. The Anisotropic displacement factor exponent takes the form: $-2\pi^2[h^2a^{*2}U_{11}+2hka^*b^*U_{12}+\ldots]$.

Atom	U_{11}	U_{22}	U_{33}	U_{23}	U_{13}	U_{12}
Cu1	14.4(2)	9.2(2)	15.5(3)	-0.2(3)	2.96(19)	-0.5(3)
N2	20.1(11)	10.9(15)	13.3(11)	-1.2(10)	4.9(9)	-0.5(10)
N3	17.7(11)	17.6(15)	14.1(13)	-1.0(10)	3.7(10)	1.1(10)
N4	16.2(18)	14.9(11)	16(2)	0.0(11)	5.1(16)	0.2(11)
N1	14.2(14)	15.9(13)	16.5(12)	0.3(11)	4.0(10)	1.5(13)
C17	23.5(12)	10(2)	22.0(12)	0.4(12)	5.9(10)	3.6(13)
C25	15.4(18)	17.0(12)	17.0(17)	2.5(12)	1.4(14)	-0.5(12)
C2	21.6(11)	11(2)	19.5(17)	-1.7(15)	7.9(10)	-0.7(12)
C5	17.5(11)	21.5(18)	15.1(15)	-1.5(13)	3.2(10)	1.3(11)
C16	21.7(12)	11.2(18)	21.8(10)	0.6(10)	7.2(8)	4.1(11)
C12	25(2)	15.2(14)	16.0(17)	-2.5(13)	-0.3(14)	2.0(13)
C21	24.4(12)	17(2)	27.5(12)	2.2(14)	11.6(10)	5.4(13)
C24	15.4(16)	15.3(10)	16.0(16)	1.2(10)	1.2(14)	-0.3(10)
C23	17(2)	15.0(10)	16(2)	-0.7(11)	7.0(18)	-0.1(11)
C20	29.8(14)	17(3)	27.6(13)	2.1(13)	13.6(10)	3.4(15)
C18	28.9(14)	15(2)	22.2(12)	-0.5(13)	7.6(10)	1.1(14)
C19	31.9(15)	11(2)	27.5(14)	2.5(15)	12.0(10)	3.1(14)
C1	19.2(15)	13(2)	19.5(18)	0.2(17)	9.0(14)	-2.9(16)
C22	24(2)	17.2(14)	24(2)	2.2(15)	9.2(17)	4.2(15)
C7	22.6(13)	22.0(15)	17.5(13)	1.5(9)	7.9(10)	2.1(10)
C29	19.9(19)	15.9(11)	18.5(18)	0.2(11)	3.7(14)	-0.5(11)
C6	17.9(18)	24(2)	16.9(12)	-1.6(12)	3.2(11)	2.9(15)
C4	16.7(15)	15.0(15)	13.5(14)	-2.9(11)	2.7(13)	-0.8(12)
C27	19.4(18)	16.7(13)	20.9(18)	2.7(12)	1.5(15)	-0.4(13)
C26	19(2)	17.3(12)	23.5(19)	2.2(12)	4.2(15)	-1.8(11)
C8	28.9(19)	29.4(17)	26(2)	9.6(14)	14.0(17)	9.2(16)
C13	21.9(12)	21(2)	18.0(19)	-1.1(15)	2.2(13)	3.1(14)
C15	18.7(16)	16.5(13)	21.7(11)	0.3(10)	6.1(10)	3.4(12)
C28	23.5(19)	15.9(11)	21.7(19)	-0.2(12)	4.4(16)	-1.6(12)
C3	20(2)	12.1(15)	15.2(13)	-2.6(10)	5.0(14)	-0.1(14)
C9	22.4(12)	21(2)	20.8(19)	1.0(15)	9.5(13)	1.0(12)
C11	22.8(11)	13.3(14)	15.8(12)	-0.8(9)	2.3(9)	2.1(10)
C14	34(2)	15.7(15)	17.1(17)	1.6(14)	5.2(15)	3.7(15)
C10	27(2)	28.6(18)	22.3(15)	-4.1(15)	13.6(16)	-3.8(17)
S1	21.1(6)	16.5(6)	22.0(7)	-4.3(5)	9.5(5)	-2.9(5)
F1	31.0(19)	20.2(17)	39(2)	-15.1(15)	9.6(16)	-4.0(14)
F2	18.9(16)	25.4(19)	60(3)	-7.5(18)	8.6(16)	3.4(14)
F3	46(2)	42(2)	29(2)	9.0(17)	0.6(17)	-4.9(18)
O1	39(2)	22(2)	27(2)	-1.7(17)	14.4(19)	-4.8(18)
O2	22(2)	36(3)	35(2)	-9(2)	12.4(18)	-3.0(18)
O3	35(2)	18(2)	39(2)	-7.4(18)	17(2)	-5.4(17)
C30	25(3)	17(3)	32(3)	-2(2)	11(2)	-1(2)

Table 4 Bond Lengths for CutBu2sec-PhEttacnNCPhOTf.

Atom	Atom	Length/Å	Atom	Atom	Length/Å
Cu1	N2	2.135(4)	C21	C20	1.384(8)
Cu1	N3	2.144(4)	C24	C23	1.435(7)
Cu1	N4	1.875(4)	C24	C29	1.391(7)

Cu1	N1	2.147(4)	C20	C19	1.367(8)
N2	C2	1.486(7)	C18	C19	1.383(8)
N2	C3	1.508(6)	C22	C15	1.528(8)
N2	C11	1.510(6)	C7	C8	1.530(7)
N3	C5	1.492(6)	C7	C9	1.532(8)
N3	C7	1.519(7)	C7	C10	1.519(8)
N3	C4	1.476(6)	C29	C28	1.386(7)
N4	C23	1.145(6)	C4	C3	1.523(7)
N1	C1	1.493(7)	C27	C26	1.376(8)
N1	C6	1.496(6)	C27	C28	1.395(8)
N1	C15	1.502(7)	C13	C11	1.527(8)
C17	C16	1.378(7)	C11	C14	1.539(7)
C17	C18	1.390(8)	S1	O1	1.438(4)
C25	C24	1.395(7)	S1	O2	1.427(4)
C25	C26	1.393(7)	S1	O3	1.437(4)
C2	C1	1.526(7)	S1	C30	1.825(6)
C5	C6	1.530(7)	F1	C30	1.335(6)
C16	C21	1.395(8)	F2	C30	1.329(7)
C16	C15	1.525(8)	F3	C30	1.337(7)
C12	C11	1.527(7)			

Table 5 Bond Angles for CutBu2sec-PhEttacnNCPhOTf.

Atom	**Atom**	**Atom**	**Angle/°**	**Atom**	**Atom**	**Atom**	**Angle/°**
N2	Cu1	N3	86.33(16)	C19	C18	C17	120.0(5)
N2	Cu1	N1	86.62(17)	C20	C19	C18	119.7(6)
N3	Cu1	N1	87.22(16)	N1	C1	C2	114.2(4)
N4	Cu1	N2	133.62(17)	N3	C7	C8	109.0(4)
N4	Cu1	N3	126.52(18)	N3	C7	C9	109.0(4)
N4	Cu1	N1	122.17(19)	N3	C7	C10	112.1(4)
C2	N2	Cu1	102.3(3)	C8	C7	C9	107.3(5)
C2	N2	C3	108.7(4)	C10	C7	C8	110.2(5)
C2	N2	C11	112.6(4)	C10	C7	C9	109.1(5)
C3	N2	Cu1	105.8(3)	C28	C29	C24	119.4(5)
C3	N2	C11	112.8(4)	N1	C6	C5	113.3(4)
C11	N2	Cu1	113.9(3)	N3	C4	C3	113.2(4)
C5	N3	Cu1	105.0(3)	C26	C27	C28	120.1(5)
C5	N3	C7	112.6(4)	C27	C26	C25	120.9(5)
C7	N3	Cu1	114.7(3)	N1	C15	C16	111.9(4)
C4	N3	Cu1	102.4(3)	N1	C15	C22	112.5(4)
C4	N3	C5	109.6(4)	C16	C15	C22	109.0(4)
C4	N3	C7	111.8(4)	C29	C28	C27	120.0(5)
C23	N4	Cu1	170.5(4)	N2	C3	C4	113.7(4)
C1	N1	Cu1	105.4(3)	N2	C11	C12	110.0(4)
C1	N1	C6	109.6(4)	N2	C11	C13	108.6(4)
C1	N1	C15	111.7(4)	N2	C11	C14	112.6(4)
C6	N1	Cu1	100.6(3)	C12	C11	C14	108.2(4)
C6	N1	C15	108.5(4)	C13	C11	C12	107.2(4)
C15	N1	Cu1	120.2(3)	C13	C11	C14	110.1(4)
C16	C17	C18	120.8(5)	O1	S1	C30	102.5(3)
C26	C25	C24	118.6(5)	O2	S1	O1	114.9(3)
N2	C2	C1	113.3(4)	O2	S1	O3	115.6(3)
N3	C5	C6	114.3(4)	O2	S1	C30	103.0(3)
C17	C16	C21	118.5(5)	O3	S1	O1	115.1(3)

C17	C16	C15	121.6(5)	O3	S1	C30	103.1(3)
C21	C16	C15	119.9(5)	F1	C30	S1	111.8(4)
C20	C21	C16	120.4(5)	F1	C30	F3	106.8(5)
C25	C24	C23	119.2(5)	F2	C30	S1	111.5(4)
C29	C24	C25	121.0(5)	F2	C30	F1	107.3(5)
C29	C24	C23	119.7(5)	F2	C30	F3	106.9(5)
N4	C23	C24	176.7(5)	F3	C30	S1	112.1(4)
C19	C20	C21	120.5(6)				

Table 6 Torsion Angles for CutBu2sec-PhEttacnNCPhOTf.

A	**B**	**C**	**D**	**Angle/°**	**A**	**B**	**C**	**D**	**Angle/°**
Cu1	N2	C2	C1	-43.5(4)	C23	C24	C29	C28	176.3(5)
Cu1	N2	C3	C4	-21.7(5)	C18	C17	C16	C21	-1.5(8)
Cu1	N2	C11	C12	-50.0(5)	C18	C17	C16	C15	-179.2(5)
Cu1	N2	C11	C13	67.1(4)	C1	N1	C6	C5	65.7(5)
Cu1	N2	C11	C14	-170.7(3)	C1	N1	C15	C16	-46.8(6)
Cu1	N3	C5	C6	-21.6(5)	C1	N1	C15	C22	-169.9(4)
Cu1	N3	C7	C8	64.3(5)	C7	N3	C5	C6	103.9(5)
Cu1	N3	C7	C9	-52.5(5)	C7	N3	C4	C3	-167.4(4)
Cu1	N3	C7	C10	-173.4(3)	C6	N1	C1	C2	-129.5(4)
Cu1	N3	C4	C3	-44.2(4)	C6	N1	C15	C16	-167.7(4)
Cu1	N1	C1	C2	-22.0(5)	C6	N1	C15	C22	69.2(5)
Cu1	N1	C6	C5	-45.1(5)	C4	N3	C5	C6	-131.0(5)
Cu1	N1	C15	C16	77.4(5)	C4	N3	C7	C8	-179.7(4)
Cu1	N1	C15	C22	-45.6(5)	C4	N3	C7	C9	63.5(5)
N2	C2	C1	N1	47.3(6)	C4	N3	C7	C10	-57.4(5)
N3	C5	C6	N1	48.7(6)	C26	C25	C24	C23	-176.6(5)
N3	C4	C3	N2	47.4(6)	C26	C25	C24	C29	0.6(7)
C17	C16	C21	C20	0.0(8)	C26	C27	C28	C29	-0.2(8)
C17	C16	C15	N1	-59.6(6)	C15	N1	C1	C2	110.2(5)
C17	C16	C15	C22	65.5(6)	C15	N1	C6	C5	-172.1(4)
C17	C18	C19	C20	-0.3(8)	C15	C16	C21	C20	177.8(5)
C25	C24	C29	C28	-0.9(7)	C28	C27	C26	C25	-0.1(8)
C2	N2	C3	C4	-130.9(4)	C3	N2	C2	C1	68.0(5)
C2	N2	C11	C12	65.9(5)	C3	N2	C11	C12	-170.5(4)
C2	N2	C11	C13	-177.1(4)	C3	N2	C11	C13	-53.5(5)
C2	N2	C11	C14	-54.8(5)	C3	N2	C11	C14	68.7(5)
C5	N3	C7	C8	-55.7(6)	C11	N2	C2	C1	-166.2(4)
C5	N3	C7	C9	-172.6(4)	C11	N2	C3	C4	103.4(5)
C5	N3	C7	C10	66.6(6)	O1	S1	C30	F1	58.4(5)
C5	N3	C4	C3	66.9(5)	O1	S1	C30	F2	-61.8(4)
C16	C17	C18	C19	1.6(8)	O1	S1	C30	F3	178.3(4)
C16	C21	C20	C19	1.3(8)	O2	S1	C30	F1	-61.2(5)
C21	C16	C15	N1	122.7(5)	O2	S1	C30	F2	178.6(4)
C21	C16	C15	C22	-112.3(5)	O2	S1	C30	F3	58.8(5)
C21	C20	C19	C18	-1.2(8)	O3	S1	C30	F1	178.2(4)
C24	C25	C26	C27	-0.1(7)	O3	S1	C30	F2	58.0(4)
C24	C29	C28	C27	0.7(8)	O3	S1	C30	F3	-61.8(5)

Table 7 Hydrogen Atom Coordinates (Å×10^4) and Isotropic Displacement Parameters (Å^2×10^3) for CutBu2sec-PhEttacnNCPhOTf.

Atom	*x*	*y*	*z*	U(eq)
H17	5087.66	5214.62	5838.81	22
H25	748.78	3761.79	8634.5	20
H2A	5795.81	7732.84	5949.96	20
H2B	5480.07	6791.58	5560.65	20
H5A	6170.66	7050.81	10678.33	22
H5B	6256.68	7572.29	9467.95	22
H12A	3514.62	6422.7	4457.98	29
H12B	1696.15	6518.13	4138.4	29
H12C	2511.92	6019.14	5344.88	29
H21	9680.35	5392.42	6462.32	26
H20	9596.7	5155.76	4370.37	28
H18	5010.95	5035.39	3728.46	26
H19	7277.86	4999.57	2998.75	27
H1A	7787.97	6803	6929.38	20
H1B	7160.85	7387.5	7875.44	20
H22A	7059.53	4711.76	9176.16	32
H22B	7559.53	4196.07	8091.27	32
H22C	5862.51	4554.57	7903.6	32
H29	3245.45	3252.02	6037.48	22
H6A	8044.76	6544.08	9580.79	23
H6B	6866.34	5855.44	9823.63	23
H4A	3857.16	8131.78	9347.46	18
H4B	2474.77	7620.82	8540.46	18
H27	930.87	1433.73	7365.11	23
H26	43.79	2371.77	8632.66	24
H8A	3676.16	5547.15	11383.45	40
H8B	5301.67	5922.29	11293.33	40
H8C	4332.11	5414.19	10155.25	40
H13A	1222.01	6910.53	6646.04	31
H13B	390.89	7340.6	5380.85	31
H13C	1286.69	7888.43	6504.2	31
H15	8551.17	5543.62	8152.9	22
H28	2542.22	1867.25	6067.02	25
H3A	3478.15	8374.27	7146.48	19
H3B	5189.66	8129.9	7786.71	19
H9A	1269.99	6883.03	9417.73	31
H9B	1361.12	6091.83	10292.03	31
H9C	1821.17	6019.46	8970.64	31
H14A	2991.68	8519.01	5179.15	33
H14B	1957.64	8034.9	4045.52	33
H14C	3773.16	7924.56	4336.19	33
H10A	4553.63	7369.82	11677.83	37
H10B	3011.67	6980.52	11942.94	37
H10C	2933.76	7709.48	10957.93	37

Crystal Data for $C_{30}H_{44}CuF_3N_4O_3S$ (*M* =661.29 g/mol): monoclinic, space group $P2_1$ (no. 4), *a* = 8.9545(15) Å, *b* = 16.264(3) Å, *c* = 11.0384(18) Å, *β* = 102.006(3)°, *V* = 1572.4(4) Å^3, *Z* = 2, *T* = 100(2) K, μ(MoKα) = 0.816 mm^{-1}, *Dcalc* = 1.397 g/cm^3, 13943 reflections measured (4.528° ≤ 2Θ ≤ 61.324°), 8349 unique (R_{int} = 0.0475, R_{sigma} = 0.0962) which were used in all calculations. The final R_1 was 0.0583 (I > 2σ(I)) and wR_2 was 0.1283 (all data).

Compound Name: **[Cu(*t*Bu$_2$menthyl)(MeCN)]PF$_6$**

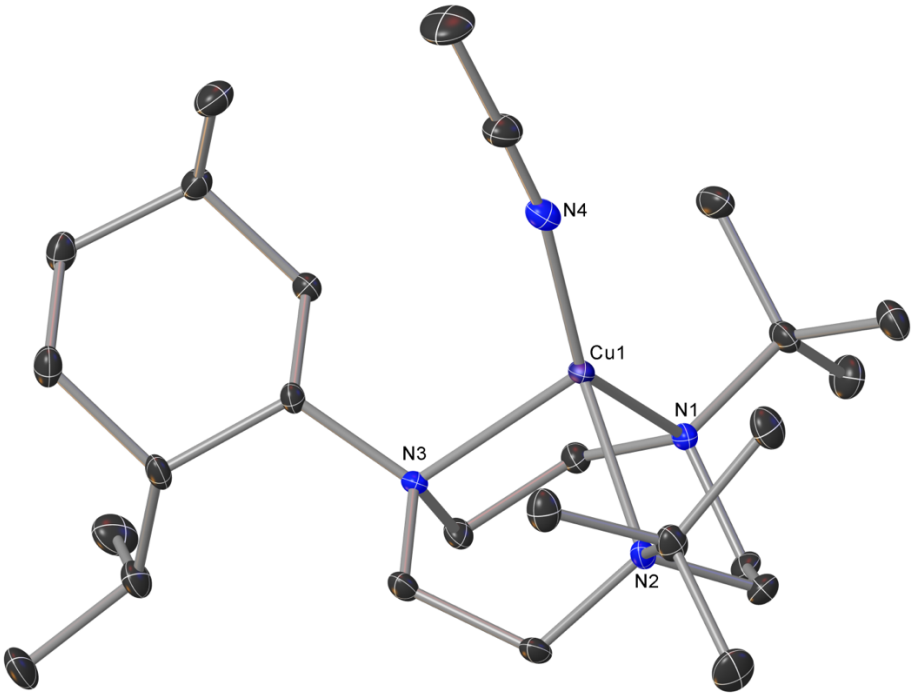

Table 1 Crystal data and structure refinement for **[Cu(*t*Bu$_2$menthyl)(MeCN)]PF$_6$**

Identification code	CutBu2menthyltacnMeCN-PF6
Empirical formula	$C_{26}H_{52}CuF_6N_4P$
Formula weight	629.22
Temperature/K	100.15
Crystal system	orthorhombic
Space group	$P2_12_12_1$
a/Å	11.0432(9)
b/Å	14.3106(12)
c/Å	19.0855(15)
α/°	90
β/°	90
γ/°	90
Volume/Å^3	3016.2(4)
Z	4
ρ_{calc}g/cm^3	1.386
μ/mm^{-1}	0.837
F(000)	1336.0
Crystal size/mm^3	0.771 × 0.406 × 0.32
Radiation	MoKα (λ = 0.71073)
2Θ range for data collection/°	3.558 to 59.146
Index ranges	$-15 \le h \le 15$, $-19 \le k \le 19$, $-26 \le l \le 26$
Reflections collected	38005
Independent reflections	8452 [R_{int} = 0.0496, R_{sigma} = 0.0434]
Data/restraints/parameters	8452/138/353
Goodness-of-fit on F^2	1.022
Final R indexes [I>=2σ (I)]	R_1 = 0.0299, wR_2 = 0.0792
Final R indexes [all data]	R_1 = 0.0327, wR_2 = 0.0806
Largest diff. peak/hole / e Å^{-3}	0.64/-0.40
Flack parameter	0.020(4)

Table 2 Fractional Atomic Coordinates ($\times 10^4$) and Equivalent Isotropic Displacement Parameters ($Å^2 \times 10^3$) for CutBu2menthyltacnMeCN-PF6. U_{eq} is defined as 1/3 of of the trace of the orthogonalised U_{IJ} tensor.

Atom	***x***	***y***	***z***	**U(eq)**
Cu1	4406.5(2)	5707.9(2)	6697.8(2)	8.29(7)
P1	593.6(5)	4413.2(4)	8246.7(3)	17.67(12)
F1	1570.9(16)	4310.4(14)	8856.9(9)	35.3(4)
F2	-396.4(15)	4497.1(14)	7630.2(9)	37.3(4)
F3	-263.2(17)	3682.7(15)	8639.0(10)	40.7(5)
F4	1437.0(17)	5137.4(13)	7832.1(10)	35.1(4)
F5	1227.2(18)	3573.8(13)	7826.5(9)	37.0(4)
F6	-43(2)	5245.6(15)	8651.5(10)	47.9(6)
N1	5765.4(15)	5695.4(12)	5917.2(9)	9.3(3)
N3	3765.5(15)	4414.8(11)	6221.4(9)	8.3(3)
N2	5617.1(17)	4842.6(11)	7301.4(9)	10.2(3)
N4	3224.3(18)	6517.8(13)	7065.7(10)	13.1(4)
C8	1756(2)	3521.8(14)	5986.0(12)	12.3(3)
C12	2162.1(19)	5183.6(14)	5506.4(11)	10.4(3)
C6	5174.7(19)	5155.8(14)	5341.9(11)	11.2(4)
C5	4543.6(19)	4264.2(14)	5596.8(11)	11.2(3)
C18	4312(2)	4751.5(15)	8352.7(12)	16.2(4)
C7	2429.0(19)	4469.3(13)	6079.1(11)	9.1(3)
C17	5560(2)	5026.9(15)	8086.9(11)	13.3(3)
C2	6821(2)	5077.1(15)	7001.4(11)	12.7(4)
C19	5715(2)	6080.8(15)	8217.7(12)	16.4(4)
C1	6802.4(19)	5145.4(14)	6201.6(11)	11.8(4)
C13	342(2)	5979.2(16)	6059.5(13)	16.7(4)
C4	4020(2)	3752.5(14)	6805.7(12)	12.3(4)
C9	389.4(19)	3744.1(15)	5902.9(12)	14.6(4)
C14	2259(2)	2786.1(15)	5463.3(13)	15.9(4)
C11	800.3(19)	5393.3(15)	5447.8(12)	12.6(3)
C22	7007(2)	6651.0(17)	5049.3(13)	18.0(4)
C3	5291(2)	3862.0(14)	7113.6(12)	12.5(4)
C25	2417(2)	6876.2(15)	7321.6(13)	16.3(4)
C23	4988(2)	7216.8(15)	5469.4(14)	17.6(4)
C26	1368(2)	7309.8(19)	7657.4(15)	26.3(6)
C15	2099(2)	2966.3(17)	4674.8(13)	21.3(5)
C20	6553(2)	4493.3(17)	8491.4(13)	20.1(4)
C10	92(2)	4480.7(15)	5347.5(12)	14.6(4)
C21	6137(2)	6667.9(15)	5677.6(12)	12.8(3)
C24	6735(2)	7176.7(15)	6292.2(12)	16.4(4)
C16	1737(2)	1822.1(16)	5633.2(15)	22.6(5)

Table 3 Anisotropic Displacement Parameters ($Å^2 \times 10^3$) for CutBu2menthyltacnMeCN-PF6. The Anisotropic displacement factor exponent takes the form: $-2\pi^2[h^2a^{*2}U_{11}+2hka^*b^*U_{12}+\ldots]$.

Atom	**U_{11}**	**U_{22}**	**U_{33}**	**U_{23}**	**U_{13}**	**U_{12}**
Cu1	7.75(11)	6.2(1)	10.90(12)	-0.80(9)	0.52(10)	0.54(9)
P1	14.9(3)	23.0(3)	15.1(3)	1.8(2)	2.5(2)	1.7(2)
F1	30.3(9)	51.5(10)	24.1(8)	-1.2(8)	-7.8(7)	4.0(8)
F2	20.7(8)	60.6(12)	30.5(9)	10.0(8)	-4.4(7)	0.4(8)
F3	40.7(11)	52.3(11)	29.0(9)	10.8(8)	9.8(8)	-14.5(9)
F4	32.8(10)	36.0(9)	36.5(10)	9.2(8)	1.4(8)	-10.6(8)

F5	46.1(11)	38.0(10)	26.9(9)	-5.1(8)	4.7(8)	15.3(8)
F6	62.8(14)	44.1(11)	36.7(11)	-6.6(9)	11.0(10)	26.6(10)
N1	7.7(7)	7.6(6)	12.7(7)	-0.1(5)	0.8(5)	-0.4(5)
N3	8.1(6)	5.7(7)	11.1(7)	0.3(6)	-0.1(6)	0.5(5)
N2	9.8(7)	7.9(6)	13.0(5)	0.8(5)	-3.8(5)	-1.5(7)
N4	15.7(8)	9.8(8)	14.0(9)	-0.6(6)	-0.3(7)	0.2(7)
C8	13.2(7)	9.2(6)	14.4(8)	2.2(6)	-2.9(7)	-4.5(5)
C12	10.2(7)	8.6(8)	12.4(9)	1.0(6)	-0.2(6)	-0.6(6)
C6	10.3(8)	10.0(7)	13.3(8)	-1.2(6)	0.1(6)	-0.5(6)
C5	11.3(8)	9.0(7)	13.4(9)	-3.1(6)	0.9(7)	-0.8(7)
C18	16.6(7)	18.2(9)	13.7(8)	0.8(8)	-1.7(7)	-4.1(6)
C7	9.1(6)	8.7(7)	9.4(8)	-0.3(6)	-1.2(6)	-2.1(5)
C17	14.6(7)	13.3(6)	12.1(6)	1.2(5)	-3.7(6)	-2.2(5)
C2	8.9(9)	13.2(9)	15.9(10)	0.4(8)	-2.2(8)	1.3(8)
C19	19.9(10)	15.1(6)	14.3(9)	-2.7(6)	-2.6(9)	-4.3(6)
C1	7.0(9)	11.7(9)	16.7(10)	-2.4(8)	0.8(8)	1.8(7)
C13	12.5(10)	19.1(9)	18.6(9)	-1.6(7)	-1.2(8)	3.4(7)
C4	14.0(9)	7.4(8)	15.4(10)	2.1(7)	-3.0(8)	-1.1(7)
C9	12.1(8)	16.1(8)	15.7(9)	2.1(7)	-1.8(7)	-4.8(7)
C14	16.4(9)	11.2(6)	20.3(7)	-3.0(6)	-4.7(7)	-3.2(6)
C11	9.9(7)	13.2(7)	14.7(8)	2.0(6)	-1.7(6)	0.3(6)
C22	13.8(9)	20.5(10)	19.7(9)	1.7(8)	4.4(8)	-3.0(8)
C3	13.8(10)	7.0(8)	16.7(10)	1.4(8)	-4.8(8)	0.9(7)
C25	17.1(10)	13.4(9)	18.6(11)	-2.9(8)	-0.4(8)	2.7(8)
C23	15.3(8)	11.7(9)	25.8(12)	4.8(8)	2.7(8)	0.7(7)
C26	22.7(12)	25.7(13)	30.6(14)	-7.5(11)	6.8(11)	10.4(10)
C15	27.8(12)	16.5(10)	19.5(7)	-5.3(6)	-4.4(8)	0.9(9)
C20	19.6(8)	23.0(9)	17.6(9)	4.0(8)	-8.5(8)	0.2(7)
C10	11.9(8)	17.2(8)	14.8(10)	0.4(7)	-3.2(8)	-2.8(6)
C21	13.0(7)	8.4(6)	17.1(7)	1.0(5)	2.5(6)	-1.8(5)
C24	17.5(10)	12.5(9)	19.1(9)	-1.3(7)	2.2(8)	-4.5(8)
C16	23.9(11)	11.3(6)	32.6(12)	-1.0(7)	-9.5(10)	-6.0(7)

Table 4 Bond Lengths for CutBu2menthyltacnMeCN-PF6.

Atom	**Atom**	**Length/Å**	**Atom**	**Atom**	**Length/Å**
Cu1	N1	2.1146(17)	C8	C7	1.556(3)
Cu1	N3	2.1800(17)	C8	C9	1.551(3)
Cu1	N2	2.1558(18)	C8	C14	1.553(3)
Cu1	N4	1.8817(19)	C12	C7	1.525(3)
P1	F1	1.5945(17)	C12	C11	1.538(3)
P1	F2	1.6107(18)	C6	C5	1.533(3)
P1	F3	1.5963(18)	C18	C17	1.521(3)
P1	F4	1.6025(18)	C17	C19	1.538(3)
P1	F5	1.6050(18)	C17	C20	1.543(3)
P1	F6	1.5845(19)	C2	C1	1.530(3)
N1	C6	1.492(3)	C13	C11	1.524(3)
N1	C1	1.492(3)	C4	C3	1.530(3)
N1	C21	1.521(3)	C9	C10	1.530(3)
N3	C5	1.485(3)	C14	C15	1.537(3)
N3	C7	1.503(3)	C14	C16	1.530(3)
N3	C4	1.490(3)	C11	C10	1.534(3)

N2	C17	1.523(3)	C22	C21	1.537(3)
N2	C2	1.486(3)	C25	C26	1.462(3)
N2	C3	1.492(3)	C23	C21	1.544(3)
N4	C25	1.138(3)	C21	C24	1.531(3)

Table 5 Bond Angles for CutBu2menthyltacnMeCN-PF6.

Atom	**Atom**	**Atom**	**Angle/°**	**Atom**	**Atom**	**Atom**	**Angle/°**
N1	Cu1	N3	85.95(7)	C3	N2	Cu1	105.21(12)
N1	Cu1	N2	86.08(7)	C3	N2	C17	112.91(16)
N2	Cu1	N3	86.37(6)	C25	N4	Cu1	168.75(19)
N4	Cu1	N1	139.51(7)	C9	C8	C7	107.31(17)
N4	Cu1	N3	116.95(8)	C9	C8	C14	114.92(18)
N4	Cu1	N2	125.78(8)	C14	C8	C7	119.56(19)
F1	P1	F2	178.98(11)	C7	C12	C11	111.83(17)
F1	P1	F3	89.90(10)	N1	C6	C5	113.32(17)
F1	P1	F4	91.54(10)	N3	C5	C6	113.39(16)
F1	P1	F5	90.05(10)	N3	C7	C8	116.37(17)
F3	P1	F2	89.37(10)	N3	C7	C12	110.74(17)
F3	P1	F4	178.36(11)	C12	C7	C8	114.19(17)
F3	P1	F5	90.15(11)	N2	C17	C19	108.96(16)
F4	P1	F2	89.17(10)	N2	C17	C20	112.19(19)
F4	P1	F5	89.08(10)	C18	C17	N2	108.71(18)
F5	P1	F2	89.24(10)	C18	C17	C19	107.51(19)
F6	P1	F1	90.79(11)	C18	C17	C20	110.40(18)
F6	P1	F2	89.93(11)	C19	C17	C20	108.97(19)
F6	P1	F3	90.03(12)	N2	C2	C1	112.76(17)
F6	P1	F4	90.72(12)	N1	C1	C2	114.03(17)
F6	P1	F5	179.15(11)	N3	C4	C3	113.29(17)
C6	N1	Cu1	102.27(12)	C10	C9	C8	114.88(18)
C6	N1	C21	111.71(16)	C15	C14	C8	118.30(19)
C1	N1	Cu1	107.03(12)	C16	C14	C8	109.9(2)
C1	N1	C6	109.28(16)	C16	C14	C15	108.4(2)
C1	N1	C21	112.65(16)	C13	C11	C12	112.13(18)
C21	N1	Cu1	113.29(12)	C13	C11	C10	113.24(19)
C5	N3	Cu1	105.67(12)	C10	C11	C12	109.96(17)
C5	N3	C7	115.51(16)	N2	C3	C4	114.18(16)
C5	N3	C4	113.53(16)	N4	C25	C26	178.3(3)
C7	N3	Cu1	110.50(12)	C9	C10	C11	113.00(18)
C4	N3	Cu1	99.59(12)	N1	C21	C22	112.87(17)
C4	N3	C7	110.70(16)	N1	C21	C23	108.74(17)
C17	N2	Cu1	113.63(13)	N1	C21	C24	108.73(18)
C2	N2	Cu1	102.66(12)	C22	C21	C23	108.73(19)
C2	N2	C17	112.14(17)	C24	C21	C22	109.59(18)
C2	N2	C3	109.59(17)	C24	C21	C23	108.06(18)

Table 6 Torsion Angles for CutBu2menthyltacnMeCN-PF6.

A	**B**	**C**	**D**	**Angle/°**	**A**	**B**	**C**	**D**	**Angle/°**
Cu1	N1	C6	C5	-46.00(18)	C7	C8	C14	C16	161.0(2)
Cu1	N1	C1	C2	-21.6(2)	C7	C12	C11	C13	72.7(2)

Cu1	N1	C21	C22	-172.95(14)	C7	C12	C11	C10	-54.3(2)
Cu1	N1	C21	C23	-52.2(2)	C17	N2	C2	C1	-164.86(17)
Cu1	N1	C21	C24	65.23(19)	C17	N2	C3	C4	103.7(2)
Cu1	N3	C5	C6	-20.28(19)	C2	N2	C17	C18	-178.89(17)
Cu1	N3	C7	C8	-159.62(14)	C2	N2	C17	C19	64.2(2)
Cu1	N3	C7	C12	67.78(18)	C2	N2	C17	C20	-56.5(2)
Cu1	N3	C4	C3	-47.59(18)	C2	N2	C3	C4	-130.56(19)
Cu1	N2	C17	C18	65.24(18)	C1	N1	C6	C5	67.2(2)
Cu1	N2	C17	C19	-51.6(2)	C1	N1	C21	C22	65.4(2)
Cu1	N2	C17	C20	-172.39(14)	C1	N1	C21	C23	-173.88(18)
Cu1	N2	C2	C1	-42.52(19)	C1	N1	C21	C24	-56.4(2)
Cu1	N2	C3	C4	-20.8(2)	C13	C11	C10	C9	-73.9(2)
N1	Cu1	N4	C25	156.1(10)	C4	N3	C5	C6	-128.38(18)
N1	C6	C5	N3	47.5(2)	C4	N3	C7	C8	-50.3(2)
N3	Cu1	N4	C25	37.8(10)	C4	N3	C7	C12	177.14(16)
N3	C4	C3	N2	50.3(3)	C9	C8	C7	N3	175.73(17)
N2	Cu1	N4	C25	-68.4(10)	C9	C8	C7	C12	-53.3(2)
N2	C2	C1	N1	46.0(2)	C9	C8	C14	C15	56.0(3)
C8	C9	C10	C11	-53.3(3)	C9	C8	C14	C16	-69.2(2)
C12	C11	C10	C9	52.4(2)	C14	C8	C7	N3	-51.1(3)
C6	N1	C1	C2	-131.61(18)	C14	C8	C7	C12	79.9(2)
C6	N1	C21	C22	-58.1(2)	C14	C8	C9	C10	-84.5(2)
C6	N1	C21	C23	62.7(2)	C11	C12	C7	N3	-169.01(17)
C6	N1	C21	C24	-179.90(17)	C11	C12	C7	C8	57.3(2)
C5	N3	C7	C8	80.5(2)	C3	N2	C17	C18	-54.5(2)
C5	N3	C7	C12	-52.1(2)	C3	N2	C17	C19	-171.37(18)
C5	N3	C4	C3	64.3(2)	C3	N2	C17	C20	67.9(2)
C7	N3	C5	C6	102.2(2)	C3	N2	C2	C1	68.9(2)
C7	N3	C4	C3	-163.91(17)	C21	N1	C6	C5	-167.48(17)
C7	C8	C9	C10	51.1(2)	C21	N1	C1	C2	103.6(2)
C7	C8	C14	C15	-73.8(3)					

Table 7 Hydrogen Atom Coordinates (Å×10^4) and Isotropic Displacement Parameters (Å^2×10^3) for CutBu2menthyltacnMeCN-PF6.

Atom	***x***	***y***	***z***	**U(eq)**
H8	1819.33	3212.9	6454.59	15
H12A	2460.18	4942.1	5051.93	12
H12B	2602.58	5770	5610.17	12
H6A	5795.43	4984.71	4990.3	13
H6B	4571	5560.49	5107.51	13
H5A	4039.98	4011.52	5211.8	13
H5B	5166.48	3790.78	5711.53	13
H18A	3690.74	5046.62	8060.58	24
H18B	4218.12	4959.58	8838.86	24
H18C	4223.75	4070.77	8330	24
H7	2075.38	4746.54	6514.41	11
H2A	7411.94	4592.22	7142.97	15
H2B	7096.76	5680.97	7197.79	15
H19A	6518.11	6278.86	8056.88	25
H19B	5635.4	6209.78	8719.86	25
H19C	5091.27	6425.25	7959.69	25

H1A	7567.51	5436.89	6042.52	14
H1B	6770.19	4506.25	6004.05	14
H13A	444.63	5629.72	6497.03	25
H13B	-518.18	6121.66	5990.41	25
H13C	803.35	6563.08	6084.46	25
H4A	3922.64	3104.96	6632.02	15
H4B	3416.77	3852.2	7182.02	15
H9A	-41.37	3159.2	5782.14	18
H9B	72.83	3961.58	6360.02	18
H14	3150.65	2746.25	5549.94	19
H11	682.86	5773.13	5013.28	15
H22A	7734.11	6294.26	5172.49	27
H22B	7236.35	7291.96	4926.51	27
H22C	6605.94	6355.92	4648.24	27
H3A	5354.2	3468.71	7538.77	15
H3B	5887.99	3625.28	6769.42	15
H23A	4685.24	6984.69	5019.17	26
H23B	5184.36	7882.22	5427.57	26
H23C	4364.71	7131.73	5829.45	26
H26A	809.69	7539.28	7297.3	39
H26B	1637.36	7833.51	7949.28	39
H26C	954.11	6847.32	7950.69	39
H15A	1238.79	2926.24	4553.18	32
H15B	2553.41	2496.85	4408.87	32
H15C	2404.18	3590.87	4559.59	32
H20A	6482.01	3823.09	8394.31	30
H20B	6454.62	4602.93	8995.09	30
H20C	7351.41	4715.03	8341.81	30
H10A	-785.71	4618.77	5364.08	18
H10B	277.21	4222.66	4878.33	18
H24A	6181.18	7182.89	6693.3	25
H24B	6923.55	7820.24	6154.6	25
H24C	7484.03	6852.69	6422.18	25
H16A	1800.41	1706.88	6138.06	34
H16B	2192.44	1342.36	5378.5	34
H16C	884.55	1799.55	5491.97	34

Crystal Data for $C_{26}H_{52}CuF_6N_4P$ (M =629.22 g/mol): orthorhombic, space group $P2_12_12_1$ (no. 19), a = 11.0432(9) Å, b = 14.3106(12) Å, c = 19.0855(15) Å, V = 3016.2(4) Å^3, Z = 4, T = 100.15 K, μ(MoKα) = 0.837 mm^{-1}, *Dcalc* = 1.386 g/cm^3, 38005 reflections measured (3.558° ≤ 2Θ ≤ 59.146°), 8452 unique (R_{int} = 0.0496, R_{sigma} = 0.0434) which were used in all calculations. The final R_1 was 0.0299 (I > 2σ(I)) and wR_2 was 0.0806 (all data).

Compound Name: ***exo*-bornyl$_2$*t*Butacn**

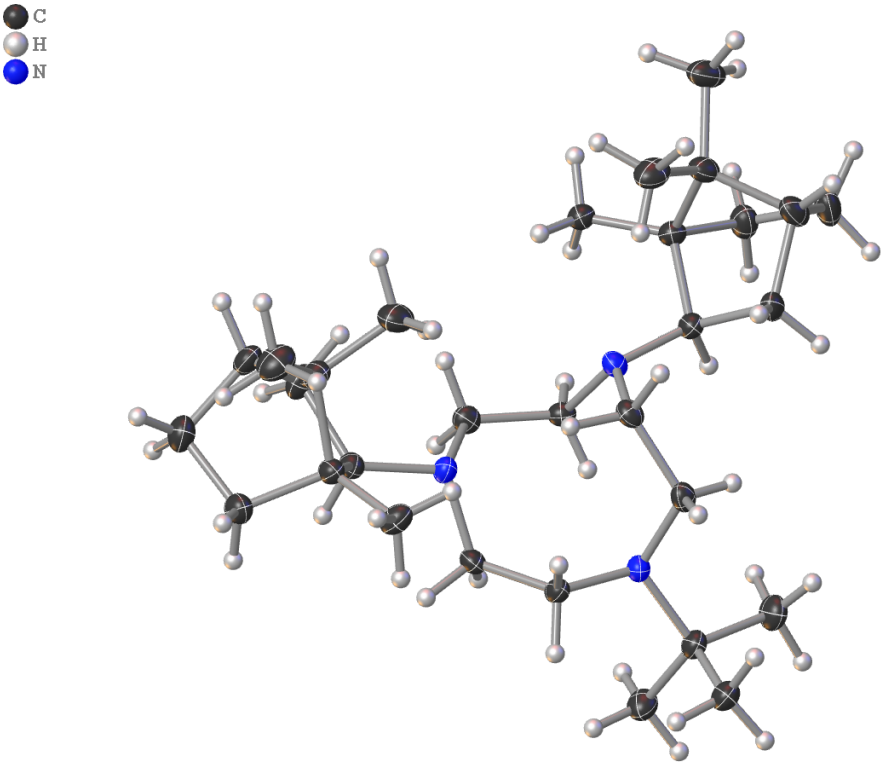

Table 1 Crystal data and structure refinement for cu_A033.

Identification code	cu_A033
Empirical formula	$C_{30}H_{55}N_3$
Formula weight	457.77
Temperature/K	100(2)
Crystal system	orthorhombic
Space group	$P2_12_12_1$
a/Å	10.5142(2)
b/Å	13.3805(2)
c/Å	19.6893(3)
α/°	90
β/°	90
γ/°	90
Volume/Å^3	2769.99(8)
Z	4
ρ_{calc}g/cm^3	1.098
μ/mm^{-1}	0.470
F(000)	1024.0
Crystal size/mm^3	0.3 × 0.2 × 0.2
Radiation	CuKα (λ = 1.54178)
2Θ range for data collection/°	7.988 to 130.138
Index ranges	$-12 \leq h \leq 12$, $-15 \leq k \leq 15$, $-23 \leq l \leq 22$
Reflections collected	18900
Independent reflections	4692 [R_{int} = 0.0707, R_{sigma} = 0.0420]
Data/restraints/parameters	4692/0/339
Goodness-of-fit on F^2	1.043
Final R indexes [I>=2σ (I)]	R_1 = 0.0424, wR_2 = 0.1118

Final R indexes [all data]	R_1 = 0.0460, wR_2 = 0.1143
Largest diff. peak/hole / e Å^{-3}	0.24/-0.19
Flack parameter	-0.1(2)

Table 2 Fractional Atomic Coordinates (×10^4) and Equivalent Isotropic Displacement Parameters (Å^2×10^3) for cu_A033. U_{eq} is defined as 1/3 of of the trace of the orthogonalised U_{IJ} tensor.

Atom	*x*	*y*	*z*	U(eq)
N(2)	-7251.5(18)	-2974.1(14)	-3275.4(9)	18.6(4)
N(1)	-9782.2(18)	-4061.7(13)	-3680.2(9)	17.9(4)
N(3)	-9330.2(18)	-1647.5(14)	-4046.4(9)	19.0(4)
C(3)	-7453(2)	-2801.4(18)	-4005.9(11)	19.8(5)
C(2)	-8460(2)	-2971.3(17)	-2898.2(11)	17.9(5)
C(1)	-9254(2)	-3902.7(17)	-2996.2(11)	20.5(5)
C(7)	-10446(2)	-5035.8(16)	-3756.8(12)	19.7(5)
C(26)	-6179(2)	-3769.8(17)	-1994.3(11)	21.1(5)
C(17)	-6298(2)	-2347.6(17)	-2924.7(11)	19.7(5)
C(00A)	-9906(3)	-268.0(18)	-4867.6(12)	25.9(5)
C(6)	-10640(2)	-3232.4(17)	-3872.2(12)	19.8(5)
C(16)	-10223(3)	-4808.7(17)	-5082.1(11)	24.5(5)
C(00D)	-9814(2)	-605.9(16)	-4124.3(12)	21.4(5)
C(12)	-9983(3)	-5921.3(17)	-3297.4(12)	27.4(6)
C(18)	-5506(2)	-2931.8(17)	-2369.6(11)	20.0(5)
C(4)	-7991(2)	-1793.3(18)	-4228.8(12)	20.4(5)
C(5)	-10136(2)	-2417.7(16)	-4355.7(11)	18.8(5)
C(00I)	-11127(2)	-536.3(18)	-3787.6(13)	27.6(6)
C(00J)	-8934(3)	110.4(18)	-3739.9(13)	28.5(6)
C(8)	-10381(2)	-5515.2(17)	-4487.1(12)	20.3(5)
C(22)	-5218(2)	-1888.9(18)	-3371.1(12)	24.1(5)
C(23)	-4282(2)	-3249.9(18)	-2765.1(12)	25.2(5)
C(24)	-4505(3)	-3986.7(19)	-3348.3(13)	30.3(6)
C(9)	-11580(2)	-6174.4(18)	-4529.2(13)	26.2(6)
C(15)	-7996(2)	-5888(2)	-4308.8(15)	33.0(6)
C(19)	-4975(3)	-2109.0(19)	-1899.2(12)	26.9(5)
C(13)	-9321(2)	-6324.0(18)	-4416.8(12)	24.7(5)
C(14)	-9234(3)	-7053(2)	-5020.4(13)	34.7(6)
C(11)	-9935(3)	-6803.2(17)	-3786.4(12)	25.4(5)
C(25)	-3238(3)	-3704(2)	-2318.5(15)	35.3(6)
C(21)	-3990(2)	-2180(2)	-2999.7(13)	27.8(6)
C(10)	-11298(3)	-7035.1(19)	-4026.5(13)	30.7(6)
C(20)	-3934(3)	-1591(2)	-2336.2(14)	34.4(6)

Table 3 Anisotropic Displacement Parameters (Å^2×10^3) for cu_A033. The Anisotropic displacement factor exponent takes the form: $-2\pi^2[h^2a^{*2}U_{11}+2hka^*b^*U_{12}+\ldots]$.

Atom	U_{11}	U_{22}	U_{33}	U_{23}	U_{13}	U_{12}
N(2)	14.7(9)	19.7(9)	21.4(9)	-0.1(8)	0.0(7)	-1.3(8)
N(1)	19.3(10)	14.2(9)	20.3(9)	0.3(7)	-1.5(8)	-1.3(8)
N(3)	17(1)	15.5(9)	24.4(10)	0.2(7)	-0.8(8)	-2.0(8)
C(3)	15.4(12)	23.3(12)	20.8(11)	-2.4(9)	2.7(9)	-0.7(10)
C(2)	17.8(12)	18.4(11)	17.6(11)	-0.3(9)	-0.5(9)	2.8(9)
C(1)	20.8(12)	22.6(11)	18.0(11)	2.3(9)	0.7(9)	-0.6(10)

C(7)	16.1(11)	17.3(11)	25.7(12)	-0.7(9)	1.5(9)	0.1(9)
C(26)	19.6(12)	18.5(11)	25.1(11)	2.8(9)	-1.1(9)	1.2(10)
C(17)	18.7(12)	15.9(11)	24.5(11)	0.4(9)	-1.1(9)	0.2(9)
C(00A)	27.0(13)	17.9(11)	33.0(13)	2.8(10)	-2.1(11)	0.4(10)
C(6)	13.7(11)	20.5(12)	25.3(12)	-0.3(9)	-1.2(9)	-0.6(9)
C(16)	33.2(14)	18.9(11)	21.5(11)	-0.6(9)	-2.6(10)	3.6(11)
C(00D)	23.2(12)	15.2(11)	25.8(11)	0.2(9)	-1.2(10)	-1.2(10)
C(12)	37.3(14)	20.6(12)	24.3(12)	4.8(10)	-0.2(11)	-2.8(11)
C(18)	18.5(12)	19.0(11)	22.6(11)	2.3(9)	-1.6(9)	1.4(9)
C(4)	18.8(12)	22.1(12)	20.4(12)	2.8(9)	1.0(9)	-4.6(10)
C(5)	18.9(11)	14.6(10)	22.9(10)	-0.1(9)	-3.4(9)	0.1(9)
C(00I)	25.7(13)	20.5(12)	36.4(14)	-0.9(10)	5.1(11)	2.6(10)
C(00J)	31.9(14)	19.7(12)	33.8(13)	-5(1)	-2.3(12)	-4.4(10)
C(8)	18.7(12)	17.0(11)	25.3(12)	-0.1(9)	-3.0(9)	0.3(9)
C(22)	21.0(12)	21.4(11)	29.9(12)	7.4(10)	-3(1)	-5.3(10)
C(23)	15.8(12)	28.3(13)	31.4(13)	5.8(10)	1.2(10)	2.7(10)
C(24)	27.3(14)	28.5(13)	35.2(13)	2.2(11)	7.8(11)	8.2(11)
C(9)	24.3(13)	21.9(12)	32.5(13)	-0.6(10)	-5.4(10)	-2.7(10)
C(15)	21.8(14)	35.3(14)	41.9(14)	5.6(12)	1.1(11)	5.5(12)
C(19)	28.1(14)	24.7(12)	28.0(12)	0.5(10)	-4.6(11)	-6.3(11)
C(13)	26.1(13)	19.5(11)	28.3(12)	1.4(9)	0.5(10)	4.6(10)
C(14)	42.2(17)	26.8(13)	35.1(14)	-2.9(12)	5.6(12)	8.4(13)
C(11)	31.2(13)	16.0(11)	28.9(12)	5.5(10)	-3.5(11)	0.7(10)
C(25)	21.2(13)	43.4(16)	41.2(15)	13.8(13)	0.4(12)	6.3(13)
C(21)	17.7(12)	34.7(14)	31.0(13)	8.8(11)	0.2(10)	-3.9(11)
C(10)	33.4(15)	21.4(12)	37.3(14)	2.3(11)	-0.3(12)	-6.0(11)
C(20)	30.5(15)	32.0(14)	40.8(14)	5.5(12)	-6.9(12)	-14.6(12)

Table 4 Bond Lengths for cu_A033.

Atom	Atom	Length/Å	Atom	Atom	Length/Å
N(2)	C(3)	1.472(3)	C(00D)	C(00I)	1.534(3)
N(2)	C(2)	1.472(3)	C(00D)	C(00J)	1.532(3)
N(2)	C(17)	1.478(3)	C(12)	C(11)	1.524(3)
N(1)	C(1)	1.472(3)	C(18)	C(23)	1.564(3)
N(1)	C(7)	1.486(3)	C(18)	C(19)	1.544(3)
N(1)	C(6)	1.479(3)	C(8)	C(9)	1.541(3)
N(3)	C(00D)	1.492(3)	C(8)	C(13)	1.559(3)
N(3)	C(4)	1.466(3)	C(22)	C(21)	1.533(3)
N(3)	C(5)	1.467(3)	C(23)	C(24)	1.531(4)
C(3)	C(4)	1.527(3)	C(23)	C(25)	1.532(3)
C(2)	C(1)	1.512(3)	C(23)	C(21)	1.535(3)
C(7)	C(12)	1.568(3)	C(9)	C(10)	1.547(3)
C(7)	C(8)	1.576(3)	C(15)	C(13)	1.525(4)
C(26)	C(18)	1.518(3)	C(19)	C(20)	1.555(3)
C(17)	C(18)	1.581(3)	C(13)	C(14)	1.540(3)
C(17)	C(22)	1.562(3)	C(13)	C(11)	1.539(3)
C(00A)	C(00D)	1.535(3)	C(11)	C(10)	1.541(4)
C(6)	C(5)	1.541(3)	C(21)	C(20)	1.527(4)
C(16)	C(8)	1.514(3)			

Table 5 Bond Angles for cu_A033.

Atom	Atom	Atom	Angle/°	Atom	Atom	Atom	Angle/°
C(3)	N(2)	C(17)	117.72(18)	N(3)	C(4)	C(3)	113.76(18)
C(2)	N(2)	C(3)	111.60(18)	N(3)	C(5)	C(6)	116.05(18)
C(2)	N(2)	C(17)	110.39(17)	C(16)	C(8)	C(7)	117.16(18)
C(1)	N(1)	C(7)	113.37(17)	C(16)	C(8)	C(9)	113.9(2)
C(1)	N(1)	C(6)	110.82(17)	C(16)	C(8)	C(13)	115.1(2)
C(6)	N(1)	C(7)	110.22(17)	C(9)	C(8)	C(7)	104.26(19)
C(4)	N(3)	C(00D)	115.25(18)	C(9)	C(8)	C(13)	101.08(18)
C(4)	N(3)	C(5)	111.08(18)	C(13)	C(8)	C(7)	103.45(17)
C(5)	N(3)	C(00D)	114.65(18)	C(21)	C(22)	C(17)	104.12(18)
N(2)	C(3)	C(4)	118.22(19)	C(24)	C(23)	C(18)	115.0(2)
N(2)	C(2)	C(1)	114.21(18)	C(24)	C(23)	C(25)	106.6(2)
N(1)	C(1)	C(2)	116.35(18)	C(24)	C(23)	C(21)	113.9(2)
N(1)	C(7)	C(12)	117.27(19)	C(25)	C(23)	C(18)	114.3(2)
N(1)	C(7)	C(8)	115.41(18)	C(25)	C(23)	C(21)	113.5(2)
C(12)	C(7)	C(8)	101.84(17)	C(21)	C(23)	C(18)	93.47(18)
N(2)	C(17)	C(18)	113.56(18)	C(8)	C(9)	C(10)	103.55(19)
N(2)	C(17)	C(22)	116.95(18)	C(18)	C(19)	C(20)	103.93(19)
C(22)	C(17)	C(18)	101.56(18)	C(15)	C(13)	C(8)	113.5(2)
N(1)	C(6)	C(5)	118.61(19)	C(15)	C(13)	C(14)	107.2(2)
N(3)	C(00D)	C(00A)	113.25(19)	C(15)	C(13)	C(11)	115.4(2)
N(3)	C(00D)	C(00I)	108.60(19)	C(14)	C(13)	C(8)	114.4(2)
N(3)	C(00D)	C(00J)	109.15(19)	C(11)	C(13)	C(8)	93.52(19)
C(00I)	C(00D)	C(00A)	109.7(2)	C(11)	C(13)	C(14)	112.6(2)
C(00J)	C(00D)	C(00A)	108.97(19)	C(12)	C(11)	C(13)	101.59(18)
C(00J)	C(00D)	C(00I)	107.0(2)	C(12)	C(11)	C(10)	108.6(2)
C(11)	C(12)	C(7)	103.36(18)	C(13)	C(11)	C(10)	103.07(19)
C(26)	C(18)	C(17)	117.16(19)	C(22)	C(21)	C(23)	102.2(2)
C(26)	C(18)	C(23)	115.17(19)	C(20)	C(21)	C(22)	108.0(2)
C(26)	C(18)	C(19)	113.81(19)	C(20)	C(21)	C(23)	103.39(19)
C(23)	C(18)	C(17)	102.93(17)	C(11)	C(10)	C(9)	103.0(2)
C(19)	C(18)	C(17)	104.65(18)	C(21)	C(20)	C(19)	102.5(2)
C(19)	C(18)	C(23)	101.22(19)				

Table 6 Torsion Angles for cu_A033.

A	B	C	D	Angle/°	A	B	C	D	Angle/°
N(2)	C(3)	C(4)	N(3)	-70.4(3)	C(16)	C(8)	C(13)	C(11)	-179.06(19)
N(2)	C(2)	C(1)	N(1)	-67.1(3)	C(00D)	N(3)	C(4)	C(3)	167.88(19)
N(2)	C(17)	C(18)	C(26)	-32.2(3)	C(00D)	N(3)	C(5)	C(6)	-121.3(2)
N(2)	C(17)	C(18)	C(23)	95.3(2)	C(12)	C(7)	C(8)	C(16)	-155.1(2)
N(2)	C(17)	C(18)	C(19)	-159.29(19)	C(12)	C(7)	C(8)	C(9)	78.0(2)
N(2)	C(17)	C(22)	C(21)	-128.6(2)	C(12)	C(7)	C(8)	C(13)	-27.4(2)
N(1)	C(7)	C(12)	C(11)	-136.0(2)	C(12)	C(11)	C(10)	C(9)	74.3(2)
N(1)	C(7)	C(8)	C(16)	-27.0(3)	C(18)	C(17)	C(22)	C(21)	-4.4(2)
N(1)	C(7)	C(8)	C(9)	-153.87(19)	C(18)	C(23)	C(21)	C(22)	-56.6(2)
N(1)	C(7)	C(8)	C(13)	100.8(2)	C(18)	C(23)	C(21)	C(20)	55.6(2)
N(1)	C(6)	C(5)	N(3)	-79.7(3)	C(18)	C(19)	C(20)	C(21)	-0.3(3)
C(3)	N(2)	C(2)	C(1)	74.6(2)	C(4)	N(3)	C(00D)	C(00A)	68.7(3)
C(3)	N(2)	C(17)	C(18)	-142.4(2)	C(4)	N(3)	C(00D)	C(00I)	-169.18(19)
C(3)	N(2)	C(17)	C(22)	-24.6(3)	C(4)	N(3)	C(00D)	C(00J)	-52.9(3)

C(2)	N(2)	C(3)	C(4)	64.6(3)	C(4)	N(3)	C(5)	C(6)	105.9(2)
C(2)	N(2)	C(17)	C(18)	87.9(2)	C(5)	N(3)	C(00D)	C(00A)	-62.1(3)
C(2)	N(2)	C(17)	C(22)	-154.31(19)	C(5)	N(3)	C(00D)	C(00I)	60.0(2)
C(1)	N(1)	C(7)	C(12)	-28.5(3)	C(5)	N(3)	C(00D)	C(00J)	176.28(19)
C(1)	N(1)	C(7)	C(8)	-148.49(19)	C(5)	N(3)	C(4)	C(3)	-59.6(2)
C(1)	N(1)	C(6)	C(5)	101.5(2)	C(8)	C(7)	C(12)	C(11)	-9.0(2)
C(7)	N(1)	C(1)	C(2)	174.51(18)	C(8)	C(9)	C(10)	C(11)	-3.3(2)
C(7)	N(1)	C(6)	C(5)	-132.2(2)	C(8)	C(13)	C(11)	C(12)	-58.0(2)
C(7)	C(12)	C(11)	C(13)	43.1(2)	C(8)	C(13)	C(11)	C(10)	54.4(2)
C(7)	C(12)	C(11)	C(10)	-65.2(2)	C(22)	C(17)	C(18)	C(26)	-158.6(2)
C(7)	C(8)	C(9)	C(10)	-69.5(2)	C(22)	C(17)	C(18)	C(23)	-31.2(2)
C(7)	C(8)	C(13)	C(15)	-67.9(3)	C(22)	C(17)	C(18)	C(19)	74.3(2)
C(7)	C(8)	C(13)	C(14)	168.7(2)	C(22)	C(21)	C(20)	C(19)	72.3(2)
C(7)	C(8)	C(13)	C(11)	51.9(2)	C(23)	C(18)	C(19)	C(20)	34.9(2)
C(26)	C(18)	C(23)	C(24)	63.8(3)	C(23)	C(21)	C(20)	C(19)	-35.6(3)
C(26)	C(18)	C(23)	C(25)	-59.9(3)	C(24)	C(23)	C(21)	C(22)	62.8(3)
C(26)	C(18)	C(23)	C(21)	-177.7(2)	C(24)	C(23)	C(21)	C(20)	175.0(2)
C(26)	C(18)	C(19)	C(20)	159.1(2)	C(9)	C(8)	C(13)	C(15)	-175.6(2)
C(17)	N(2)	C(3)	C(4)	-64.5(3)	C(9)	C(8)	C(13)	C(14)	60.9(3)
C(17)	N(2)	C(2)	C(1)	-152.53(18)	C(9)	C(8)	C(13)	C(11)	-55.9(2)
C(17)	C(18)	C(23)	C(24)	-64.9(2)	C(15)	C(13)	C(11)	C(12)	60.2(3)
C(17)	C(18)	C(23)	C(25)	171.4(2)	C(15)	C(13)	C(11)	C(10)	172.6(2)
C(17)	C(18)	C(23)	C(21)	53.6(2)	C(19)	C(18)	C(23)	C(24)	-172.94(19)
C(17)	C(18)	C(19)	C(20)	-71.8(2)	C(19)	C(18)	C(23)	C(25)	63.3(3)
C(17)	C(22)	C(21)	C(23)	39.4(2)	C(19)	C(18)	C(23)	C(21)	-54.5(2)
C(17)	C(22)	C(21)	C(20)	-69.3(2)	C(13)	C(8)	C(9)	C(10)	37.6(2)
C(6)	N(1)	C(1)	C(2)	-60.9(2)	C(13)	C(11)	C(10)	C(9)	-32.9(2)
C(6)	N(1)	C(7)	C(12)	-153.3(2)	C(14)	C(13)	C(11)	C(12)	-176.4(2)
C(6)	N(1)	C(7)	C(8)	86.6(2)	C(14)	C(13)	C(11)	C(10)	-63.9(3)
C(16)	C(8)	C(9)	C(10)	161.6(2)	C(25)	C(23)	C(21)	C(22)	-175.0(2)
C(16)	C(8)	C(13)	C(15)	61.2(3)	C(25)	C(23)	C(21)	C(20)	-62.9(3)
C(16)	C(8)	C(13)	C(14)	-62.3(3)					

Table 7 Hydrogen Atom Coordinates (Å×10^4) and Isotropic Displacement Parameters (Å^2×10^3) for cu_A033.

Atom	*x*	*y*	*z*	U(eq)
H(1A)	-8735	-4477	-2881	25
H(1B)	-9955	-3882	-2676	25
H(7)	-11346	-4922	-3652	24
H(26A)	-6802	-3492	-1692	32
H(26B)	-5569	-4147	-1738	32
H(26C)	-6592	-4201	-2316	32
H(17)	-6747	-1798	-2699	24
H(00A)	-9095	-351	-5084	39
H(00B)	-10150	423	-4884	39
H(00C)	-10532	-665	-5099	39
H(16A)	-10929	-4355	-5097	37
H(16B)	-10191	-5186	-5497	37
H(16C)	-9447	-4438	-5030	37
H(12A)	-9149	-5784	-3108	33
H(12B)	-10577	-6046	-2930	33

H(5A)	−9655	−2741	−4714	23
H(5B)	−10859	−2091	−4566	23
H(00D)	−11717	−955	−4027	41
H(00E)	−11419	143	−3801	41
H(00F)	−11067	−754	−3324	41
H(00G)	−8777	−147	−3293	43
H(00H)	−9331	755	−3706	43
H(00I)	−8143	172	−3980	43
H(22A)	−5233	−2166	−3826	29
H(22B)	−5302	−1168	−3400	29
H(24A)	−4624	−4646	−3167	45
H(24B)	−3781	−3984	−3645	45
H(24C)	−5249	−3792	−3598	45
H(9A)	−11704	−6428	−4986	31
H(9B)	−12331	−5804	−4393	31
H(15A)	−7679	−5631	−4731	49
H(15B)	−7436	−6401	−4146	49
H(15C)	−8039	−5357	−3981	49
H(19A)	−4611	−2396	−1491	32
H(19B)	−5635	−1639	−1772	32
H(14A)	−10049	−7357	−5095	52
H(14B)	−8617	−7562	−4922	52
H(14C)	−8981	−6694	−5420	52
H(11)	−9474	−7385	−3611	30
H(25A)	−3081	−3272	−1938	53
H(25B)	−2472	−3775	−2579	53
H(25C)	−3506	−4347	−2158	53
H(21)	−3222	−2122	−3279	33
H(10A)	−11890	−7030	−3649	37
H(10B)	−11339	−7679	−4251	37
H(20A)	−4130	−891	−2409	41
H(20B)	−3103	−1646	−2125	41
H(2A)	−8910(20)	−2383(19)	−3008(11)	13(6)
H(2B)	−8230(30)	−2958(18)	−2421(13)	16(6)
H(6A)	−11380(30)	−3531(19)	−4091(13)	20(7)
H(6B)	−10980(30)	−2880(20)	−3468(13)	23(6)
H(4A)	−7510(30)	−1320(20)	−4012(13)	23(7)
H(3A)	−6620(30)	−2883(18)	−4217(12)	17(6)
H(4B)	−7890(30)	−1747(19)	−4731(13)	18(6)
H(3B)	−8030(30)	−3360(20)	−4161(13)	24(7)

Crystal Data for $C_{30}H_{55}N_3$ (M =457.77 g/mol): orthorhombic, space group $P2_12_12_1$ (no. 19), a = 10.5142(2) Å, b = 13.3805(2) Å, c = 19.6893(3) Å, V = 2769.99(8) Å^3, Z = 4, T = 100(2) K, μ(CuKα) = 0.470 mm^{-1}, *Dcalc* = 1.098 g/cm^3, 18900 reflections measured (7.988° ≤ 2Θ ≤ 130.138°), 4692 unique (R_{int} = 0.0707, R_{sigma} = 0.0420) which were used in all calculations. The final R_1 was 0.0424 (I > 2σ(I)) and wR_2 was 0.1143 (all data).

Compound Name: **[Cu(*t*Bu$_2$Htacn)(MeCN)]PF**

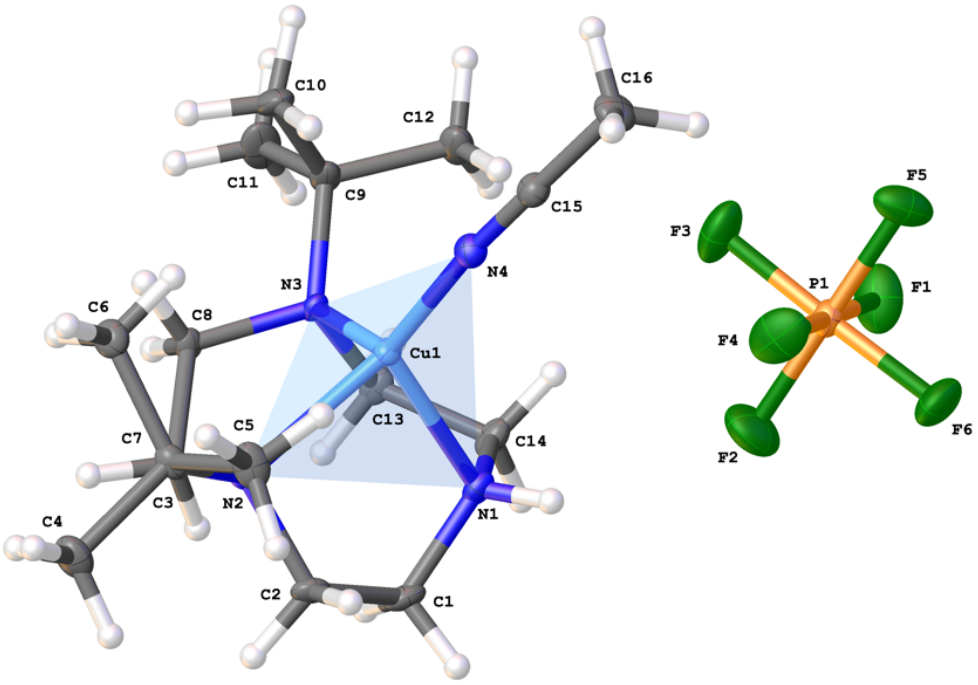

Crystal data and structure refinement for [Cu(*t*Bu$_2$Htacn)(MeCN)]PF

Formula	$C_{16}H_{34}CuF_6N_4P$	V/Å^3	2146.4(4)
$D_{calc.}$/ g cm^{-3}	1.519	Z	4
μ/mm^{-1}	1.152	Z'	1
Formula Weight	490.98	Θ_{min}/°	1.84
Colour	colorless	Θ_{max}/°	30.513
Shape	prism	Measured Refl.	9886
Max Size/mm	0.76	Independent Refl.	6165
Mid Size/mm	0.3	Reflections Used	5772
Min Size/mm	0.25	R_{int}	0.0254
T/K	100(2)	Parameters	265
Crystal System	orthorhombic	Restraints	1
Flack Parameter	0.578(11)	Largest Peak	0.656
Hooft Parameter	0.572(6)	Deepest Hole	-0.595
Space Group	$P2_12_12_1$	GooF	1.055
a/Å	8.3173(9)	wR_2 (all data)	0.085
b/Å	13.6535(15)	wR_2	0.0823
c/Å	18.901(2)	R_1 (all data)	0.0367
α/°	90	R_1	0.0334
β/°	90		
γ/°	90		

Table 1: Fractional Atomic Coordinates (×10^4) and Equivalent Isotropic Displacement Parameters (Å^2×10^3) for **TCP-1-186**. U_{eq} is defined as 1/3 of the trace of the orthogonalised U_{ij}.

Atom	x	y	z	U_{eq}
Cu1	6546.6(3)	4469.5(2)	2795.2(2)	11.16(8)
P1	3335.5(8)	4363.7(5)	575.0(4)	16.47(14)
F4	3919(3)	3299.8(15)	816.7(13)	38.2(5)
F5	4041(3)	4157.7(15)	-202.2(11)	33.8(5)
F6	1651(2)	3902.2(17)	329.0(12)	38.2(5)
F2	2632(3)	4571.1(19)	1348.6(11)	44.7(6)
F1	2757(3)	5420.7(16)	312.7(12)	39.6(5)

Atom	x	y	z	U_{eq}
F3	5019(3)	4836.6(17)	797.3(13)	40.7(6)
N3	7104(2)	5980.4(17)	3055.2(12)	11.8(4)
N2	6419(3)	4241.6(15)	3908.9(11)	11.3(4)
N1	4115(3)	4919.2(17)	2879.4(13)	14.9(4)
N4	7239(3)	3764.5(18)	1999.4(12)	15.3(4)
C8	7756(3)	5904(2)	3785.3(14)	12.8(5)
C3	7482(3)	3421(2)	4169.0(14)	13.5(5)
C14	4193(3)	5959(2)	2678.7(16)	17.1(5)
C9	8306(3)	6447(2)	2553.9(14)	17.4(5)
C12	7555(4)	6514(2)	1819.2(16)	23.5(6)
C4	7281(4)	3222(2)	4968.2(16)	22.4(6)
C1	3569(3)	4730(2)	3613.8(15)	17.8(5)
C15	7522(3)	3425(2)	1462.8(15)	15.7(5)
C6	9239(3)	3699(2)	4023.2(16)	18.2(6)
C10	9796(3)	5789(3)	2496.4(17)	25.1(7)
C5	7107(4)	2476(2)	3757.9(16)	21.0(6)
C7	6793(3)	5204.2(19)	4253.9(13)	12.9(5)
C16	7868(4)	3000(2)	773.3(16)	22.9(6)
C2	4675(3)	4013(2)	4002.4(15)	16.1(5)
C13	5527(3)	6499(2)	3072.6(15)	15.4(5)
C11	8820(4)	7477(2)	2800.3(19)	29.6(7)

Table 2: Anisotropic Displacement Parameters (×10^4) **TCP-1-186**. The anisotropic displacement factor exponent takes the form: $-2\pi^2[h^2a^{*2} \times U_{11} + \ldots + 2hka^* \times b^* \times U_{12}]$

Atom	U_{11}	U_{22}	U_{33}	U_{23}	U_{13}	U_{12}
Cu1	10.97(12)	11.34(15)	11.17(13)	-1.49(11)	0.30(11)	0.34(11)
P1	15.9(3)	15.4(3)	18.0(3)	-0.7(2)	-3.2(2)	0.9(3)
F4	36.6(11)	21.1(11)	57.0(14)	17.7(10)	-3.7(10)	2.5(8)
F5	46.6(12)	25.6(11)	29.1(10)	-5.3(8)	15.8(9)	-9.3(9)
F6	20.1(8)	50.8(13)	43.6(12)	-6.4(10)	-4.1(9)	-10.3(10)
F2	56.9(14)	55.0(15)	22.3(10)	-9.5(10)	8.5(10)	-4.6(13)
F1	49.8(12)	24.1(11)	44.8(12)	-3.3(9)	-15.4(10)	14(1)
F3	31.7(10)	35.9(13)	54.5(15)	5.5(10)	-19.9(10)	-12.6(9)
N3	9.1(8)	12.6(11)	13.6(10)	1.9(8)	-1.8(7)	-3.0(7)
N2	13.1(9)	8.5(10)	12.3(9)	-1.2(7)	1.6(8)	-1.4(7)
N1	11.1(9)	13.6(11)	19.9(12)	-0.1(9)	-2.6(8)	-2.9(8)
N4	15.4(10)	14.7(11)	15.9(11)	-0.2(8)	-0.7(8)	1.6(8)
C8	14.3(10)	10.5(12)	13.5(12)	0.2(9)	-2.6(9)	-3.1(9)
C3	19.3(12)	8.8(12)	12.4(12)	1.2(9)	-0.4(9)	2.1(9)
C14	11.9(10)	12.6(13)	26.8(15)	3.1(11)	-4.9(10)	0.7(9)
C9	16.4(11)	20.0(14)	15.8(12)	6.6(10)	-2(1)	-8.9(11)
C12	25.6(14)	26.6(16)	18.3(14)	9.7(12)	-4.5(11)	-9.8(12)
C4	32.1(15)	18.4(15)	16.9(13)	6.0(11)	-1.6(12)	-2.0(12)
C1	9.8(10)	18.5(14)	25.2(13)	-1.1(10)	4.8(10)	-1.9(9)
C15	14.3(11)	15.0(13)	17.8(13)	0.8(10)	-1.2(9)	1.9(10)
C6	18.6(12)	17.1(14)	18.8(14)	2.4(11)	-1.9(10)	4.9(10)
C10	12.0(11)	40(2)	23.0(14)	8.8(13)	2.9(10)	-5.0(11)
C5	31.1(14)	11.4(14)	20.7(14)	-0.5(10)	-4.3(11)	2.1(11)
C7	17.3(12)	9.7(12)	11.5(11)	-2.1(9)	1.3(9)	-0.5(9)
C16	26.7(13)	24.9(17)	17.2(14)	-6.5(11)	4.8(11)	2.5(12)
C2	14.0(11)	15.1(13)	19.2(13)	0.2(10)	5.5(9)	-4.6(10)
C13	14.6(11)	10.0(12)	21.5(13)	3.2(10)	-3.2(10)	1.2(9)
C11	36.2(16)	25.4(17)	27.3(15)	7.6(14)	-7.0(14)	-20.7(13)

Table 3: Bond Lengths in Å for **TCP-1-186**.

Atom	Atom	Length/Å
Cu1	N3	2.171(2)
Cu1	N2	2.131(2)
Cu1	N1	2.120(2)
Cu1	N4	1.876(2)
P1	F4	1.598(2)
P1	F5	1.607(2)
P1	F6	1.605(2)
P1	F2	1.600(2)
P1	F1	1.600(2)
P1	F3	1.598(2)
N3	C8	1.486(3)
N3	C9	1.517(3)
N3	C13	1.492(3)
N2	C3	1.509(3)
N2	C7	1.500(3)
N2	C2	1.494(3)
N1	C14	1.471(4)
N1	C1	1.483(4)
N4	C15	1.140(4)
C8	C7	1.530(4)
C3	C4	1.544(4)
C3	C6	1.535(4)
C3	C5	1.538(4)
C14	C13	1.526(4)
C9	C12	1.526(4)
C9	C10	1.534(4)
C9	C11	1.543(4)
C1	C2	1.532(4)
C15	C16	1.455(4)

Table 4: Bond Angles in ° for **TCP-1-186**.

Atom	Atom	Atom	Angle/°
N2	Cu1	N3	85.75(8)
N1	Cu1	N3	84.94(8)
N1	Cu1	N2	85.45(9)
N4	Cu1	N3	127.11(9)
N4	Cu1	N2	137.09(9)
N4	Cu1	N1	120.11(10)
F4	P1	F5	89.51(13)
F4	P1	F6	89.49(12)
F4	P1	F2	90.62(13)
F4	P1	F1	178.56(14)
F4	P1	F3	91.48(12)
F6	P1	F5	89.15(12)
F2	P1	F5	179.88(15)
F2	P1	F6	90.87(13)
F2	P1	F1	90.78(14)
F1	P1	F5	89.10(12)
F1	P1	F6	90.10(13)
F3	P1	F5	89.49(13)
F3	P1	F6	178.31(13)
F3	P1	F2	90.50(13)
F3	P1	F1	88.89(12)
C8	N3	Cu1	102.81(16)
C8	N3	C9	111.64(19)
C8	N3	C13	109.5(2)
C9	N3	Cu1	113.46(17)
C13	N3	Cu1	105.57(15)
C13	N3	C9	113.2(2)
C3	N2	Cu1	113.64(15)
C7	N2	Cu1	106.93(15)
C7	N2	C3	112.78(19)
C2	N2	Cu1	101.30(16)
C2	N2	C3	112.0(2)
C2	N2	C7	109.5(2)
C14	N1	Cu1	102.58(15)
C14	N1	C1	115.0(2)

Atom	Atom	Atom	Angle/°
C1	N1	Cu1	108.18(16)
C15	N4	Cu1	170.2(2)
N3	C8	C7	113.0(2)
N2	C3	C4	112.7(2)
N2	C3	C6	108.4(2)
N2	C3	C5	109.8(2)
C6	C3	C4	108.8(2)
C6	C3	C5	108.0(2)
C5	C3	C4	108.9(2)
N1	C14	C13	111.9(2)
N3	C9	C12	108.9(2)
N3	C9	C10	109.3(2)
N3	C9	C11	112.1(2)
C12	C9	C10	107.5(3)
C12	C9	C11	109.5(2)
C10	C9	C11	109.4(2)
N1	C1	C2	112.1(2)
N4	C15	C16	179.3(3)
N2	C7	C8	113.9(2)
N2	C2	C1	113.1(2)
N3	C13	C14	113.5(2)

Table 5: Hydrogen Fractional Atomic Coordinates ($\times 10^4$) and Equivalent Isotropic Displacement Parameters ($Å^2 \times 10^3$) for **TCP-1-186**. U_{eq} is defined as 1/3 of the trace of the orthogonalised U_{ij}.

Atom	x	y	z	U_{eq}
H8A	7757	6563	4005	15
H8B	8884	5675	3761	15
H14A	3149	6275	2784	21
H14B	4385	6010	2163	21
H12A	7163	5866	1676	35
H12B	8365	6741	1480	35
H12C	6656	6977	1829	35
H4A	7651	3793	5237	34
H4B	7920	2648	5101	34
H4C	6146	3099	5074	34
H1A	2465	4460	3603	21
H1B	3536	5357	3877	21
H6A	9378	3833	3518	27
H6B	9943	3156	4162	27
H6C	9519	4284	4297	27
H10A	10381	5796	2946	38
H10B	10497	6032	2119	38
H10C	9461	5117	2388	38
H5A	6079	2207	3920	32
H5B	7963	1996	3840	32
H5C	7040	2623	3251	32
H7A	7408	5080	4693	15
H7B	5771	5525	4389	15
H16A	7003	3167	443	34
H16B	7947	2287	817	34
H16C	8889	3262	596	34
H2A	4414	4025	4513	19
H2B	4466	3342	3826	19
H13A	5661	7158	2861	18

Atom	x	y	z	U_{eq}
H13B	5197	6589	3572	18
H11A	7871	7900	2834	44
H11B	9579	7756	2458	44
H11C	9337	7431	3265	44
H1	3490(30)	4600(20)	2565(15)	8(7)

Crystal Data. $C_{16}H_{34}CuF_6N_4P$, M_r = 490.98, orthorhombic, $P2_12_12_1$ (No. 19), a = 8.3173(9) Å, b = 13.6535(15) Å, c = 18.901(2) Å, $\alpha = \beta = \gamma = 90^{\circ}$, V = 2146.4(4) Å^3, T = 100(2) K, Z = 4, Z' = 1, μ(MoK_α) = 1.152, 9886 reflections measured, 6165 unique (R_{int} = 0.0254) which were used in all calculations. The final wR_2 was 0.0850 (all data) and R_1 was 0.0334 (I > 2(I)).

Compound Name: **[Cu(*t*BuH$_2$tacn)(MeCN)]OTf**

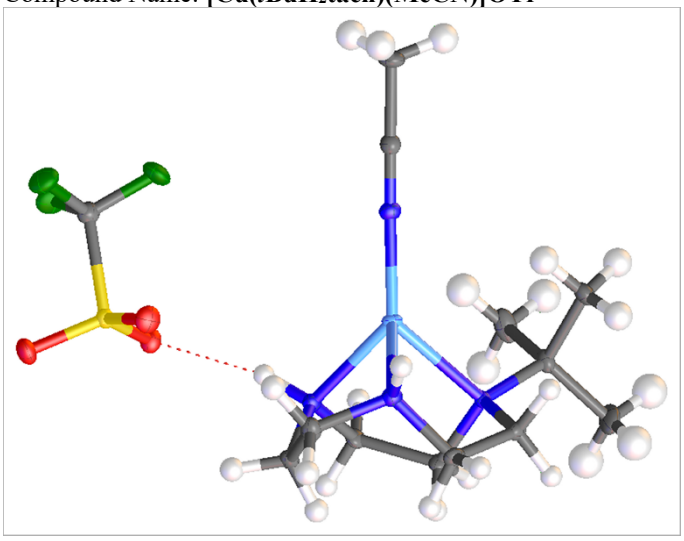

Table 1. Crystal data and structure refinement for **[Cu(*t*BuH$_2$tacn)(MeCN)]OTf**.

Empirical formula	C13 H26 Cu F3 N4 O3 S	
Formula weight	438.98	
Temperature	110(2) K	
Wavelength	0.71073 Å	
Crystal system	Monoclinic	
Space group	P 1 21/n 1	
Unit cell dimensions	a = 8.2740(5) Å	α = 90°.
	b = 25.9552(15) Å	β = 100.6790(10)°
	c = 8.8914(5) Å	γ = 90°.
Volume	1876.39(19) Å3	
Z	4	
Density (calculated)	1.554 Mg/m3	
Absorption coefficient	1.323 mm-1	
F(000)	912	
Crystal size	0.535 x 0.376 x 0.356 mm3	
Theta range for data collection	2.460 to 30.534°.	
Index ranges	-11<=h<=11, -33<=k<=37, -12<=l<=10	
Reflections collected	22286	
Independent reflections	5727 [R(int) = 0.0351]	
Completeness to theta = 26.000°	100.00%	
Absorption correction	Semi-empirical from equivalents	
Max. and min. transmission	0.7461 and 0.5636	
Refinement method	Full-matrix least-squares on F2	
Data / restraints / parameters	5727 / 0 / 230	
Goodness-of-fit on F2	1.04	
Final R indices [I>2sigma(I)]	R1 = 0.0314, wR2 = 0.0786	
R indices (all data)	R1 = 0.0387, wR2 = 0.0822	
Extinction coefficient	n/a	
Largest diff. peak and hole	0.598 and -0.304 e.Å-3	

Table 2. Atomic coordinates (x 10^4) and equivalent isotropic displacement parameters ($Å^2$x 10^3) for TCP-Cu(tButacn)(MeCN). U(eq) is defined as one third of the trace of the orthogonalized U^{ij} tensor.

Atom	x	y	z	U(eq)
Cu(01)	4229(1)	6205(1)	6352(1)	11(1)
S(1)	6664(1)	6442(1)	1802(1)	11(1)
F(2)	7130(1)	5483(1)	2717(1)	24(1)
F(1)	6762(1)	5578(1)	267(1)	25(1)
F(3)	9080(1)	5788(1)	1672(1)	25(1)
O(1)	4910(1)	6355(1)	1627(1)	16(1)
O(2)	7470(1)	6592(1)	3317(1)	19(1)
O(3)	7159(1)	6726(1)	562(1)	19(1)
N(2)	1926(1)	6461(1)	6987(1)	10(1)
N(4)	5240(2)	5562(1)	6616(2)	13(1)
N(1)	3499(2)	6656(1)	4378(1)	12(1)
N(3)	5197(2)	6906(1)	7324(2)	13(1)
C(9)	1688(2)	6654(1)	4167(2)	14(1)
C(11)	5931(2)	5182(1)	6865(2)	14(1)
C(5)	2578(2)	6801(1)	8305(2)	12(1)
C(10)	1090(2)	6774(1)	5657(2)	13(1)
C(6)	3911(2)	7172(1)	7996(2)	14(1)
C(12)	6823(2)	4697(1)	7203(2)	19(1)
C(13)	7448(2)	5790(1)	1598(2)	16(1)
C(4)	836(2)	6039(1)	7432(2)	14(1)
C(7)	5661(2)	7180(1)	6009(2)	16(1)
C(8)	4245(2)	7174(1)	4636(2)	15(1)
C(3)	1809(2)	5717(1)	8733(2)	18(1)
C(1)	321(2)	5686(1)	6045(2)	24(1)
C(2)	-702(2)	6253(1)	7949(2)	25(1)

Table 3. Bond lengths [Å] and angles [°] for TCP-Cu(tButacn)(MeCN).

Cu(01)-N(2)	2.1883(11)	C(6)-N(3)-Cu(01)	108.66(9)
Cu(01)-N(4)	1.8629(13)	C(6)-N(3)-H(3)	110.3
Cu(01)-N(1)	2.1025(13)	C(7)-N(3)-Cu(01)	102.97(9)
Cu(01)-N(3)	2.1082(13)	C(7)-N(3)-H(3)	110.3
S(1)-O(1)	1.4485(11)	C(7)-N(3)-C(6)	114.03(12)
S(1)-O(2)	1.4416(12)	N(1)-C(9)-H(9A)	109.2
S(1)-O(3)	1.4474(12)	N(1)-C(9)-H(9B)	109.2
S(1)-C(13)	1.8332(16)	N(1)-C(9)-C(10)	111.90(12)
F(2)-C(13)	1.3380(19)	H(9A)-C(9)-H(9B)	107.9
F(1)-C(13)	1.3335(19)	C(10)-C(9)-H(9A)	109.2
F(3)-C(13)	1.3397(17)	C(10)-C(9)-H(9B)	109.2
N(2)-C(5)	1.4867(19)	N(4)-C(11)-C(12)	179.26(17)
N(2)-C(10)	1.4937(19)	N(2)-C(5)-H(5A)	108.8

N(2)-C(4)	1.5174(19)	N(2)-C(5)-H(5B)	108.8
N(4)-C(11)	1.141(2)	N(2)-C(5)-C(6)	113.66(12)
N(1)-H(1)	1	H(5A)-C(5)-H(5B)	107.7
N(1)-C(9)	1.4752(18)	C(6)-C(5)-H(5A)	108.8
N(1)-C(8)	1.4807(19)	C(6)-C(5)-H(5B)	108.8
N(3)-H(3)	1	N(2)-C(10)-C(9)	113.50(11)
N(3)-C(6)	1.4831(18)	N(2)-C(10)-H(10A)	108.9
N(3)-C(7)	1.478(2)	N(2)-C(10)-H(10B)	108.9
C(9)-H(9A)	0.99	C(9)-C(10)-H(10A)	108.9
C(9)-H(9B)	0.99	C(9)-C(10)-H(10B)	108.9
C(9)-C(10)	1.530(2)	H(10A)-C(10)-H(10B)	107.7
C(11)-C(12)	1.461(2)	N(3)-C(6)-C(5)	112.07(12)
C(5)-H(5A)	0.99	N(3)-C(6)-H(6A)	109.2
C(5)-H(5B)	0.99	N(3)-C(6)-H(6B)	109.2
C(5)-C(6)	1.526(2)	C(5)-C(6)-H(6A)	109.2
C(10)-H(10A)	0.99	C(5)-C(6)-H(6B)	109.2
C(10)-H(10B)	0.99	H(6A)-C(6)-H(6B)	107.9
C(6)-H(6A)	0.99	C(11)-C(12)-H(12A)	109.5
C(6)-H(6B)	0.99	C(11)-C(12)-H(12B)	109.5
C(12)-H(12A)	0.98	C(11)-C(12)-H(12C)	109.5
C(12)-H(12B)	0.98	H(12A)-C(12)-H(12B)	109.5
C(12)-H(12C)	0.98	H(12A)-C(12)-H(12C)	109.5
C(4)-C(3)	1.530(2)	H(12B)-C(12)-H(12C)	109.5
C(4)-C(1)	1.532(2)	F(2)-C(13)-S(1)	110.73(11)
C(4)-C(2)	1.535(2)	F(2)-C(13)-F(3)	107.21(13)
C(7)-H(7A)	0.99	F(1)-C(13)-S(1)	111.69(11)
C(7)-H(7B)	0.99	F(1)-C(13)-F(2)	107.68(13)
C(7)-C(8)	1.527(2)	F(1)-C(13)-F(3)	107.49(13)
C(8)-H(8A)	0.99	F(3)-C(13)-S(1)	111.81(11)
C(8)-H(8B)	0.99	N(2)-C(4)-C(3)	109.70(11)
C(3)-H(3A)	0.98	N(2)-C(4)-C(1)	108.24(12)
C(3)-H(3B)	0.98	N(2)-C(4)-C(2)	112.47(14)
C(3)-H(3C)	0.98	C(3)-C(4)-C(1)	108.10(14)
C(1)-H(1A)	0.98	C(3)-C(4)-C(2)	108.67(13)
C(1)-H(1B)	0.98	C(1)-C(4)-C(2)	109.57(14)
C(1)-H(1C)	0.98	N(3)-C(7)-H(7A)	109.5
C(2)-H(2A)	0.98	N(3)-C(7)-H(7B)	109.5
C(2)-H(2B)	0.98	N(3)-C(7)-C(8)	110.73(12)
C(2)-H(2C)	0.98	H(7A)-C(7)-H(7B)	108.1
N(4)-Cu(01)-N(2)	129.19(5)	C(8)-C(7)-H(7A)	109.5

N(4)-Cu(01)-N(1)	131.01(5)	C(8)-C(7)-H(7B)	109.5
N(4)-Cu(01)-N(3)	126.48(5)	N(1)-C(8)-C(7)	111.62(12)
N(1)-Cu(01)-N(2)	85.28(5)	N(1)-C(8)-H(8A)	109.3
N(1)-Cu(01)-N(3)	83.73(5)	N(1)-C(8)-H(8B)	109.3
N(3)-Cu(01)-N(2)	85.12(5)	C(7)-C(8)-H(8A)	109.3
O(1)-S(1)-C(13)	102.17(7)	C(7)-C(8)-H(8B)	109.3
O(2)-S(1)-O(1)	115.05(7)	H(8A)-C(8)-H(8B)	108
O(2)-S(1)-O(3)	115.28(7)	C(4)-C(3)-H(3A)	109.5
O(2)-S(1)-C(13)	103.32(7)	C(4)-C(3)-H(3B)	109.5
O(3)-S(1)-O(1)	114.65(7)	C(4)-C(3)-H(3C)	109.5
O(3)-S(1)-C(13)	103.91(7)	H(3A)-C(3)-H(3B)	109.5
C(5)-N(2)-Cu(01)	100.21(8)	H(3A)-C(3)-H(3C)	109.5
C(5)-N(2)-C(10)	110.42(12)	H(3B)-C(3)-H(3C)	109.5
C(5)-N(2)-C(4)	111.74(11)	C(4)-C(1)-H(1A)	109.5
C(10)-N(2)-Cu(01)	104.96(8)	C(4)-C(1)-H(1B)	109.5
C(10)-N(2)-C(4)	112.84(11)	C(4)-C(1)-H(1C)	109.5
C(4)-N(2)-Cu(01)	115.81(9)	H(1A)-C(1)-H(1B)	109.5
C(11)-N(4)-Cu(01)	175.20(13)	H(1A)-C(1)-H(1C)	109.5
Cu(01)-N(1)-H(1)	110	H(1B)-C(1)-H(1C)	109.5
C(9)-N(1)-Cu(01)	103.42(9)	C(4)-C(2)-H(2A)	109.5
C(9)-N(1)-H(1)	110	C(4)-C(2)-H(2B)	109.5
C(9)-N(1)-C(8)	114.01(12)	C(4)-C(2)-H(2C)	109.5
C(8)-N(1)-Cu(01)	109.20(9)	H(2A)-C(2)-H(2B)	109.5
C(8)-N(1)-H(1)	110	H(2A)-C(2)-H(2C)	109.5
Cu(01)-N(3)-H(3)	110.3	H(2B)-C(2)-H(2C)	109.5

Table 4. Anisotropic displacement parameters ($Å^2 x\ 10^3$) for TCP-Cu(tButacn)(MeCN).
The anisotropic displacement factor exponent takes the form: $-2\pi^2[\ h^2\ a^{*2}U^{11} + \ldots + 2\ h\ k\ a^*\ b^*\ U^{12}\ ]$

Atom	U^{11}	U^{22}	U^{33}	U^{23}	U^{13}	U^{12}
Cu(01)	12(1)	8(1)	12(1)	0(1)	1(1)	2(1)
S(1)	13(1)	12(1)	9(1)	-1(1)	2(1)	-2(1)
F(2)	32(1)	16(1)	25(1)	8(1)	6(1)	1(1)
F(1)	33(1)	21(1)	20(1)	-11(1)	-1(1)	0(1)
F(3)	17(1)	26(1)	33(1)	-1(1)	6(1)	6(1)
O(1)	13(1)	20(1)	14(1)	0(1)	2(1)	0(1)
O(2)	20(1)	22(1)	14(1)	-5(1)	0(1)	-3(1)
O(3)	24(1)	18(1)	16(1)	3(1)	7(1)	-4(1)
N(2)	10(1)	11(1)	9(1)	2(1)	1(1)	0(1)
N(4)	14(1)	12(1)	13(1)	-1(1)	2(1)	1(1)
N(1)	15(1)	10(1)	11(1)	0(1)	3(1)	0(1)

N(3)	13(1)	12(1)	14(1)	-1(1)	2(1)	0(1)
C(9)	15(1)	15(1)	9(1)	3(1)	0(1)	2(1)
C(11)	13(1)	14(1)	13(1)	0(1)	2(1)	-1(1)
C(5)	15(1)	13(1)	10(1)	-2(1)	3(1)	2(1)
C(10)	12(1)	15(1)	12(1)	2(1)	0(1)	4(1)
C(6)	18(1)	11(1)	12(1)	-3(1)	2(1)	1(1)
C(12)	20(1)	13(1)	23(1)	3(1)	2(1)	5(1)
C(13)	17(1)	16(1)	14(1)	-1(1)	2(1)	0(1)
C(4)	13(1)	17(1)	13(1)	2(1)	3(1)	-3(1)
C(7)	20(1)	14(1)	16(1)	-2(1)	5(1)	-5(1)
C(8)	21(1)	9(1)	15(1)	1(1)	6(1)	-1(1)
C(3)	22(1)	15(1)	16(1)	5(1)	4(1)	-2(1)
C(1)	28(1)	27(1)	16(1)	-1(1)	3(1)	-15(1)
C(2)	15(1)	36(1)	28(1)	9(1)	11(1)	4(1)

Table 5. Hydrogen coordinates (x 10^4) and isotropic displacement parameters ($Å^2$x 10^3) for TCP-Cu(tButacn)(MeCN).

Atom	x	y	z	U(eq)
H(1)	3858	6488	3482	14
H(3)	6191	6841	8129	16
H(9A)	1269	6311	3786	16
H(9B)	1236	6913	3385	16
H(5A)	3035	6584	9198	15
H(5B)	1659	7004	8575	15
H(10A)	1277	7144	5900	16
H(10B)	-109	6710	5504	16
H(6A)	3400	7445	7286	16
H(6B)	4428	7339	8968	16
H(12A)	6844	4512	6246	28
H(12B)	6272	4486	7868	28
H(12C)	7952	4770	7721	28
H(7A)	6637	7012	5725	19
H(7B)	5957	7540	6301	19
H(8A)	3394	7423	4813	18
H(8B)	4657	7284	3710	18
H(3A)	2868	5618	8475	26
H(3B)	1184	5406	8878	26
H(3C)	1998	5919	9679	26
H(1A)	-379	5878	5224	35
H(1B)	-291	5391	6339	35
H(1C)	1303	5563	5685	35
H(2A)	-370	6486	8818	38
H(2B)	-1344	5967	8259	38
H(2C)	-1373	6441	7102	38

Crystal Data for $C_{13}H_{26}CuF_3N_4O_3S$ (M =438.98 g/mol): monoclinic, space group $P2_1/n$ (no. 14), a = 8.2740(5) Å, b = 25.9552(15) Å, c = 8.8914(5) Å, β = 100.6790(10)°, V = 1876.39(19) $Å^3$, Z = 4, T = 110(2) K, μ(MoKα) = 1.323 mm^{-1}, $Dcalc$ = 1.554 g/cm^3, 22286 reflections measured (4.92° ≤ 2Θ ≤ 61.068°), 5727 unique (R_{int} = 0.0351, R_{sigma} = 0.0327) which were used in all calculations. The final R_1 was 0.0314 (I > 2σ(I)) and wR_2 was 0.0822 (all data).

1.6 References

[1] a) P. Chaudhuri, K. Wieghardt. The Chemistry of 1,4,7-Triazacyclononane and Related Tridentate Macrocyclic Compounds. *Progress in Inorganic Chemistry* **1987**, *35*, 329; b) K. P. Wainwright. Synthetic and structural aspects of the chemistry of saturated polyaza macrocyclic ligands bearing pendant coordinating groups attached to nitrogen. *Coordination Chemistry Reviews* **1997**, *166*, 35-90; c) R. I. Haines. Pendant-Arm Tri- and Tetraazamacrocycles: Synthesis, Structure and Properties of their First-Row Transition Metal Complexes. *Reviews in Inorganic Chemistry* **2001**, *21*, 165-206.

[2] a) R. Hage, J. E. Iburg, J. Kerschner, J. H. Koek, E. L. M. Lempers, R. J. Martens, U. S. Racherla, S. W. Russell, T. Swarthoff, M. R. P. van Vliet, J. B. Warnaar, L. v. d. Wolf, B. Krijnen. Efficient manganese catalysts for low-temperature bleaching. *Nature* **1994**, *369*, 637-639; b) R. Hage, J. W. de Boer, F. Gaulard, K. Maaijen. Chapter Three - Manganese and Iron Bleaching and Oxidation Catalysts. In *Advances in Inorganic Chemistry, Vol. 65* (Eds.: R. van Eldik, C. D. Hubbard), Academic Press, **2013**, pp. 85-116.

[3] J. E. Richman, T. J. Atkins. Nitrogen analogs of crown ethers. *Journal of the American Chemical Society* **1974**, *96*, 2268-2270.

[4] a) N. Luk'yanenko, S. Basok, L. Filonova, N. Kulikov, V. Pastushok. Macroheterocycles. 51. Synthesis of macrocyclic polyamines in a biphasic system. *Chemistry of Heterocyclic Compounds* **1990**, *26*, 346-349; b) J. F. Wei, X. Y. Shi, D. P. He, Y. Zhang. A Rapid Detosylation of N, N', N', N''-Tetra-(p-tosyl)-1, 4, 7, 10-tetraazacyclod odecane under Microwave Irradiation and Normal Pressure. *Chinese Journal of Organic Chemistry* **2003**, *23*, 1142-1145; c) P. Désogère, Y. Rousselin , S. Poty, C. Bernhard, C. Goze, F. Boschetti, F. Denat. Efficient Synthesis of 1,4,7-Triazacyclononane and 1,4,7-Triazacyclononane-Based Bifunctional Chelators for Bioconjugation. *European Journal of Organic Chemistry* **2014**, *2014*, 7831-7838; d) S. A. Madison, D. J. Batal, Lever Brothers Co, U.S. Pat. 5,284,944, **1994**.

[5] a) G. R. Weisman, D. J. Vachon, V. B. Johnson, D. A. Gronbeck. Selective N-protection of medium-ring triamines. *Journal of the Chemical Society, Chemical Communications* **1987**, 886-887; b) I. Lázár, Z. Takács. Convenient synthesis of mono-and ditosylated 1, 4, 7-triazacyclononane. *Synthetic Communications* **2001**, *31*, 3141-3144; c) H. S. Winchell, J. Y. Klein, E. D. Simhon, R. L. Cyjon, O. Klein, H. Zaklad, U.S. Pat. 5874573 A, **1999**.

[6] a) C. Bolm, D. Kadereit, M. Valacchi. Enantioselective olefin epoxidation with chiral manganese/1, 4, 7-triazacyclononane complexes. *Synlett* **1997**, *1997*, 687-688; b) G. Argouarch, C. L. Gibson, G. Stones, D. C. Sherrington. The synthesis of chiral annulet 1,4,7-triazacyclononanes. *Tetrahedron Letters* **2002**, *43*, 3795-3798; c) C. Bolm, N. Meyer, G. Raabe, T. Weyhermuller, E. Bothe. A novel enantiopure proline-derived triazacyclononane: synthesis, structure and application of its manganese complex. *Chemical Communications* **2000**, 2435-2436; d) S. Pulacchini, K. F. Sibbons, K. Shastri, M. Motevalli, M. Watkinson, H. Wan, A. Whiting, A. P. Lightfoot. Synthesis of C2-symmetric aza- and azaoxa-macrocyclic ligands derived from (1R,2R)-1,2-diaminocyclohexane and their applications in catalysis. *Dalton Transactions* **2003**, 2043-2052; e) G. Stones, G. Argouarch, A. R. Kennedy, D. C. Sherrington, C. L. Gibson. The synthesis of an isopropyl substituted 1,4,7-triazacyclononane via an in situ sequential macrocyclisation method. *Organic and Biomolecular Chemistry* **2003**, *1*, 2357-2363; f)

G. Stones, R. Tripoli, C. L. McDavid, K. Roux-Duplâtre, A. R. Kennedy, D. C. Sherrington, C. L. Gibson. Investigation of macrocyclisation routes to 1, 4, 7-triazacyclononanes: efficient syntheses from 1, 2-ditosylamides. *Organid and Biomolecular Chemistry* **2008**, *6*, 374-384; g) V. B. Romakh, B. Therrien, G. Süss-Fink, G. B. Shul'pin. Dinuclear Manganese Complexes Containing Chiral 1,4,7-Triazacyclononane-Derived Ligands and Their Catalytic Potential for the Oxidation of Olefins, Alkanes, and Alcohols. *Inorganic Chemistry* **2007**, *46*, 1315-1331.

[7] a) J. Robb, R. D. Peacock. Preparation of the chiral hexadentate ligand N,N′,N″-tris[(S)-2-hydroxypropyl]-1,4,7-triazacyclononane and preparation and circular dichroism spectra of its Co(III) complexes. *Inorganica Chimica Acta* **1986**, *121*, L15-L17; b) P. Rossi, F. Felluga, P. Scrimin. A new ligand α-amino acid: (S)-2-amino-3-[1-(1,4,7-triazacyclononane)]propanoic acid. *Tetrahedron Letters* **1998**, *39*, 7159-7162.

[8] a) J. E. W. Scheuermann, F. Ronketti, M. Motevalli, D. V. Griffiths, M. Watkinson. The synthesis of C2-symmetric 1,4,7-triazacyclononane ligands derived from chiral aziridines. *New Journal of Chemistry* **2002**, *26*, 1054-1059; b) M. Beller, A. Tafesch, R. W. Fischer, B. Scharbert, German Pat. 19523891, **1995**; c) B. M. Kim, S. M. So, H. J. Choi. A Concise, Modular Synthesis of Chiral Peraza-Macrocycles Using Chiral Aziridines. *Organic Letters* **2002**, *4*, 949-952; d) J. Koek, E. Kohlen, S. Russell. L. van derWolf, PF ter Steeg, JC Hellemons. *Inorganica Chimica Acta* **1999**, *295*, 189-199; e) P. Graham, D. Weatherburn. The preparation of C-methyl-substituted triazamacrocyclic ligands. *Australian Journal of Chemistry* **1983**, *36*, 2349-2354; f) J. P. L. Cox, A. S. Craig, I. M. Helps, K. J. Jankowski, D. Parker, M. A. W. Eaton, A. T. Millican, K. Millar, N. R. A. Beeley, B. A. Boyce. Synthesis of a kinetically stable yttrium-90 labelled macrocycle–antibody conjugate. *Journal of the Chemical Society, Perkin Transactions 1* **1996**, 2567–2576; g) S. W. Golding, T. W. Hambley, G. A. Lawrence, S. M. Luther, M. Maeder, P. J. Turner. Synthesis and some octahedral complexes of a chiral triaza macrocycle. *Journal of the Chemical Society, Dalton Transactions: Inorganic Chemistry* **1999**, 1975–1980; h) J. E. W. Scheuermann, K. F. Sibbons, D. M. Benoit, M. Motevalli, M. Watkinson. The synthesis of unsymmetrically N-substituted chiral 1,4,7-triazacyclononanes. *Organic and Biomolecular Chemistry* **2004**, *2*, 2664-2670; i) A. F. Drake, R. Kuroda, S. F. Mason. Single-crystal, vacuum-ultraviolet, and lon-association circular-dichroism spectra of the bis[(2R)-2-methyl-1,4,7-triazacyclononane]cobalt(III) lon. *Journal of the Chemical Society, Dalton Transactions* **1979**, 1095-1100; j) M. Nonoyama. [(R)-2-Methyl-1, 4, 7-triazacyclononane][1, 1, 1-tris (aminomethyl) ethane]-cobalt (III) and some Mono [(R)-2-methyl-1, 4, 7-triazacyclononane]-cobalt (III) Complexes. *Transition Metal Chemistry* **1980**, *5*, 269-271; k) S. Kamioka, S. Sugiyama, T. Takahashi, T. Doi. Synthesis of chiral polyazamacrocycles of variable ring size. *Organic and Biomolcular Chemistry* **2010**, *8*, 2529-2536.

[9] K. Wieghardt, P. Chaudhuri, B. Nuber, J. Weiss. New triply hydroxo-bridged complexes of chromium (III), cobalt (III), and rhodium (III): crystal structure of tris (. mu.-hydroxo) bis [(1, 4, 7-trimethyl-1, 4, 7-triazacyclononane) chromium (III)] triiodide trihydrate. *Inorganic Chemistry* **1982**, *21*, 3086-3090.

[10] A. Thangavel, M. Wieliczko, J. Bacsa, C. C. Scarborough. 1,4,7-Triazacyclononane Ligands Bearing Tertiary Alkyl Nitrogen Substituents. *Inorganic Chemistry* **2013**, *52*, 13282-13287.

[11] a) J. S. Bradshaw, K. E. Krakowiak, R. M. Izatt. Convenient syntheses of N-[2-(2-hydroxyethoxy)ethyl]-substituted polyaza-crown ethers and cyclams without the need for a hydroxy blocking group. *Tetrahedron Letters* **1989**, *30*, 803-806; b) J. S. Bradshaw, K. E. Krakowiak, R. M. Izatt. A simple crab-like cyclization procedure to prepare polyaza-crowns and cyclams with one or two unsubstituted macroring nitrogen atoms or with a hydroxy group. *Journal of Heterocyclic Chemistry* **1989**, *26*, 1431-1435; c) K. E. Krakowiak, J. S. Bradshaw, R. M. Izatt. Preparation of triaza-, tetraaza- and peraza-crown compounds containing aminoalkyl side groups or unsubstituted ring nitrogen atoms. *Journal of Organic Chemistry* **1990**, *55*, 3364-3368.

[12] A. Grenz, S. Ceccarelli, C. Bolm. Synthesis and application of novel catalytically active polymers containing 1,4,7-triazacyclononanes. *Chemical Communications* **2001**, 1726-1727.

[13] M. J. Belousoff, M. B. Duriska, B. Graham, S. R. Batten, B. Moubaraki, K. S. Murray, L. Spiccia. Synthesis, X-ray crystal structures, magnetism, and phosphate ester cleavage properties of copper (II) complexes of N-substituted derivatives of 1, 4, 7-triazacyclononane. *Inorganic Chemistry* **2006**, *45*, 3746-3755.

[14] S. V. Pronin, C. A. Reiher, R. A. Shenvi. Stereoinversion of tertiary alcohols to tertiary-alkyl isonitriles and amines. *Nature* **2013**, *501*, 195.

[15] A. J. Blake, I. A. Fallis, R. O. Gould, S. Parsons, S. A. Ross, M. Schroder. Selective derivatisation of aza macrocycles. *Journal of the Chemical Society, Dalton Transactions* **1996**, 4379-4387.

[16] R. Hage, J. H. Koek, S. W. Russell, X. Wang, L. V. D. Wolf, J. Zhang, W. Zhao, WO Pat. 2012003598 A1, **2012**.

[17] a) I. Prat, L. Gómez, M. Canta, X. Ribas, M. Costas. An Iron Catalyst for Oxidation of Alkyl C-H Bonds Showing Enhanced Selectivity for Methylenic Sites. *Chemistry: A European Journal* **2013**, *19*, 1908-1913; b) T. Corona, S. K. Padamati, F. Acuna-Pares, C. Duboc, W. R. Browne, A. Company. Trapping of superoxido cobalt and peroxido dicobalt species formed reversibly from CoII and O2. *Chemical Communications* **2017**, *53*, 11782-11785; c) M. Soler, M. Gonzalez-Bartulos, E. Figueras, A. Massaguer, L. Feliu, M. Planas, X. Ribas, M. Costas. Delivering aminopyridine ligands into cancer cells through conjugation to the cell-penetrating peptide BP16. *Organic and Biomolecular Chemistry* **2016**, *14*, 4061-4070; d) A. Draksharapu, Z. Codolà, L. Gómez, J. Lloret-Fillol, W. R. Browne, M. Costas. Spectroscopic Analyses on Reaction Intermediates Formed during Chlorination of Alkanes with NaOCl Catalyzed by a Nickel Complex. *Inorganic Chemistry* **2015**, *54*, 10656-10666; e) A. Company, L. Gómez, M. Güell, X. Ribas, J. M. Luis, L. Que, M. Costas. Alkane Hydroxylation by a Nonheme Iron Catalyst that Challenges the Heme Paradigm for Oxygenase Action. *Journal of the American Chemical Society* **2007**, *129*, 15766-15767; f) I. Garcia-Bosch, A. Company, X. Fontrodona, X. Ribas, M. Costas. Efficient and Selective Peracetic Acid Epoxidation Catalyzed by a Robust Manganese Catalyst. *Organic Letters* **2008**, *10*, 2095-2098; g) A. Company, L. Gómez, X. Fontrodona, X. Ribas, M. Costas. A Novel Platform for Modeling Oxidative Catalysis in Non-Heme Iron Oxygenases with Unprecedented Efficiency. *Chemistry: A European Journal* **2008**, *14*, 5727-5731; h) X. S. Ribas, M. S. Costas, I. B. Garcia, A. C. Company, L. M. Gomez, Spanish Pat. ES 2336746 A1, **2010**.

[18] a) R. Hage, A. Lienke. Applications of transition-metal catalysts to textile and wood-pulp bleaching. *Angewandte Chemie International Edition* **2006**, *45*, 206-222; b) R.

Hage, A. Lienke. Anwendung von Übergangsmetallkomplexen zum Bleichen von Textilien und Holzpulpe. *Angewandte Chemie* **2006**, *118*, 212-229.

[19] a) K. Wieghardt, W. Schmidt, B. Nuber, J. Weiss. Neue μ-Hydroxo-Übergangsmetallkomplexe, I. Darstellung und Struktur des trans-Diaqua-di-μ-hydroxo-bis [(1, 4, 7-triazacyclononan) cobalt (III)]-Kations; Kinetik und Mechanismus seiner Bildung. *Chemische Berichte* **1979**, *112*, 2220-2230; b) A. McAuley, P. Norman, O. Olubuyide. Preparation, characterization, and outer-sphere electron-transfer reactions of nickel complexes of 1, 4, 7-triazacyclononane. *Inorganic Chemistry* **1984**, *23*, 1938-1943; c) G. Searle, R. Geue. Improved Richman-Atkins syntheses of cyclic polyamines particularly 1,4,7-Triazacyclononane (tacn) and 1,4,7-Triazacyclodecane (tacd), with the aid of cation-exchange in purification and isolation. *Australian Journal of Chemistry* **1984**, *37*, 959-970; d) R. Yang, L. J. Zompa. Metal complexes of cyclic triamines. 1. Complexes of 1, 4, 7-triazacyclononane ([9] aneN3) with nickel (II), copper (II), and zinc (II). *Inorganic Chemistry* **1976**, *15*, 1499-1502.

[20] S. Bambirra, D. van Leusen, C. G. J. Tazelaar, A. Meetsma, B. Hessen. Rare Earth Metal Alkyl Complexes with Methyl-Substituted Triazacyclononane-amide Ligands: Ligand Variation and Ethylene Polymerization Catalysis. *Organometallics* **2007**, *26*, 1014-1023.

[21] N. Armanino, E. M. Carreira. Ruthenium-Catalyzed Intramolecular Hydrocarbamoylation of Allylic Formamides: Convenient Access to Chiral Pyrrolidones. *Journal of the American Chemical Society* **2013**, *135*, 6814-6817.

[22] Y. Zhou, J. Dong, F. Zhang, Y. Gong. Synthesis of C1-Symmetric Chiral Secondary Diamines and Their Applications in the Asymmetric Copper(II)-Catalyzed Henry (Nitroaldol) Reactions. *Journal of Organic Chemistry* **2011**, *76*, 588-600.

[23] D. M. K., H. Azardokht, Z. Feng-Lan. Steric and Electronic Effects in the Dimerization of Wanzlick Carbenes: The Alkyl Effect. *European Journal of Inorganic Chemistry* **2007**, *2007*, 3527-3534.

[24] W. O. Lin, J. A. de Azeredo Figueira, H. G. Alt. New multidentate potential ionophors of ether-amide type. *Monatshefte für Chemie / Chemical Monthly* **1985**, *116*, 217-221.

[25] P. Malatesta, G. Migliaccio. Aralkyl glycinamides and urethans with probable anesthetic action. *Annali di Chimica* **1958**, *48*, 776-782.

[26] L. F. Fieser, M. Fieser, *Reagents for Organic Synthesis*, **1967**, 581-595.

[27] C. A. Barta, S. R. Bayly, P. W. Read, B. O. Patrick, R. C. Thompson, C. Orvig. Molecular Architectures for Trimetallic d/f/d Complexes: Structural and Magnetic Properties of a LnNi2 Core. *Inorganic Chemistry* **2008**, *47*, 2280-2293.

[28] G. Bartoli, G. Di Antonio, R. Giovannini, S. Giuli, S. Lanari, M. Paoletti, E. Marcantoni. Efficient Transformation of Azides to Primary Amines Using the Mild and Easily Accessible CeCl3 7H2O/NaI System. *The Journal of Organic Chemistry* **2008**, *73*, 1919-1924.

Chapter 2

Esterification by Redox Dehydration Using Diselenides as Catalytic Organooxidants

Adapated from: T. C. Pickel, S. M. Akondi, L. S. Liebeskind. Esterification by Redox Dehydration Using Diselenides as Catalytic Organooxidants. *J. Org. Chem.* **2019**, *84*, 4954-4960.

2.1 Abstract. Ortho functionalized aryl diselenides are catalytic (5.0 mol %) oxidants for the redox dehydrative construction of esters from carboxylic acids and alcohols in the presence of stoichiometric triethylphosphite and dioxygen in air as the terminal redox reagents. The reaction proceeds through the intermediacy of the anhydride and requires the presence of 10% DMAP to drive the esterification.

2.2 Introduction

Esters are common functional groups in natural and synthetic molecules. They are found in compounds used in flavoring, fragrance and cosmetic formulations, pharmaceuticals, and are the backbone of triglycerides and the many polymers that are collectively referred to as polyesters.[1] Additionally, esters are frequently used as protecting groups for carboxylic acids and alcohols in organic synthesis.[2] Because esters are so ubiquitous, the development of methods for their mild and efficient synthesis remains an area of active research. Esters are accessible via a variety of synthetic pathways, though the dehydrative coupling of the parent alcohol and carboxylic acid is the most straightforward approach. Classically, these coupling reactions proceed via loss of water with the aid of a strong Brønsted or Lewis acid catalyst, or by preactivation of the carboxylic acid to generate a more potent electrophile.[3] A mechanistically distinct approach, originally described by Mukaiyama and later by Mitsunobu, involves a "redox" coupling via removal of the elements of "H_2" and "O" with a P^{III} reductant and an oxidant such as a sulfenamide, disulfide, or azo compound.[4] These protocols, termed "oxidation-reduction condensations" or redox condensations, tend to be more mild than classical procedures since they proceed at nearly neutral pH and the requisite redox reagents are compatible with a broad range of functionalities.

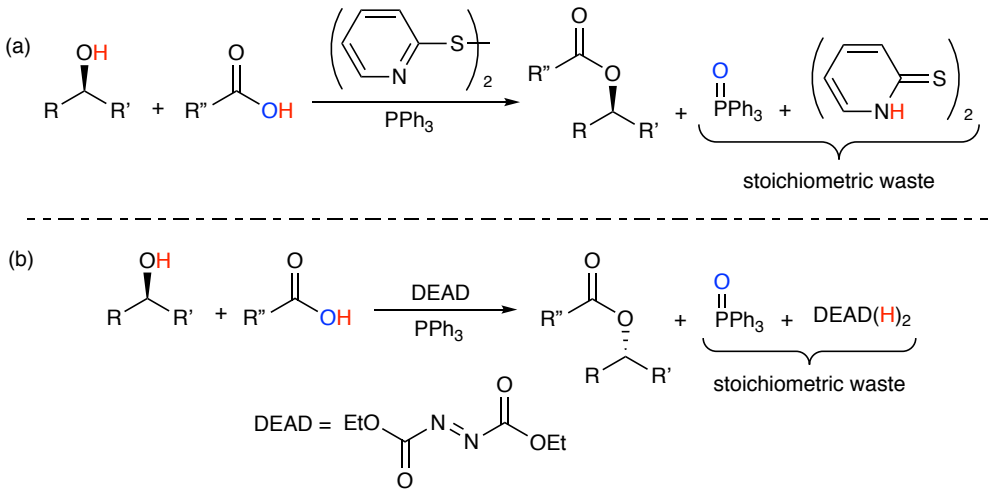

Scheme 2-1. Redox condensation protocols reported by Mukaiyama (a) and Mitsunobu (b).

Nonetheless, the synthetic utility of redox condensation reactions is limited by the requirement for a stoichiometric reductant and oxidant waste they produce, which compromises atom economy and can complicate isolation of the coupling product. To address these issues, recent efforts have focused on catalytic recycling the stoichiometric redox reagents *in situ* using mild, earth-abundant terminal oxidants and reductants.[5] To date, progress has largely centered around catalytic recycling of the organoreductant. For example, O'Brien and Aldrich have reported Mitsunobu reactions in which catalytic phenylphospholane reductants are recycled with cost effective and environmentally benign silanes (Scheme 2-2).[6]

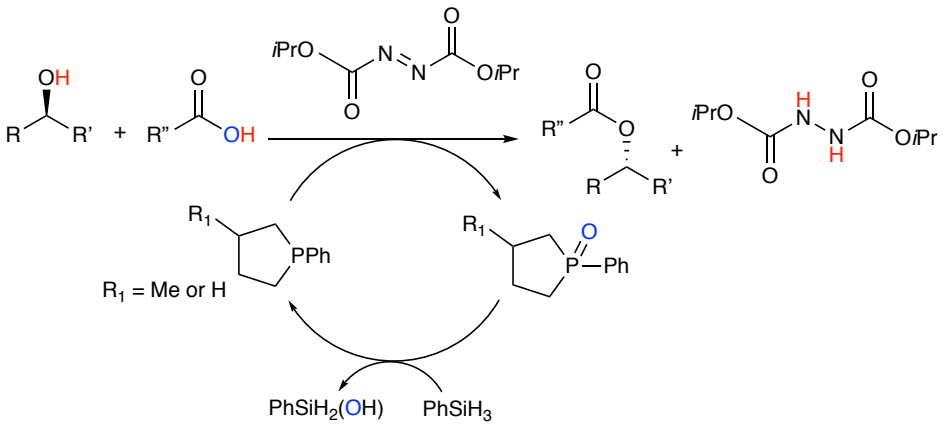

Scheme 2-2. Phosphine recycling system developed by O'Brien.

Similar conditions have proven effective in a number of other reactions that typically require stoichiometric phosphines, including Wittig, Aza-Wittig, and Staudinger reactions, among others.[7] In contrast, there are only three reports of redox dehydration reactions that are catalytic in the organooxidant. The first, reported by Toy and coworkers in 2006, was a Mitsunobu reaction catalytic in diethylazodicarboxylate (DEAD) with iodosobenzene diacetate serving as the terminal oxidant (Scheme 2-3a).[8] While competent for the formation of certain esters, iodosobenzene diacetate is an atom inefficient terminal oxidant, and its propensity to competitively oxidize secondary alcohols limits the synthetic utility of Toy's catalytic protocol. In 2011, Taniguchi described a redox dehydration esterification utilizing catalytic Fe(Pc) (iron(II) phthalocyanine) in the presence of a catalytic pyridine N-oxide and O_2 as the terminal oxidant (Scheme 2-3b).[5b] The combination of Fe(Pc) and O_2 also proved useful for recycling certain specialized mixed aryl azo carboxylate reagents, enabling the development of a catalytic Mitsunobu reaction (Scheme 2-3c).[9] However, in both of the reactions reported by Taniguchi, the substrate scope and yields were diminished relative to the analogous stoichiometric methods owing to complications associated with the use of Fe(Pc) catalyst. In view of these examples, progress towards a more sustainable redox dehydration protocol would require the development of a more effective catalytic oxidant. We assessed that this oxidant would, in the ideal case, be non-toxic, compatible with P^{III} reductants, active at low catalyst loadings, and able to utilize O_2 as a terminal oxidant.

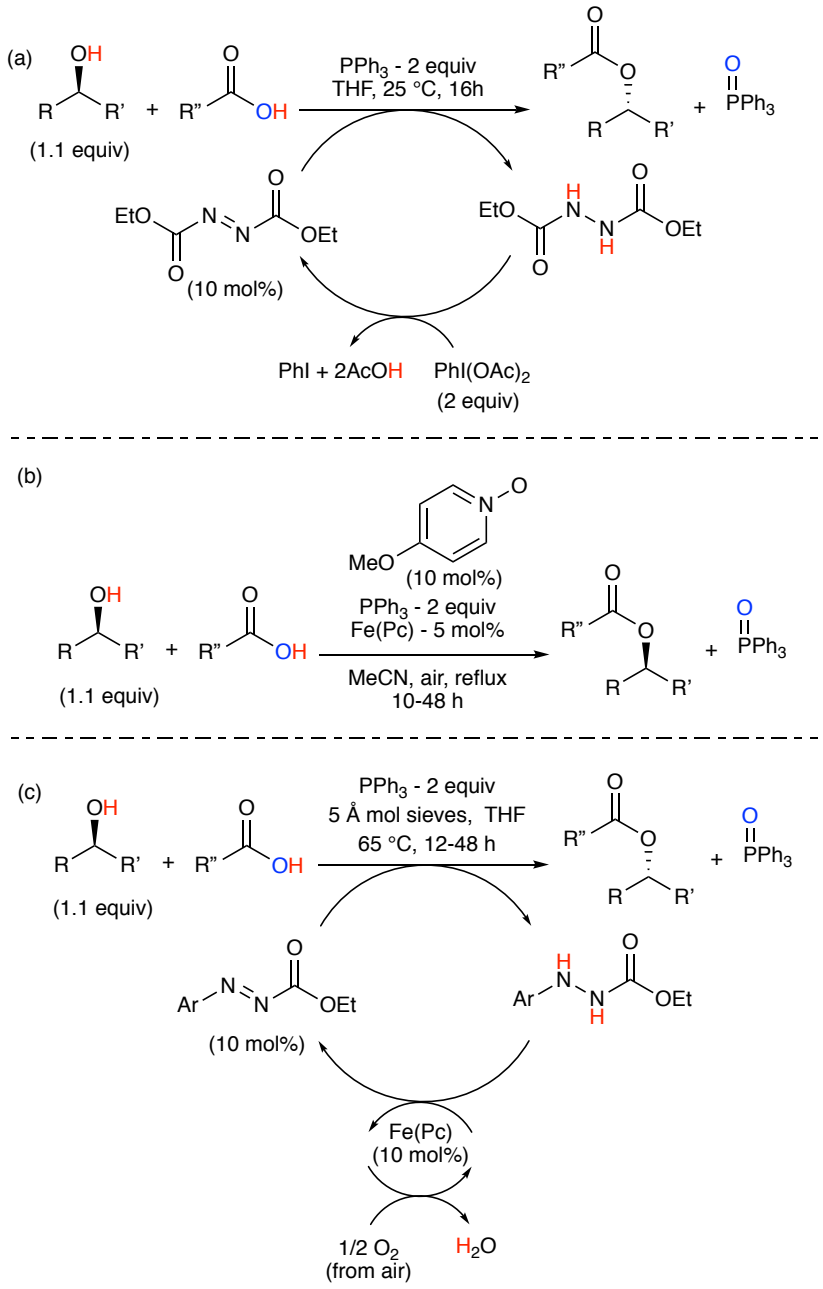

Scheme 2-3. Mitsunobu reaction catalytic in azo reagent reported by Toy (a). Redox esterification (b) and Mitsunobu reaction catalytic in aryl carboxylate azo reagent (c), with catalytic Fe(Pc) and O_2 as terminal oxidant, reported by Taniguchi.

While investigating new synthetic approaches to thioesters, Liebeskind and Srogl demonstrated that S-acyl thiosalicylamides can be generated by the reductive acylation of benzoisothiazolones

(BITs) with a carboxylic acid and P^{III} reagent.[10] In a separate study, Kanai and coworkers established that free thiosalicylamides oxidatively cyclize to regenerate the parent BIT in the presence of O_2 and a copper catalyst[11] thus suggesting a catalytic cyclic based on a benzoisothiazolone-thiosalicylamide interconversion.

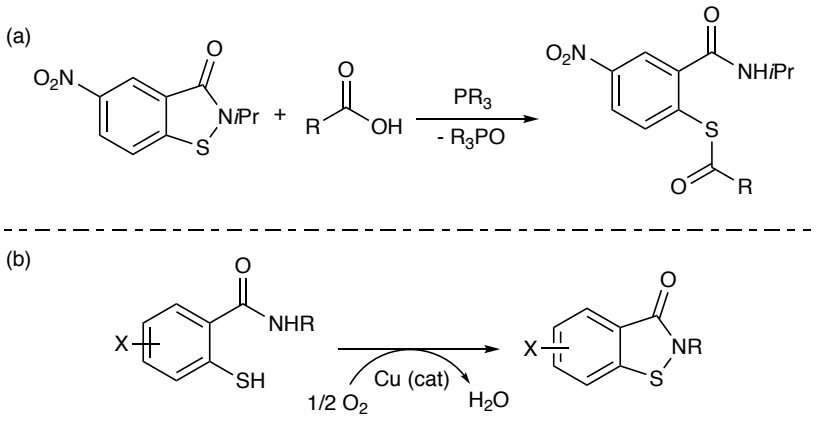

Scheme 2-4. Reductive acylation of BITs to give thioesters (a), and copper catalyzed aerobic oxidation of thiosalcylamides to BITs.

With these precedents, Gangireddy and coworkers found that BITs catalyzed the redox dehydrative coupling of amines and carboxylic acids in the presence of triethyl phosphite as a terminal reductant and co-catalytic copper with O_2 as a terminal oxidant.[12] The reaction mechanism is assumed to proceed via reduction of the BIT with triethylphosphite to generate P^V intermediate **2.02** (Scheme 2-5), which undergoes proton transfer and nucleophilic addition by a carboxylate to give a pentavalent P^V intermediate. The intermediate rapidly decomposes to give triethyl phosphate and thioester **2.03**, which transfers its acyl moiety to an amine nucleophile, giving the amide product and thiophenol **2.04**. Finally, **2.04** is oxidized to the starting BIT by O_2 in a copper-catalyzed process proceeding through disulfide intermediate **2.05** (see Scheme 2-5). Studies aimed at optimizing the BIT structure revealed that electron-withdrawing substituents para to the sulfur on the aryl ring were beneficial, likely owing to attenuation of the nucleophilicity of the thiophenol

intermediate, which is prone to side-reaction via Arbuzov-like ethylation with triethoxy phosphonium intermediates. Additionally, N-alkyl substituted BITs were more stable than those with N-aryl groups, since the N-aryl moiety favors a deoxygenative side-reaction leading to BIT destruction.[13] Ultimately, **2.01** was identified as the most effective BIT for the redox dehydration reaction, allowing the formation of a broad scope of amides and peptides in yields ranging from 61-91%. Nonetheless, the system suffered from three significant drawbacks, including high BIT catalyst loadings (20 mol%), the requirement of a copper co-catalyst, and protracted reaction times of up to 36 hours.[12] In an effort to improve the efficiency and overall rate of BIT catalysis, the Liebeskind lab sought strategies to hasten the rate limiting step, which is the regeneration of the BIT by oxidation of the thiosalicylamide intermediate.[14]

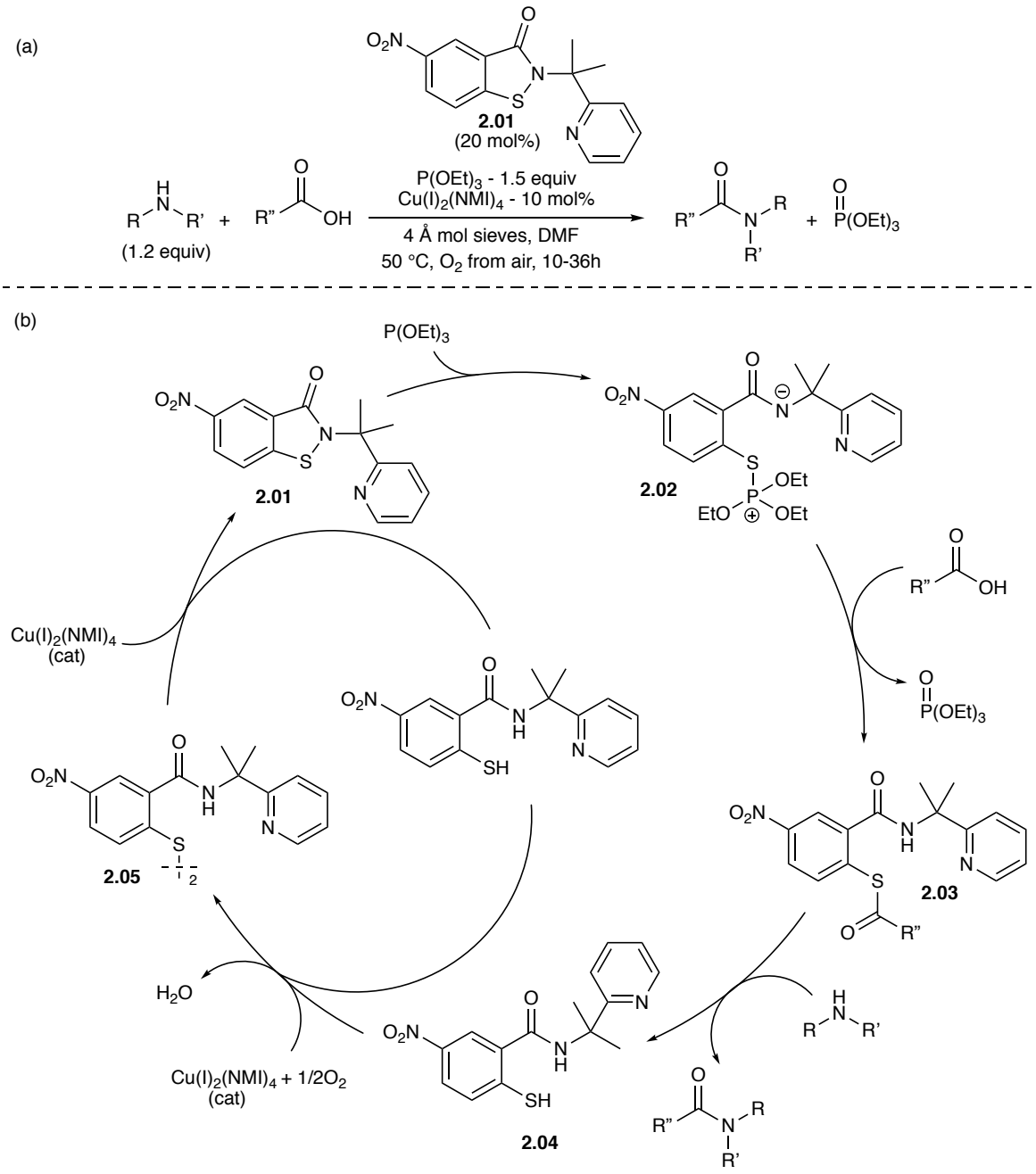

Scheme 2-5. BIT catalyzed amidation reaction (a) and catalytic cycle (b).

In contrast to thiols, selenols are known to undergo direct oxidation with O_2 to generate the corresponding diselenide at ambient pressure and temperatures. This reactivity is highlighted in the selenocystamine catalyzed aerobic oxidation of glutathione to glutathione disulfide (Scheme 2-6, a).[15] Under the conditions described by Chaudiere and coworkers, a 0.2 mM solution of

glutathione was quantitatively oxidized to glutathione disulfide by 120 μM selenocystamine in under 15 minutes, with O_2 from air as the terminal oxidant. Notably, reduction of selenocystamine by glutathione, not oxidation of the selenol intermediate, was the rate limiting step, suggesting that selenol oxidation to the diselenide is rapid. Based on these and other related precedents,[16] replacing the sulfur atom of the BIT with a selenium atom was considered, as it was anticipated that the selenol analogue of **2.04** would undergo oxidation more quickly than thiophenol **2.04**.

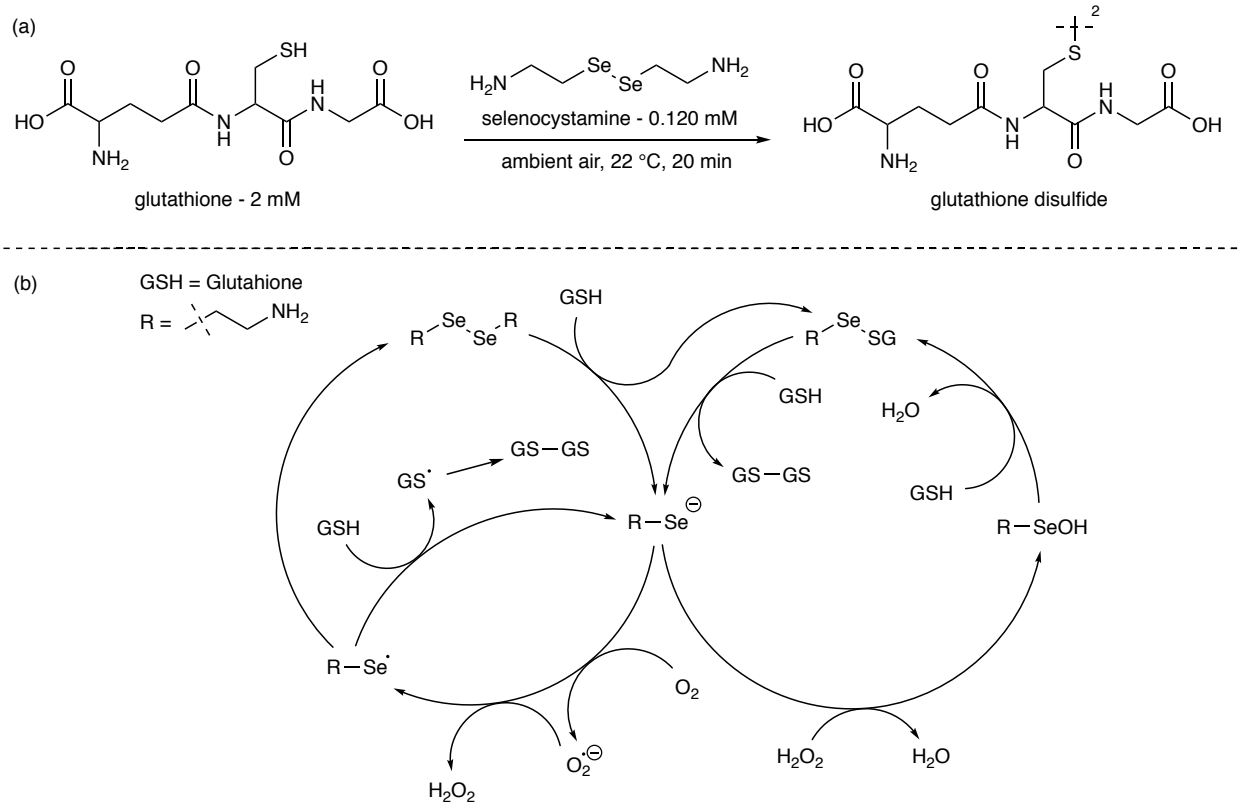

Scheme 2-6. Reaction conditions (a) and catalytic cycle (b) of selenocystamine catalyzed aerobic oxidation of glutathione to glutathione disulfide.

After preparing benzoisoselenazolones **2.07** and **2.08** as shown in Scheme 2-7, Akondi and coworkers evaluated them under the previously optimized conditions for catalytic BIT amidation with the notable exception that they were employed at 5 mol % loading (BIT catalyzed amidation reactions employed 20 mol % of **2.01**). Under these conditions, the benzoisoselenazolone

catalyzed dehydrative coupling of *p*-toluic acid and benzylamine to the corresponding amide was completed within eight hours and in 93% yield.[17]

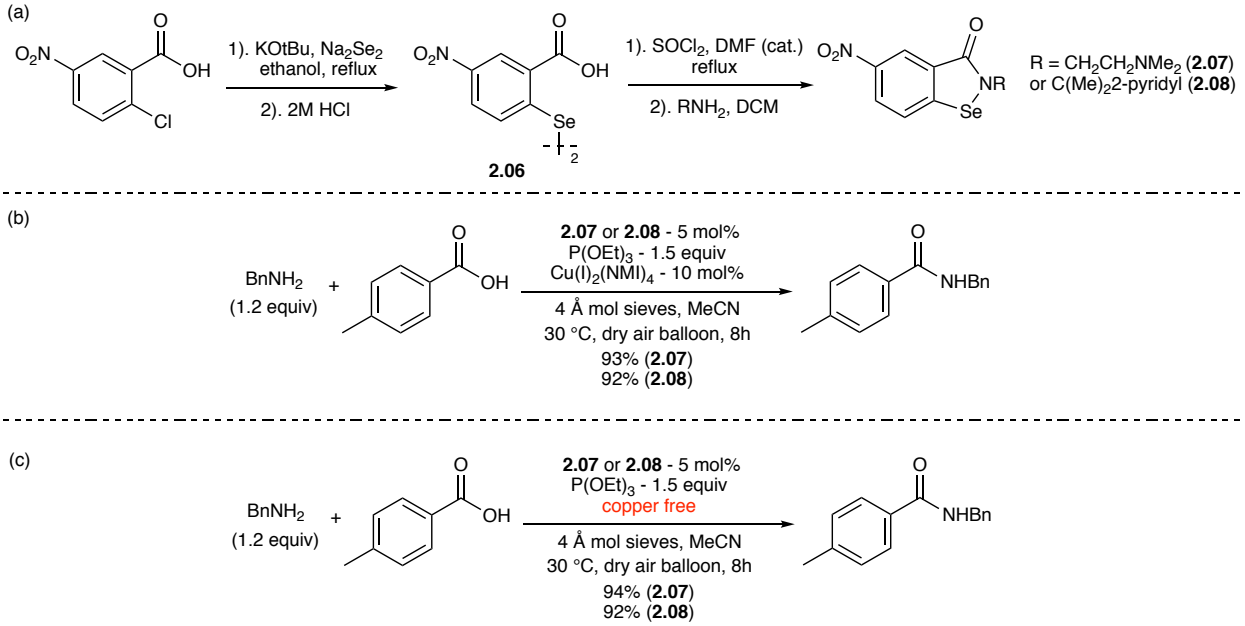

Scheme 2-7. Synthesis of benzoisoselenazolones (a) and catalytic amidation with benzoisoselenazolones in the presence of copper co-catalyst (b) and under copper free conditions (c).

With these results in hand, the role of copper in the benzoisoselenazolone catalyzed amidation reaction was probed. Because selenols tend to undergo oxidation with O_2 relatively quickly in the absence of a transition metal catalyst, it was postulated that the catalytic amidation reaction may proceed in the absence of a copper cocatalyst. Under copper free conditions that were otherwise identical to those shown in Scheme 2-7b, the benzoisoselenazolone catalyzed coupling of toluic acid and benzylamine occurred in similar yield and on a similar time scale to that of the copper containing reactions (scheme 2-7c). This observation is consistent with the hypothesis that selenol intermediate **2.09** should undergo direct oxidation with O_2 without the need for a facilitating co-catalytic metal. Moreover, the fact that benzoisoselenazolone catalysis proceeds in the absence of

copper suggests that these compounds operate via a different catalytic cycle than their sulfur counterparts. We hypothesize that after initial reduction of the benzoisoselenazolone, the resultant selenophenol is oxidized directly with O_2 to generate a disulfide, which is analogous to the copper catalyzed oxidation of thiophenol intermediates to disulfides presumed to take place in the BIT catalytic cycle. However, while disulfides are fated to undergo copper catalyzed disproportionation back to BITs, diselenides are stable to disproportionation in the absence of copper. Therefore, it is likely that diselenides are the catalytically active oxidants and that benzoisoselenazolones serve as precatalysts. Evidence for this theory was obtained when it was demonstrated that tertiary amide diselenides, which are incapable of forming the benzoisoselenazolone heterocycle, are also competent for the coupling of toluic acid and benzylamine.

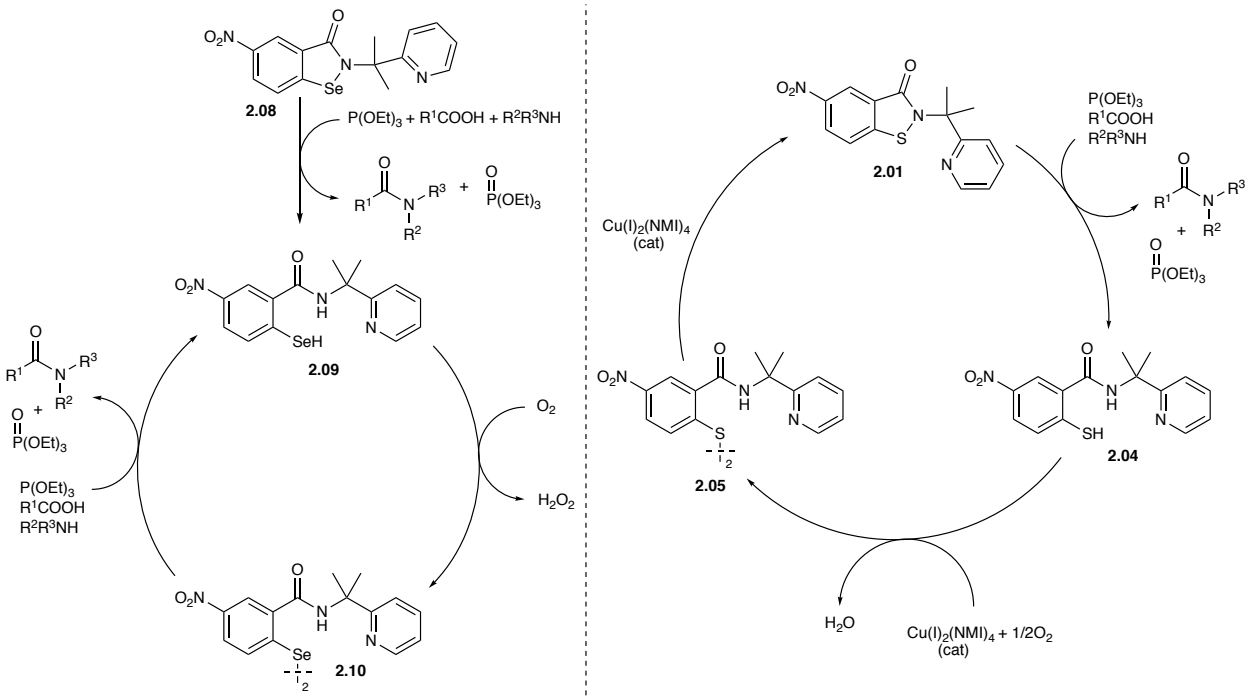

Scheme 2-8: Comparison of diselenide (left) and BIT (right) catalytic cycles.

Following this observation, several diselenides were screened for catalytic activity in the redox dehydration amidation reaction. As was the case with BIT catalysts, *p*-nitro substituted diselenides

performed better than those without an electron withdrawing substituent on the aryl ring. Interestingly, despite not playing an obvious role in diselenide catalysis, ortho substitution of the aryl ring was associated with a substantial improvement in yield of coupling product, and both secondary and tertiary amides were viable. The most effective amide substituents possessed a basic pendant nitrogen atom positioned five atoms away from the aryl ring, possibly due to an increase in the rate of diselenide reduction resulting from an attractive non-bonded interaction between the selenium and nitrogen atoms (Scheme 2-9). Similar hypervalent interactions between divalent selenium and nitrogen donors have been observed and extensively characterized by Tomoda,[18] Silvestru,[19] and others.[20]

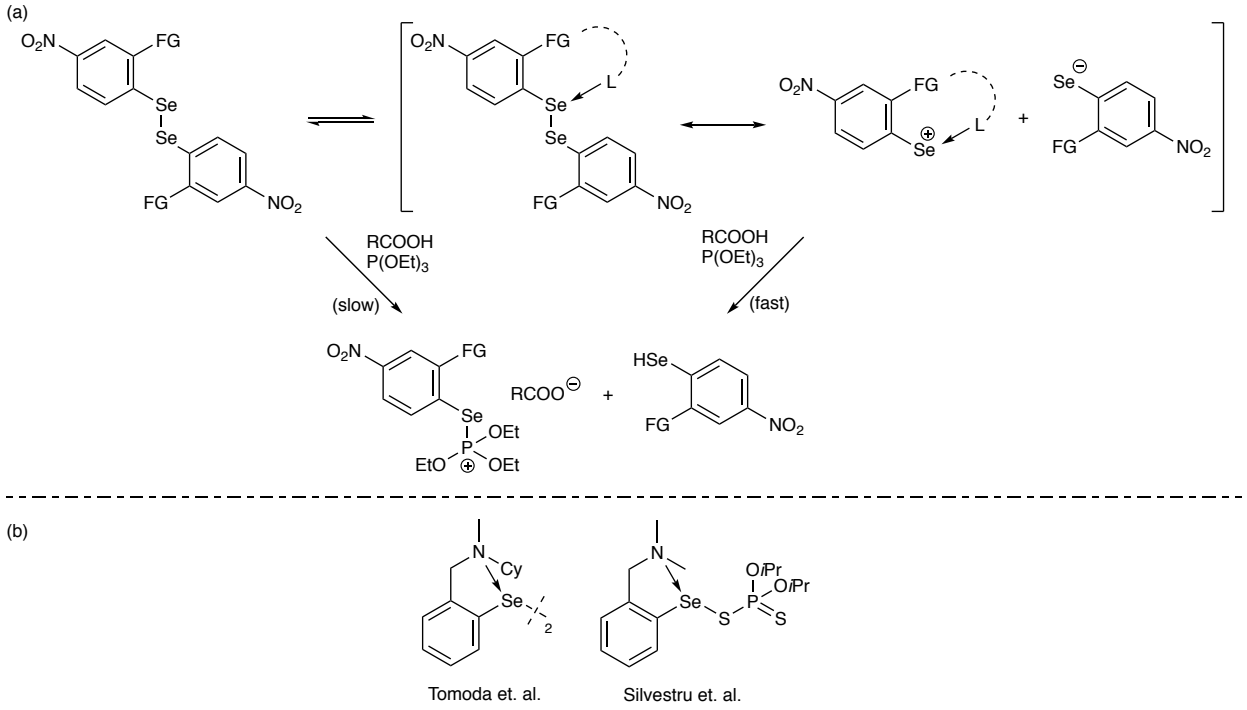

Scheme 2-9. Proposed coordination of divalent selenium with pendant nitrogen (a), and molecular structures of divalent selenium compounds interacting with a nitrogen donor reported by Tomoda and Silvestru (b). Note, the N-Se interaction was, in both cases, confirmed by X-ray crystallography.

Consistent with these observations, diselenide **2.11** was identified as the most efficient catalyst, and the amidation reaction with **2.11** was optimized utilizing benzylamine and *p*-toluic acid as substrates. Under optimal conditions, *p*-toluic benzylamide was generated in 91% yield in only six hours at 30 °C, with 4 Å mol sieves (to scavenge water generated during the selenol reoxidation process) 1.5 equivalents of triethyl phosphite as the terminal reductant, O_2 from air as the terminal oxidant, and only 2.5 mol% of **2.11** as catalytic oxidant.[17] This method proved to be a quite general and mild approach to amidation, tolerating unprotected alcohols and phenols, epimerizable stereocenters, as well as acid and base labile functionalities.

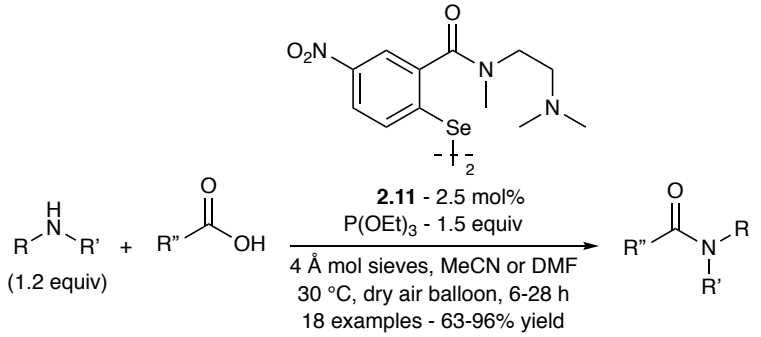

Scheme 2-10. Diselenide catalyzed aerobic amidation conditions.

Given the utility of this amidation protocol, we were interested in extending the substrate scope to include the coupling of alcohols and carboxylic acids. Described below are our efforts toward a redox dehydration esterification reaction employing diselenides as catalytic oxidants.

2.3 Results and Discussion

Treatment of 1 equiv of *p*-toluic acid and 1.2 equiv of 4-methoxyphenethyl alcohol under the conditions previously established for effective amidation and peptidation[17] (2.5 mol % diaryldiselenide **2.11**, 1.5 equiv triethylphosphite, dry air, freshly dried and activated 4Å mol sieves, room temp. in MeCN) over 14 h generated predominantly *p*-toluic anhydride (50%) along

with 31% of the desired ester product, traces of recovered *p*-toluic acid, and 10% of ethyl *p*-toluate (Table 2-1). Inclusion of 10 mol % of the acyl transfer catalyst DMAP[21] within the reaction mixture avoided buildup of the anhydride; the desired ester was formed in 65% yield along with smaller quantities of unreacted *p*-toluic acid (16%) and ethyl *p*-toluate (11%). Raising the reaction temperature to 50 °C improved the conversion to ester (80%) leaving similar quantities of ethyl *p*-toluate (10%) and only minor traces of unreacted *p*-toluic acid.

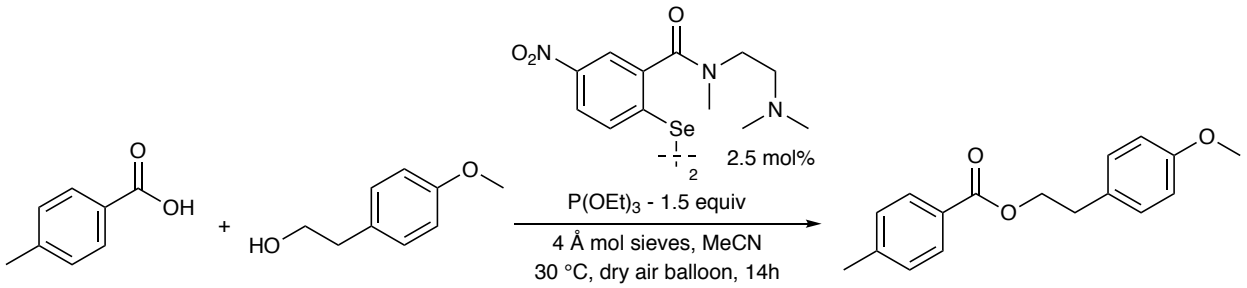

% **1**	°C	additives	% ester	other*
2.5	25	---	31	10, 50, trace
2.5	25	10% DMAP	65	11, 0, 16
2.5	50	10% DMAP	80	10, 0, trace
2.5	50	10% DMAP, 1.1 equiv Et_3N	74	trace, 0, 14
5.0	50	10% DMAP, 1.1 equiv Et_3N	84	trace, 0, trace

*Table 2-1. Optimization of Aerobic, Diselenide-Catalyzed Esterification Conditions. *Yields of ethyl ester, p-toluic anhydride, recovered p-toluic acid, respectively.*

The undesired ethyl ester can be formed in one of two ways: either by carboxylate reacting in an S_N2 reaction with active Arbuzov-like intermediates that are generated during the reaction process when triethylphosphite cleaves the diselenide (i.e. $ArSeP^+(OEt)_3$), or by liberation of free ethanol

during the reaction through the very rapid, acid-catalyzed hydrolysis[22] (or transesterification) of triethylphosphite.

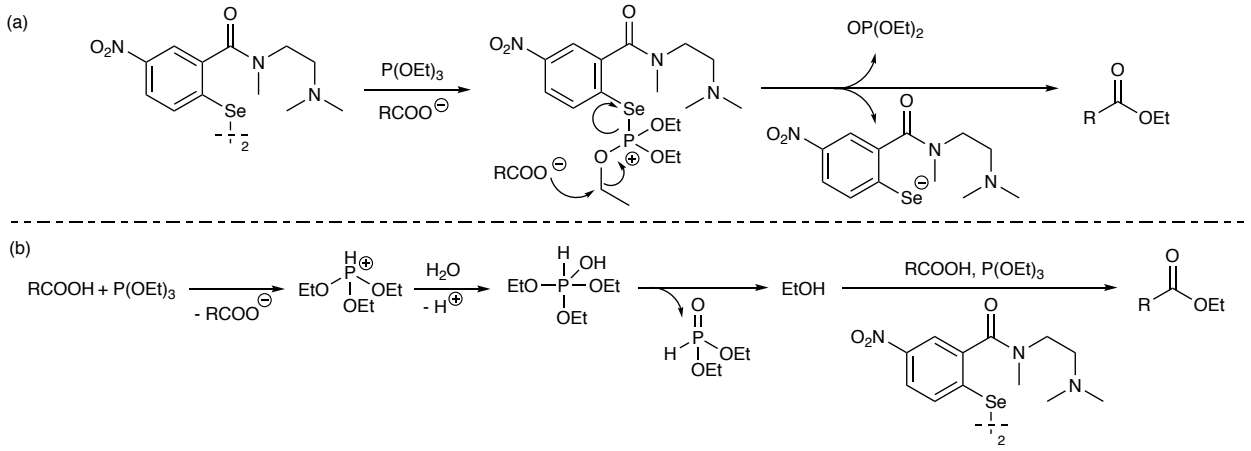

Scheme 2-11. Formation of ethyl ester byproducts resulting from the S_N2 reaction of carboxylic acids with Arbuzov-like intermediates (a) or diselenide catalyzed coupling of carboxylic acids with ethanol generated by acid promoted decomposition of triethylphosphite (b).

Addressing the latter possibility, 1.1 equiv of Et_3N was added to buffer the carboxylate acidity. While this tactic slightly slowed the rate of overall reaction, it effectively mitigated formation of the undesired ethyl ester pointing to acid-catalyzed hydrolysis/alcoholysis of triethylphosphite as the problematic side reaction. Thus, after 14 h the desired ester was formed in 74% yield with 14% of *p*-toluic acid remaining. Optimum conditions were achieved by raising the diselenide loading to 5 mol %. At 5 mol % diselenide, 10 mol % DMAP and 1.1 equiv of Et_3N amine at 50 °C in 14 h, the ester was generated in 84% yield. Only very minor traces of the ethyl ester and *p*-toluic acid were evident. For comparison, the same reactants generated the ester in 78% yield when treated under the Steglich conditions[23] with 1.5 equiv of EDCI (N-(3-Dimethylaminopropyl)-N′-ethylcarbodiimide hydrochloride), 1.5 equiv of Et_3N and catalytic DMAP in CH_2Cl_2 at room temperature for 3 hr.

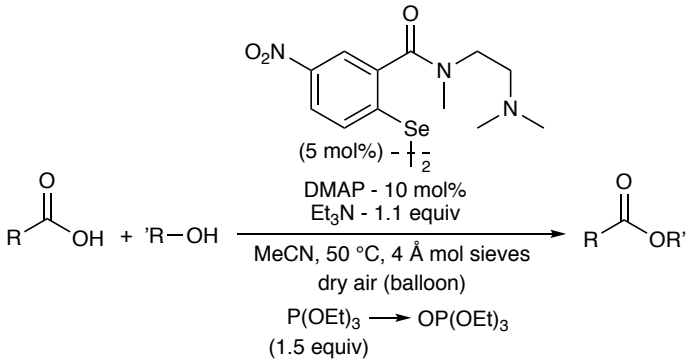

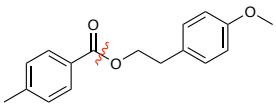
Entry 1, 83%, 12h

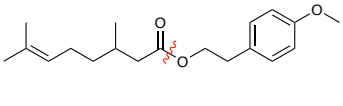
Entry 2, 86%,[a] 10h

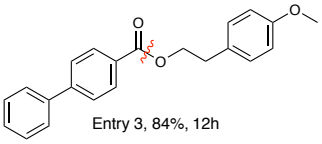
Entry 3, 84%, 12h

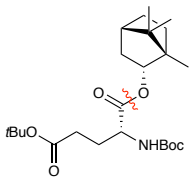

Entry 4, 85%, 14h

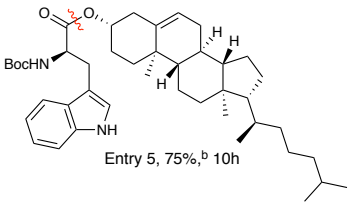

Entry 5, 75%,[b] 10h

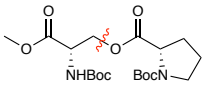

Entry 6, 82%,[b] 10h

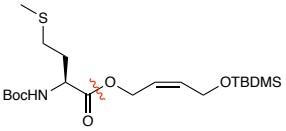

Entry 7, 74%, 12h

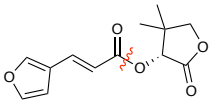
Entry 8, 79%, 12h

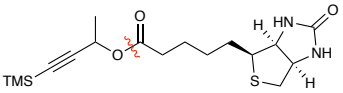

Entry 9, 88%,[c] 14h

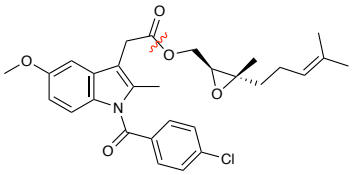

Entry 10, 86%, 11h

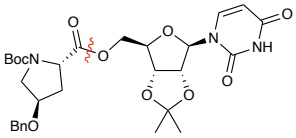

Entry 11, 72%, 12h

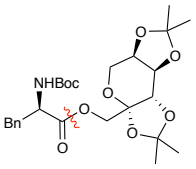

Entry 12, 79%,[b] 10h

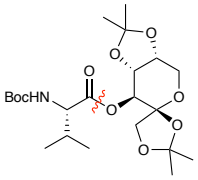

Entry 13, 82%,[b] 10h

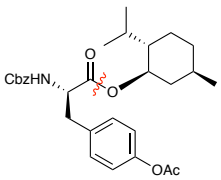

Entry 14, 77%,[b] 10h

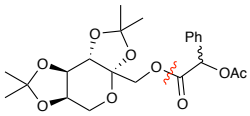

Entry 15, 83%,[b,d] 10h

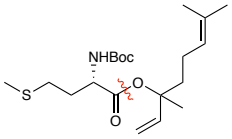

Entry 16, 0%, 12h

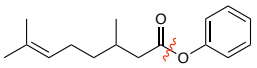
Entry 17, 41%,[a] 8h

Table 2-2. Esterification conducted using aerobic, diselenide catalyzed redox dehydration. Reaction conditions: 1.0 equiv of carboxylic acid, 1.1 equiv of alcohol, 1.5 equiv of $P(OEt)_3$, 10 mol % DMAP, 1.1 equiv Et_3N, 5.0 mol % catalyst, solvent, dry air balloon and 4 Å mol sieves (1.0 x wt % of acid). Solvent, temperature and reaction time are given in the Table entries. [a] *Reaction in the absence of triethylamine.* [b] *EtOAc was used as reaction solvent in place of MeCN.* [c] *DMF was used as reaction solvent in place of MeCN.* [d] *Mixture of diastereomers (1:0.6 dr).*

The Taniguchi procedure[5b] (1.0 equivalent of toluic acid, 1.1 equivalents of *p*-methoxyphenethyl alcohol, 2.0 equivalents of PPh_3, 10 mol % *p*-methoxypyridine N-oxide, and 5 mol % Fe(Pc) in MeCN (0.5 M), reflux for 24h under an air balloon) provided the ester in only 48% yield. In addition to the greater yield of *p*-methoxyphenethyl *p*-toluate, the esterification protocol described here has a number of advantages over Taniguchi's method, including shorter reaction times, lower reaction temperature (50 °C vs ~80 °C), and a broader effective substrate scope. Furthermore, the triethylphosphite reductant utilized in this protocol gives a phosphate byproduct that is easily removed via aqueous workup, whereas the triphenylphosphine oxide byproduct produced in the Taniguchi protocol is not water soluble and can be challenging to separate from relatively hydrophobic esters.

Having identified the optimal conditions for the esterification of *p*-toluic acid and *p*-methoxyphenethyl alcohol, the scope of the reaction was investigated (Table 2-2). Citronellic acid (Entry 2, triethylamine not required) and biphenyl-4-carboxylic acid (Entry 3) reacted smoothly with *p*-methoxyphenethyl alcohol to provide the desired esters in 86% and 84% yield, respectively. Attempted esterification of cholesterol with N-Boc-tryptophan was unsuccessful in MeCN, owing to the poor solubility of cholesterol in this solvent. A switch to EtOAc as solvent gave the anticipated ester in 75% yield (Entry 5). An attempted coupling of N-Boc-serine methyl ester with N-Boc-proline in MeCN was compromised by competitive dehydration of serine to dehydroalanine. Again, switching from MeCN to the less polar EtOAc as solvent was beneficial and delivered the desired product in 82% yield (Entry 6) with no trace of the dehydroalanine byproduct. The esterification of biotin was challenging because of its poor solubility in MeCN. Switching to DMF provided product in 88% yield (Entry 9). Entries 12, 14, and 15 of Table 2-2 were first attempted in MeCN, but in each case the ester products were partially epimerized.

Changing the solvent from MeCN to EtOAc completely suppressed the epimerization in Entries 12 and 14, resulting in the formation of single diastereomers, although partial epimerization was unavoidable with the more C-H acidic product in Entry 15 (1:0.6 dr). Attempts to engage a tertiary alcohol in esterification (Entry 16) were unsuccessful. The esterification of phenols was briefly investigated. Attempts to esterify phenol or methyl-4-hydroxybenzoate with citronellic acid resulted in substantial disappearance of the phenol, full consumption of triethylphosphite, and destruction of the diselenide catalyst, but none of the desired phenolic ester was generated.

To determine how the diselenide and phenol were decaying, a control experiment was conducted with 1.0 equivalent of methyl-4-hydroxybenzoate, 0.5 equivalents of diselenide, 10 mol % DMAP, 1.1 equivalents of triethylamine, and 1.5 equivalents of triethylphosphite (Scheme 2-12a). The reaction was monitored by ^{31}P for changes in triethylphosphite concentration and freed of solvent after 8 hours. Following chromatographic separation of the reaction constituents, selenoether **2.12** was obtained in 68 % yield along with methyl-4-((ethoxy(ethoxymethyl)phosphoryl)oxy)benzoate (**2.13**) in 80% yield. It appears that the selenophosphonium intermediate **2.14**, generated from triethylphosphite and the diselenide, undergoes exchange with the phenol under basic reaction conditions to generate arylselenide **2.15** and aryloxyphosphonium intermediate **2.16**. These react together to generate the observed products **2.12** and **2.13**.

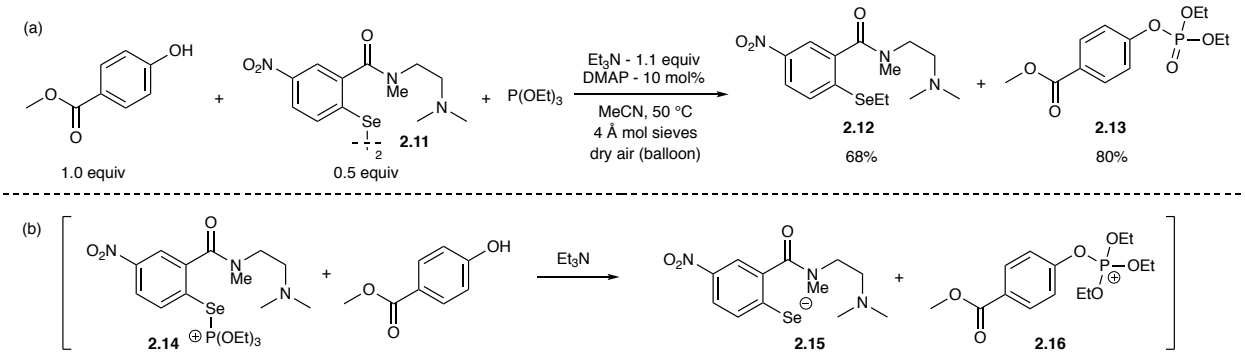

Scheme 2-12. Attempted phenol esterification (a) and key intermediates (b).

In the absence of triethylamine as a catalyst, transesterification of the phenol with the selenophosphonium species does not occur and the selenol does not undergo ethylation. Therefore, the esterification of phenol and citronellic acid was carried out in the absence of triethylamine, providing 41% yield of the phenolic ester after 8 hours (Table 2-2, Entry 17). No attempt was made to optimize this reaction.

The mechanisms of the diselenide catalyzed reactions (amidation[17] and esterification[24]) and the BIT catalyzed reactions[12-13] (amidation) are each distinct, and it is likely that there is a unique active acylating agent under each set of conditions. In the presence of triethylphosphite and a carboxylic acid, BITs undergo reduction presumably to give thiophosphonium intermediates (**2.02**, Scheme 2-12) which would react further with carboxylic acids to generate an acyloxyphosphonium intermediate. Intramolecular decomposition of the acyloxyphosphonium results in the formation of discrete, isolable thioesters (**2.03,** Scheme 2-12). These thioesters are competent acylating agents for amines in stoichiometric reactions and could serve as the active acylating agent in the BIT catalyzed amidation reactions. However, under the BIT catalyzed amidation conditions, it is possible that the amine intercepts the acyloxyphosphonium intermediate prior to the formation of a thioester. In contrast, the reaction between diselenide **2.11,** triethylphosphite, and a carboxylic acid produces the corresponding carboxylic anhydride with no observable selenoester. It is

possible that in lieu of the formation of a selenoester, an acyloxyphosphonium is the active acylating agent. Another possibility is that the selenoester is generated under the conditions but rapidly acylates carboxylate nucleophiles, precluding its detection. In the presence of amines, the formation of anhydrides is not observed. This is likely because amines undergo acylation with either the acyloxyphosphonium or selenoester intermediate more rapidly than carboxylates, which is consistent with the greater nucleophilicity of amines compared to carboxylates. However, when alcohols are used as nucleophiles in place of amines, the anhydride forms preferentially as the carboxylate anion more readily intercepts the activated acyl donor (either selenoester or acyloxyphosphonium) than the neutral alcohol. Consequently, an acyl transfer reagent (DMAP) is necessary to catalyze the reaction between the anhydride and alcohol.

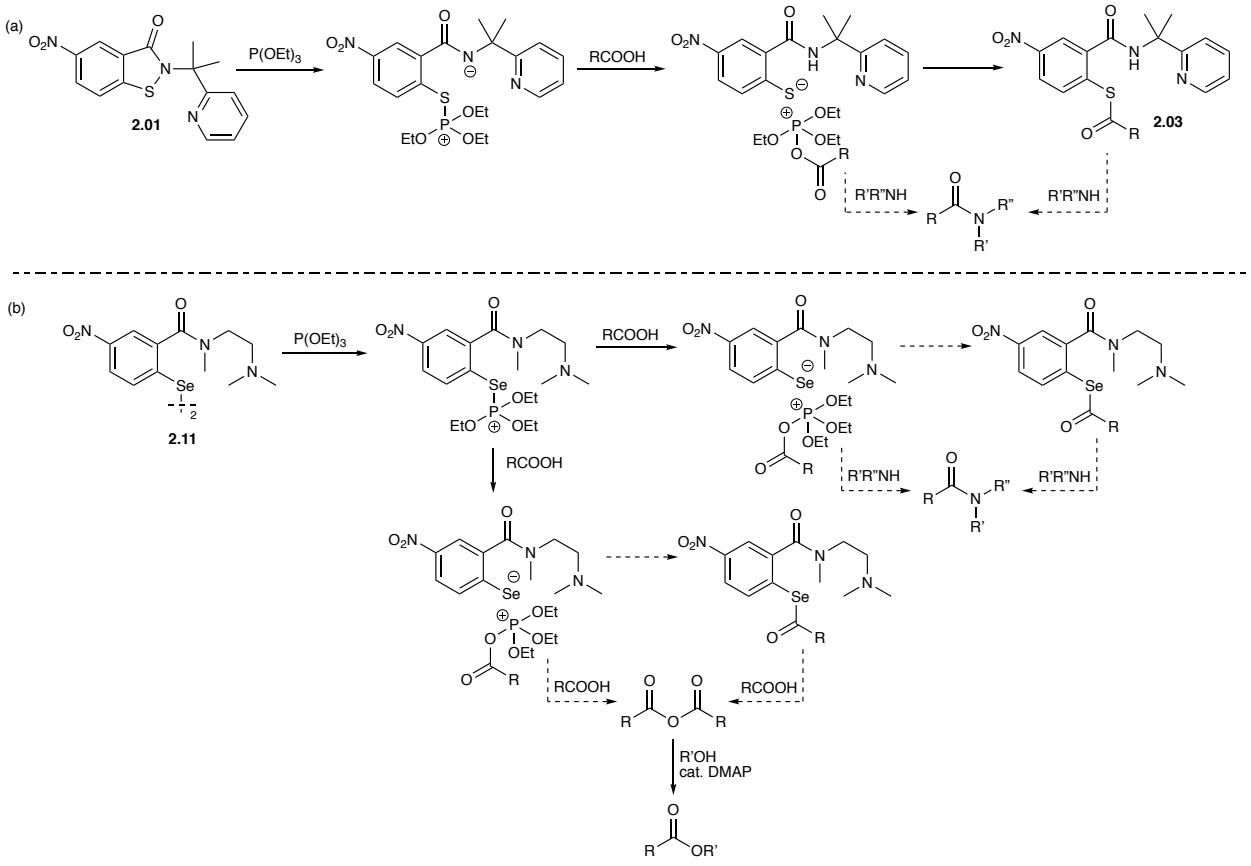

Scheme 1-13. Comparison of reaction pathways in BIT (a) and diselenide (b) catalyzed amidation and esterification reactions.

2.4 Conclusions

We have demonstrated an aerobic, diselenide-catalyzed redox dehydrative generation of O-esters from carboxylic acids and 1° and 2° alcohols, with triethylphosphite as reductant and O_2 from air as a terminal oxidant. Slight deviations from the protocol that was previously described for diselenide catalyzed amidation were necessary. These include the addition of an equivalent of triethylamine to inhibit acid-catalyzed decomposition of triethylphosphite, and inclusion of 10 mol % DMAP to promote acylation of alcohol substrates by *in situ* generated anhydrides. The formation of anhydrides is, itself, a divergence from the reaction pathway that takes place in the amide system, likely resulting from the lowered nucleophilicity of alcohols relative to amines. Our optimized conditions were not generally applicable to the esterification of phenolic substrates, since phenolate, generated under slightly basic conditions, competitively intercepted the acyloxyphosphonium intermediate, leading to the formation of a phenylphosphate byproduct. When triethylamine was omitted from esterification reactions employing a phenolic substrate, the desired ester was obtained in modest yield.

2.5 Experimental Information and Characterization Data

General information

All solvents were purchased from Fisher Scientific and dried over 4Å mol sieves. Mol sieves were activated via heating in a microwave oven for three minutes and dried under reduced pressure for five minutes. Unless otherwise noted, all commercially available reagents and substrates were used directly as received. Compressed dry air was obtained from Nexair and used as received. Thin layer chromatography was performed on Merck silica gel plates and visualized by UV light/$KMnO_4$. ^{1}H, ^{13}C, and ^{31}P NMR spectra were recorded on Bruker 600, Varian INOVA 600,

INOVA 500, INOVA 400, and Mercury 300 spectrometers. Residual solvent resonances were treated as internal reference signals. IR spectra were recorded on a Nicolet iS10 FT-IR spectrometer and the absorption peaks were reported in cm^{-1}. A Thomas capillary melting point apparatus was used to determine the melting points (uncorrected). High resolution mass spectra were obtained with a Thermo LTQ-FTMS instrument equipped with tandem ion trap - ICR mass analyzers at the Emory University Mass Spec Facility Inc. 8-(4-Chlorophenylsulfonamido)-4-(3-(pyridin-3-yl)propyl)octanoic acid was obtained from Novartis (as a gift to the Emory University Center for C-H Functionalization).

General Experimental Procedure for Ester Bond Formation. A 12 mL test tube was charged with 4 Å molecular sieves (100 mg) previously activated in a microwave oven for three minutes and dried under reduced pressure for five minutes. Then the carboxylic acid (0.21 mmol), diselenide **2.11**[17] (0.011 mmol), and 4-dimethylaminopyridine (2.6 mg, 0.021 mmol) were added followed by dry CH_3CN, EtOAc, or DMF (1.0 mL, 0.2M, moisture content <25 ppm). The alcohol (0.23 mmol), 4-dimethylaminopyridine (0.021 mmol), triethylamine, (0.23 mmol) and triethylphosphite (0.32 mmol) were added sequentially. The reaction mixture was stirred for 10 – 18 h at 50 °C (temperature controlled with an aluminum block on a hot plate) under a dry air atmosphere (balloon). Upon complete conversion of carboxylic acid as monitored by TLC, the reaction mixture was filtered, and the molecular sieves thoroughly washed with CH_2Cl_2 (DCM). The combined filtrate was concentrated under reduced pressure and the crude product was purified by flash column chromatography using the eluents mentioned below to obtain the ester product.

Experimental Procedure for Reactions Reported in Table 2-1. A 12 mL test tube was charged with 4 Å molecular sieves (100 mg) previously activated in a microwave oven for three minutes and dried under reduced pressure for five minutes. Then toluic acid (29 mg, 0.21 mmol) and diselenide **2.11** (3.6 mg, 0.0055 mmol or 7.2 mg, 0.011 mmol) were added. For the reactions in which 4-dimethylaminopyridine (2.6 mg, 0.021 mmol) was employed, it was added followed by dry CH_3CN (1.0 mL, 0.2M, moisture content <25 ppm) and *p*-methoxy-phenethyl alcohol (35 mg, 0.23 mmol). If triethylamine (33 μL, 0.23 mmol) was employed, it was added followed by triethylphosphite (0.32 mmol). Lastly, 1,3,5-trimethoxybenzene was added and used as an internal standard. The reaction was stirred at either 25 or 50 °C (temperature controlled with an aluminum block on a hot plate) under a dry air atmosphere (balloon) and stopped after 14 h, at which time the reaction mixtures were concentrated under reduced pressure and analyzed by ^{1}H NMR. Reported yields are based on NMR integration of product peaks versus the internal standard.

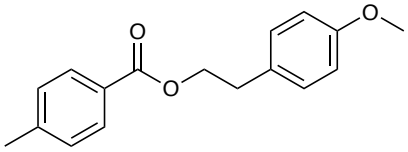

4-Methoxyphenethyl 4-methylbenzoate - (Table 2-2, Entry 1). A mixture of *p*-toluic acid (29 mg, 0.21 mmol), diselenide **2.11** (7.2 mg, 0.011 mmol), 4-dimethylaminopyridine (2.6 mg, 0.021 mmol), and 4 Å molecular sieves (100 mg) in dry CH_3CN (1 mL, 0.2M) was treated with *p*-methoxy-phenethyl alcohol (35 mg, 0.231 mmol), triethylamine (33 μL, 0.231 mmol), and $P(OEt)_3$ (54 μL, 0.32 mmol) according to the general procedure. The coupling reaction was stirred for 10 h under dry air at 50 °C and purified by flash column chromatography using SiO_2 and 7% EtOAc in hexanes to give the pure ester as a colorless oil (47 mg, 83% yield). ^{1}H NMR (400 MHz, chloroform-*d*) δ 7.95 – 7.87 (m, 2H), 7.25 – 7.22 (m, 2H), 7.22 – 7.18 (m, 2H), 6.88 – 6.84 (m,

2H), 4.47 (t, J = 7.0 Hz, 2H), 3.80 (s, 3H), 3.01 (t, J = 7.0 Hz, 2H), 2.41 (s, 3H). ^{13}C NMR (150 MHz, chloroform-*d*) δ 166.7, 158.5, 143.7, 130.2, 130.1, 129.7, 129.2, 127.8, 114.1, 65.7, 55.4, 34.5, 21.8. IR (neat, cm^{-1}): 1710. HRMS (ESI) Calcd for $C_{17}H_{19}O_3$ $[M+H]^+$: 271.1329. Found: 271.1328.

***O*-Esterification Comparison Results.**

Steglich Conditions.[23] To a test tube under N_2 containing a magnetic stir bar and *p*-toluic acid (29 mg, 0.21 mmol), *p*-methoxyphenethyl alcohol (0.231, 0.231 mmol), and DMAP (2.5 mg, 0.021 mmol) in dichloromethane (1 mL, 0.2 M), Et_3N (44 uL, 0.315 mmol) was added N-(3-dimethylaminopropyl)-N′-ethylcarbodiimide hydrochloride (60 mg, 0.315 mmol) under a stream of nitrogen. The reaction was stirred at room temperature for 3 h and determined to be complete by TLC (7% EtOAc in hexanes). The crude reaction mixture was filtered over silica and the silica washed with dichloromethane to furnish the pure ester as a colorless oil (44 mg, 78% yield).

Taniguchi Conditions. Following the procedure reported by Taniguchi and coworkers,[5b] a mixture of p-toluic acid (29 mg, 0.21 mmol), *p*-methoxyphenethyl alcohol (0.231, 0.231 mmol), triphenylphosphine (110 mg, 0.42 mmol), iron(II) phthalocyanine (6.2 mg, 0.011 mmol), and 4-methoxypyridine N-oxide (2.6 mg, 0.021 mmol) in MeCN (0.5 mL, 0.5 M) was heated at reflux with an aluminum block on hot plate under dry air (balloon) for 24 h. The mixture was filtered, and the solvent was removed under reduced pressure. The residue was purified by filtration over silica gel, eluting with dichloromethane to give the pure ester as a colorless oil (27 mg, 48% yield).

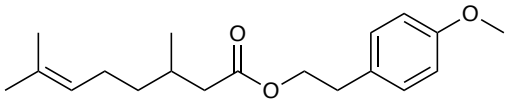

4-Methoxyphenethyl 3,7-dimethyloct-6-enoate - (Table 2-2, Entry 2). A mixture of racemic citronellic acid (36 mg, 0.21 mmol, 94% pure), diselenide **2.11** (7.2 mg, 0.011 mmol), 4-dimethylaminopyridine (2.6 mg, 0.021 mmol), and 4 Å molecular sieves (100 mg) in dry CH_3CN (1 mL, 0.2M) was treated with *p*-methoxyphenethyl alcohol (35 mg, 0.231 mmol), triethylamine (33 µL, 0.23 mmol), and $P(OEt)_3$ (54 µL, 0.32 mmol) according to the general procedure. The coupling reaction was stirred for 10 h under dry air at 50 °C and purified by flash column chromatography using SiO_2 and 5% EtOAc in hexanes to give the pure ester as a colorless oil (55 mg, 86% yield). ^{1}H NMR (600 MHz, chloroform-*d*) δ 7.14 (AA' of AA'XX', 2H), 6.84 (XX' of AA'XX', 2H), 5.08 (tp, *J* = 7.1, 1.4 Hz, 1H), 4.25 (t, *J* = 7.1 Hz, 2H), 3.79 (s, 3H), 2.88 (t, *J* = 7.1 Hz, 2H), 2.30 (dd, *J* = 14.7, 5.9 Hz, 1H), 2.10 (dd, *J* = 14.7, 8.2 Hz, 1H), 2.04 – 1.89 (m, 3H), 1.68 (q, *J* = 1.3 Hz, 3H), 1.60 (d, *J* = 1.3 Hz, 3H), 1.36 – 1.29 (m, 1H), 1.20 (dddd, *J* = 13.6, 9.4, 7.8, 5.9 Hz, 1H), 0.91 (d, *J* = 6.7 Hz, 3H). ^{13}C NMR (150 MHz, chloroform-*d*) δ 173.4,158.4, 131.7, 130.04, 129.98, 124.4, 114.1, 65.0, 55.4, 42.0, 36.9, 34.4, 30.2, 25.9, 25.6, 19.7, 17.8. IR ($CDCl_3$, cm^{-1}): 1733. HRMS (ESI) Calcd for $C_{19}H_{32}NO_3$ $[M+NH_4]^+$: 322.2377. Found: 322.2379.

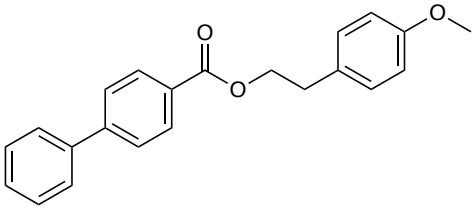

4-Methoxyphenethyl [1,1'-biphenyl]-4-carboxylate - (Table 2-2, Entry 3). A mixture of biphenyl-4-carboxylic acid (42 mg, 0.21 mmol, 95% pure), diselenide **2.11** (7.2 mg, 0.011 mmol), 4-dimethylaminopyridine (2.6 mg, 0.021 mmol), and 4 Å molecular sieves (100 mg) in dry CH_3CN (1 mL, 0.2M) was treated with *p*-methoxyphenethyl alcohol (35 mg, 0.231 mmol), triethylamine

(33 μL, 0.23 mmol), and $P(OEt)_3$ (54 μL, 0.32 mmol) according to the general procedure. The coupling reaction was stirred for 12 h under dry air at 50 °C and purified by flash column chromatography using SiO_2 and 7% EtOAc in hexanes to give the pure ester as a crystalline white solid (56 mg, 84% yield). ^{1}H NMR (600 MHz, chloroform-*d*) δ 8.10 – 8.07 (m, 2H), 7.68 – 7.64 (m, 2H), 7.64 – 7.61 (m, 2H), 7.50 – 7.45 (m, 2H), 7.40 (ddt, *J* = 8.1, 6.7, 1.3 Hz, 1H), 7.25 – 7.20 (m, 2H), 6.90 – 6.86 (m, 2H), 4.52 (t, *J* = 7.0 Hz, 2H), 3.80 (s, 3H), 3.04 (t, *J* = 7.0 Hz, 2H). ^{13}C NMR (150 MHz, chloroform-*d*) δ 166.6, 158.5, 145.8, 140.2, 130.2, 130.1, 129.2, 129.1, 128.3, 127.4, 127.2, 114.1, 65.9, 55.4, 34.6. IR ($CDCl_3$, cm^{-1}): 1711. HRMS (ESI) Calcd for $C_{22}H_{21}O_3$ $[M+H]^+$: 333.1485. Found: 333.1490. Melting point: 127-128 °C (recrystallized from EtOAc/hexanes).

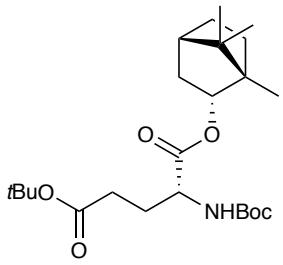

5-(*tert*-Butyl) 1-((1*S*,2*R*,4*S*)-1,7,7-trimethylbicyclo[2.2.1]heptan-2-yl) (*tert*-butoxycarbonyl)-*D*-glutamate - (Table 2-2, Entry 4). A mixture of Boc-L-glutamic acid 1-tert-butyl ester (64 mg, 0.21 mmol), diselenide **2.11** (7.2 mg, 0.011 mmol), 4-dimethylaminopyridine (2.6 mg, 0.021 mmol), and 4 Å molecular sieves (100 mg) in dry CH_3CN (1 mL, 0.2M) was treated with (1S,2R,4S)-1,7,7-trimethylbicyclo[2.2.1]heptan-2-ol (36 mg, 0.23 mmol), triethylamine (33 μL, 0.23 mmol), and $P(OEt)_3$ (54 μL, 0.32 mmol) according to the general procedure. The coupling reaction was stirred for 14 h under dry air at 50 °C and purified by flash column chromatography using SiO_2 and 10% EtOAc in hexanes to give the pure ester as a colorless oil (78 mg, 85% yield). ^{1}H NMR (600 MHz, chloroform-*d*) δ 5.09 (d, *J* = 8.4 Hz, 1H), 4.94 (ddd, *J* = 10.0, 3.5, 2.2 Hz,

1H), 4.38 – 4.28 (m, 1H), 2.35 (ddd, *J* = 16.3, 8.6, 6.7 Hz, 2H), 2.27 (ddd, *J* = 16.3, 8.6, 6.3 Hz, 1H), 2.18 – 2.10 (m, 1H), 1.97 – 1.88 (m, 2H), 1.75 (ddq, *J* = 12.2, 8.1, 4.0 Hz, 1H), 1.69 (t, *J* = 4.6 Hz, 1H), 1.45 (s, 9H), 1.44 (s, 9H), 1.34 – 1.23 (m, 2H), 1.02 (dd, *J* = 13.8, 3.4 Hz, 1H), 0.90 (s, 3H), 0.88 (s, 3H), 0.83 (s, 3H). ^{13}C NMR (150 MHz, chloroform-*d*) δ 172.8, 172.2, 155.5, 81.4, 80.8, 80.0, 53.5, 49.1, 48.1, 45.0, 36.7, 31.8, 28.5, 28.2, 28.13, 28.11, 27.3, 19.8, 19.0, 13.7.IR ($CDCl_3$, cm^{-1}): 3361, 1734, 1717, 1700. HRMS (ESI) Calcd for $C_{24}H_{42}NO_6$ $[M+H]^+$: 440.3007. Found: 440.3013.

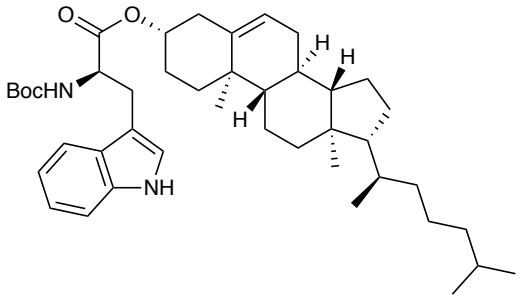

(3*S*,8*S*,9*S*,10*R*,13*R*,14*S*,17*R*)-10,13-Dimethyl-17-((*R*)-6-methylheptan-2-yl)-2,3,4,7,8,9,10,11,12,13,14,15,16,17-tetradecahydro-1*H*-cyclopenta[*a*]phenanthren-3-yl (*tert*-butoxycarbonyl)-*D*-tryptophanate - (Table 2-2, Entry 5). A mixture of N-α-Boc-D-tryptophan (64 mg, 0.21 mmol), diselenide **2.11** (7.2 mg, 0.011 mmol), 4-dimethylaminopyridine (2.6 mg, 0.021 mmol), and 4 Å molecular sieves (100 mg) in dry EtOAc (1 mL, 0.2M) was treated with cholesterol (89 mg, 0.23 mmol), triethylamine (33 µL, 0.23 mmol), and $P(OEt)_3$ (54 µL, 0.32 mmol) according to the general procedure. The coupling reaction was stirred for 14 h under dry air at 50 °C and purified by flash column chromatography using SiO_2 and 3% EtOAc in DCM to give the pure ester as a white foam (106 mg, 75% yield). ^{1}H NMR (600 MHz, chloroform-d) δ 8.05 (s, 1H), 7.59 (d, J = 6.9 Hz, 1H), 7.35 (d, J = 8.2 Hz, 1H), 7.19 (ddd, J = 8.1, 7.0, 1.1 Hz, 1H), 7.12 (t, J = 7.5 Hz, 1H), 7.02 (d, J = 2.4 Hz, 1H), 5.33 (d, J = 5.7 Hz, 1H), 5.07 (d, J = 8.3 Hz, 1H), 4.67 – 4.49 (m, 2H), 3.38 – 3.18 (m, 2H), 2.20 (d, J = 10.1 Hz, 2H), 2.00 (dt, J = 12.6, 3.5 Hz, 1H),

1.99 – 1.93 (m, 1H), 1.82 (dtd, J = 13.2, 6.3, 3.5 Hz, 2H), 1.75 – 1.67 (m, 1H), 1.61 – 1.23 (m, 21H), 1.19 – 0.89 (m, 16H), 0.87 (d, J = 2.8 Hz, 3H), 0.86 (d, J = 2.7 Hz, 3H), 0.67 (s, 3H). ^{13}C NMR (150 MHz, chloroform-*d*) δ 171.8, 155.4, 139.6, 136.2, 128.1, 122.9, 122.8, 122.3, 119.7, 119.2, 111.2, 110.7, 79.8, 75.2, 56.8, 56.3, 54.6, 50.1, 42.5, 39.9, 39.7, 38.0, 37.1, 36.7, 36.3, 35.9, 32.04, 31.99, 28.5, 28.4, 28.2, 27.7, 24.4, 24.0, 23.0, 22.7, 21.2, 19.4, 18.9, 12.0. IR ($CDCl_3$, cm^{-1}): 3415, 3349, 1696. HRMS (ESI) Calcd for $C_{43}H_{63}N_2O_4$ [M-H]$^-$: 671.4793. Found: 671.4799. Melting point: 87-89 °C (recrystallized from ether/hexanes).

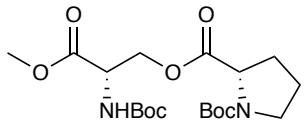

2-((S)-2-((tert-Butoxycarbonyl)amino)-3-methoxy-3-oxopropyl) 1-(tert-butyl) (S)-pyrrolidine-1,2-dicarboxylate - (Table 2-2, Entry 6). A mixture of N-Boc-L-proline (45 mg, 0.21 mmol), diselenide **2.11** (7.2 mg, 0.011 mmol), 4-dimethylaminopyridine (2.6 mg, 0.021 mmol), and 4 Å molecular sieves (100 mg) in dry EtOAc (1 mL, 0.2M) was treated with N-Boc-L-serine methyl ester (51 mg, 0.23 mmol), triethylamine (33 μL, 0.23 mmol), and $P(OEt)_3$ (54 μL, 0.32 mmol) according to the general procedure. The coupling reaction was stirred for 10 h under dry air at 50 °C and purified by flash column chromatography using SiO_2 and 30% EtOAc in hexanes to give the pure ester as a colorless oil (70 mg, 82% yield). ^{1}H NMR (400 MHz, chloroform-*d*) δ 5.60, 5.24 (d, *J* = 8.6 Hz, 1H, rotamers), 4.63 – 4.50 (m, 2H), 4.41 (dtd, *J* = 33.9, 11.2, 3.8 Hz, 2H), 4.29, 4.21 (dd, *J* = 8.6, 4.0 Hz, 1H, rotamers), 3.75 (s, 3H), 3.60 – 3.31 (m, 2H), 2.20 (ddq, *J* = 16.0, 12.4, 8.2 Hz, 1H), 2.05 – 1.81 (m, 3H), 1.48, 1.40 (s, 9H rotamers), 1.44 (s, 9H). ^{13}C NMR (150 MHz, chloroform-*d*) δ 172.8, 172.5, 170.4, 170.2, 155.5, 155.2, 154.7, 153.7, 80.5, 80.2, 80.1, 64.9, 64.8, 59.2, 59.0, 53.05, 53.02, 52.8, 52.7, 46.7, 46.4, 31.0, 30.1, 28.6, 28.42, 28.38, 24.5,

23.6. IR ($CDCl_3$, cm^{-1}): 3347, 1755, 1737, 1712, 1693. HRMS (ESI) Calcd for $C_{19}H_{36}N_3O_8$ $[M+NH_4]^+$: 434.2497. Found: 434.2492.

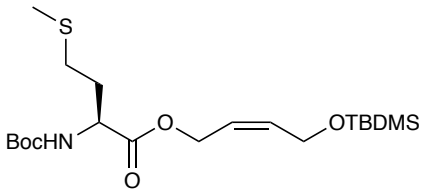

(*Z*)-4-((*tert*-Butyldimethylsilyl)oxy)but-2-en-1-yl (*tert*-butoxycarbonyl)-*L*-methioninate - (Table 2-2, Entry 7). A mixture of N-Boc-L-methionine (52 mg, 0.21 mmol), diselenide **2.11** (7.2 mg, 0.011 mmol), 4-dimethylaminopyridine (2.6 mg, 0.021 mmol), and 4 Å molecular sieves (100 mg) in dry CH_3CN (1 mL, 0.2M) was treated with (*Z*)-4-((*tert*-butyldimethylsilyl)oxy)but-2-en-1-ol (47 mg, 0.23 mmol), triethylamine (33 uL, 0.231 mmol), and $P(OEt)_3$ (54 µL, 0.32 mmol) according to the general procedure. The coupling reaction was stirred for 12 h under dry air at 50 °C and purified by flash column chromatography using SiO_2 and 15% EtOAc in hexanes to give the pure ester as a colorless oil (68 mg, 74% yield). ^{1}H NMR (600 MHz, chloroform-*d*) δ 5.75 (dtt, *J* = 11.5, 5.8, 1.5 Hz, 1H), 5.56 (dtt, *J* = 11.3, 6.8, 1.8 Hz, 1H), 5.11 (d, *J* = 8.2 Hz, 1H), 4.78 – 4.70 (m, 2H), 4.44 – 4.38 (m, 1H), 4.28 (ddt, *J* = 5.8, 1.8, 0.9 Hz, 2H), 2.57 – 2.50 (m, 2H), 2.17 – 2.10 (m, 1H), 2.09 (s, 3H), 1.92 (dq, *J* = 14.6, 7.6 Hz, 1H), 1.44 (s, 9H), 0.90 (s, 9H), 0.08 (s, 6H). ^{13}C NMR (150 MHz, chloroform-*d*) δ 172.2, 155.4, 134.7, 123.6, 80.2, 61.5, 59.7, 52.3, 32.4, 30.1, 28.5, 26.1, 18.5, 15.7, -5.1. IR (neat, cm^{-1}): 3351, 1714. HRMS (ESI) Calcd for $C_{20}H_{40}NO_5SSi$ $[M+H]^+$: 434.2391. Found: 434.2389.

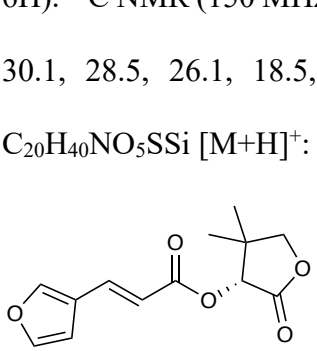

(*R*)-4,4-Dimethyl-2-oxotetrahydrofuran-3-yl (*E*)-3-(furan-3-yl)acrylate - (Table 2-2, Entry 8). A mixture of (*E*)-3-(furan-3-yl)acrylic acid (29 mg, 0.21 mmol), diselenide **2.11** (7.2 mg, 0.011

mmol), 4-dimethylaminopyridine (2.6 mg, 0.021 mmol), and 4 Å molecular sieves (100 mg) in dry CH_3CN (1 mL, 0.2M) was treated with (*R*)-3-hydroxy-4,4-dimethyldihydrofuran-2(3*H*)-one (30 mg, 0.23 mmol), triethylamine (33 µL, 0.23 mmol), and $P(OEt)_3$ (54 µL, 0.32 mmol) according to the general procedure. The coupling reaction was stirred for 12 h under dry air at 50 °C and purified by flash column chromatography using SiO_2 and 30% EtOAc in hexanes to give the pure ester as a colorless oil (40 mg, 79% yield). ^{1}H NMR (400 MHz, chloroform-*d*) δ 7.76 – 7.62 (m, 2H), 7.45 (ddd, *J* = 2.1, 1.5, 0.8 Hz, 1H), 6.61 (dt, *J* = 1.9, 0.7 Hz, 1H), 6.25 (dd, *J* = 15.8, 0.5 Hz, 1H), 5.49 (s, 1H), 4.09 (d, *J* = 9.0 Hz, 1H), 4.06 (d, *J* = 9.3 Hz, 2H), 1.24 (s, 3H), 1.16 (s, 3H). ^{13}C NMR (150 MHz, chloroform-*d*) δ 172.7, 165.8, 145.3, 144.8, 137.0, 122.6, 116.2, 107.5, 76.4, 75.2, 40.6, 23.3, 20.1. IR ($CDCl_3$, cm^{-1}): 1781, 1716, 1684. HRMS (ESI) Calcd for $C_{13}H_{15}O_5$ $[M+H]^+$: 251.0914. Found: 251.0913.

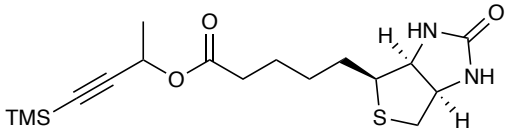

4-(Trimethylsilyl)but-3-yn-2-yl 5-((3aS,4S,6aR)-2-oxohexahydro-1H-thieno[3,4-d]imidazol-4-yl)pentanoate - (Table 2-2, Entry 9). A mixture of biotin (51 mg, 0.21 mmol), diselenide **2.11** (7.2 mg, 0.011 mmol), 4-dimethylaminopyridine (2.6 mg, 0.021 mmol), and 4 Å molecular sieves (100 mg) in dry DMF (1 mL, 0.2M) was treated with racemic 4-(trimethylsilyl)but-3-yn-2-ol (33 mg, 0.23 mmol), triethylamine (33 µL, 0.23 mmol), and $P(OEt)_3$ (54 µL, 0.32 mmol) according to the general procedure. The coupling reaction was stirred for 14 h under dry air at 50 °C and purified by triturating the crude mixture with H_2O to remove triethylphosphate, followed by flash column chromatography using SiO_2 and 7% MeOH in DCM to give the ester as white gummy semi-solid (68 mg, 88% yield, 1:1 mixture of diastereomers). ^{1}H NMR (400 MHz, chloroform-*d*) δ 5.95 (s, 1H), 5.46 (q, *J* = 6.7 Hz, 1H), 5.36 (s, 1H), 4.58 – 4.44 (m, 1H), 4.30 (ddd, *J* = 7.9, 4.6, 1.5 Hz,

1H), 3.15 (ddd, *J* = 8.2, 6.3, 4.5 Hz, 1H), 2.90 (dd, *J* = 12.8, 4.9 Hz, 1H), 2.75 (d, *J* = 12.8 Hz, 1H), 2.35 (td, *J* = 7.5, 2.2 Hz, 2H), 1.80 – 1.57 (m, 4H), 1.51– 1.39 (m, 5H), 0.16 (s, 9H). ^{13}C NMR (100 MHz, chloroform-*d*) δ 172.6, 163.7, 103.7, 89.6, 62.1, 60.7, 60.2, 55.6, 40.7, 34.0, 28.40, 28.38, 28.35, 28.33, 24.8, 24.8, 21.7. IR ($CDCl_3$, cm^{-1}): 3206, 1737, 1695. HRMS (ESI) Calcd for $C_{17}H_{29}N_2O_3SSi$ $[M+H]^+$: 369.1663. Found: 369.1660.

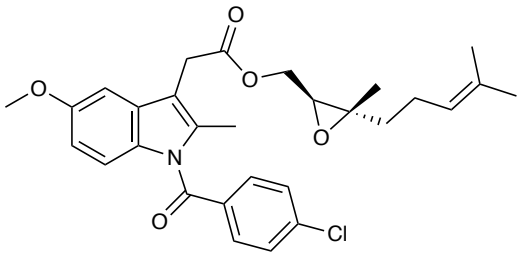

((2*S*,3*S*)-3-Methyl-3-(4-methylpent-3-en-1-yl)oxiran-2-yl)methyl 2-(1-(4-chlorobenzoyl)-5-methoxy-2-methyl-1*H*-indol-3-yl)acetate - (Table 2-2, Entry 10). A mixture of 2-(1-(4-chlorobenzoyl)-5-methoxy-2-methyl-1*H*-indol-3-yl)acetic acid (75 mg, 0.21 mmol), diselenide **2.11** (7.2 mg, 0.011 mmol), 4-dimethylaminopyridine (2.6 mg, 0.021 mmol), and 4 Å molecular sieves (100 mg) in dry CH_3CN (1 mL, 0.2M) was treated with ((2*S*,3*S*)-3-methyl-3-(4-methylpent-3-en-1-yl)oxiran-2-yl)methanol (39 mg, 0.23 mmol), triethylamine (33 μL, 0.23 mmol), and $P(OEt)_3$ (54 μL, 0.32 mmol) according to the general procedure. The coupling reaction was stirred for 11 h under dry air at 50 °C and purified by flash column chromatography using SiO_2 and 15% EtOAc in hexanes to give the pure ester as a pale-yellow oil (93 mg, 86% yield). ^{1}H NMR (500 MHz, Chloroform-*d*) δ 7.69 – 7.63 (m, 2H), 7.50 – 7.43 (m, 2H), 6.97 (d, *J* = 2.5 Hz, 1H), 6.87 (dd, *J* = 9.0, 0.5 Hz, 1H), 6.67 (dd, *J* = 9.0, 2.5 Hz, 1H), 5.06 (ddq, *J* = 8.6, 5.7, 1.5 Hz, 1H), 4.36 (dd, *J* = 12.1, 4.0 Hz, 1H), 4.07 (dd, *J* = 12.1, 7.1 Hz, 1H), 3.84 (s, 3H), 3.72 (s, 2H), 2.98 (dd, *J* = 7.1, 4.0 Hz, 1H), 2.39 (s, 3H), 2.11 – 1.96 (m, 2H), 1.68 (d, *J* = 1.3 Hz, 3H), 1.67 – 1.61 (m, 1H), 1.59 (d, *J* = 1.2 Hz, 3H), 1.45 (ddd, *J* = 13.8, 9.7, 6.8 Hz, 1H), 1.28 (s, 3H). ^{13}C NMR (150 MHz,

Chloroform-*d*) δ 170.8, 168.4, 156.2, 139.4, 136.2, 134.0, 132.4, 131.3, 131.0, 130.7, 129.3, 123.3, 115.1, 112.4, 111.9, 101.4, 64.2, 60.7, 59.7, 55.9, 38.4, 30.3, 25.8, 23.7, 17.8, 17.0, 13.5. IR (neat, cm^{-1}): 1737, 1681. HRMS (ESI) Calcd for $C_{29}H_{33}ClNO_5$ $[M+H]^+$: 510.2042. Found: 510.2048.

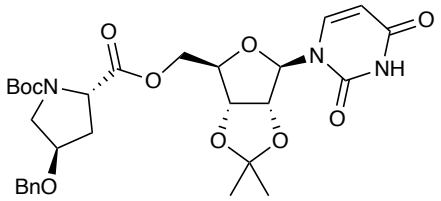

1-(*tert*-Butyl) 2-(((3a*R*,4*R*,6*R*,6a*R*)-6-(2,4-dioxo-3,4-dihydropyrimidin-1(2*H*)-yl)-2,2-dimethyltetrahydrofuro[3,4-*d*][1,3]dioxol-4-yl)methyl) (2*S*,4*R*)-4-(benzyloxy)pyrrolidine-1,2-dicarboxylate - (Table 2-2, Entry 11). A mixture of (2*S*,4*R*)-4-(benzyloxy)-1-(*tert*-butoxycarbonyl)pyrrolidine-2-carboxylic acid (68 mg, 0.21 mmol), diselenide **2.11** (7.2 mg, 0.011 mmol), 4-dimethylaminopyridine (2.6 mg, 0.021 mmol), and 4 Å molecular sieves (100 mg) in dry CH_3CN (1 mL, 0.2M) was treated with 1-((3a*R*,4*R*,6*R*,6a*R*)-6-(hydroxymethyl)-2,2-dimethyltetrahydrofuro[3,4-*d*][1,3]dioxol-4-yl)pyrimidine-2,4(1*H*,3*H*)-dione (66 mg, 0.23 mmol), triethylamine (33 μL, 0.23 mmol), and $P(OEt)_3$ (54 μL, 0.32 mmol) according to the general procedure. The coupling reaction was stirred for 12 h under dry air at 50 °C and purified by flash column chromatography using SiO_2 and 70% EtOAc in hexanes to give the pure ester as a white foam (89 mg, 72% yield). ^{1}H NMR (600 MHz, chloroform-*d*) δ 8.17, 8.14 (s, 1H, rotamers), 7.38 – 7.27, 7.21– 7.18 (m, 6H rotamers), 5.76 – 5.71, 5.59 – 5.57 (m, 2H rotamers), 5.01, 4.86 (dd, *J* = 6.4, 1.8 Hz, and dd, *J* = 6.4, 2.6 Hz, 1H rotamers), 4.79 (dt, *J* = 6.6, 3.7 Hz, 1H), 4.55 – 4.26 (m, 6H), 4.20 – 4.13 (m, 1H), 3.74 – 3.70, 3.61 – 3.54 (m, 2H), 2.47 – 2.33 (m, 1H), 2.11 – 2.02 (m, 1H), 1.56 (s, 3H), 1.45, 1.40 (s, 9H, rotamers), 1.35 (s, 3H). ^{13}C NMR (150 MHz, chloroform-*d*) δ 172.8, 172.6, 162.7, 162.5, 154.6, 153.9, 149.9, 149.7, 142.6, 141.7, 137.8, 137.9, 128.70, 128.67, 128.1, 128.0, 127.8, 127.7, 114.9, 114.9, 103.0, 102.8, 95.4, 93.5, 85.5, 84.6, 84.5, 84.4,

81.3, 80.7, 80.6, 76.1, 71.4, 71.3, 64.8, 64.5, 58.2, 57.8, 52.1, 51.5, 37.0, 35.9, 28.6, 28.4, 27.4, 27.3, 25.54, 25.48. IR (neat, cm^{-1}): 3194, 1746, 1687. HRMS (ESI) Calcd for $C_{29}H_{36}N_3O_{10}$ $[M-H]^-$: 586.2406. Found: 586.2415. Melting point: 74-78 °C (recrystallized from EtOAc/hexanes).

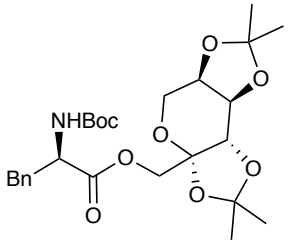

((3a*S*,5a*R*,8a*R*,8b*S*)-2,2,7,7-Tetramethyltetrahydro-3a*H*-bis([1,3]dioxolo)[4,5-*b*:4',5'-*d*]pyran-3a-yl)methyl (*tert*-butoxycarbonyl)-*D*-phenylalaninate - (Table 2-2, Entry 12). A mixture of N-Boc-*D*-phenylalanine (58 mg, 0.21 mmol), diselenide **2.11** (7.2 mg, 0.011 mmol), 4-dimethylaminopyridine (2.6 mg, 0.021 mmol), and 4 Å molecular sieves (100 mg) in dry EtOAc (1 mL, 0.2M) was treated with ((3a*S*,5a*R*,8a*R*,8b*S*)-2,2,7,7-tetramethyltetrahydro-3a*H*-bis([1,3]dioxolo)[4,5-*b*:4',5'-*d*]pyran-3a-yl)methanol (60 mg, 0.23 mmol), triethylamine (33 µL, 0.23 mmol), and $P(OEt)_3$ (54 µL, 0.32 mmol) according to the general procedure. The coupling reaction was stirred for 10 h under dry air at 50 °C and purified by flash column chromatography using SiO_2 and 20% EtOAc in hexanes to give the pure ester a colorless oil (84 mg, 79% yield). ^{1}H NMR (600 MHz, chloroform-*d*) δ 7.31 (t, *J* = 7.3 Hz, 2H), 7.26 (t, *J* = 7.4 Hz, 1H), 7.15 (d, *J* = 6.9 Hz, 2H), 5.02 (d, *J* = 8.4 Hz, 1H), 4.69 (dt, *J* = 8.6, 5.6 Hz, 1H), 4.63 (dd, *J* = 7.9, 2.7 Hz, 1H), 4.29 (d, *J* = 11.7 Hz, 1H), 4.28 – 4.24 (m, 2H), 4.20 (d, *J* = 11.6 Hz, 1H), 3.95 (dd, *J* = 13.0, 1.9 Hz, 1H), 3.80 (d, *J* = 13.0 Hz, 1H), 3.22 – 3.08 (m, 2H), 1.57 (s, 3H), 1.43 (s, 9H), 1.42 (s, 3H), 1.37 (s, 3H). ^{13}C NMR (150 MHz, chloroform-*d*) δ 171.3, 155.1, 135.9, 129.6, 128.8, 127.2, 109.4, 109.1, 101.3, 80.1, 70.9, 70.5, 70.1, 66.3, 61.5, 54.5, 38.4, 28.5, 26.7, 26.1, 25.5, 24.2. IR ($CDCl_3$, cm^{-1}): 3355, 1746, 1711. HRMS (ESI) Calcd for $C_{26}H_{38}NO_9$ $[M+H]^+$: 508.2541. Found: 508.2543.

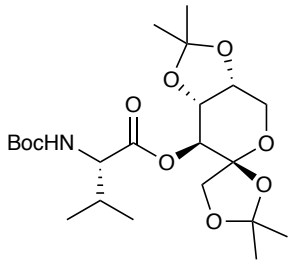

(3a'*R*,4*S*,7'*S*,7a'*R*)-2,2,2',2'-Tetramethyltetrahydrospiro[[1,3]dioxolane-4,6'-[1,3]dioxolo[4,5-*c*]pyran]-7'-yl (*tert*-butoxycarbonyl)-*L*-valinate - (Table 2-2, Entry 13). A mixture of N-Boc-*L*-valine (46 mg, 0.21 mmol), diselenide **2.11** (7.2 mg, 0.011 mmol), 4-dimethylaminopyridine (2.6 mg, 0.021 mmol), and 4 Å molecular sieves (100 mg) in dry EtOAc (1 mL, 0.2M) was treated with (3a'*R*,4*S*,7'*S*,7a'*S*)-2,2,2',2'-tetramethyltetrahydrospiro[[1,3]dioxolane-4,6'-[1,3]dioxolo[4,5-*c*]pyran]-7'-ol (60 mg, 0.23 mmol), triethylamine (33 μL, 0.23 mmol), and $P(OEt)_3$ (54 μL, 0.32 mmol) according to the general procedure. The coupling reaction was stirred for 10 h under dry air at 50 °C and purified by flash column chromatography using SiO_2 and 20% EtOAc in hexanes to give the pure ester as a white solid (79 mg, 82% yield). ^{1}H NMR (500 MHz, chloroform-*d*) δ 5.15 (d, *J* = 7.7 Hz, 1H), 5.04 (d, *J* = 9.2 Hz, 1H), 4.34 (dd, *J* = 9.2, 4.4 Hz, 1H), 4.29 (dd, *J* = 7.8, 5.4 Hz, 1H), 4.25 – 4.21 (m, 1H), 4.13 (dd, *J* = 13.5, 2.5 Hz, 1H), 4.07 (d, *J* = 13.4 Hz, 1H), 3.96 (d, *J* = 9.3 Hz, 1H), 3.82 (d, *J* = 9.3 Hz, 1H), 2.21 (pd, *J* = 6.9, 4.6 Hz, 1H), 1.54 (s, 3H), 1.47 (s, 3H), 1.44 (s, 9H), 1.41 (s, 3H), 1.35 (s, 3H), 1.00 (d, *J* = 6.8 Hz, 3H), 0.90 (d, *J* = 6.9 Hz, 3H). ^{13}C NMR (100 MHz, chloroform-*d*) δ 171.7, 155.5, 112.1, 109.8, 103.6, 79.9, 74.8, 73.8, 72.2, 71.3, 60.8, 58.9, 31.6, 28.4, 27.8, 26.48, 26.46, 26.2, 19.4, 17.3. IR (neat, cm^{-1}): 3393, 1746, 1688. HRMS (ESI) Calcd for $C_{22}H_{38}NO_9$ $[M+H]^+$: 460.2541. Found: 460.2542. Melting point: 106 – 108 °C (recrystallized from ether/hexanes).

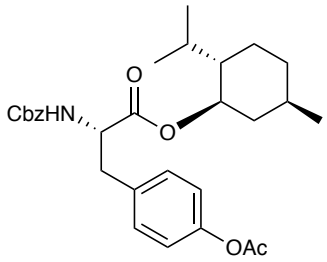

(1*R*,2*S*,5*R*)-2-Isopropyl-5-methylcyclohexyl (*S*)-3-(4-acetoxyphenyl)-2-(((benzyloxy)carbonyl)amino)propanoate - (Table 2-2, Entry 14). A mixture of O-acetyl-N-Cbz-*L*-tyrosine (75 mg, 0.21 mmol), diselenide **2.11** (7.2 mg, 0.011 mmol), 4-dimethylaminopyridine (2.6 mg, 0.021 mmol), and 4 Å molecular sieves (100 mg) in dry EtOAc (1 mL, 0.2M) was treated with (-)-Menthol (36 mg, 0.23 mmol), triethylamine (33 μL, 0.23 mmol), and $P(OEt)_3$ (54 μL, 0.32 mmol) according to the general procedure. The coupling reaction was stirred for 10 h under dry air at 50 °C and purified by flash column chromatography using SiO_2 and 20% EtOAc in hexanes to give the pure ester as a colorless oil (80 mg, 77% yield). ^{1}H NMR (600 MHz, chloroform-*d*) δ 7.39 – 7.28 (m, 5H), 7.16 – 7.11 (m, 2H), 7.01 – 6.96 (m, 2H), 5.26 (d, *J* = 8.1 Hz, 1H), 5.10 (s, 2H), 4.70 (td, *J* = 10.9, 4.4 Hz, 1H), 4.61 (dt, *J* = 8.1, 5.9 Hz, 1H), 3.13 (dd, *J* = 14.0, 6.0 Hz, 1H), 3.07 (dd, *J* = 14.0, 5.8 Hz, 1H), 2.28 (s, 3H), 1.94 – 1.83 (m, 1H), 1.73 (pd, *J* = 6.9, 2.2 Hz, 1H), 1.69 – 1.63 (m, 2H), 1.51 – 1.41 (m, 1H), 1.34 (ddt, *J* = 14.4, 11.2, 3.2 Hz, 1H), 1.02 (qd, *J* = 13.4, 12.7, 3.7 Hz, 1H), 0.96 – 0.80 (m, 8H), 0.71 (d, *J* = 6.9 Hz, 3H). ^{13}C NMR (75 MHz, $CDCl_3$) δ 171.0, 169.5, 155.7, 149.8, 136.4, 133.5, 130.6, 128.6, 128.3, 128.3, 121.7, 76.0, 67.1, 54.8, 46.9, 40.8, 37.7, 34.1, 31.5, 26.2, 23.4, 22.1, 21.3, 20.8, 16.3. IR ($CDCl_3$, cm^{-1}): 3362, 1751, 1721, 1688. HRMS (ESI) Calcd for $C_{29}H_{38}NO_6$ $[M+H]^+$: 496.2694. Found: 496.2687.

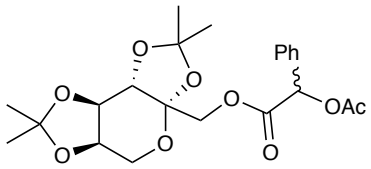

((3a*S*,5a*R*,8a*R*,8b*S*)-2,2,7,7-Tetramethyltetrahydro-3a*H*-bis([1,3]dioxolo)[4,5-*b*:4',5'-*d*]pyran-3a-yl)methyl 2-acetoxy-2-phenylacetate - (Table 2-2, Entry 15). A mixture of (S)-(+)-O-acetylmandelic acid (40 mg, 0.21 mmol), diselenide **2.11** (7.2 mg, 0.011 mmol), 4-dimethylaminopyridine (2.6 mg, 0.021 mmol), and 4 Å molecular sieves (100 mg) in dry EtOAc (1 mL, 0.2M) was treated with ((3a*S*,5a*R*,8a*R*,8b*S*)-2,2,7,7-tetramethyltetrahydro-3a*H*-bis([1,3]dioxolo)[4,5-*b*:4',5'-*d*]pyran-3a-yl)methanol (60 mg, 0.23 mmol), triethylamine (33 µL, 0.23 mmol), and $P(OEt)_3$ (54 µL, 0.32 mmol) according to the general procedure. The coupling reaction was stirred for 10 h under dry air at 50 °C and purified by flash column chromatography using SiO_2 and 25% EtOAc in hexanes to give the pure ester as a colorless oil (76 mg, 83% yield, 1:0.6 mixture of diastereomers based on integration of ^{1}H NMR spectrum). ^{1}H NMR (400 MHz, chloroform-*d*) δ 7.51 – 7.34 (m, 5H), 6.04, 5.96 (s, 1H, mixture of diastereomers), 4.59, 4.53 (dd, *J* = 7.9, 2.7 Hz, 1H, mixture of diastereomers), 4.46 – 4.02 (m, 4H), 3.89, 3.86 (d, *J* = 1.9 Hz, 1H, diastereomers), 3.73, 3.70 (dd, *J* = 4.6, 0.8 Hz, 1H mixture of diastereomers), 2.18, 2.17 (s, 3H, mixture of diastereomers), 1.50, 1.46 (s, 3H, mixture of diastereomers), 1.45 (s, 3H,), 1.33, 1.31 (s, 3H, mixture of diastereomers), 1.26, 1.05 (s, 3H, mixture of diastereomers). ^{13}C NMR (100 MHz, chloroform-*d*) δ 196.4, 170.4, 170.1, 168.3, 168.3, 133.9, 133.5, 129.56, 129.55, 129.03, 128.98, 128.21, 128.15, 109.30, 109.25, 109.1, 109.0, 101.23, 101.16, 74.6, 74.4, 70.9, 70.8, 70.3, 70.12, 70.09, 70.05, 65.61, 65.56, 61.42, 61.38, 26.60, 26.57, 26.01, 26.00, 25.2, 25.0, 24.19, 24.17, 20.9. IR ($CDCl_3$, cm^{-1}): 1743. HRMS (ESI) Calcd for $C_{22}H_{27}O_9$ $[M-H]^-$: 435.1661. Found: 435.1660.

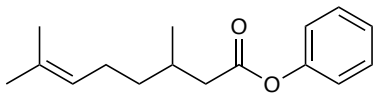

Phenyl 3,7-dimethyloct-6-enoate - (Table 2-2, Entry 17). A mixture of racemic citronellic acid (36 mg, 0.21 mmol), diselenide **2.11** (7.2 mg, 0.011 mmol), 4-dimethylaminopyridine (2.6 mg, 0.021 mmol), and 4 Å molecular sieves (100 mg) in dry CH_3CN (1 mL, 0.2M) was treated with phenol (22 mg, 0.23 mmol) and $P(OEt)_3$ (54 μL, 0.32 mmol) according to the general procedure. The coupling reaction was stirred for 9 h under dry air at 50 °C and purified by flash column chromatography using SiO_2 and 10% EtOAc in hexanes to give the pure ester as a colorless oil (21 mg, 41% yield). ^{1}H NMR (400 MHz, chloroform-*d*) δ 7.42 – 7.34 (m, 2H), 7.25 – 7.19 (m, 1H), 7.11 – 7.05 (m, 2H), 5.13 (tp, *J* = 10.7, 2.2 Hz, 1H), 2.57 (dd, *J* = 14.7, 6.0 Hz, 1H), 2.37 (dd, *J* = 14.8, 8.2 Hz, 1H), 2.16 – 1.99 (m, 3H), 1.70 (q, *J* = 1.3 Hz, 3H), 1.62 (d, *J* = 1.2 Hz, 3H), 1.46 (dddd, *J* = 13.5, 9.2, 6.7, 5.7 Hz, 1H), 1.32 (dddd, *J* = 13.6, 9.1, 7.8, 6.2 Hz, 1H), 1.06 (d, *J* = 6.7 Hz, 3H). ^{13}C NMR (100 MHz, chloroform-*d*) δ 171.8, 150.9, 131.9, 129.5, 125.9, 124.3, 121.8, 77.5, 77.2, 76.8, 41.9, 36.9, 30.3, 25.9, 25.6, 19.8, 17.8. IR (neat, cm^{-1}): 1755. HRMS (ESI) Calcd for $C_{16}H_{22}O_2$ $[M+H]^+$: 247.1693. Found: 247.1691.

Experimental Details for Reaction Described in Scheme 2-11. A mixture of methyl-4-hydroxybenzoate (15 mg, 0.099 mmol), diselenide **2.11** (32 mg, 0.049 mmol), 4-dimethylaminopyridine (1.0 mg, 0.001 mmol), and 4 Å molecular sieves (100 mg) in dry CH_3CN (1 mL, 0.2M) was treated with triethylamine (15 μL, 0.11 mmol) and $P(OEt)_3$ (26 μL, 0.15 mmol) according to the general procedure. The coupling reaction was stirred for 12h under dry air at 50 °C and the components separated by SiO_2 and 30% EtOAc in hexanes (phosphate ester, colorless oil, 24 mg, 84% yield) followed by 10% MeOH in DCM (ethyl selenoether, yellow gummy solid, 24 mg, 68% yield).

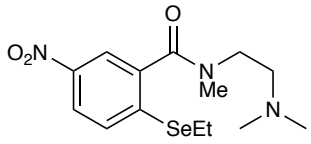

***N*-(2-(Dimethylamino)ethyl)-2-(ethylselanyl)-*N*-methyl-5-nitrobenzamide. – (2.12)** ^{1}H NMR (300 MHz, chloroform-*d*) δ 8.16 – 7.99 (m, 2H), 7.54 (d, *J* = 8.7 Hz, 1H), 3.67 (t, *J* = 6.9 Hz, 1H), 3.20 (t, *J* = 6.8 Hz, 1H), 3.14, 2.91 (s, 3H, rotamers), 3.05 (q, *J* = 7.5 Hz, 2H), 2.63 (t, *J* = 6.9 Hz, 1H), 2.42 (d, *J* = 7.0 Hz, 1H), 2.33 (s, 3H), 2.06 (s, 3H), 1.49 (t, *J* = 7.5 Hz, 3H). ^{13}C NMR (150 MHz, chloroform-*d*) δ 168.6, 168.0, 146.0, 145.8, 140.3, 139.8, 139.5, 139.1, 130.5, 130.2, 123.7, 122.4, 121.7, 57.5, 56.5, 49.2, 45.8, 45.6, 37.4, 33.2, 29.8, 21.3, 21.1, 20.9, 14.8. IR ($CDCl_3$, cm^{-1}): 1639, 1632. HRMS (ESI) Calcd for $C_{14}H_{22}O_3N_3Se$ $[M+H]^+$: 360.0821. Found: 360.0818.

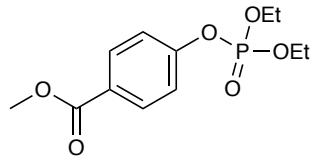

Methyl 4-((diethoxyphosphoryl)oxy)benzoate. – (2.13) ^{1}H NMR (400 MHz, chloroform-*d*) δ 8.03 (AA' of AA'XX', 2H), 7.27 (XX' of AA'XX', 2H), 4.22 (dqd, *J* = 8.2, 7.1, 2.0 Hz, 4H), 3.90 (s, 3H), 1.35 (td, *J* = 7.1, 1.1 Hz, 6H). ^{13}C NMR (150 MHz, $CDCl_3$) δ 166.4, 154.53, 154.49, 131.7, 127.0, 119.9, 119.9, 77.4, 77.2, 77.0, 65.01, 64.97, 52.3, 16.23, 16.19. ^{31}P NMR (121 MHz, chloroform-*d*) δ -6.89. IR ($CDCl_3$, cm^{-1}): 1721. HRMS (ESI) Calcd for $C_{12}H_{18}O_6P$ $[M+H]^+$: 289.0836. Found: 289.0832.

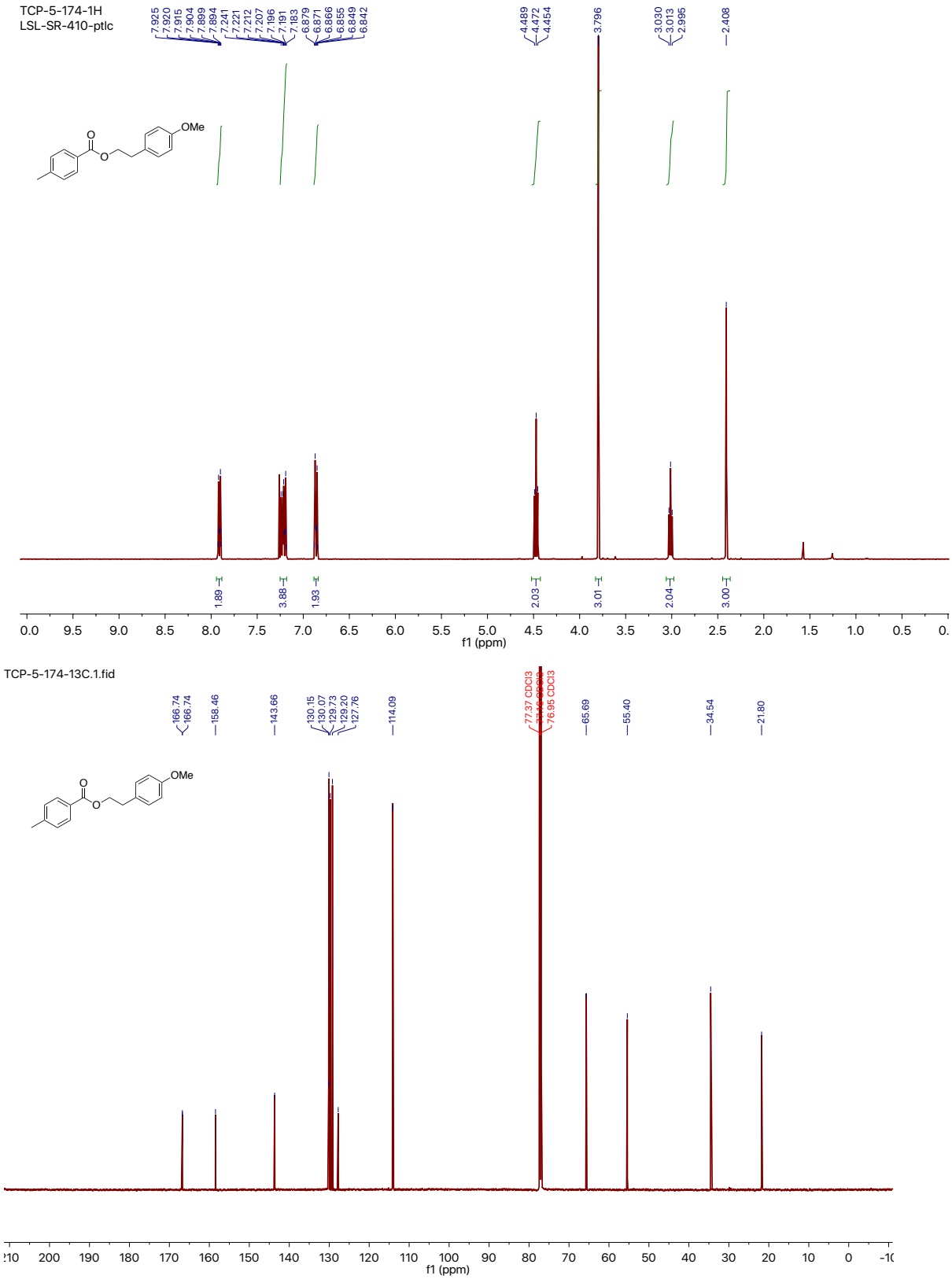

Figure S2-1: ^{1}H NMR spectrum in $CDCl_3$ at 400 MHz (top) and ^{13}C NMR spectrum in $CDCl_3$ at 150 MHz (bottom) for entry 1, Table 2-2.

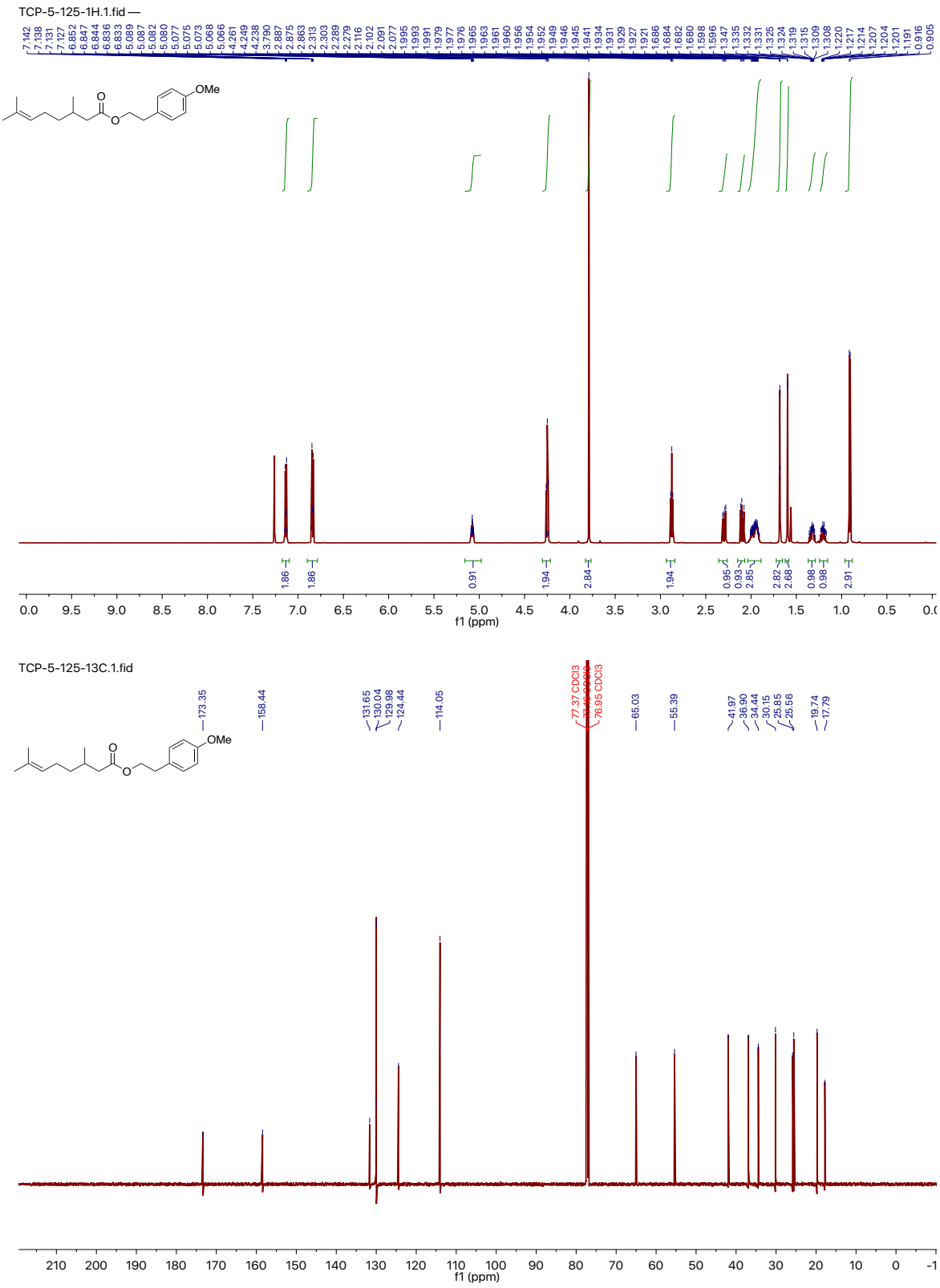

Figure S2-2: ^{1}H NMR spectrum in $CDCl_3$ at 600 MHz (top) and ^{13}C NMR spectrum in $CDCl_3$ at 150 MHz (bottom) for entry 2, Table 2-2.

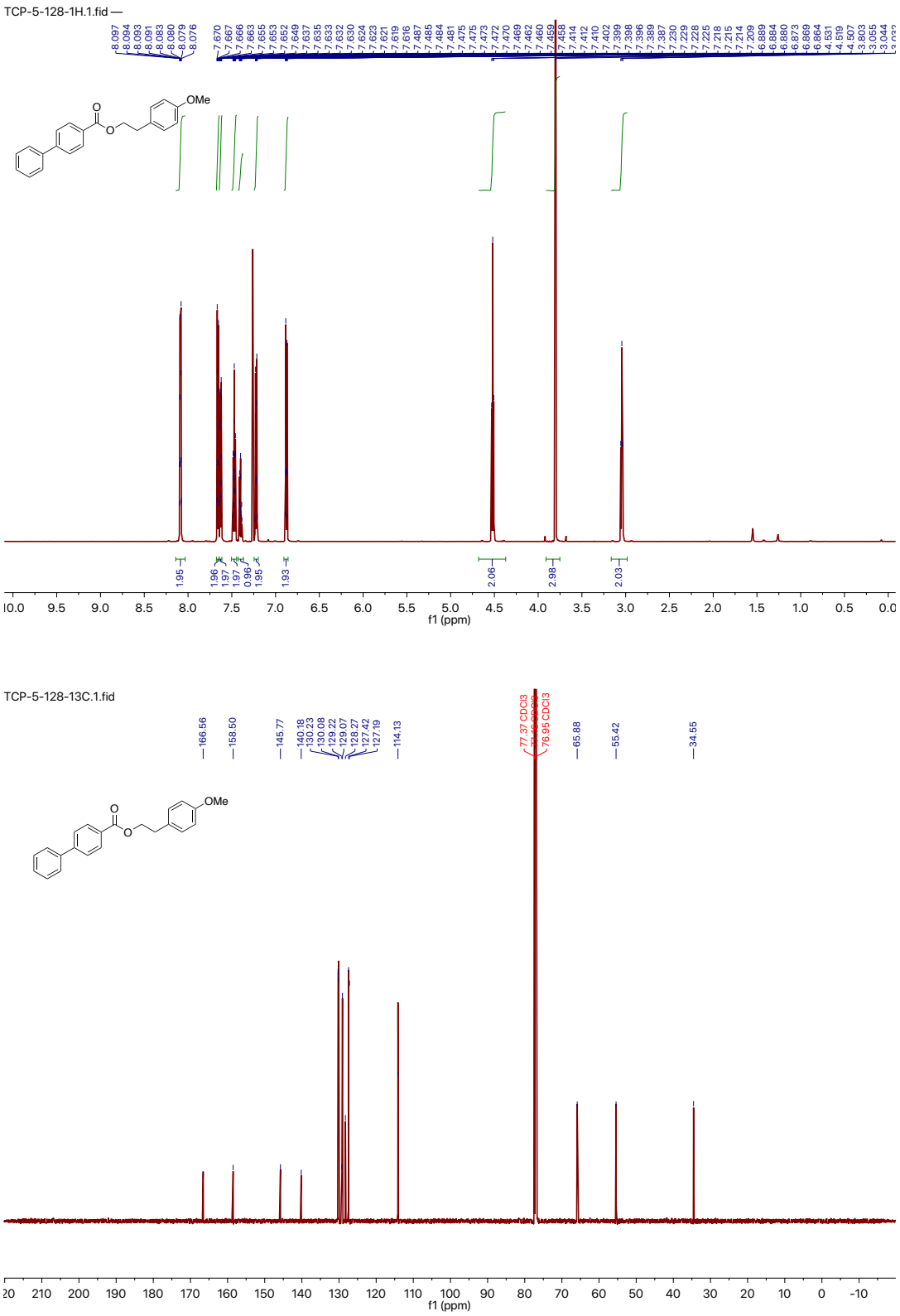

Figure S2-3: ^{1}H NMR spectrum in $CDCl_3$ at 600 MHz (top) and ^{13}C NMR spectrum in $CDCl_3$ at 150 MHz (bottom) for entry 3, Table 2-2.

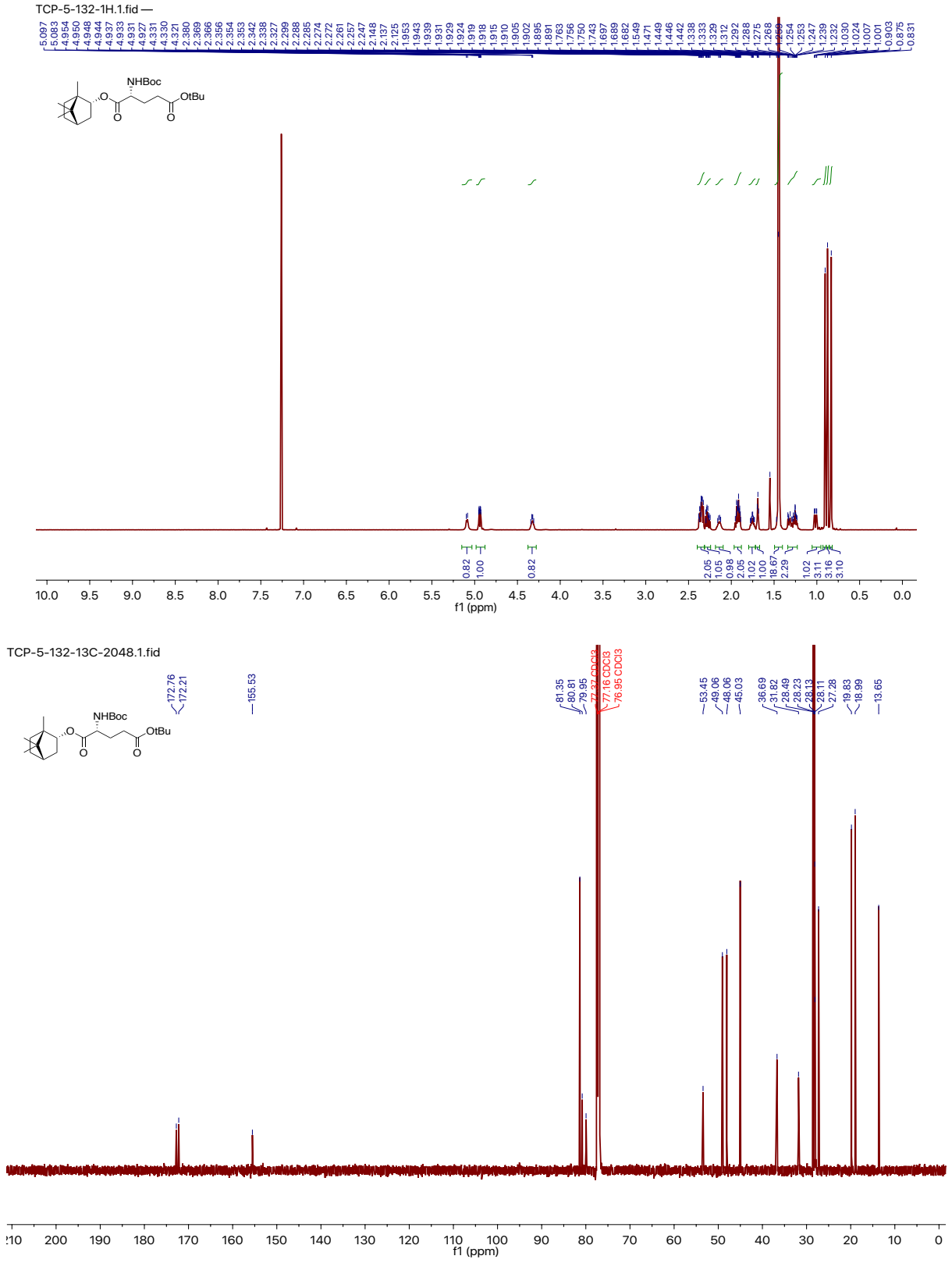

Figure S2-4: ^{1}H NMR spectrum in $CDCl_3$ at 600 MHz (top) and ^{13}C NMR spectrum in $CDCl_3$ at 150 MHz (bottom) for entry 4, Table 2-2.

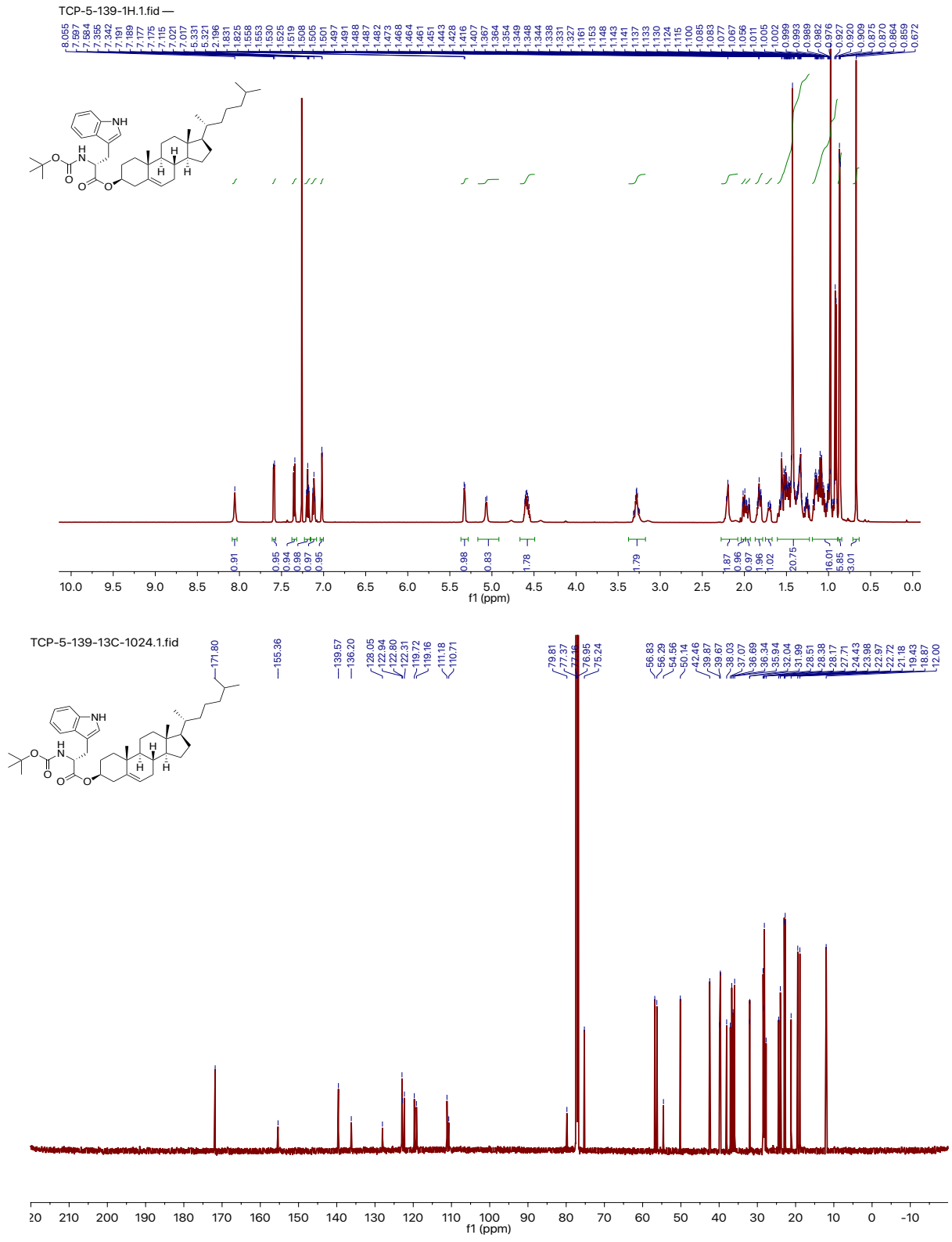

Figure S2-5: ^{1}H NMR spectrum in $CDCl_3$ at 600 MHz (top) and ^{13}C NMR spectrum in $CDCl_3$ at 150 MHz (bottom) for entry 5, Table 2-2.

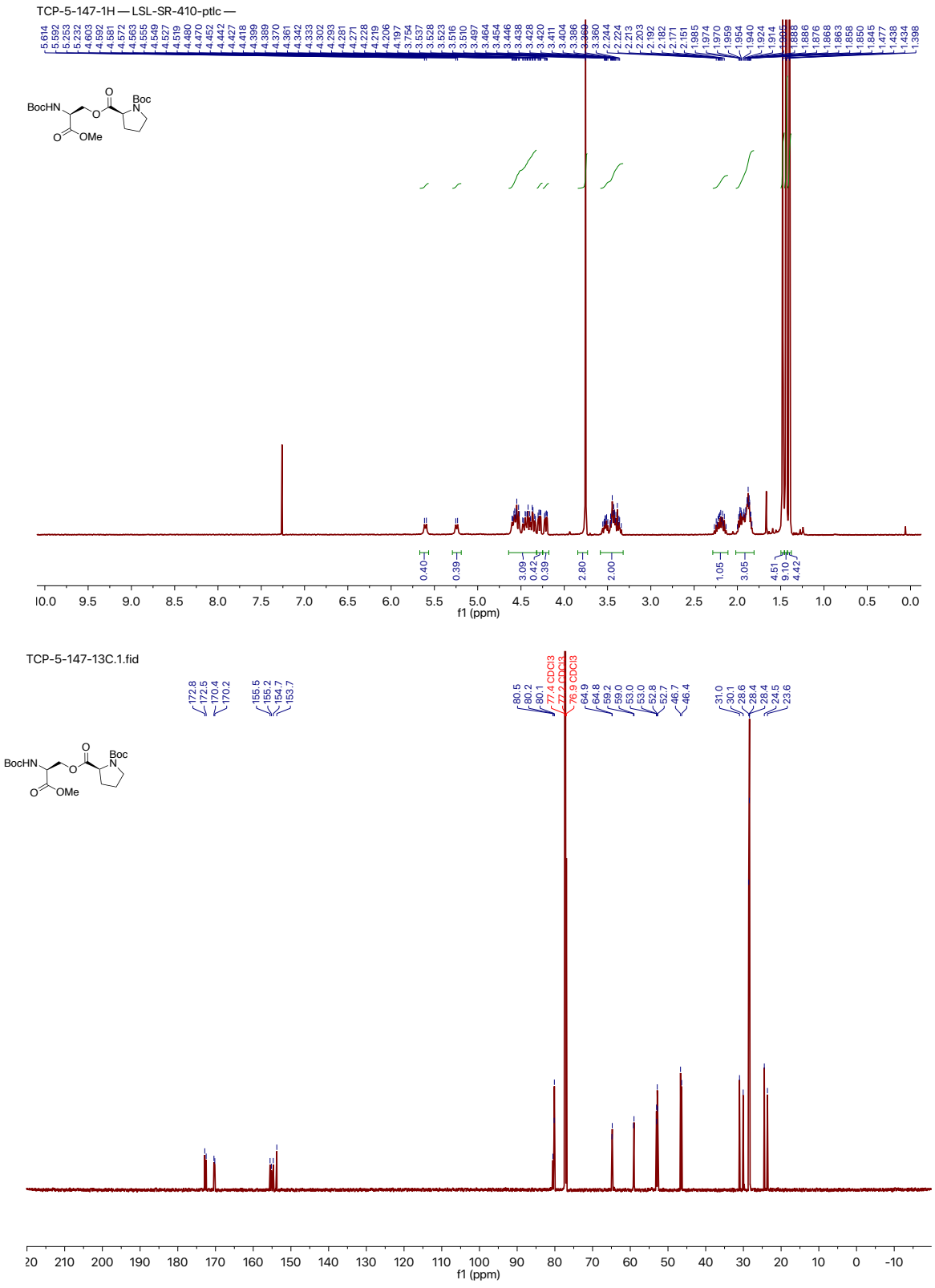

Figure S2-6: ^{1}H NMR spectrum in $CDCl_3$ at 400 MHz (top) and ^{13}C NMR spectrum in $CDCl_3$ at 150 MHz (bottom) for entry 6, Table 2-2.

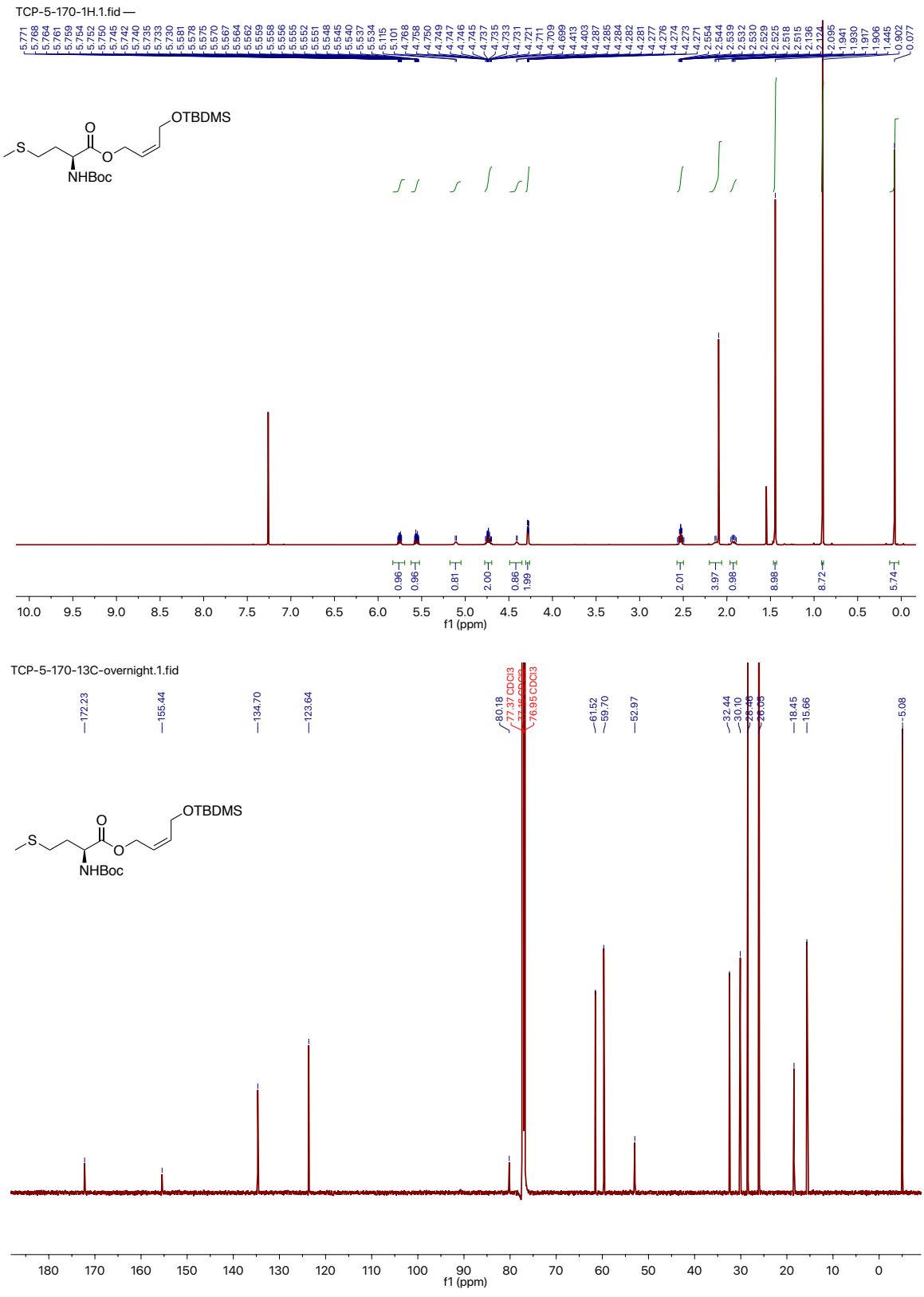

Figure S2-7: ^{1}H NMR spectrum in $CDCl_3$ at 600 MHz (top) and ^{13}C NMR spectrum in $CDCl_3$ at 150 MHz (bottom) for entry 7, Table 2-2.

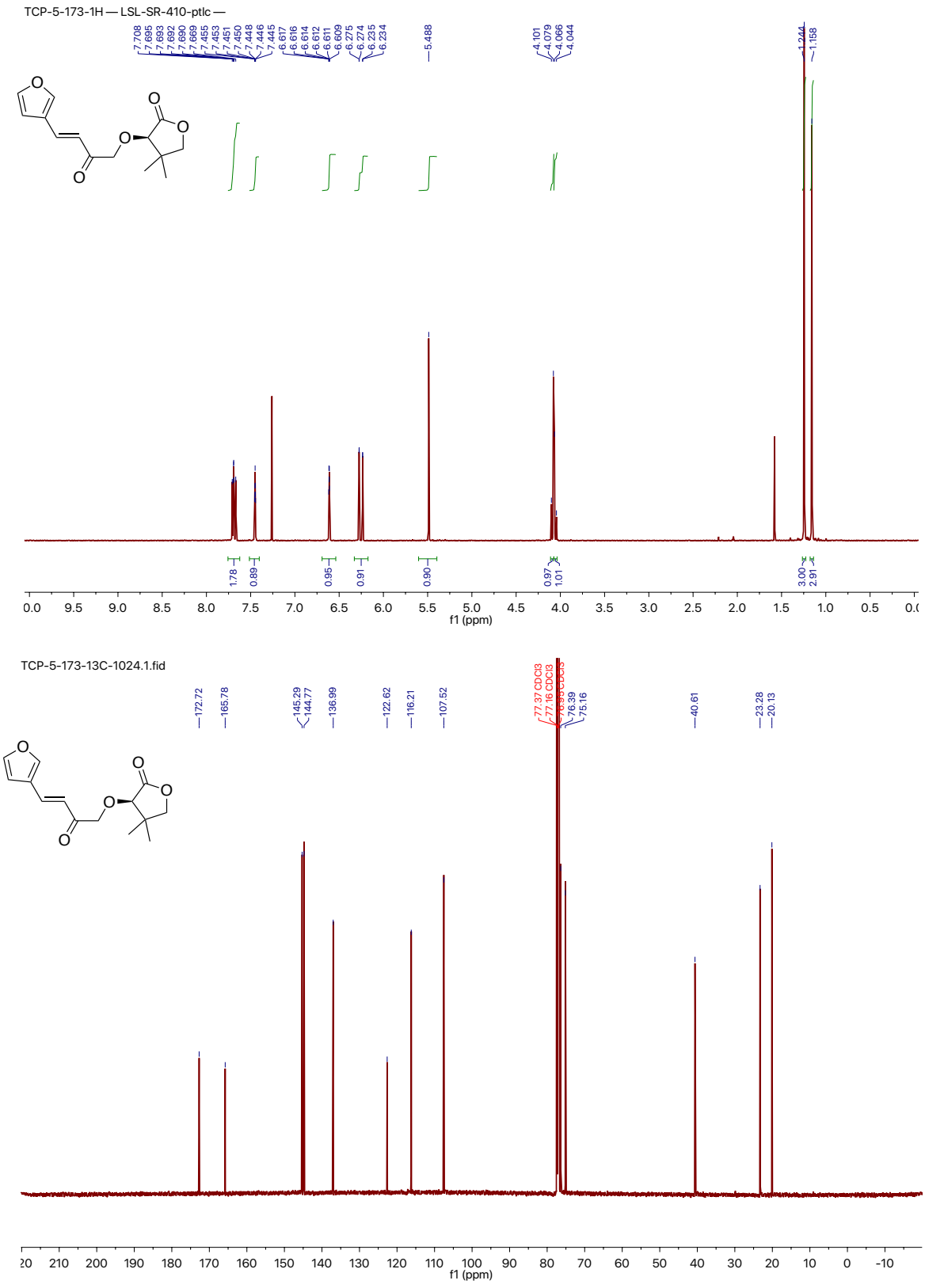

Figure S2-8: ^{1}H NMR spectrum in $CDCl_3$ at 400 MHz (top) and ^{13}C NMR spectrum in $CDCl_3$ at 150 MHz (bottom) for entry 8, Table 2-2.

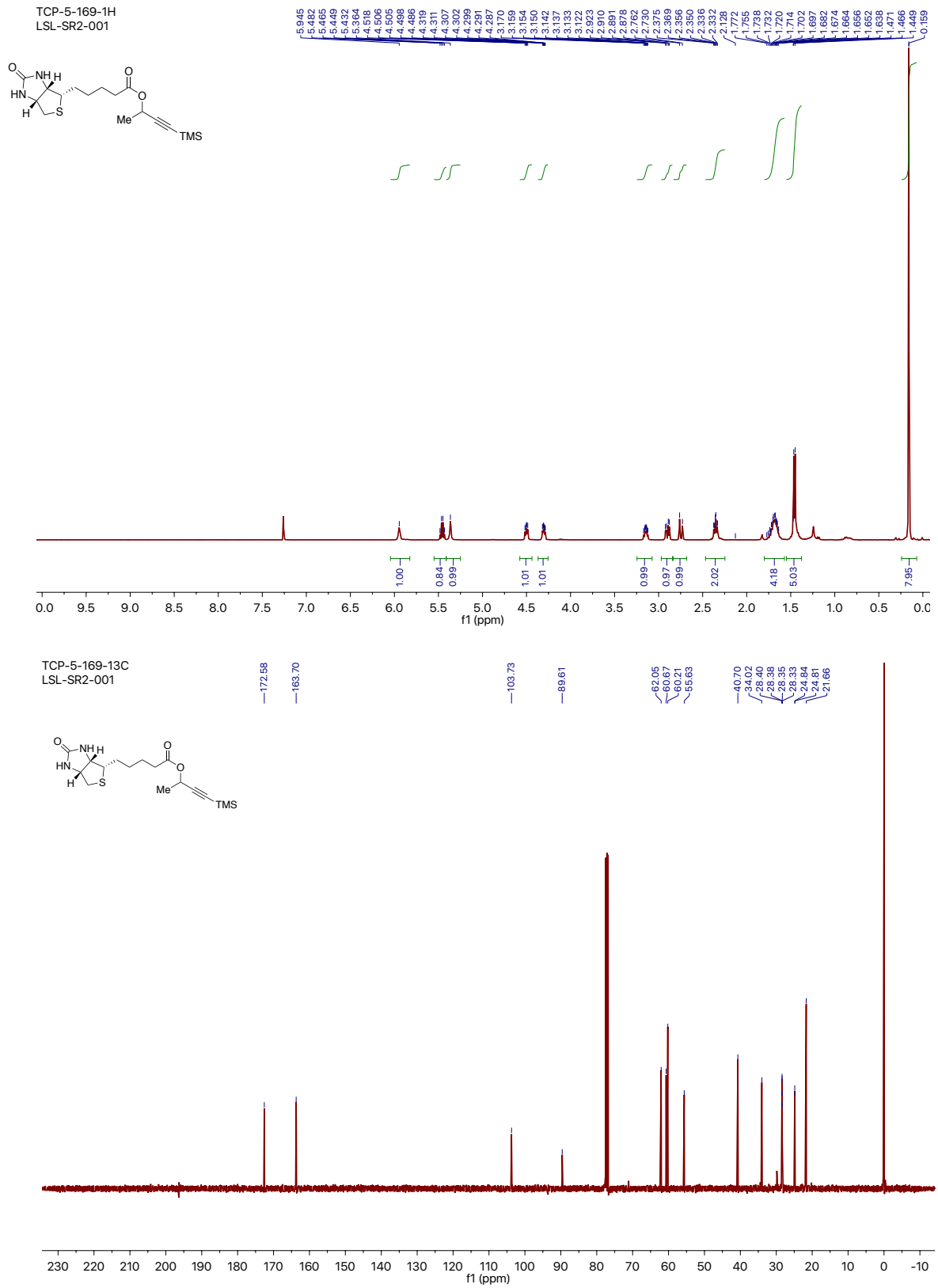

Figure S2-9: ^{1}H NMR spectrum in $CDCl_3$ at 400 MHz (top) and ^{13}C NMR spectrum in $CDCl_3$ at 100 MHz (bottom) for entry 9, Table 2-2.

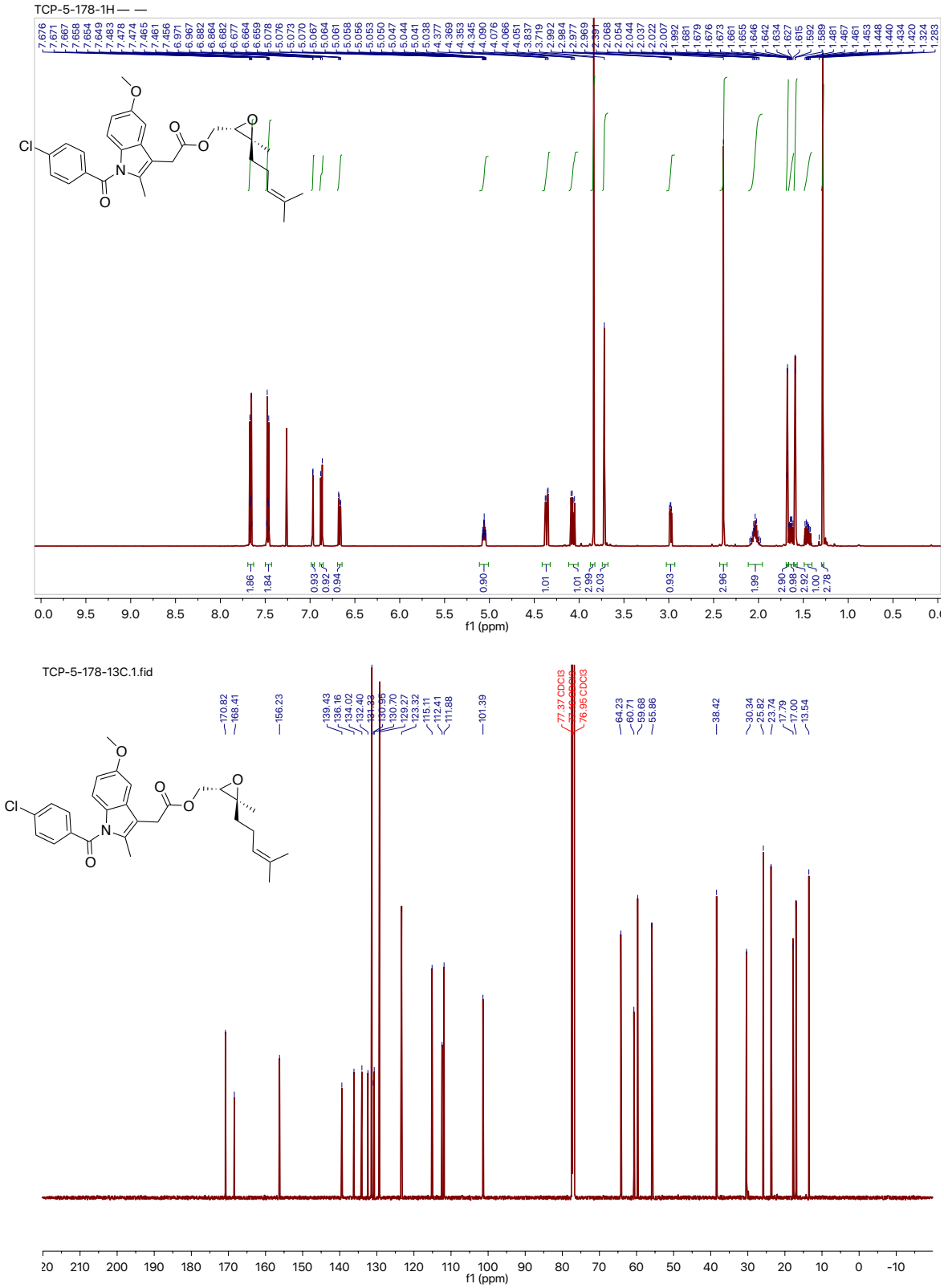

Figure S2-10: ^{1}H NMR spectrum in $CDCl_3$ at 500 MHz (top) and ^{13}C NMR spectrum in $CDCl_3$ at 150 MHz (bottom) for entry 10, Table 2-2.

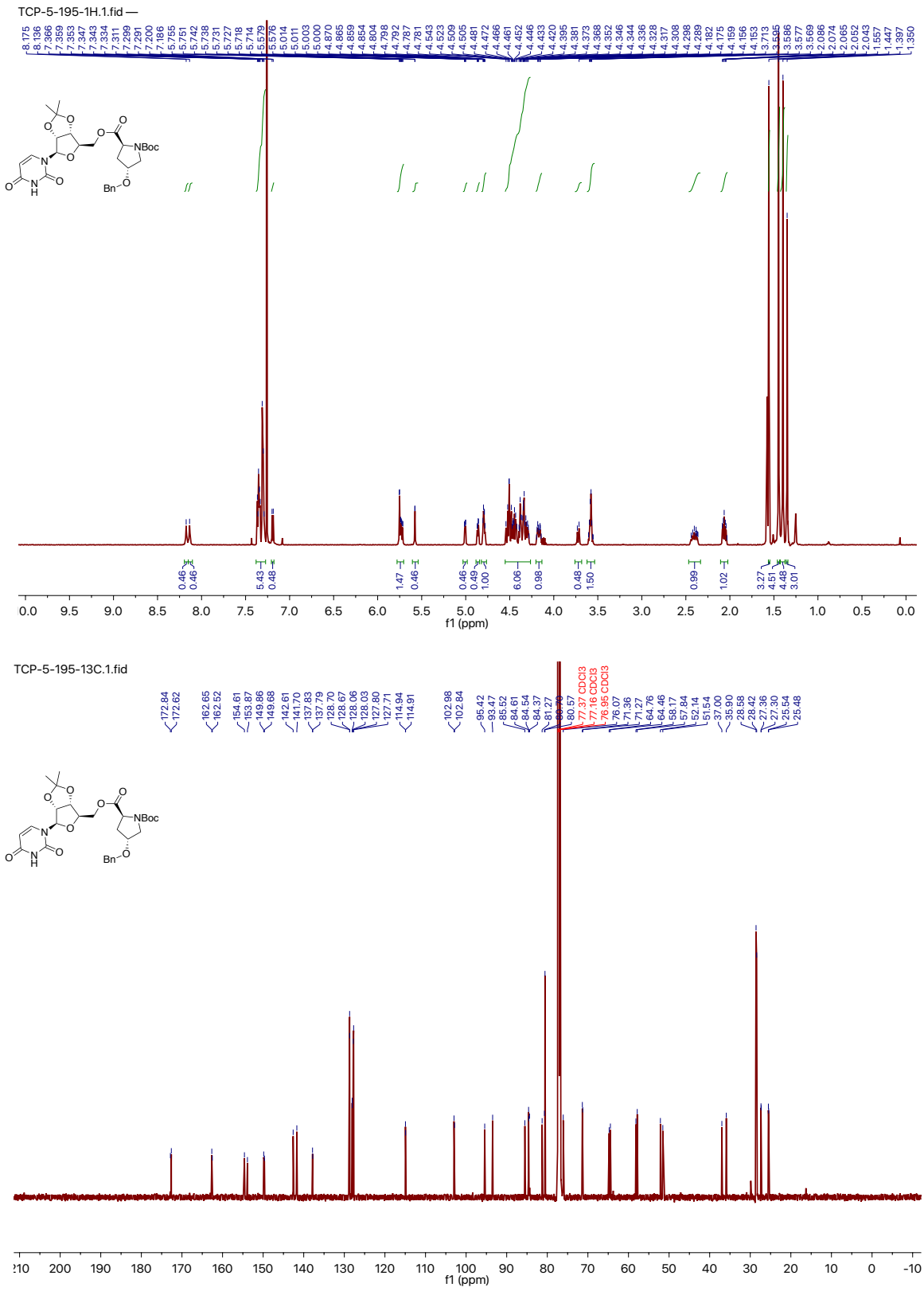

Figure S2-11: ^{1}H NMR spectrum in $CDCl_3$ at 600 MHz (top) and ^{13}C NMR spectrum in $CDCl_3$ at 150 MHz (bottom) for entry 11, Table 2-2.

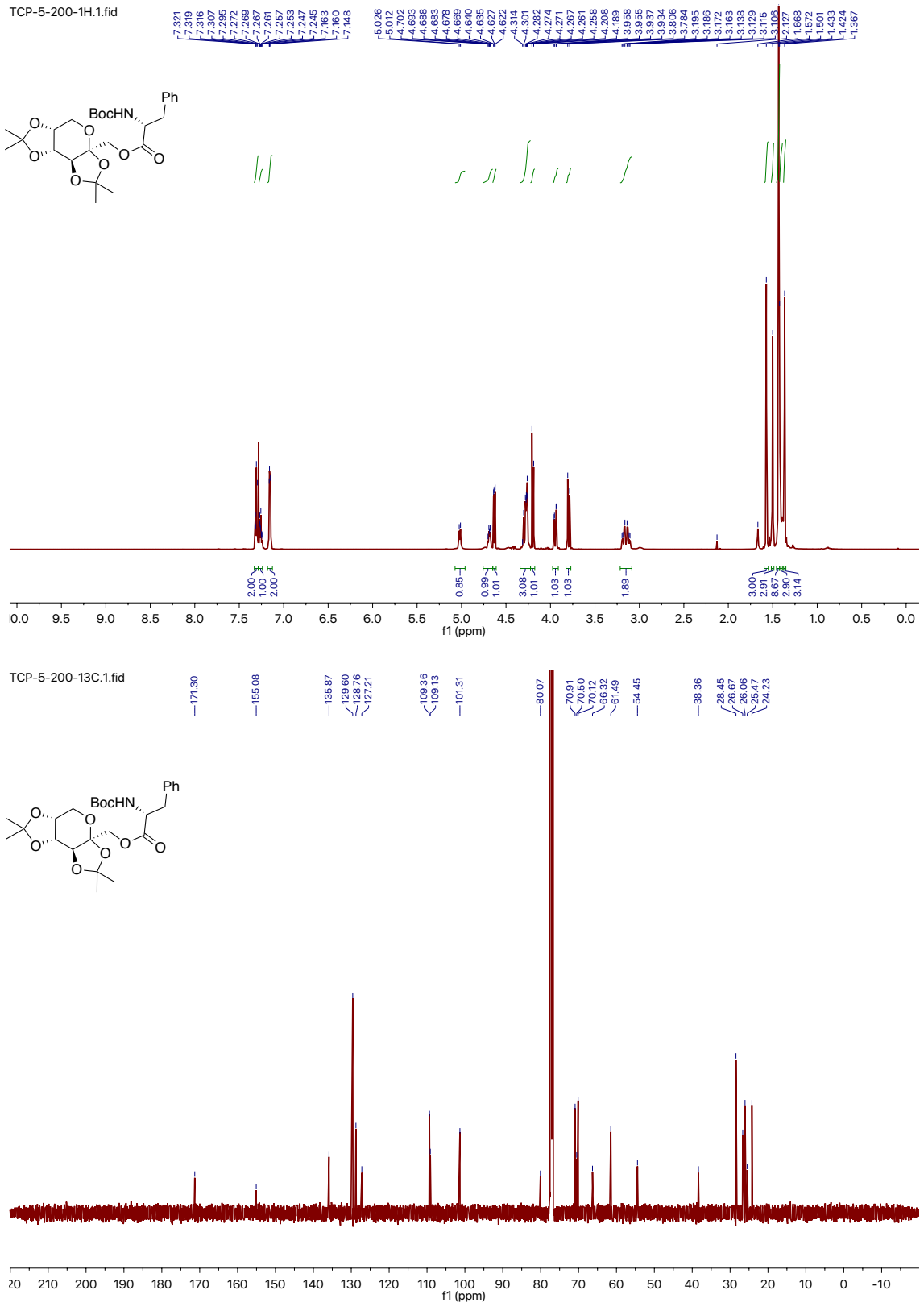

Figure S2-12: ^{1}H NMR spectrum in $CDCl_3$ at 600 MHz (top) and ^{13}C NMR spectrum in $CDCl_3$ at 150 MHz (bottom) for entry 12, Table 2-2.

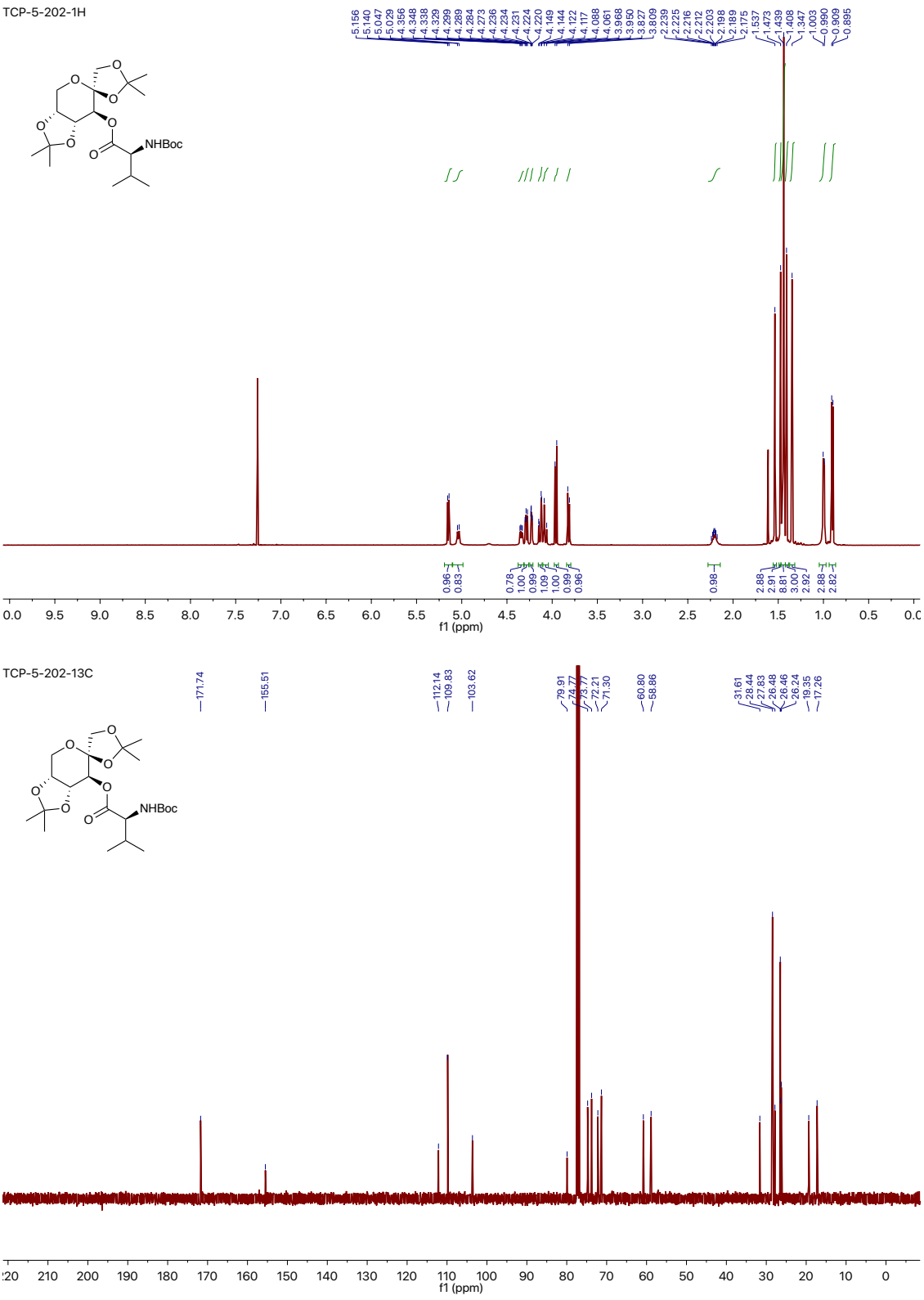

Figure S2-13: ^{1}H NMR spectrum in $CDCl_3$ at 500 MHz (top) and ^{13}C NMR spectrum in $CDCl_3$ at 100 MHz (bottom) for entry 13, Table 2-2.

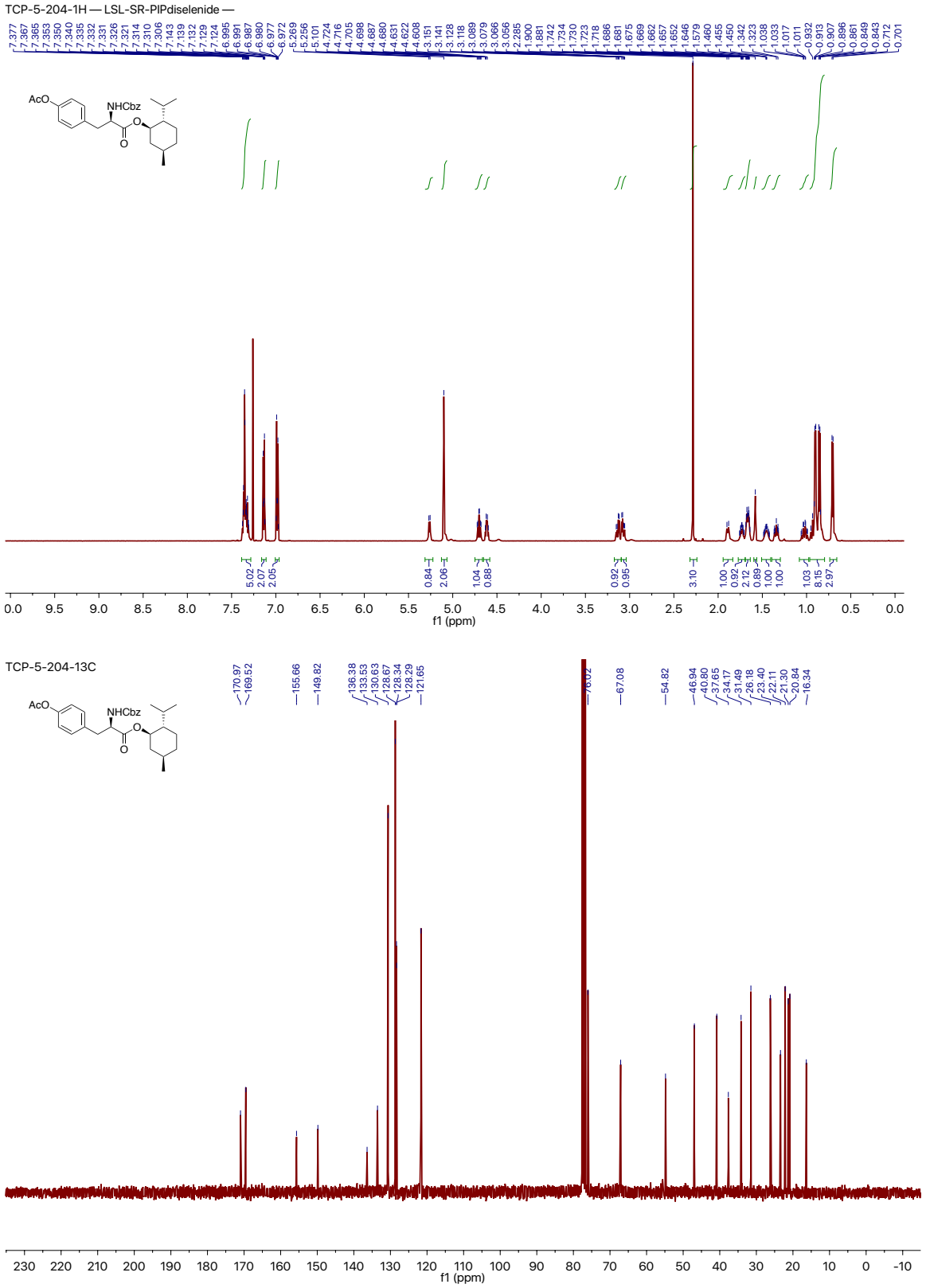

Figure S2-14: ^{1}H NMR spectrum in $CDCl_3$ at 600 MHz (top) and ^{13}C NMR spectrum in $CDCl_3$ at 75 MHz (bottom) for entry 14, Table 2-2.

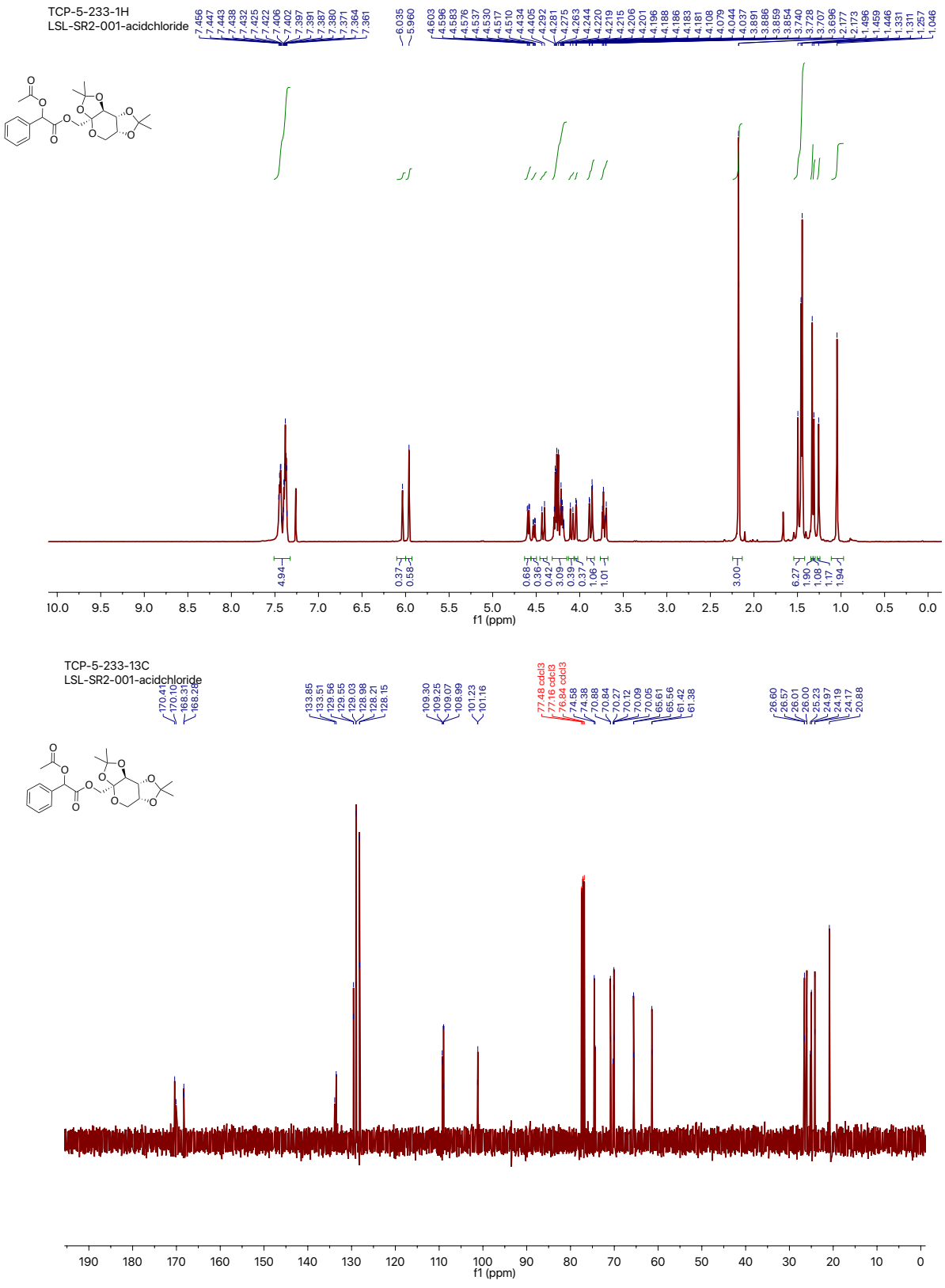

Figure S2-15: ^{1}H NMR spectrum in $CDCl_3$ at 400 MHz (top) and ^{13}C NMR spectrum in $CDCl_3$ at 100 MHz (bottom) for entry 15, Table 2-2.

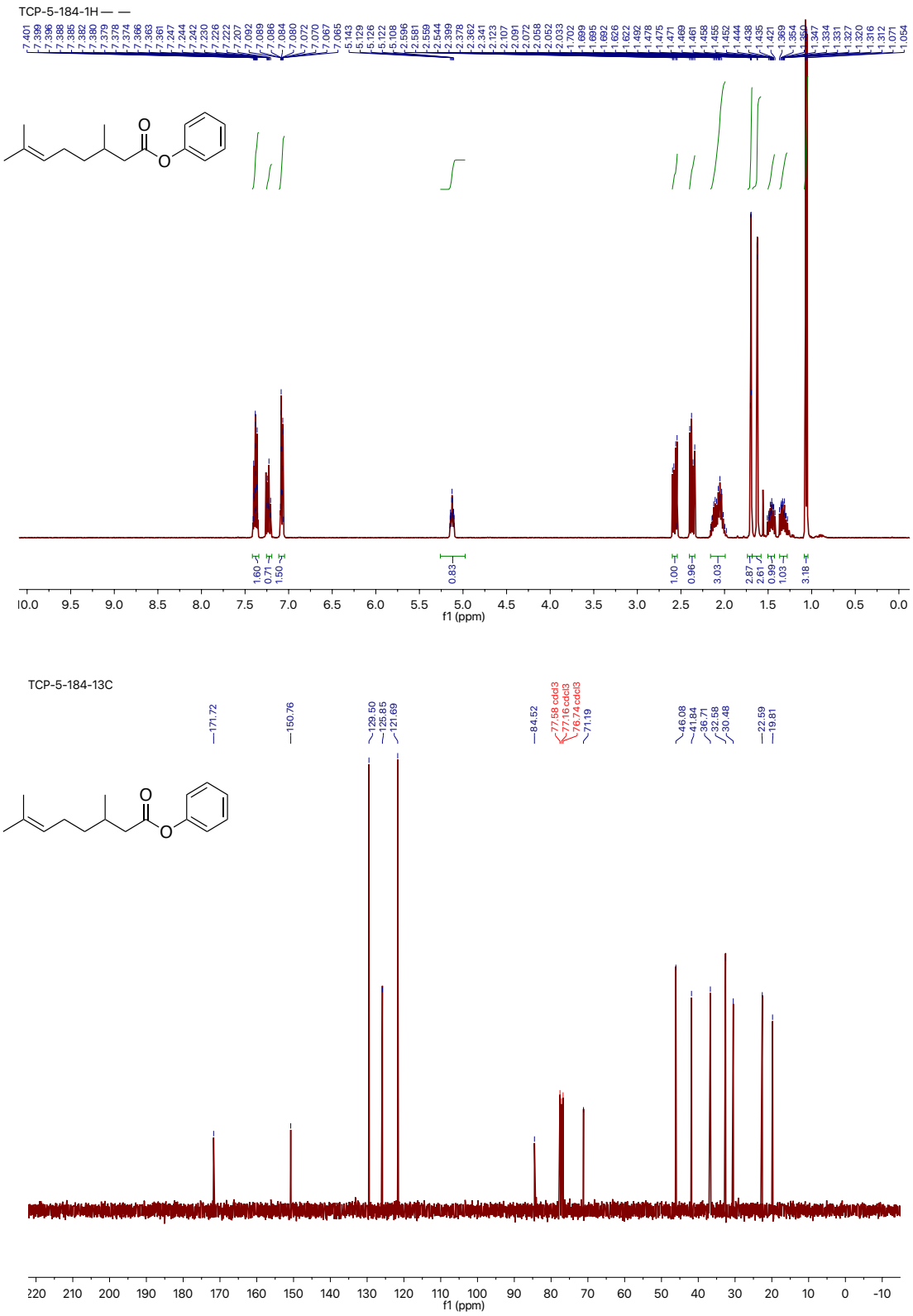

Figure S2-16: ^{1}H NMR spectrum in $CDCl_3$ at 400 MHz (top) and ^{13}C NMR spectrum in $CDCl_3$ at 100 MHz (bottom) for entry 17, Table 2-2.

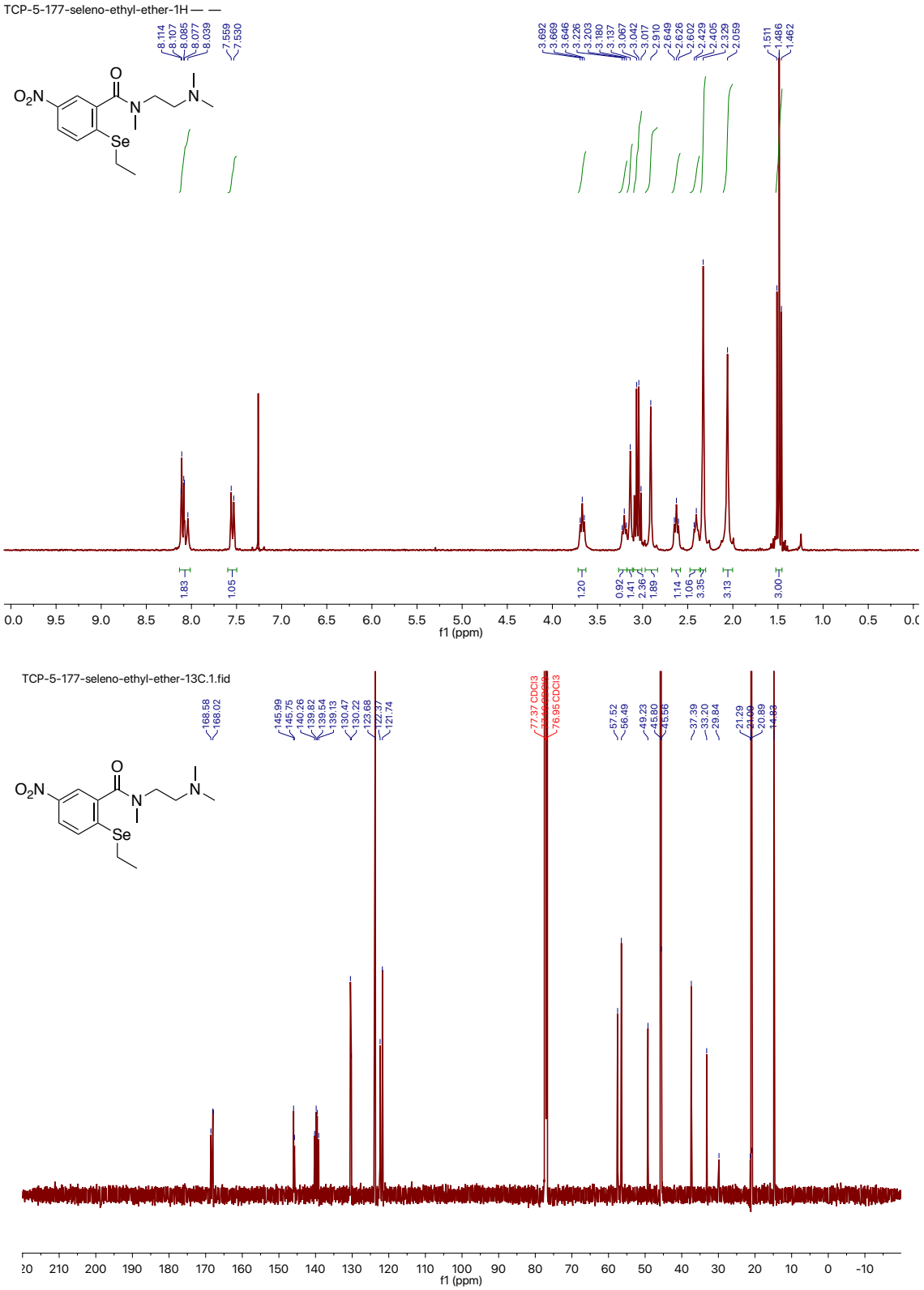

Figure S2-17: ^{1}H NMR spectrum in $CDCl_3$ at 400 MHz (top) and ^{13}C NMR spectrum in $CDCl_3$ at 100 MHz (bottom) of compound **2.12**.

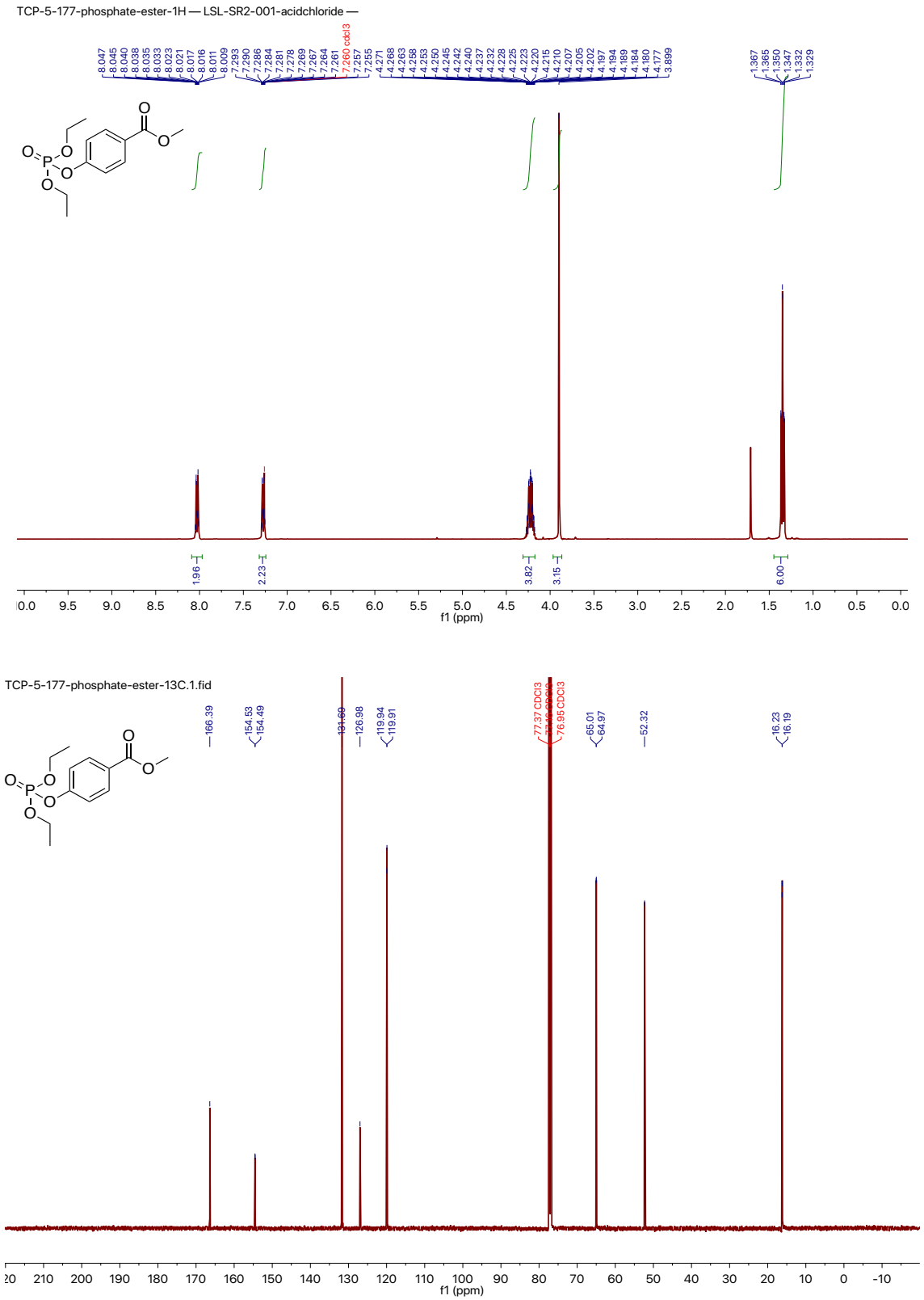

Figure S2-18: ^{1}H NMR spectrum in $CDCl_3$ at 400 MHz (top) and ^{13}C NMR spectrum in $CDCl_3$ at 100 MHz (bottom) of compound **2.13**.

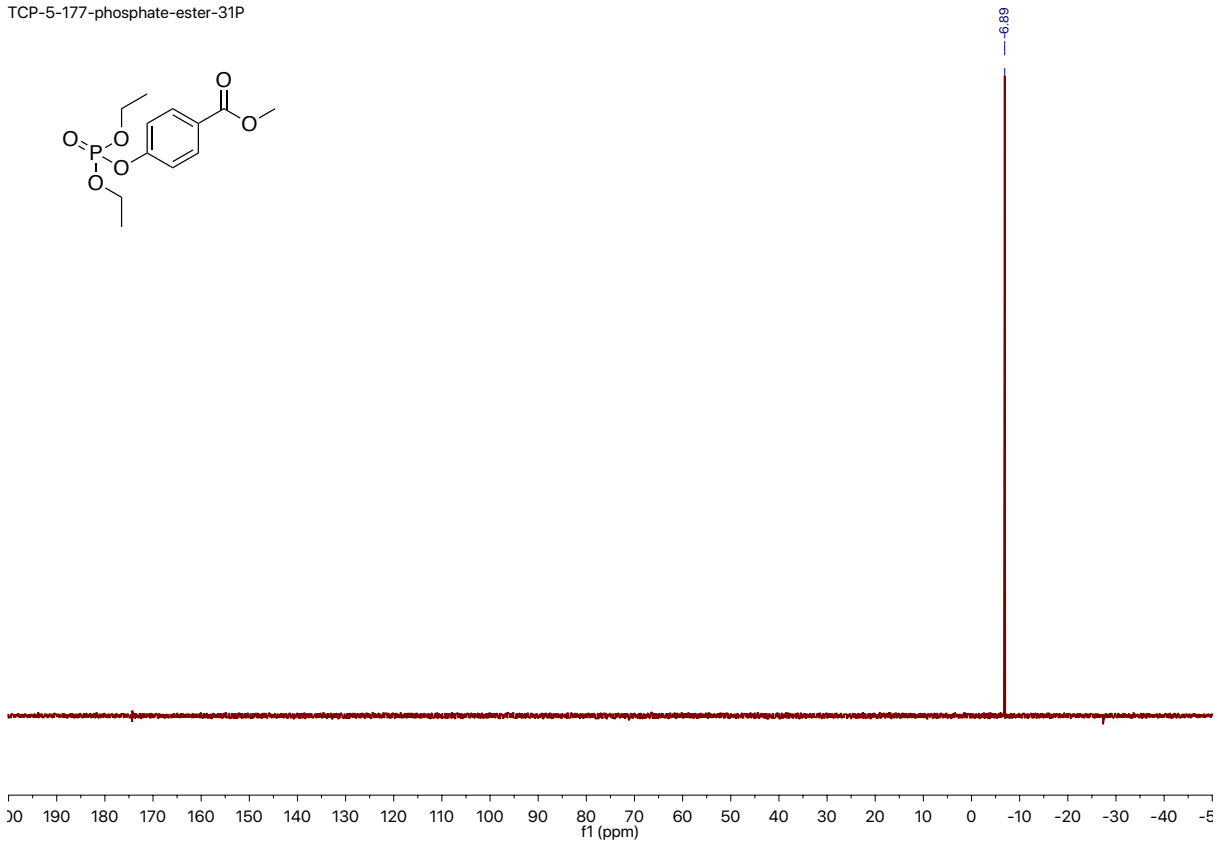

Figure S2-19: ^{31}P NMR spectrum at 121 MHz of compound **2.13**.

2.6 References

[1] J. Otera, J. Nishikido, *Esterification: methods, reactions, and applications*, John Wiley & Sons, **2009**.

[2] P. G. Wuts, T. W. Greene, *Greene's protective groups in organic synthesis*, John Wiley & Sons, **2006**.

[3] a) K. Matsumoto, R. Yanagi, Y. Oe. Recent Advances in the Synthesis of Carboxylic Acid Esters. In *Carboxylic Acid-Key Role in Life Sciences*, IntechOpen, **2018**; b) P. Siengalewicz, J. Mulzer, U. Rinner. Synthesis of esters and lactones. In *Comprehensive Organic Synthesis: Second Edition* (Eds.: P. Knochel, G. A. Molander), Elsevier Ltd., **2014**; c) Carboxylic Acid Derivatives Synthesis. In *Name Reactions for Functional Group Transformations* (Eds.: J. J. Li, E. J. Corey), **2010**.

[4] a) T. Mukaiyama. Oxidation-reduction condensation. *Angewandte Chemie, International Edition in English* **1976**, *15*, 94-103; b) D. Hughes. The Mitsunobu Reaction. In *Org. React., Vol. 42*, **1992**, pp. 335-656; c) T. Y. S. But, P. H. Toy. The Mitsunobu Reaction: Origin, Mechanism, Improvements, and Applications. *Chemistry: An Asian Journal* **2007**, *2*, 1340-1355; d) K. K. Swamy, N. B. Kumar, E. Balaraman, K. P. Kumar. Mitsunobu and related reactions: advances and applications. *Chemical Reviews* **2009**, *109*, 2551-2651; e) T. Mukaiyama, K. Kuroda, Y. Maruyama. A new type of oxidation-reduction condensation by the combined use of phenyl diphenylphosphinite and oxidant. *Heterocycles* **2010**, *80*, 63-82; f) T. Mukaiyama. Explorations into new reaction chemistry. *Angewandte Chemie International Edition* **2004**, *43*, 5590-5614.

[5] a) R. H. Beddoe, H. F. Sneddon, R. M. Denton. The catalytic Mitsunobu reaction: a critical analysis of the current state-of-the-art. *Organic and biomolecular chemistry* **2018**, *16*, 7774-7781; b) T. Taniguchi, D. Hirose, H. Ishibashi. Esterification via iron-catalyzed activation of triphenylphosphine with air. *ACS Catalysis* **2011**, *1*, 1469-1474.

[6] a) C. J. O'Brien, (Univ. Texas, USA), WO 2010/118042A3, **2010**; b) J. A. Buonomo, C. G. Eiden, C. C. Aldrich. Chemoselective Reduction of Phosphine Oxides by 1, 3-Diphenyl-Disiloxane. *Chemistry--A European Journal* **2017**, *23*, 14434-14438.

[7] a) C. J. O'Brien, J. L. Tellez, Z. S. Nixon, L. J. Kang, A. L. Carter, S. R. Kunkel, K. C. Przeworski, G. A. Chass. Recycling the Waste: The Development of a Catalytic Wittig Reaction. *Angewandte Chemie International Edition* **2009**, *48*, 6836-6839; b) Z. Lao, P. H. Toy. Catalytic Wittig and Aza-Wittig Reactions. *Beilstein Journal of Organic Chemistry* **2016**, *12*, 2577-2587; c) L. Wang, Y. Wang, M. Chen, M.-W. Ding. Reversible P(III)/P(V) Redox: Catalytic Aza-Wittig Reaction for the Synthesis of 4(3H)-Quinazolinones and the Natural Product Vasicinone. *Advanced Synthesis & Catalysis* **2014**, *356*, 1098-1104; d) D. C. Lenstra, J. J. Wolf, J. Mecinovic. Catalytic Staudinger Reduction at Room Temperature. *The Journal of Organic Chemistry* **2019**; e) T. V. Nykaza, T. S. Harrison, A. Ghosh, R. A. Putnik, A. T. Radosevich. A Biphilic Phosphetane Catalyzes N–N Bond-Forming Cadogan Heterocyclization via PIII/PV=O Redox Cycling. *Journal of the American Chemical Society* **2017**, *139*, 6839-6842.

[8] T. Y. S. But, P. H. Toy. Organocatalytic Mitsunobu reactions. *Journal of the American Chemical Society* **2006**, *128*, 9636-9637.

[9] D. Hirose, T. Taniguchi, H. Ishibashi. Recyclable Mitsunobu reagents: Catalytic Mitsunobu reactions with an iron catalyst and atmospheric oxygen. *Angewandte Chemie International Edition* **2013**, *52*, 4613-4617.

[10] a) A. Henke, J. Srogl. Thioimides: new reagents for effective synthesis of thiolesters from carboxylic acids. *The Journal of Organic Chemistry* **2008**, *73*, 7783-7784; b) J. M. Villalobos. Aerobic, Medal Mediated Ketone Synthesis from Thiol Esters and Boronic Acids. Ph.D. Dissertation, Emory University, Atlanta, Georgia, **2007**.

[11] Z. Wang, Y. Kuninobu, M. Kanai. Copper-Catalyzed Intramolecular N–S Bond Formation by Oxidative Dehydrogenative Cyclization. *The Journal of Organic Chemistry* **2013**, *78*, 7337-7342.

[12] L. S. Liebeskind, P. Gangireddy, M. G. Lindale. Benzoisothiazolone Organo/Copper-Cocatalyzed Redox Dehydrative Construction of Amides and Peptides from Carboxylic Acids using (EtO)3P as the Reductant and O2 in Air as the Terminal Oxidant. *Journal of the American Chemical Society* **2016**, *138*, 6715-6718.

[13] P. Gangireddy, V. Patro, L. Lam, M. Morimoto, L. S. Liebeskind. Mechanism of Acylative Oxidation–Reduction–Condensation Reactions Using Benzoisothiazolones as Oxidant and Triethylphosphite as Stoichiometric Reductant. *The Journal of Organic Chemistry* **2017**, *82*, 3513-3529.

[14] M. G. Lindale. Desulfitative Coupling Reactions for the Mild Construction of Carbon-Carbon, Carbon-Nitrogen, and Carbon-Oxygen Bonds. Ph.D. Dissertation, Emory University, Atlanta, Georgia, **2015**.

[15] J. Chaudiere, O. Courtin, J. Leclaire. Glutathione oxidase activity of selenocystamine: a mechanistic study. *Archives of Biochemistry and Biophysics* **1992**, *296*, 328-336.

[16] H. J. Reich, R. J. Hondal. Why Nature Chose Selenium. *ACS Chemical Biology* **2016**, *11*, 821-841.

[17] S. M. Akondi, P. Gangireddy, T. C. Pickel, L. S. Liebeskind. Aerobic, Diselenide-Catalyzed Redox Dehydration: Amides and Peptides. *Organic Letters* **2018**, *20*, 538-541.

[18] a) M. Iwaoka, S. Tomoda. Direct observation of intramolecular interaction between a divalent selenium and a tertiary amine by means of single crystal X-ray analysis and NMR spectroscopy. *Phosphorus, Sulfur, and Silicon and the Related Elements* **1992**, *67*, 125-130; b) M. Iwaoka, S. Tomoda. Nature of the Intramolecular Se···N Nonbonded Interaction of 2-Selenobenzylamine Derivatives. An Experimental Evaluation by 1H, 77Se, and 15N NMR Spectroscopy. *Journal of the American Chemical Society* **1996**, *118*, 8077-8084; c) M. Iwaoka, S. Tomoda. Structural Characterization of areneselenenyl chloride stabilized by the stereoelectronic Effect of an intramolecular nitrogen atom. *The Journal of Organic Chemistry* **1995**, *60*, 5299-5302.

[19] C. Deleanu, J. E. Drake, M. B. Hursthouse, M. Kulcsar, M. E. Light, A. Silvestru. Hypervalent selenium compounds containing N→ Se intramolecular interactions: synthesis, characterization and X-ray structures of [2-(Me2NCH2) C6H4] SeS (S) PR2 (R= Ph, OiPr). *Applied Organometallic Chemistry* **2002**, *16*, 727-731.

[20] a) H. Fujihara, H. Mima, N. Furukawa. First Isolation and Crystal Structure of Heavier Chalcogenenium Cations (RSe+, RTe+) Stabilized by Two Neighboring Amino Groups. *Journal of the American Chemical Society* **1995**, *117*, 10153-10154; b) H. Fujihara, H. Mima, M. Ikemori, N. Furukawa. New hypervalent .sigma.-selenanes with a transannular selenium-nitrogen bond from N-methyl-5H,7H-dibenzo[b,g][1,5]selenazocine. *Journal of the American Chemical Society* **1991**, *113*, 6337-6338; c) A. Panda, G. Mugesh, H. B. Singh, R. J. Butcher. Synthesis, Structure, and Reactivity of Organochalcogen (Se, Te) Compounds Derived from 1-(N,N-Dimethylamino)naphthalene and N,N-Dimethylbenzylamine. *Organometallics* **1999**, *18*, 1986-1993; d) R. Kaur, H. B. Singh,

R. P. Patel. Synthesis, characterisation and reactions of bis[2-(dimethylaminomethyl)-phenyl] diselenide: its structure and that of [2-(dimethylaminomethyl)phenyl]-selenium bromide. *Journal of the Chemical Society, Dalton Transactions* **1996**, 2719-2726; e) Y. Miyake, M. Oda, A. Oyamada, H. Takada, K. Ohe, S. Uemura. Asymmetric imidation of organic selenides into selenimides. *Journal of Organometallic Chemistry* **2000**, *611*, 475-487.

[21] A. C. Spivey, S. Arseniyadis. Amine, Alcohol and Phosphine Catalysts for Acyl Transfer Reactions. In *Asymmetric Organocatalysis, Vol. 291* (Ed.: B. List), Springer Berlin Heidelberg, Berlin, Heidelberg, **2009**, pp. 233-280.

[22] F. Westheimer, S. Huang, F. Covitz. Rates and mechanisms of hydrolysis of esters of phosphorous acid. *Journal of the American Chemical Society* **1988**, *110*, 181-185.

[23] a) B. Neises, W. Steglich. Simple Method for the Esterification of Carboxylic Acids. *Angewandte Chemie International Edition in English* **1978**, *17*, 522-524; b) J. C. Sheehan, J. J. Hlavka. The use of water-soluble and basic carbodiimides in peptide synthesis. *The Journal of Organic Chemistry* **1956**, *21*, 439-441.

[24] T. C. Pickel, S. M. Akondi, L. S. Liebeskind. Esterification by Redox Dehydration Using Diselenides as Catalytic Organooxidants. *The Journal of Organic Chemistry* **2019**, *84*, 4954-4960.

Chapter 3

Synthesis and Biological Evaluation of the Stereoisomers of 1-Amino-3,4-difluorocyclopentane-1-carboxylic acid (3,4-DFACPC) as PET Imaging Agents

Collaborative project with Professor Mark M. Goodman, PhD, Emory University School of Medicine, Department of Radiology.

Ronald Voll, PhD, Department of Radiology, performed the radiosynthesis of **[^{18}F]3.09, 3.23, and 3.33**.

Weiping Yu, PhD, Department of Radiology, performed *in vitro* cancer cell uptake assays.

Jaekeun Park, PhD, Wallace H. Coulter Department of Biomedical Engineering collected and processed Positron Emission Tomography and Computed Tomography data.

John Nye, PhD, Department of Radiology, performed Positron Emission Tomography image analysis and provided biodistribution data.

Zhaobin Zhang, Emory University School of Medicine, Department of Neurosurgery, provided animals and cancer cells for *in vitro* and *in vivo* studies.

3.1 Abstract: Positron emission tomography (PET) has emerged as a valuable technique for imaging a variety of oncological disorders, though there is a need for the development of new PET radiotracers for intracranial and prostate tumors. Reported herein is the cold synthesis, ^{18}F radiosynthesis, and biological evaluation of the four stereoisomers of 1-amino-3,4-difluorocyclopentane-1-carboxylic acid (3,4-DFACPC), a series of rationally designed non-natural amino acids. *In vitro* 9L, U87 ΔEGFR, and DU145 cancer cell line assays demonstrated that each stereoisomer of 3,4-DFACPC is a substrate primarily for system L transport, with s3ome transport occurring via system ASC. In Fischer rats bearing 9L gliosarcoma tumors, the stereoisomers of [^{18}F]3,4-DFACPC each showed high affinity for uptake by tumor cells and good tumor to normal brain tissue ratios, suggesting that these compounds may be useful as PET radiotracers for imaging brain tumors. Additionally, biodistribution studies in normal Fischer rats as well as uptake in DU145 cells collectively suggest that [^{18}F]3,4-DFACPCs show promise for imaging prostate cancer.

3.2 Introduction

In clinical oncology, non-invasive techniques that are able to provide a visual representation of anatomical and physiological features serve an essential role in the diagnosis and treatment of disorders. Accordingly, imaging is one of the most common practices in oncological medicine, with an estimated 5 billion procedures conducted worldwide as of 2010.[1] Imaging modalities can be stratified into two categories: anatomical and functional. Anatomical modalities such as magnetic resonance imaging (MRI), computed tomography (CT), ultrasound, and optical imaging, detect morphological changes associated with disorder. These modalities offer high resolution but are generally limited to the detection of relatively well-developed tumors with a diameter of at least 1 cm, because smaller structural anomalies tend not to produce a readily identified

morphological abnormality.[2] In contrast, functional imaging modalities, such as positron emission tomography (PET), provide insight into the molecular biology of tissues across the body.[3] Cancer cells generally present with greatly altered metabolism relative to healthy cells, a disparity that functional imaging techniques leverage to identify oncological disorder. Because metabolic processes can be monitored at the molecular level rather than at the tissue level, it is possible to detect smaller quantities of cells via PET than by anatomical methods. Consequently, PET has the potential to be a more sensitive modality than its anatomical counterparts. Additionally, insight into the metabolic behavior of the tumor is inherently useful for staging, prognostic evaluation, and assessing response to therapy. While this increased sensitivity and utility presents great opportunities for oncological imaging, the efficacy of PET in clinical settings is limited relative to its potential.[2b, 4] This is because the capacity of PET to image a particular tumor type is dependent on the selectivity of the imaging agent that is used. In PET, imaging agents, also called radiotracers, are molecules bearing a radionuclide, which exploit the metabolic variance between healthy and cancer cells to allow for selective uptake in the latter. At present, there is a lack of effective PET radiotracers for imaging brain and prostate tumors.[5] It is particularly crucial that these can be accurately imaged, as there is a risk of unnecessary loss of functionally indispensable tissue during radiotherapy or surgical resection due to poor delineation of lesion boundaries.[6] Additionally, developing an appropriate treatment plan following initial medical intervention is contingent upon differentiating between necrotic or inflamed tissue and recurrent tumors, though such distinctions remain challenging with current technology.[7] These issues can be addressed by the development of PET radiotracers that are capable of selectively identifying intracranial and prostate tumors in the presence of healthy tissue. Below, a brief overview of the principles of PET is provided, followed by an introduction to the concepts related

to radiotracer development and a critical analysis of some commercial and experimental oncological imaging agents. Finally, the synthesis of the stereoisomers of ^{18}F labeled 1-amino-3,4-difluorocyclopentane-1-carboxylic acids and preliminary evaluation of their utility as PET radiotracers is described.

Principles of PET

There are many radionuclides capable of emitting positrons, including ^{11}C (maximum kinetic energy of emitted positron, Emax = 970 keV, $t_{1/2}$ = 20.4 min), ^{13}N (Emax = 1.30 MeV, $t_{1/2}$ = 10.0 min), ^{15}O (Emax = 1.72 MeV, $t_{1/2}$ = 2.04 min), ^{18}F (Emax = 635 keV, $t_{1/2}$ = 110 min), ^{64}Cu (Emax = 657 keV, $t_{1/2}$ = 12.7 hours), ^{68}Ga (Emax = 1.90 MeV, $t_{1/2}$ = 67.7 min), and ^{124}I (Emax = 2.13 MeV, $t_{1/2}$ = 4.2 days). ^{18}F has a favorable half-life, a relatively low beta decay energy, which allows for a short positron linear range (positron linear range is inversely correlated with resolution, *vide infra*), and is easily incorporated into small molecules.[8] Additionally, the electronegativity of fluorine is similar to that of oxygen, and it is sterically similar to hydrogen. For these reasons, ^{18}F is often the radionuclide of choice in the development of experimental radiotracers and is by far the most commonly employed radionuclide in clinical settings, owing to the widespread use of 2-deoxy-2-[^{18}F]fluoroglucose ([^{18}F]FDG).[3b, 7] ^{18}F is the product of a nuclear reaction between $H_2{}^{18}O$ and a high energy (10-15 MeV) proton beam (Scheme 3-1), which is generated by a cyclotron, as described below.

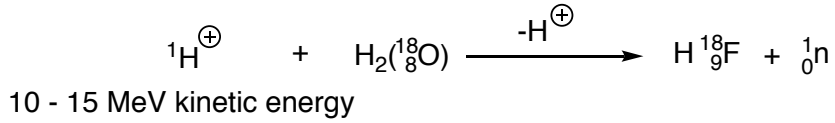

Scheme 3-1: Nuclear reaction between ^{18}O bearing H_2O and a proton with high kinetic energy yielding ^{18}F.

Within a cyclotron, a Penning Ion Gauge ionizes hydrogen gas, generating hydride ions. The ions are injected into the center of a region flanked by two electrodes, called dees, which rapidly alternate in polarity of voltage. The hydride ions travel toward the positively charged dee, though they travel along a curved path instead of a straight line, owing to the influence of an applied magnetic field. As the ions approach the trailing edge of the positively charged dee, its sign changes, repelling the ions and accelerating them toward the opposing dee. With each iteration, the ions gain greater speed and bend further away from the center of the chamber, following an approximately spiral shaped path until they reach the outer edge of the chamber. At this juncture, a carbon foil intercepts the beam of hydride ions, stripping them of their electron pairs and generating protons. The protons are directed toward a port leading out of the acceleration chamber, where they are brought into contact with $H_2{}^{18}O$, generating a solution of $H^{18}F$ in $H_2{}^{18}O$. Once generated, $H^{18}F$ is often converted to an alkali metal salt for immediate use in the synthesis of molecular tracers, generally via an S_N2 displacement of a halide or pseudohalide.

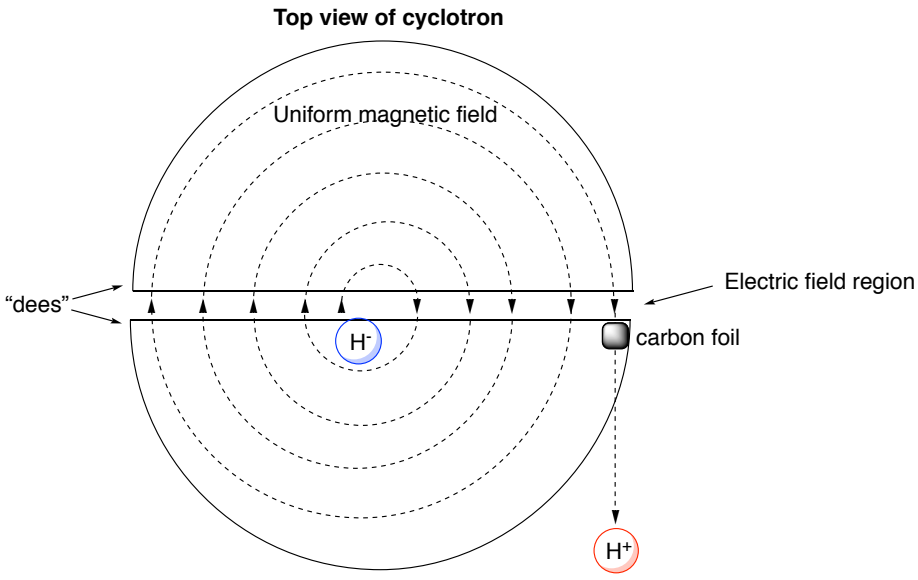

Figure 3-1. Illustration of the production of high kinetic energy H^+ ions by a cyclotron.

Once the tracer is synthesized and purified, a dose containing the requisite quantity of radioactivity is prepared as an aqueous solution and administered intravenously to the patient. The ^{18}F labeled compound travels through the body, and, ideally, is selectively transported into tumor cells in the presence of healthy tissues. Spontaneous beta-plus decay of the unstable ^{18}F nucleus results in the formation of a high energy positron, which travels a distance of up to 2 mm before meeting an electron, resulting in an annihilation event that produces two 511 keV photons. The photons travel away from the point of annihilation in an antiparallel and linear fashion until they are detected by a PET scanner outside of the body. The scanner contains an array of scintillation crystals composed of inorganic salts, which convert a single 511 keV photon into thousands of photons in the UV-vis energy regime. The signal is amplified further as the photons are directed to a photomultiplier tube before a final output is transmitted to the electronic components of the scanner. Because the annihilation event produces two photons travelling at a 180° angle with respect to each other, in the absence of any perturbing physical occurrences, both photons will strike the detector arrays at approximately the same time, with small variations in timing arising from annihilations that are closer in proximity to one side of the detector. If two photons are detected within a 6-12 ns timeframe, the detection is considered to be a true-coincidence event, and the line between the photons is called the line of response (LOR). If only a single photon is detected over the course of the coincidence timeframe, the detection is discarded. Therefore, the number of coincident events is proportional to the concentration of radiotracer along a given LOR, and when all LOR are considered as an ensemble, a three-dimensional depiction of the distribution of the radiotracer can be constructed.[9]

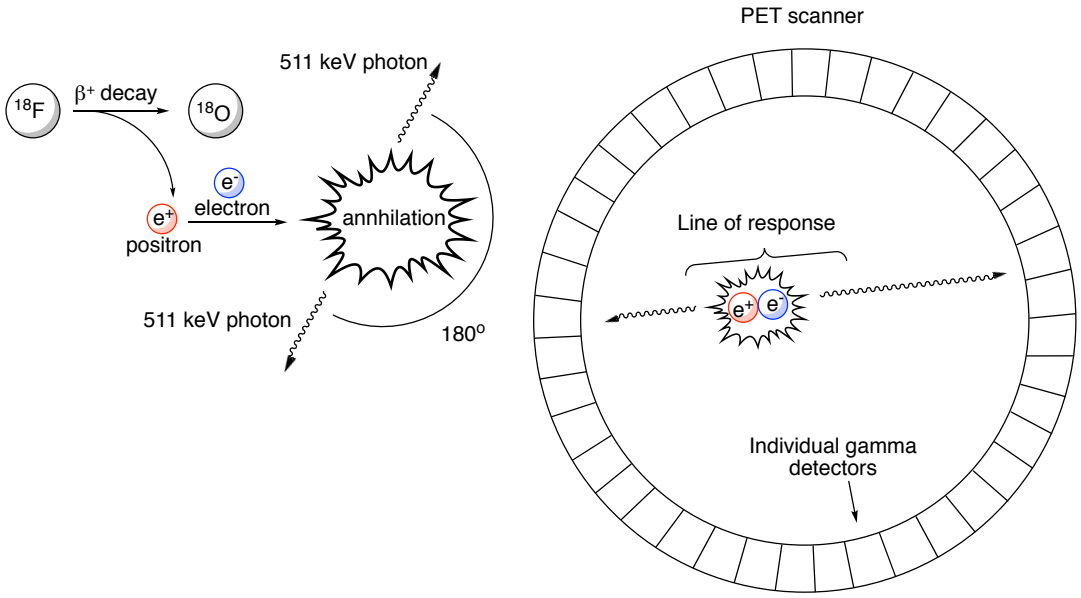

Figure 3-2. Illustration of gamma ray detection by a PET scanner.

The spatial resolution of PET is constrained by the accuracy of the determination of the point of positron emission, which, according to the description of the PET imaging process outlined above, is a function of three factors: (1) the distance the positron travels away from the site of beta decay (emission) to the point of annihilation, (2) confounding physical effects, such as the deflection of photons away from the real LOR, which result in the false detection of true-coincidence events, and (3) fidelity in the detection of incident photons by the scintillation crystals. In practice, these factors limit PET to a modest spatial resolution of 1-3 mm.[10] By comparison, MRI and CT offer spatial resolutions of 10-100 and 50-200 μm, respectively. However, because each photon produced by positron annihilation is sufficiently energetic to produce thousands of UV-vis photons in a scintillator, there is an inherent amplification of signal associated with beta decay events. Additionally, the condition that detected photons must be coincident in order to be distinguished as valid intrinsically provides an efficient form of electronic collimation, obviating the need for a physical collimator, which would result in a loss of signal.[11] Consequently, PET is much more

sensitive than anatomic modalities, with radiotracers detectable at concentrations as low as 0.1 pM.[2b]

PET Radiotracers for Imaging Brain and Prostate Cancer

All imaging modalities rely on some form of contrast to distinguish between healthy tissue and oncological disorder. For example, ^{1}H magnetic resonance T1 and T2 relaxation times and water content vary according to tissue type, providing the basis for contrast and detection of tumors via MRI.[12] In the case of PET, contrast is based on the differential uptake or binding of a radiotracer to cancer cells versus healthy cells. Because the molecular biology of cancer cells varies greatly from that of healthy cells, there are many approaches to engineering radiotracers such that they may differentiate between the two.

The first and, until 2012, only radiotracer approved for clinical oncological use was [^{18}F]FDG, a fluorinated glucose derivative, which is a substrate for transmembrane glucose transporters (GLUT).[3b] Cancer cells have an increased energy demand relative to healthy cells and GLUT are indirectly responsible for providing cells with energy equivalents, since cellular transport of authentic glucose provides substrates for glycolysis, which produces ATP. Under aerobic conditions, a single equivalent of glucose is capable of producing 36 equivalents of adenosine triphosphate (ATP), while only two equivalents are produced under anaerobic conditions. Uncontrolled cell proliferation coupled with a lack of adequate blood supply often results in hypoxic conditions for solid tumors, rendering them unable to utilize the more energy efficient aerobic glycolytic pathway and further increasing their appetite for glucose. Many types of tumors upregulate GLUT in order to meet energy demands and maintain rapid rates of cell proliferation. Once transported into the cell, [^{18}F]FDG undergoes phosphorylation, though it is not a substrate for glycolysis, and without other metabolic pathways to traverse or a mode of efflux, [^{18}F]FDG-6-

phosphate remains trapped within the cell. Accordingly, [^{18}F]FDG-6-phosphate accumulates to some extent within all cells, but upregulation of GLUT in cancer cells results in greater [^{18}F]FDG avidity relative to healthy cells, which is the basis for detection of tumors by [^{18}F]FDG-PET.[3b]

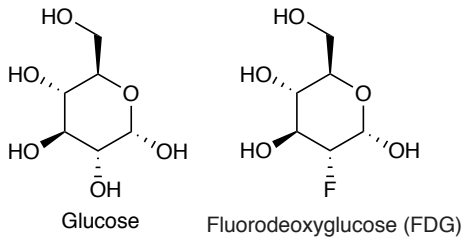

Figure 3-3. Molecular structures of glucose and FDG.

Because GLUT are so ubiquitous, [^{18}F]FDG-PET has proven to be a powerful method for imaging a diverse array of oncological disorders including breast, lung, head and neck, esophageal, colorectal, cervical, and ovarian cancers, as well as lymphoma.[3b, 7] However, there are substantial limitations associated with the use of [^{18}F]FDG. Firstly, [^{18}F]FDG-PET is unable to distinguish cancer cells from benign cells that have heightened metabolic rates, such as benign neoplastic cells or those associated with inflammation or infection. Because inflammation is a common side effect of radiation therapy, [^{18}F]FDG-PET is often ineffective in distinguishing recurrent tumors from radionecrosis. Secondly, in healthy brain tissue, high basal [^{18}F]FDG uptake causes poor signal-to-noise ratios or obscures tumors entirely, resulting in false-negatives and poor delineation of tumor boundaries.[7] Lastly, the prostate is often obscured by proximal bladder activity arising from rapid urinary excretion of [^{18}F]FDG, resulting in poor sensitivity and specificity in the detection of primary prostate cancer.[13] In addition to GLUT, other metabolic targets for detecting oncological disorder have been investigated, including tumor hypoxia,[14] angiogenesis,[15] tumor proliferation (via nucleoside metabolism),[16] and amino acid transport.[17] Of these, amino acid transport is the most promising target for addressing the shortcomings associated with [^{18}F]FDG-PET.

Natural amino acids (AAs) are ubiquitous substrates that are essential to many cellular processes including protein synthesis, energy metabolism, cell signaling, cellular proliferation, and regulating gene expression. Generally, AAs are obtained by recycling partially degraded proteins into their constituent residues, by *de novo* synthesis from glycolysis or citric acid cycle intermediates, or by abduction from the extracellular environment. AAs are unable to freely diffuse through cell membranes and require substrate specific amino acid transporters (AATs) to mediate their passage into the cell.[18] The expression of AATs varies according to cell type, though, like GLUT, AATs are upregulated in most types of cancer cells due to their enhanced demand for both protein synthesis and cellular respiration substrates. Accordingly, AATs are considered to be viable targets for the detection of cancer cells with PET radiotracers.

AATs consist of several transmembrane domains that operate in concert to create channels that mediate the influx and efflux of specific AAs. An empirically derived classification system developed by Christensen and coworkers based on functional properties such as ion dependence, pH sensitivity, and substrate specificity identified three principal AAT systems: L, A, and ASC. Each of the three systems is named for the type of AA it prefers to transport: L for "leucine preferring", is an Na^+ independent transporter and obligatory exchanger (meaning that for each system L substrate transported into the cell, another substrate is transported out of the cell) of neutral AAs with bulky aliphatic and aromatic side chains, such as L-leucine, L-valine, L-isoleucine, L-methionine, L-asparagine, L-tyrosine, L-phenylalanine, L-tryptophan, and L-histidine. A for "alanine preferring", is a Na^+ dependent and unidirectional transporter of neutral AAs with sterically diminutive sidechains, such as L-serine and L-alanine. And ASC, for "alanine, serine, and cysteine preferring", is a Na^+ dependent obligatory exchange transporter of L-alanine, L-serine, and L-cysteine, though this system also recognizes L-glutamine and L-threonine.[19] Of

all AATs, LAT1 (large amino acid transporter 1; a protein from the system L family) and ASCT2 (alanine, serine, and cysteine transporter 2; a protein from the system ASC family) are the most highly expressed in most types of cancer cells.[20] Particularly noteworthy is the increased expression of these two AATs in brain cancer and prostate cancer, which are challenging to image with [^{18}F]FDG, as described above.[21] Furthermore, LAT1 is expressed in the lumen of the blood brain barrier and is principally responsible for mediating AA transport into the brain, thereby allowing system L substrates to access intracranial tissue.[22] Therefore, radiotracers with a high affinity for active transport by ASCT2, and especially LAT1, are of interest.

In principle, any of the naturally occurring AAs that are known to undergo transport by LAT1 and ASCT2 could serve as effective radiotracers for tumor imaging, provided that the molecular structure of the AA is amenable to the time-sensitive introduction of a radionuclide suitable for PET. ^{11}C and ^{13}N are the only such radionuclides with promise for natural AA incorporation, since fluorine is not a constituent of these compounds. While ^{13}N has seen clinical use in the form of [^{13}N]NH_3,[23] its 10-minute half-life is not sufficient to allow for the reliable synthesis of [^{13}N]AAs in clinical settings. ^{11}C also has a short half-life (20.4 minutes), though a few highly optimized processes have been developed that allow production of ^{11}C labeled compounds.[24] These processes center around the conversion of [^{11}C]CH_4 to [^{11}C]CH_3I for methylation of nucleophilic substrates, or to [^{11}C]HCN for addition to an electrophile followed by hydrolysis to the corresponding carboxylic acid. Nearly all naturally occurring AAs can be radiolabeled with ^{11}C by one of these two methods, though methylation of L-homocysteine thiolactone with $^{13}CH_3I$ to give [^{11}C]L-methionine ([^{11}C]MET) is the only transformation that is sufficiently straightforward to allow for significant clinical use. Accordingly, [^{11}C]MET was the first [^{11}C]AA oncologic PET

radiotracer to be evaluated in humans and has been extensively studied as a PET radiotracer for the detection of brain and prostate tumors.[6, 25]

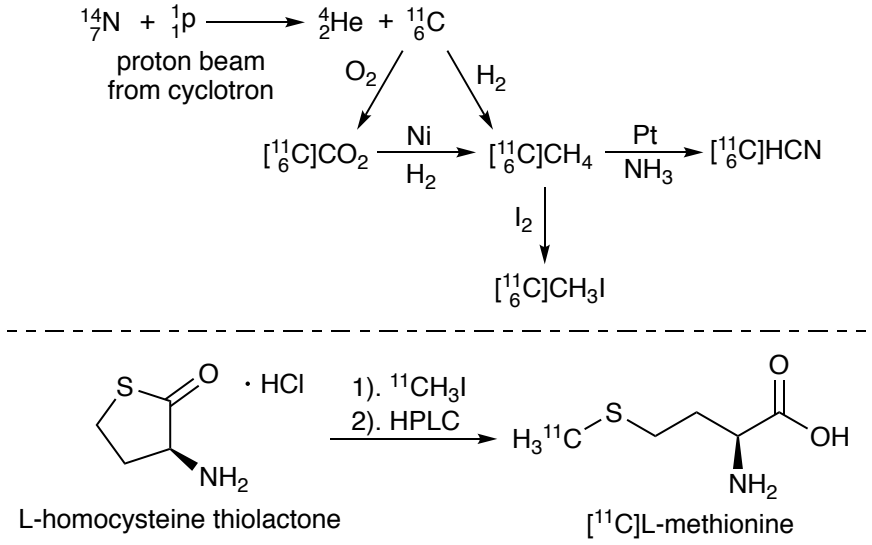

Scheme 3-2. Conversion of $^{11}CO_2$ to [^{11}C]HCN and [^{11}C]CH_3I (top). Synthesis of [^{11}C]L-methionine (bottom).

One such study conducted by Iwama and coworkers, in which patients with primary glioma were imaged with both [^{11}C]MET-PET and [^{18}F]FDG-PET, demonstrated that only 3-6% of patients with low grade tumors presented with increased [^{18}F]FDG uptake, while 72-76% presented with increased [^{11}C]MET uptake. In patients with grade II (diffuse astrocytoma), III (anaplastic astrocytoma), and IV (glioblastoma multiforme) glioma, ^{11}[C]MET uptake in tumor versus normal contralateral tissue (T/N ratio; a measure of contrast) was 2.24 ± 0.90, 3.03 ± 1.02, and 5.03 ± 1.65 respectively, while [^{18}F]FDG gave T/N ratios of 0.79 ± 0.08, 1.27 ± 0.46, and 1.88 ± 0.78, respectively.[25d] Additionally, [^{11}C]MET-PET was found to be more useful than [^{18}F]FDG-PET for staging, prognostic prediction, and delineation of tumor boundaries, as well as differentiation between non-neoplastic lesions and malignant brain tumors.[6, 25b, e] These data are consistent with

the notion that targeting LAT1 overexpression is a feasible approach to imaging tumors that have been challenging to image with [^{18}F]FDG-PET and highlight the potential value of AA radiotracers. Nonetheless, there are two substantial drawbacks associated with the use of [^{11}C]MET. Firstly, [^{11}C]MET studies require an onsite cyclotron, since the half-life of ^{11}C is not long enough to allow for synthesis and transport of [^{11}C]AAs from a remote location. Secondly, radiolabeled natural AAs are substrates for normal metabolic processes and protein synthesis. Quantitation of protein synthesis provides less clinically valuable information than does quantitation of AA transport and analysis of PET data is often complicated by both the variable rate of AA metabolism between individuals and the appearance of radiolabeled metabolites in the blood and tissue.[6, 8]

To address the issues associated with [^{11}C]MET-PET, α,α disubstituted ^{18}F labeled AAs have been investigated as PET imaging agents. AAs with the α,α substitution pattern are metabolically stable and are not recognized as substrates for protein synthesis. Additionally, the use of ^{18}F as a radionuclide provides the compound with a substantially longer half-life compared to ^{11}C. The first application of α,α substituted AAs as experimental PET imaging agents occurred in 1978 in the lab of Washburn, who conducted a study on a series of ^{14}C labeled 1-amino-cycloalkane-1-carboxylic acids ranging in size from three to six-membered rings.[26] Washburn identified the cyclobutane (ACBC)[27] and cyclopentane (ACPC)[28] analogues as having high affinity for a variety of types of tumors in humans, including intracranial tumors.[29] Building on these studies, in 1999, Goodman and coworkers reported the synthesis and biological evaluation of 1-amino-3-[^{18}F]-fluorocyclobutane-1-carboxylic acid anti-3-[^{18}F]FACBC, a fluorinated analogue of ACBC and the first ^{18}F labeled α,α disubstituted AA.[30] *In vitro* cell assays demonstrated that anti-3-[^{18}F]FACBC is a substrate for transport by ASC transporters, with some affinity for system L.

Since its discovery, anti-3-[^{18}F]FACBC has been evaluated in a humans with a variety of different types of tumor including breast,[31] lung,[32] prostate,[33] and brain cancer.[25a, 34] To date, anti-3-[^{18}F]FACBC has been approved by the FDA for detection of suspected recurrent prostate cancer and is in phase II clinical trials for imaging glioma.[34a, b] Relative to [^{11}C]MET-PET, anti-3-[^{18}F]FACBC-PET shows similar uptake in a variety of tumors, but gives lower background uptake in healthy brain, which may be explained by the fact that it is not metabolized and therefore accumulates in healthy tissues to a lesser extent.[25a]

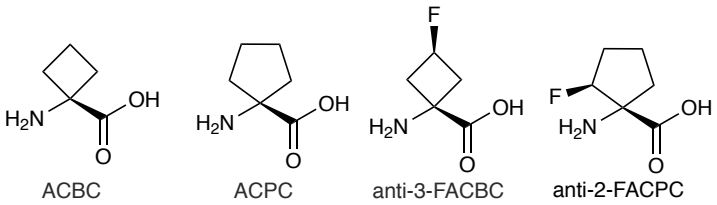

Figure 3-4. Non-natural α,α disubstituted alicyclic AAs for PET imaging as described by Washburn and Goodman.

In 2010, Goodman reported the synthesis of racemic anti-2-[^{18}F]fluorocyclopentane carboxylic acid (anti-2-[^{18}F]FACPC), a slightly bulkier analogue of anti-3-[^{18}F]FACBC and demonstrated that it was transported primarily by system L, with lesser contribution from system ASC. In Fischer rats bearing intracranial 9L gliosarcoma, anti-2-[^{18}F]FACPC and anti-3-[^{18}F]FACBC showed similar tumor uptake at various time points, though the relatively lower uptake of anti-2-[^{18}F]FACPC in healthy brain tissue resulted in T/N ratios of 12:1, an approximate two-fold increase over the T/N ratios obtained with anti-3-[^{18}F]FACBC.[35] These data suggest that anti-2-[^{18}F]FACPC may provide a greater degree of differentiation between brain tumors and normal tissue, potentially allowing for more accurate detection and localization of lesions. However, the biodistribution of anti-2-[^{18}F]FACPC is not ideal for whole body imaging, as significant and rapid accumulation in the bladder is observed and would complicate the detection of tumors near the

genitourinary tract, such as primary prostate cancer. While it may not be obvious that such an impediment could hinder the development of a radiotracer with promise for imaging intracranial tissues, the drug development process is time intensive and costly, and in the ideal case, candidate radiotracers would address both areas of concern that are not covered by [^{18}F]FDG, which include brain and prostate cancer. Notably, both anti-2-[^{18}F]FACBC and 2-[^{18}F]FACPC concentrate in the bladder at early time points in the PET scan, while anti-3-[^{18}F]FACBC accumulates in the bladder much more slowly and to a lesser extent.[36] We speculate that, in the former two compounds, the proximity of the fluorine atom to the amine and carboxylate functionalities alters the isoelectric point relative to the latter two, contributing to the observed variance in biodistribution. Based on this analysis, we anticipate that 3-[^{18}F]FACPC would exhibit a biodistribution profile more similar to anti-3-[^{18}F]FACBC, and thus represents an attractive target for development as a radiotracer. However, 3-[^{18}F]FACPC exists as two pairs of enantiomers and there are likely to be synthetic challenges associated with the isolation of a single enantiomer. Alternatively, the difluorinated ACPC derivative 1-amino-3,4-difluorocyclopentane-1-carboxylic acid (3,4-DFACPC) exists as a pair of achiral cis-difluoro meso diastereomers, in addition to a set of trans difluoro enantiomers. Ostensibly, the meso stereoisomers of 3,4-DFACPC would be more straightforward to isolate than the enantiomers of 3-[^{18}F]FACPC, which would facilitate biological evaluation. Therefore, with the goal of developing a metabolically stable radiotracer with high affinity for system L and ASC transport and an improved biodistribution profile with less rapid urinary excretion relative to 2-[^{18}F]FACPC, we targeted the synthesis of the stereoisomers of [^{18}F]3,4-DFACPC.

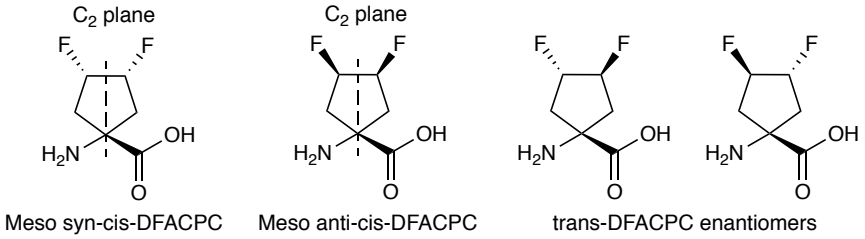

Figure 3-5. Stereoisomers of 3,4-DFACPC.

3.3 Results and Discussion

Synthesis of Non-Radioactive ("Cold") Compounds

Synthetic routes are often optimized around the most efficient and most practical series of steps to a desired final compound irrespective of the order of transformations leading to the compound, though there are additional considerations to attend to in the design of synthetic routes to PET imaging agents. For example, here we describe the synthesis of 1-amino-3,4-difluorocylopentane-1-carboxylic acids (3,4-DFACPCs), which can, in theory, be accessed via a variety of different synthetic approaches. However, because the ultimate goal of these studies is to incorporate the ^{18}F radionuclide into 3,4-DFACPCs, the only viable routes are those that allow for fluorine incorporation in the penultimate step of the synthesis, leaving only a rapid deprotection for the final step. Routes that would incorporate the ^{18}F radionuclide earlier in the synthesis are not feasible, since decay of the resultant radioactive intermediates would preclude the synthesis of useful quantities of the desired [^{18}F]3,4-DFACPC. With this in mind, we assessed that ethyl 1-amino-cyclopent-3-ene-1-carboxylate could provide access to all four stereoisomers of 3,4-DFACPC, proceeding through a route that makes use of an S_N2 displacement of a pseudohalide in the penultimate step, and which utilizes protecting groups that are easily and rapidly cleaved under acidic conditions. Therefore, we began by preparing an N-benzoyl protected derivative of this compound according to the method previously reported by Cativiela. In accordance with

Cativiela's report, hippuric acid was dehydrated with N,N'-dicyclohexylcarbodiimide to give **3.01**, which underwent nucleophilic addition to two equivalents of allyl bromide to give di-allylated intermediate **3.02**. Treatment with sodium ethoxide cleaved the oxazolone moiety, resulting in the formation of an N-benzoyl, ethyl ester protected amino acid **3.03** in 54% yield over three steps. The cyclopentene moiety was established with a ring-closing Grubbs metathesis, furnishing **3.04** in 94% yield on gram scale (Scheme 3-3).

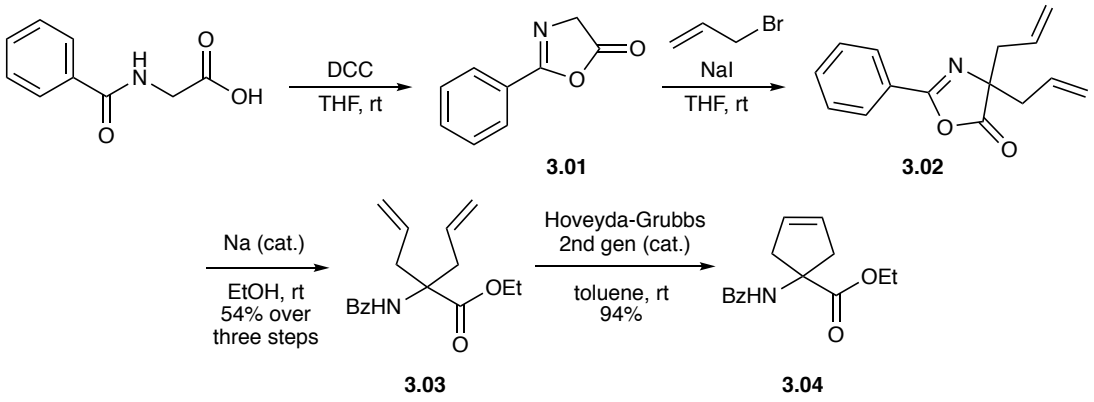

*Scheme 3-3. Synthesis of N-benzoyl protected ethyl 1-amino-cyclopent-3-ene-1carboxylate (**3.04**).*[37]

With the cyclopentene amino acid in hand, we first targeted the synthesis of **anti-cis-3,4-DFACPC**, since this stereoisomer would naturally result from sequential consecutive fluorinations of the syn-epoxide, which we anticipated to form preferentially in the oxidation of **3.04**. Indeed, m-CPBA oxidation of **3.04** provided a 9:1 mixture of epoxide diastereomers, favoring the syn-epoxide (**3.05**). The diastereomers were easily separable by column chromatography and **3.06** was obtained in 78% yield. Fluorination of **3.05** with HF-pyridine resulted in the formation of the desired racemic fluorohydrin **3.06** in 54% yield. As described above, both fluorohydrin enantiomers will be converted to the same C2 symmetric difluoride product, so there is no incentive to pursue an enantioselective fluorination of **3.05**. The hydroxyl moiety of **3.06** was converted to triflate **3.07** with triflic anhydride in 83% yield in preparation for fluorination with

triethylamine trihydrofluoride, which proceeded to give the C2 symmetric difluoride **3.08** in 26% yield. Finally, the benzoyl and ethyl ester protecting groups were removed via acidic hydrolysis at 90 °C with concentrated HCl. When the reaction mixture was allowed to cool to room temperature, **anti-cis-3,4-DFACPC** (**3.09**) crystallized spontaneously in 90% yield (Scheme 3-4, Figure 3-6).

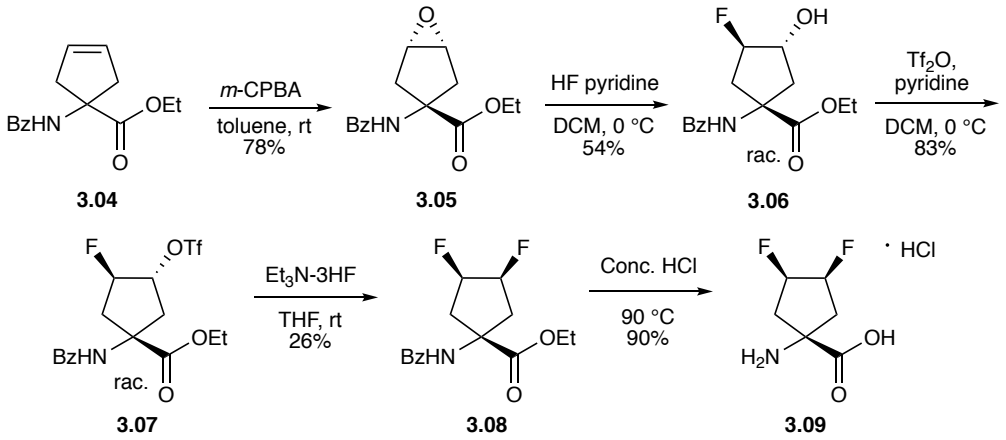

*Scheme 3-4. Synthesis of **3.09** cold standard.*

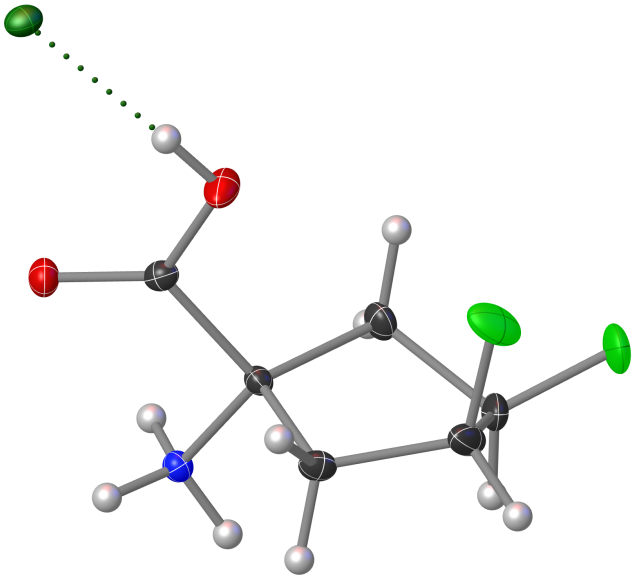

*Figure 3-6. X-ray crystal structure of **anti-cis-3,4-DFACPC (3.09).** Atom labels are as follows: white = hydrogen, black = carbon, red = oxygen, blue = nitrogen, light green = fluorine, dark green = chlorine.*

This route was effective for generating authentic **[^{19}F]3.09** to be used as a "cold" standard, though the acidolysis of the benzoyl group was sluggish and therefore not ideal for the synthesis of **[^{18}F]3.09**, since the radioactive compound decays quickly. Consequently, we replaced the benzoyl moiety with a more labile *t*-butyl carbamate N-protecting group. This manipulation proceeded over three steps, beginning with acidic hydrolysis of the amine and carboxylate protecting groups to give the free amino acid hydrochloride **3.10**.

The ethyl ester was then reinstalled under Fischer conditions, and the resultant amine **3.11** was treated with di-*tert*-butyl dicarbonate, furnishing **3.12** in 51% yield over the course of the three-step sequence (Scheme 3-5).

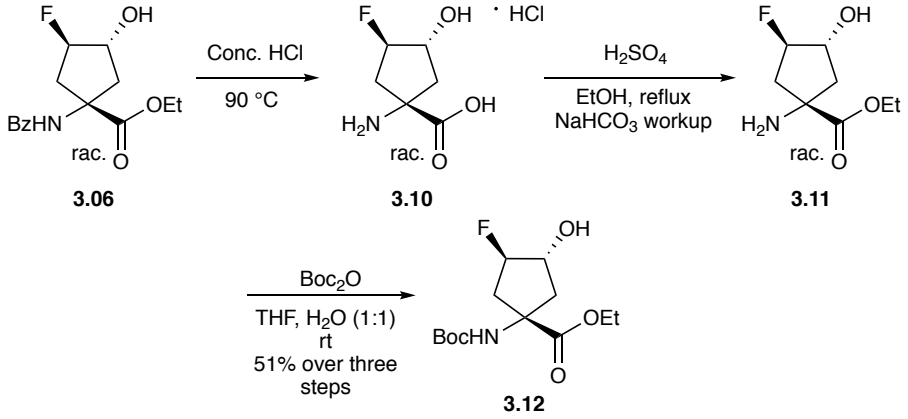

*Scheme 3-5. Conversion of N-benzoyl fluorohydrin **3.06** to N-Boc protected fluorohydrin **3.12**.*

While we were able to attain reasonable quantities of **3.12**, losing ~50% of our material to a circuitous deprotection and reprotection sequence at the end of the route was considered to be inelegant and likely unnecessary. Therefore, we considered alternative approaches that would allow for the direct synthesis of an N-Boc protected derivative of **3.06**. One such route, originally reported by Kurth, provides the N-deprotected amino acid **3.15** in 62% yield over three steps (Scheme 3-6).

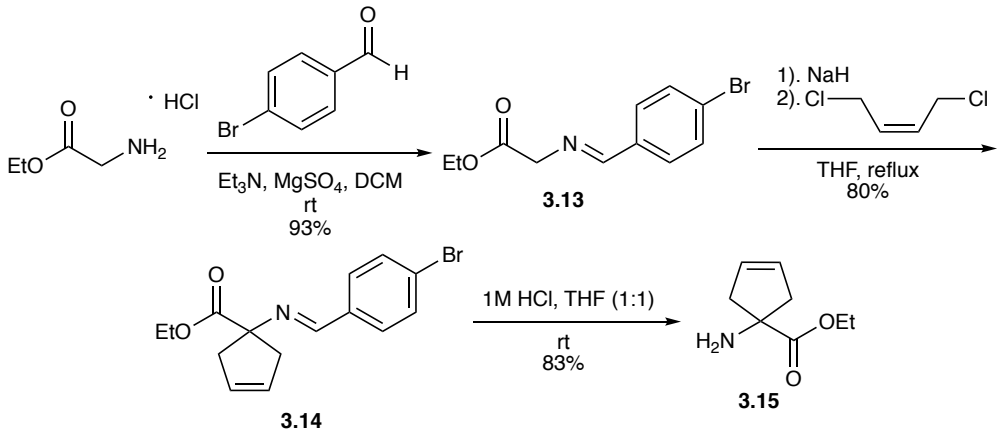

*Scheme 3-6. Synthesis of **3.15** as reported by Kurth.[38]*

Utilizing Kurth's route, we found that more than 10 g of **3.15** was readily produced in a single batch. N-Boc protection of this compound gave cyclopentene **3.16**, which, much like **3.04**, underwent oxidation with *m*-CPBA favoring the formation of the syn-epoxide by a ratio of 5:1. Again, the epoxide diastereomers were easily separable by chromatography and **3.17** was isolated in 76% yield.

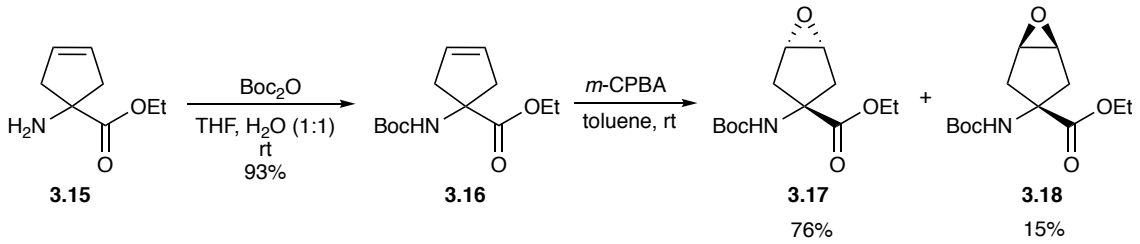

*Scheme 3-7. Synthesis of syn-epoxide **3.17** and anti-epoxide **3.18**.*

With **3.17** in hand, we began exploring methods for ring opening fluorination of the epoxide. In contrast to benzamide **3.05**, which was fairly robust to acidic conditions, the N-Boc bearing compound **3.17** generated complex mixtures on addition of HF-pyridine or triethylamine trihydrofluoride, presumably due to the lability of the Boc group. However, fluorination with triethylamine trihydrofluoride proceeded well with the aid of two equivalents of triethylamine, providing fluorohydrin **3.12** in 86% yield. This route, which proceeded in six steps from glycine

ethyl ester hydrochloride and provided **3.12** in 38% yield over six steps, constitutes a substantial improvement over the previous route, which afforded **3.12** in 11% yield over 10 steps. With access to sufficient quantities of **3.12**, we attempted to convert it to the triflate, though this was not as straightforward as the analogous conversion of **3.06**. On addition of triflic anhydride to **3.06**, TLC analysis indicated that reaction had gone to completion within minutes at 0 °C, and the R_f of the primary spot as determined by charring with $KMnO_4$ was consistent with the formation of the triflate **3.19**. Given that we anticipated the triflate to be unstable to aqueous conditions, we opted not to perform an aqueous workup and pushed the reaction mixture directly through a silica plug instead. The white solid thus obtained gave a proton NMR consistent with loss of the Boc moiety, indicating that if **3.19** was produced, it likely decomposed via an acid mediated process. We attempted the same procedure with a silica plug that had been pretreated with a 1 % triethylamine in DCM, though the same white solid was obtained. We hypothesized that since it was likely excess pyridinium triflate promoting the decomposition of **3.19**, precipitating this compound by diluting the reaction media with hexanes prior to chromatography may solve this issue. Indeed, on completion of the triflation reaction as determined by TLC, addition of hexanes caused a white solid to precipitate, and after filtration and chromatographic purification of the resultant supernatant, **3.19** was isolated in 74% yield. **3.19** is the direct precursor to ^{18}F radionuclide incorporation to generate **[^{18}F]3.09 (anti-cis-3,4-[^{18}F]-DFACPC)**, as is described in the radiosynthesis section below.

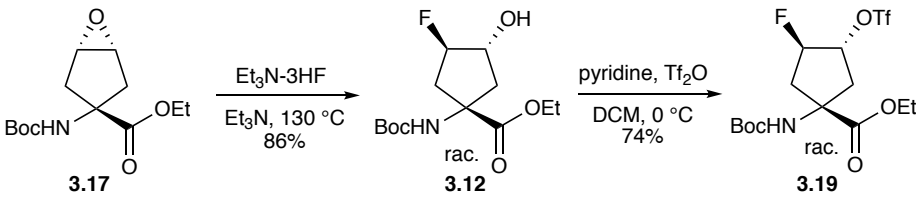

*Scheme 3-8. Synthesis of triflate precursor (**3.19**) to **[^{18}F]3.09 (anti-cis-3,4-[^{18}F]-DFACPC)**.*

We next targeted the synthesis of the *trans*-3,4-DFACPC stereoisomers, since they should be easily accessible from fluorohydrin **3.12**, which is readily produced on gram scale. Thus, **3.19** was taken up in THF and treated with saturated aqueous sodium bicarbonate, resulting in clean S_N2 inversion hydrolysis of the triflate to give racemic fluorohydrin **3.20** in nearly quantitative yield. **3.20** was converted to racemic triflate **3.21** utilizing the same procedure described for **3.19**, though unlike **3.19**, **3.21** is highly unstable and was not purified by chromatography but used directly in subsequent fluorination reactions. Our attempts to fluorinate **3.21** were unsuccessful under a variety of conditions, owing to the formation of olefinic byproducts via elimination of the triflate. Ultimately, a particularly mild method described by Kim,[36c, 39] which involves the use of cesium fluoride in tertiary alcohol solvents, proved to be an efficient method for the introduction of fluoride and racemic trans-difluoride **3.22** was generated in 38% yield over two steps from **3.20**. **3.22** was then treated with concentrated HCl at 90 °C to remove the Boc and ethyl ester protecting groups, giving racemic difluoride **3.23** (**trans-3,4-DFACPC**) in 93% yield (Scheme 3-9). As was the case with **3.09**, crystals of **3.23** grew spontaneously from the reaction mixture when it was cooled from 90 °C to room temperature, and an X-ray crystal structure was obtained (Figure 3-7). We were content to develop a racemic synthesis of **3.23** as the synthesis is scalable and provides access to both enantiomers, which are separable by chiral chromatography (see Figure S3-42). Furthermore, we were able to proceed with biological testing of **3.23** as the racemate, which allowed us to evaluate the utility of the mixture of enantiomers in a single set of studies.

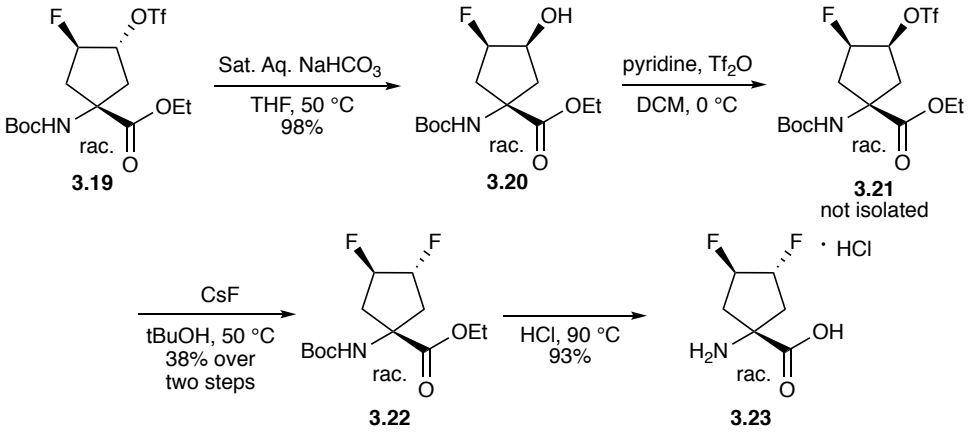

*Scheme 3-9. Synthesis of triflate precursor **3.21** and racemic **trans-3,4-DFACPC (3.23)**.*

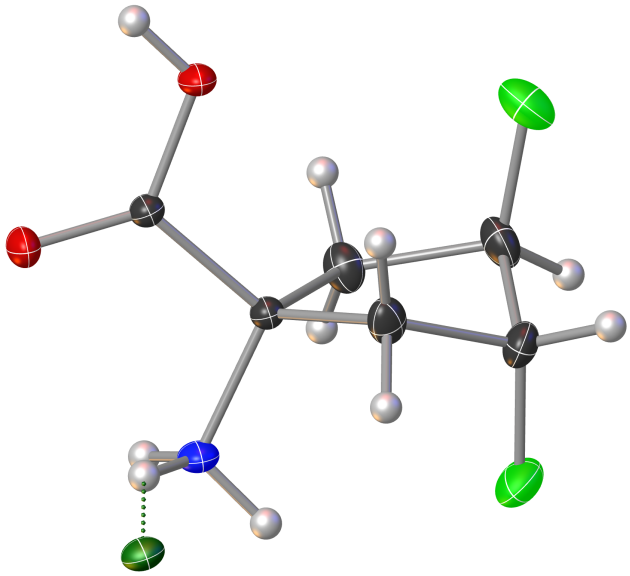

*Figure 3-7. X-ray crystal structure of racemic **trans-3,4-DFACPC (3.23)**. Atom labels are as follows: white = hydrogen, black = carbon, red = oxygen, blue = nitrogen, light green = fluorine, dark green = chlorine.*

Finally, we turned our attention to the synthesis of **syn-cis-3,4-DFACPC**. This compound presents a challenge in that the desired stereochemistry arises from fluorination of anti-epoxide **3.18**, though this epoxide is only a minor product of the oxidation of cyclopentene **3.16**, which preferentially generates the syn-epoxide by a ratio of 5:1. Notably, the epoxidation of ethyl cyclopent-3-ene-1-carboxylate effected with *m*-CPBA gives the anti-isomer in 70% yield (3:1 dr). We considered

functionalizing the amine with a bulky group, intending to favor the preferential formation of the anti-epoxide via steric blocking of the syn face, though such routes rendered epoxidation slow and low yielding, or suppressed the reaction altogether. A brief survey of epoxidizing agents and reaction conditions also failed to improve selectivity in the conversion of **3.16** to anti-epoxide **3.18**. Thus, we resigned to obtain reasonable quantities of **3.18** by way of scale up and consider alternative routes for its synthesis after generating the **syn-cis-3,4-DFACPC** cold standard, if necessary. To this end, **3.18** was treated with triethylamine trihydrofluoride to afford **3.24** in 21% yield (Scheme 3-10).

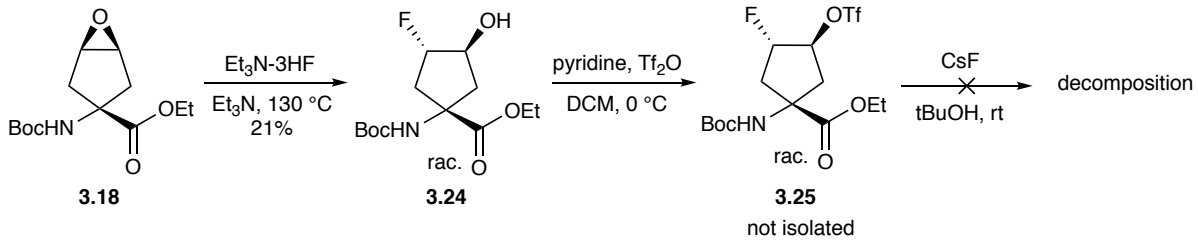

*Scheme 3-10. Attempted synthesis of N-Boc protected **syn-cis-3,4,-DFACPC** from triflate precursor **3.25.***

3.24 was treated with triflic anhydride to furnish the highly unstable triflate **3.25**, which could not be isolated. Attempts to displace the triflate moiety of **3.25** with fluoride met with failure. Crude NMR and LCMS analysis of these failed reactions was consistent with the formation of a byproduct in which the Boc and triflate moieties had been lost. Notably, the relatively stable triflates **3.07** and **3.19** have a syn relationship between the triflate group and the N-benzoyl or N-Boc group, whereas labile triflates **3.21** and **3.25** bear these functionalities in a trans disposition. We speculate that **3.25** may decompose via an intramolecular decomposition pathway in which the triflate moiety is displaced by the carbamate oxygen followed by extrusion of isobutylene, generating a cyclic carbamate byproduct. Based on this analysis, it was necessary to consider alternate protecting group strategies. Our goal was to identify a protecting group that would not

promote the conjectured mode of decay, but which was also able to undergo rapid cleavage under operationally simple conditions. The phthaloyl protecting group seemed to meet these criteria, as we anticipated that it would not participate in nucleophilic displacement of the triflate group, and Goodman and coworkers previously reported that N-phthaloyl, O-ethyl ester protected amino acids were efficiently deprotected in 10 minutes with aqueous solutions of hydrazine.[40] Therefore, **3.15** and phthalic anhydride were combined in a Dean-Stark apparatus with refluxing toluene resulting in the formation of phthalimide **3.26** in 67% yield. Epoxidation of **3.26** with *m*-CPBA was slightly more selective for the anti-epoxide than it was in the case of **3.04** and **3.16**, resulting in a 2.6:1 mixture of syn and anti-epoxide diastereomers, respectively. However, in contrast to the epoxide diastereomers described earlier, **3.27** and **3.28** were quite challenging to separate by chromatography, though they could be obtained in pure form by crystallization. Compound **3.27** thus obtained was treated with triethylamine trihydrofluoride to afford racemic fluorohydrin **3.29** in 43% yield. **3.29** was uneventfully converted to racemic triflate **3.30**, which, as anticipated, was stable at room temperature and isolated in 85% yield following chromatographic purification. Fluorination of **3.30** proved challenging as elimination byproducts formed preferentially over the desired difluoride.

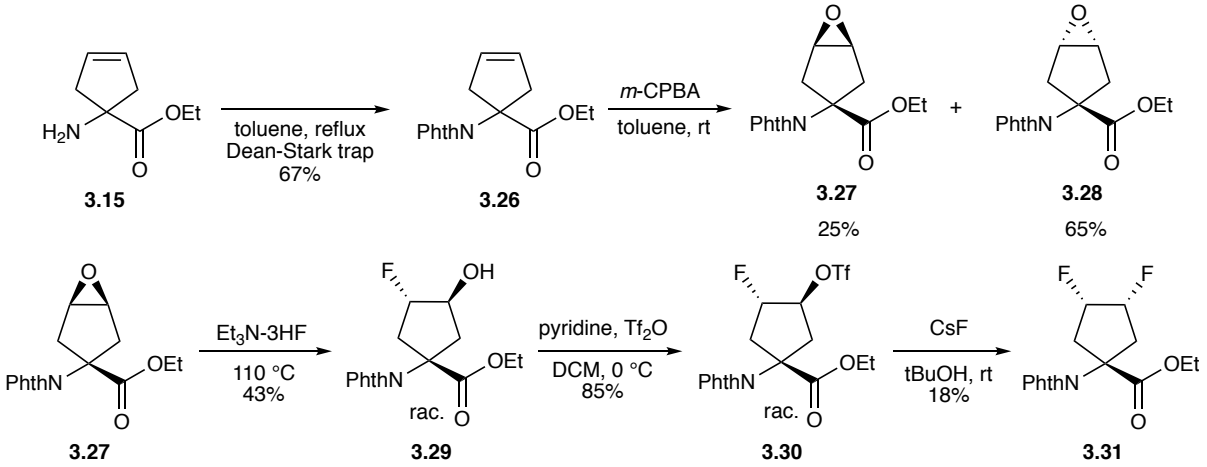

Scheme 3-11. Synthesis of phthalimide protected ***syn-cis-3,4-DFACPC (3.31)****.*

Nonetheless, difluoride **3.31** was obtained in 18% yield utilizing Kim's cesium fluoride in *tert*-butanol system. With **3.31** in hand, we attempted to remove the phthaloyl and ester protecting groups with aqueous hydrazine. LCMS analysis of this reaction mixture indicated the formation of one product with a mass that was consistent with the loss of the phthaloyl and ethyl groups, as well as incorporation of hydrazine, suggesting the formation of an amino hydrazide rather than the desired amino acid. Hydrazides are reticent to undergo hydrolysis under acidic or basic conditions, though they are labile to oxidation and can be displaced in aqueous media to reveal the parent carboxylic acid.[41] Thus, we attempted the two step, one pot deprotection of **3.31** by first treating the compound with aqueous hydrazine to generate the hydrazide, then evacuating the reaction vessel at 100 °C under a flow of inert gas, before finally adding 1M HCl (to protonate the free amine) and N-bromosuccinimide oxidant. We were able to generate the **syn-cis-3,4-DFACPC** cold standard with this procedure, though it was difficult to carry out with ^{18}F labeled **3.31**, owing to the inherent challenges associated with handling radioactive materials.

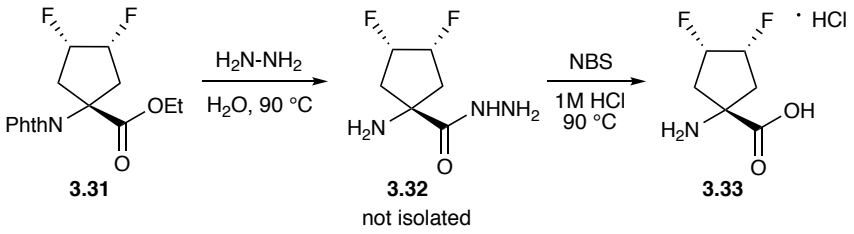

Scheme 3-12. Two step hydrazine, NBS deprotection procedure for generating ***syn-cis-3,4-DFACPC (3.33)*** *from phthalimide* ***3.31****.*

Consequently, we considered other methods of deprotection, bearing in mind that the rate of deprotection is of the utmost importance. Acidic hydrolysis of both the phthaloyl and ethyl ester functional groups presented a simple and attractive option, though phthaloyl groups are slow to hydrolyze under acidic conditions due to the poor basicity of the phthaloyl carbonyl oxygen. Therefore, we considered hydrolyzing the ester and phthaloyl moieties first with aqueous base to

give an *o*-carboxybenzamide, which could then be quickly cleaved with aqueous acid. Indeed, we found that treating **3.31** with 2M aqueous sodium hydroxide at 140 °C for five minutes, followed by addition of concentrated HCl with heating at 140 °C for another 15 minutes resulted in the clean formation of amino acid **3.33** in 88% yield (Scheme 3-13). The manipulations associated with this protocol proved straightforward enough to be translated to the radiochemistry lab, allowing for the synthesis of **syn-cis-3,4-[^{18}F]-DFACPC**. Finally, the stereochemistry of **3.33** was confirmed by single crystal X-ray diffraction (Figure 3-8).

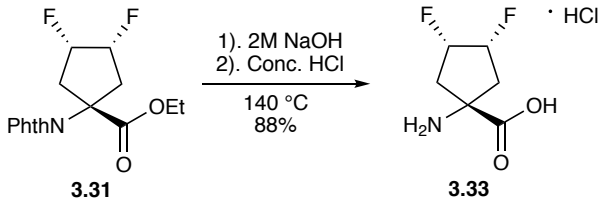

3.31 **3.33**

*Scheme 3-13. Synthesis of **syn-cis-3,4-DFACPC (3.33)** by aqueous hydrolysis of **3.31**.*

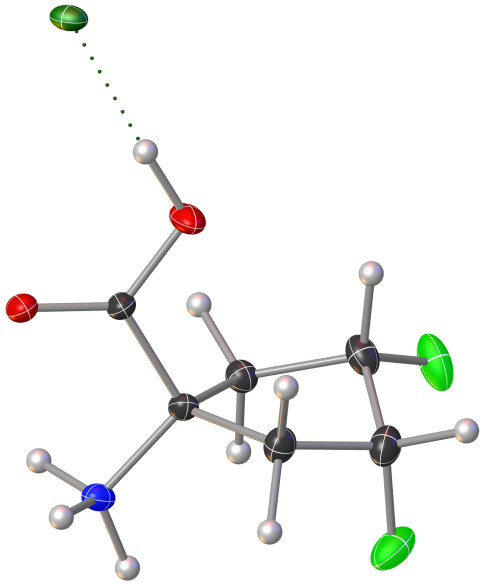

*Figure 3-8. X-ray crystal structure of **syn-cis-3,4-DFACPC (3.33)**. Atom labels are as follows: white = hydrogen, black = carbon, red = oxygen, blue = nitrogen, light green = fluorine, dark green = chlorine.*

Synthesis of ^{18}F Radionuclide Bearing ("Hot") Compounds

The handling of ^{18}F containing compounds in quantities sufficient for radiological use poses a significant risk of overexposure to gamma radiation. To mitigate such risks and ensure the safety of laboratory personnel, the synthesis and purification of ^{18}F labeled materials takes place inside specialized hoods fitted with leaded doors and leaded glass windows, which effectively contain the ionizing radiation. In the Goodman laboratory, where the radiosynthesis described herein was carried out, there are two types of fume hoods for preclinical radiosynthetic use. One hood contains a computer process control unit (CPCU), a programmable system that carries out various steps in the radiolabeling process. The other hood, referred to as a "hot-cell", is fitted with a pair of mechanical arms that allow laboratory personnel to manually perform synthetic manipulations inside the hood while standing behind a closed leaded door. The hot-cell also contains a dose calibrator (gamma counter) that is used to determine the quantity of radioactivity within a particular vessel. In practice, the CPCU is generally used for the introduction of $^{18}F^-$, simple deprotection reactions, and filtration of the labeled compound through various adsorbents, while more complicated synthetic procedures, purification steps involving fraction collection, and preparation of doses are handled in the hot-cell. A schematic of the CPCU, adapted from an article written by McConathy, Goodman, and coworkers, is shown in Figure 3-9.[42]

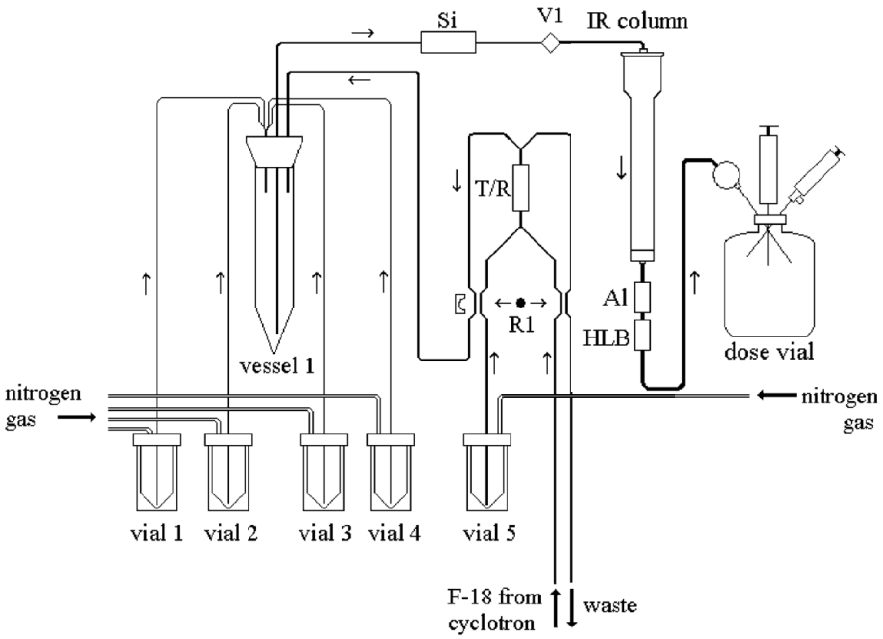

Figure 3-9. General schematic of the chemistry process control unit (CPCU) used to synthesize the ^{18}F radiolabeled compounds described herein. Adapted with permission, copyright © Elsevier.[42]

The synthesis of **[^{18}F]3.09** (**anti-cis-3,4-[^{18}F]-DFACPC**) was achieved under conditions similar to those employed in the CPCU automated preparation of [^{18}F]FDG.[42] Prior to the start of the synthesis, each vial in the CPCU was charged with the necessary mixture of solutions and reagents and equipped with a silicone rubber septum secured with an aluminum crimp top, an inlet line for inert gas to pressurize the vial, and Teflon outlet lines for transfer of the vials contents to the reaction vessel or to the ion exchange "trap and release" cartridge. The reaction vessel was equipped similarly to allow for transfer of its contents to the ion retard resin, alumina, and Oasis HLB cartridge chain used for purification. Approximately 790 mCi of ^{18}F as [^{18}F]HF was transferred from the cyclotron to the trap and release cartridge, and an aqueous solution of potassium carbonate from vial 5 was flushed through the cartridge to generate an aqueous solution of [^{18}F]KF, which eluted into vessel 1. A solution of Cryptand 222 in acetonitrile from vial 1 was

then transferred to the reaction vessel, and the vessel was heated with an oil bath (not depicted) under a flow of inert gas to evaporate the acetonitrile with azeotropic removal of water. A second aliquot of acetonitrile (from vial 2) was added and evaporated to ensure that the contents of vessel 1 were free of residual water. A solution containing 9 mg (0.021 mmol) of triflate precursor **3.19** in acetonitrile was then transferred to the reaction vessel from vial 3, and the reaction was heated to reflux for 10 minutes. The reaction was terminated after 10 minutes by the evaporation of acetonitrile under inert gas flow. A 6M solution of HCl was transferred to vessel 1 from vial 4 and heated for 10 minutes to cleave the N-Boc and ethyl ester protecting groups, giving crude **[^{18}F]3.09**. The contents of vessel 1 were then pushed through ion retard resin, alumina, and Oasis HLB (reverse phase) cartridges, and vessel 1 was rinsed with an aliquot of saline (from a vial not depicted in Figure 3-9) that was also passed through the chain of adsorbent containing cartridges to ensure that all of the **[^{18}F]3.09** was collected and eluted. The line carrying the eluent terminated inside the hot-cell where fractions were collected manually, and the most concentrated fractions were used as doses for in vivo and in vitro use. The identity of the radioactive species in the dose vials was assayed by comparison of the R_f (on silica) of the ^{18}F labeled material to the authentic cold racemic **3.09.** Because the concentration of ^{18}F is low (1 Ci of ^{18}F is approximately 80 nanomoles), the direct detection of **[^{18}F]3.09** by UV or staining of the TLC plate was not feasible. Instead, a radiometric TLC scanner was used to determine the R_f of the radioactive compounds on the silica TLC plate. The radiometric TLC chromatogram showed a small peak at the baseline consistent with residual $^{18}F^-$, and a much larger peak with an R_f value consistent with that of the authentic **3.09** standard, indicating that **[^{18}F]3.09** was obtained in > 99% radiochemical purity (see Figure S3-41).

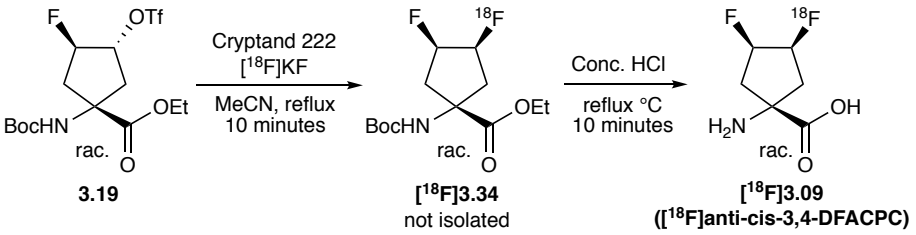

Scheme 3-14. Synthesis of ***[^{18}F]3.09 (anti-cis-3,4-[^{18}F]-DFACPC)*** *from triflate* ***3.19****.*

50 mCi of **[^{18}F]3.09** were obtained in 12 mL of saline solution, affording a decay corrected yield of 10%. The specific activity, a measure of the quantity of radioactivity arising from a particular compound in a sample of a given mass, was estimated to be no less than 2.4 Ci/mmol based on the assumption that all of the starting precursor (which was used in approximately 300 fold excess relative to [^{18}F]CsF) that was not converted to **[^{18}F]3.09** remained in the dose as a non-radioactive amino acid byproduct. The concentration of the dose is significant because the sample volume that can be administered in both *in vitro* and *in vivo* assays is finite, and a dose that is not sufficiently concentrated will prevent the study from proceeding with the intended quantity of radioactive compound. For example, the rats employed in these studies can be injected with a dose of up to ~ 0.4 mL, and we intended to dose each specimen with approximately 250 μCi of ^{18}F amino acid. Therefore, each dose should have a theoretical minimum concentration of 625 μCi/mL of ^{18}F amino acid at the end of synthesis, though in practice the dose should be more concentrated to account for radiochemical decay that inevitably takes place during administration to test subjects. The synthesis of racemic **[^{18}F]3.23** (**trans-3,4-[^{18}F]-DFACPC**) proceeded similarly to **[^{18}F]3.09**, with a few changes to the reagents employed in the CPCU. Initially, we attempted to use [^{18}F]KF as the nucleophilic fluoride source, though these reactions were unsuccessful, likely owing to competitive decomposition of the triflate under heating. This result was somewhat unsurprising given that we noted that triflate **3.21** decomposed much more rapidly than **3.19**, as described above.

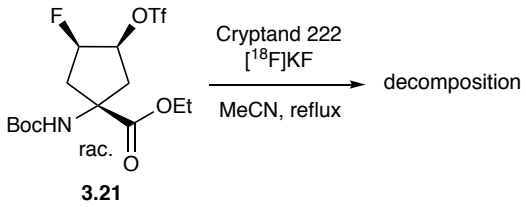

*Scheme 3-15. Failed attempt at fluorination of triflate **3.21** with [^{18}F]KF.*

Seeking a more gentle fluorination protocol, we turned to the cesium fluoride in *tert*-butanol system described by Kim[36c] which had already proven to be a valuable method for installing fluoride in the cold synthesis of racemic **3.23**. Indeed, [^{18}F]CsF in 1:1 *tert*-butanol/acetonitrile solvent proved to be an effective system for labeling triflate **3.21** (20 mg, 0.047 mmol) to give racemic **[^{18}F]3.23**. Operationally, the CPCU automated synthesis of racemic **[^{18}F]3.23** was very comparable to the protocol used to prepare **[^{18}F]3.09**; the only notable changes in protocol include the use of cesium carbonate in vial 5, resulting in the formation of [^{18}F]CsF rather than [^{18}F]KF, the use of a mixture of 1:1 *tert*-butanol/acetonitrile solvent in vial 3 rather than pure acetonitrile. After the reaction was carried out and purified as described above, the contents of the dose were compared with authentic **3.23** using chiral analytical HPLC with an inline UV detector and radiation counter. HPLC analysis indicated that **[^{18}F]3.23** was obtained in > 99% radiochemical purity (see Figure S3-42). 12 mCi of racemic **[^{18}F]3.23** were obtained in 7 mL of saline solution, affording a decay corrected yield of 1.3%, and the specific activity was estimated to be no less than 0.26 Ci/mmol based on the approximation outlined above.

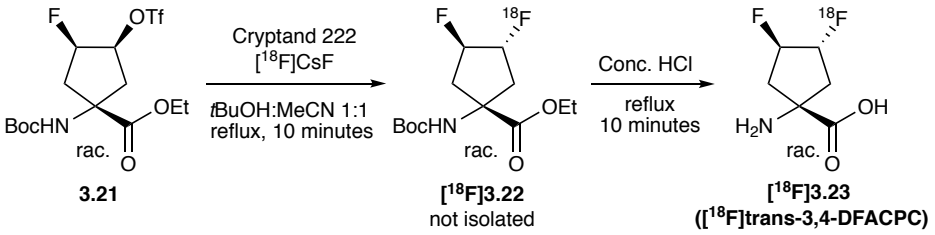

*Scheme 3-16: Synthesis of racemic **[^{18}F]3.23 (trans-3,4-[^{18}F]-DFACPC)** from triflate **3.21**.*

The remaining stereoisomer, **[^{18}F]3.33** (**syn-cis-3,4-[^{18}F]-DFACPC**), proved to be more difficult to prepare and required significant departures from the protocols used for the other 3,4-DFACPC stereoisomers owing to the challenges associated with deprotection of the phthalimide moiety. As was the case with triflate **3.21**, triflate **3.30** failed to produce the desired labeled amino acid under the typical conditions used for [^{18}F]FDG production ([^{18}F]KF, Cryptand 222, acetonitrile solvent).

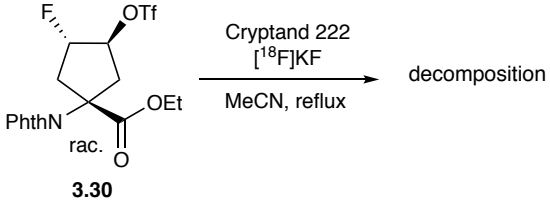

*Scheme 3-17. Attempted fluorination of triflate **3.30** with [^{18}F]KF.*

However, we were pleased to find that Kim's cesium fluoride system,[36c] which enabled the fluorination of triflate **3.21,** also proved to be effective for the conversion of triflate **3.30** to difluoride **3.31**. The CPCU was equipped as follows: an aqueous solution of cesium carbonate in vial 5, Cryptand 222 in acetonitrile in vial 1, acetonitrile in vial 2, triflate **3.30** in a 1:1 mixture of *tert*-butanol/acetonitrile in vial 3, and another volume of acetonitrile in vial 4. 1460 mCi of [^{18}F]HF was transferred from the cyclotron onto the trap and release cartridge and it was washed with the contents of vial 5, generating an aqueous solution of [^{18}F]CsF in reaction vessel 1. The contents of vial 1 were added to the reaction vessel and the solvent was removed via heating under a flow of

inert gas. This drying procedure was repeated after a second aliquot of acetonitrile from vial 2 was added to vessel 1. The *tert*-butanol/acetonitrile mixture containing triflate **3.30** (20 mg, 0.044 mmol) in vial 3 was then added to vessel 1, and the mixture was heated to reflux for 10 minutes. In contrast to the previous two procedures, the contents of vessel 1 were not concentrated and treated with aqueous HCl at this stage. Instead, the crude mixture containing difluoride **[^{18}F]3.31** was loaded onto a chain of two alumina cartridges. The reaction vessel was rinsed with acetonitrile from vial 4, and this solution was used to elute the remaining material from the alumina cartridges into the hot-cell where fractions were collected manually. The most concentrated fractions were combined in a single v-vial and concentrated at reflux under a flow of inert gas. At this stage, the contents of the reaction mixture were examined by radiometric TLC on silica. Two peaks were observed in the radiometric TLC chromatogram; a small peak at the baseline corresponding to residual unreacted [^{18}F]CsF, and a second, much larger peak with an R_f consistent with that of the authentic difluoride **3.31** in the same solvent system, verifying that we'd successfully prepared difluoride **[^{18}F]3.31**. Initially, we attempted to deprotect this compound by first reacting it with a 1:1 solution of hydrazine and water, assuming that these conditions would generate amino hydrazide **[^{18}F]3.32**. After 10 minutes at 90 °C, the reaction was concentrated at reflux under inert gas flow and the mixture was treated with 1M HCl to protonate the amine of **[^{18}F]3.32**. Excess N-bromo succinimide was then added to the crude **[^{18}F]3.32**, and the mixture was heated to reflux for another 10 minutes at 90 °C, then cooled to room temperature. Despite the fact that this two-step procedure was able to reliably produce the cold standard **3.33** in pure form, radiometric TLC analysis of the crude mixture showed that multiple [^{18}F] containing compounds were obtained. Given the time constraints and other difficulties associated with handling [^{18}F] labeled molecules, purification of the mixture was considered to be infeasible. Additionally, further optimization of

the protocol was challenging since the formation of **3.33** related byproducts could not be reproduced in the cold chemistry.

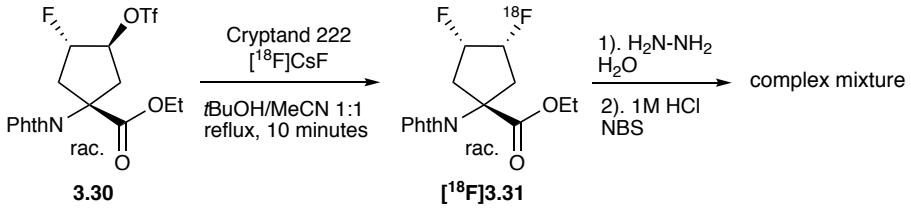

Scheme 3-18. Attempted synthesis of ***[18F]3.33*** *employing a hydrazine hydrate and N-bromosuccinimide (NBS) protocol to deprotect difluoride* ***[18F]3.31****.*

Consequently, we identified another two-step protocol for the deprotection of **[18F]3.31**, which involved basic hydrolysis with 2M NaOH to give followed by acidic hydrolysis with conc. HCl. While this procedure was effective in the cold chemistry, it too was challenging to carry out in the hot-cell, since the hydrolysis reactions required heating at 140 °C in order to proceed on the necessary time scale. Typically, heating solutions beyond their boiling point can be achieved with a sealed tube or other suitable apparatus fitted with an appropriate screw cap that is capable of withstanding high pressures, though the mechanical arms in the hot-cell do not articulate in such a way that an operator would be able to affix a screw cap onto a vessel. Since we were unable to use a sealed tube, the hot-cell was instead charged with screw capped v-vials with thick Teflon coated septa prior to the transfer of radioactive material from the CPCU. We anticipated that solutions of **[18F]3.31** could be syringed into a sealed v-vial, then briefly heated to 140 °C to allow the reaction to occur while the septa remained intact. Thus, once **[18F]3.31** was transferred from the CPCU into the hot-cell as a solution in acetonitrile, it was syringed into a screw capped v-vial fitted with a Teflon septum. The vial was placed in a pie plate maintained at 140 °C, fitted with an outlet needle and a second needle connected to an inert gas line, and the acetonitrile solvent was

removed under inert gas flow. After evaporation, both needles were removed, 2M NaOH was syringed into the reaction, and the mixture was allowed to stand for 5 minutes at 140 °C. After cooling briefly, concentrated HCl was syringed into the reaction vial, and the mixture was heated for 15 minutes at 140 °C then evaporated under inert gas flow (the outlet needle was fitted with a line that was submerged in saturated aqueous potassium carbonate to neutralize the HCl fumes and prevent etching of the leaded glass doors). At this stage, the integrity of Teflon septum was severely compromised, and it no longer acted as an effective seal, which rendered pressure induced cannulation from the reaction vessel in the following purification steps inefficient and negatively impacted the radiochemical yield. Nonetheless, water was syringed through the septum into the reaction vial to dissolve the crude **[^{18}F]3.33**, and the mixture was cannulated under pressure into a chain of Oasis HLB (reverse phase) and alumina cartridges. The eluent was collected in fractions, and the fractions with the greatest concentration of radioactivity were used for in vitro and in vivo studies. The contents of the dose solution were assayed by analytical HPLC, utilizing **[^{18}F]3.23** as a reference standard (see Figure S3-43). HPLC analysis indicated that **[^{18}F]3.33** was obtained in > 99% radiochemical purity. 8.4 mCi of **[^{18}F]3.33** were obtained in 5 mL of water, affording a decay corrected yield of 1.7%, and the specific activity was estimated to be no less than 0.19 Ci/mmol based on the approximation outlined above.

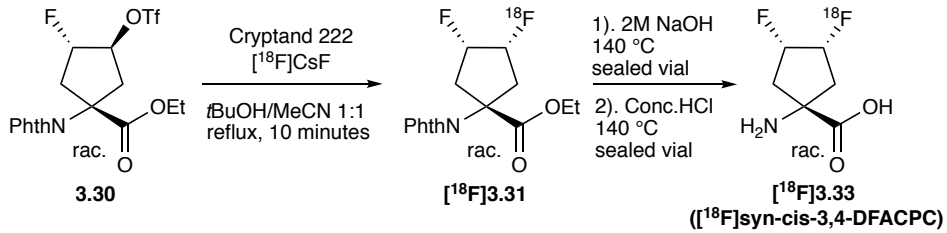

*Scheme 3-19. Synthesis of **[^{18}F]3.33 (syn-cis-3,4-[^{18}F]-DFACPC)** from triflate **3.30**.*

Cell Uptake Studies

Amino acids enter cells, both healthy and neoplastic, via functionally and biochemically distinct amino acid transporters (AATs) that are categorized based on their selectivity for particular amino acids as well as their physico-chemical properties. AATs from system L, ASC, and A are the most abundant AATs in the majority of mammalian cells and are overexpressed in a variety of cancers. For example, systems L and ASC are most highly expressed in brain, breast, ovary, lung, liver, pancreas, and prostate cancers,[20] while system A is overexpressed in prostate, glioma, hepatocellular carcinoma, hilar cholangiocarcinoma, and breast cancer.[20c, 43] AAs containing a positron emitting element that have a high affinity for an overexpressed AAT can be used to identify tumors via PET, since the AA will tend to concentrate in the tumor to a greater extent than in healthy cells. Consistent with this reasoning, having knowledge of which systems take part in transporting a particular AA is of value, since this information can be used to determine which tumor types the AA may be useful for imaging. To establish which systems are responsible for transporting a particular AA, cell uptake inhibition studies are performed. In these studies, a known number of cells of a certain line are suspended in a media containing a known quantity of an AA radiotracer and incubated for a set period to allow for the AA to be transported into the cells. The cells are then collected, centrifuged, and rinsed to separate them from the remaining tracer that did not undergo cellular transport. The radioactivity present within the cells after rinsing is measured and expressed as a normalized percent uptake of the radioactive AA dose that the cells were initially exposed to. This experiment establishes the degree to which a given AA is taken up by a group of cells in the absence of any perturbing conditions and serves as the control. With this information in hand, the cell uptake experiment is performed again, but in the presence of an excess of a substrate known to have a high affinity for a particular transport system. The excess substrate

floods the targeted system, competitively inhibiting the transport of other AAs. Consequently, any reduction in cellular uptake of radioactivity relative to the control experiment is assumed to arise from loss of AA transport by the inhibited system. It follows that if inhibition of a transport system results in reduced uptake of a given AA, then that system contributes to cellular transport of the AA. Furthermore, the degree to which the system participates in transport can be roughly evaluated by the percent loss (inhibition) of AA uptake relative to the control. In addition to delineating transport mechanisms, cell uptake studies provide insight into the avidity of a particular cell line for an AA.

Given that we were interested in evaluating the potential of **[^{18}F]3.09**, **[^{18}F]3.23**, and **[^{18}F]3.33** as PET radiotracers for imaging brain and prostate cancer, cell uptake studies with rat 9L gliosarcoma, human U87 ΔEGFR glioblastoma, and human DU145 androgen-independent prostate carcinoma were performed. Uptake data for anti-3-[^{18}F]-FACBC were also collected under the same conditions for comparison, since this compound is the state-of-the-art radiotracer for PET imaging of recurrent prostate cancer[33b, c] and has shown promise for imaging glioma in ongoing clinical trials. Methylaminoisobutyric acid (MeAIB) was used as a competitive inhibitor for system A transport, 2-amino-bicyclo[2.2.1]heptane2-carboxylic acid (BCH) was used to inhibit system L, and the combination of alanine, serine, and cysteine was used for inhibition of system ASC.[44] The results of these studies are shown in Table 3-1 and Figure 3-10.

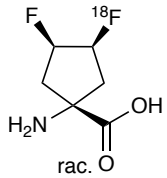

[^{18}F]3.09

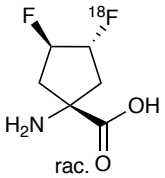

[^{18}F]3.23

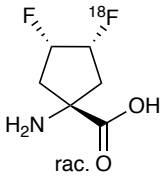

[^{18}F]3.33

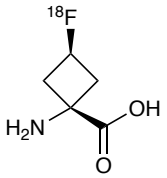

anti-3-[^{18}F]-FACBC

Tracer		Tumor cell line		
		9L	U87 ΔEGFR	DU145
[^{18}F]3.09	Control	23.4 ± 3.0	7.53 ± 1.2	17.7 ± 3.0
	BCH	4.71 ± 0.25*	3.75 ± 0.26*	3.42 ± 0.31*
	MeAIB	23.7 ± 2.1**	7.92 ± 0.84**	20.5 ± 4.0*
	ASC	9.11 ± 1.1*	1.64 ± 0.29*	4.10 ± 0.33*
[^{18}F]3.23	Control	23.5 ± 1.5	6.45 ± 0.46	34.0 ± 4.1
	BCH	3.91 ± 0.72*	2.16 ± 0.11*	2.03 ± 0.19*
	MeAIB	24.8 ± 2.3**	5.47 ± 0.16**	31.9 ± 1.4**
	ASC	11.1 ± 0.54*	2.34 ± 0.18*	5.68 ± 0.60*
[^{18}F]3.33	Control	7.82 ± 0.37	4.29 ± 0.29	12.2 ± 0.46
	BCH	2.11 ± 0.04*	1.93 ± 0.11*	1.70 ± 0.09*
	MeAIB	9.96 ± 0.27*	4.27 ± 0.24**	14.5 ± 0.65*
	ASC	4.43 ± 0.19*	2.44 ± 0.16*	3.85 ± 0.19*
[^{18}F]-FACBC‡	Control	23.2 ± 2.6	6.19 ± 1.22	20.2 ± 3.4
	BCH	12.4 ± 1.7*	3.95 ± 0.90*	8.84 ± 0.31*
	MeAIB	26.3 ± 4.3*	7.18 ± 0.74**	19.8 ± 2.9**
	ASC	6.19 ± 0.75*	1.36 ± 0.15*	2.58 ± 0.22*

*Table 3-1. 9L, U87 ΔEGFR, and DU145cell uptake of **[^{18}F]3.09**, **[^{18}F]3.23**, and **[^{18}F]3.33** with and without inhibitors after 30 min of incubation. Data are presented as percent ligand uptake of the initial dose per 0.5 million cells (%ID/5×10^{5} cells) ± standard deviation (n = 3-4) and normalized for the dose and number of cells. p values represent comparisons of uptake in the presence of inhibitor to control uptake using two-tailed paired t-tests. $p < 0.05$ is considered statistically significant. * $p < 0.05$. ** $p \geq 0.05$. ‡ [^{18}F]-FACBC denotes anti-3-[^{18}F]-FACBC.*

The uptake levels of **[^{18}F]3.09**, **[^{18}F]3.23**, and **[^{18}F]3.33** were relatively high, ranging between approximately 4–34 % of the initial dose per 0.5 million cells (%ID/5×10^{5} cells) across all cell lines tested, compared to 6–20 %ID/5×10^{5} cells with anti-3-[^{18}F]-FACBC. **[^{18}F]3.09** and **[^{18}F]3.23** showed greater uptake than **[^{18}F]3.33** in all cell lines, particularly in rat 9L gliosarcoma and human

DU145 androgen-independent prostate carcinoma cells. The uptake of **[^{18}F]3.09** and **[^{18}F]3.23** was similar in rat 9L gliosarcoma and U87 ΔEGFR glioblastoma cells, and these uptake data were comparable to those obtained for anti-3-[^{18}F]-FACBC. In DU145 androgen-independent prostate carcinoma cells, the uptake of **[^{18}F]3.23** (34 %ID/5×10^5 cells) was nearly double that of **[^{18}F]3.09** (18 %ID/5×10^5 cells) and was also substantially higher than the uptake of anti-3-[^{18}F]-FACBC (20 %ID/5×10^5 cells). With regard to transport mechanism, data from each of the three cell lines used in this study demonstrate that **[^{18}F]3.09**, **[^{18}F]3.23**, and **[^{18}F]3.33** undergo transport predominantly by system L (50–94% inhibition by BCH) with some transport occurring through system ASC (43–83% inhibition by alanine, serine, and cysteine, Figure 3-10). The lone exception is **[^{18}F]3.09** in U87 ΔEGFR glioblastoma cells, as 78% of uptake was inhibited by alanine, serine, and cysteine in this cell line, compared to 50% inhibition with BCH. MeAIB did not result in significant uptake inhibition for any of the stereoisomers of 3,4-[^{18}F]-DFACPC. These results are similar to those obtained in 9L gliosarcoma cells for anti-2-[^{18}F]-FACPC, which is transported by system L (71% inhibition by BCH) and ASC (65% inhibition by alanine, serine, and cysteine), though it is also transported to a lesser degree by system A (38% inhibition by MeAIB).[35] Consistent with previous reports[8] and the smaller steric profile of anti-3-[^{18}F]-FACBC relative to 3,4-[^{18}F]-DFACPCs, it undergoes some transport by system L (36–56% inhibition by BCH) in all cell lines, though it is primarily a substrate for system ASC (73–87% inhibition by alanine, serine, and cysteine).

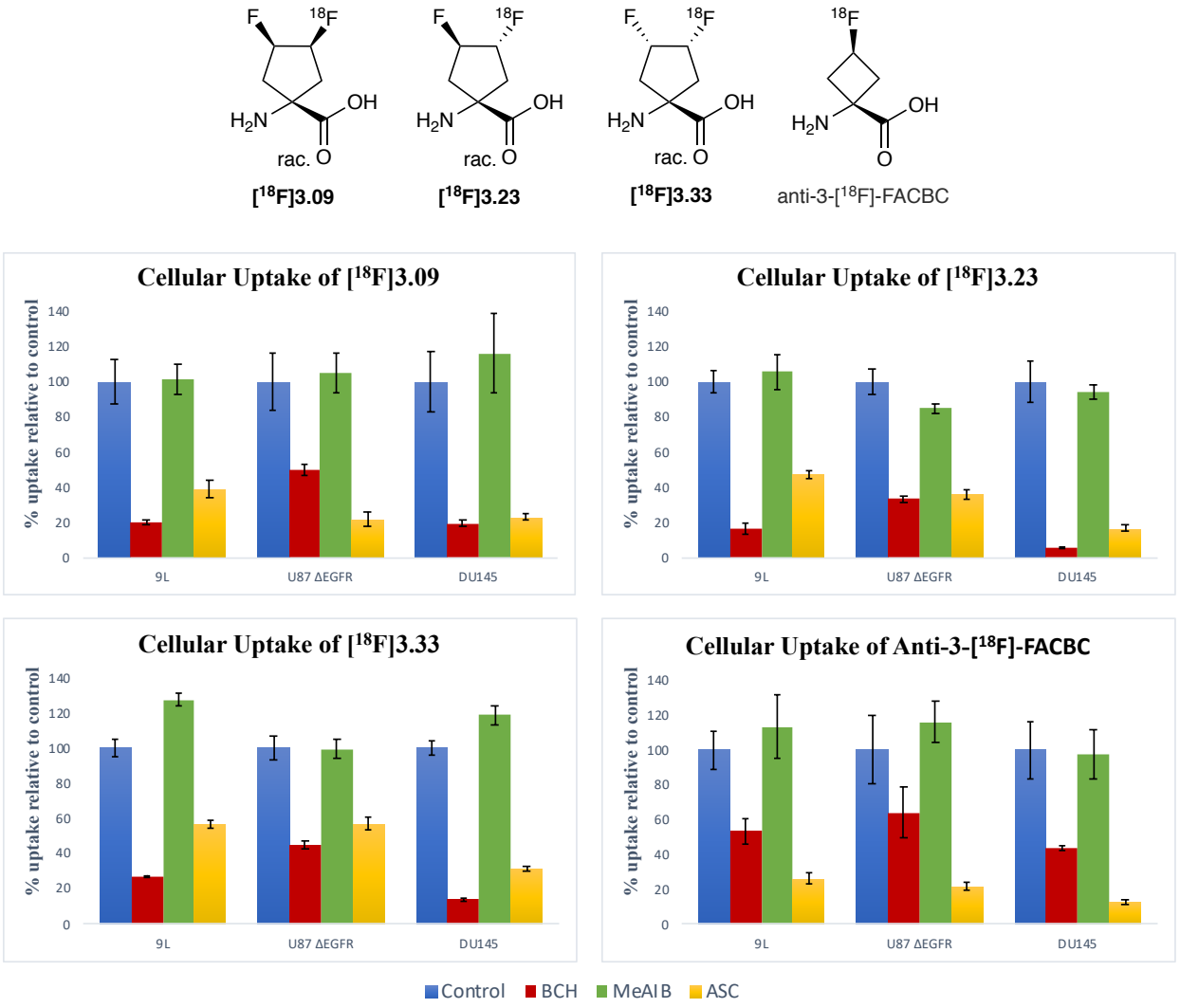

Figure 3-10. Percent uptake and inhibition of ***[18F]3.09****,* ***[18F]3.23****, and* ***[18F]3.33*** *in tumor cells relative to control condition. Error bars indicate ± standard deviation (n = 3-4). These data are a representation of the cell uptake data shown in Table 3-1.*

Biodistribution Studies in Normal Fischer Rats and Fischer Rats with Intracranial 9L Gliosarcoma Tumors

In the context of PET radiotracer development, biodistribution refers to the extent of radiotracer distribution in the tissues of an *in vivo* test subject. An ideal biodistribution profile is one in which the tracer is broadly bioavailable and maintains a consistent and low concentration in all normal

tissues throughout the course of the PET study. Low levels of radiotracer uptake in normal tissues with comparatively high tumor uptake is desirable, since contrast in uptake between tumors and adjacent normal tissues is the basis for tumor visualization via PET. Therefore, high uptake in normal tissues is problematic. For example, despite being a useful radiotracer for the localization of a wide variety of tumors, [^{18}F]FDG is not an effective imaging agent for brain and prostate tumors owing to its high uptake in normal brain tissue and in the bladder, which is proximal to the prostate. For tracers intended to image brain tissue, an additional consideration is the permeability of the blood-brain barrier (BBB). Charged small molecules such as amino acids are not able to freely diffuse through the BBB but can be brought into the brain by facilitated transport. Of the ubiquitous AAT systems, only system L is present in the lumen of the brain, thus only radiotracers that undergo system L transport hold promise for imaging intracranial tumors.

To gain insight into the biodistribution profiles of **[^{18}F]3.09**, **[^{18}F]3.23**, and **[^{18}F]3.33** each was administered to Fischer rats bearing intracranial 9L gliosarcoma tumors, which have been used extensively as models for human glioma.[45] The data from these studies are provided in the tables below.

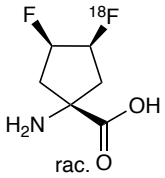

[^{18}F]3.09

Tissue	4.5 min	12.5 min	22.5 min	32.5 min	42.5 min	52.5 min
Liver	2.70 ± 0.50	2.60 ± 0.48	2.30 ± 0.41	2.05 ± 0.44	1.88 ± 0.40	1.75 ± 0.35
Heart	2.54 ± 0.63	1.84 ± 0.48	1.60 ± 0.38	1.49 ± 0.34	1.41 ± 0.36	1.33 ± 0.31
Lung	1.83 ± 0.58	1.30 ± 0.30	1.15 ± 0.26	1.08 ± 0.25	1.02 ± 0.21	0.99 ± 0.19
Muscle	0.69 ± 0.23	0.81 ± 0.25	0.89 ± 0.25	0.94 ± 0.25	1.00 ± 0.26	1.03 ± 0.28
Brain	0.59 ± 0.12*	0.76 ± 0.18*	0.86 ± 0.20*	0.92 ± 0.24*	0.96 ± 0.26*	0.95 ± 0.23*
Tumor	2.05 ± 0.44*	2.22 ± 0.45*	2.21 ± 0.61*	2.13 ± 0.62*	2.10 ± 0.63*	2.04 ± 0.59*
Bone	2.79 ± 0.69	2.21 ± 0.52	1.92 ± 0.48	1.81 ± 0.45	1.77 ± 0.47	1.67 ± 0.42
Spine	1.64 ± 0.54	1.42 ± 0.42	1.34 ± 0.35	1.32 ± 0.34	1.29 ± 0.31	1.28 ± 0.29
L/N‡	3.5	2.9	2.6	2.3	2.2	2.1

Table 3-2. Biodistribution as percent of injected dose per gram (%ID/g) of radioactivity in tissues of 9L tumor-bearing Fischer rats following intravenous administration of ***[^{18}F]3.09****. Data are reported as mean percent dose per gram ± standard deviation (n = 5) at each time point. p values represent comparisons of uptake in the 9L tumor and normal brain using two-tailed paired t-tests. $p < 0.05$ is considered statistically significant. * $p < 0.05$. ‡ L/N denotes tumor to brain ratio.*

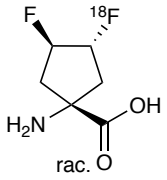

[^{18}F]3.23

Tissue	4.5 min	12.5 min	22.5 min	32.5 min	42.5 min	52.5 min
Liver	1.36 ± 0.14	0.97 ± 0.09	0.75 ± 0.08	0.68 ± 0.06	0.63 ± 0.03	0.62 ± 0.05
Heart	1.42 ± 0.10	0.98 ± 0.12	0.83 ± 0.10	0.74 ± 0.09	0.68 ± 0.07	0.67 ± 0.08
Lung	0.84 ± 0.08	0.64 ± 0.06	0.59 ± 0.10	0.58 ± 0.11	0.57 ± 0.09	0.59 ± 0.11
Muscle	0.56 ± 0.15	0.61 ± 0.12	0.65 ± 0.13	0.67 ± 0.13	0.69 ± 0.13	0.68 ± 0.12
Brain	0.39 ± 0.03*	0.43 ± 0.04*	0.47 ± 0.04*	0.48 ± 0.04*	0.47 ± 0.05*	0.46 ± 0.05*
Tumor	1.00 ± 0.22*	1.20 ± 0.43*	1.18 ± 0.46*	1.15 ± 0.45*	1.15 ± 0.43*	1.11 ± 0.40*
Bone	0.68 ± 0.23	0.75 ± 0.16	0.76 ± 0.12	0.77 ± 0.10	0.79 ± 0.09	0.80 ± 0.09
Spine	0.80 ± 0.26	0.75 ± 0.11	0.75 ± 0.12	0.76 ± 0.14	0.74 ± 0.14	0.75 ± 0.15
L/N‡	2.6	2.8	2.5	2.4	2.4	2.4

Table 3-3. Biodistribution as percent of injected dose per gram (%ID/g) of radioactivity in tissues of 9L tumor-bearing Fischer rats following intravenous administration of ***[^{18}F]3.23****. Data are reported as mean percent dose per gram ± standard deviation (n = 4) at each time point. p values represent comparisons of uptake in the 9L tumor and normal brain using two-tailed paired t-tests. $p < 0.05$ is considered statistically significant. * $p < 0.05$. ‡ L/N denotes tumor to brain ratio.*

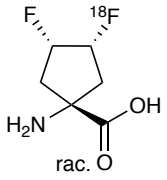

[^{18}F]3.33

Tissue	4.5 min	12.5 min	22.5 min	32.5 min	42.5 min	52.5 min
Liver	1.40 ± 0.19	0.90 ± 0.05	0.66 ± 0.04	0.57 ± 0.03	0.54 ± 0.04	0.51 ± 0.04
Heart	1.24 ± 0.24	0.84 ± 0.07	0.68 ± 0.04	0.60 ± 0.03	0.55 ± 0.02	0.52 ± 0.02
Lung	0.94 ± 0.09	0.66 ± 0.05	0.54 ± 0.02	0.48 ± 0.04	0.45 ± 0.04	0.42 ± 0.04
Muscle	0.48 ± 0.04	0.55 ± 0.03	0.58 ± 0.03	0.57 ± 0.02	0.55 ± 0.03	0.54 ± 0.02
Brain	0.28 ± 0.02*	0.33 ± 0.02*	0.36 ± 0.01*	0.37 ± 0.02*	0.37 ± 0.02*	0.36 ± 0.01*
Tumor	1.21 ± 0.22*	1.16 ± 0.15*	1.04 ± 0.10*	0.91 ± 0.07*	0.85 ± 0.08*	0.78 ± 0.04*
Bone	0.67 ± 0.14	0.65 ± 0.21	0.65 ± 0.20	0.63 ± 0.19	0.61 ± 0.18	0.58 ± 0.17
Spine	0.70 ± 0.23	0.63 ± 0.11	0.57 ± 0.05	0.54 ± 0.05	0.52 ± 0.06	0.50 ± 0.06
L/N‡	4.3	3.5	2.9	2.5	2.3	2.2

*Table 3-4. Biodistribution as percent of injected dose per gram (%ID/g) of radioactivity in tissues of 9L tumor-bearing Fischer rats following intravenous administration of **[^{18}F]3.33**. Data are reported as mean percent dose per gram ± standard deviation (n = 3 - 4) at each time point. p values represent comparisons of uptake in the 9L tumor and normal brain using two-tailed paired t-tests. $p < 0.05$ is considered statistically significant. * $p < 0.05$. ‡ L/N denotes tumor to brain ratio.*

With each tracer, uptake in 9L tumors was higher than in normal brain tissue at all time points, peaking near the 12.5-minute time point. Tumor uptake was highest with **[^{18}F]3.09** and stayed fairly constant at 2.0-2.2% injected dose per gram of tissue (%ID/g) throughout the course of the study. Lower uptake was observed with **[^{18}F]3.23** and **[^{18}F]3.33**, both of which peaked at 1.2 %ID/g, though the concentration of radioactivity in the 9L tumors fell more rapidly with the latter compound, dropping to 0.8 %ID/g by the final time point while uptake of **[^{18}F]3.23** remained nearly constant (1.1% ID/g during the final scan). While absolute uptake in tumors was highest

with **[^{18}F]3.09**, background uptake in healthy brain was also highest with this stereoisomer, ranging from 0.59-0.96% %ID/g, compared to uptake values of 0.39-0.46 and 0.28-0.36 %ID/g obtained with **[^{18}F]3.23** and **[^{18}F]3.33**, respectively. Despite the lower absolute tumor uptake observed with **[^{18}F]3.33**, this stereoisomer gave the highest L/N ratio of 4.3 at the 4.5-minute time point, though this value fell in each following time point owing to the progressive loss of activity in the 9L tumor over the course of the study. The highest L/N ratio obtained with **[^{18}F]3.09** also occurred at the 4.5-minute time point (L/N of 3.5) and similarly decreased over time, though this resulted from accumulation of radioactivity in normal brain rather than loss of activity in the tumor. **[^{18}F]3.23** reached a maximum at the 12.5-minute mark (L/N of 2.8), and its concentration in the 9L tumor and normal brain remained steady over the course of the study (L/N of 2.4 at 52.5 minutes). These uptake profiles are consistent with system L and ASC mediated transport. Because these systems transport via exchange rather than unidirectional flow of AA substrates into the cell, it is often the case that system L and ASC substrates will reach their peak concentration in tissues at early time points and remain relatively steady, or slowly decrease with time. Nonetheless, the relatively high absolute uptake of **[^{18}F]3.09**, **[^{18}F]3.23**, and **[^{18}F]3.33** in 9L tumors coupled with low background uptake in normal brain suggests that these compounds may have promise for imaging glioma.

In addition to the microPET studies performed on tumor-bearing Fischer rats, the biodistribution of **[^{18}F]3.09** and **[^{18}F]3.33** has also been measured in normal Fischer rats (these data have not yet been collected with **[^{18}F]3.23** but will be reported shortly). The purpose of acquiring this additional data is two-fold. In previous studies using Fischer rats, the 9L tumor seemed to have little impact on tracer distribution in normal tissues relative to normal rats.[46] Nonetheless, biodistribution studies in normal rats serve as a control in the absence of a tumor that could, in theory, alter uptake

in normal tissues. Additionally, bladder and 9L tumor uptake data are challenging to collect simultaneously, since the microPET scanner's field of view does not have sufficient breadth to image both in a single scan. This issue is conveniently addressed by obtaining bladder uptake data in biodistribution studies with normal rats. The data obtained from these studies is shown in the tables below.

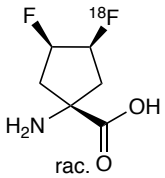

[^{18}F]3.09

Tissue	4.4 min	13.3 min	23.7 min	35.6 min	41.5 min	53.4 min
Liver	2.73 ± 0.77	2.41 ± 0.57	2.06 ± 0.44	1.76 ± 0.36	1.68 ± 0.36	1.51 ± 0.26
Heart	2.86 ± 0.86	1.82 ± 0.48	1.46 ± 0.23	1.26 ± 0.23	1.24 ± 0.15	1.13 ± 0.22
Lung	1.81 ± 0.45	1.20 ± 0.20	0.99 ± 0.17	0.90 ± 0.16	0.91 ± 0.18	0.86 ± 0.14
Kidney	9.55 ± 2.14	16.0 ± 3.05	17.5 ± 1.47	15.5 ± 1.74	14.5 ± 2.02	12.5 ± 1.73
Bladder	0.46 ± 0.18	2.43 ± 3.57	6.85 ± 8.94	15.8 ± 13.5	20.7 ± 14.7	30.2 ± 15.7
Muscle	0.54 ± 0.25	0.66 ± 0.20	0.70 ± 0.04	0.70 ± 0.03	0.72 ± 0.03	0.66 ± 0.09
Brain	0.65 ± 0.19	0.68 ± 0.18	0.81 ± 0.16	0.82 ± 0.14	0.85 ± 0.12	0.87 ± 0.10
Bone	1.52 ± 0.55	1.17 ± 0.36	1.12 ± 0.35	1.00 ± 0.26	1.01 ± 0.25	0.95 ± 0.20
Bowel	1.32 ± 0.31	0.90 ± 0.29	0.75 ± 0.28	0.75 ± 0.26	0.72 ± 0.25	0.66 ± 0.23
Testes	0.78 ± 0.23	1.00 ± 0.23	0.99 ± 0.22	0.92 ± 0.23	0.93 ± 0.16	0.87 ± 0.16
Spine	1.62 ± 0.27	1.36 ± 0.24	1.26 ± 0.20	1.23 ± 0.16	1.16 ± 0.12	1.18 ± 0.14

Table 3-5. Biodistribution of radioactivity in tissues of normal Fischer rats following intravenous administration of ***[^{18}F]3.09****. Data are reported as mean percent dose per gram ± standard deviation (n = 3) at each time point.*

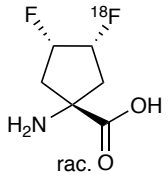

[^{18}F]3.33

Tissue	4.4 min	13.3 min	23.7 min	35.6 min	41.5 min	53.4 min
Liver	1.91 ± 0.06	1.23 ± 0.10	0.92 ± 0.08	0.84 ± 0.05	0.79 ± 0.05	0.74 ± 0.07
Heart	1.75 ± 0.05	1.16 ± 0.03	1.01 ± 0.04	0.92 ± 0.08	0.73 ± 0.06	0.73 ± 0.07
Lung	1.52 ± 0.09	0.96 ± 0.09	0.76 ± 0.04	0.68 ± 0.07	0.63 ± 0.01	0.63 ± 0.05
Kidney	4.16 ± 0.60	7.55 ± 0.41	6.82 ± 1.61	6.18 ± 1.60	5.62 ± 0.75	5.41 ± 0.34
Bladder	0.29 ± 0.06	2.94 ± 0.20	7.67 ± 0.35	11.1 ± 2.95	17.5 ± 5.23	22.3 ± 7.94
Muscle	0.80 ± 0.16	0.79 ± 0.12	0.73 ± 0.04	0.76 ± 0.02	0.75 ± 0.03	0.74 ± 0.05
Brain	0.37 ± 0.04	0.46 ± 0.03	0.50 ± 0.08	0.52 ± 0.02	0.51 ± 0.02	0.50 ± 0.04
Bone	1.11 ± 0.09	0.97 ± 0.01	0.94 ± 0.05	0.88 ± 0.08	0.82 ± 0.08	0.82 ± 0.12
Bowel	1.18 ± 0.42	0.78 ± 0.06	0.60 ± 0.06	0.56 ± 0.04	0.48 ± 0.00	0.50 ± 0.01
Testes	0.51 ± 0.17	0.73 ± 0.12	0.72 ± 0.16	0.71 ± 0.15	0.69 ± 0.19	0.67 ± 0.15
Spine	0.92 ± 0.03	0.80 ± 0.01	0.79 ± 0.01	0.74 ± 0.03	0.71 ± 0.00	0.69 ± 0.05

Table 3-6. Biodistribution of radioactivity in tissues of normal Fischer rats following intravenous administration of ***[^{18}F]3.33****. Data are reported as mean percent dose per gram ± standard deviation (n = 2) at each time point.*

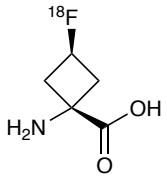

anti-3-[^{18}F]-FACBC

Tissue	4.4 min	13.3 min	23.7 min	35.6 min	41.5 min	53.4 min
Liver	2.24 ± 0.46	2.18 ± 0.42	1.95 ± 0.33	1.78 ± 0.27	1.68 ± 0.29	1.65 ± 0.27
Heart	2.43 ± 0.02	1.86 ± 0.25	1.60 ± 0.15	1.53 ± 0.13	1.48 ± 0.11	1.41 ± 0.09
Lung	1.59 ± 0.42	1.28 ± 0.33	1.21 ± 0.27	1.06 ± 0.21	1.06 ± 0.12	1.06 ± 0.14
Kidney	3.72 ± 0.04	3.14 ± 0.04	2.78 ± 0.14	2.36 ± 0.05	2.03 ± 0.11	1.94 ± 0.10
Bladder	0.51 ± 0.13	0.66 ± 0.11	0.76 ± 0.04	0.82 ± 0.02	0.88 ± 0.06	0.90 ± 0.10
Muscle	0.49 ± 0.05	0.70 ± 0.14	0.83 ± 0.10	0.98 ± 0.21	1.04 ± 0.19	1.09 ± 0.25
Brain	0.56 ± 0.06	0.48 ± 0.00	0.56 ± 0.04	0.64 ± 0.02	0.66 ± 0.05	0.68 ± 0.08
Bone	2.30 ± 0.69	1.79 ± 0.38	1.78 ± 0.32	1.70 ± 0.32	1.62 ± 0.37	1.63 ± 0.29
Bowel	1.11 ± 0.49	0.94 ± 0.45	0.79 ± 0.25	0.70 ± 0.23	0.71 ± 0.21	0.68 ± 0.18
Testes	0.54 ± 0.01	0.69 ± 0.02	0.78 ± 0.11	0.83 ± 0.11	0.85 ± 0.12	0.84 ± 0.14
Spine	1.80 ± 0.44	1.61 ± 0.41	1.48 ± 0.25	1.46 ± 0.19	1.44 ± 0.18	1.47 ± 0.20

Table 3-7. Biodistribution of radioactivity in tissues of normal Fischer rats following intravenous administration of anti-3-[^{18}F]-FACBC. Data are reported as mean percent dose per gram ± standard deviation (n = 2) at each time point.

The biodistribution profiles of **[^{18}F]3.09** and **[^{18}F]3.33** in normal tissue were similar, though **[^{18}F]3.09** generally concentrated in most tissues to a slightly greater degree than did **[^{18}F]3.33**. A crucial element of this study was the hypothesis that the proximity of the fluorine atom to the carboxylic acid and amine moieties in anti-2-[^{18}F]-FACPC produced an altered isoelectric point relative to ACPC, which resulted in rapid urinary excretion of the former compound. We postulated that the inductive impact of the fluorine atom on the carboxylate and amine moieties may be sufficiently attenuated in the 3,4-[^{18}F]-DFACPC compounds such that the urinary excretion observed with anti-2-[^{18}F]-FACPC occurs to a lesser extent. Indeed, while urinary excretion was significant with both **[^{18}F]3.09** and **[^{18}F]3.33**, it occurred at substantially later time points

compared to what has previously been observed with anti-2-[^{18}F]-FACPC.[47] Unfortunately, there are no available biodistribution data with anti-2-[^{18}F]-FACPC in normal Fischer rats, though the biodistribution of this compound has been evaluated in humans, for which Fischer rats are a reasonable proxy.[46a, 48] The human biodistribution data collected for anti-2-[^{18}F]-FACPC shows that this compound undergoes urinary excretion within 10 minutes of administration, at which point activity in the bladder is approximately 5-fold greater than in any other tissue other than the kidneys. Notably, 4.4 minutes after the start of the study, bladder uptake of **[^{18}F]3.09** and **[^{18}F]3.33** is less than 0.5 %ID/g and is similar to that of anti-3-FACBC at the same time point.

High kidney uptake was observed with **[^{18}F]3.09** and **[^{18}F]3.33**, which is consistent with the biodistribution profiles of other system L substrates,[49] though **[^{18}F]3.09** concentrated in the renal system to a greater degree (9.6-16 %ID/g) than **[^{18}F]3.33** (4.2-76 %ID/g) at all time points. With both **[^{18}F]3.09** and **[^{18}F]3.33**, activity in the bone and spine decreased over the course of the study, indicating that these compounds are stable to defluoration *in vivo*. Uptake in other normal tissues was similar for both compounds and in line with uptake values observed with anti-3-FACBC in the same animal model.

These data seem to validate the hypothesis that moving the fluorine atom away from the carboxylate and amine moieties is a viable strategy for improving upon the biodistribution profile of anti-2-[^{18}F]-FACPC. With the exception of the kidneys, uptake of **[^{18}F]3.09** and **[^{18}F]3.33** is relatively low in normal tissues, including the bladder at sufficiently early time points, indicating that these compounds may be useful for imaging tumors outside of the brain.

3.4 Conclusions

The synthesis of each stereoisomer of 3,4-DFACPC has been described. Both stereoisomers in which the fluorine atoms have a cis relationship (cis-anti-3,4-DFACPC, **3.09** and cis-syn-DFACPC, **3.33**) were isolated as single diastereomers, while the trans-3,4-DFACPC enantiomers were obtained as a racemic mixture (**3.23**). Each compound was ^{18}F radiolabeled and while the radiolabeling reactions generally proceeded in modest yields, the labeled compounds were obtained in high radiochemical purity. Each ^{18}F labeled 3,4-DFACPC was subjected to biological evaluation in cells and in healthy Fischer rats in addition to those bearing 9L gliosarcoma. Cell uptake inhibition studies demonstrated that each stereoisomer is transported primarily by system L with a lesser degree of transport occurring via system ASC. Cell uptake levels were relatively high for each stereoisomer in each of the cell lines tested, which included 9L gliosarcoma, human U87 ΔEGFR glioblastoma, and human DU145 androgen-independent prostate carcinoma, though **[^{18}F]3.09** and **[^{18}F]3.23** were taken up to a greater extent than **[^{18}F]3.33** in all cell lines. The level of cell uptake of **[^{18}F]3.09**, **[^{18}F]3.23**, and anti-3-[^{18}F]FACBC was generally very similar, with the notable exception that DU145 cells displayed a substantially greater avidity for **[^{18}F]3.23** than for the other compounds tested. These data suggest that **[^{18}F]3.23** may have promise for imaging prostate cancer, though the rate of urinary excretion of these compounds has not yet been established. Therefore, biodistribution studies in normal rats constitute an important next step in the evaluation of **[^{18}F]3.23**. Additionally, it is possible that the enantiomers of **[^{18}F]3.23** have distinct cell uptake and biodistribution profiles, and on this basis isolation and biological evaluation of the isolated enantiomers may be warranted. Biodistribution studies in Fischer rats bearing 9L gliosarcoma were performed with each stereoisomer of 3,4-DFACPC. Absolute uptake in the 9L tumor was greater than 1 %ID/g for each compound tested within the first several minutes

of the PET scan, and at all time points tumor to normal brain tissue uptake ratios were greater than 2. Biodistribution studies with **[^{18}F]3.09** and **[^{18}F]3.33** showed substantially delayed urinary excretion relative to 2-anti-[^{18}F]-FACPC,[47] consistent with the hypothesis that the rapid accumulation of 2-anti-[^{18}F]-FACPC in the bladder could be attenuated by moving the fluorine atom further away from the carboxylate and amine substituents of the ACPC moiety. Taken together, the data presented here suggest that **[^{18}F]3.09**, **[^{18}F]3.23**, and **[^{18}F]3.33** are promising preclinical candidates for further evaluation as oncological PET imaging agents.

3.5 Experimental Information and Characterization Data

General information

All solvents were purchased from Fisher Scientific or Sigma Aldrich and dried over 4 Å mol sieves (8-12 mesh, Sigma Aldrich). Unless otherwise noted, all commercially available reagents and substrates were used directly as received. Ultra-High Purity dry air was purchased from nexAir LLC. Thin layer chromatography was performed on Merck silica gel plates and visualized by UV light and or potassium permanganate. ^{1}H NMR and ^{13}C and ^{19}F NMR spectra were recorded on Bruker 600, Varian INOVA 600, INOVA 500 and INOVA 400 spectrometers. Residual solvent resonances were treated as internal reference signals. ^{19}F spectra were referenced to either trifluoroacetic acid (-76.55 ppm) or fluorobenzene (-113.15 ppm). IR spectra were recorded on a Nicolet iS10 FT-IR spectrometer and the absorption peaks were reported in cm^{-1}. The purification of products was performed via flash chromatography[50] unless otherwise noted. A Thomas capillary melting point apparatus was used to determine the melting points (uncorrected). High resolution mass spectra were obtained from the Emory University Mass Spec Facility Inc. X-ray crystal structure data was obtained from Dr. John Bacsa of the Emory University X-ray

Crystallography Center. The [^{18}F]fluoride was produced at Emory University Center for Systems Imaging with an 11MeV Siemens RDS 111 negative-ion cyclotron (Knoxville, TN) by the ^{18}O(p, n) ^{18}F reaction using [^{18}O]H_2O (95%). Alumina N SepPaks and HLB Oasis cartridges were purchased from Waters, Inc. (Milford, MA). The ion retardation (IR) chromatography columns and the IR resin AG 11A8 (50-100 mesh) were purchased from BioRad Laboratories (Hercules, CA). Trap/release cartridges model DW-TRC were purchased from D&W, Inc. (Oakdale, TN). Radiometric TLC was performed with the same type of silica plates from Whatman and analyzed using a Raytest system (model Rita Star, Germany). Isolated radiochemical yields were determined using a dose-calibrator (Capintec CRC-712M). Analytical HPLC experiments were performed with a Waters Breeze HPLC system equipped with a Bioscan flowcount radioactivity detector and an inline UV detector set to monitor wavelengths 210 nm, 230 nm, and 254 nm (Astec chirobiotic T column, Sigma-Aldrich part number 12021AST; mobile phase: MeOH). All animal experiments were carried out under humane conditions and were approved by the Institutional Animal Use and Care Committee (IUCAC) and Radiation Safety Committees at Emory University.

Cold Chemistry

2-Phenyloxazol-5(4*H*)-one (**3.01**),[37] ethyl (*E*)-2-((4-bromobenzylidene)amino)acetate (**3.13**),[38] ethyl (*Z*)-1-((4-bromobenzylidene)amino)cyclopent-3-ene-1-carboxylate (**3.14**),[38] and ethyl 1-aminocyclopent-3-ene-1-carboxylate (**3.15**),[38] were prepared according to previously reported procedures.

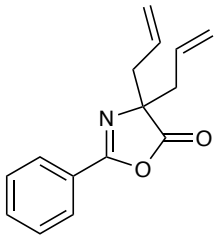

4,4-Diallyl-2-phenyloxazol-5(4*H*)-one (3.02) was prepared from 2-phenyloxazol-5(4*H*)-one with a slight modification to the reported procedure.[37]

To a round-bottomed flask under N_2 containing a magnetic stir bar and a solution of 2-phenyloxazol-5(4*H*)-one (74.1 g, 459.8 mmol, 1 equiv) in DMF (1 L, 0.5 M), NaI (3.45 g, 23.0 mmol, 0.05 equiv), and allyl bromide (79.5 mL, 111.3 g, 920 mmol, 2 equiv) were added sequentially. Diisopropylethylamine (DIPEA) (160.3 mL, 118.9 g, 920 mmol, 2 equiv) was then added dropwise. Immediately upon addition of DIPEA, the reaction began to exotherm and developed a dark green color. Upon complete addition of DIPEA, the reaction was left to stir at room temperature overnight. The reaction was diluted with ethyl acetate (1 L) and washed with 5 x 500 mL portions of brine. The organic layers were collected, dried over anhydrous Na_2SO_4, and concentrated to give an orange oil that was used without further purification.

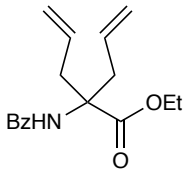

Ethyl 2-allyl-2-benzamidopent-4-enoate (**3.03**). To a round-bottomed flask under N_2 containing a magnetic stir bar and EtOH (100 mL), sodium (0.11 g, 4.6 mmol, 0.01 equiv) was added. The mixture was stirred until the evolution of H_2 gas ceased, at which time crude **4,4-diallyl-2-phenyloxazol-5(4*H*)-one** (**3.02**) was added as a solution in EtOH (100 mL). After stirring for 3 hours at room temperature, the reaction was concentrated, and the remaining oily residue was taken

up in CH_2Cl_2 (DCM) and washed with one portion of H_2O and one portion of brine. The organics were dried over anhydrous Na_2SO_4, filtered, and concentrated to give an orange oil. The oil was taken up in a minimum quantity of hot hexanes, gravity filtered, and stored at 0 °C overnight, resulting in the formation of pale-yellow crystals. The supernatant was removed by vacuum filtration and the crystals were washed with cold hexanes, then freed of residual solvent *in vacuo*. Pale yellow crystalline solid, 74.8 g, 260.3 mmol, 54% yield over three steps from 480 mmol of hippuric acid. ^{1}H NMR (400 MHz, chloroform-*d*) δ 7.83 – 7.72 (m, 2H), 7.54 – 7.47 (m, 1H), 7.47 – 7.39 (m, 2H), 7.12 (s, 1H), 5.72 – 5.57 (m, 2H), 5.24 – 4.84 (m, 4H), 4.27 (q, *J* = 7.1 Hz, 2H), 3.41 (dd, *J* = 13.7, 7.4 Hz, 2H), 2.61 (dd, *J* = 13.7, 7.4 Hz, 2H), 1.32 (t, *J* = 7.1 Hz, 3H). ^{13}C NMR (150 MHz, chloroform-*d*) δ 173.4, 166.5, 135.2, 132.4, 131.6, 128.7, 127.0, 119.3, 64.7, 62.2, 39.3, 14.4. IR (neat, cm^{-1}): 3254, 1740, 1632. HRMS (ESI) Calcd. for $C_{17}H_{22}O_3N$ $(M+H)^+$: 288.15942. Found: 288.15959. Melting point: 54-55 °C.

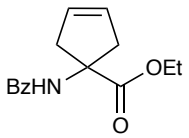

Ethyl 1-benzamidocyclopent-3-ene-1-carboxylate (**3.04**)**.** To a round-bottomed flask under N_2 containing a magnetic stir bar and a solution of **ethyl 2-allyl-2-benzamidopent-4-enoate** (**3.03**) (3.60 g, 12.6 mmol, 1 equiv) in toluene (60 mL, 0.2 M), dichloro[1,3-bis(2,4,6-trimethylphenyl)-2-imidazolidinylidene](2-isopropoxyphenylmethylene)ruthenium(II) (120 mg, 0.192 mmol, 0.015 equiv) was added and the mixture was stirred at room temperature for 10 hours. The contents of the reaction vessel were filtered over Celite™ and the filtrate was concentrated. The resulting black solid was subjected to silica gel flash chromatography, eluting the desired compound with 30% EtOAc in hexanes gradient (R_f = 0.3). White solid, 3.08 g, 11.88 mmol, 94% yield. Alternatively,

the crude material can be purified by crystallization from EtOAc/hexanes. ^{1}H NMR (400 MHz, chloroform-*d*) δ 7.81 – 7.76 (m, 2H), 7.55 – 7.47 (m, 1H), 7.47 – 7.40 (m, 2H), 6.78 (s, 1H), 5.71 (s, 2H), 4.25 (q, *J* = 7.1 Hz, 2H), 3.15 (d, *J* = 15.2 Hz, 2H), 2.82 (d, *J* = 15.2 Hz, 2H), 1.26 (t, *J* = 7.1 Hz, 3H). ^{13}C NMR (125 MHz, chloroform-*d*) δ 174.0, 167.0, 134.3, 131.8, 128.7, 128.1, 127.1, 64.5, 61.8, 44.8, 14.3. IR (neat, cm^{-1}): 3381, 3284, 1732, 1718, 1654, 1631. HRMS (ESI) Calcd. for $C_{15}H_{18}O_3N$ $(M+H)^+$: 260.12812. Found: 260.12823. Melting point: 101-102 °C.

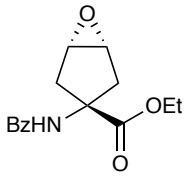

Ethyl (1*R*,3*R*,5*S*)-3-benzamido-6-oxabicyclo[3.1.0]hexane-3-carboxylate (**3.05**). To a round-bottomed flask under N_2 containing a magnetic stir bar and **ethyl 1-benzamidocyclopent-3-ene-1-carboxylate** (**3.04**) (2.00 g, 7.71 mmol, 1.0 equiv) suspended in toluene (60 mL, 0.1 M), *meta*-chloroperoxybenzoic acid (2.60 g, 11.57 mmol, 1.5 equiv) was added at once. The reaction was stirred at room temperature for 24 hours. Saturated aqueous sodium bicarbonate (30 mL) was added and the mixture was stirred for another 30 minutes, then it was diluted with 60 mL of DCM. The organics were separated, washed with another 30 mL portion of saturated aqueous sodium bicarbonate, and then with brine. The organics were collected, dried over anhydrous Na_2SO_4, filtered, and concentrated. Purification of the crude oily residue was achieved by silica gel flash chromatography, eluting the desired compound with 60/40 EtOAc hexanes gradient (R_f = 0.3). White solid, 1.66 g, 6.04 mmol, 78% yield. ^{1}H NMR (400 MHz, chloroform-*d*) δ 7.79 – 7.71 (m, 2H), 7.54 – 7.46 (m, 1H), 7.46 – 7.39 (m, 2H), 6.53 (s, 1H), 4.21 (q, *J* = 7.1 Hz, 2H), 3.68 (s, 2H), 2.57 (d, *J* = 15.8 Hz, 2H), 2.44 (d, *J* = 15.5 Hz, 2H), 1.24 (t, *J* = 7.1 Hz, 3H). ^{13}C NMR (125 MHz, chloroform-*d*) δ 171.5, 166.4, 133.9, 131.8, 128.7, 127.2, 62.2, 61.9, 56.9, 38.8, 14.3. IR (neat, cm^{-}

[1]): 3361, 1721, 1651. HRMS (ESI) Calcd. for $C_{15}H_{18}O_4N$ $(M+H)^+$: 276.12303. Found: 276.12315. Melting point: 110-112 °C.

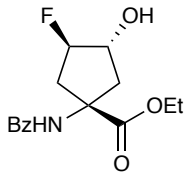

Racemic ethyl 1-benzamido-3-fluoro-4-hydroxycyclopentane-1-carboxylate (**3.06**). A plastic vial under N_2 containing a magnetic stir bar and a solution of **ethyl-3-benzamido-6-oxabicyclo[3.1.0]hexane-3-carboxylate** (**3.05**) (1.60 g, 5.81 mmol) in DCM (40 mL, 0.1 M) was chilled with an ice water bath. To this solution, HF pyridine (2 mL) was added dropwise with a plastic syringe. The mixture was stirred for 2 h at 0 °C, then slowly poured onto a slurry of ice and saturated aqueous sodium bicarbonate. Once the evolution of gas had ceased, the mixture was transferred to a separatory funnel and the organic layer was collected. The aqueous phase was washed 2 times with 20 mL of DCM, and the organic layers were combined and collectively dried over anhydrous Na_2SO_4, filtered, and concentrated. The resulting residue was purified by silica gel flash chromatography, eluting the desired compound with a 60/40 EtOAc/hexanes gradient (R_f = 0.3). Tan oil, 924 mg, 3.13 mmol, 54% yield. ^{1}H NMR (400 MHz, chloroform-*d*) δ 7.83 – 7.75 (m, 3H), 7.58 – 7.51 (m, 1H), 7.49 – 7.43 (m, 2H), 5.65 (d, *J* = 9.5 Hz, 1H), 5.15 (ddd, *J* = 51.3, 5.1, 1.5 Hz, 1H), 4.52 – 4.41 (m, 1H), 4.32 (qd, *J* = 7.1, 2.4 Hz, 2H), 3.01 – 2.83 (m, 2H), 2.50 (dd, *J* = 24.0, 15.9 Hz, 1H), 2.27 (d, *J* = 15.4 Hz, 1H), 1.33 (t, *J* = 7.1 Hz, 3H). ^{13}C NMR (125 MHz, chloroform-*d*) δ 174.5, 166.6, 133.9, 132.3, 128.9, 127.1, 99.7 (d, *J* = 181.3 Hz), 77.0, 65.2, 63.0, 44.5, 40.87 (d, *J* = 21.9 Hz), 14.08. ^{19}F NMR (376 MHz, chloroform-*d,* trifluoroacetic acid reference standard) δ -179.6 (dddd, *J* = 51.0, 34.7, 23.8, 11.0 Hz). IR (neat, cm^{-1}): 3354, 1728, 1636. HRMS (ESI) Calcd. for $C_{15}H_{19}O_4NF$ $(M+H)^+$: 296.12926. Found: 296.12940.

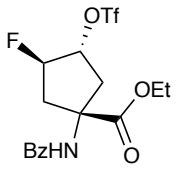

Racemic ethyl-1-benzamido-3-fluoro-4-(((trifluoromethyl)sulfonyl)oxy)cyclopentane-1-carboxylate (**3.07**). A scintillation vial under N_2 containing a stir bar and racemic **ethyl-1-benzamido-3-fluoro-4-hydroxycyclopentane-1-carboxylate** (**3.06**) (400 mg, 1.35 mmol, 1 equiv) and pyridine (240 µL, 2.97 mmol, 2.2 equiv) in DCM (5 mL) was cooled to 0 °C. A separate vial containing trifluoromethanesulfonic anhydride (385 µL, 2.70 mmol, 2.0 equiv) in DCM (1.5 mL) was cooled to 0 °C, and this mixture was added dropwise to the fluorohydrin solution with vigorous stirring. The mixture was stirred at 0 °C for 15 minutes, then diluted with hexanes (10 mL). A white powder precipitated and was filtered away, and the supernatant was concentrated at 0 °C. The crude residue was purified with a silica plug, eluting the desired compound with a 30/70 EtOAc/hexanes gradient (R_f = 0.3). Colorless oil, 481 mg, 1.13 mmol, 83% yield. Note, these compounds are thermally unstable. They should be isolated from the reaction mixture as quickly as possible and used immediately, or stored as a solution in benzene at < 0 °C. ^{1}H NMR (400 MHz, chloroform-*d*) δ 7.78 – 7.74 (m, 2H), 7.57 – 7.51 (m, 1H), 7.48 – 7.43 (m, 2H), 5.62 (ddd, *J* = 8.4, 6.3, 5.2 Hz, 1H), 5.50 (dtd, *J* = 15.7, 7.8, 5.3 Hz, 1H), 4.34 (qd, *J* = 7.1, 4.7 Hz, 2H), 2.90 – 2.78 (m, 3H), 2.51 (ddd, *J* = 23.3, 15.0, 6.5 Hz, 1H), 1.34 (t, *J* = 7.1 Hz, 3H). ^{13}C NMR (100 MHz, chloroform-*d*) δ 172.8, 166.9, 133.5, 132.4, 129.0, 118.6 (q, *J* = 320 Hz), 94.1 (d, *J* = 188 Hz), 89.8 (d, *J* = 25 Hz), 63.3, 61.9 (d, *J* = 5.0 Hz), 39.5 (d, *J* = 22 Hz), 38.2 (d, *J* = 3.4 Hz), 14.1. ^{19}F NMR (376 MHz, chloroform-*d,* fluorobenzene reference standard) δ -74.5 (s, 3F), -184.7 (ddd, *J* = 53.6, 23.7, 12.4 Hz, 1F). IR (neat, cm^{-1}): 3301, 1737, 1636. HRMS (ESI) Calcd. for $C_{16}H_{18}O_6NF_4S$ $(M+H)^+$: 428.07855. Found: 428.07894.

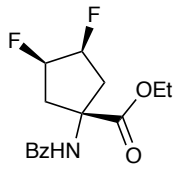

Ethyl (1*s*,3*R*,4*S*)-1-benzamido-3,4-difluorocyclopentane-1-carboxylate (**3.08**). To a scintillation vial under N_2 containing a stir bar and a mixture of racemic **ethyl-1-benzamido-3-fluoro-4-(((trifluoromethyl)sulfonyl)oxy)cyclopentane-1-carboxylate** (**3.07**) (370 mg, 1.09 mmol, 1 equiv) in THF (10 mL, 0.1 M), triethylamine trihydrofluoride (0.60 mL, 10.9 mmol, 10.0 equiv) was added at once and the reaction was stirred overnight at room temperature. The reaction was diluted with DCM (20 mL) and washed with two portions of saturated aqueous sodium bicarbonate (10 mL), then brine (10 mL). The organic phase was dried over anhydrous Na_2SO_4, filtered, and concentrated *in vacuo*. The crude residue was purified by silica gel flash chromatography, eluting the desired compound with a 20/80 EtOAc/hexanes gradient (R_f = 0.4). Colorless oil, 67 mg, 0.23 mmol, 26% yield. ^{1}H NMR (600 MHz, chloroform-*d*) δ 7.78 – 7.71 (m, 2H), 7.53 (t, *J* = 7.2 Hz, 1H), 7.45 (t, *J* = 7.7 Hz, 2H), 7.33 (s, 1H), 5.65 – 5.37 (m, 2H), 4.32 (q, *J* = 7.1 Hz, 2H), 2.88 – 2.71 (m, 2H), 2.58 (ddd, *J* = 18.8, 14.7, 5.5 Hz, 2H), 1.33 (t, *J* = 7.1 Hz, 3H). ^{13}C NMR (150 MHz, chloroform-*d*) δ 173.6, 167.3, 133.7, 132.3, 128.9, 127.0, 92.2 (dd, *J* = 188.7, 15.1 Hz), 63.1, 61.7 (t, *J* = 4.8 Hz), 40.3 – 40.1 (four-line multiplet, magnetic inequivalence), 14.1. ^{19}F NMR (376 MHz, chloroform-*d,* fluorobenzene reference standard) δ -198.5 – -198.9 (m). IR (neat, cm^{-1}): 3312, 1739, 1632. HRMS (ESI) Calcd. for $C_{15}H_{18}O_3NF_2$ $(M+H)^+$: 298.12493. Found 298.12509.

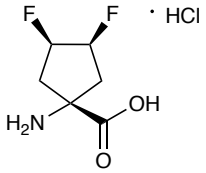

(1*s*,3*R*,4*S*)-1-Amino-3,4-difluorocyclopentane-1-carboxylic acid hydrochloride (**3.09**). To a scintillation vial open to air containing a stir bar and **ethyl (1*s*,3*R*,4*S*)-1-benzamido-3,4-difluorocyclopentane-1-carboxylate** (**3.08**) (33 mg, 0.111 mmol), concentrated aqueous HCl (1 mL) was added. The vial was sealed with a plastic cap and allowed to stir at 90 °C for 10 hours. Upon cooling to room temperature, colorless crystals formed spontaneously. These crystals were collected by filtration, washed with diethyl ether, and freed of residual solvent *in vacuo*. Colorless crystals, 20.1 mg, 0.100 mmol, 90% yield. ^{1}H NMR (400 MHz, Deuterium Oxide) δ 5.40 – 5.17 (m, 2H), 2.81 (ddt, *J* = 18.4, 15.9, 5.1 Hz, 1H), 2.40 (ddd, *J* = 18.5, 14.2, 5.4 Hz, 2H). ^{13}C NMR (125 MHz, deuterium oxide) δ 173.3, 91.3 (dd, *J* = 186.9, 15.6 Hz), 60.3 (t, *J* = 4.2 Hz), 37.7 – 37.4 (four-line multiplet, magnetic inequivalence). ^{19}F NMR (376 MHz, deuterium oxide, trifluoroacetic acid reference standard) δ -201.3 – -201.6 (m). IR (neat, cm^{-1}): 3196, 3067, 1712. HRMS (ESI) Calcd. for $C_6H_9O_2NClF_2$ $(M-H)^-$: 200.02954. Found 200.03002. Melting point: 242-244 °C (decomposes).

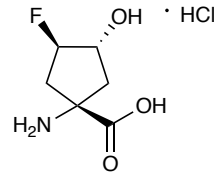

Racemic 1-amino-3-fluoro-4-hydroxycyclopentane-1-carboxylic acid hydrochloride (**3.10**). To a mixture of racemic **ethyl-1-benzamido-3-fluoro-4-hydroxycyclopentane-1-carboxylate** (**3.06**) (800 mg, 2.71 mmol) in a scintillation vial with a magnetic stir bar and open to air, concentrated aqueous HCl was added (3.0 mL). The vial was sealed with a plastic cap and heated

to 90 °C overnight. The reaction was removed from heat, concentrated *in vacuo* and washed with ether. A white solid (519 mg) was obtained that was carried forward without further purification. ^{1}H NMR (600 MHz, deuterium oxide) δ 5.12 (d, *J* = 49.8 Hz, 1H), 4.59 – 4.45 (m, 1H), 2.77 – 2.46 (m, 3H), 2.12 (d, *J* = 14.8 Hz, 1H). ^{13}C NMR (125 MHz, deuterium oxide) δ 173.7, 97.1 (d, *J* = 179.9 Hz), 74.8 (d, *J* = 26.7 Hz), 63.3, 40.5 (d, *J* = 23.5), 40.5.

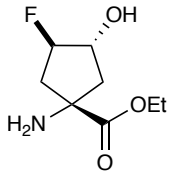

Racemic ethyl (1S,3R,4R)-1-amino-3-fluoro-4-hydroxycyclopentane-1-carboxylate (**3.11**).

To a round-bottomed flask under N_2 fitted with a reflux condenser and stir bar and containing a crude mixture of racemic **1-amino-3-fluoro-4-hydroxycyclopentane-1-carboxylic acid hydrochloride** (**3.10**) (519 mg) in dry ethanol, H_2SO_4 (0.1 mL) was added, and the reaction was heated to reflux for 10 hours. Ethanol was removed *in vacuo* and the crude residue was taken up in water (10 mL) and washed with three portions of DCM (10 mL). The organic layers were discarded, and the aqueous phase was treated with 30 mL of saturated aqueous sodium bicarbonate, then extracted with three portions of DCM (30 mL). The organics were collected, dried over anhydrous Na_2SO_4, filtered, and concentrated *in vacuo*. A pale-yellow oil (320 mg) was obtained which was carried forward without further purification. ^{1}H NMR (300 MHz, chloroform-*d*) δ 5.13 (dddd, *J* = 51.6, 6.0, 2.7, 1.8 Hz, 1H), 4.28 (dd, *J* = 9.2, 4.6 Hz, 1H), 4.19 (q, *J* = 7.2 Hz, 2H), 2.53 – 2.32 (m, 2H), 2.22 (dddd, *J* = 25.2, 15.7, 6.0, 2.1 Hz, 1H), 1.82 (d, *J* = 13.9 Hz, 1H), 1.28 (t, *J* = 7.1 Hz, 3H). ^{13}C NMR (75 MHz, chloroform-*d*) δ 175.8, 99.3 (d, *J* = 180.8 Hz), 77.2 (d, *J* = 27.7 Hz), 64.5, 61.9, 44.4 (d, *J* = 24.6 Hz), 42.9, 14.3.

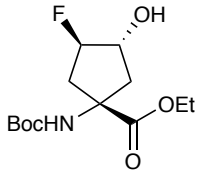

Racemic ethyl-1-((*tert*-butoxycarbonyl)amino)-3-fluoro-4-hydroxycyclopentane-1-carboxylate (**3.12**). To a scintillation vial under N_2 containing crude racemic **ethyl-1-amino-3-fluoro-4 hydroxycyclopentane-1-carboxylate** (**3.11**) (320 mg) in 10 mL of a 1:1 mixture of THF and water (10 mL) di-*tert*-butyl dicarbonate (290 mg, 1.32 mmol) was added. The mixture was stirred at room temperature for 8 h, then extracted with 3 portions of DCM (20 mL). The organic layers were combined, dried over anhydrous Na_2SO_4, filtered, and concentrated *in vacuo*. The resulting crude residue was purified by silica gel flash chromatography, eluting the desired compound with a 40/60 EtOAc/hexanes gradient ($R_f = 0.3$). White solid, 401 mg, 1.38 mmol, 51% yield over three steps.

Alternatively, **ethyl (1*R*,3*r*,5*S*)-3-((*tert*-butoxycarbonyl)amino)-6-oxabicyclo[3.1.0]hexane-3-carboxylate** (**3.17**) (820 mg, 3.02 mmol, 1.0 equiv) was suspended in 3 mL of benzene and stirred under high vacuum to allow for the azeotropic distillation of residual water. Once all of the benzene was removed, this compound was then added to a thick-walled glass tube with a stir bar and the tube was purged with N_2. Triethylamine (4.2 mL, 30.2 mmol, 10.0 equiv) and triethylamine trihydrofluoride were added (2.5 mL, 15.1 mmol, 5.0 equiv) sequentially and the tube was sealed with a screw cap then heated to 130 °C for 8 hours. After cooling to room temperature, DCM (30 mL) and saturated aqueous sodium bicarbonate (30 mL) were added and the biphasic mixture was stirred vigorously for several minutes. The mixture was transferred to a seperatory funnel and the organics were separated, and the aqueous phase was washed with DCM (30 mL). The organics were combined, washed with brine (30 mL), dried over Na_2SO_4, filtered, and concentrated in vacuo. The resulting crude residue was purified by silica gel flash chromatography, eluting the

desired compound with a 40/60 EtOAc/hexanes gradient (R_f = 0.3). Off-white solid, 755 mg, 2.59 mmol, 86% yield. ^{1}H NMR (400 MHz, chloroform-*d*) δ 5.82 (s, 1H), 5.16 – 4.91 (m, 1H), 4.63 (s, 1H), 4.36 (dq, *J* = 14.9, 7.1 Hz, 1H), 4.24 (q, *J* = 7.1 Hz, 2H), 2.81 (dd, *J* = 15.5, 6.5 Hz, 1H), 2.72 – 2.41 (m, 2H), 2.07 (d, *J* = 15.1 Hz, 1H), 1.43 (s, 9H), 1.29 (t, *J* = 7.1 Hz, 3H). ^{13}C NMR (150 MHz, chloroform-*d*) δ 173.9, 155.0, 99.3 (d, *J* = 181 Hz), 81.0, 76.7 (d, *J* = 27 Hz), 64.5, 62.5, 43.9, 41.4 (d, *J* = 18.8 Hz), 28.4, 14.1. ^{19}F NMR (282 MHz, chloroform-*d*, fluorobenzene reference standard) δ -179.2. IR ($CDCl_3$, cm^{-1}): 3374, 1717, 1695. HRMS (ESI) Calcd. for $C_{13}H_{23}O_5NF$ $(M+H)^+$: 292.15548. Found: 292.15567. Melting point: 48-51 °C.

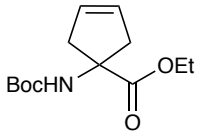

Ethyl 1-((*tert*-butoxycarbonyl)amino)cyclopent-3-ene-1-carboxylate (**3.16**). To a round-bottomed flask under N_2 containing a stir bar and **ethyl 1-aminocyclopent-3-ene-1-carboxylate** (**3.15**) (2.01 g, 12.95 mmol, 1.0 equiv) in 1:1 mixture of THF and water (40 mL, 0.3 M), di-tert-butyl dicarbonate (3.11 g, 14.24 mmol, 1.1 equiv) was added, and the mixture was stirred at room temperature for 8 hours. EtOAc was added (100 mL) and the organic layer was separated, washed with brine (50 mL), dried over Na_2SO_4, filtered, and concentrated *in vacuo*. The crude residue was purified by silica gel flash chromatography, eluting the desired compound with a 15/85 EtOAc/hexanes gradient (R_f = 0.4). White solid, 3.08 g, 12.06 mmol, 93% yield. ^{1}H NMR (400 MHz, chloroform-*d*) δ 5.64 (s, 2H), 5.10 (d, *J* = 13.1 Hz, 1H), 4.20 (q, *J* = 7.1 Hz, 2H), 3.08 – 3.01 (m, 2H), 2.60 (d, *J* = 17.2 Hz, 2H), 1.42 (s, 9H), 1.26 (t, *J* = 7.1 Hz, 3H).^{13}C NMR (150 MHz, chloroform-*d*) δ 174.4, 155.0, 127.8, 79.9, 64.3, 61.6, 45.0, 28.4, 14.3. IR (neat, cm^{-1}): 3272, 3139, 1733, 1698. HRMS (ESI) Calcd. for $C_{13}H_{22}O_4N$ $(M+H)^+$:256.15433. Found 256.15430. Melting

point: 75-76 °C. Known compound; spectroscopic data matches literature, lit. melting point: 82 °C. [51]

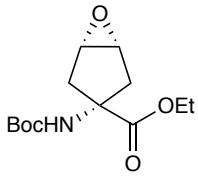

Ethyl (1*R*,3*r*,5*S*)-3-((*tert*-butoxycarbonyl)amino)-6-oxabicyclo[3.1.0]hexane-3-carboxylate (3.17). To a round-bottomed flask under N_2 containing a stir bar and **ethyl 1-((*tert*-butoxycarbonyl)amino)cyclopent-3-ene-1-carboxylate (3.16)** (550 mg, 2.16 mmol, 1.0 equiv) in toluene (20 mL, 0.1 M), *meta*-chloroperoxybenzoic acid (725 mg, 3.23 mmol, 1.5 equiv) was added in one portion. The reaction was stirred at room temperature for 24 hours. Saturated aqueous sodium bicarbonate (15 mL) was added and the mixture was stirred for another 30 minutes, then it was diluted with 30 mL of DCM. The organics were separated, washed with another 15 mL portion of saturated aqueous sodium bicarbonate, and then with brine (15 mL). The organics were collected, dried over anhydrous Na_2SO_4, filtered, and concentrated. Purification of the crude oily residue was achieved by silica gel flash chromatography, eluting the desired compound with 30/70 EtOAc/hexanes gradient (R_f = 0.3). White solid, 446 mg, 1.64 mmol, 76% yield. ^{1}H NMR (400 MHz, chloroform-*d*) δ 5.02 (s, 1H), 4.19 (q, *J* = 7.1 Hz, 2H), 3.61 (s, 2H), 2.46 (d, *J* = 15.3 Hz, 2H), 2.27 (d, *J* = 15.3 Hz, 2H), 1.41 (s, 9H), 1.24 (t, *J* = 7.1 Hz, 3H). ^{13}C NMR (125 MHz, chloroform-*d*) δ 172.3, 154.6, 80.0, 62.3, 61.8, 57.0, 38.8, 28.4, 14.2. IR (neat, cm^{-1}): 3380, 1735, 1709. HRMS (ESI) Calcd. for $C_{13}H_{22}O_5N$ $(M+H)^+$: 272.14925. Found 272.14922. Melting point: 62-63 °C.

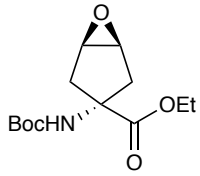

Ethyl (1*R*,3*s*,5*S*)-3-((*tert*-butoxycarbonyl)amino)-6-oxabicyclo[3.1.0]hexane-3-carboxylate (**3.18**). To a round-bottomed flask under N_2 containing a stir bar and **ethyl 1-((*tert*-butoxycarbonyl)amino)cyclopent-3-ene-1-carboxylate** (**3.16**) (550 mg, 2.16 mmol, 1.0 equiv) in toluene (20 mL, 0.1 M), *meta*-chloroperoxybenzoic acid (725 mg, 3.23 mmol, 1.5 equiv) was added in one portion. The reaction was stirred at room temperature for 24 hours. Saturated aqueous sodium bicarbonate (15 mL) was added and the mixture was stirred for another 30 minutes, then it was diluted with 30 mL of DCM. The organics were separated, washed with another 15 mL portion of saturated aqueous sodium bicarbonate, and then with brine (15 mL). The organics were collected, dried over anhydrous Na_2SO_4, filtered, and concentrated. Purification of the crude oily residue was achieved by silica gel flash chromatography, eluting the desired compound with 30/70 EtOAc/hexanes gradient (R_f = 0.25). White solid, 85 mg, 0.313 mmol, 15% yield. ^{1}H NMR (400 MHz, chloroform-*d*) δ 5.08 (s, 1H), 4.20 (q, *J* = 7.1 Hz, 2H), 3.57 (s, 2H), 2.88 (d, *J* = 14.8 Hz, 2H), 2.08 (d, *J* = 14.8 Hz, 2H), 1.42 (s, 9H), 1.27 (t, *J* = 7.1 Hz, 3H). ^{13}C NMR (125 MHz, chloroform-*d*) δ 173.1, 154.6, 80.4, 64.0, 61.9, 56.8, 38.8, 28.4, 14.2. IR (neat, cm^{-1}): 3358, 1734, 1701. HRMS (ESI) Calcd. for $C_{13}H_{22}O_5N$ $(M+H)^+$: 272.14925. Found 272.14920. Melting point: 108 – 109 °C.

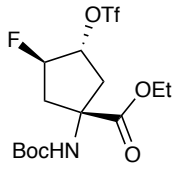

Racemic ethyl-1-((*tert*-butoxycarbonyl)amino)-3-fluoro-4 (((trifluoromethyl)sulfonyl)oxy)cyclopentane-1-carboxylate (**3.19**) (A scintillation vial under N_2 containing a stir bar and a mixture of racemic **1-((*tert*-butoxycarbonyl)amino)-3-fluoro-4-hydroxycyclopentane-1-carboxylate** (**3.12**) (70 mg, 0.24 mmol, 1 equiv) and pyridine (40 µL, 0.53 mmol, 2.2 equiv) in DCM (1.5 mL) was cooled to 0 °C. A separate vial containing trifluoromethanesulfonic anhydride (70 µL, 0.48 mmol, 2.0 equiv) in DCM (1.5 mL) was cooled to 0 °C, and this mixture was added dropwise to the fluorohydrin solution with vigorous stirring. The mixture was stirred at 0 °C for 15 minutes, then diluted with hexanes (3 mL). A white powder precipitated and was filtered away, and the supernatant was concentrated at 0 °C. The crude residue was purified with a silica plug, eluting the desired compound with a 20/80 EtOAc/hexanes gradient (R_f= 0.3). Colorless oil, 75 mg, 0.177 mmol, 74% yield. Note, these compounds are thermally unstable, decomposing over the course of one evening at room temperature. Care should be taken to purify these compounds as quickly as possible, at which point they should be used immediately, or taken up in benzene and stored at < 0 °C. ^{1}H NMR (600 MHz, chloroform-*d*) δ 5.54 – 5.25 (m, 3H), 4.27 (q, *J* = 7.1 Hz, 2H), 2.95 – 2.35 (m, 4H), 1.44 (d, 9H), 1.31 (t, *J* = 7.1 Hz, 3H). ^{13}C NMR (100 MHz, chloroform-*d*) δ 172.4, 154.6, 118.6 (q, *J* = 319 Hz), 94.6 (d, *J* = 188 Hz), 92.2, 89.9 (d, *J* = 26 Hz), 62.8, 58.1, 40.2 (d, *J* = 22 Hz), 39.2, 28.4, 14.1. ^{19}F NMR (376 MHz, chloroform-*d*, fluorobenzene reference standard) δ -74.6 (s, 3F), -184.6 (m, 1F). IR ($CDCl_3$, cm^{-1}): 3353, 1716. HRMS (ESI) Calcd. for $C_{14}H_{22}O_7NF_4S$ $(M+H)^+$: 424.10476. Found: 424.10539.

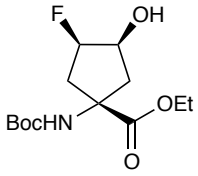

Racemic ethyl 1-((*tert*-butoxycarbonyl)amino)-3-fluoro-4-hydroxycyclopentane-1-carboxylate (**3.20**). To a scintillation vial open to air containing a stir bar and racemic **ethyl 1-((*tert*-butoxycarbonyl)amino)-3-fluoro-4-(((trifluoromethyl)sulfonyl)oxy)cyclopentane-1-carboxylate** (**3.19**) (131 mg, 0.309 mmol) in THF (2 mL, 0.15 M), saturated aqueous sodium bicarbonate (2 mL) was added. The biphasic mixture was heated to 50 °C and stirred vigorously for 16h. After cooling to room temperature, the contents of the reaction were poured into a seperatory funnel, and the contents were diluted with ethyl acetate (10 mL). The organics were separated, washed with brine (5 mL), dried over Na_2SO_4, filtered, and concentrated *in vacuo.* The resulting crude residue was purified by silica gel flash chromatography, eluting the desired compound with a 50/50 EtOAc/hexanes gradient (R_f = 0.4). White solid, 88 mg, 0.302 mmol, 98% yield. ^{1}H NMR (400 MHz, chloroform-*d*) δ 5.14 – 4.94 (m, 2H), 4.47 – 4.34 (m, 1H), 4.22 (qd, *J* = 7.1, 1.3 Hz, 2H), 2.80 (ddd, *J* = 27.5, 15.9, 3.1 Hz, 1H), 2.47 – 2.17 (m, 4H), 1.43 (s, 9H), 1.28 (t, *J* = 7.1 Hz, 3H). ^{13}C NMR (150 MHz, chloroform-*d*) δ 173.6, 155.2, 93.9 (d, *J* = 179.5 Hz), 80.6, 73.0 (d, *J* = 17.8 Hz), 62.2, 61.8, 42.8, 41.4 (d, *J* = 17.4 Hz), 28.4, 14.2. ^{19}F NMR (282 MHz, chloroform-*d,* fluorobenzene reference standard) δ -195.4 – -196.2 (m). IR (neat, cm^{-1}): 3355, 1709, 1692. HRMS (ESI) Calcd. for $C_{13}H_{23}O_5NF$ $(M+H)^+$: 292.15548. Found: 292.15546. Melting point: 72 – 74 °C.

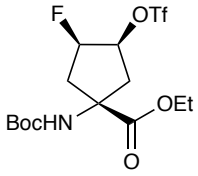

Racemic ethyl-1-((*tert*-butoxycarbonyl)amino)-3-fluoro-4 (((trifluoromethyl)sulfonyl)oxy)cyclopentane-1-carboxylate (**3.21**). A scintillation vial under N_2 containing a stir bar and racemic **ethyl 1-((*tert*-butoxycarbonyl)amino)-3-fluoro-4-hydroxycyclopentane-1-carboxylate** (**3.20**) (50 mg, 0.17 mmol, 1 equiv) and pyridine (30 µL, 0.38 mmol, 2.2 equiv) in DCM (0.5 mL) was cooled to 0 °C. A separate vial containing trifluoromethanesulfonic anhydride (50 µL, 0.34 mmol, 2.0 equiv) in DCM (0.5 mL) was cooled to 0 °C, and this mixture was added dropwise to the fluorohydrin solution with vigorous stirring. The mixture was stirred at 0 °C for 15 minutes, then diluted with hexanes (1 mL). A white powder precipitated and was filtered away, and the supernatant was concentrated at 0 °C to give 54 mg of crude, colorless oil. As the triflate is highly unstable, it was used directly without further purification.

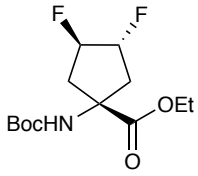

Racemic ethyl-1-((*tert*-butoxycarbonyl)amino)-3,4-difluorocyclopentane-1-carboxylate (**3.22**). To a scintillation vial under N_2 containing a stir bar and crude racemic **ethyl-1-((*tert*-butoxycarbonyl)amino)-3-fluoro-4 (((trifluoromethyl)sulfonyl)oxy)cyclopentane-1-carboxylate** (**3.21**) (54 mg), *tert*-butanol (2 mL) was added. Cesium fluoride (78 mg, 0.515 mmol) was then added under a stream of N_2 and the reaction was heated to 50 °C for 12 hours. The mixture was diluted with water (5 mL) and DCM (5 mL) and the phases were separated. The aqueous phase

was washed with another portion of DCM (5 mL) and the organics were collected and dried over Na_2SO_4, filtered, and concentrated. The resulting crude residue was purified by silica gel flash chromatography, eluting the desired compound with a 20/80 EtOAc/hexanes gradient (R_f = 0.4). White solid, 19 mg, 0.065 mmol, 38% yield over two steps. ^{1}H NMR (500 MHz, chloroform-*d*) δ 5.40 – 5.04 (m, 3H), 4.22 (q, *J* = 7.1 Hz, 2H), 2.83 – 2.47 (m, 3H), 2.29 (t, *J* = 19.1 Hz, 1H), 1.43 (s, 9H), 1.27 (t, *J* = 7.1 Hz, 3H). ^{13}C NMR (125 MHz, chloroform-*d*) δ 172.7, 154.82, 96.6 (dd, *J* = 179.2, 29.2 Hz), 95.9 (dd, *J* = 180.5, 30.0 Hz), 80.5, 63.7, 62.2, 41.6, 40.8, 28.4, 14.2. ^{19}F NMR (376 MHz, chloroform-*d,* fluorobenzene reference standard) δ -183.2 (broad s, 1F), -184.8 (dddd, *J* = 60.1, 35.0, 13.0, 9.1 Hz, 1F). IR (neat, cm^{-1}): 3281, 1735, 1688, 1671. HRMS (ESI) Calcd. for $C_{13}H_{22}O_4NF_2$ $(M+H)^+$: 294.15114. Found: 294.15129. Melting point: 64 – 66 °C.

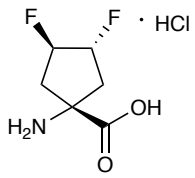

Racemic 1-amino-3,4-difluorocyclopentane-1-carboxylic acid hydrochloride (**3.23**). To a scintillation vial containing a racemic **ethyl-1-((*tert*-butoxycarbonyl)amino)-3,4-difluorocyclopentane-1-carboxylate** (**3.22**) (19 mg, 0.065 mmol), concentrated HCl (1 mL) was added. The reaction was heated to 90 °C for 1h and then allowed to cool to room temperature. On cooling, colorless crystals formed spontaneously. The supernatant was carefully removed with a small gauge needle and the crystals were freed of further solvent *in vacuo*. Colorless crystals, 10 mg, 0.061 mmol, 93% yield. ^{1}H NMR (600 MHz, deuterium oxide) δ 5.40 – 5.35 (m, 1H), 5.32 – 5.27 (m, 1H), 2.80 (ddt, *J* = 40.7, 16.2, 3.6 Hz, 1H), 2.71 (dd, *J* = 27.5, 16.5 Hz, 1H), 2.57 (ddd, *J* = 31.2, 16.7, 6.0 Hz, 1H), 2.42 (dd, *J* = 19.2, 17.3 Hz, 1H). ^{13}C NMR (125 MHz, deuterium oxide) δ 173.6, 96.2 (dd, *J* = 172.7, 31.1 Hz), 94.9 (dd, *J* = 177.1, 32.0 Hz), 63.4, 40.6 (d, *J* = 23.5 Hz),

39.7 (d, J = 20.9 Hz). ^{19}F NMR (376 MHz, chloroform-*d,* trifluoroacetic acid reference standard) δ -184.6 – -185.1 (m), -187.6 – -188.1 (m). IR (neat, cm^{-1}): 2919 (broad), 1746. HRMS (ESI) Calcd. for $C_6H_{10}O_2NF_2$ $(M+H)^+$: 166.06741. Found: 166.06783. Melting point (decomposes): 260 °C.

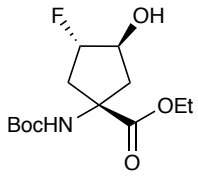

Racemic 1-((*tert*-butoxycarbonyl)amino)-3-fluoro-4-hydroxycyclopentane-1-carboxylate (**3.24**). A thick-walled glass tube purged with N_2, containing a stir bar and **ethyl (1*R*,3*s*,5*S*)-3-((*tert*-butoxycarbonyl)amino)-6-oxabicyclo[3.1.0]hexane-3-carboxylate** (**3.18**) (350 mg, 1.20 mmol, 1.0 equiv), was treated with 3 mL of benzene and stirred under high vacuum to allow for the azeotropic distillation of residual water. Once all of the benzene was removed, triethylamine (1.79 mL, 12.9 mmol, 10.0 equiv) and triethylamine trihydrofluoride (1.05 mL, 6.45 mmol, 5.0 equiv) were added sequentially. The tube was sealed with a screw cap and the mixture was heated to 130 °C for 8 hours. After cooling to room temperature, DCM (20 mL) and saturated aqueous sodium bicarbonate (20 mL) were added and the biphasic mixture was stirred vigorously for several minutes. The mixture was transferred to a seperatory funnel and the organics were separated, and the aqueous phase was washed with DCM (20 mL). The organics were combined, washed with brine (20 mL), dried over Na_2SO_4, filtered, and concentrated in vacuo. The resulting crude residue was purified by silica gel flash chromatography, eluting the desired compound with a 40/60 EtOAc/hexanes gradient (R_f = 0.3). Colorless oil, 68 mg, 0.252 mmol, 21% yield. ^{1}H NMR (400 MHz, chloroform-*d*) δ 5.13 (s, 1H), 4.96 (dd, J = 51.0, 4.7 Hz, 1H), 4.49 – 4.34 (m, 1H), 4.30 – 4.16 (m, 2H), 3.16 (d, J = 7.4 Hz, 1H), 2.68 (ddd, J = 35.4, 15.8, 5.0 Hz, 1H), 2.58 (d, J = 15.9

Hz, 1H), 2.35 (ddd, J = 14.8, 6.2, 2.1 Hz, 1H), 2.16 (dd, J = 23.2, 15.7 Hz, 1H), 1.43 (s, 9H), 1.29 (t, J = 7.1 Hz, 3H). ^{13}C NMR (150 MHz, chloroform-*d*) δ 176.4, 155.9, 98.7 (d, J = 178.9 Hz), 80.4, 76.0 (d, J = 27.2 Hz), 64.0, 62.6, 44.4, 42.7 (d, J = 22.3 Hz), 28.4, 14.9. ^{19}F NMR (282 MHz, chloroform-*d,* fluorobenzene reference standard) δ -176.5 – -179.3 (m). IR (neat, cm^{-1}): 3348, 1737, 1692. HRMS (ESI) Calcd. for $C_{13}H_{23}O_5NF$ $(M+H)^+$: 292.15548. Found: 292.15551.

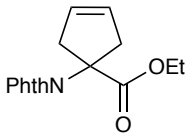

Ethyl 1-(1,3-dioxoisoindolin-2-yl)cyclopent-3-ene-1-carboxylate (**3.26**). To a two necked round-bottomed flask under N_2, fitted with a dean stark apparatus, and containing a stir bar, **ethyl 1-aminocyclopent-3-ene-1-carboxylate** (**3.15**) (7.01 g, 45.2 mmol, 1.0 equiv), and toluene (200 mL), phthalic anhydride (7.35 g, 49.7 mmol, 1.1 equiv) was added. The mixture was heated to 110 °C for 24 hours. The mixture was cooled to room temperature and diluted with 200 mL of DCM. The organics were washed with water (100 mL), brine (100 mL), and dried over Na_2SO_4, before being filtered and concentrated *in vacuo*. The crude residue was purified by silica gel flash chromatography, eluting the desired compound with a 15/85 EtOAc/hexanes gradient (R_f = 0.3). White needles, 8.66 g, 30.4 mmol, 67% yield. ^{1}H NMR (400 MHz, chloroform-*d*) δ 7.83 – 7.78 (m, 2H), 7.74 – 7.67 (m, 2H), 5.76 (s, 2H), 4.18 (q, J = 7.1 Hz, 2H), 3.43 (d, J = 16.0 Hz, 2H), 3.27 (d, J = 16.1 Hz, 2H), 1.20 (t, J = 7.1 Hz, 3H). ^{13}C NMR (100 MHz, chloroform-*d*) δ 172.5, 168.8, 134.2, 132.0, 127.9, 123.3, 68.3, 62.0, 42.4, 14.1. IR (neat, cm^{-1}): 1775, 1707. HRMS (ESI) Calcd. for $C_{16}H_{16}O_4N$ $(M+H)^+$: 286.10738. Found: 286.10765. Melting point (crystallized from diethyl ether): 57-59 °C.

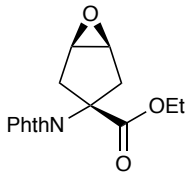

Ethyl (1*R*,3*s*,5*S*)-3-(1,3-dioxoisoindolin-2-yl)-6-oxabicyclo[3.1.0]hexane-3-carboxylate (**3.27**). To a round-bottomed flask containing a stir bar and **ethyl 1-(1,3-dioxoisoindolin-2-yl)cyclopent-3-ene-1-carboxylate** (**3.26**) (4.00 g, 14.02 mmol, 1.0 equiv) in toluene (140 mL), *meta*-chloroperoxybenzoic acid was added (5.20 g, 21.03 mmol, 1.5 equiv) and the mixture was stirred at room temperature for 12 hours. The reaction was quenched by the addition of saturated aqueous sodium bicarbonate (100 mL) and diluted with DCM (150 mL) and stirred for several minutes. The phases were separated, the organic phase was dried over Na_2SO_4, filtered, and concentrated. Analysis of the proton NMR of the crude mixture suggests that a mixture of syn and anti-epoxides were formed in a 1:0.4 ratio. The crude residue was taken up in a minimum quantity of refluxing diethyl ether and allowed to stand for several hours at room temperature, then chilled to 0 °C overnight. Crystalline white blocks were obtained, which were determined to be a mixture of syn and anti-epoxide diastereomers (1:0.4) by proton NMR. The desired anti diastereomer was obtained by column chromatography eluting with a 30/70 EtOAc/hexanes gradient (R_f = 0.2). White solid, 1.06 g, 3.51 mmol, 25% yield. ^{1}H NMR (400 MHz, chloroform-*d*) δ 7.83 – 7.77 (m, 2H), 7.75 – 7.69 (m, 2H), 4.24 (q, *J* = 7.1 Hz, 2H), 3.63 (s, 2H), 3.33 (d, *J* = 14.8 Hz, 2H), 2.66 (d, *J* = 14.8 Hz, 2H), 1.26 (t, *J* = 7.1 Hz, 3H). ^{13}C NMR (100 MHz, chloroform-*d*) δ 170.4, 168.0, 134.4, 131.6, 123.4, 65.7, 62.2, 55.7, 36.0, 14.1. IR (neat, cm^{-1}): 1778, 1719. HRMS (ESI) Calcd. for $C_{16}H_{16}O_5N$ $(M+H)^+$: 302.10230. Found: 302.10261. Melting point (crystallized from diethyl ether): 128 °C.

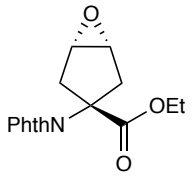

Ethyl (1*R*,3*r*,5*S*)-3-(1,3-dioxoisoindolin-2-yl)-6-oxabicyclo[3.1.0]hexane-3-carboxylate (**3.28**). Prepared as described above. Purified by column chromatography eluting with a 30/70 EtOAc/hexanes gradient (R_f = 0.25). White solid, 2.74 g, 9.09 mmol, 65% yield. ^{1}H NMR (600 MHz, chloroform-*d*) δ 7.81 – 7.75 (m, 2H), 7.70 – 7.65 (m, 2H), 4.16 (q, *J* = 7.1 Hz, 2H), 3.65 (s, 2H), 3.48 (d, *J* = 15.1 Hz, 2H), 2.49 (d, *J* = 14.9 Hz, 2H), 1.17 (t, *J* = 7.1 Hz, 3H). ^{13}C NMR (100 MHz, chloroform-*d*) δ 171.6, 168.4, 134.1, 131.8, 123.2, 66.2, 62.4, 56.1, 36.4, 14.1. IR (neat, cm^{-1}): 1778, 1732, 1721, 1712. HRMS (ESI) Calcd. for $C_{16}H_{16}O_5N$ $(M+H)^+$: 302.10230. Found: 302.10256. Melting point (crystallized from diethyl ether): 115 °C.

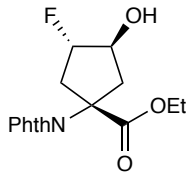

Racemic ethyl-1-(1,3-dioxoisoindolin-2-yl)-3-fluoro-4-hydroxycyclopentane-1-carboxylate (**3.29**). A scintillation vial purged with N_2 and containing a stir bar and **ethyl (1*R*,3*s*,5*S*)-3-(1,3-dioxoisoindolin-2-yl)-6-oxabicyclo[3.1.0]hexane-3-carboxylate** (**3.27**) (942 mg, 3.13 mmol) was treated with 10 mL of benzene and stirred under high vacuum to allow for the azeotropic distillation of residual water. Once all of the benzene was removed, triethylamine trihydrofluoride (5 mL) was added. The mixture was heated to 110 °C for 8 hours. After cooling to room temperature, DCM (50 mL) and saturated aqueous sodium bicarbonate (50 mL) were added and the biphasic mixture was stirred vigorously for several minutes. The mixture was transferred to a separatory funnel and the organics were separated, and the aqueous phase was washed with DCM

(50 mL). The organics were combined, washed with brine (50 mL), dried over Na_2SO_4, filtered, and concentrated in vacuo. The resulting crude residue was purified by silica gel flash chromatography, eluting the desired compound with a 40/60 EtOAc/hexanes gradient (R_f = 0.4). Colorless oil, 429 mg, 1.34 mmol, 43% yield. ^{1}H NMR (400 MHz, chloroform-*d*) δ 7.89 – 7.80 (m, 2H), 7.79 – 7.71 (m, 2H), 5.06 (ddt, *J* = 51.5, 5.1, 2.4 Hz, 1H), 4.59 – 4.36 (m, 1H), 4.20 (q, *J* = 7.1 Hz, 2H), 3.41 (d, *J* = 8.3 Hz, 1H), 3.40 – 3.26 (m, 1H), 3.19 (ddd, *J* = 15.2, 6.4, 2.1 Hz, 1H), 2.97 (ddd, *J* = 32.5, 16.2, 5.3 Hz, 1H), 2.69 (dd, *J* = 15.3, 2.8 Hz, 1H), 1.17 (t, *J* = 7.1 Hz, 3H). ^{13}C NMR (100 MHz, chloroform-*d*) δ 174.7, 168.7, 134.5, 131.8, 123.5, 99.0 (d, *J* = 179.6 Hz), 75.8 (d, *J* = 27.2 Hz), 67.3, 63.2, 42.7 (d, *J* = 1.7 Hz), 40.1 (d, *J* = 23.3 Hz), 14.1. ^{19}F NMR (282 MHz, chloroform-*d,* fluorobenzene reference standard) δ -176.8 – -177.3 (m). IR (neat, cm^{-1}): 3467, 1779, 1713. HRMS (ESI) Calcd. for $C_{16}H_{17}O_5NF$ $(M+H)^+$: 322.10853. Found: 322.10881.

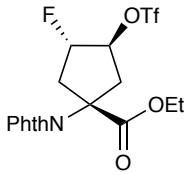

Racemic ethyl-1-(1,3-dioxoisoindolin-2-yl)-3-fluoro-4-(((trifluoromethyl)sulfonyl)oxy)cyclopentane-1-carboxylate. (**3.30**) A scintillation vial under N_2 containing a stir bar, racemic **ethyl-1-(1,3-dioxoisoindolin-2-yl)-3-fluoro-4-hydroxycyclopentane-1-carboxylate** (**3.29**) (170 mg, 0.529 mmol, 1 equiv) and pyridine (94 µL, 1.17 mmol, 2.2 equiv) in DCM (2.5 mL) was cooled to 0 °C. A separate vial containing trifluoromethanesulfonic anhydride (200 µL, 1.06 mmol, 2.0 equiv) in DCM (2.5 mL) was cooled to 0 °C, and this mixture was added dropwise to the fluorohydrin solution with vigorous stirring. The mixture was stirred at 0 °C for 15 minutes, then diluted with hexanes (5 mL). A white powder precipitated and was filtered away, and the supernatant was concentrated *in vacuo*. The resulting

crude residue was purified by silica gel flash chromatography, eluting the desired compound with a 15/85 EtOAc/hexanes gradient (R_f = 0.2). White solid, 203 mg, 0.448 mmol, 85% yield. ^{1}H NMR (400 MHz, C_6D_6) δ 7.47 – 7.28 (m, 2H), 6.86 – 6.72 (m, 2H), 5.72 – 5.54 (m, 1H), 5.07 – 4.78 (m, 1H), 3.85 – 3.70 (m, 2H), 3.43 (dd, *J* = 15.4, 8.4 Hz, 1H), 2.95 (ddd, *J* = 21.6, 15.4, 6.6 Hz, 1H), 2.71 (ddd, *J* = 20.5, 15.4, 5.1 Hz, 1H), 2.55 (dd, *J* = 15.4, 5.8 Hz, 1H), 0.76 (t, *J* = 7.1 Hz, 3H). ^{13}C NMR (150 MHz, C_6D_6) δ 170.2, 168.2, 134.2, 131.8, 128.4, 123.3, 119.2 (q, *J* = 319.7 Hz), 96.0 (d, *J* = 185.3 Hz), 90.4 (d, *J* = 29.4 Hz), 66.0 (d, *J* = 3.1 Hz), 62.8, 39.6 (d, *J* = 3.4 Hz), 39.4 (d, *J* = 22.6 Hz), 13.7. ^{19}F NMR (282 MHz, chloroform-*d,* fluorobenzene reference standard) δ -75.5, -181.9 (s, 3F), (dq, *J* = 51.4, 20.2 Hz, 1F). IR (neat, cm^{-1}): 1774, 1736, 1720, 1709. HRMS (ESI) Calcd. for $C_{17}H_{16}O_7NF_4S$ $(M+H)^+$: 454.05781. Found: 454.05808. Melting point: 91-94 °C.

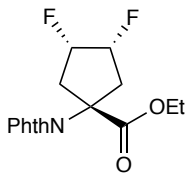

Ethyl (1*r*,3*R*,4*S*)-1-(1,3-dioxoisoindolin-2-yl)-3,4-difluorocyclopentane-1-carboxylate (**3.31**)

To a scintillation vial under N_2 containing a stir bar and racemic **ethyl-1-(1,3-dioxoisoindolin-2-yl)-3-fluoro-4-(((trifluoromethyl)sulfonyl)oxy)cyclopentane-1-carboxylate** (**3.30**) (261 mg, 0.576 mmol), *tert*-butanol (1 mL) was added. Cesium fluoride (262 mg, 1.73 mmol) was then added under a stream of N_2 and the reaction was stirred at room temperature for 28 hours. The mixture was concentrated under reduced pressure, then diluted with DCM (5 mL) and washed with water (5 mL). The phases were separated, and the aqueous phase was washed with another portion of DCM (5 mL). The organics were combined and dried over Na_2SO_4, filtered, and concentrated. The resulting crude residue was purified by preparative thin layer chromatography, eluting the desired compound with a 15/85 EtOAc/hexanes gradient (R_f = 0.3). Colorless oil, 34 mg, 0.105

mmol, 18% yield. ^{1}H NMR (300 MHz, chloroform-*d*) δ 7.89 – 7.81 (m, 2H), 7.78 – 7.71 (m, 2H), 5.31 – 5.02 (m, 2H), 4.17 (q, *J* = 7.1 Hz, 2H), 3.33 – 3.11 (m, 2H), 3.11 – 2.92 (m, 2H), 1.18 (t, *J* = 7.1 Hz, 3H). ^{13}C NMR (100 MHz, chloroform-*d*) δ 172.4, 168.7, 134.5, 131.8, 123.5, 90.5 (dd, *J* = 188.6, 15.7), 63.4 (t, *J* = 5.2 Hz), 62.9, 38.5 – 38.1 (four-line multiplet, magnetic inequivalence), 14.1. ^{19}F NMR (282 MHz, chloroform-*d,* fluorobenzene reference standard) δ -198.6 – -199.2 (m). IR (neat, cm^{-1}): 1780, 1717. HRMS (ESI) Calcd. for $C_{16}H_{16}O_4NF_2$ $(M+H)^+$: 324.10419. Found: 324.10473.

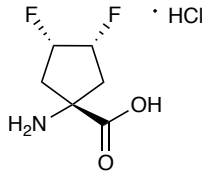

(1*r*,3*R*,4*S*)-1-amino-3,4-difluorocyclopentane-1-carboxylic acid hydrochloride (**3.33**).

To a scintillation vial open to air containing a stir bar and **ethyl (1*r*,3*R*,4*S*)-1-(1,3-dioxoisoindolin-2-yl)-3,4-difluorocyclopentane-1-carboxylate** (**3.31**) (19 mg, 0.059 mmol), 2 M NaOH (0.5 mL) was added. The vial was sealed with a plastic cap and allowed to stir at 140 °C for 5 minutes. Upon cooling to room temperature, concentrated HCl (2 mL) was added, and the mixture was again heated to 140 °C. After heating for 15 minutes, the solvent was removed under air flow at 140 °C and the concentrated residue was allowed to cool to room temperature. The mixture was taken up in water and loaded onto a Biotage™ SNAP Ultra C18 column, then eluted with water to separate the compound of interest from NaCl. Once the fractions containing the amino acid were collected and concentrated, coeluted phthalic acid was removed by trituration with ether (3x5 mL). The remaining solid was freed of residual water and ether *in vacuo*. White solid, 10.4 mg, 0.052 mmol, 88% yield.

Alternatively, to a scintillation vial open to air containing a stir bar and **ethyl (1*r*,3*R*,4*S*)-1-(1,3-dioxoisoindolin-2-yl)-3,4-difluorocyclopentane-1-carboxylate** (**3.31**) (21 mg, 0.065 mmol), concentrated HCl was added and the mixture was heated to 100 °C for 16 hours. During this time, colorless crystals deposited along the bottom of the scintillation vial. The reaction mixture was decanted away from the crystalline material, and the crystals were triturated with ether (3x5 mL). Colorless crystals, 4.5 mg, 0.022 mmol, 34% yield.

Another method for the deprotection of **3.33** is effected with hydrazine and n-bromosuccinimide (NBS). To a scintillation vial open to air containing a stir bar and **ethyl (1*r*,3*R*,4*S*)-1-(1,3-dioxoisoindolin-2-yl)-3,4-difluorocyclopentane-1-carboxylate** (**3.31**) (5 mg, 0.015 mmol), hydrazine (0.5 mL) and water (0.5 mL) were added. The vial was stirred and heated to 75 °C for 10 minutes, then the hydrazine and water were removed under air flow. 1M aqueous HCl (1 mL) was added, followed by NBS (27 mg, 0.15 mmol), and the reaction was heated to 75 °C for another 10 minutes. The solvent was evaporated under air flow. The crude reaction mixture was analyzed by ^{1}H NMR in D_2O, which indicated the formation of the desired amino acid product. ^{1}H NMR (400 MHz, Deuterium Oxide) δ 5.38 – 5.17 (m, 2H), 2.73 (ddd, J = 22.9, 15.6, 5.3 Hz, 2H), 2.36 (tt, J = 17.4, 4.5 Hz, 2H). ^{13}C NMR (125 MHz, Deuterium Oxide) δ 173.7, 92.2 (dd, J = 184.9, 15.7 Hz), 60.5, 37.8 – 37.5 (four-line multiplet, magnetic inequivalence). ^{19}F NMR (282 MHz, Deuterium Oxide, trifluoroacetic acid reference standard) δ -199.4 – -199.9 (m). IR (neat, cm^{-1}): 3045 (broad), 1718. HRMS (ESI) Calcd. for $C_6H_{10}O_2NF_2$ $(M+H)^+$: 166.06741. Found: 166.06740. Melting point: 251-252 °C (decomposes: effervesces and takes on brown color).

Radiochemistry

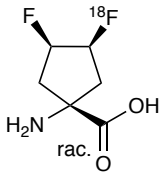

anti-cis-3,4-[^{18}F]-DFACPC (**[^{18}F]3.09**). The preparation of **[^{18}F]3.09** was based on the previously reported automated synthesis of anti-[^{18}F]FACBC. To a glass vessel containing a solution of Cryptand 222 in MeCN (5.0 mg/mL) (1.0 mL) was added 790 mCi of no-carrier-added [^{18}F]HF through a trap/release (T/R) cartridge by using a solution of K_2CO_3/H_2O (1.5 mg/mL) (0.6 mL). The solvent was removed at 110 °C with a nitrogen flow, and additional MeCN (3.5 mL) was added followed by evaporation of the solvent with a nitrogen flow to remove residual H_2O. Triflate precursor **3.19** (9 mg, 0.021 mmol) in dry MeCN (1 mL) was added to the vial, and the reaction mixture was heated at 110 °C for 10 min. The intermediate product was treated with 6 N HCl (0.5 mL) at 110 °C for 10 min and purified by passing through an IR column assembly consisting of a 7 mm x 120 mm bed of AG 11A8 IR resin column, a neutral alumina SepPak (preconditioned with water), and an HLB Oasis reverse phase cartridge (preconditioned with water). **[^{18}F]3.09** eluted in series through the assembly with three successive portions of sterile saline (~4.0 mL), into dose vials and was ready for in vitro and in vivo studies. Evidence of the identity of **[^{18}F]3.09** was achieved by comparing the R_f of the radioactive product visualized with radiometric TLC with the R_f of the authentic cold compound visualized with ninhydrin stain, using the solvent system $MeCN/H_2O/CH_3OH$ = 2:1:1 (R_f = 0.6, Whatman silica gel plates). The only peak present on radiometric TLC analysis corresponded to **[^{18}F]3.09**, and the radiochemical purity of the product exceeded 99% (see Figure S3-41). The pH of the final dose solution was tested with pH paper and found to be 6-7. The isolated radiochemical yield was 50 mCi in 12 mL of saline as determined

using a dose calibrator, affording a 10% decay corrected radiochemical yield based on a synthesis time of approximately 70 minutes, which proceeded immediately upon the end of cyclotron bombardment.

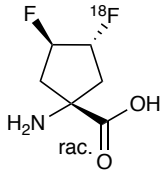

Racemic **trans-3,4-[^{18}F]-DFACPC** (**[^{18}F]3.23**). The preparation of racemic **[^{18}F]3.23** was based on the previously reported automated synthesis of anti-[^{18}F]FACBC. To a glass vessel containing a solution of Cryptand 222 in MeCN (22 mg/mL) (1.0 mL) was added 1460 mCi of no-carrier-added [^{18}F]HF through a trap/release (T/R) cartridge by using a solution of Cs_2CO_3/H_2O (20 mg mg/mL) (0.6 mL). The solvent was removed at 110 °C with a nitrogen flow, and additional MeCN (3.5 mL) was added followed by evaporation of the solvent with a nitrogen flow to remove residual H_2O. Racemic triflate precursor **3.21** (20 mg, 0.047 mmol) in dry *t*BuOH (0.5 mL) and MeCN (0.5 mL) was added to the vial, and the reaction mixture was heated at 110 °C for 10 min. The intermediate product was treated with 6 N HCl (0.5 mL) at 110 °C for 10 min and purified by passing through an IR column assembly consisting of a 7 mm x 120 mm bed of AG 11A8 IR resin, two neutral alumina SepPaks (preconditioned with water) and an HLB Oasis reverse phase cartridge (preconditioned with water). Racemic **[^{18}F]3.23** eluted in series through the assembly with three successive portions of sterile saline (~4.0 mL), into dose vials and was ready for in vitro and in vivo studies. Based on analytical chiral HPLC data comparing the dose solution with authentic **3.23**, **[^{18}F]3.23** was obtained in > 99% radiochemical purity (see Figure S3-42). The pH of the final dose solution was tested with pH paper and found to be 6-7. The isolated radiochemical

yield was 12 mCi in 7 mL of saline as determined using a dose calibrator, affording a 1.3% decay corrected radiochemical yield based on a synthesis time of approximately 83 minutes, which proceeded immediately upon the end of cyclotron bombardment.

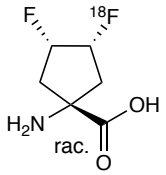

syn-cis-3,4-[^{18}F]-DFACPC (**[^{18}F]3.33**). The preparation of **[^{18}F]3.33** was based on the previously reported automated synthesis of anti-[^{18}F]FACBC. To a glass vessel containing a solution of Cryptand 222 in MeCN (22 mg/mL) (1.0 mL) was added 1460 mCi of no-carrier-added [^{18}F]HF through a trap/release (T/R) cartridge by using a solution of Cs_2CO_3/H_2O (20 mg mg/mL) (0.6 mL). The solvent was removed at 110 °C with a nitrogen flow, and additional MeCN (3.5 mL) was added followed by evaporation of the solvent with a nitrogen flow to remove residual H_2O. Triflate precursor **3.30** (20 mg, 0.044 mmol) in dry *t*BuOH (0.5 mL) and MeCN (0.5 mL) was added to the vial, and the reaction mixture was heated at 110 °C for 10 min. The reaction mixture was diluted with 2 mL of acetonitrile, passed through two neutral alumina SepPaks (preconditioned with acetonitrile), and eluted with 10 mL of acetonitrile into a vented vial in a hot cell. The solvent was removed from the vial under a flow of nitrogen at 140 °C. 0.5 mL of 2M NaOH was added to the vial which was sealed with a Teflon septum capped with an aluminum crimp top, and the mixture was heated to 140 °C for 5 minutes. The vial was cooled and 2 mL of concentrated HCl was added, and the sealed vial was again heated for 15 minutes at 140 °C. Then vial was vented, and the solvent was removed under inert gas flow at 140 °C. The resultant solid was taken up in H_2O (5 mL) and cannulated through a chain composed of one Waters HLB Oasis cartridge and two alumina SepPaks (both preconditioned with water). A second aliquot of water

(5 mL) was passed through the chain, and the eluent containing **[^{18}F]3.33** was collected in a dose vial. The contents of the dose solution were assessed by analytical HPLC, utilizing **[^{18}F]3.23** as a reference (see Figure S3-43). HPLC analysis indicated that **[^{18}F]3.33** was obtained in > 99% radiochemical purity. The pH of the final dose solution was tested with pH paper and found to be 6-7. The isolated radiochemical yield was 8.4 mCi in 5 mL of water as determined using a dose calibrator, affording a 1.7% decay corrected radiochemical yield based on a synthesis time of approximately 135 minutes, which proceeded 35 minutes after the end of cyclotron bombardment (total time from end of bombardment to measurement of radiochemical yield was 170 minutes).

Cells and culture

The cancer cells used in the study include 9L gliosarcoma (rat), DU145 androgen-independent prostate carcinoma (human), and U87 glioblastoma tumor cell lines (human). Cells were cultured as described previously.[52] The tumor cells were cultured in Dulbecco's Modified Eagle's Medium (DMEM) supplemented with 10% fetal calf serum, 100 U/mL penicillin and 100 μg/mL streptomycin, maintained in T-150 tissue culture flasks under humidified incubator conditions (37 °C, 5% CO_2/95% air) and were routinely passaged at confluence.[53] Cells thus prepared would be used in cell uptake and inhibition assays and in mice tumor implantations.

Amino acid uptake and inhibition

Amino acid uptake and inhibition experiments were performed as described previously.[52] At the time of the experiments, the medium was exchanged to amino acid free Hank's balanced salt solution (HBSS) and cells were adjusted to a final concentration of 5×10^7 cells/mL. The following standard condition applied to each study (refer to Supplementary Data for optimization

information). Approximately 5×10^5 cells were exposed to 5 μCi of **[^{18}F]3.09**, **[^{18}F]3.23**, and **[^{18}F]3.33** respectively, in 0.1 mL of amino acid/serum-free HBSS in the absence (control condition) or presence of transport inhibitors for 30 minutes under incubator conditions (37 °C, 5% CO_2/95% air) in 1.5 mL conical tubes. 10 mM final concentrations of MeAIB were used to inhibit uptake mediated by system A AATs. 10 mM final concentrations of 2-amino-bicyclo[2.2.1]heptane-2-carboxylic acid (BCH) were used to inhibit uptake mediated by system L AATs. The combination of 10 mM alanine-cysteine-serine (ACS, 3.3 mM of each amino acid) was used for uptake inhibition of system ACS AATs. After incubation, cells were twice centrifuged (75 G for 5 minutes) and rinsed with ice-cold HBSS to remove residual activity in the supernatant. Each assay condition was performed in triplicate. The activity in tubes was counted in a Packard Cobra II Auto-Gamma counter, the raw counts decay corrected, and the activity per cell number determined. The data from these studies were expressed and normalized as percent uptake of the initial dose per 0.5 million cells (% ID/5×10^5 cells) ± standard deviation (SD).

Tumor Induction and Animal Preparation

Rat 9L gliosarcoma cells for intracranial implantation experiments were cultured and prepared the same way as the uptake and inhibition assays and then were washed with phosphate buffer solution (PBS) and were made a final concentration of 5 x 10^4/5 μL in PBS. Rat 9L gliosarcoma cells were implanted into the brains of male Fischer 344 rats (160-210 g) as described previously.[46a] Briefly, following anesthesia with an intramuscular injection of ketamine (60 mg/mL) and xylazine (7.5 mg/mL) solution, rats were placed in a stereotactic head holder and were injected with 5 μL suspension of rat 9L gliosarcoma cells (5 x 10^4 cells per rat) in a location 3 mm right of midline and 1 mm anterior to the bregma at 4 mm deep to the outer table. The injection was performed

over the course of 2 min, and the needle was withdrawn over the course of 1 min to minimize the backflow of tumor cells. The burr hole and scalp incision were closed, and the animals were returned to their original cages after recovering from the procedure. Intracranial tumors developed that produced weight loss, apathy, and hunched posture in the tumor-bearing rats. Typically, among 25 animals implanted with tumor cells, 20 would develop tumors visible to the naked eye upon dissection in approximately 10-12 days and were used in the study.[54]

Anesthesia

Anesthesis was carried out as described previously.[55] Rats were anesthetized using isoflurane gas. Anesthesia was initiated 10 minutes ahead of imaging experiments by placing the animal in a cage ventilated with oxygen containing 1-2% isoflurane. Body temperature was held at 37 ºC using a temperature-controlled warm air convection system.

Injection of the Radiotracer

The tracer was administered as described previously.[55] A catheter placed in the tail vein prior to imaging experiments was filled with isotonic sodium chloride solution. The racer was diluted with saline to a final volume of 0.4 mL and injected via the catheter.

Biodistribution Studies in Normal Male Fischer Rats (160-210 g) and Male Fischer Rats Bearing 9L Intracranial Tumors

The microPET imaging process was carried out as described previously.[55] The rats were injected through the tail vein catheter with 200 – 250 μCi of **[^{18}F]3.09**, **[^{18}F]3.23**, or **[^{18}F]3.33** in 0.4 mL of isotonic saline (pH = 6-7). PET Imaging MicroPET data was acquired with a Siemens Inveon

PET/CT system (Siemens Medical Solutions, Knoxville, TN, USA). After anesthesia and placement of the tail vein catheter, the animal was placed with its body located at the center of the field of view. Radioactivity in the syringe was measured before and after the tracer was injected into the tail vein catheter using a Capintec CRC 15R (Capintec Inc, 6 Arrow Road Ramsey, NJ) dose calibrator. Data acquisition was performed for 60 minutes starting immediately following tracer injection. The emission data were normalized and corrected for decay and dead time. The images were reconstructed using an attenuation correction with a cobalt source into fifteen 1 minute frames followed by nine 5 minute frames. The image volume consisted of 128 x 128 x 159 voxels, each of a size of 0.78 x 0.78 x 0.80 mm. After PET imaging, all animals underwent CT scan in the same position as the acquired PET data. Data Processing and Co-Registration MicroPET data and CT data were co-registered using ASIPro. The CT template was used for definition of regions-of-interest (ROIs). The regions of interest were drawn around the tumor in the right hemisphere of the brain and compared to the symmetrical contralateral region in the left hemisphere. The time-activity curves represent the mean activity in the regions-of-interest over time.

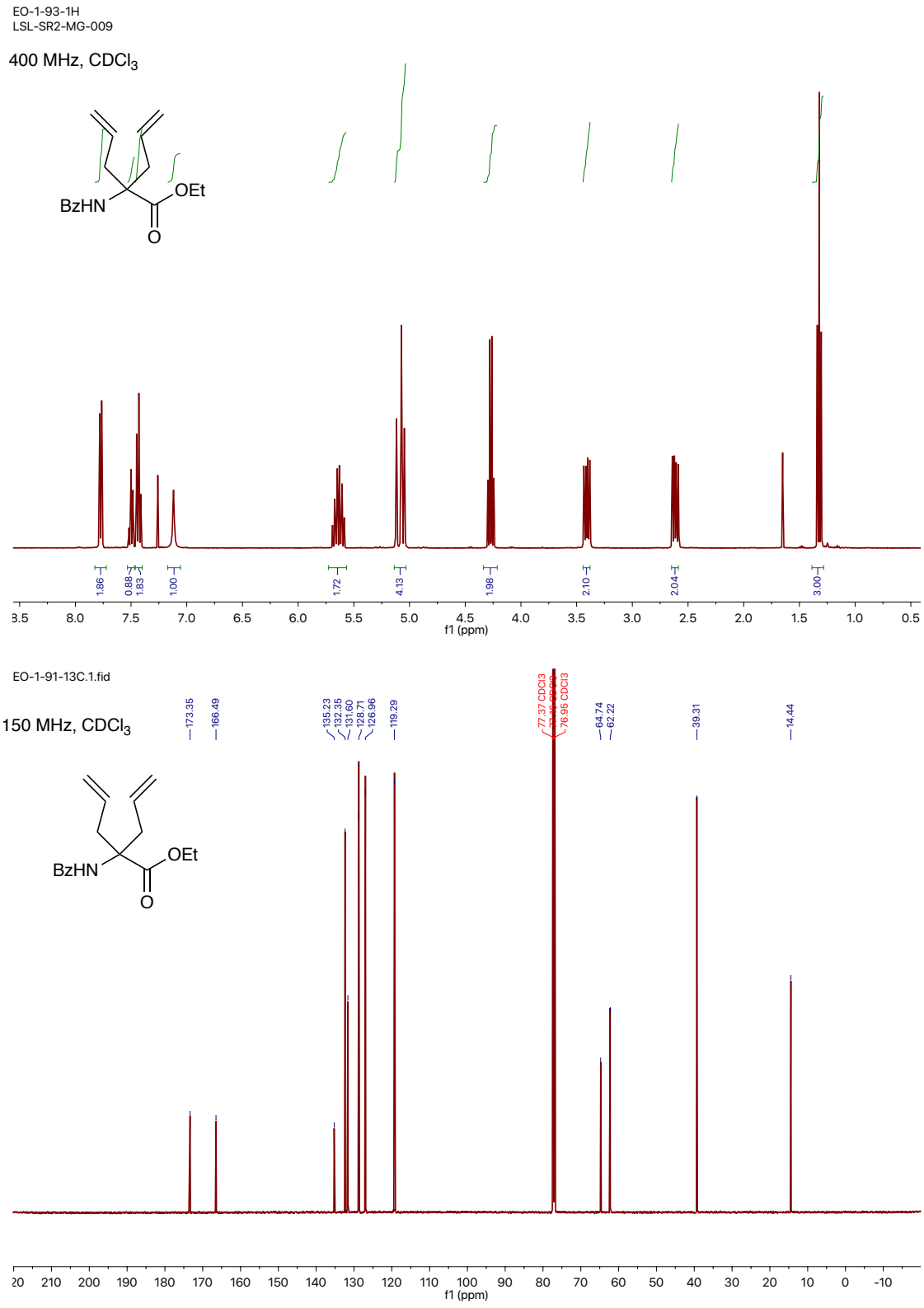

Figure S3-1. ^{1}H NMR (top) and ^{13}C NMR (bottom) of **3.03**.

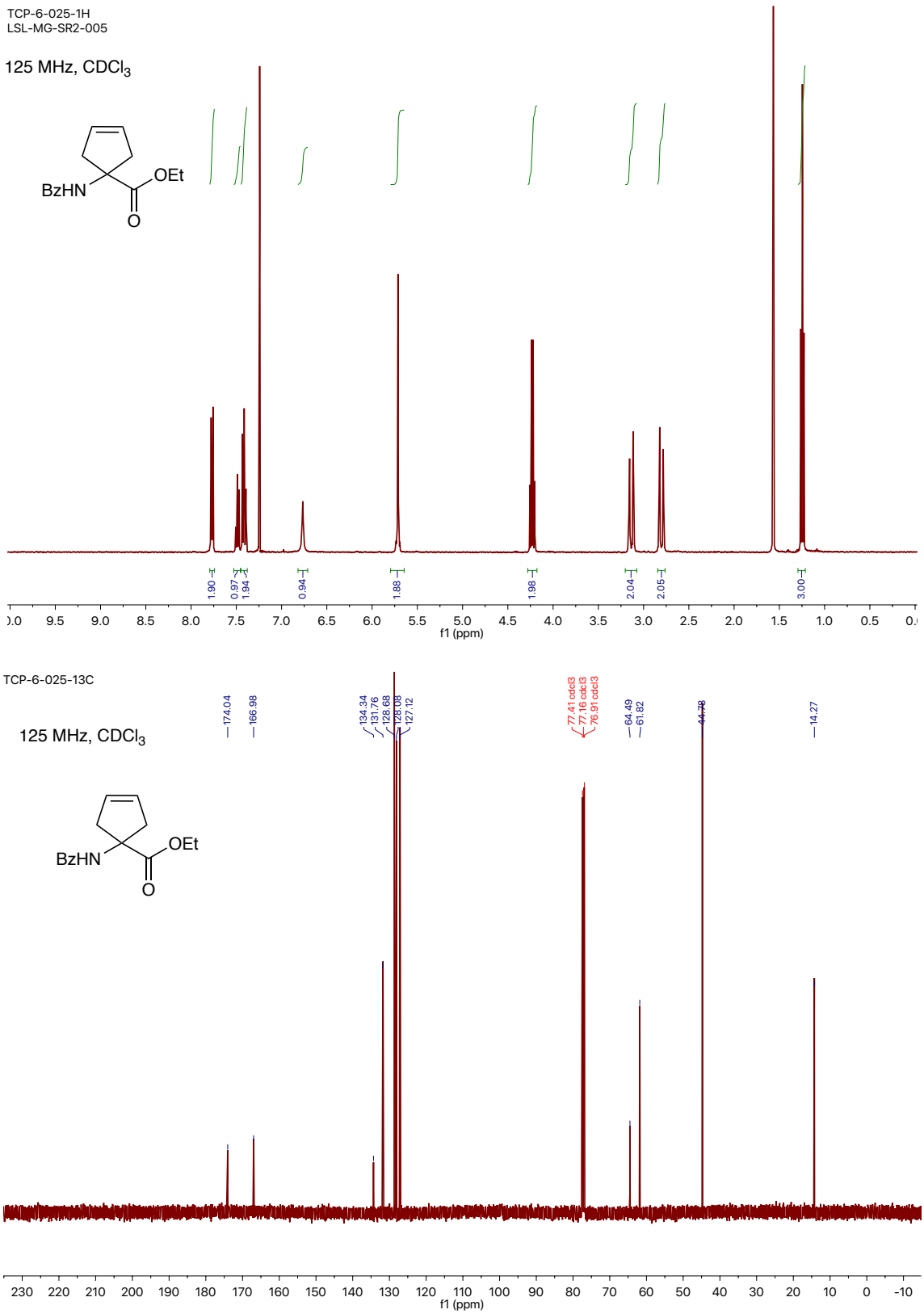

Figure S3-2. ^{1}H NMR (top) and ^{13}C NMR (bottom) of **3.04**.

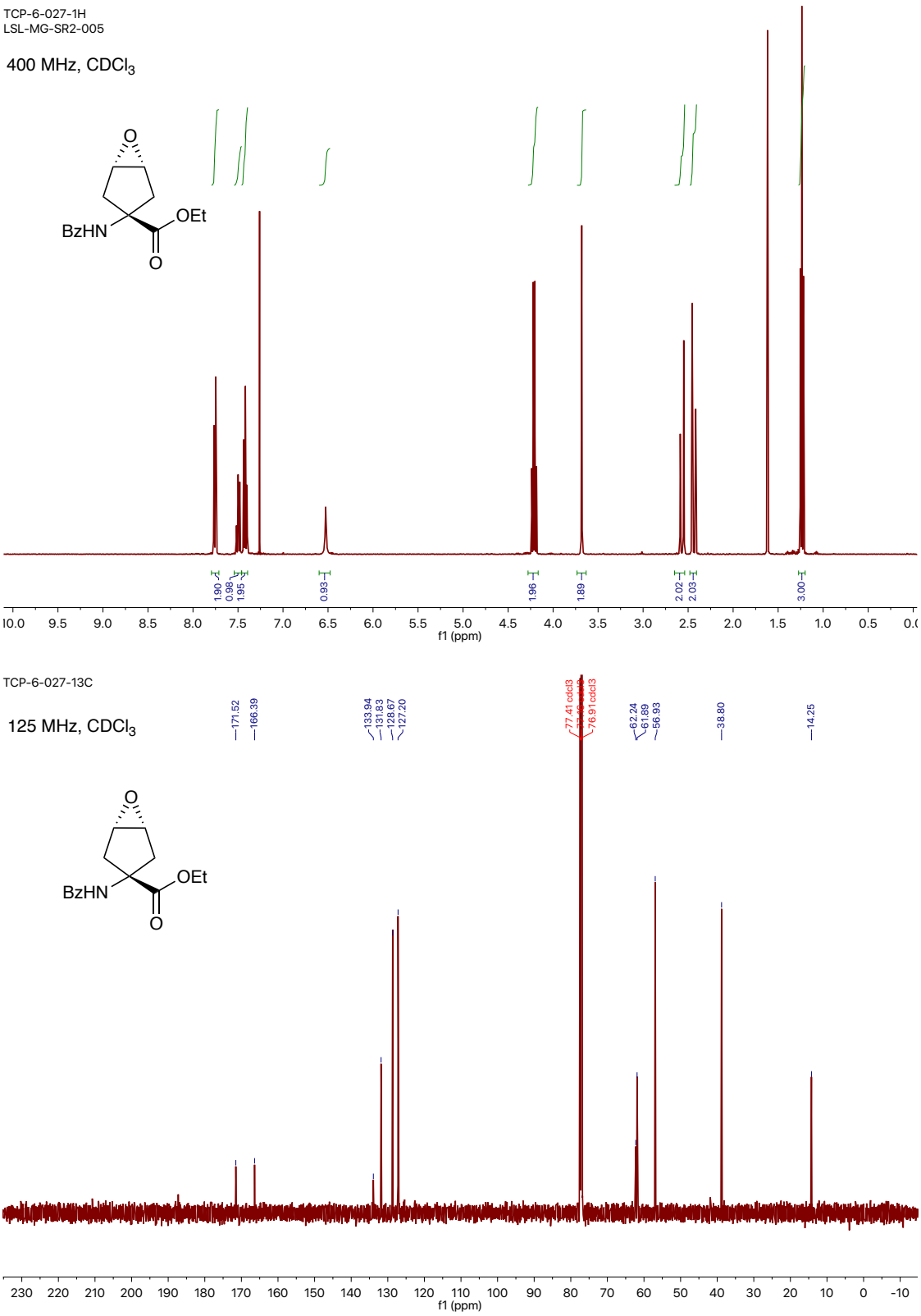

Figure S3-3. ^{1}H NMR (top) and ^{13}C NMR (bottom) of **3.05**.

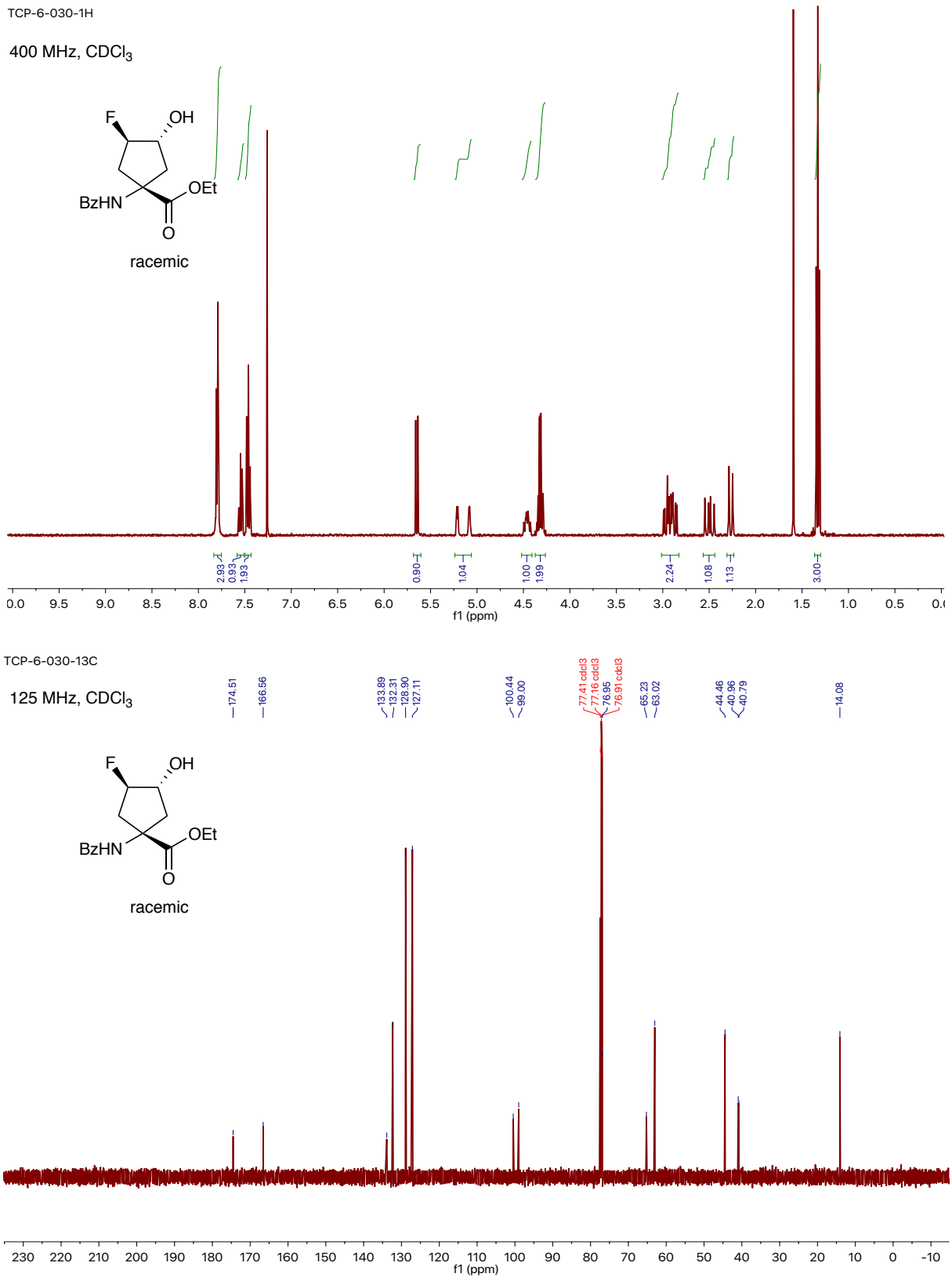

Figure S3-4. ^{1}H NMR (top) and ^{13}C NMR (bottom) of **3.06**.

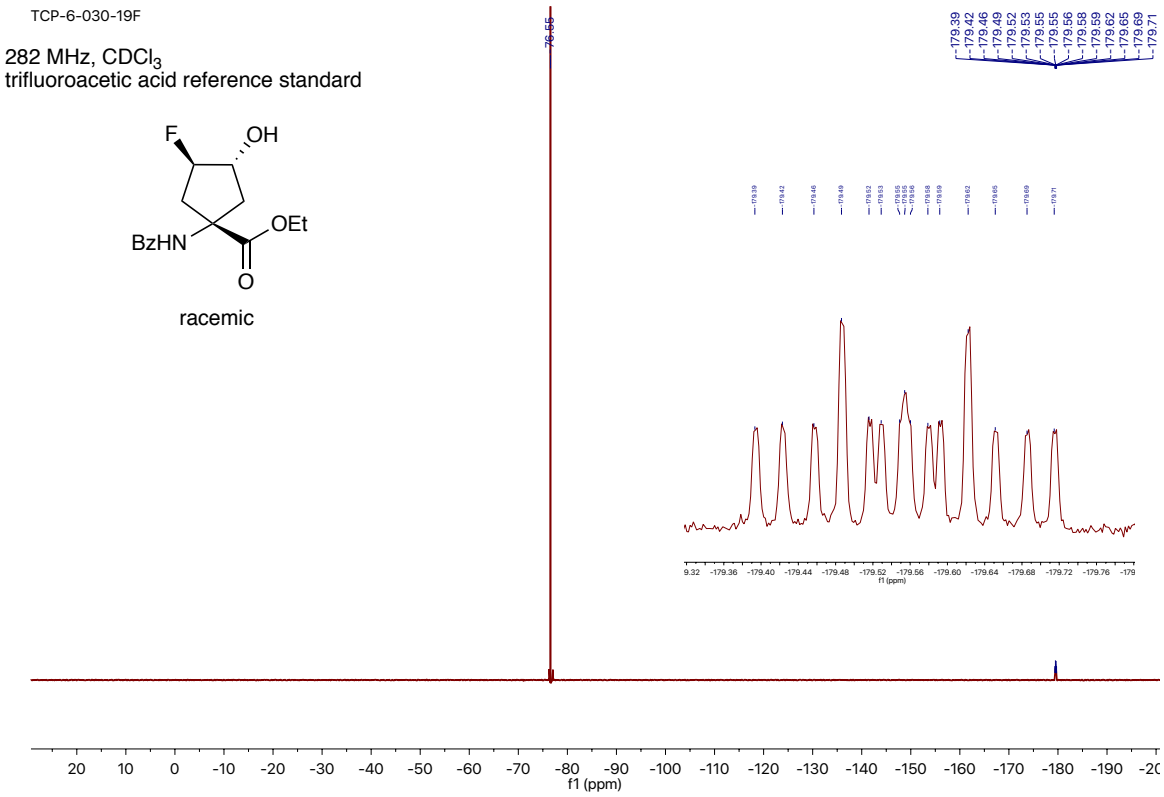

Figure S3-5. ^{19}F NMR of **3.06**.

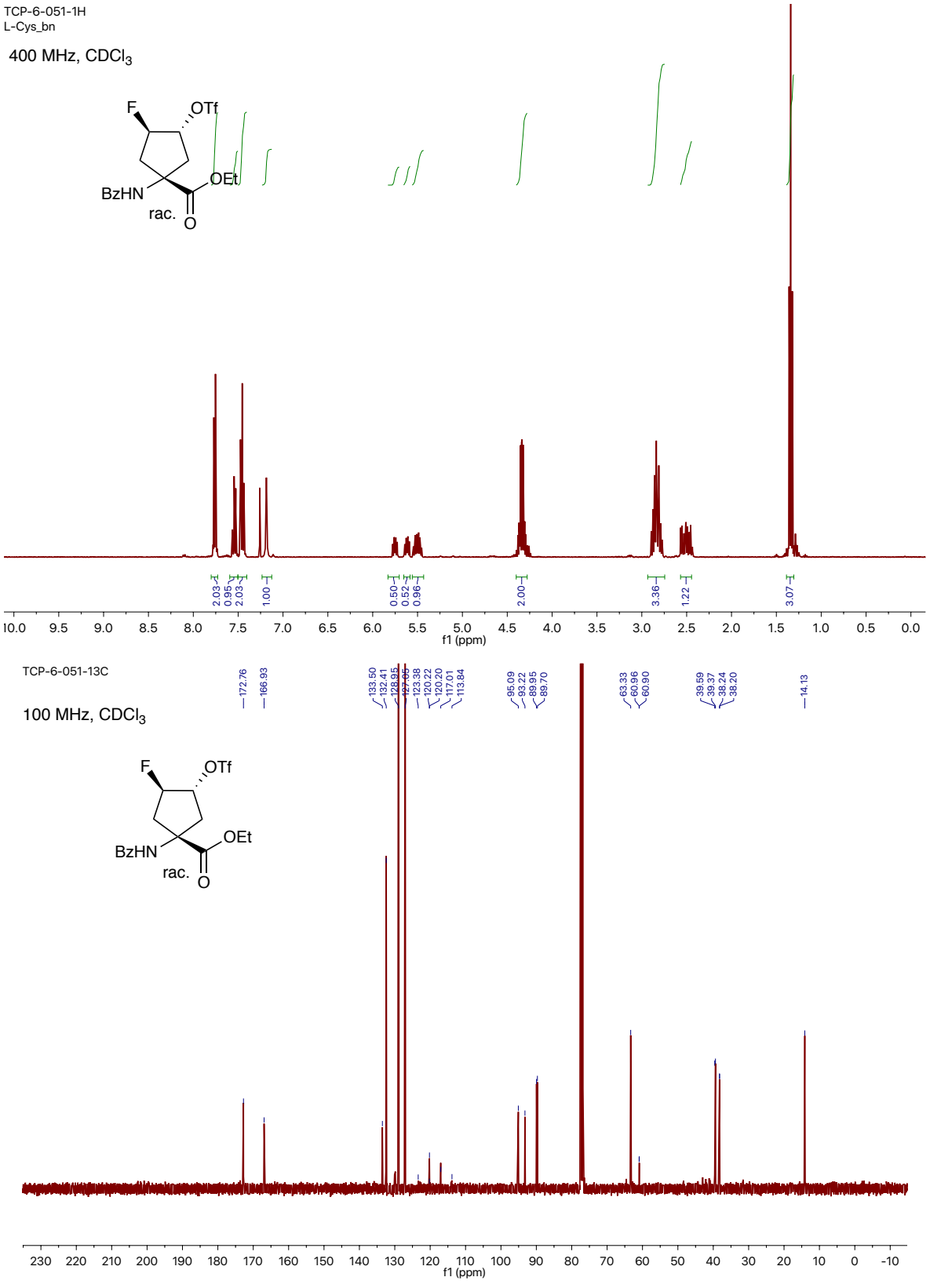

Figure S3-6. ^{1}H NMR (top) and ^{13}C NMR (bottom) of **3.07**.

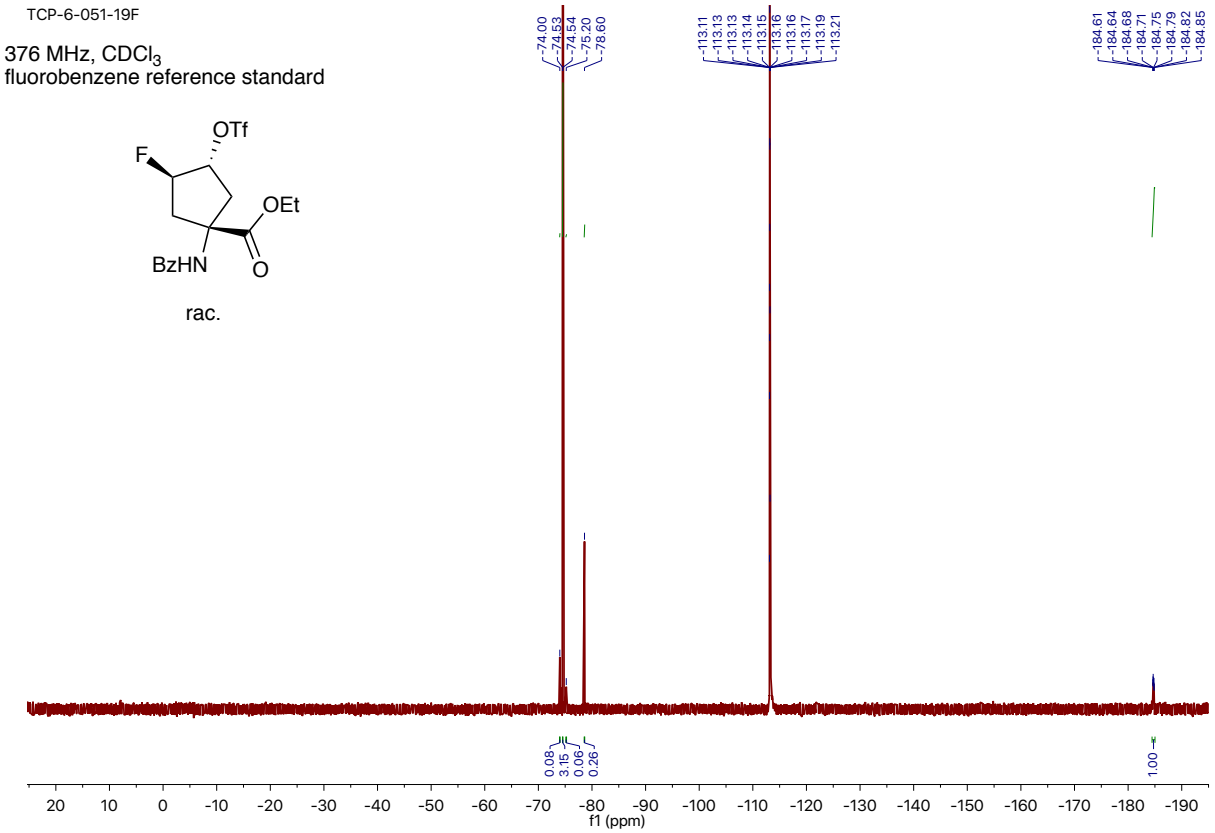

Figure S3-7. ^{19}F NMR of **3.07**.

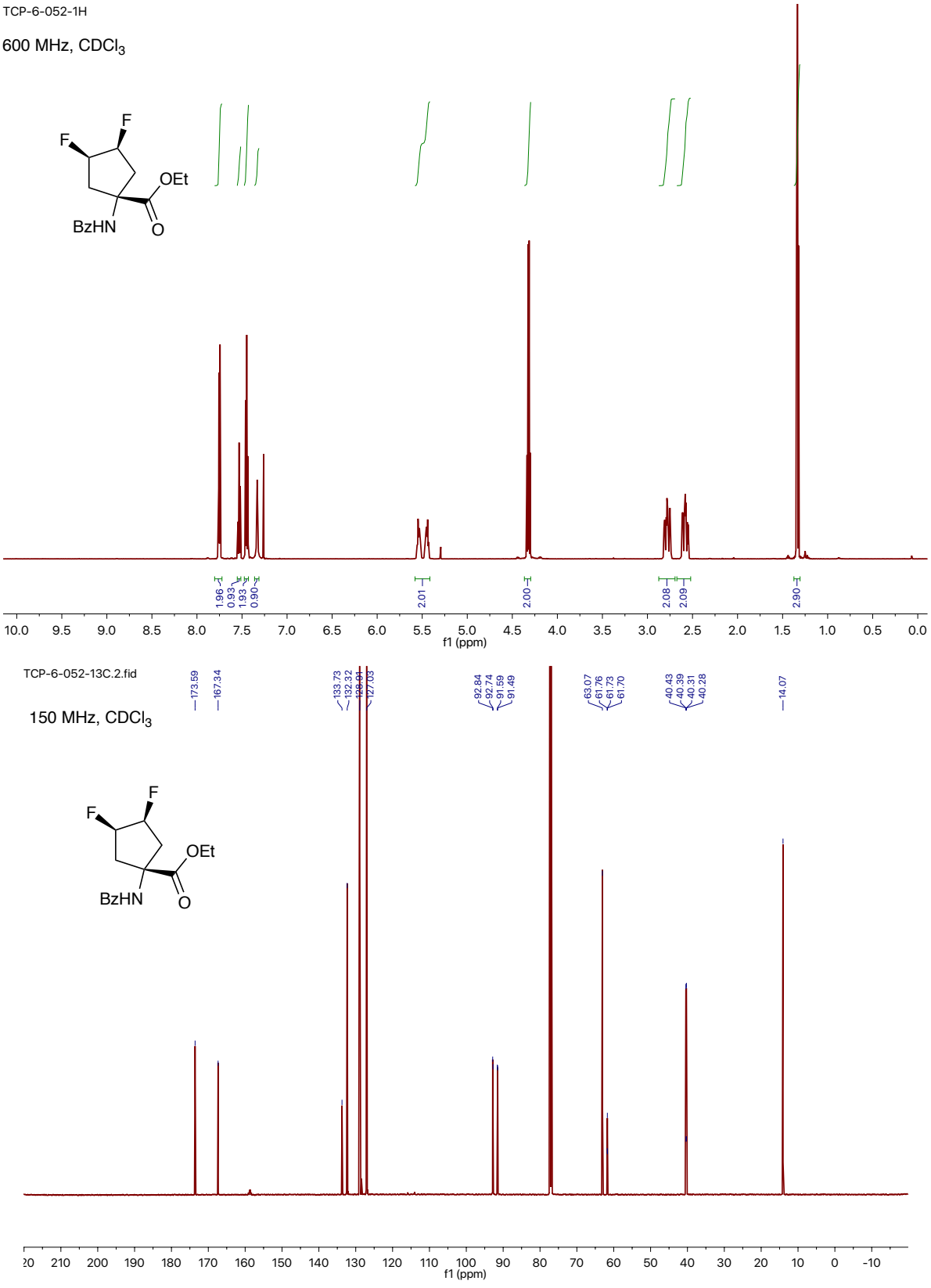

Figure S3-8. ^{1}H NMR (top) and ^{13}C NMR (bottom) of **3.08**.

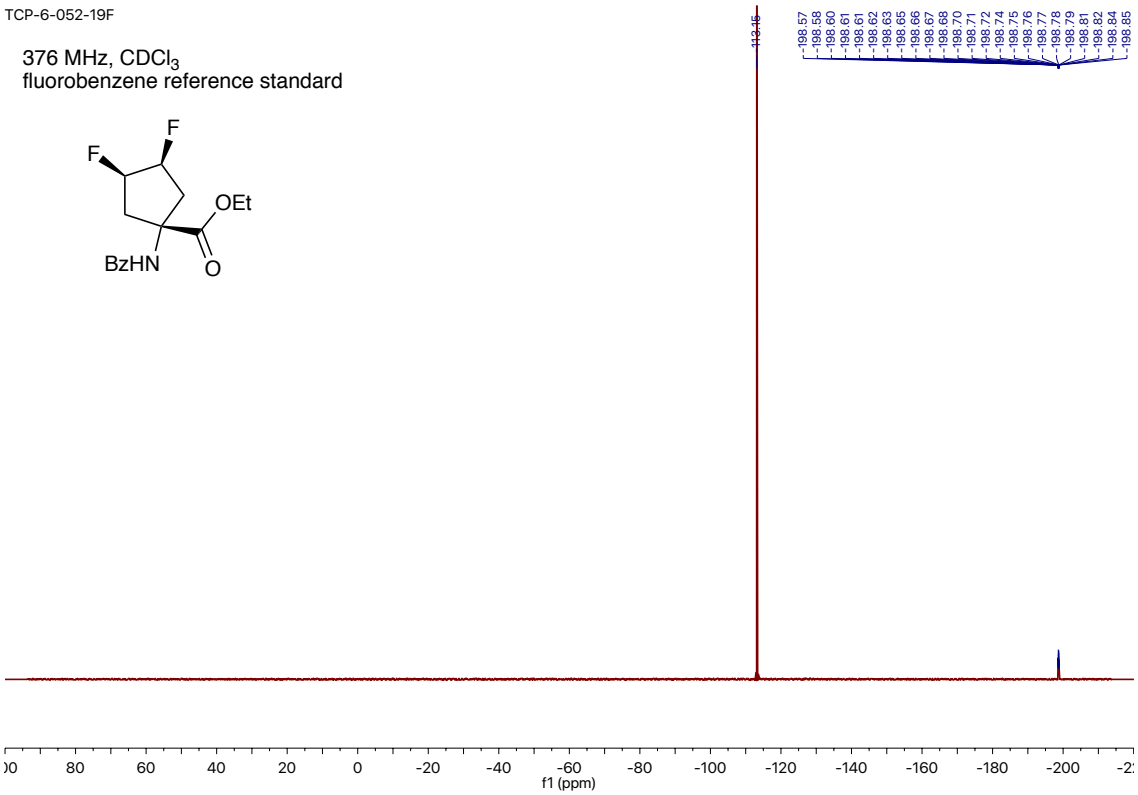

Figure S3-9. ^{19}F NMR of **3.08**.

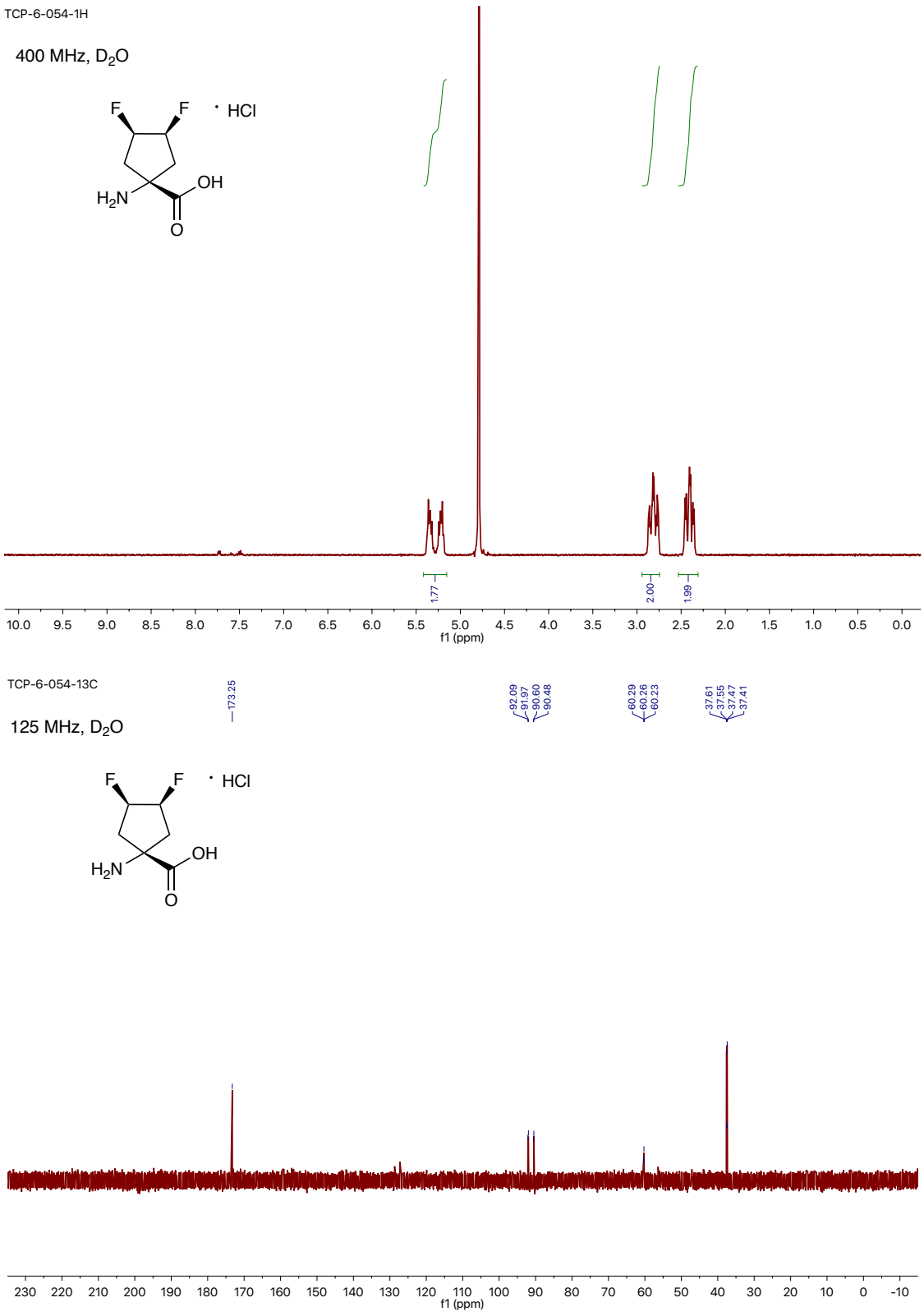

Figure S3-10 ^{1}H NMR (top) and ^{13}C NMR (bottom) of **3.09**.

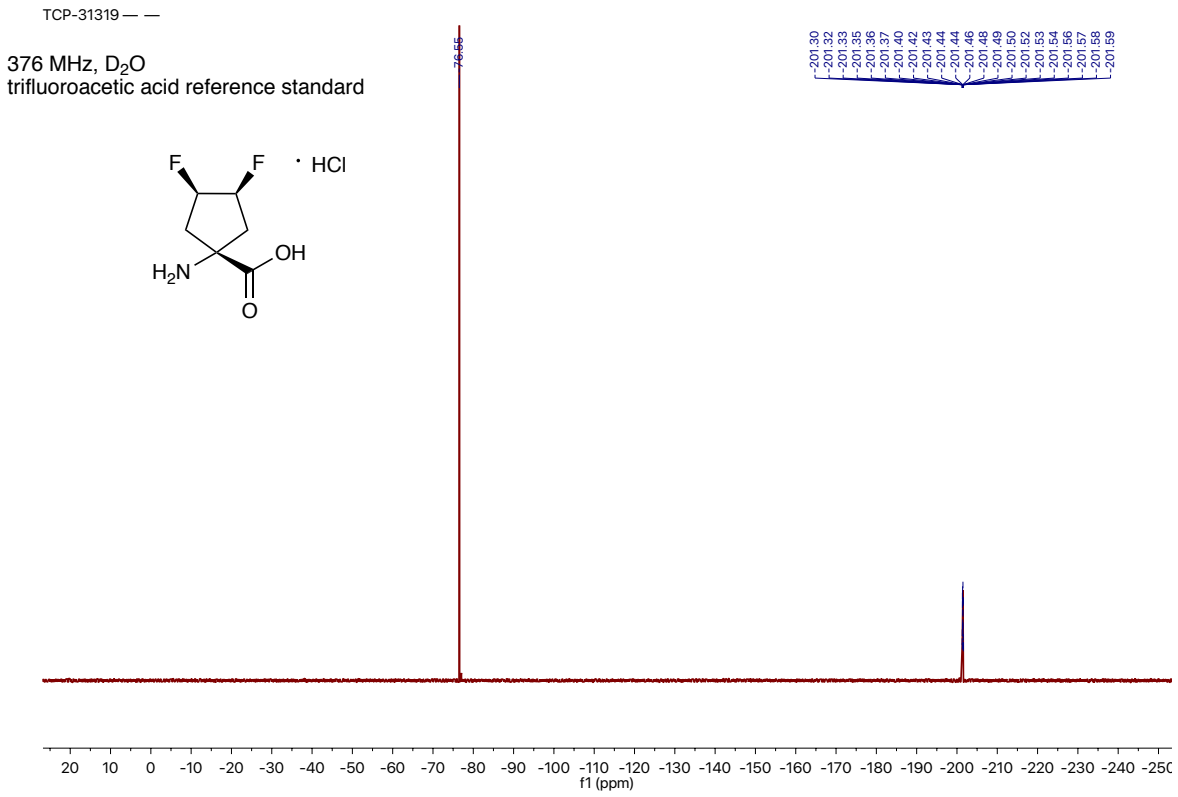

Figure S3-11. ^{19}F NMR of **3.09**.

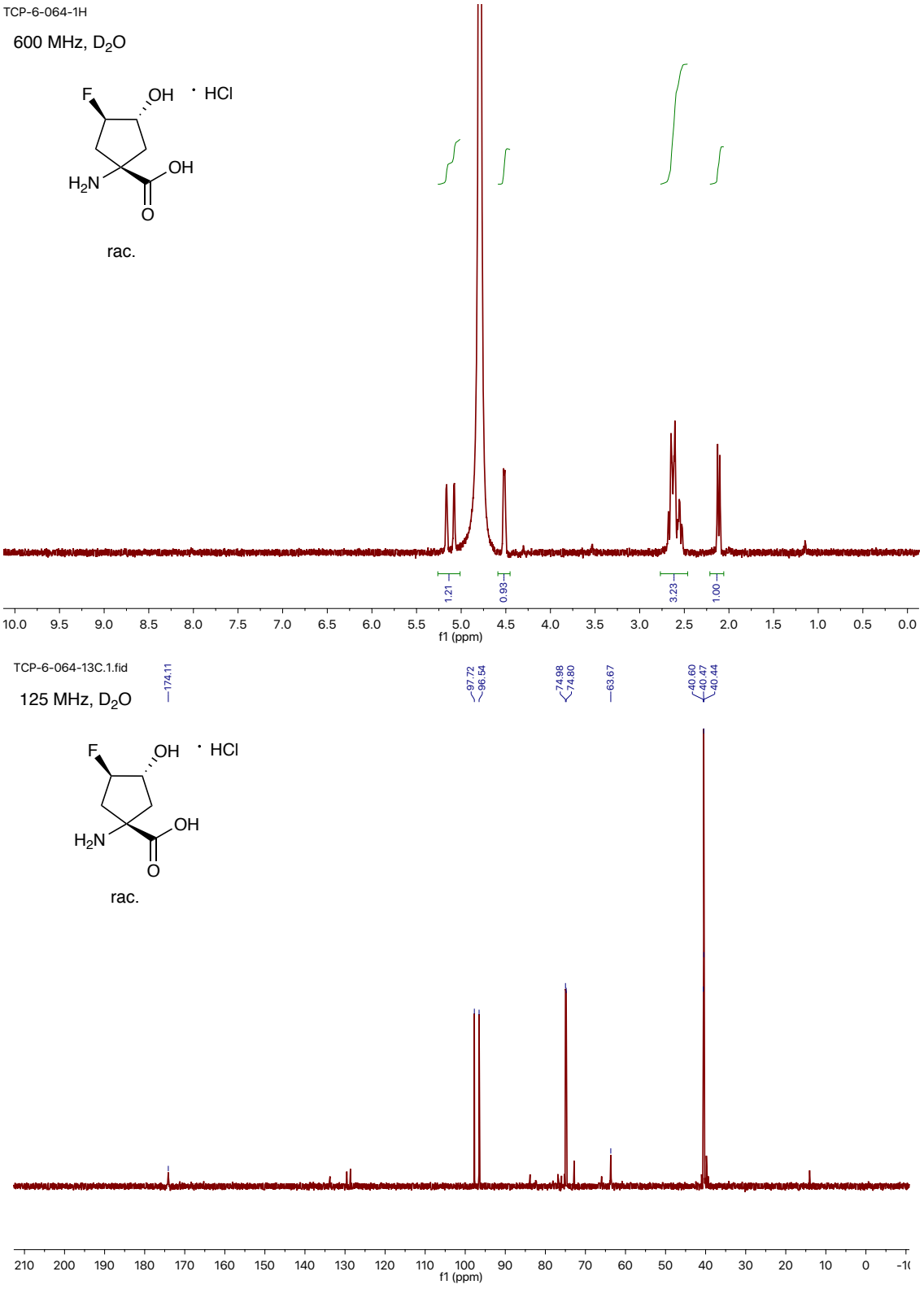

Figure S3-12. ^{1}H NMR (top) and ^{13}C NMR (bottom) of crude **3.10**.

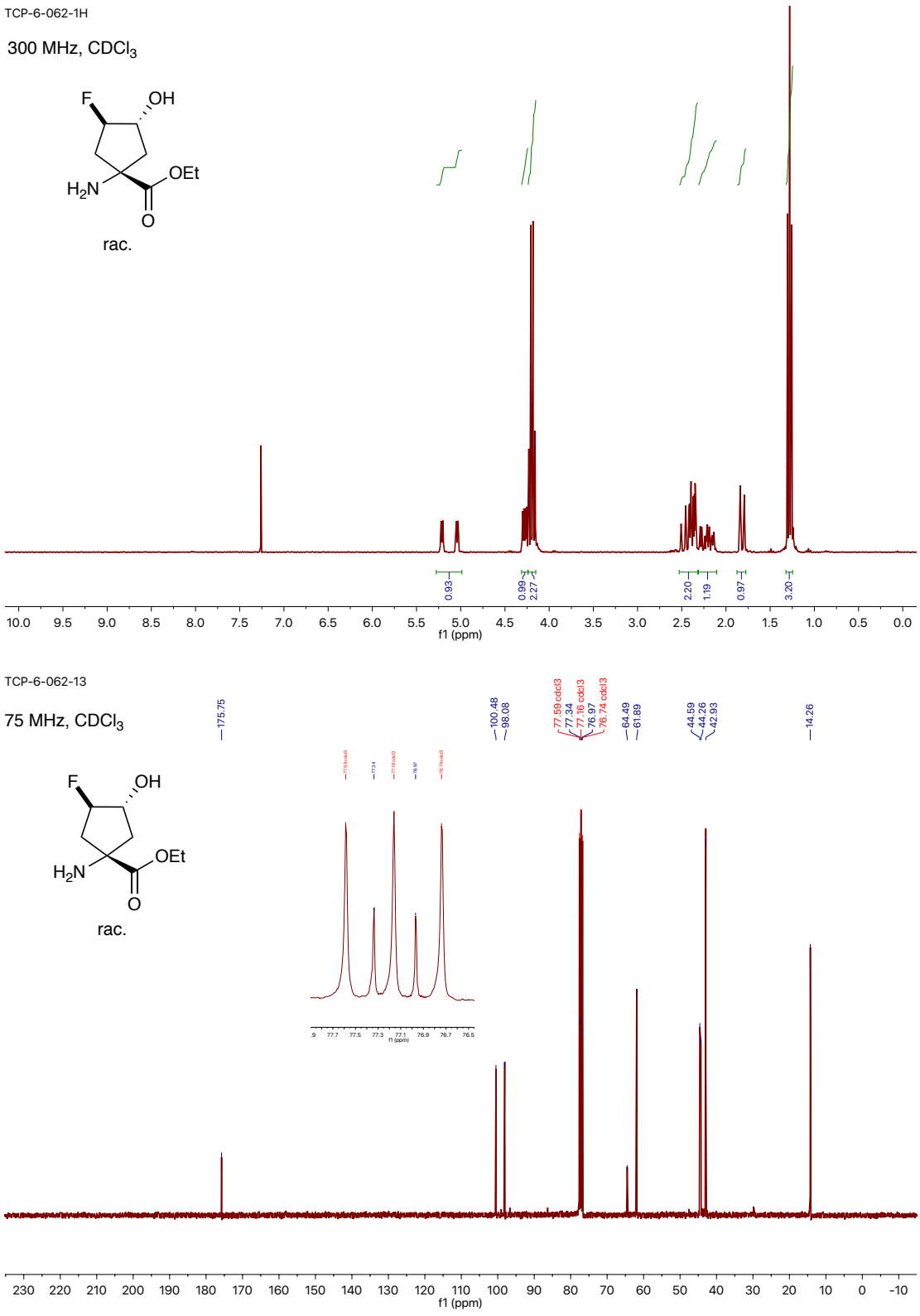

Figure S3-13. ^{1}H NMR (top) and ^{13}C NMR (bottom) of crude **3.11**.

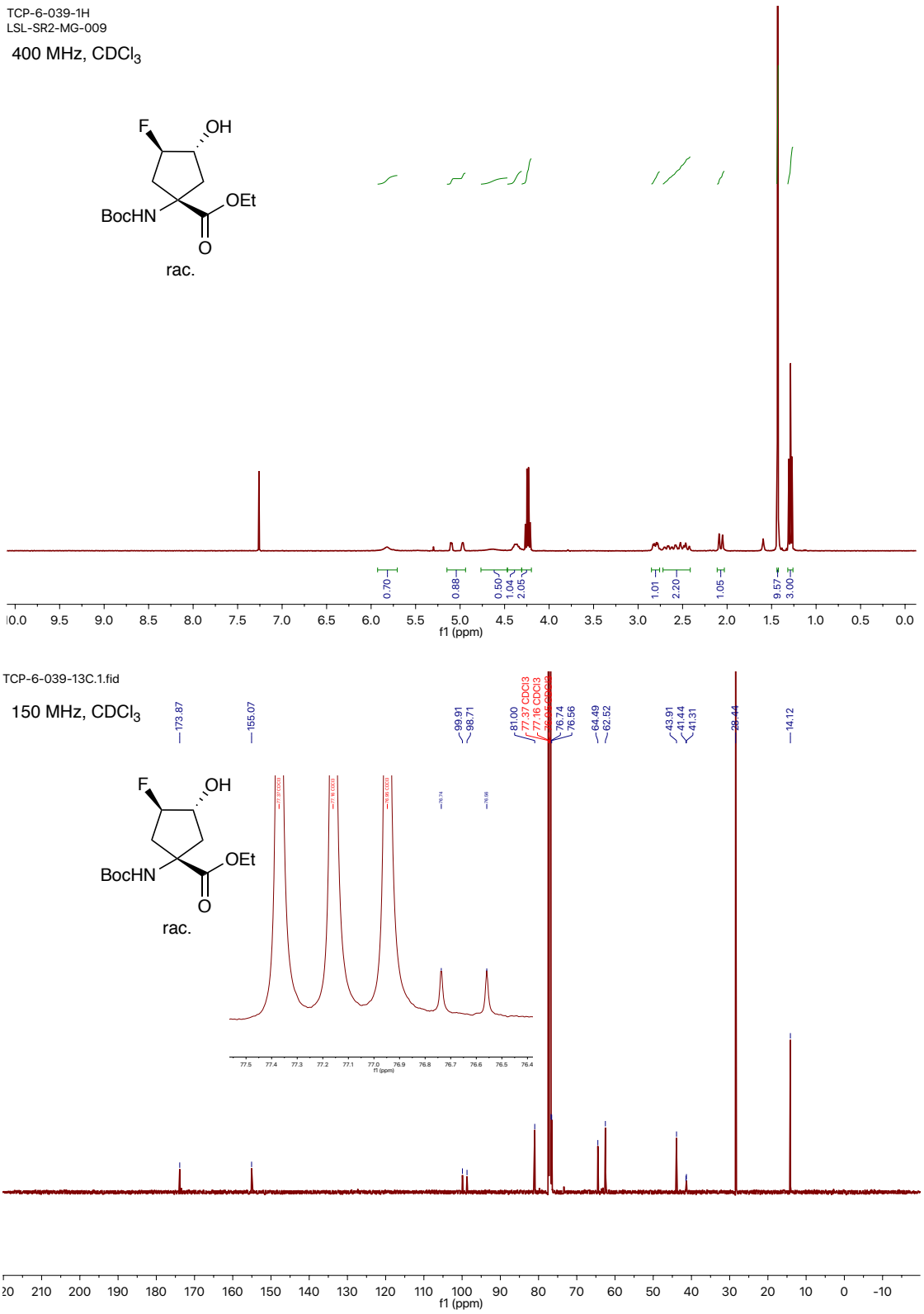

Figure S3-14. ^{1}H NMR (top) and ^{13}C NMR (bottom) of **3.12**.

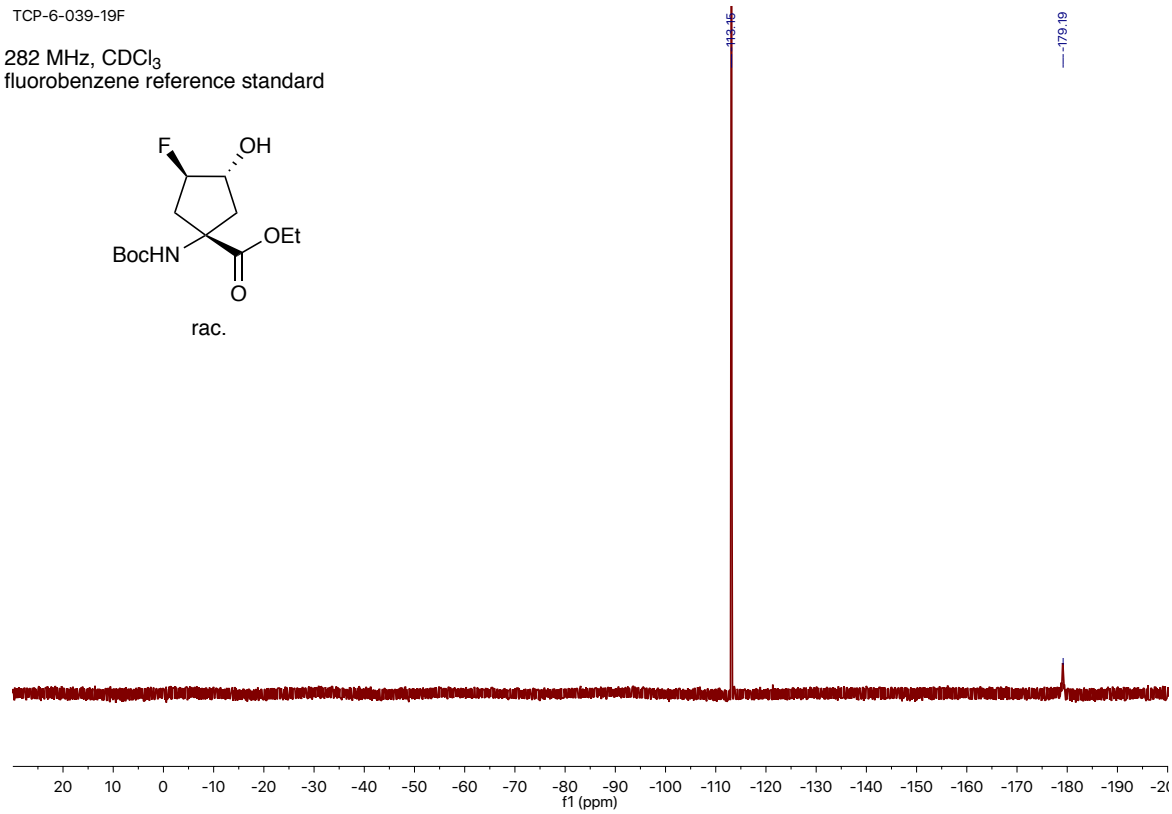

Figure S3-15. ^{19}F NMR of **3.12**.

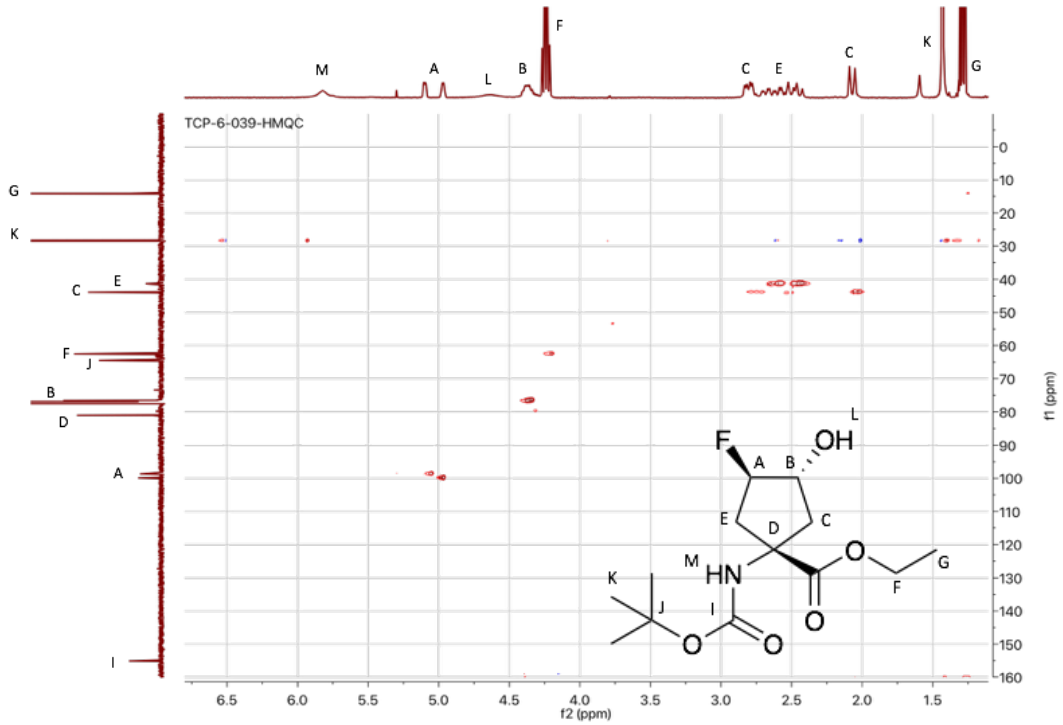

Figure S3-16. HMQC of **3.12**.

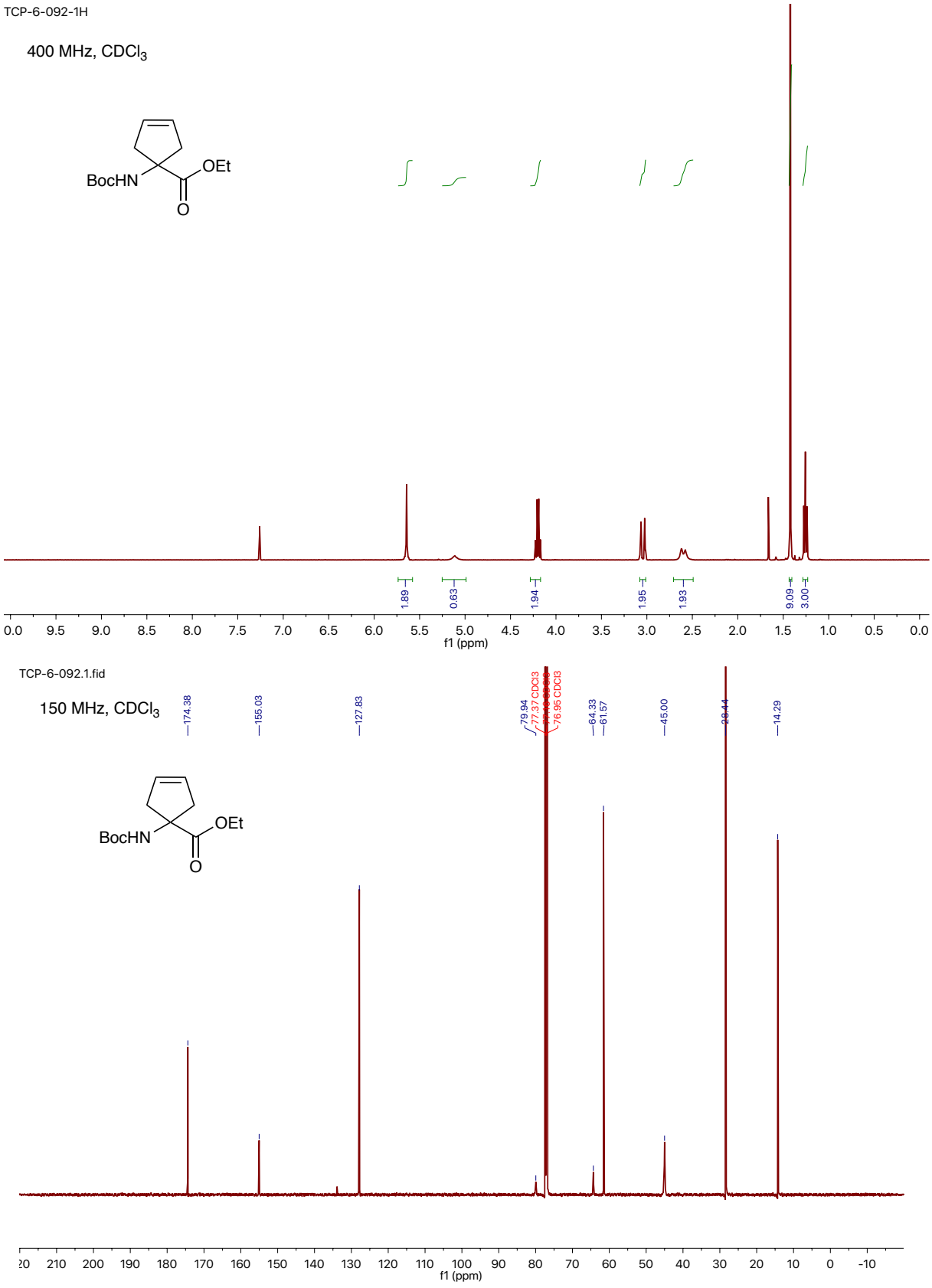

Figure S3-17. ^{1}H NMR (top) and ^{13}C NMR (bottom) of **3.16**.

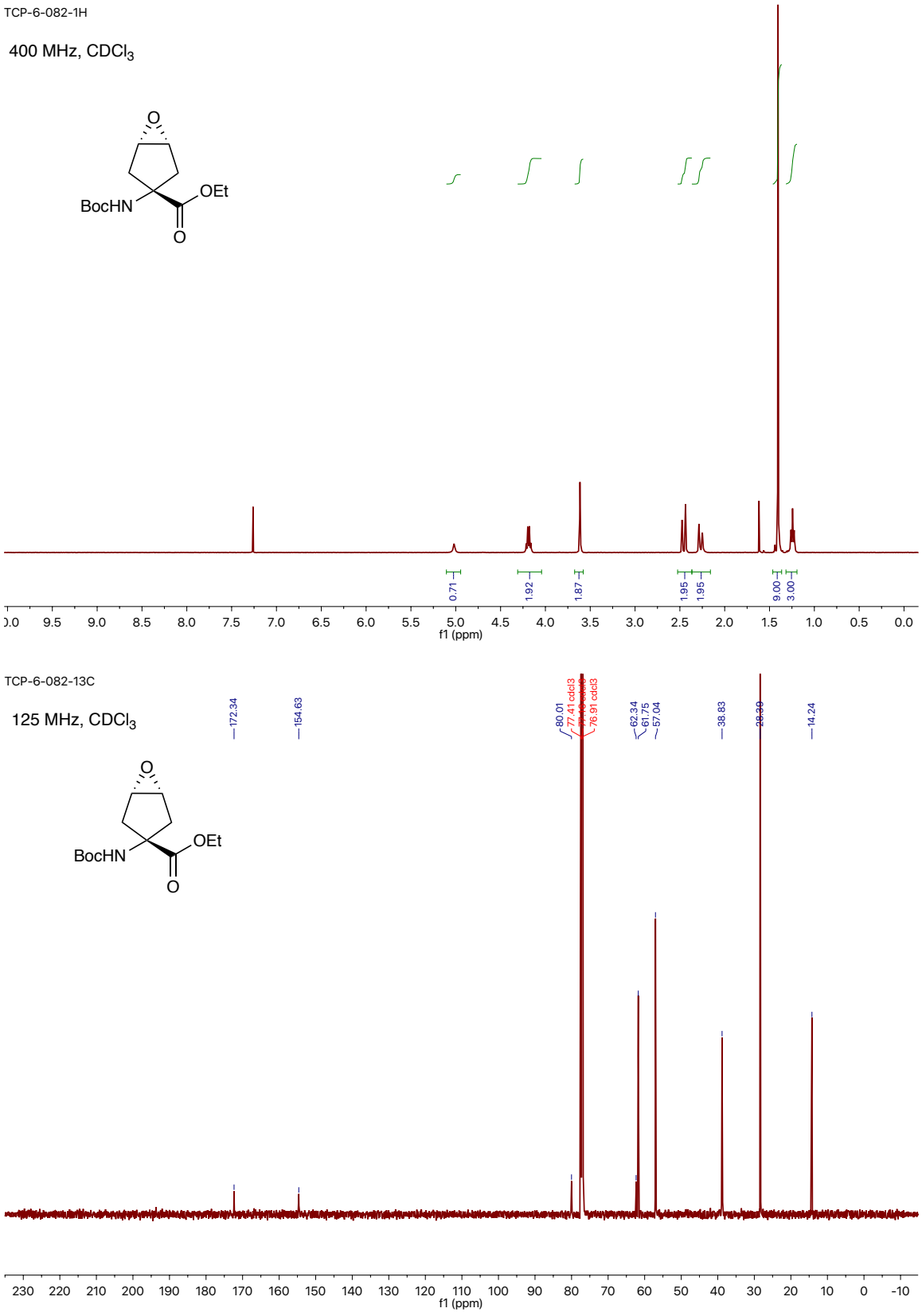

Figure S3-18. ^{1}H NMR (top) and ^{13}C NMR (bottom) of **3.17**.

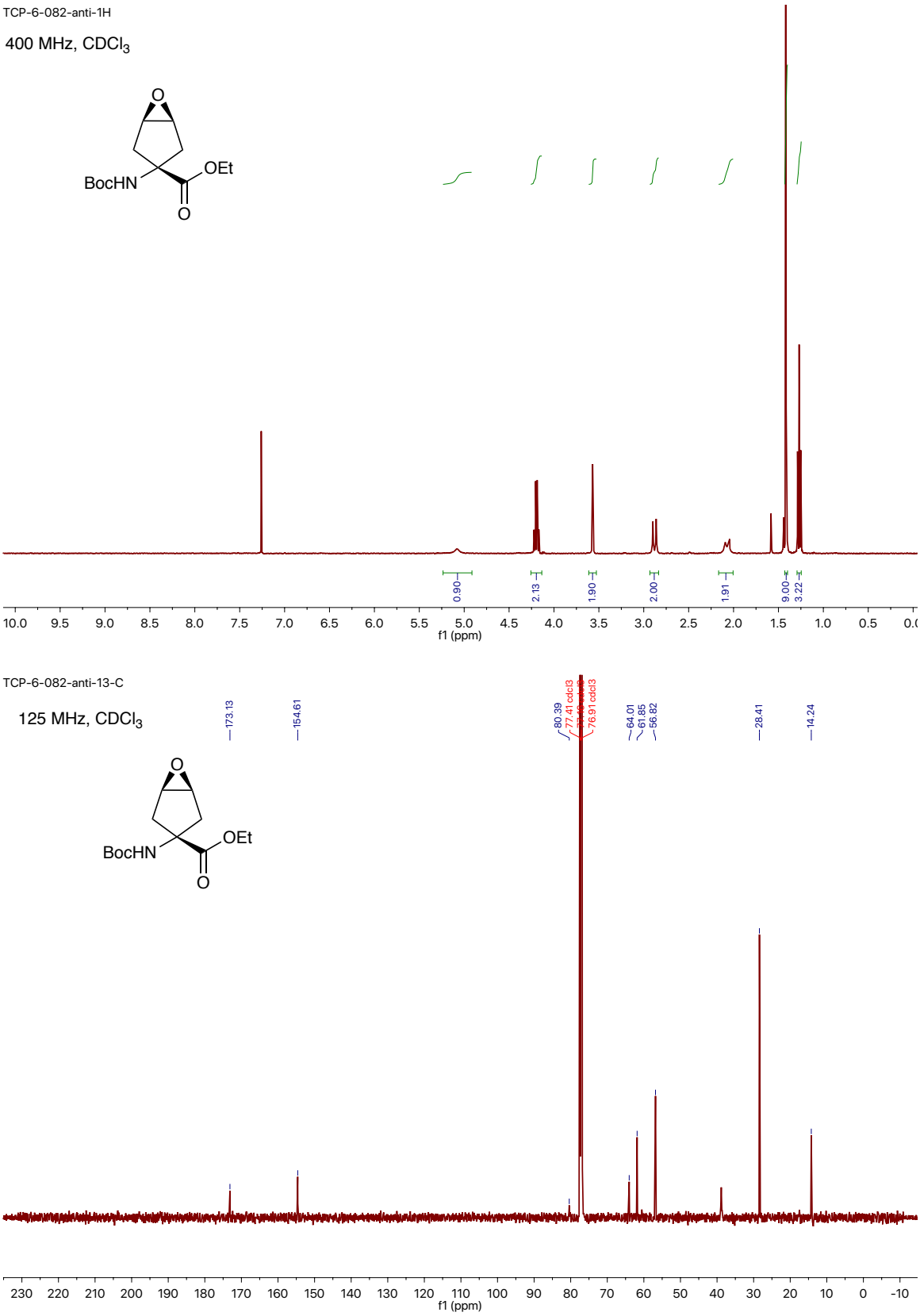

Figure S3-19. ^{1}H NMR (top) and ^{13}C NMR (bottom) of **3.18**.

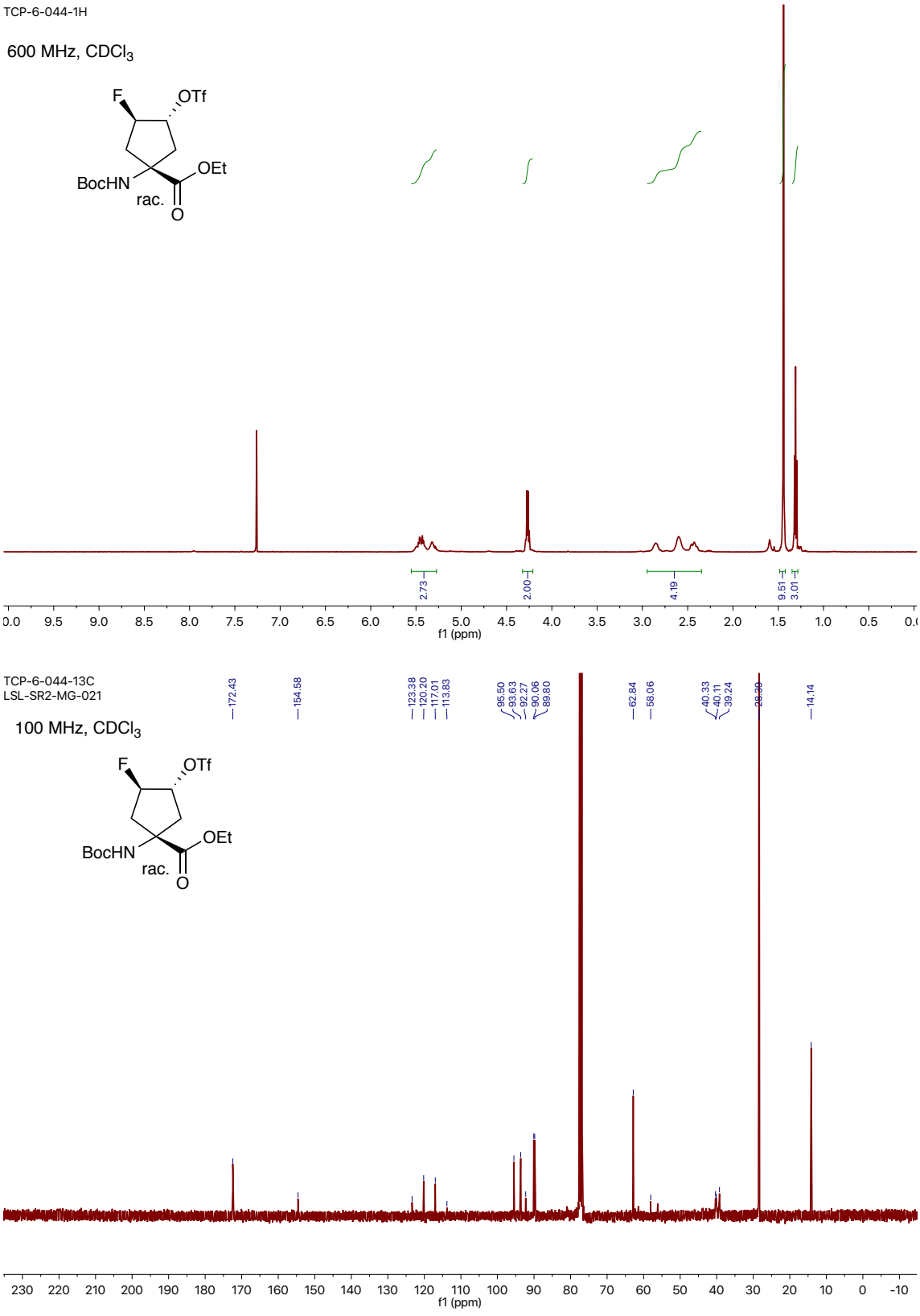

Figure S3-20. ^{1}H NMR (top) and ^{13}C NMR (bottom) of **3.19**.

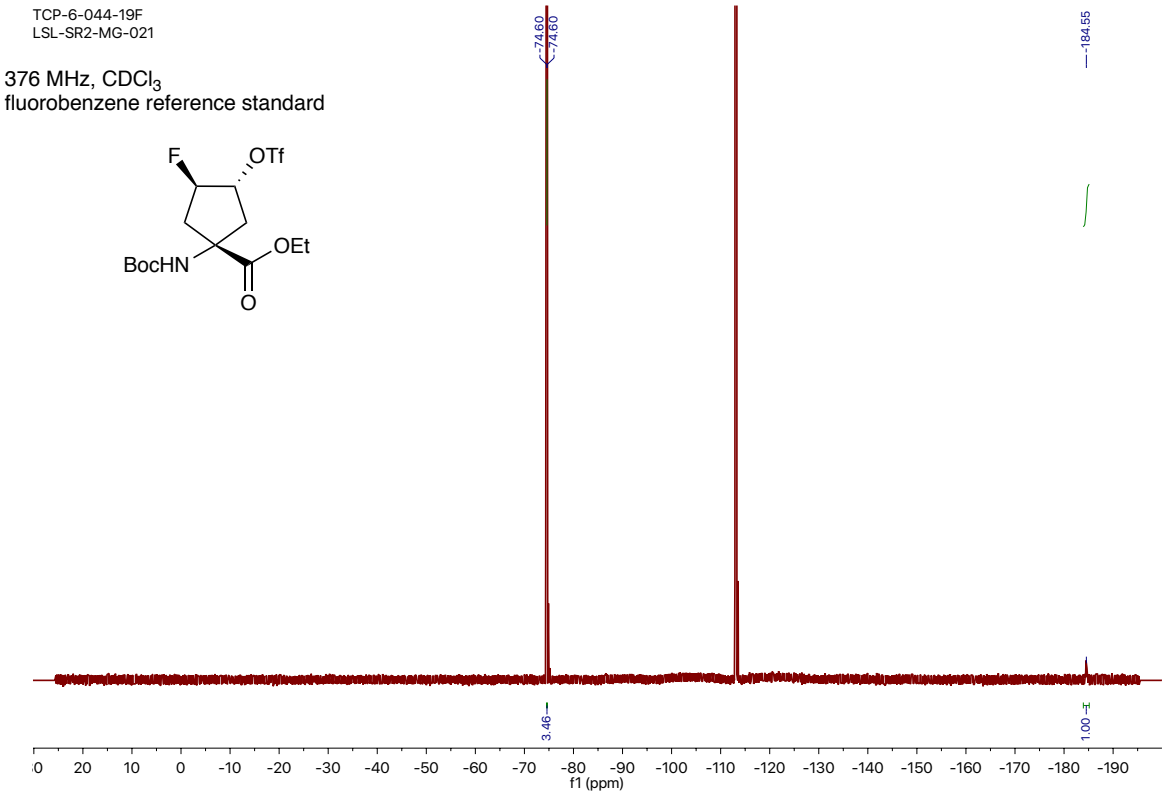

Figure S3-21. ^{19}F NMR of **3.19**.

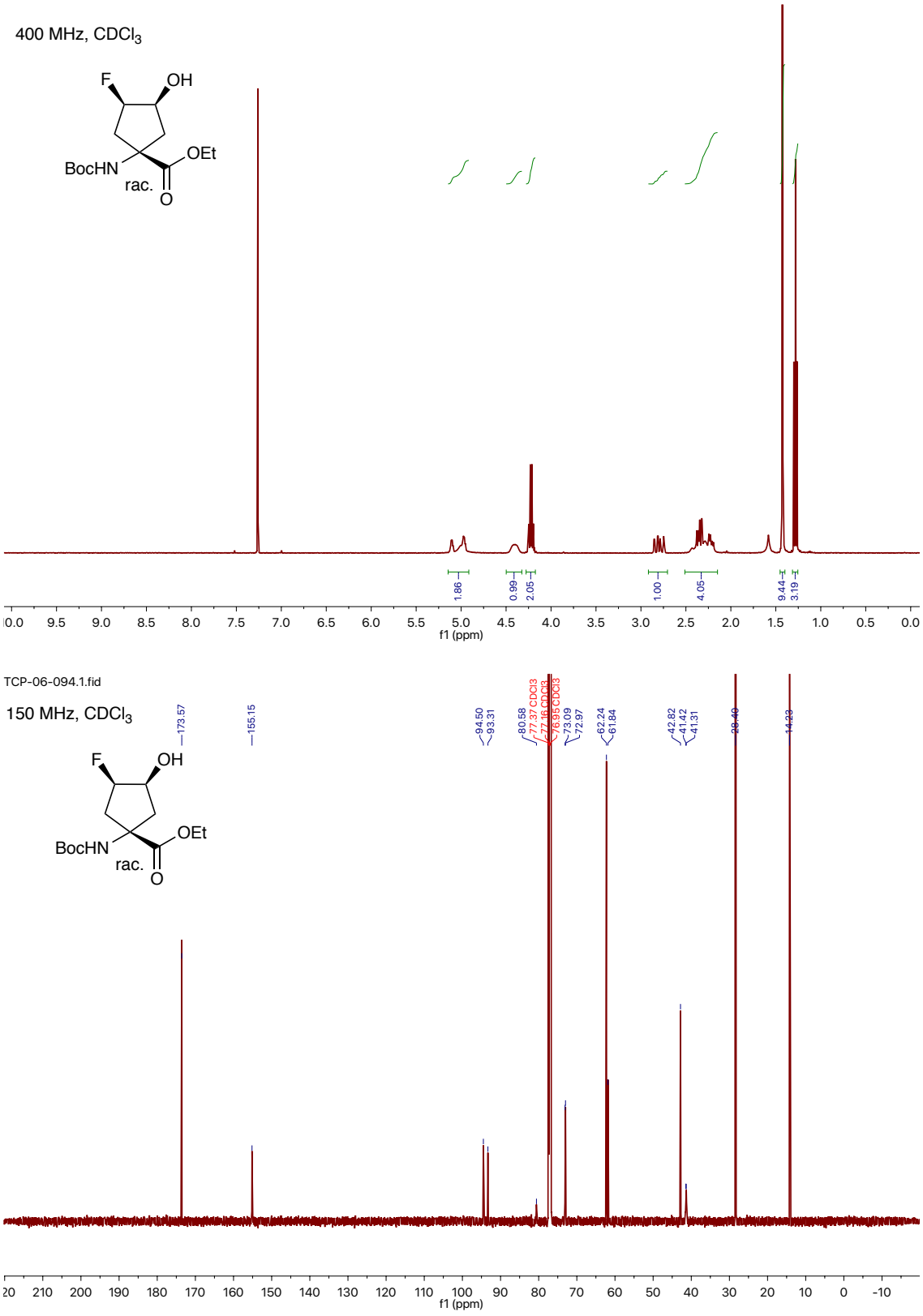

Figure S3-22. ^{1}H NMR (top) and ^{13}C NMR (bottom) of **3.20**.

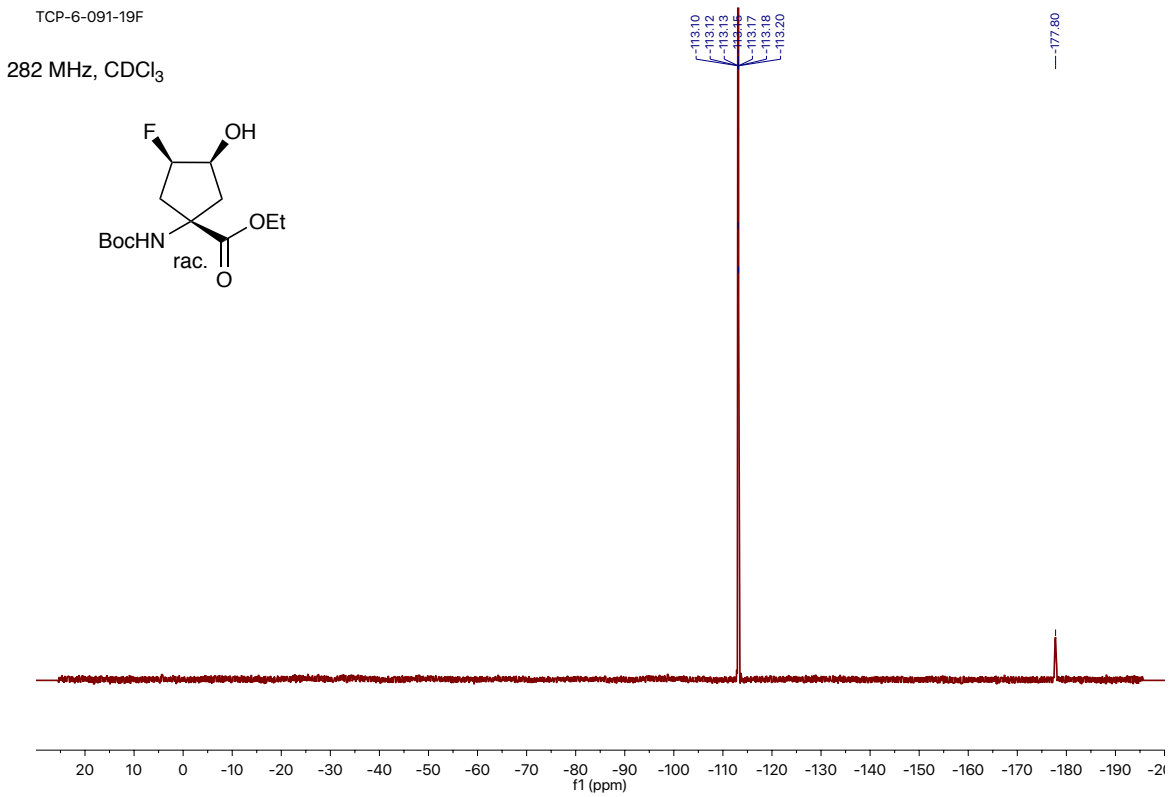

Figure S3-23. ^{19}F NMR of **3.20**.

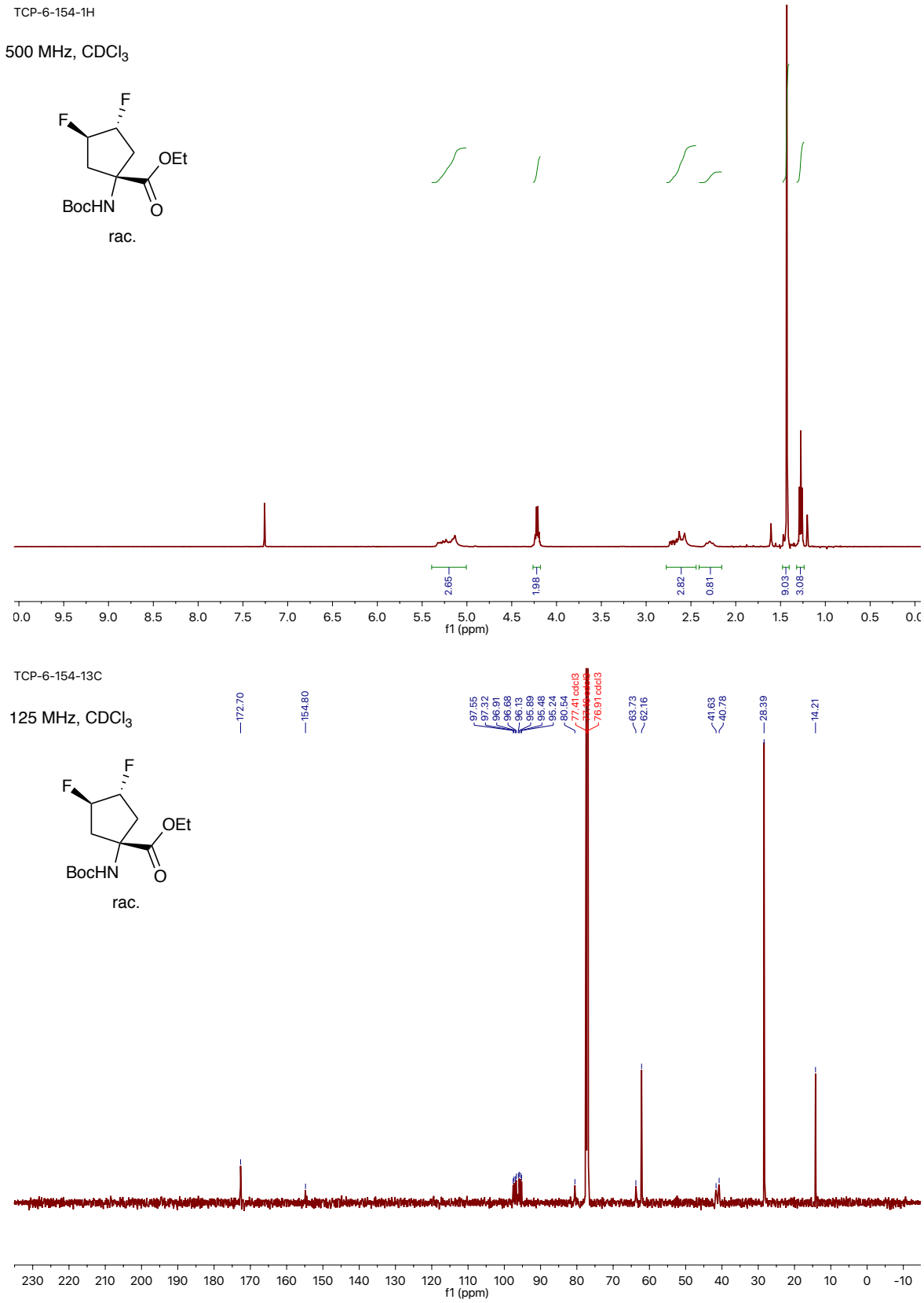

Figure S3-24. ^{1}H NMR (top) and ^{13}C NMR (bottom) of **3.22**.

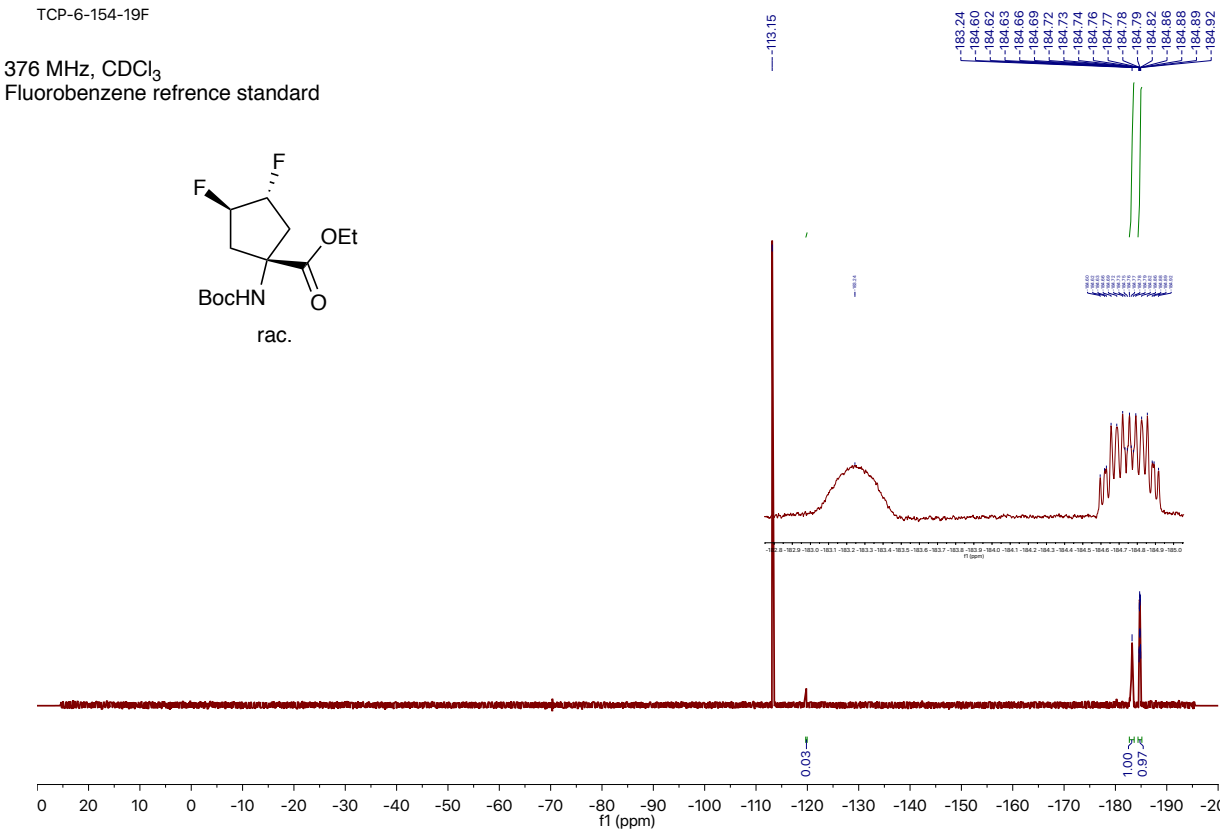

Figure S3-25. ^{19}F NMR of **3.22**.

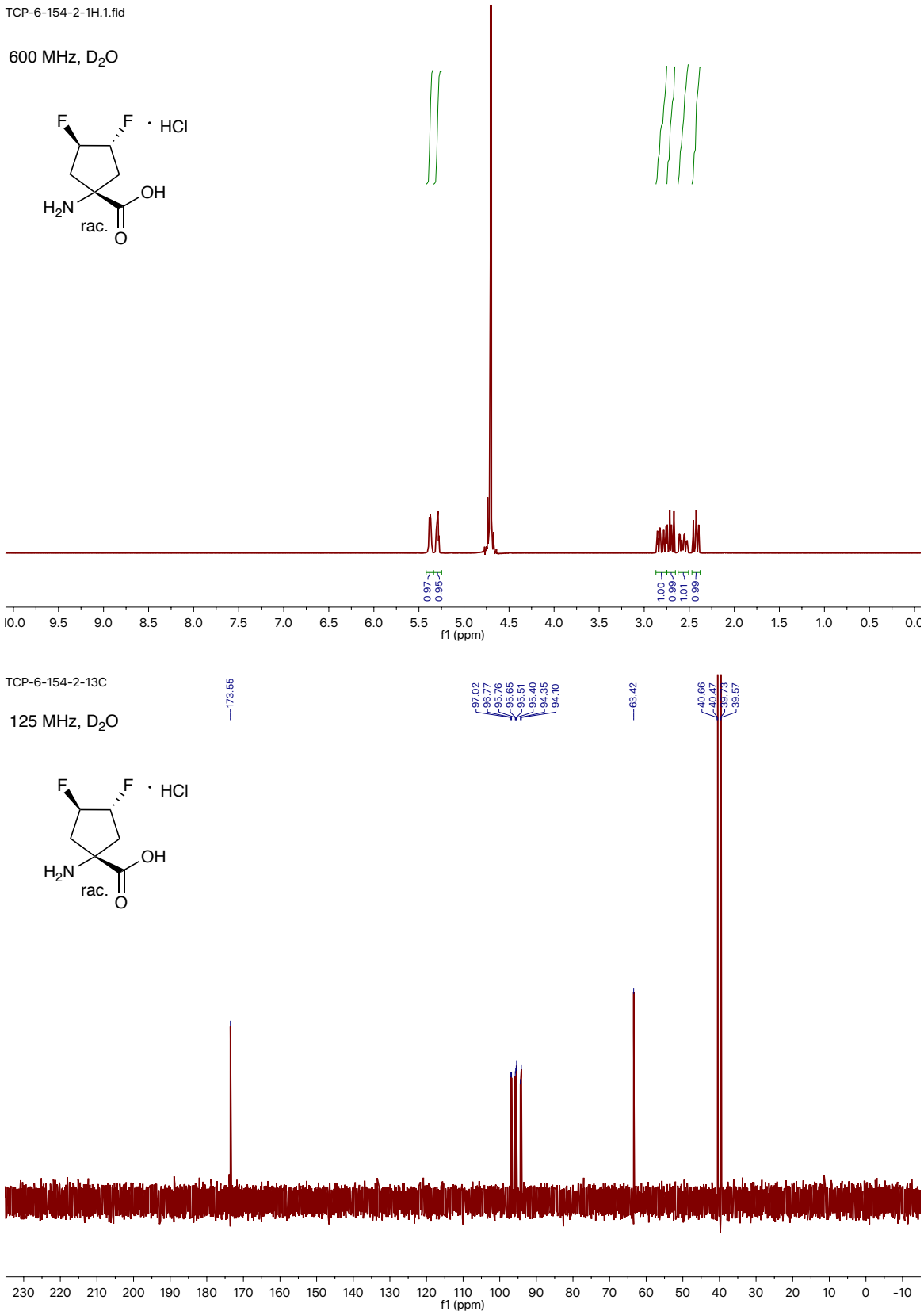

Figure S3-26. ^{1}H NMR (top) and ^{13}C NMR (bottom) of **3.23**.

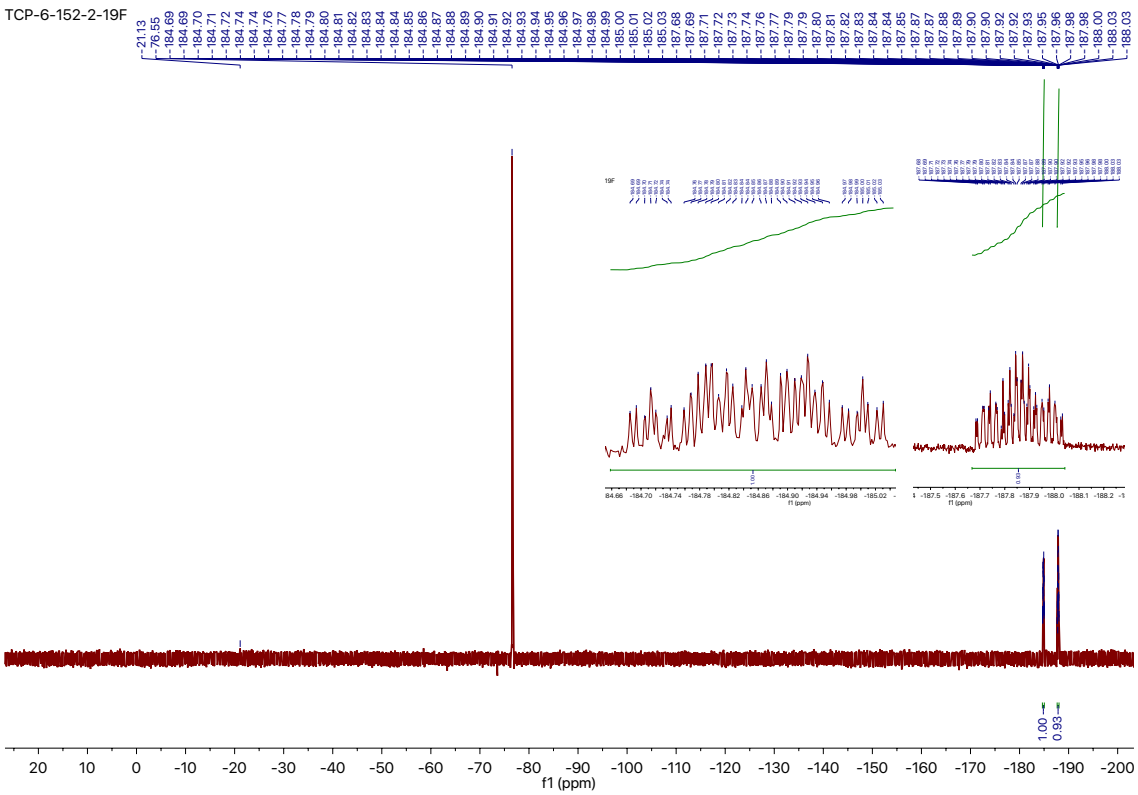

Figure S3-27. ^{19}F NMR of **3.23**.

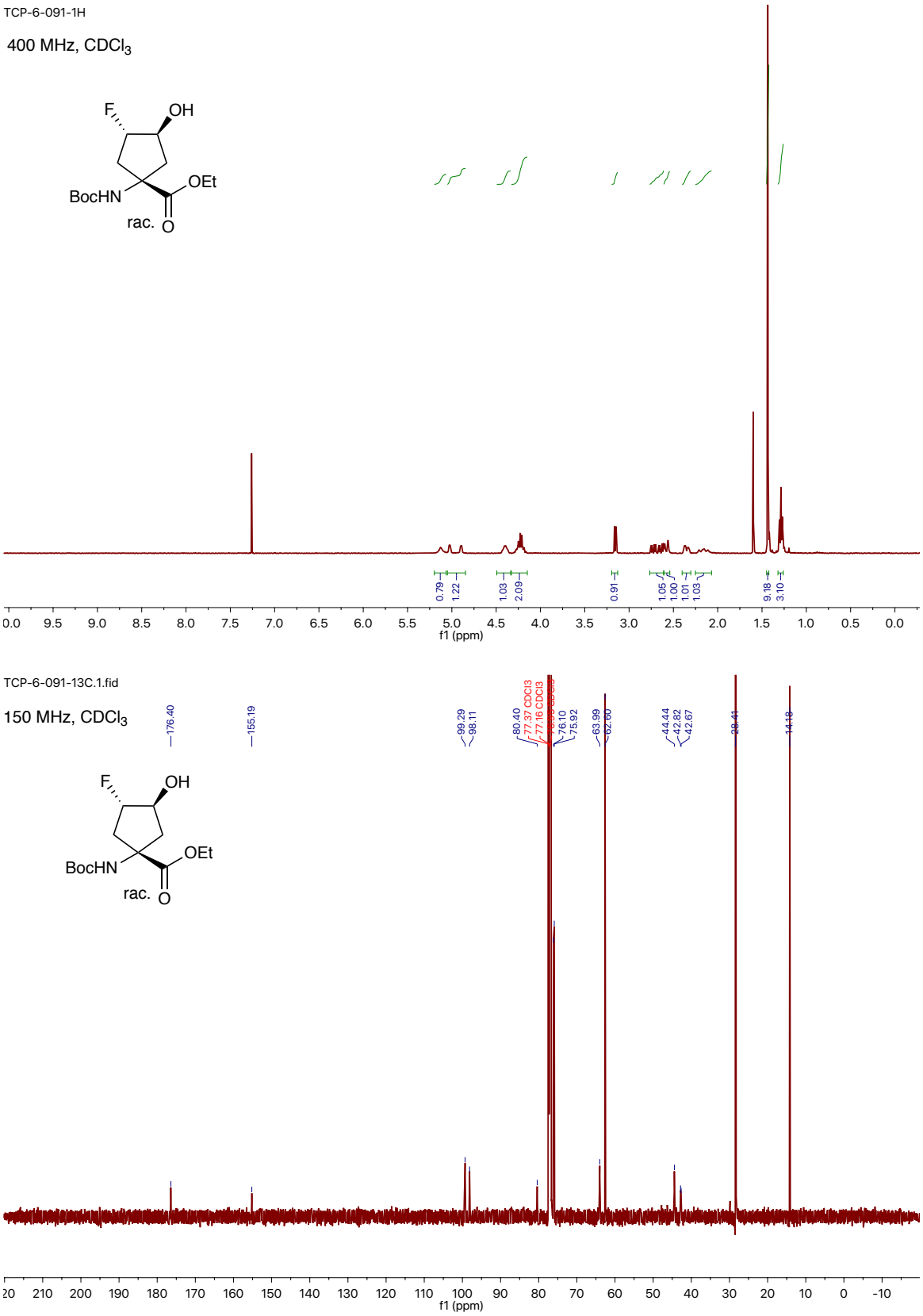

Figure S3-28. ^{1}H NMR (top) and ^{13}C NMR (bottom) of **3.24**.

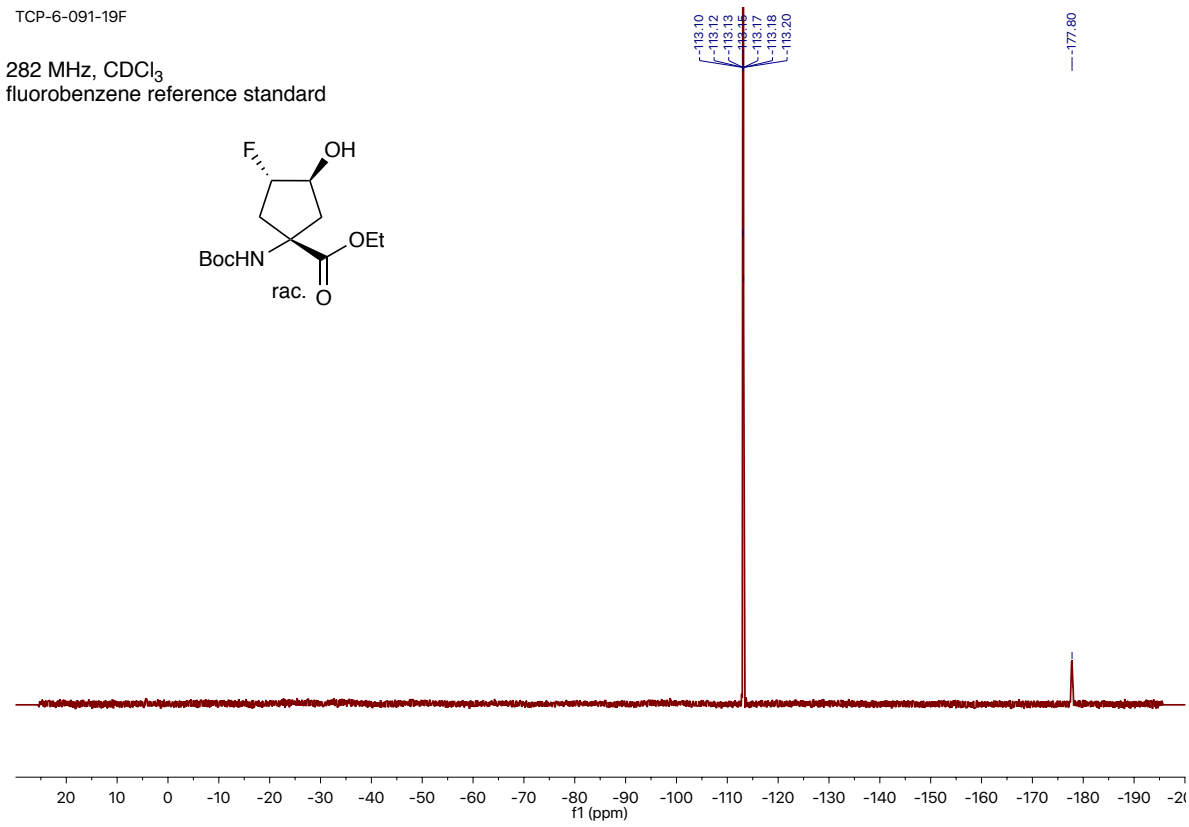

Figure S3-29. ^{19}F NMR of **3.24**.

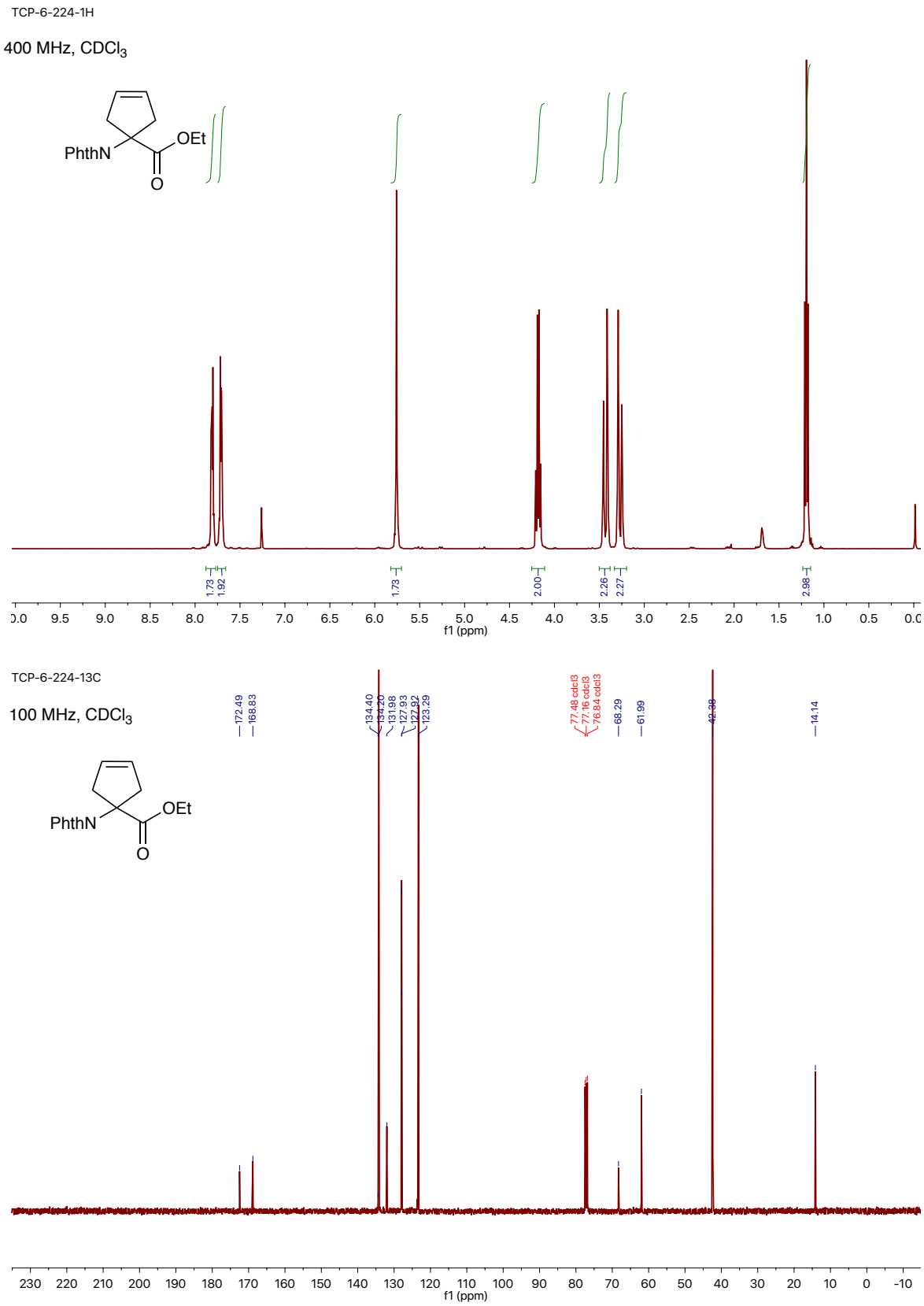

Figure S3-30. ^{1}H NMR (top) and ^{13}C NMR (bottom) of **3.26**.

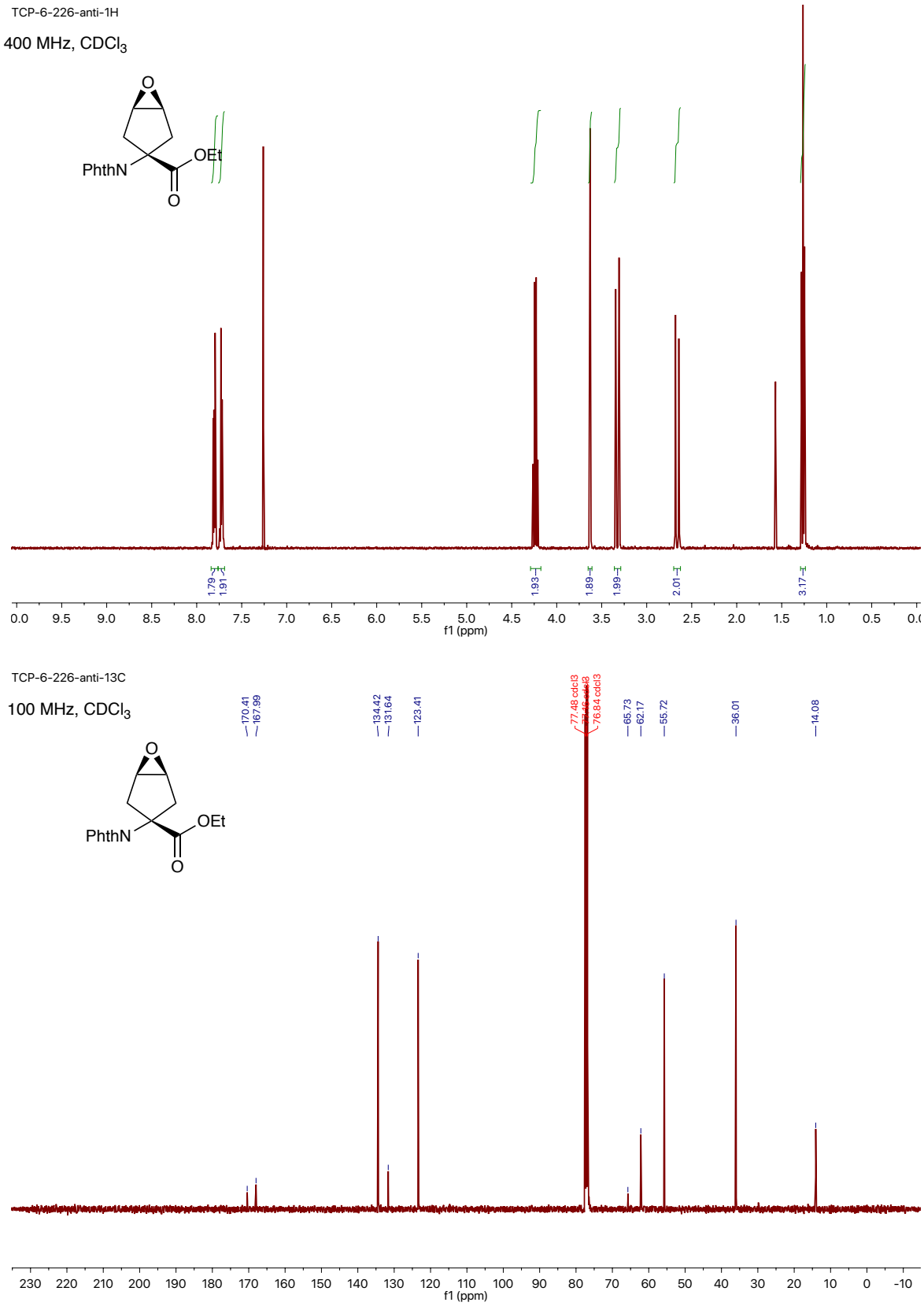

Figure S3-31. ^{1}H NMR (top) and ^{13}C NMR (bottom) of **3.27**.

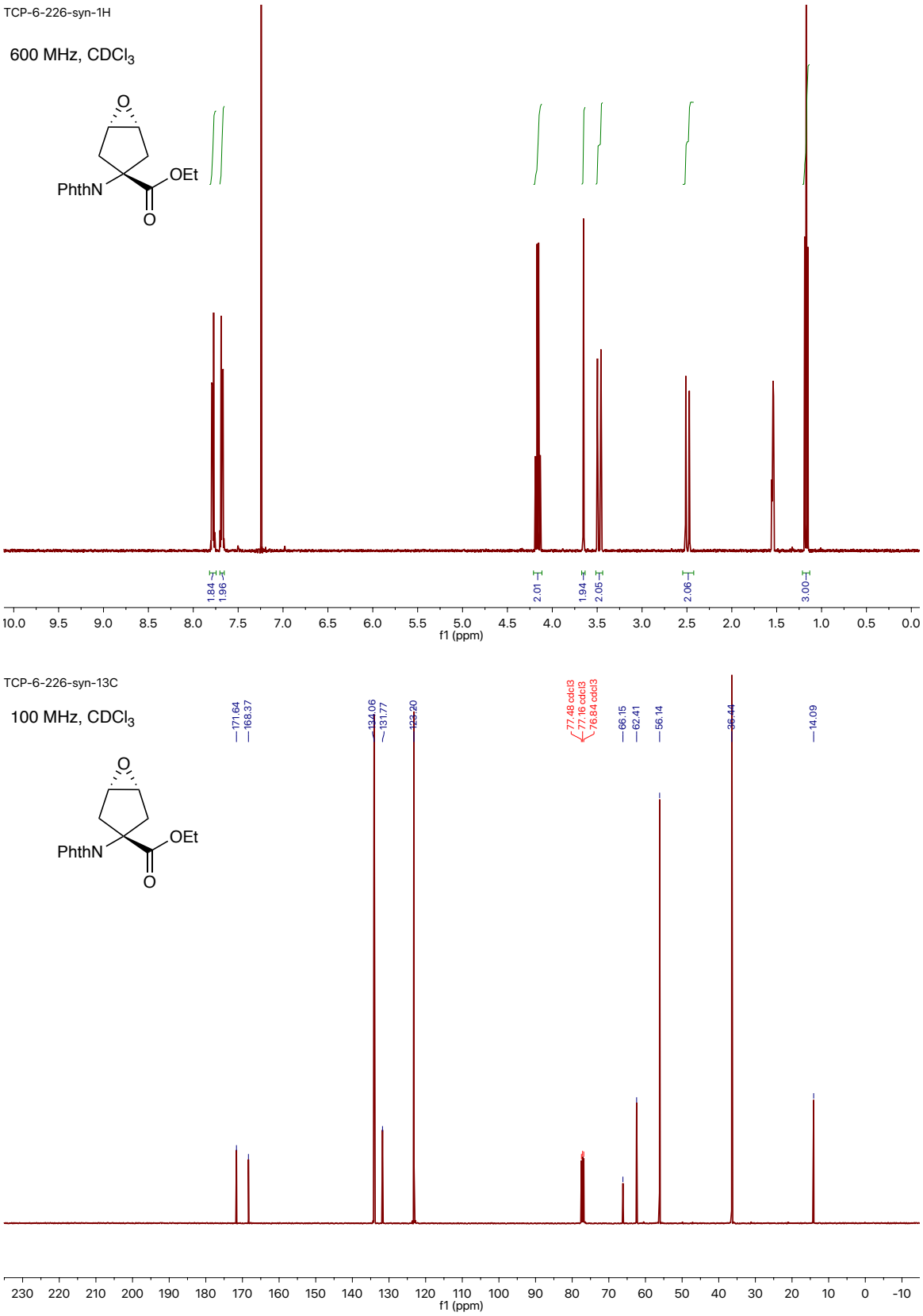

Figure S3-32. ^{1}H NMR (top) and ^{13}C NMR (bottom) of **3.28**.

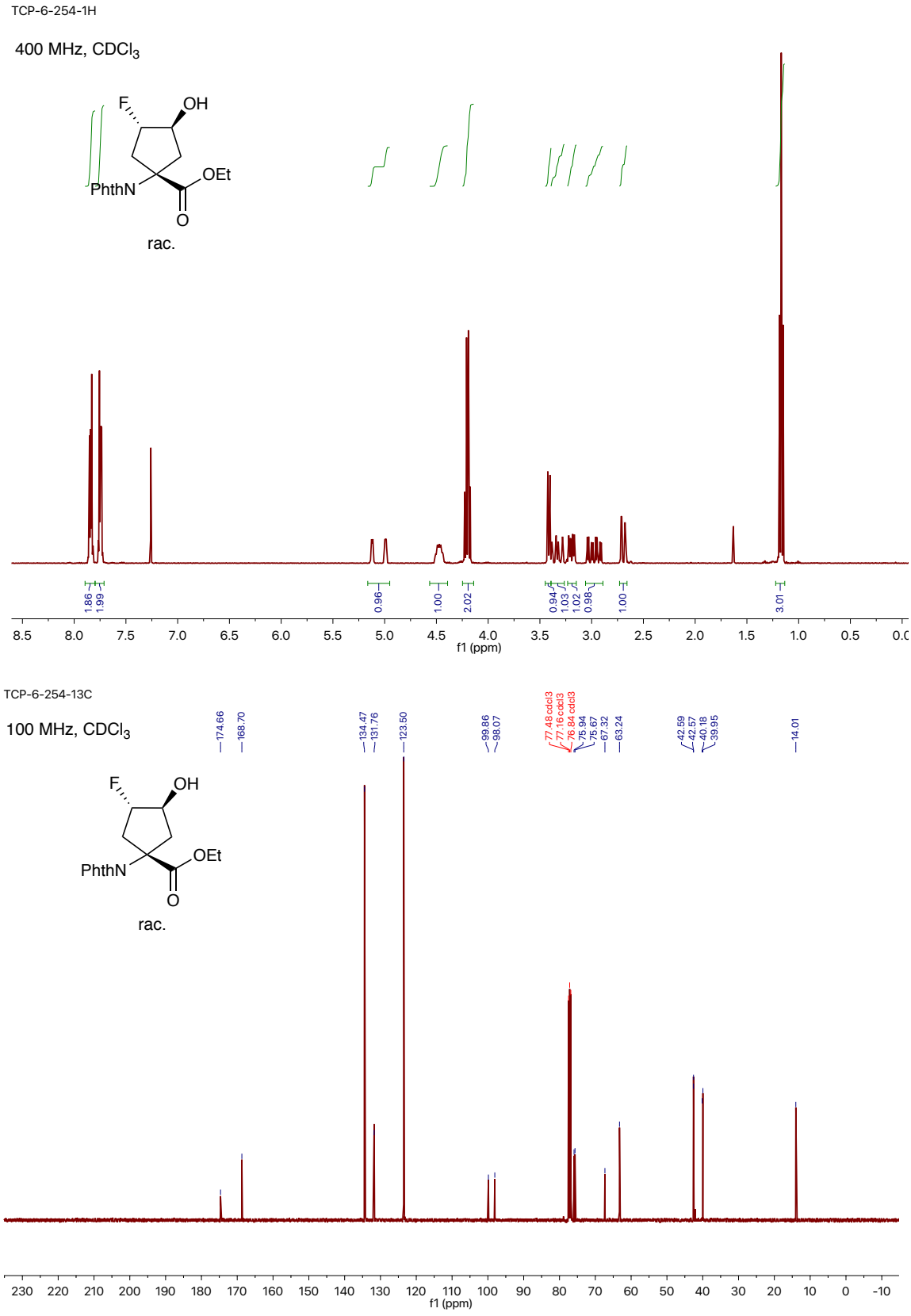

Figure S3-33. ^{1}H NMR (top) and ^{13}C NMR (bottom) of **3.29**.

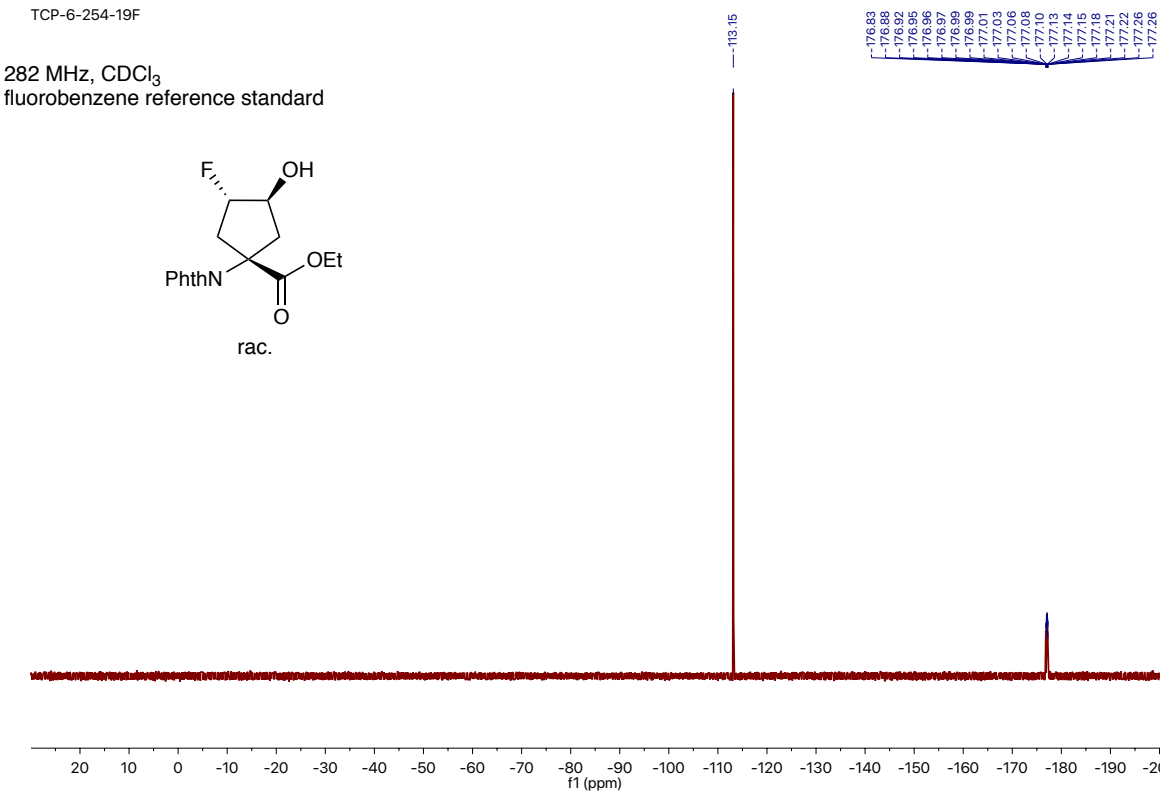

Figure S3-34. ^{19}F NMR of **3.29**.

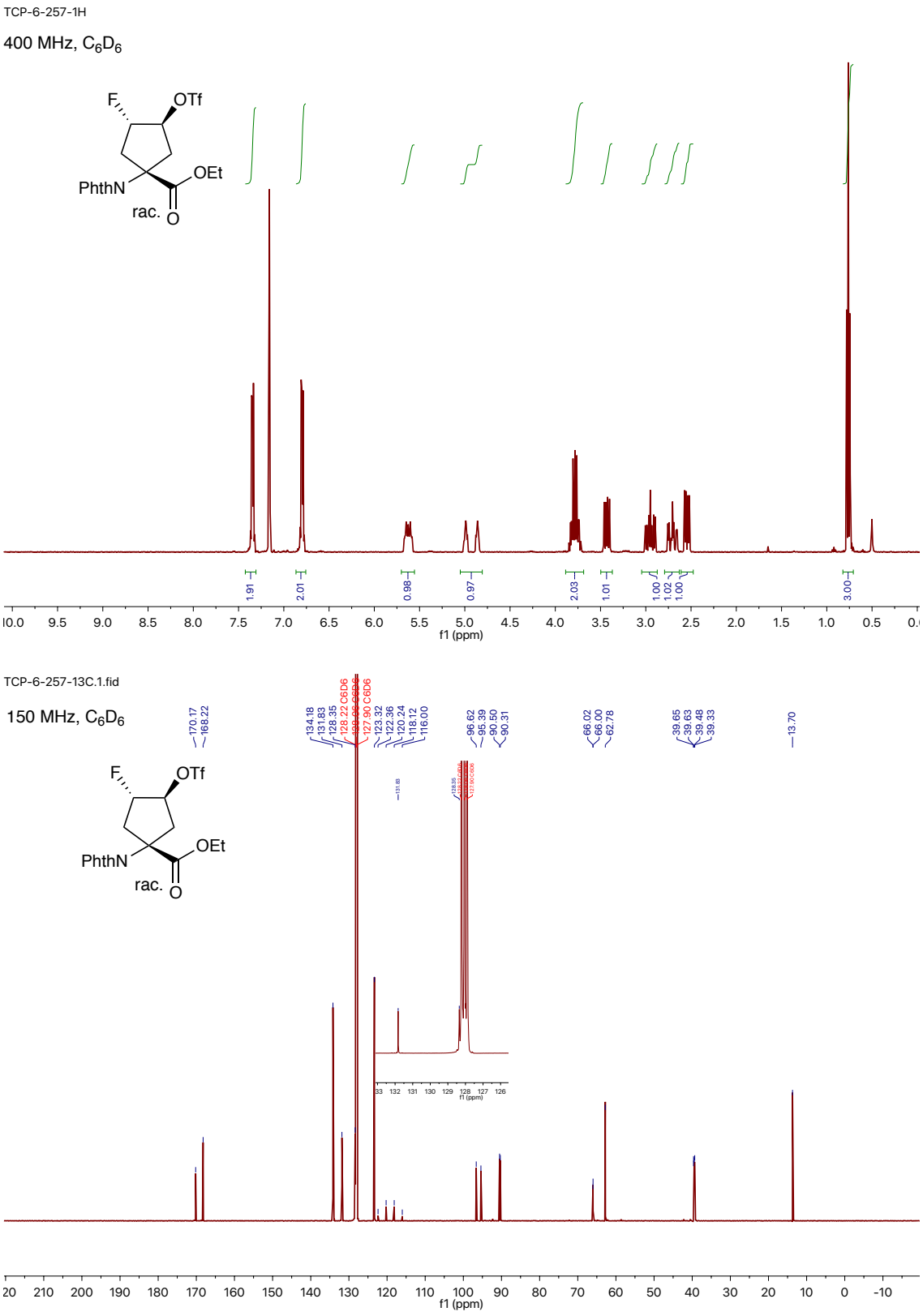

Figure S3-35. ^{1}H NMR (top) and ^{13}C NMR (bottom) of **3.30**.

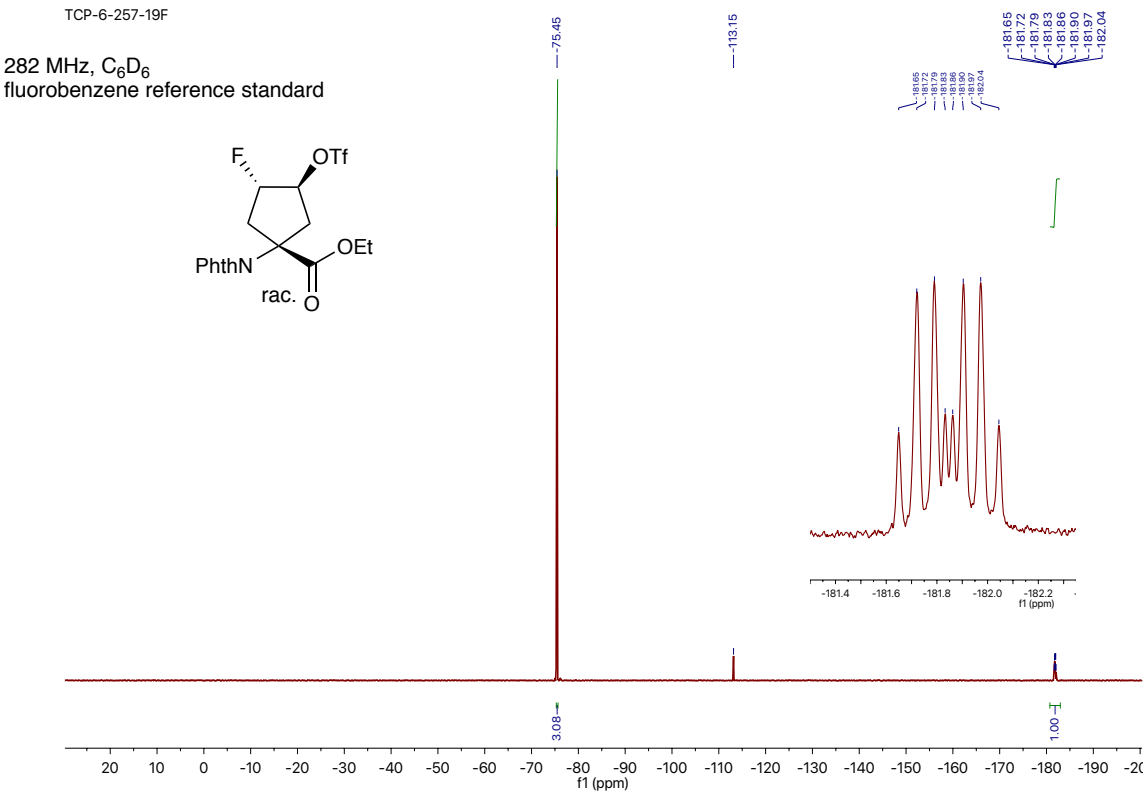

Figure S3-36. ^{19}F NMR of **3.30**.

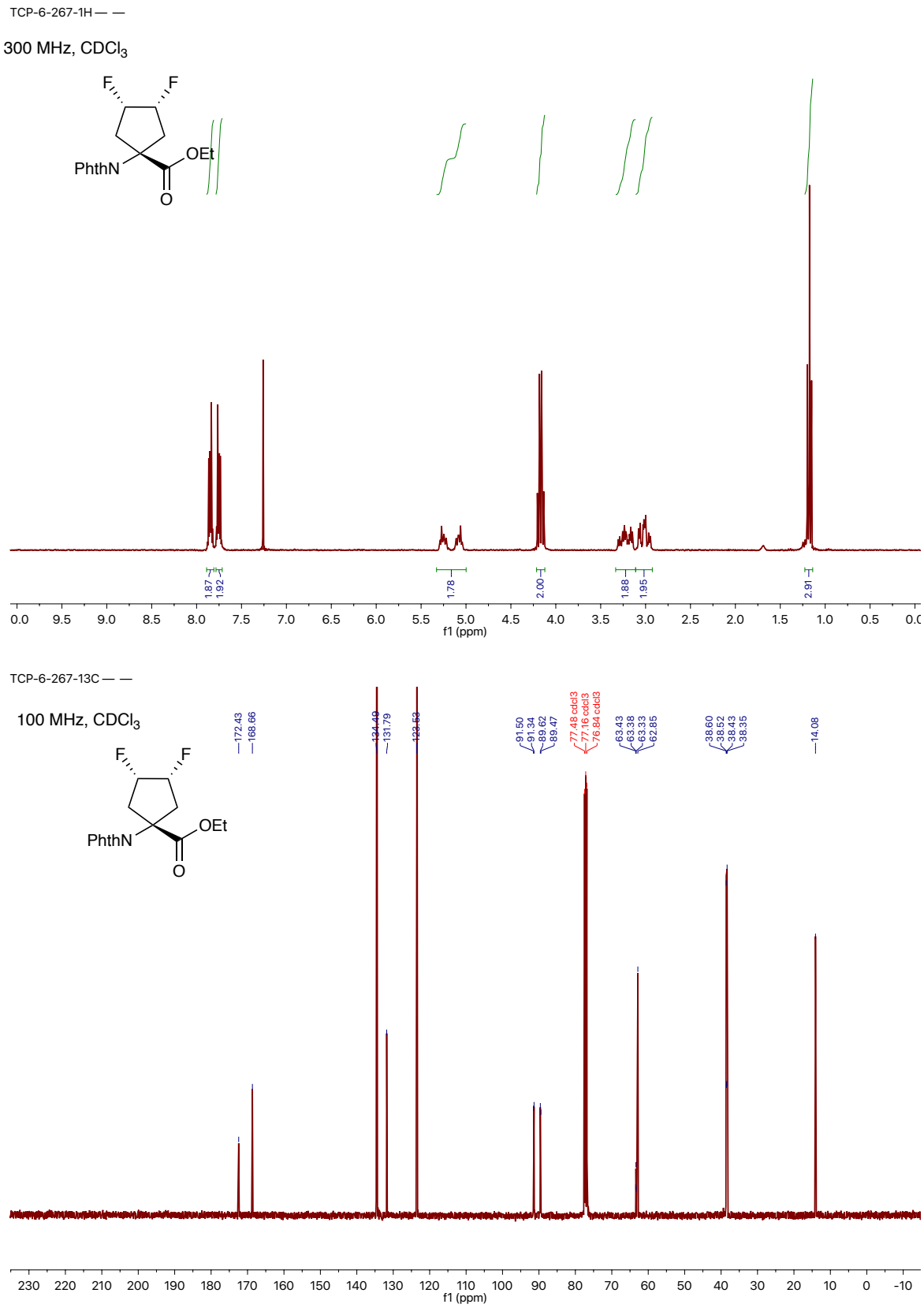

Figure S3-37. ^{1}H NMR (top) and ^{13}C NMR (bottom) of **3.31**.

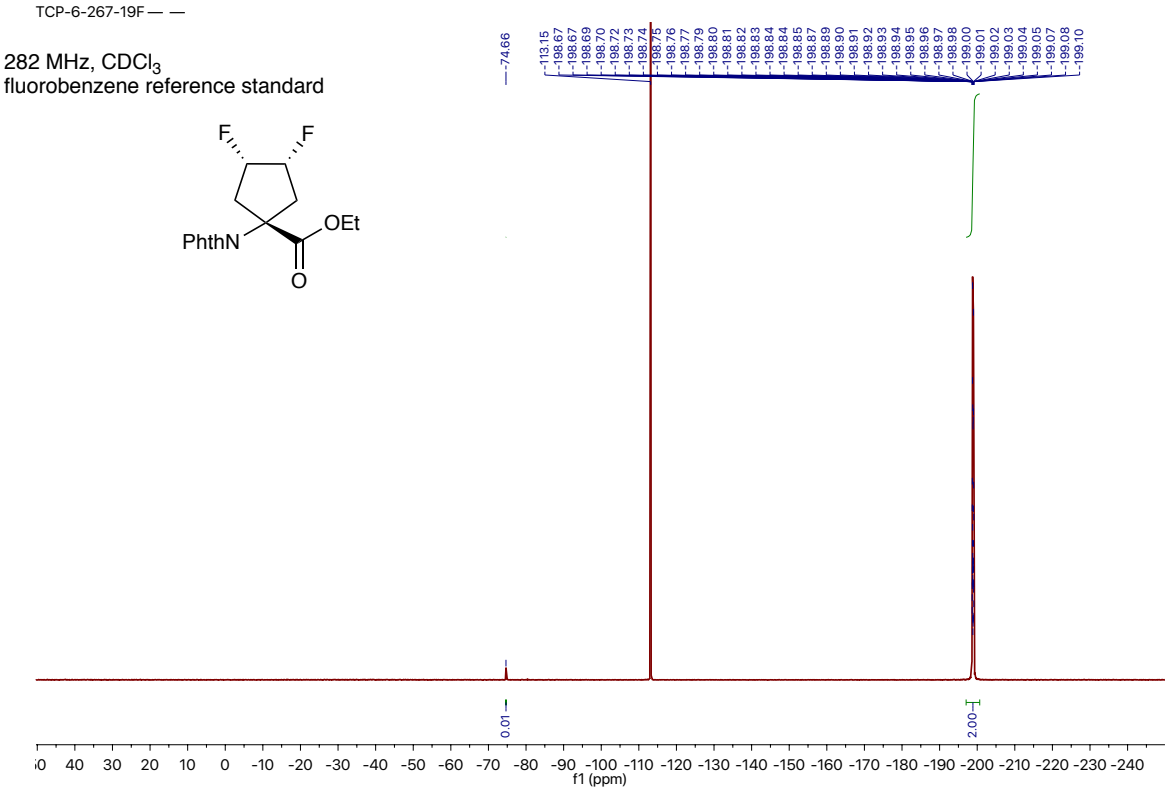

Figure S3-38. ^{19}F NMR of **3.31**.

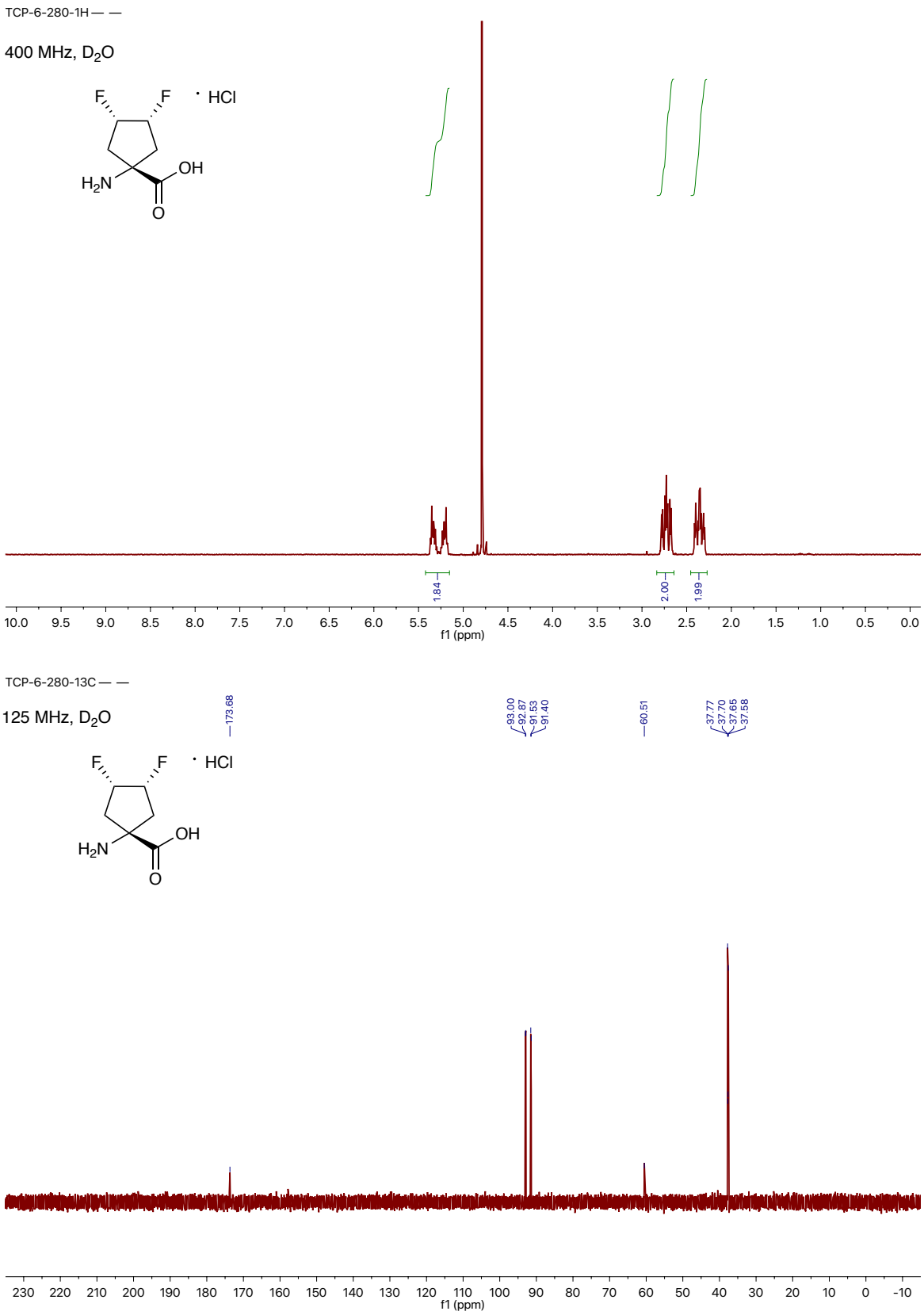

Figure S3-39. ^{1}H NMR (top) and ^{13}C NMR (bottom) of **3.33**.

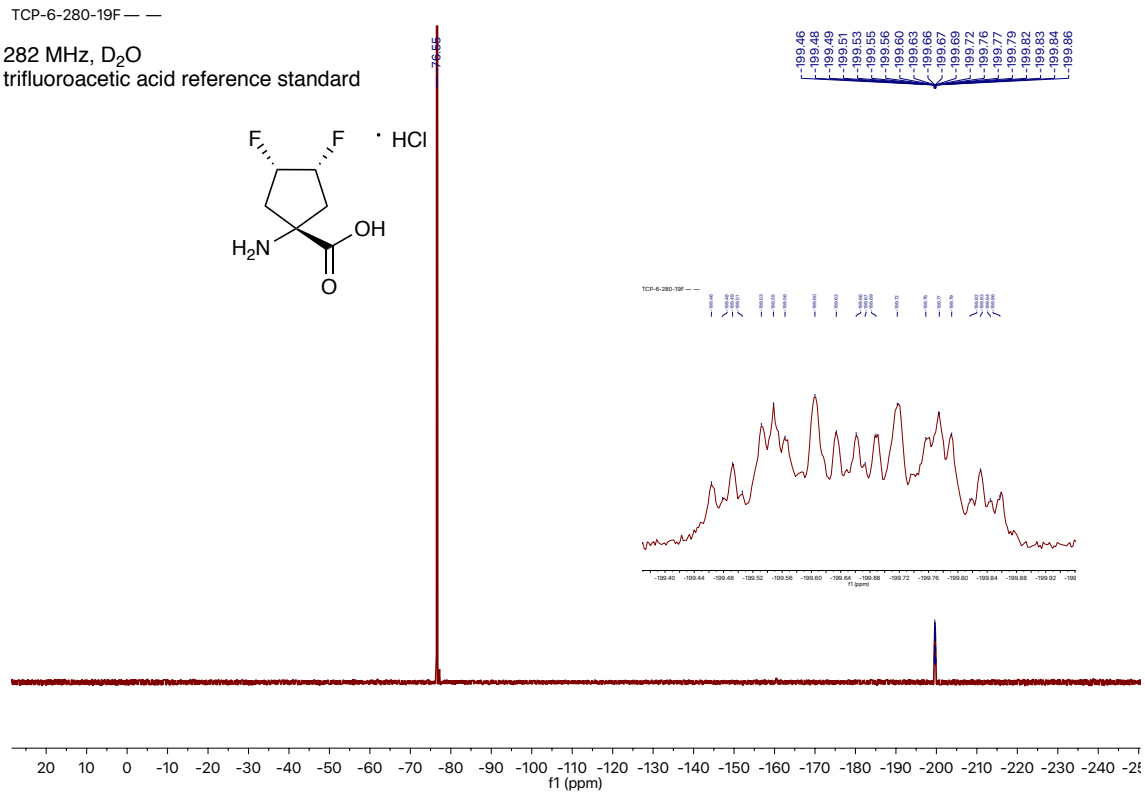

Figure S3-40. ^{19}F NMR of **3.33**.

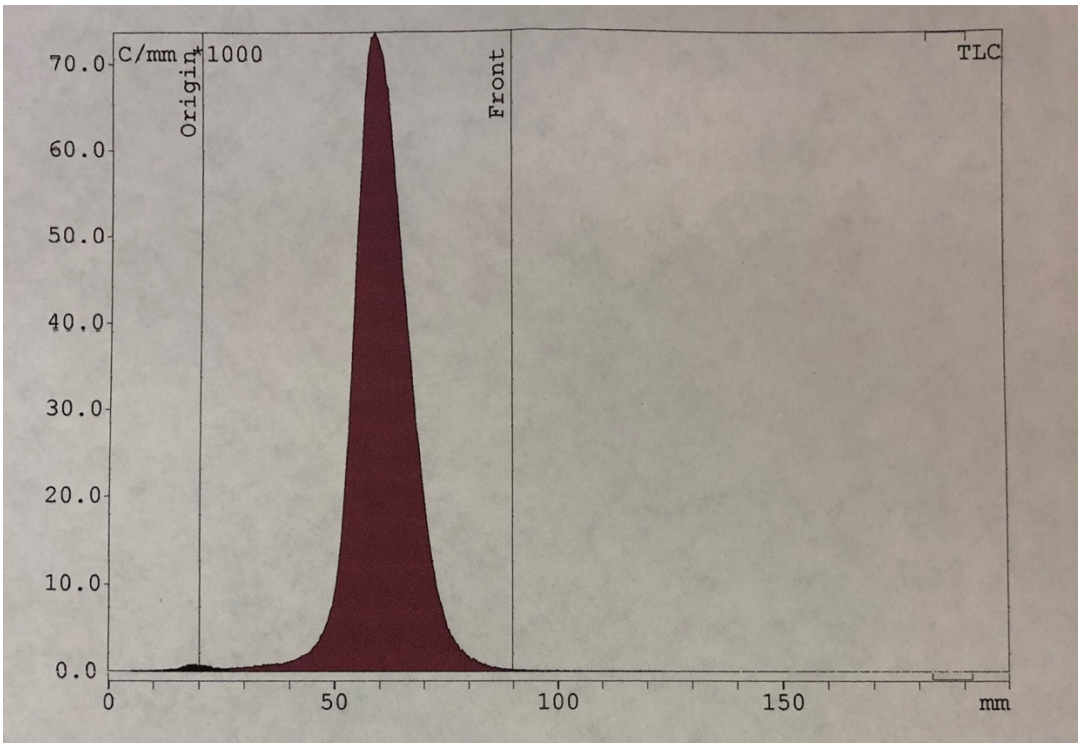

Figure S3-41. Radiometric TLC chromatogram of **[^{18}F]3.09**. Solvent system: MeCN/H_2O/CH_3OH = 2:1:1 (R_f = 0.6, Whatman silica gel plates).

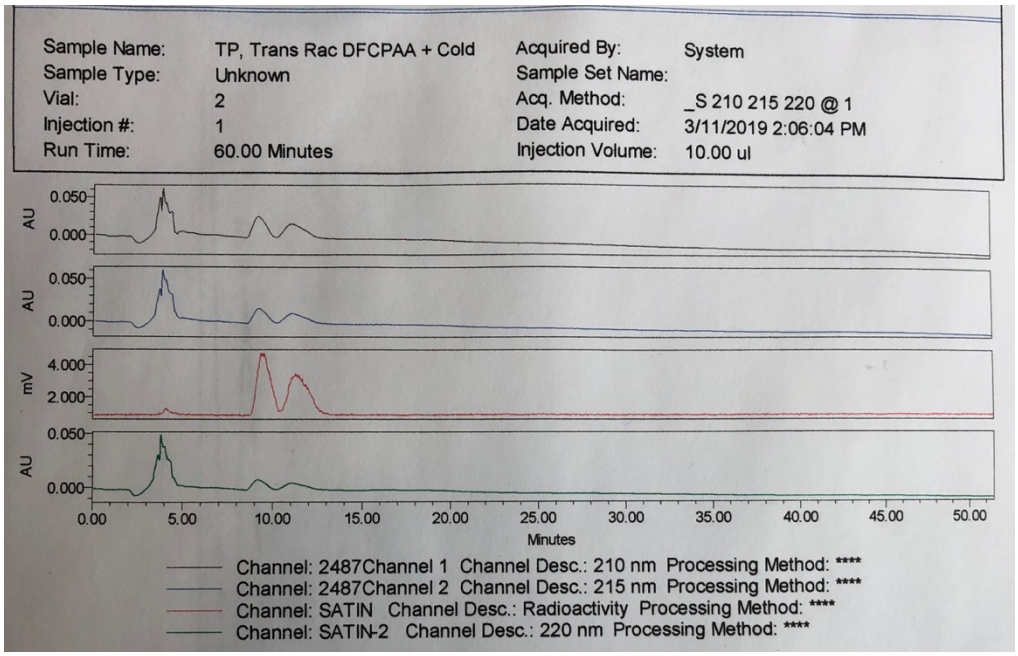

Figure S3-42. HPLC chromatogram of co-injected **3.23** and **[^{18}F]3.23** (Astec chirobiotic T column, MeOH solvent). **3.23** is observed in the UV windows (black - 210 nm, blue - 215 nm, and green - 220 nm) and **[^{18}F]3.23** is observed in the radiocounter window (red).

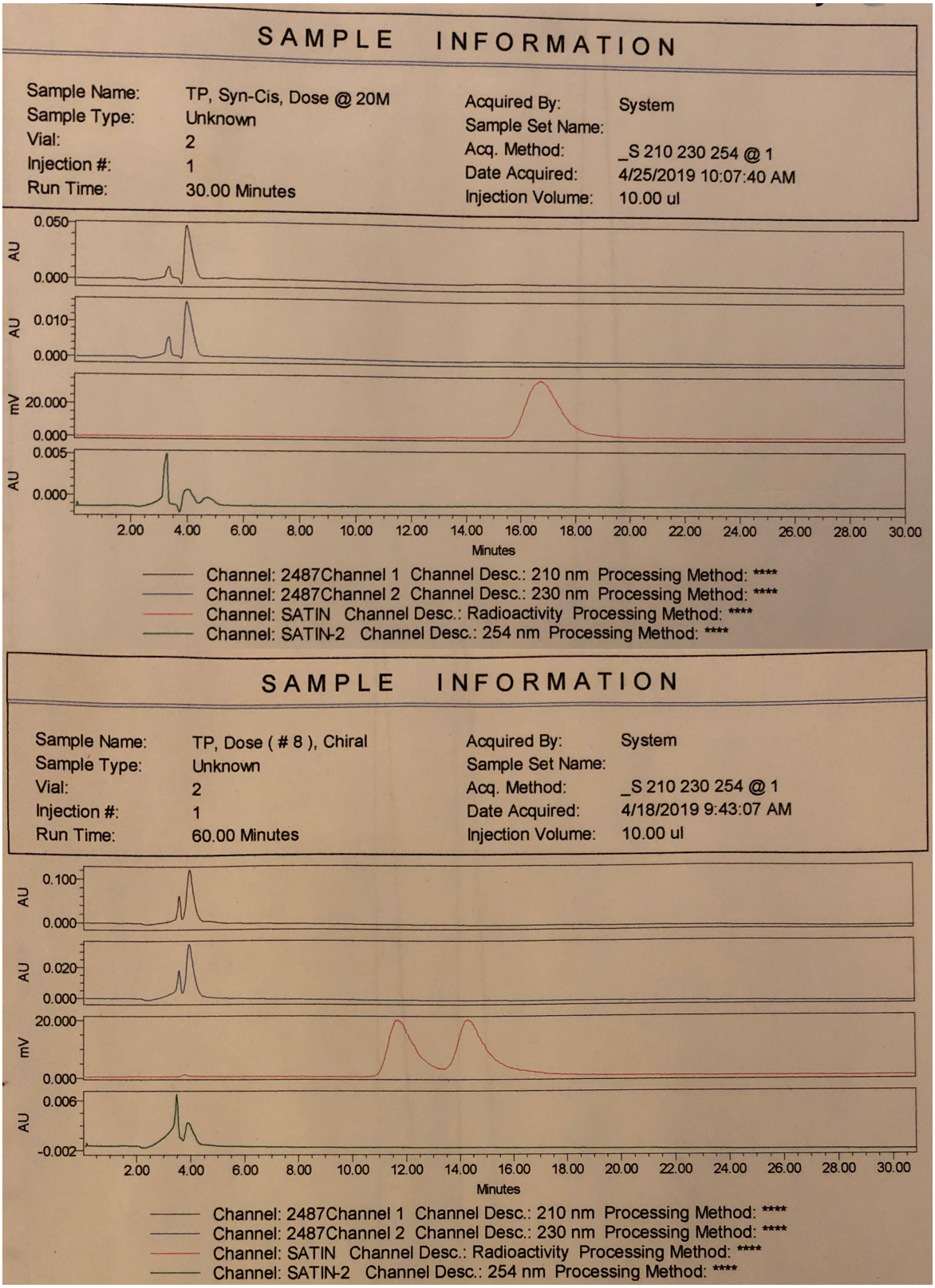

Figure S3-43. HPLC chromatogram of **[^{18}F]3.33** (16.7 minute retention time, top scan) and **[^{18}F]3.23** (11.7 and 14.3 minute retention time, bottom scan) (Astec chirobiotic T column, MeOH solvent). Both runs were performed with the same method.

Anti-cis-3,4-DFACPC

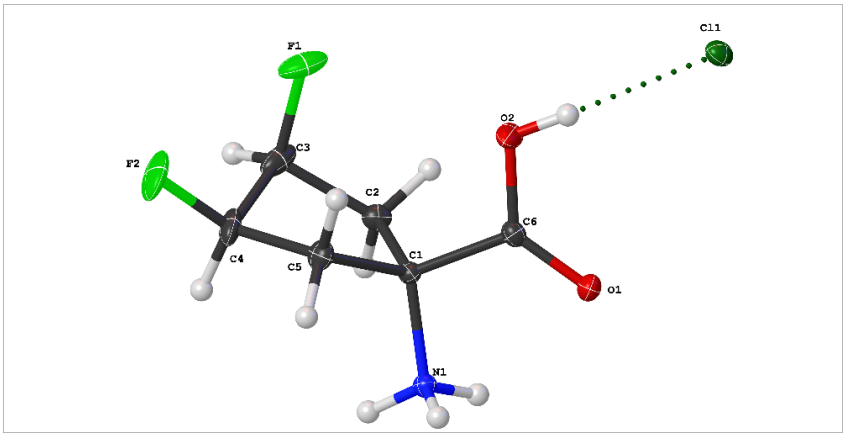

Table 1: Crystal Data and Structure Refinement for **anti-cis-3,4-DFACPC**.

Identification code	TCP-6-054
Empirical formula	$C_6H_{10}ClF_2NO_2$
Formula weight	201.60
Temperature/K	99.9(6)
Crystal system	monoclinic
Space group	$P2_1$
a/Å	6.41583(13)
b/Å	5.94388(12)
c/Å	10.9879(2)
α/°	90
β/°	96.3458(18)
γ/°	90
Volume/Å^3	416.456(15)
Z	2
ρ_{calc}g/cm^3	1.608
μ/mm^{-1}	4.112
F(000)	208.0
Crystal size/mm^3	0.453 × 0.372 × 0.074
Radiation	CuKα (λ = 1.54184)
2Θ range for data collection/°	8.096 to 140.116
Index ranges	$-7 \leq h \leq 7, -7 \leq k \leq 7, -11 \leq l \leq 13$
Reflections collected	3889
Independent reflections	1568 [R_{int} = 0.0293, R_{sigma} = 0.0290]
Data/restraints/parameters	1568/1/111
Goodness-of-fit on F^2	1.052
Final R indexes [I>=2σ (I)]	R_1 = 0.0397, wR_2 = 0.1030
Final R indexes [all data]	R_1 = 0.0405, wR_2 = 0.1038
Largest diff. peak/hole / e Å^{-3}	0.25/-0.26
Flack parameter	-0.01(2)

Table 2: Fractional Atomic Coordinates ($\times 10^4$) and Equivalent Isotropic Displacement Parameters ($Å^2 \times 10^3$) for **anti-cis-3,4-DFACPC**. U_{eq} is defined as 1/3 of of the trace of the orthogonalised U_{IJ} tensor.

Atom	*x*	*y*	*z*	U(eq)
Cl1	9986(1)	8812.2(11)	8621.3(6)	13.6(3)
F1	5530(4)	2179(4)	5674(2)	27.4(6)
F2	1479(4)	2610(5)	4732.0(19)	31.2(6)
O2	6384(4)	6112(5)	7521(2)	20.5(6)
O1	5170(4)	6494(5)	9352(2)	14.2(5)
N1	2042(4)	3712(5)	8872(2)	10.4(5)
C6	5097(5)	5673(6)	8345(3)	11.5(7)
C1	3464(4)	3910(6)	7883(3)	9.8(6)
C5	2196(5)	4528(6)	6648(3)	14.5(7)
C2	4516(5)	1598(6)	7667(3)	12.9(7)
C3	4034(6)	1119(6)	6309(3)	19.7(8)
C4	1939(6)	2277(7)	5985(3)	19.8(8)

Table 3: Anisotropic Displacement Parameters ($Å^2 \times 10^3$) for **anti-cis-3,4-DFACPC**. The Anisotropic displacement factor exponent takes the form: $-2\pi^2[h^2a^{*2}U_{11}+2hka^*b^*U_{12}+...]$.

Atom	U_{11}	U_{22}	U_{33}	U_{23}	U_{13}	U_{12}
Cl1	12.4(4)	12.1(4)	16.7(4)	-0.3(3)	3.2(2)	-2.3(3)
F1	40.1(13)	23.4(13)	22.7(11)	4.0(9)	20.9(10)	4.8(11)
F2	50.7(15)	32.0(14)	8.7(11)	-1.2(10)	-6.7(10)	-11.3(12)
O2	20.9(13)	25.5(16)	16.6(13)	-6.2(11)	8.5(10)	-14.6(11)
O1	14.2(11)	17.2(13)	11.0(12)	-2.3(10)	0.9(8)	-1.8(10)
N1	10.3(11)	10.9(13)	9.9(12)	0.3(12)	1.0(9)	0.5(12)
C6	10.2(15)	10.4(16)	13.5(15)	1.1(13)	-0.2(12)	-0.2(12)
C1	10.0(13)	11.1(14)	8.2(13)	0.8(13)	1.1(10)	-0.5(14)
C5	16.0(16)	16.5(18)	10.2(15)	1.8(13)	-1.7(12)	1.1(13)
C2	14.1(16)	10.2(16)	14.9(17)	1.9(13)	3.2(12)	1.3(13)

C3	36(2)	10.7(17)	14.3(17)	-1.1(14)	9.8(15)	-2.2(15)
C4	29.5(19)	19.7(19)	9.1(16)	-1.3(14)	-2.4(14)	-9.6(16)

Table 4: Bond Lengths for **anti-cis-3,4-DFACPC**.

Atom	Atom	Length/Å	Atom	Atom	Length/Å
F1	C3	1.398(4)	C1	C5	1.547(4)
F2	C4	1.390(4)	C1	C2	1.561(5)
O2	C6	1.317(4)	C5	C4	1.524(5)
O1	C6	1.205(4)	C2	C3	1.518(5)
N1	C1	1.498(3)	C3	C4	1.517(6)
C6	C1	1.528(5)			

Table 5: Bond Angles for **anti-cis-3,4-DFACPC**.

Atom	Atom	Atom	Angle/°	Atom	Atom	Atom	Angle/°
O2	C6	C1	111.5(3)	C4	C5	C1	103.3(3)
O1	C6	O2	125.9(3)	C3	C2	C1	105.6(3)
O1	C6	C1	122.6(3)	F1	C3	C2	109.3(3)
N1	C1	C6	105.2(3)	F1	C3	C4	108.6(3)
N1	C1	C5	110.5(2)	C4	C3	C2	103.0(3)
N1	C1	C2	110.4(3)	F2	C4	C5	110.4(3)
C6	C1	C5	113.8(3)	F2	C4	C3	112.5(3)
C6	C1	C2	111.2(2)	C3	C4	C5	103.9(3)
C5	C1	C2	105.7(3)				

Table 6: Hydrogen Bonds for **anti-cis-3,4-DFACPC**.

D	H	A	d(D-H)/Å	d(H-A)/Å	d(D-A)/Å	D-H-A/°
N1	H1A	O1[1]	0.89	2.01	2.824(4)	152.3

[1]1-X,-1/2+Y,2-Z

Table 7: Hydrogen Atom Coordinates (Å×10⁴) and Isotropic Displacement Parameters (Å²×10³) for **anti-cis-3,4-DFACPC**.

Atom	*x*	*y*	*z*	U(eq)
H2	7331	6932.96	7822.75	31
H1A	2799.01	3400.69	9579.8	16
H1B	1119.87	2613.34	8684.94	16
H1C	1363.61	5004.86	8937.07	16
H5A	844.08	5165.35	6773.77	17
H5B	2955.91	5591.48	6194.12	17
H2A	6018.99	1677.3	7895.49	16
H2B	3941.47	427.65	8147.45	16
H3	3951.37	-498.41	6138.41	24
H4	819.47	1402.34	6299.47	24

Crystal Data for $C_6H_{10}ClF_2NO_2$ (M=201.60 g/mol): monoclinic, space group $P2_1$ (no. 4), a = 6.41583(13) Å, b = 5.94388(12) Å, c = 10.9879(2) Å, β = 96.3458(18)°, V = 416.456(15) Å^3, Z = 2, T = 99.9(6) K, μ(CuKα) = 4.112 mm, $Dcalc$ = 1.608 g/cm^3, 3889 reflections measured (8.096° ≤ 2Θ ≤ 140.116°), 1568 unique (R_{int} = 0.0293, R_{sigma} = 0.0290) which were used in all calculations. The final R_1 was 0.0397 (I > 2σ(I)) and wR_2 was 0.1038 (all data).

Racemic-Trans-3,4-DFACPC

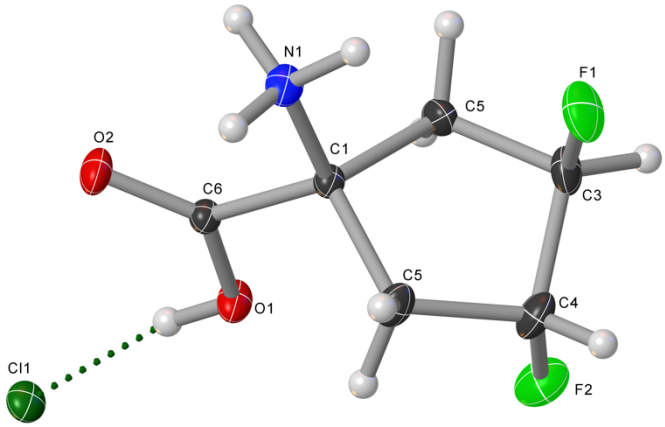

Table 1: Crystal Data and Structure Refinement for **Trans-DFACPC**

Compound	**Trans-DFACPC**
Formula	$C_6H_{10}ClF_2NO_2$
$D_{calc.}$/ g cm^{-3}	1.630
μ/mm^{-1}	0.458
Formula Weight	201.60
Colour	colourless
Shape	prism
Size/mm^3	0.21×0.13×0.12
T/K	106(7)
Crystal System	orthorhombic
Space Group	*Pnam*
a/Å	14.2673(4)
b/Å	9.3624(3)
c/Å	6.1491(2)
α/°	90
β/°	90
γ/°	90
V/Å^3	821.37(5)
Z	4
Z'	0.5
Wavelength/Å	0.71073
Radiation type	MoK_α
Θ_{min}/°	2.602
Θ_{max}/°	37.765
Measured Refl.	15683
Independent Refl.	2279
Reflections with I > 2(I)	2060
R_{int}	0.0577

Parameters	96
Restraints	25
Largest Peak	0.525
Deepest Hole	-0.376
GooF	1.159
wR_2 (all data)	0.1061
wR_2	0.1043
R1 (all data)	0.0456
R1	0.0408

Structure Quality Indicators

Reflections: d min (Mo) 0.58 | I/σ 31.4 | Rint 5.77% | complete 100% (IUCr) 100%

Refinement: Shift -0.001 | Max Peak 0.5 | Min Peak -0.4 | GooF 1.159

Images of the Crystal on the Diffractometer

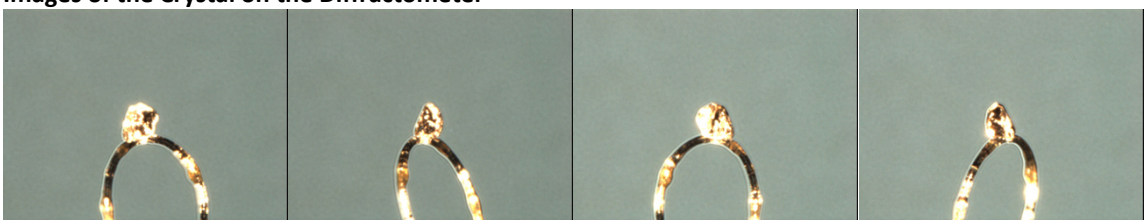

Reflection Statistics

Total reflections (after filtering)	16494	Unique reflections	2279
Completeness	0.965	Mean I/σ	20.96
hkl_{max} collected	(24, 15, 10)	hkl_{min} collected	(-22, -15, -10)
hkl_{max} used	(24, 15, 10)	hkl_{min} used	(0, 0, 0)
Lim d_{max} collected	100.0	Lim d_{min} collected	0.36
d_{max} used	9.36	d_{min} used	0.58
Friedel pairs	3725	Friedel pairs merged	1
Inconsistent equivalents	0	R_{int}	0.0577
R_{sigma}	0.0319	Intensity transformed	0
Omitted reflections	0	Omitted by user (OMIT hkl)	0
Multiplicity	(6976, 3670, 611, 60, 16, 3, 1)	Maximum multiplicity	24
Removed systematic absences	811	Filtered off (Shel/OMIT)	0

Table 2: Fractional Atomic Coordinates (×10^4) and Equivalent Isotropic Displacement Parameters (Å^2×10^3)

for **Trans-DFACPC**. U_{eq} is defined as 1/3 of the trace of the orthogonalised U_{ij}.

Atom	x	y	z	U_{eq}
Cl1	4674.6(3)	-3307.1(3)	2500	16.81(9)
O1	3897.8(8)	-355.1(11)	2500	16.6(2)
O2	5299.6(8)	746.3(13)	2500	18.9(2)
N1	4579.1(9)	3340.3(13)	2500	16.9(2)
C1	3882.8(9)	2143.5(14)	2500	11.7(2)
C6	4453.4(9)	770.8(14)	2500	12.2(2)
C5	3226.8(7)	2265.6(12)	4498.5(18)	17.99(18)
F2	1831.1(11)	1023.8(17)	1760(3)	27.4(3)
F1	2623.1(11)	4503.2(15)	3011(3)	28.6(4)
C4	2231.1(13)	2367(2)	1337(4)	20.6(4)
C3	2384.5(14)	3077(2)	3501(4)	19.7(4)

Table 3: Anisotropic Displacement Parameters ($\times 10^4$) for **Trans-DFACPC**. The anisotropic displacement factor exponent takes the form: $-2\pi^2[h^2a^{*2} \times U_{11} + \ldots + 2hka^* \times b^* \times U_{12}]$.

Atom	U_{11}	U_{22}	U_{33}	U_{23}	U_{13}	U_{12}
Cl1	18.02(15)	9.32(13)	23.10(16)	0	0	0.47(10)
O1	13.3(4)	9.0(4)	27.5(5)	0	0	-0.6(3)
O2	10.5(4)	14.9(4)	31.1(6)	0	0	0.6(3)
N1	15.8(5)	9.1(4)	26.0(6)	0	0	-1.0(4)
C1	10.9(5)	9.7(4)	14.5(5)	0	0	0.1(4)
C6	11.5(5)	9.8(5)	15.2(5)	0	0	0.2(4)
C5	14.7(4)	23.3(4)	16.1(4)	-5.0(3)	2.0(3)	0.8(3)
F2	22.4(6)	29.7(6)	30.1(7)	2.8(6)	-1.8(5)	-10.2(5)
F1	26.5(6)	16.2(5)	43.1(13)	0.8(5)	7.0(6)	5.9(4)
C4	11.2(7)	25.7(7)	24.8(9)	4.2(7)	-1.7(7)	-2.2(5)
C3	14.9(7)	17.0(5)	27.1(10)	-0.9(6)	3.4(7)	5.4(5)

Table 4: Bond Lengths in Å for **Trans-DFACPC**.

Atom	Atom	Length/Å
O1	C6	1.3188(17)
O2	C6	1.2076(17)
N1	C1	1.4975(18)
C1	C6	1.5214(18)
C1	C5[1]	1.5489(13)
C1	C5	1.5489(13)
C5	C4[1]	1.514(2)
C5	C3	1.548(2)
F2	C4	1.405(2)
F1	C3	1.411(2)
C4	C3	1.504(3)

[1]+x,+y,1/2-z

Table 5: Bond Angles in ° for **Trans-DFACPC**.

Atom	Atom	Atom	Angle/°
N1	C1	C6	106.08(11)

Atom	Atom	Atom	Angle/°
N1	C1	C5	110.22(8)
N1	C1	C5[1]	110.22(8)
C6	C1	C5	112.68(8)
C6	C1	C5[1]	112.68(8)
C5[1]	C1	C5	105.01(11)
O1	C6	C1	110.70(11)
O2	C6	O1	125.86(13)
O2	C6	C1	123.44(13)
C4[1]	C5	C1	107.61(12)
C4[1]	C5	C3	26.67(12)
C3	C5	C1	101.00(12)
F2	C4	C5[1]	112.83(17)
F2	C4	C3	106.91(19)
C3	C4	C5[1]	101.03(15)
F1	C3	C5	111.21(16)
F1	C3	C4	105.34(19)
C4[1]	C3	C5	73.9(2)
C4	C3	C5	104.28(15)
C4[1]	C3	F1	174.3(3)
C4[1]	C3	C4	70.4(3)

[1]+x,+y,1/2-z

Table 6: Hydrogen Fractional Atomic Coordinates (×10[4]) and Equivalent Isotropic Displacement Parameters (Å[2]×10[3]) for **Trans-DFACPC**. U_{eq} is defined as 1/3 of the trace of the orthogonalised U_{ij}.

Atom	x	y	z	U_{eq}
H1	4201(18)	-1120(30)	2500	25
H1A	4875.4	3363.45	1226.78	20
H1B	4993.51	3203.85	3561.76	20
H1C	4282.37	4164.82	2711.46	20
H5A	3159(13)	1372(15)	5180(30)	28(3)
H5B	3439(12)	2946(17)	5510(30)	28(3)
H3	1823(13)	3020(20)	4480(40)	31(5)

Table 7: Atomic Occupancies for all atoms that are not fully occupied in **Trans-DFACPC**.

Atom	Occupancy
H1A	0.5
H1B	0.5
H1C	0.5
F2	0.5
F1	0.5
C4	0.5
C3	0.5

Syn-cis-3,4-DFACPC

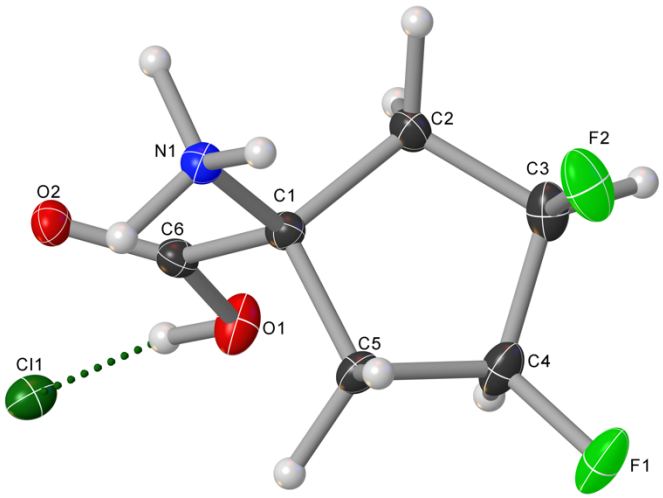

Table 1: Crystal Data and Structure Refinement for **Syn-cis-DFACPC**.

Compound	**Syn-cis-DFACPC**
Formula	$C_6H_{10}ClF_2NO_2$
$D_{calc.}$/ g cm^{-3}	1.587
m/mm^{-1}	4.06
Formula Weight	201.6
Colour	colourless
Shape	needle
Size/mm^3	0.42×0.08×0.04
T/K	100(2)
Crystal System	monoclinic
Flack Parameter	-0.009(16)
Hooft Parameter	-0.004(7)
Space Group	$P2_1$
a/Å	6.54423(13)
b/Å	5.90852(13)
c/Å	11.0924(3)
a/°	90
b/°	100.404(2)
g/°	90
V/Å^3	421.857(16)
Z	2
Z'	1
Wavelength/Å	1.54184
Radiation type	CuK_α

$Q_{min}/^{\circ}$	4.052
$Q_{max}/^{\circ}$	77.226
Measured Refl.	4999
Independent Refl.	1676
Reflections with I > 2σ(I)	1643
R_{int}	0.0346
Parameters	110
Restraints	1
Largest Peak	0.36
Deepest Hole	-0.219
GooF	1.061
wR_2 (all data)	0.087
wR_2	0.0853
R_1 (all data)	0.0335

Structure Quality Indicators

Reflections: d min (Cu) 0.79 | I/σ 32.4 | Rint 3.46% | complete 100% (IUCr) 100%

Refinement: Shift 0.000 | Max Peak 0.4 | Min Peak -0.2 | GooF 1.061 | Flack -.009(16)

Images of the Crystal on the Diffractometer

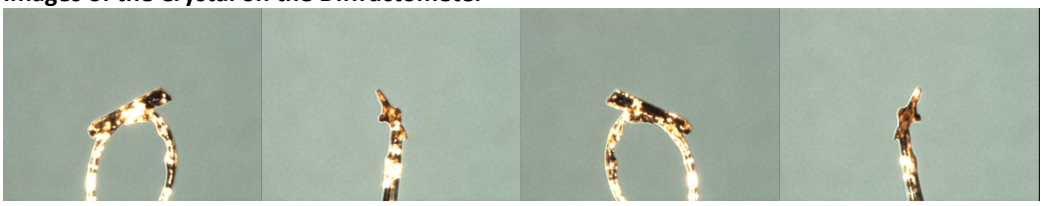

Reflection Statistics

Total reflections (after filtering)	4999	Unique reflections	1676
Completeness	0.943	Mean I/σ	29.43
hkl_{max} collected	(7, 7, 12)	hkl_{min} collected	(-8, -7, -13)
hkl_{max} used	(8, 7, 13)	hkl_{min} used	(-8, -7, 0)
Lim d_{max} collected	100.0	Lim d_{min} collected	0.77
d_{max} used	10.91	d_{min} used	0.79
Friedel pairs	561	Friedel pairs merged	0
Inconsistent equivalents	13	R_{int}	0.0346
R_{sigma}	0.0309	Intensity transformed	0
Omitted reflections	0	Omitted by user (OMIT hkl)	0
Multiplicity	(925, 564, 296, 181, 116, 63,	Maximum multiplicity	9

	36, 11, 4)		
Removed systematic absences	0	Filtered off (Shel/OMIT)	0

Table 2: Fractional Atomic Coordinates (×10^4) and Equivalent Isotropic Displacement Parameters (Å^2×10^3) for **Syn-cis-DFACPC**. U_{eq} is defined as 1/3 of the trace of the orthogonalised U_{ij}.

Atom	x	y	z	U_{eq}
Cl1	130.41	375.8	6309.5	19.1(2)
F1	5600(4)	9669(4)	9185.4(19)	33.1(5)
F2	9391(3)	7919(4)	9143.7(19)	33.3(5)
O2	4914(3)	2567(4)	5631.0(18)	18.0(5)
O1	3588(3)	3347(4)	7320(2)	23.3(5)
N1	8044(3)	5408(5)	6167.1(19)	15.4(4)
C6	4965(4)	3558(5)	6592(3)	15.7(5)
C5	5729(4)	7552(5)	7343(3)	16.8(6)
C3	7790(5)	6370(6)	9243(3)	22.4(6)
C1	6665(4)	5239(6)	7102(2)	14.3(5)
C4	5742(5)	7503(5)	8711(3)	21.7(6)
C2	7909(5)	4442(6)	8369(3)	18.9(6)

Table 3: Anisotropic Displacement Parameters (×10^4) for **Syn-cis-DFACPC**. The anisotropic displacement factor exponent takes the form: $-2\pi^2[h^2a^{*2} \times U_{11} + ... + 2hka^* \times b^* \times U_{12}]$

Atom	U_{11}	U_{22}	U_{33}	U_{23}	U_{13}	U_{12}
Cl1	16.1(3)	16.1(3)	26.5(3)	-1.0(3)	7.7(2)	-2.7(2)
F1	57.8(13)	19.4(9)	26.3(10)	-4.1(8)	19.0(9)	3.6(8)
F2	34.0(10)	32.8(11)	29.0(10)	0.7(9)	-5.2(8)	-16.5(9)
O2	15.5(8)	20.9(11)	17.1(10)	-3.2(9)	2.2(7)	-2.2(8)
O1	23.2(10)	26.2(12)	23.1(11)	-6.8(10)	11.2(8)	-10.7(9)
N1	12.8(9)	16.8(10)	17.2(10)	-0.2(12)	4.2(8)	-2.0(11)
C6	13.6(12)	15.6(13)	17.4(14)	0.6(12)	1.2(10)	0.3(11)
C5	18.2(12)	13.8(13)	19.2(14)	-2.0(11)	5.4(11)	-0.2(10)
C3	29.9(15)	20.2(14)	16.9(14)	-0.3(12)	3.3(11)	-6.6(12)
C1	14.1(10)	15.4(12)	13.8(11)	0.9(13)	3.9(9)	1.0(12)
C4	31.9(15)	15.5(13)	19.7(14)	-2.1(12)	9.7(12)	-1.4(12)
C2	21.4(12)	18.9(13)	15.2(14)	1.2(12)	-0.2(11)	3.0(10)

Table 4: Bond Lengths in Å for **Syn-cis-DFACPC**.

Atom	Atom	Length/Å
F1	C4	1.393(4)
F2	C3	1.411(4)
O2	C6	1.211(4)
O1	C6	1.320(3)
N1	C1	1.496(3)
C6	C1	1.523(4)
C5	C1	1.540(4)
C5	C4	1.517(4)
C3	C4	1.519(4)
C3	C2	1.507(5)

Atom	Atom	Length/Å
C1	C2	1.564(4)

Table 5: Bond Angles in ° for **Syn-cis-DFACPC**.

Atom	Atom	Atom	Angle/°
O2	C6	O1	125.4(3)
O2	C6	C1	123.0(3)
O1	C6	C1	111.6(2)
C4	C5	C1	103.0(2)
F2	C3	C4	107.4(3)
F2	C3	C2	108.4(3)
C2	C3	C4	103.2(3)
N1	C1	C6	106.1(2)
N1	C1	C5	111.7(2)
N1	C1	C2	111.2(2)
C6	C1	C5	110.9(2)
C6	C1	C2	111.4(2)
C5	C1	C2	105.7(2)
F1	C4	C5	111.8(2)
F1	C4	C3	111.9(3)
C5	C4	C3	104.0(2)
C3	C2	C1	105.8(3)

Table 6: Torsion Angles in ° for **Syn-cis-DFACPC**.

Atom	Atom	Atom	Atom	Angle/°
F2	C3	C4	F1	-49.3(3)
F2	C3	C4	C5	71.5(3)
F2	C3	C2	C1	-85.1(3)
O2	C6	C1	N1	2.5(4)
O2	C6	C1	C5	124.0(3)
O2	C6	C1	C2	-118.6(3)
O1	C6	C1	N1	-177.1(2)
O1	C6	C1	C5	-55.7(3)
O1	C6	C1	C2	61.7(3)
N1	C1	C2	C3	116.8(3)
C6	C1	C2	C3	-125.0(3)
C5	C1	C2	C3	-4.5(3)
C1	C5	C4	F1	160.4(2)
C1	C5	C4	C3	39.5(3)
C4	C5	C1	N1	-142.4(2)
C4	C5	C1	C6	99.5(3)
C4	C5	C1	C2	-21.3(3)
C4	C3	C2	C1	28.6(3)
C2	C3	C4	F1	-163.7(2)
C2	C3	C4	C5	-42.8(3)

Table 7: Hydrogen Fractional Atomic Coordinates ($\times 10^4$) and Equivalent Isotropic Displacement Parameters ($Å^2 \times 10^3$) for **Syn-cis-DFACPC**. U_{eq} is defined as 1/3 of the trace of the orthogonalised U_{ij}.

Atom	x	y	z	U_{eq}
H5A	6780	9030	7120	37(6)
H1A	9159.99	6700	6340	46(7)
H1B	7040	5890	5380	46(7)
H1C	8700	3730	6050	46(7)
H5B	4150	7910	6740	37(6)
H2A	9600	4039.99	8390	37(6)
H2B	7230.01	2820	8670.01	37(6)
H3	7920	5840	10250.02	40(13)
H4	4489.99	6460	8930.01	38(12)
H1	2480	2150	6990	57

Table 8: Hydrogen Bond information for **Syn-cis-DFACPC**.

D	H	A	d(D-H)/Å	d(H-A)/Å	d(D-A)/Å	D-H-A/deg
N1	H1B	O2[1]	1.033(2)	1.8321(19)	2.821(3)	158.92(16)

[1]1-x,1/2+y,1-z

3.6 References

[1] C. A. Roobottom, G. Mitchell, G. Morgan-Hughes. Radiation-reduction strategies in cardiac computed tomographic angiography. *Clinical Radiology* **2010**, *65*, 859-867.

[2] a) A. Zhu, D. Lee, H. Shim. Metabolic positron emission tomography imaging in cancer detection and therapy response. *Seminars in oncology* **2011**, *38*, 55-69; b) J. V. Frangioni. New technologies for human cancer imaging. *Journal of clinical oncology : official journal of the American Society of Clinical Oncology* **2008**, *26*, 4012-4021.

[3] a) V. Kapoor, B. M. McCook, F. S. Torok. An introduction to PET-CT imaging. *Radiographics* **2004**, *24*, 523-543; b) A. Almuhaideb, N. Papathanasiou, J. Bomanji. 18F-FDG PET/CT imaging in oncology. *Annals of Saudi medicine* **2011**, *31*, 3-13; c) K. K. S. Sai, Z. Zachar, P. M. Bingham, A. Mintz. Metabolic PET Imaging in Oncology. *American Journal of Roentgenology* **2017**, *209*, 270-276.

[4] K. Chen, X. Chen, in *Seminars in oncology, Vol. 38*, Elsevier, **2011**, pp. 70-86.

[5] a) M. M. D'Souza, R. Sharma, M. Tripathi, P. Panwar, A. Jaimini, A. Mondal. Novel positron emission tomography radiotracers in brain tumor imaging. *The Indian journal of radiology & imaging* **2011**, *21*, 202-208; b) K. L. Wallitt, S. R. Khan, S. Dubash, H. H. Tam, S. Khan, T. D. Barwick. Clinical PET Imaging in Prostate Cancer. *RadioGraphics* **2017**, *37*, 1512-1536.

[6] T. Singhal, T. K. Narayanan, V. Jain, J. Mukherjee, J. Mantil. 11C-l-Methionine Positron Emission Tomography in the Clinical Management of Cerebral Gliomas. *Molecular Imaging and Biology* **2008**, *10*, 1-18.

[7] T. Belhocine, K. Spaepen, M. Dusart, C. Castaigne, K. Muylle, P. Bourgeois, D. Bourgeois, L. Dierickx, P. Flamen. 18FDG PET in oncology: the best and the worst. *International Journal of Oncology* **2006**, *28*, 1249-1261.

[8] M. M. Goodman, W. Yu, N. Jarkas. Synthesis and biological properties of radiohalogenated α, α-disubstituted amino acids for PET and SPECT imaging of amino acid transporters (AATs). *Journal of Labelled Compounds and Radiopharmaceuticals* **2018**, *61*, 272-290.

[9] S. S. Gambhir. Molecular imaging of cancer with positron emission tomography. *Nature Reviews Cancer* **2002**, *2*, 683-693.

[10] W. W. Moses. Fundamental Limits of Spatial Resolution in PET. *Nuclear instruments & methods in physics research. Section A, Accelerators, spectrometers, detectors and associated equipment* **2011**, *648 Supplement 1*, S236-S240.

[11] S. D. Metzler, S. Matej, J. S. Karp. Resolution Enhancement in PET Reconstruction Using Collimation. *IEEE transactions on nuclear science* **2013**, *60*, 65-75.

[12] A. Berger. Magnetic resonance imaging. *BMJ (Clinical research ed.)* **2002**, *324*, 35-35.

[13] H. Jadvar. Imaging evaluation of prostate cancer with 18F-fluorodeoxyglucose PET/CT: utility and limitations. *European Journal of Nuclear Medicine and Molecular Imaging* **2013**, *40*, 5-10.

[14] C.-T. Lee, M.-K. Boss, M. W. Dewhirst. Imaging tumor hypoxia to advance radiation oncology. *Antioxidants & redox signaling* **2014**, *21*, 313-337.

[15] G. Niu, X. Chen. PET Imaging of Angiogenesis. *PET clinics* **2009**, *4*, 17-38.

[16] M. Peck, H. A. Pollack, A. Friesen, M. Muzi, S. C. Shoner, E. G. Shankland, J. R. Fink, J. O. Armstrong, J. M. Link, K. A. Krohn. Applications of PET imaging with the

proliferation marker [18F]-FLT. *Quarterly Journal of Nuclear Medicine and Molecular Imaging* **2015**, *59*, 95-104.

[17] C. Huang, J. McConathy. Radiolabeled amino acids for oncologic imaging. *Journal of Nuclear Medicine* **2013**, *54*, 1007-1010.

[18] a) H. N. Christensen. Role of amino acid transport and countertransport in nutrition and metabolism. *Physiological reviews* **1990**, *70*, 43-77; b) H. N. Christensen, M. Liang, E. G. Archer. A distinct Na+-requiring transport system for alanine, serine, cysteine, and similar amino acids. *Journal of Biological Chemistry* **1967**, *242*, 5237-5246; c) M. Kilberg, M. Handlogten, H. Christensen. Characteristics of an amino acid transport system in rat liver for glutamine, asparagine, histidine, and closely related analogs. *Journal of Biological Chemistry* **1980**, *255*, 4011-4019; d) D. L. Oxender, H. N. Christensen. Distinct mediating systems for the transport of neutral amino acids by the Ehrlich cell. *Journal of Biological Chemistry* **1963**, *238*, 3686-3699.

[19] R. J. Reimer, F. A. Chaudhry, A. T. Gray, R. H. Edwards. Amino acid transport System A resembles System N in sequence but differs in mechanism. *Proceedings of the National Academy of Sciences* **2000**, *97*, 7715-7720.

[20] a) Y. D. Bhutia, E. Babu, S. Ramachandran, V. Ganapathy. Amino acid transporters in cancer and their relevance to "glutamine addiction": novel targets for the design of a new class of anticancer drugs. *Cancer research* **2015**, *75*, 1782-1788; b) B. C. Fuchs, B. P. Bode. Amino acid transporters ASCT2 and LAT1 in cancer: Partners in crime? *Seminars in Cancer Biology* **2005**, *15*, 254-266; c) H. Okudaira, N. Shikano, R. Nishii, T. Miyagi, M. Yoshimoto, M. Kobayashi, K. Ohe, T. Nakanishi, I. Tamai, M. Namiki. Putative transport mechanism and intracellular fate of trans-1-amino-3-18F-fluorocyclobutanecarboxylic acid in human prostate cancer. *Journal of Nuclear Medicine* **2011**, *52*, 822-829.

[21] T. Miyagawa, T. Oku, H. Uehara, R. Desai, B. Beattie, J. Tjuvajev, R. Blasberg. "Facilitated" Amino Acid Transport is Upregulated in Brain Tumors. *Journal of Cerebral Blood Flow & Metabolism* **1998**, *18*, 500-509.

[22] a) R. J. Boado, J. Y. Li, M. Nagaya, C. Zhang, W. M. Pardridge. Selective expression of the large neutral amino acid transporter at the blood-brain barrier. *Proceedings of the National Academy of Sciences of the United States of America* **1999**, *96*, 12079-12084; b) H. Matsuo, S. Tsukada, T. Nakata, A. Chairoungdua, D. K. Kim, S. H. Cha, J. Inatomi, H. Yorifuji, J. Fukuda, H. Endou. Expression of a system L neutral amino acid transporter at the blood–brain barrier. *Neuroreport* **2000**, *11*, 3507-3511.

[23] R. Nakazato, D. S. Berman, E. Alexanderson, P. Slomka. Myocardial perfusion imaging with PET. *Imaging in medicine* **2013**, *5*, 35-46.

[24] K. Dahl, C. Halldin, M. Schou. New methodologies for the preparation of carbon-11 labeled radiopharmaceuticals. *Clinical and translational imaging* **2017**, *5*, 275-289.

[25] a) N. Tsuyuguchi, Y. Terakawa, T. Uda, K. Nakajo, Y. Kanemura. Diagnosis of Brain Tumors Using Amino Acid Transport PET Imaging with (18)F-fluciclovine: A Comparative Study with L-methyl-(11)C-methionine PET Imaging. *Asia Oceania journal of nuclear medicine & biology* **2017**, *5*, 85-94; b) T. Nariai, Y. Tanaka, H. Wakimoto, M. Aoyagi, M. Tamaki, K. Ishiwata, M. Senda, K. Ishii, K. Hirakawa, K. Ohno. Usefulness of l-[methyl-11C] methionine—positron emission tomography as a biological monitoring tool in the treatment of glioma. *Journal of neurosurgery* **2005**, *103*, 498-507; c) A. W. Glaudemans, R. H. Enting, M. A. Heesters, R. A. Dierckx, R. W. van Rheenen,

A. M. Walenkamp, R. H. Slart. Value of 11 C-methionine PET in imaging brain tumours and metastases. *European journal of nuclear medicine and molecular imaging* **2013**, *40*, 615-635; d) T. Kato, J. Shinoda, N. Nakayama, K. Miwa, A. Okumura, H. Yano, S. Yoshimura, T. Maruyama, Y. Muragaki, T. Iwama. Metabolic Assessment of Gliomas Using [11C]-Methionine, [18F]-Fluorodeoxyglucose, and [11C]-Choline Positron-Emission Tomography. *American Journal of Neuroradiology* **2008**, *29*, 1176-1182; e) K. Herholz, T. Hölzer, B. Bauer, R. Schröder, J. Voges, R. I. Ernestus, G. Mendoza, G. Weber-Luxenburger, J. Löttgen, A. Thiel, K. Wienhard, W. D. Heiss. [11C]-methionine PET for differential diagnosis of low-grade gliomas. *Neurology* **1998**, *50*, 1316-1322; f) G. Tóth, Z. Lengyel, L. Balkay, M. A. Salah, L. Tron, C. Toth. Detection of prostate cancer with 11C-methionine positron emission tomography. *The Journal of urology* **2005**, *173*, 66-69.

[26] L. C. Washburn, T. T. Sun, J. B. Anon, R. L. Hayes. Effect of structure on tumor specificity of alicyclic α-amino acids. *Cancer research* **1978**, *38*, 2271-2273.

[27] a) L. C. Washburn, T. T. Sun, B. Byrd, R. L. Hayes, T. A. Butler. 1-aminocyclobutane [11C] carboxylic acid, a potential tumor-seeking agent. *Journal of nuclear medicine: official publication, Society of Nuclear Medicine* **1979**, *20*, 1055-1061; b) K. Hübner, J. Thie, G. Smith, G. Kabalka, I. Keller, A. Kliefoth, S. Campbell, E. Buonocore. Positron emission tomography (PET) with 1-aminocyclobutane-1-[11C] carboxylic acid (1-[11C]-ACBC) for detecting recurrent brain tumors. *Clinical Positron Imaging* **1998**, *1*, 165-173.

[28] a) R. L. Hayes, L. C. Washburn, B. W. Wieland, T. T. Sun, R. R. Turtle, T. A. Butler. Carboxyl-labeled 11C-1-aminocyclopentanecarboxylic acid, a potential agent for cancer detection. *Journal of nuclear medicine: official publication, Society of Nuclear Medicine* **1976**, *17*, 748-751; b) K. F. Hübner, G. A. Andrews, L. Washburn, B. W. Wieland, W. D. Gibbs, R. L. Hayes, T. A. Butler, J. D. Winebrenner. Tumor location with 1-aminocyclopentane [11C] carboxylic acid: preliminary clinical trials with single-photon detection. *Journal of nuclear medicine: official publication, Society of Nuclear Medicine* **1977**, *18*, 1215-1221.

[29] K. F. Hübner, S. Krauss, L. Washburn, W. D. Gibbs, E. C. Holloway. Tumor detection with 1-aminocyclopentane and 1-aminocyclobutane C-11-carboxylic acid using positron emission computerized tomography. *Clinical nuclear medicine* **1981**, *6*, 249-252.

[30] T. M. Shoup, M. M. Goodman. Synthesis of [F-18]-1-amino-3-fluorocyclobutane-1-carboxylic acid (FACBC): a PET tracer for tumor delineation. *Journal of Labelled Compounds and Radiopharmaceuticals: The Official Journal of the International Isotope Society* **1999**, *42*, 215-225.

[31] F. I. Tade, M. A. Cohen, T. M. Styblo, O. A. Odewole, A. I. Holbrook, M. S. Newell, B. Savir-Baruch, X. Li, M. M. Goodman, J. A. Nye. Anti-3-18F-FACBC (18F-Fluciclovine) PET/CT of breast cancer: an exploratory study. *Journal of Nuclear Medicine* **2016**, *57*, 1357-1363.

[32] R. Amzat, P. Taleghani, D. L. Miller, J. J. Beitler, L. M. Bellamy, J. A. Nye, W. Yu, B. Savir-Baruch, A. O. Osunkoya, Z. Chen. Pilot study of the utility of the synthetic PET amino-acid radiotracer anti-1-amino-3-[18 F] fluorocyclobutane-1-carboxylic acid for the noninvasive imaging of pulmonary lesions. *Molecular Imaging and Biology* **2013**, *15*, 633-643.

[33] a) D. M. Schuster, P. T. Nieh, A. B. Jani, R. Amzat, F. D. Bowman, R. K. Halkar, V. A. Master, J. A. Nye, O. A. Odewole, A. O. Osunkoya. Anti-3-[18F] FACBC positron

emission tomography-computerized tomography and 111In-capromab pendetide single photon emission computerized tomography-computerized tomography for recurrent prostate carcinoma: results of a prospective clinical trial. *The Journal of urology* **2014**, *191*, 1446-1453; b) O. A. Odewole, F. I. Tade, P. T. Nieh, B. Savir-Baruch, A. B. Jani, V. A. Master, P. J. Rossi, R. K. Halkar, A. O. Osunkoya, O. Akin-Akintayo, C. Zhang, Z. Chen, M. M. Goodman, D. M. Schuster. Recurrent prostate cancer detection with anti-3-[18F]FACBC PET/CT: comparison with CT. *European Journal of Nuclear Medicine and Molecular Imaging* **2016**, *43*, 1773-1783; c) C. Nanni, R. Schiavina, E. Brunocilla, S. Boschi, M. Borghesi, L. Zanoni, C. Pettinato, G. Martorana, S. Fanti. 18F-fluciclovine PET/CT for the detection of prostate cancer relapse: a comparison to 11C-choline PET/CT. *Clinical nuclear medicine* **2015**, *40*, e386-e391.

[34] a) T. Wakabayashi, T. Iuchi, N. Tsuyuguchi, R. Nishikawa, Y. Arakawa, T. Sasayama, K. Miyake, T. Nariai, Y. Narita, N. Hashimoto. Diagnostic performance and safety of positron emission tomography using 18F-fluciclovine in patients with clinically suspected high-or low-grade gliomas: a multicenter phase IIb trial. *Asia Oceania Journal of Nuclear Medicine and Biology* **2017**, *5*, 10; b) A. Kondo, H. Ishii, S. Aoki, M. Suzuki, H. Nagasawa, K. Kubota, R. Minamimoto, A. Arakawa, M. Tominaga, H. Arai. Phase IIa clinical study of [18 F] fluciclovine: efficacy and safety of a new PET tracer for brain tumors. *Annals of nuclear medicine* **2016**, *30*, 608-618; c) E. E. Parent, M. Benayoun, I. Ibeanu, J. J. Olson, C. G. Hadjipanayis, D. J. Brat, V. Adhikarla, J. Nye, D. M. Schuster, M. M. Goodman. [(18)F]Fluciclovine PET discrimination between high- and low-grade gliomas. *EJNMMI research* **2018**, *8*, 67-67.

[35] N. Jarkas, R. J. Voll, L. Williams, V. M. Camp, M. M. Goodman. (R, S)-anti-1-Amino-2-[18F] Fluorocyclopentyl-1-carboxylic Acid: Synthesis from Racemic 2-Benzyloxycyclopentanone and Biological Evaluation for Brain Tumor Imaging with Positron Emission Tomography. *Journal of Medicinal Chemistry* **2010**, *53*, 6603-6607.

[36] a) D. M. Schuster, P. T. Nieh, A. B. Jani, R. Amzat, F. D. Bowman, R. K. Halkar, V. A. Master, J. A. Nye, O. A. Odewole, A. O. Osunkoya, B. Savir-Baruch, P. Alaei-Taleghani, M. M. Goodman. Anti-3-[(18)F]FACBC positron emission tomography-computerized tomography and (111)In-capromab pendetide single photon emission computerized tomography-computerized tomography for recurrent prostate carcinoma: results of a prospective clinical trial. *The Journal of urology* **2014**, *191*, 1446-1453; b) W. Seo, R. Voll, L. Williams, V. Camp, E. Malveaux, M. Goodman. Synthesis and biological evaluation of 1S,2R- and 1R,2S-1-amino-2-[18F]fluorocyclobutyl-1-carboxylic acid (2-FACBC) as PET tumor imaging agents. *Journal of Nuclear Medicine* **2010**, *51*, 361; c) D. W. Kim, D.-S. Ahn, Y.-H. Oh, S. Lee, H. S. Kil, S. J. Oh, S. J. Lee, J. S. Kim, J. S. Ryu, D. H. Moon, D. Y. Chi. A New Class of SN2 Reactions Catalyzed by Protic Solvents: Facile Fluorination for Isotopic Labeling of Diagnostic Molecules. *Journal of the American Chemical Society* **2006**, *128*, 16394-16397.

[37] D. Casabona, C. Cativiela. Simple and efficient multigram scale synthesis of 1-aminocyclopent-3-ene-1-carboxylic acid. *Synthesis* **2006**, *2006*, 2440-2443.

[38] K.-H. Park, M. M. Olmstead, M. J. Kurth. Diastereoselective Synthesis of Cyclopentanoids with Hydantoin and Isoxazoline Substituents. *The Journal of Organic Chemistry* **1998**, *63*, 113-117.

[39] D. W. Kim, Jeong, S. T. Lim, M.-H. Sohn, J. A. Katzenellenbogen, D. Y. Chi. Facile Nucleophilic Fluorination Reactions Using tert-Alcohols as a Reaction Medium:

Significantly Enhanced Reactivity of Alkali Metal Fluorides and Improved Selectivity. *The Journal of Organic Chemistry* **2008**, *73*, 957-962.

[40] W. Yu, L. Williams, V. M. Camp, E. Malveaux, J. J. Olson, M. M. Goodman. Stereoselective synthesis and biological evaluation of syn-1-amino-3-[18F]fluorocyclobutyl-1-carboxylic acid as a potential positron emission tomography brain tumor imaging agent. *Bioorganic & Medicinal Chemistry* **2009**, *17*, 1982-1990.

[41] a) H. Cheung, E. Blout. The Hydrazide as a Carboxylic-Protecting Group in Peptide Synthesis1. *The Journal of Organic Chemistry* **1965**, *30*, 315-316; b) K. J. Hale, L. Lazarides, J. Cai. A synthetic strategy for the cyclodepsipeptide core of the antitumor antibiotic verucopeptin. *Organic Letters* **2001**, *3*, 2927-2930.

[42] J. McConathy, R. J. Voll, W. Yu, R. J. Crowe, M. M. Goodman. Improved synthesis of anti-[18F]FACBC: improved preparation of labeling precursor and automated radiosynthesis. *Applied Radiation and Isotopes* **2003**, *58*, 657-666.

[43] a) H. Okudaira, T. Nakanishi, S. Oka, M. Kobayashi, H. Tamagami, D. M. Schuster, M. M. Goodman, Y. Shirakami, I. Tamai, K. Kawai. Kinetic analyses of trans-1-amino-3-[18F] fluorocyclobutanecarboxylic acid transport in Xenopus laevis oocytes expressing human ASCT2 and SNAT2. *Nuclear medicine and biology* **2013**, *40*, 670-675; b) M. Sidoryk, E. Matyja, A. Dybel, M. Zielinska, J. Bogucki, D. J. Jaskólski, P. P. Liberski, P. Kowalczyk, J. Albrecht. Increased expression of a glutamine transporter SNAT3 is a marker of malignant gliomas. *Neuroreport* **2004**, *15*, 575-578; c) N. Kondoh, N. Imazeki, M. Arai, A. Hada, K. Hatsuse, H. Matsuo, O. Matsubara, S. Ohkura, M. Yamamoto. Activation of a system A amino acid transporter, ATA1/SLC38A1, in human hepatocellular carcinoma and preneoplastic liver tissues. *International Journal of Oncology* **2007**, *31*, 81-87; d) W. L. Yu, W. M. Cong, Y. Zhang, Y. Chen, F. Wang, G. Yu. Overexpression of ATA1/SLC38A1 predicts future recurrence and death in Chinese patients with hilar cholangiocarcinoma. *Journal of Surgical Research* **2011**, *171*, 663-668; e) K. Wang, F. Cao, W. Fang, Y. Hu, Y. Chen, H. Ding, G. Yu. Activation of SNAT1/SLC38A1 in human breast cancer: correlation with p-Akt overexpression. *BMC cancer* **2013**, *13*, 343.

[44] M. Palacín, R. Estévez, J. Bertran, A. Zorzano. Molecular Biology of Mammalian Plasma Membrane Amino Acid Transporters. *Physiological Reviews* **1998**, *78*, 969-1054.

[45] a) R. F. Barth. Rat brain tumor models in experimental neuro-oncology: the 9L, C6, T9, F98, RG2 (D74), RT-2 and CNS-1 gliomas. *Journal of neuro-oncology* **1998**, *36*, 91-102; b) V. L. Jacobs, P. A. Valdes, W. F. Hickey, J. A. De Leo. Current review of in vivo GBM rodent models: emphasis on the CNS-1 tumour model. *ASN neuro* **2011**, *3*, e00063-e00063.

[46] a) T. M. Shoup, J. Olson, J. M. Hoffman, J. Votaw, D. Eshima, L. Eshima, V. M. Camp, M. Stabin, D. Votaw, M. M. Goodman. Synthesis and Evaluation of [18F] 1-Amino-3-fluorocyclobutane 1-carboxylic Acid to Image Brain Tumors. *therapy* **1999**, *1*, 2; b) L. Martarello, J. McConathy, V. M. Camp, E. J. Malveaux, N. E. Simpson, C. P. Simpson, J. J. Olson, G. D. Bowers, M. M. Goodman. Synthesis of syn-and anti-1-amino-3-[18F] fluoromethyl-cyclobutane-1-carboxylic acid (FMACBC), potential PET ligands for tumor detection. *Journal of Medicinal Chemistry* **2002**, *45*, 2250-2259.

[47] J. A. Nye, N. Jarkas, D. M. Schuster, B. Savir-Baruch, R. J. Voll, V. M. Camp, M. M. Goodman. Biodistribution and human dosimetry of enantiomer-1 of the synthetic leucine

analog anti-1-amino-2-fluorocyclopentyl-1-carboxylic acid. *Nuclear medicine and biology* **2011**, *38*, 1035-1041.

[48] J. A. Nye, D. M. Schuster, W. Yu, V. M. Camp, M. M. Goodman, J. R. Votaw. Biodistribution and radiation dosimetry of the synthetic nonmetabolized amino acid analogue anti-18F-FACBC in humans. *Journal of Nuclear Medicine* **2007**, *48*, 1017-1020.

[49] a) L. Martarello, J. McConathy, V. M. Camp, E. J. Malveaux, N. E. Simpson, C. P. Simpson, J. J. Olson, G. D. Bowers, M. M. Goodman. Synthesis of syn- and anti-1-Amino-3-[18F]fluoromethyl-cyclobutane-1-carboxylic Acid (FMACBC), Potential PET Ligands for Tumor Detection. *Journal of Medicinal Chemistry* **2002**, *45*, 2250-2259; b) J. McConathy, L. Martarello, E. J. Malveaux, V. M. Camp, N. E. Simpson, C. P. Simpson, G. D. Bowers, Z. Zhang, J. J. Olson, M. M. Goodman. Synthesis and evaluation of 2-amino-4-[18F]fluoro-2-methylbutanoic acid (FAMB): relationship of amino acid transport to tumor imaging properties of branched fluorinated amino acids. *Nuclear Medicine and Biology* **2003**, *30*, 477-490; c) P. Heiss, S. Mayer, M. Herz, H.-J. Wester, M. Schwaiger, R. Senekowitsch-Schmidtke. Investigation of transport mechanism and uptake kinetics of O-(2-[18F] fluoroethyl)-L-tyrosine in vitro and in vivo. *Journal of Nuclear Medicine* **1999**, *40*, 1367-1373.

[50] W. C. Still, M. Kahn, A. Mitra. Rapid chromatographic technique for preparative separations with moderate resolution. *The Journal of Organic Chemistry* **1978**, *43*, 2923-2925.

[51] K.-H. Park, M. M. Olmstead, M. J. Kurth. Diastereoselective solid-phase synthesis of novel hydantoin-and isoxazoline-containing heterocycles. *The Journal of Organic Chemistry* **1998**, *63*, 6579-6585.

[52] W. Yu, J. McConathy, J. J. Olson, M. M. Goodman. System a amino acid transport-targeted brain and systemic tumor PET imaging agents 2-amino-3-[18 F] fluoro-2-methylpropanoic acid and 3-[18 F] fluoro-2-methyl-2-(methylamino) propanoic acid. *Nuclear medicine and biology* **2015**, *42*, 8-18.

[53] W. Yu, L. Williams, V. M. Camp, E. Malveaux, J. J. Olson, M. M. Goodman. Stereoselective synthesis and biological evaluation of syn-1-amino-3-[18F] fluorocyclobutyl-1-carboxylic acid as a potential positron emission tomography brain tumor imaging agent. *Bioorganic & Medicinal Chemistry* **2009**, *17*, 1982-1990.

[54] W. Yu, J. McConathy, L. Williams, V. M. Camp, E. J. Malveaux, Z. Zhang, J. J. Olson, M. M. Goodman. Synthesis, radiolabeling, and biological evaluation of (R)-and (S)-2-amino-3-[18F] fluoro-2-methylpropanoic acid (FAMP) and (R)-and (S)-3-[18F] fluoro-2-methyl-2-N-(methylamino) propanoic acid (N MeFAMP) as potential PET radioligands for imaging brain tumors. *Journal of Medicinal Chemistry* **2009**, *53*, 876-886.

[55] A. B. Pippin, R. J. Voll, Y. Li, H. Wu, H. Mao, M. M. Goodman. Radiochemical synthesis and evaluation of 13N-labeled 5-aminolevulinic acid for PET imaging of gliomas. *ACS Medicinal Chemistry Letters* **2017**, *8*, 1236-1240.